SYNTHESIS AND STRUCTURAL STUDIES OF IRON, COBALT AND NICKEL COMPLEXES

A THESIS

Submitted in partial fulfilment of the requirements for the award of the degree of

DOCTOR OF PHILOSOPHY

in

CHEMISTRY

by

VAIBHAVE AGGARWAL

DEPARTMENT OF CHEMISTRY
INDIAN INSTITUTE OF TECHNOLOGY ROORKEE
ROORKEE - 247 667 (INDIA)

JULY, 2008

INDIAN INSTITUTE OF TECHNOLOGY ROORKEE
ROORKEE

CANDIDATE'S DECLARATION

I hereby certify that the work which is being presented in the thesis entitled, **SYNTHESIS AND STRUCTURAL STUDIES OF IRON, COBALT AND NICKEL COMPLEXES**, in partial fulfilment of the requirements for the award of the Degree of Doctor of Philosophy and submitted in the Department of Chemistry of the Indian Institute of Technology Roorkee, Roorkee is an authentic record of my own work carried out during a period from January 2005 to July 2008 under the supervision of Dr. Udai P. Singh, Professor, Department of Chemistry, Indian Institute of Technology Roorkee, Roorkee.

The matter presented in this thesis has not been submitted by me for the award of any other degree of this or any other Institute.

Vaibhave

(VAIBHAVE AGGARWAL)

This is to certify that the above statement made by the candidate is correct to the best of my knowledge.

(Udai P. Singh)
Supervisor

Date: 21.07.08

The Ph.D. Viva-Voce Examination of **Mr. Vaibhave Aggarwal**, Research Scholar, has been held on .....

Signature of Supervisor

Signature of External Examiner

ABSTRACT

The poly(pyrazolyl)borate ligands have more than 40 years old history as they were first time reported by S. Trofimenko in 1966. These ligands can be tetradentate, tridentate, bidentate or monodentate depending on the number of donor substituents on boron atom and the steric congestion around the metal. Nitrogen heterocycle other than pyrazole can also be used such as pyrrole, imidazole and indole. The pyrazole nucleus both thermally and hydrolytically is very stable and occupies a position similar to that of pyridine or ammonia in spectrochemical series. As a ligand, it coordinates to metals and metalloids through the 2-N but after deprotonation, the formed pyrazolate anions can coordinate through both nitrogen atoms as an exobidentate ligand of C_{2v} symmetry. The nucleophilicity of the nitrogen and their steric accessibility may be varied through appropriate ring substitution. Due to these attractive features, the coordination chemistry of pyrazole and its derivatives have attracted much attention. Among the different types of pyrazolylborates, hydrotris(pyrazolyl)borate (Tp^R) ligand has been widely used as supporting ligand for various inorganic and organometallic compounds.

Thioimidazole (N,N,S donor) can also be used in place of pyrazole as soft donor ligand and can bind to metal center through N or/and S atoms. In recent years, N-alkyl derivatives thioimidazoles have been directly coordinated to a variety of transition and main group metals and used as building blocks for the assembly of poly(mercaptoimidazolyl)borates. These soft analogues of Trofimenko's versatile poly(pyrazolyl)borates ligands, have been developed by Reglinski and co-workers in 1996 and also found interesting applications in the preparation of model compounds for sulfur-rich metalloenzymes such as liver alcohol dehydrogenase (LADH) and [NiFe]

hydrogenases. An important property of these ligands is the delocalized anionic charge on the thioimidazole group, which brings about the thiolate-like character of the thioimidazole sulfurs. After Reglinski's discovery of the tris(thioimidazolyl)borates (S_3 donor), Parkin and Vahrenkamp introduced the pyrazolylbis(thioimidazolyl)borates (NS_2 donor), and bis(pyrazolyl)(thioimidazolyl)borates (N_2S donor) ligands to give these coordination environment around metal centers. Further they have suggested that varying the substituents on the pyrazole and thioimidazole groups of these ligands, an appropriate electronic and geometrical environment can also be generated on metal centre. For the sake of convenience, the work embodied in the thesis is presented in the following chapter:

The **first** chapter of the thesis is the general introduction and presents an up to date survey of literature related to the various pyrazole, thioimidazole and their borate salts. The different types of metal complexes related to the present research have been posed in the context of the cited work.

The chapter **two** of the thesis deals with azido complexes of Iron (III) having hydrotris(1-pyrazolyl)borate [Tp] or hydrotris(3,5-dimethyl-pyrazolyl)borate [Tp^{Me2}] and some bidentate ligands (acetylacetonate/picolinate) as supporting ligands. To check these complexes as azide-selective, one of the iron complex [$Tp^{Me2}Fe(acac)Cl$] was used as an ionophore for the preparation of a poly(vinyl chloride) (PVC) membrane sensor for azide anion. After confirming the selectivity of azide ion, the reaction of [$Tp^{Me2}Fe(acac)Cl$] with the methanolic solution of sodium azide was performed to get single azide bonded compound [$Tp^{Me2}Fe(acac)N_3$]. The complex [$Tp^{Me2}Fe(Pz^{Me2}H)(N_3)_2$] was also synthesized by the reaction of $FeCl_3$ and KTp^{Me2} with two equivalent sodium azide in presence of 3,5-dimethylpyrazole [$Pz^{Me2}H$]. All of these compounds were

characterized by different spectroscopic methods including single crystal X-ray crystallography. The one electron electrochemically reduced product of $[Tp^{Me2}Fe(Pz^{Me2}H)(N_3)_2]$ was crystallized in ionic form $[(Tp^{Me2})_2Fe][FeCl_4]$. Further attempts have been made to prepare more ion-pair complexes by co-crystallization of nickel (II) phenanthroline complex cations and different complex anions like $[MnCl_4]^{2-}$, $[Co(tm^{t\text{-}Bu})Cl_3]^-$, $[Ni(tm^{t\text{-}Bu})Cl_3]^-$ and $[Zn(tm^{t\text{-}Bu})Cl_3]^-$ ($tm^{t\text{-}Bu}$ = N-*tert*-butyl-2-thioimidazole).

Chapter **three** deals with synthesis of some cobalt complexes using 3,5-diisopropylpyrazole $[Pz^{iPr2}H]$, hydrotris(3,5-diisopropyl-1-pyrazolyl)borate $[Tp^{iPr2}]$, substituted benzoates and N-tert-butyl-2-thioimidazole $[tm^{t\text{-}Bu}]$. The reaction of $[Tp^{iPr2}Co(NO_3)]$ with sodium para-fluorobenzoate [Na(*p*-F-OBz)] led to the formation of five coordinate complex of the type $[Tp^{iPr2}Co(p\text{-F-OBz})]$. The oxidation of this compound with H_2O_2 in the presence of $Pz^{iPr2}H$ resulted the formation of a unique compound $[\{HB(\mu\text{-}3\text{-}OCMe_2\text{-}5\text{-}Pz^{iPr})(Pz^{iPr2})_2\}Co(Pz^{iPr2}H)(p\text{-F-OBz})]$ where only one methine group of diisopropyl pyrazole ring of Tp^{iPr2} ligand was oxidized and coordinated to cobalt center. Pyrazolato bridged binuclear cobalt (II) complex $[(Pz^{iPr2}H)_2Co_2(\mu\text{-}Pz^{iPr2})_2(p\text{-F-OBz})_2]$ was formed when the reaction of cobalt (II) chloride with $Pz^{iPr2}H$ in presence of sodium *p*-fluorobenzoate was performed. The same reaction in presence of 50 equivalent of H_2O_2 resulted in the formation of host-guest complexes of the type $[(Co(3\text{-}OCMe_2,5\text{-}Pz^{iPr}H)_3].2(p\text{-X-OBz})$ (where X = F, Cl, CH_3, NO_2, CN, CHO) with different packing. Some cobalt complexes with N-tert-butyl-2-thioimidazole $[tm^{t\text{-}Bu}]$ were also synthesized and characterized.

The chapter **four** of the thesis deals with mononuclear nickel (II) complexes having hydrotris(3-phenyl-5-methyl-1-pyrazolyl)borate $[Tp^{Ph,Me}]$, 3-phenyl-5-methyl-

pyrazole [$Pz^{Ph,Me}H$] and N-tert-butyl-2-thioimidazole [$tm^{t\text{-}Bu}$] as supporting ligands. [$(Tp^{Ph,Me})_2Ni$] were synthesized by the reaction of $Tp^{Ph,Me}$ and nickel (II) chloride whereas the same reaction in presence of $Pz^{Ph,Me}H$ resulted in the formation of [$Tp^{Ph,Me}Ni(Cl)Pz^{Ph,Me}H$]. The complex [$Tp^{Ph,Me}Ni(Cl)Pz^{Ph,Me}H$] has been used as an ionophore to prepare its polymeric membrane as a sensor for benzoate anion. The different benzoate complexes of the type [$Tp^{Ph,Me}Ni(p\text{-X-OBz})Pz^{Ph,Me}H$] (X = H, F, Cl, NO_2, Me, OMe, OH, CHO, CN, NH_2) were also prepared by the reaction of [$Tp^{Ph,Me}Ni(Cl)Pz^{Ph,Me}H$] and different sodium *p*-X-benzoate for structural studies in solid state using single crystal X-ray method. In all these complexes except amino-benzoate complex, the benzoate groups are coordinated as monodentate and the uncoordinated oxygen atom of the benzoate groups form intramolecular hydrogen bonds with NH group present on pyrazole ring. The complex [$Tp^{Ph,Me}Ni(Cl)Pz^{Ph,Me}H$] has also been used as ionophores for azide and thiocyanate anions. Some nickel (II) complexes with N-tert-butyl-2-thioimidazole [$tm^{t\text{-}Bu}$] were also synthesized and characterized.

The material and reagents, synthetic procedures, experimental details and different type of spectroscopic measurements are described in chapter **five** of the thesis. Methods for the preparation of different type of ligands and their metal complexes have also been included.

ACKNOWLEDGEMENT

Pursuing a Ph.D. is like climbing a high peak, step by step, accompanied with hardships, hope and despair, encouragements and discouragements, frustration and success, and help and cooperation of the people around you. Today, as I find myself here at the summit enjoying the beautiful and serene ambience, I realize that it was in fact a teamwork that helped me reach here and so I wish to express my gratitude towards one and all who contributed to this significant journey of my career, in whatever big or small way they could.

First and foremost, I wish to take the opportunity to thanks **Prof. Udai P. Singh**, my supervisor and mentor, whose suggestions, advice, ideas and criticisms at all stages of the work, right from the formulation of the problem through the laboratory work to the completion of the final draft of the thesis, have made it possible for me to complete this work quantitatively as well as qualitatively. His exhaustive guidance, prudent support and enthusiastic interest through out the period of my research work, helped to develop a positive research attitude in me. I further extend my thanks to him for providing all the facilities and keeping me free to do research up to the maximum possible extent.

I am extremely grateful to **Prof. Kamaluddin**, Head and **Prof. Ravi Bhushan**, former Head, Department of Chemistry, for providing the basic infrastructural facilities for carrying out this research work.

I owe my sincere thanks to **Prof. A. K. Singh**, who generously gave his valuable time for detailed and constructive comments and whose in-depth knowledge on the sensor work has been highly significant for me.

I am thankful to the entire faculty and the staff members who have helped me in some way or the other during my association with the Institute and provided a healthy environment to develop my skills as a good researcher.

I express my genuine appreciation to my seniors, **Dr. Asish K. Sharma**, **Dr. Rajeev Kumar**, **Dr. Raj Kumar**, **Dr. Pooja Tyagi** for their encouragement and moral support during the course of the research work. I am thankful to my lab mates **Sujata**, **Nidhi**, **Sandeep** and **Kapil** for their continuous support, cooperation and encouragement. The last moment impetus and completion deadline has given sleepless nights to them too. Helping hands extended by them at that moment are beyond any expression.

I would also like to mention the name of **Sameena** who has been a great friend and colleague. From the very beginning she has extended her enduring help and assistance. I highly appreciate the constant encouragement, support and guidance of **Puja Mam** and **Vipin Sir** during my difficult moments. I express my wholehearted indebtedness to my friends **Aditi**, **Jitendra**, **Barkha**, **Virender**, **Nivedita** and **Saurabh**, who boosted my morale with their ever-buoyant expression and gave me a congenial environment in the department.

It will be unjust if I don't express my deep gratitude towards **God**, my **mummy** and late **papa** for their blessing which always acted as a guiding star for me at every stage of my work, and helped me to scale new heights. I wish to give special thanks to my **mummy**, who has taken a lot of pain to make me realize my dream and I owe her what I am today. This thesis would not have been possible without the sacrifice, motivation and indomitable faith of all my family members to whom I express my indebtedness and gratitude, especially my little sister **Peenu**.

I am also thankful to the financial assistance from Council of Scientific and Industrial Research, New Delhi, in the form of Junior and Senior Research Fellowship during my research work.

Last, but not the least I am thankful to **Dr. P. Venugopalan**, **Arshad**, **Shailesh Sir** and **V. Ramkumar**, whose useful suggestions eased the complicated task of solving and refining the crystal structure of my complexes and contributed in bringing this work to fruitation.

(Vaibhave Aggarwal)

LIST OF PUBLICATIONS/CONFERENCES/SYMPOSIUM

Publications:

1. Udai P. Singh , **Vaibhave Aggarwal**, Asish K.Sharma, "Mononuclear cobalt (II) carboxylate complexes: Synthesis, molecular structure and selective oxygenation study", Inorganica Chimica Acta, 360 (2007) 3226–3232..
2. Udai P. Singh and **Vaibhave Aggarwal**, "Hydrogen-bonding and π–π stacking interactions in tris(1,10-phenanthroline-κ^2N,N')nickel (II) bis{[1-tert-butyl-imidazole-2(3H)-thione-κS]trichloridonickelate (II)} acetonitrile disolvate", Acta Crystallographica Section E : Structure Reports Online, E64 (2008) m935-m936.
3. Ashok Kumar Singh, Udai P. Singh, **Vaibhave Aggarwal**, Sameena Mehtab, "Azide-selective sensor based on tripodal iron complex for direct azide determination in aqueous samples", Analytical and Bioanalytical Chemistry (2008) in press.
4. **Vaibhave Aggarwal**, Sameena Mehtab, Udai P. Singh, Ashok K. Singh, "Nickel Pyrazolyl Borate Complexes: Synthesis, Structure and Analytical Application in Biological and Environmental Samples as Anion Selective Sensors", Talanta (accepted).
5. Udai P. Singh, **Vaibhave Aggarwal**, Shailesh Upreti, "Nickel Pyrazolyl Borate Complex: Synthesis, Structure and Application as Benzoate Selective Sensors", European Journal of Inorganic Chemistry (communicated).
6. Udai P. Singh and **Vaibhave Aggarwal**, "Synthesis and structural studies of nickel (II) complexes having thioimidazole and pyrazole ligands", Journal of Structural Chemistry (communicated).

7. **Vaibhave Aggarwal**, V. Ram Kumar and Udai P. Singh, "Synthesis and molecular structure of sulfur containing cobalt compounds", Journal of Chemical Crystallography (communicated).
8. Ashok Kumar Singh, Sameena Mehtab, Udai P. Singh, **Vaibhave Aggarwal** "Comparative studies of tridentate sulphur and nitrogen-containing ligands as ionophores for construction of cadmium ion-selective membrane sensors", Electroanalysis, 19 (2007) 1213-1221.
9. Ashok Kumar Singh, Udai P. Singh, Sameena Mehtab, **Vaibhave Aggarwal** "Thiocyanate selective sensor based on tripodal zinc complex for direct determination of thiocyanate in biological samples", Sensors and Actuators B Chemical, B125(2) (2007) 453-461.
10. Ashok Kumar Singh, Sameena Mehtab, Udai P. Singh, **Vaibhave Aggarwal** "Tripodal chelating ligands based sensor for selective determination of Zn(II) in biological and environmental sample", Analytical and Bioanalytical Chemistry, 388(8) (2007) 1867-1876.
11. Ashok Kumar Singh, Sameena Mehtab, Udai P. Singh, **Vaibhave Aggarwal**, Jitendra, "Tripodal cadmium complex and macrocyclic ligand based sensors for phosphate ion determination in environmental samples", Electroanalysis, 11, (2008) 1186-1193.
12. Mamata Singh, **Vaibhave Aggarwal**, Udai. P. Singh, Nand K. Singh, "Synthesis, characterization and spectroscopic studies of a new ligand [N'-(2-methoxy-benzoyl)-hydrazine]-carbodithioic acid ethyl ester and its complexes: X-ray structural study of Mn(II) complex", Polyhedron (accepted).

Conferences/Symposium:

1. "Metal Nitrido Complexes: Synthesis and Structural Studies", 8th CRSI National Symposium in Chemistry (NSC-8), Indian Institute of Technolgy Bombay, India, P-61 (2006). **Vaibhave Aggarwal**, Pooja Tyagi and Udai P. Singh.
2. "Synthesis, Structural and Selective Oxygenation Studies of Cobalt (II) Complexes", 9th CRSI National Symposium in Chemistry (NSC-9), Univ. of Delhi, India, P-218 (2007). **Vaibhave Aggarwal**, Asish K. Sharma and Udai P. Singh.
3. "Synthesis, Structural Characterization and Superoxide Dismutase Activity of some Ni(II) Complexes" XII-Modern Trend in Inorganic Chemistry, Indian Institute of Technology, Madras, India, P-107 (2007). **Vaibhave Aggarwal** and Udai P. Singh.

CONTENTS

Chapter 1

General Introduction

The poly(pyrazolyl)borate ligands have more than 40 years old history as they were first time reported by S. Trofimenko in 1966 [1-3]. The basic skeleton of the ligand involves pyrazole units bonded to a boron apex via the nitrogen atoms. Poly(pyrazolyl)borate ligands and their analogues are also known as scorpionate ligands as the manner in which they combine with metal ions resembles the grabbing-and-stinging action of a scorpion. These ligands can behave as tetradentate, tridentate, bidentate or monodentate depending on the number of donor substituents on the boron atom and the steric congestion around the metal.

The pyrazole nucleus both thermally and hydrolytically is very stable and occupies a position similar to that of pyridine or ammonia in the spectrochemical series. As a ligand, it coordinates to metals and metalloids through the 2-N position but after deprotonation, pyrazolate anions can coordinate through both nitrogen atoms as an exobidentate ligand of C_{2v} symmetry. The nucleophilicity of the nitrogens and their steric accessibility may be varied through appropriate ring substitution. Due to these fascinating features, the coordination chemistry of pyrazole and its derivatives has attracted much attention. Several pyrazoles with substitutions at 3, 4 or 5-positions have been synthesized and the some are given below.

3-tert-butylpyrazole, 3-phenylpyrazole [4], 3-phenyl-5-methylpyrazole [5], 3-isopropylpyrazole [6], 3,5-diisopropylpyrazole [7], 3-tert-butyl-5-methylpyrazole, 3-tert-butyl-5-isopropylpyrazole [8], 3-furyl-5-methylpyrazole, 3-carboxyethyl-5-methylpyrazole [9], 3-diphenylmethylpyrazole [10], 3-(1-naphthyl)pyrazole, 3-(2-naphthyl)pyrazole [11], 3-(4-pyridyl)-5-methylpyrazole [12], 4-cyano-3-phenylpyrazole [13], 3-isopropyl-4-bromopyrazole [14, 15], 3-isopropyl-5-

methylpyrazole [16], 3-neopentylpyrazole [17], 3-thienylpyrazole [18], 3,5-diphenylpyrazole [5], 3-*p*-tolylpyrazole [19], 3-*p*-anisylpyrazole [14], 3,5-di-tert-butylphenylpyrazole [20], 3-anthrylpyrazole [21], 3-mesitylpyrazole, 3-cumyl-5-methylpyrazole [22], 3,5-trifluoromethylpyrazole [23], 3(5)-(4-methoxyphenyl)pyrazole [24], 3-(2-pyridyl)pyrazole [25], 3,5-di(4-n-butoxyphenyl)pyrazole [26], 5-amino-3-(pyrid-2-yl)-1H-pyrazole [27], 3(5)-amino-4-acetyl-5(3)-methylpyrazole [28], 3,5-dimethyl-1-carbamidopyrazole [29], 5-methyl-3-(2'-benzimidazolyl)pyrazole [30]. Most of these synthesized pyrazoles have been used for the synthesis of their dihydrobis-, hydrotris- and tetrakis(pyrazolyl)borate salts which have wide application in coordination chemistry, bioinorganic and organometallic chemistry. Some pyrazoles have also been used as powerful ditopic receptors for metal cations (through the pyridinic N atom) and anions (via the pyrrolic N-H group) [31-33].

The pyrazolylborate / scorpionate chemistry signifies a very large and growing area as these ligands are extremely versatile and the number of donor atoms can be varied from two to three while going from the bidentate ligands to the potentially tridentate ligands. The poly(pyrazolyl)borate ligands have properties lying between those of parent $[H_4\text{-}nB(Pz)_n]^-$ ligands (Pz = pyrazolyl) and the strerically hindered derivatives $[H_4\text{-}nB(3\text{-}RPz)_n]^-$, where R = tert-butyl and phenyl groups [4, 34]. The parents ligands, in particular the derivatives with n = 3, have been extensively used in inorganic and bioinorganic chemistry. However, the chemistry is severely limited because of the tendency of the first row transition metal ions to form the bis-ligated complex i.e., $M(HB(Pz)_3)_2$. On the other hand, the bulky group of the 3-R derivatives prevents formation of this type of complex. The 3-tert-butyl ligand allows no further

access to the metal ion and is a "tetrahedral enforcer", whereas the 3-phenyl derivative accommodates five coordination with trigonal-bipyramidal geometry. Although bis-ligated complex formation is prevented, the metal ion is not readily accessible to other molecules because of the steric bulk of the 3-substituents.

As the steric effect plays a significant role in the chemistry of poly(pyrazolyl)borate ligands, a large number of second-generation scorpionates with the alkyl or aryl groups at the 3- and / or 5-positions of the ring are available in literature. The most commonly used members of this family are the tris(pyrazolyl)borate ligands (generally abbreviated as Tp^R) which are formally analogous to cyclopentadienyl (Cp) ligands in that both are six-electron (ionic model) or five-electron donor (covalent model) ligands. They are weak-field hard σ-N donors which tend to form *fac*-octahedral complexes, while Cp ligands are typically 5-fold π-donors and tend to form tetrahedral complexes. Comparatively, their overall donor properties are weaker than those of the cyclopentadienyls. They are bulkier than the cyclopentadienyls and moreover in six-coordinate environment they enforce nearly octahedral coordination to the metal with N-M-N bite angles close to the ideal 90° value. The Tp^R ligands are able to grab the top half of a metal so that it is possible to do chemistry at the other half. They may act as more than simple spectators in the course of chemical reactions experienced by their compounds and have an important influence on their reactivity by means of temporary changes of denticity. They have been used in the design of functional molecules, catalysis of chiral induced asymmetric synthesis, liquid crystal materials, molecular electronic devices and biomimetic chemistry.

In the hierarchy of increasing steric hindrance around the metal in 3- or 5-substituted tris(pyrazolyl)borates, the currently known series is $H < CH_3 < C_6H_5 <$ iPr

< tBu. In terms of forming octahedral L_2M complexes, ligands with R = H and CH_3 do so rapidly whereas those with R = C_6H_5 do so reluctantly and those with R = iPr do not form L_2M complexes [4]. The ligands with R = iPr form octahedral complexes only with rearrangement of each L to $HB(3\text{-}Pz^{iPr})_2(5\text{-}Pz^{iPr})$; they also form mixed octahedral LML complexes, provided L is a relatively unhindered tris(pyrazolyl)borate ligand [35]. Finally, ligands with R = ^{t}Bu do not form octahedral complexes at all with first-row transition metals. Conversely, in terms of formation of LMX (X= halide or pseudohalide) species, ligands with R = ^{t}Bu form these stable complexes with ease and those with R = iPr, also form LMX complexes readily but possess reactivity for solvation or for displacement of X with anionic nucleophiles. The ligands with R = phenyl form LMX species, that are even more reactive towards solvation or substitution of X. When R = methyl, and even more so when R = H, the LMX species becomes progressively less stable and undergo transformation to the octahedral L_2M complexes. Some reported metal complexes of the hydrotris(pyrazolyl)borate ligands relevant to the present work are cited below.

Hydrotris(1-pyrazolyl)borate [$HB(pz)_3$ = Tp]

Calogero et al. [36] prepared a series of iron (II) or iron (III) complexes of type FeL_2 or $[FeL_2]^+ X^-$ (X = BF_4 or BPh_4) with L = hydridotris(lH-pyrazol-1-yl)borate, tetrakis(lH-pyrazol-l-yl)borate, hydridotris(3-methyl-1H-pyrazol-1-yl)borate, hydridotris-(3,5-dimethyl-1H-pyrazol-1-yl)borate, hydridotris(4-chloro-3,5-dimethyl-lH-pyrazol-l-yl)borate, hydridotris(3,4,5-trimethyl-1H-pyrazol-l-yl)borate, hydridotris(1,2,4-1H-triazol-lyl)borate and hydridotris(3a,7a-benzo-1,2,3-1H-triazol-l-yl)borate. They also characterized this series by ^{57}Fe Mössbauer effect and X-ray crystal structures of iron

(II) bis[hydridotris(3-methyl-1H-pyrazol-l-yl)borate] and iron (III) bis[hydridotris(lH-pyrazol-1-yl)borate]tetrafluoroborate (Fig. 1-1). Both complexes were in octahedral geometry.

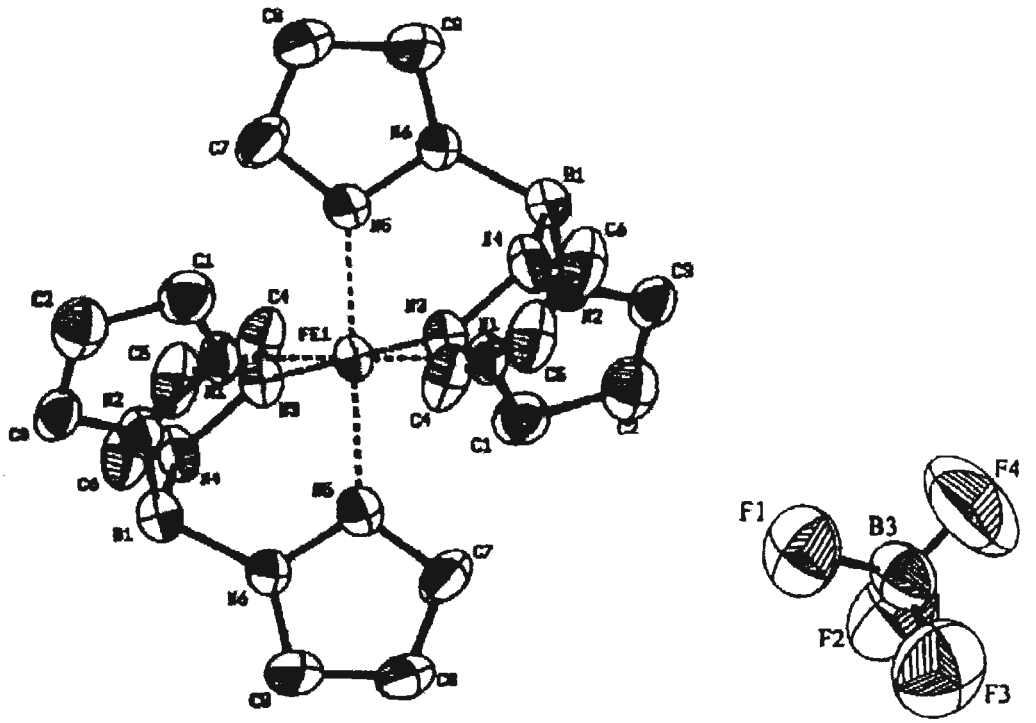

Fig. 1-1 Crystal structure of $[Fe(Tp)_2][BF_4]$

Hydrotris(3,5-dimethyl-pyrazolyl)borate [$HB(Pz^{Me2})_3 = Tp^{Me2}$]

Mason et al. [37] synthesized bis[hydrotris(3,5-dimethyl-1-pyrazolyl)borate] iron (III) complexes with different counter anions i.e., $[Fe(Tp^{Me2})_2][PF_6]$, $[Fe(Tp^{Me2})_2]$-[TCNQ].THF and $[Fe(Tp^{Me2})_2][FeBr_4]$. They succeeded in obtaining crystal structures determination of $[Fe(Tp^{Me2})_2]$ $[PF_6]$ (Fig. 1-2) and $[Fe(Tp^{Me2})_2]$[TCNQ].THF where iron centre was almost in an octahedral geometry.

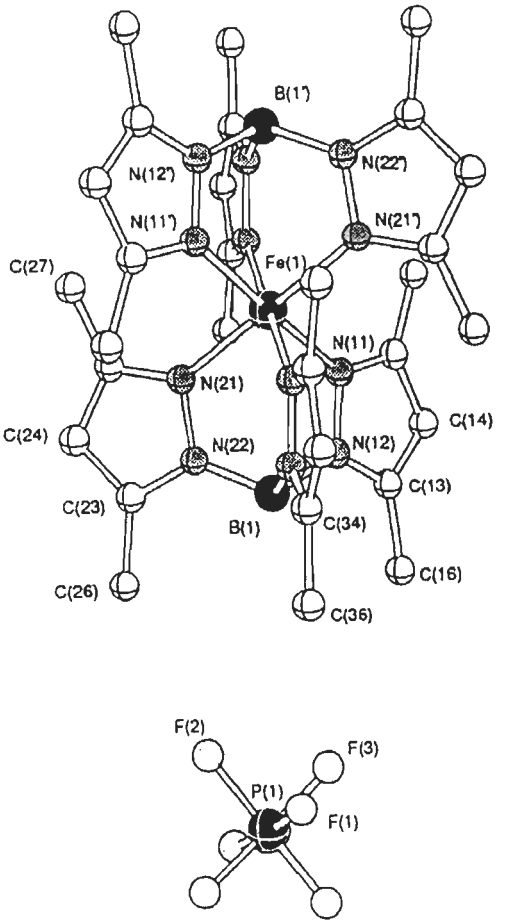

Fig. 1-2 Crystal structure of $[Fe(Tp^{Me2})_2][PF_6]$

Sun et al. [38] reported the syntheses, crystal structure and properties of a new half-sandwich mononuclear nickel (II) complex containing a single hydrotris(3,5-dimethylpyrazolyl)borate (Tp^{Me2}) ligand, nitrito and methanol co-ligands. The Ni(II) ion in the complex was coordinated to three pyrazolyl nitrogen atoms, two oxygen atoms of NO_2^- and one oxygen atom of CH_3OH to form a distorted octahedron (Fig. 1-3). The NO_2^- was coordinated in an asymmetric nitrito-O,O'-bidentate coordination mode with an O(1)–Ni–O(2) angle of 57.71(11)° and Ni–O bond lengths of 2.1882 and 2.1222 Å.

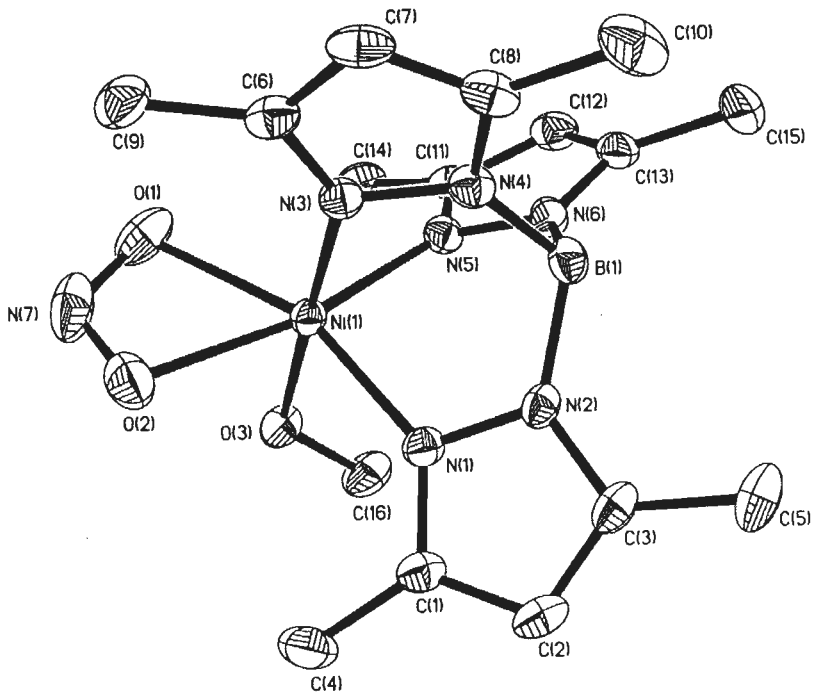

Fig. 1-3 Crystal structure of $[Tp^{Me2}Ni(\eta^2\text{-}O_2N)(CH_3OH)]$

Sun et al. further [39] reported the syntheses, crystal structures and spectroscopic properties of a series of half-sandwich nickel (II) complexes with hydrotris(3,5-dimethylpyrazolyl)borate and azide or thiocyanate i.e., $[Tp^{Me2}Ni(Pz^{Me2}H)_2(N_3)]$, $[Tp^{Me2}Ni(Pz^{Me2}H)(SCN)(H_2O)]$ and $[Tp^{Me2}Ni(SCN)(CH_3OH)_2]$ (Tp^{Me2} = hydrotris(3,5-dimethylpyrazolyl)borate; $Pz^{Me2}H$ = 3,5-dimethylpyrazole). They suggested from X-ray crystallography studies that the nickel (II) ion in $[Tp^{Me2}Ni(Pz^{Me2}H)_2(N_3)]$ was coordinated to six nitrogen atoms of Tp^{Me2} and the azide ion to form a distorted N6 octahedron (Fig. 1-4). The nickel (II) ion in $[Tp^{Me2}Ni(Pz^{Me2}H)(SCN)(H_2O)]$ was six-coordinated to five nitrogen atoms of Tp^{Me2}, $Pz^{Me2}H$, thiocyanate and one oxygen atom of water molecule to form a N5O octahedral environment.

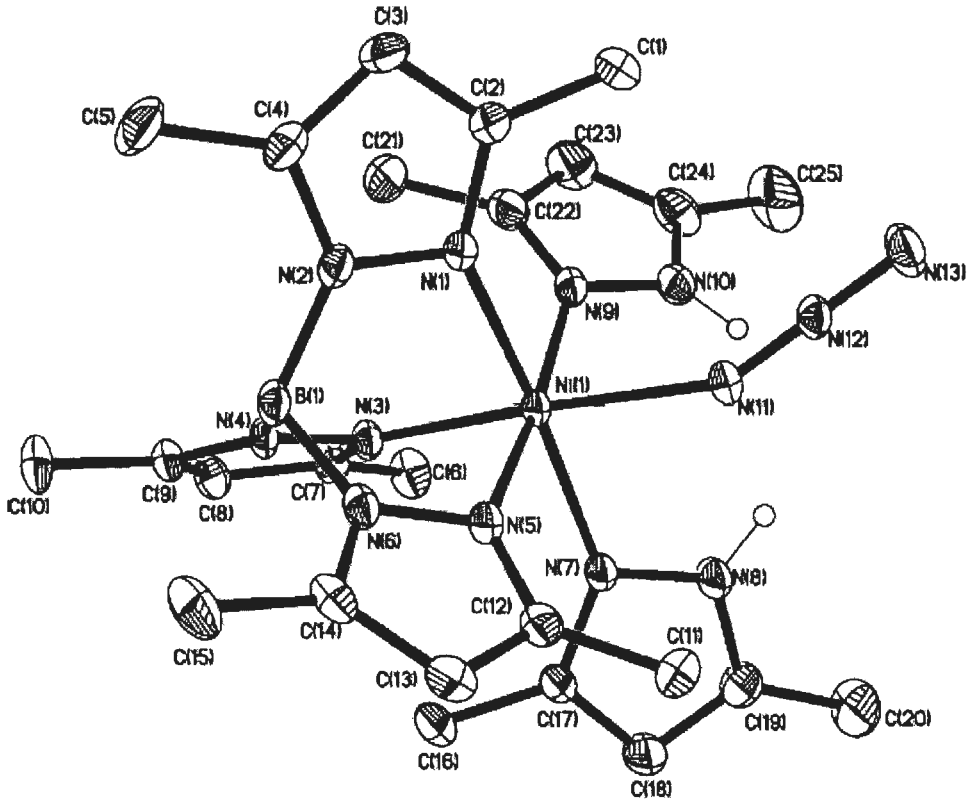

Fig. 1-4 Crystal structure of $[Tp^{Me2}Ni(Pz^{Me2})_2(N_3)]$

Sun et al. [40] also reported the synthesis, crystal structure and spectroscopic properties of a novel half-sandwich mononuclear cobalt (III) complex with hydrotris(3,5-dimethylpyrazolyl) borate ligand and thiocyanate $[Tp^{Me2}Co(Pz^{Me2}H)(NCS)_2].H_2O.\ CH_3OH$. They suggested that the cobalt (III) ion in this complex was six-coordinated with nitrogen atoms, three from Tp^{Me2}, one from 3,5-dimethylpyrazole and two from two thiocyanates, to form an octahedral environment (Fig. 1-5).

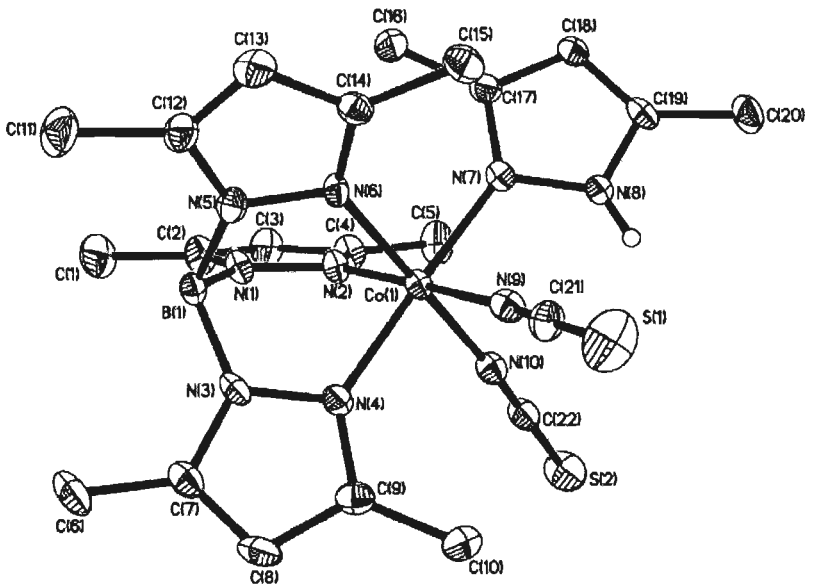

Fig. 1-5 Crystal structure of $[Tp^{Me2}Co(Pz^{Me2}H)(NCS)_2].H_2O.CH_3OH$

Hydrotris(3,5-diisopropylpyrazolyl)borate [$HB(Pz^{iPr2})_3 = Tp^{iPr2}$]

Kitajima et al. [41] synthesized and characterized a series of monomeric carboxylate ferrous complexes with a tripodal N_3 ligand i.e., hydrotris(3,5-diisopropylpyrazolyl)borate [Tp^{iPr2}] as model for the iron site in non-heme iron proteins which bind or activate dioxygen. They also reported the X-ray structures for [$Tp^{iPr2}Fe(OAc)$] (Fig. 1-6), [$Tp^{iPr2}Fe(OBz)(MeCN)$] and [$Tp^{iPr2}Fe(OOC^tBu)$].

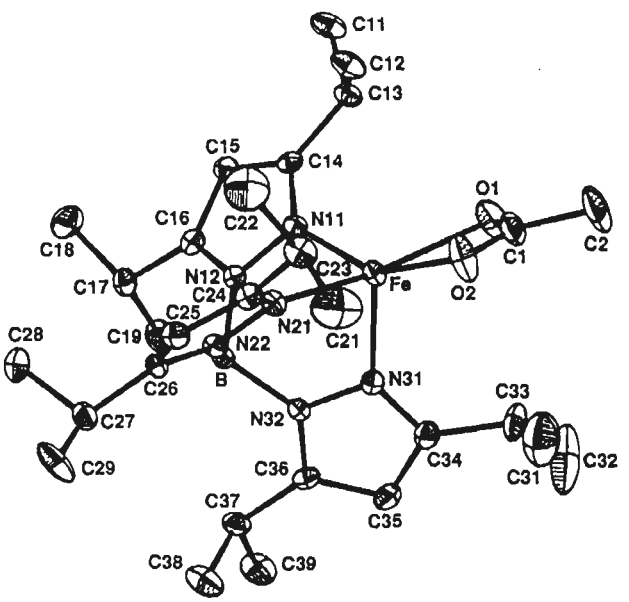

Fig. 1-6 Crystal structure of $[Tp^{iPr2}Fe(OAc)]$

Akita et al. [42] prepared coordinatively unsaturated allyl and benzyl complexes with the hydrotris(3,5-diisopropylpyrazolyl)borate ligand [Tp^{iPr2}], Tp^{iPr2}M–allyl (M = Ni, Co, Fe) and Tp^{iPr}Fe–p-methylbenzyl and characterized by X-ray crystallography. They suggested that the allyl ligand is coordinated to the Fe center in a η^1-fashion (Fig. 1-7) to form a 14e species in contrast to the η^3-coordination found for the Ni and Co complexes (Fig. 1-8).

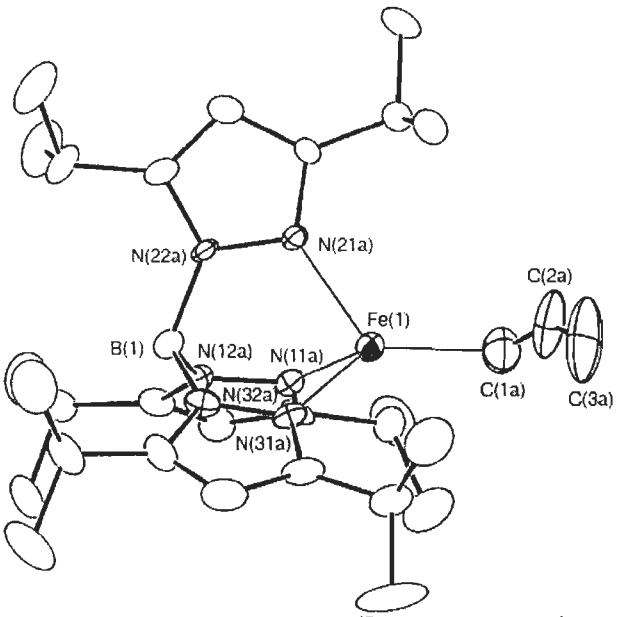

Fig. 1-7 Crystal structure of [Tp^{iPr}Fe–allyl] in η^1-fashion

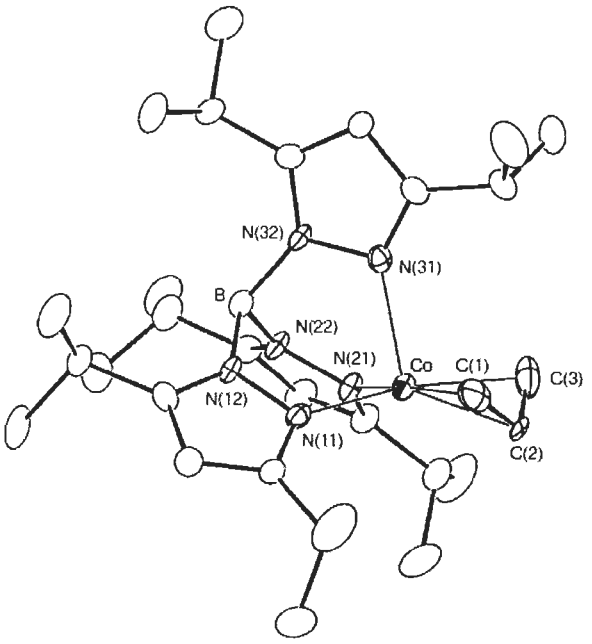

Fig. 1-8 Crystal structure of [Tp^{iPr}Co–allyl] in η^3-fashion

Singh et al. [43] synthesized both mono- and binuclear complexes of cobalt $[Tp^{iPr2}Co(X)]$ (X = NO_3 and OBz) and $[Tp^{iPr2}Co]_2(\mu\text{-}X)(\ \mu\text{-}OBz)$ (X = OH, N_3) by using the hydrotris(3,5-diisopropyl-1-pyrazolyl)borate $[Tp^{iPr2}]$. From X-ray crystallography, they found that nitrato and benzoate complexes, i.e., $[Tp^{iPr2}Co(NO_3)]$ (Fig. 1-9) and $[Tp^{iPr2}Co(OBz)]$ have distorted octahedral geometry with N4O2 donor set involving one coordinated acetonitrile molecule.

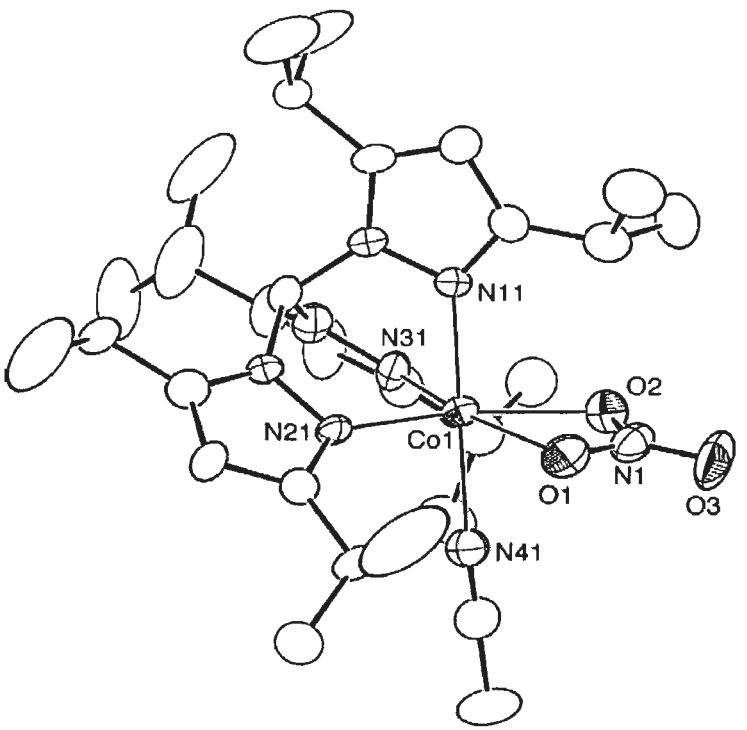

Fig. 1-9 Crystal structure of $[Tp^{iPr2}Co(NO_3)]$

Fujisawa et al. [44] recently reported the five-coordinate thiolato complexes, $[Tp^{iPr2}M(SMeIm)]$ (M = Co and Ni), (Tp^{iPr2} = hydrotris(3,5-diisopropyl-1-pyrazolyl)borate anion and HSMeIm = 2-mercapto-1-methylimidazole). These complexes were compared with the corresponding Cu(II) and Zn(II) complexes having same ligands and with the related four-coordinate complexes $[Tp^{iPr2}M(SC6F5)]$ (HSC_6F_5 = pentafluorobenzenthiol). All the complexes were characterized by X-ray

crystallography and UV–Vis absorption, IR, ^{1}H NMR and other spectroscopic techniques. All five-coordinate thiolato complexes, [Tp^{iPr2}M(SMeIm)] (M = Co, Ni, and Cu) (Fig. 1-10) formed a distorted square pyramidal structure with a high spin state and only [Tp^{iPr2}Zn(SMeIm)] has a four-coordinate structure with a distorted tetrahedral configuration.

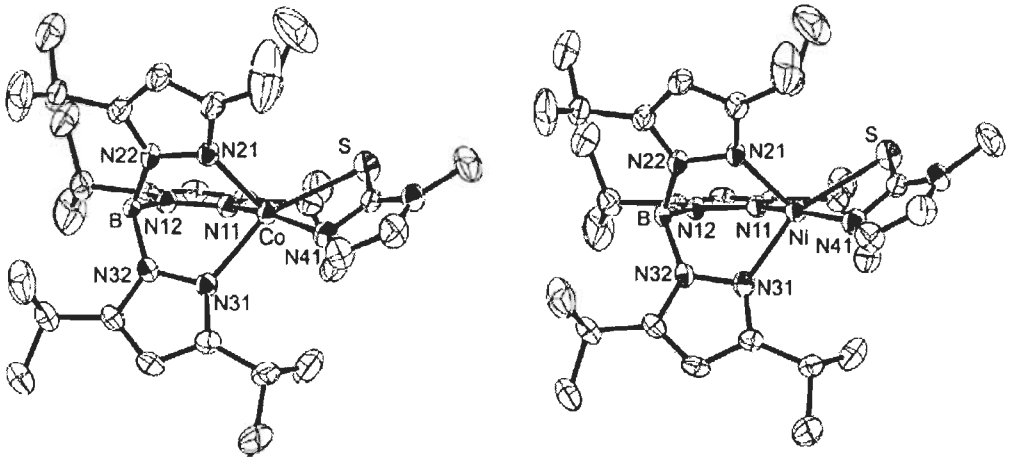

Fig. 1-10 Crystal structure of [Tp^{iPr2}M(SMeIm)] (M = Co and Ni)

Hydrotris(3-phenylpyrazolyl)borate [HB(Pz^{Ph})$_3$ = Tp^{Ph}]

Siemer et al. [45] reported the syntheses and structures of a number of complexes i.e., Tp^{Ph}Fe(SCN)(THF), Tp^{Ph}Fe(NO$_3$)$_2$, Tp^{Ph}CuCl(Pz^{Ph}H), Tp^{Ph}Cu(SCN)(Pz^{Ph}H), Bp^{Ph2}Co and Tp^{Ph}Bp^{Ph}Co containing hydrotris(3-phenylpyrazolyl)borate [Tp^{Ph}] dihydrobis(3-phenylpyrazolyl)borate [Bp^{Ph}] and 3-phenylpyrazole [Pz^{Ph}H]. Compound Tp^{Ph}Fe(SCN)(THF) displayed a trigonal bipyramidal coordination sphere, while Tp^{Ph}CuCl(Pz^{Ph}H) and Tp^{Ph}Cu(SCN)(Pz^{Ph}H) were square-pyramidal. Compound Tp^{Ph}Fe(NO$_3$)$_2$ (Fig. 1-11) contained one monodentate and one bidentate nitrate ligand in a distorted octahedral coordination sphere. Compound Bp^{Ph2}Co was tetrahedral and Tp^{Ph}Bp^{Ph}Co was octahedral with an agostic Co-H interaction in the sixth coordination site.

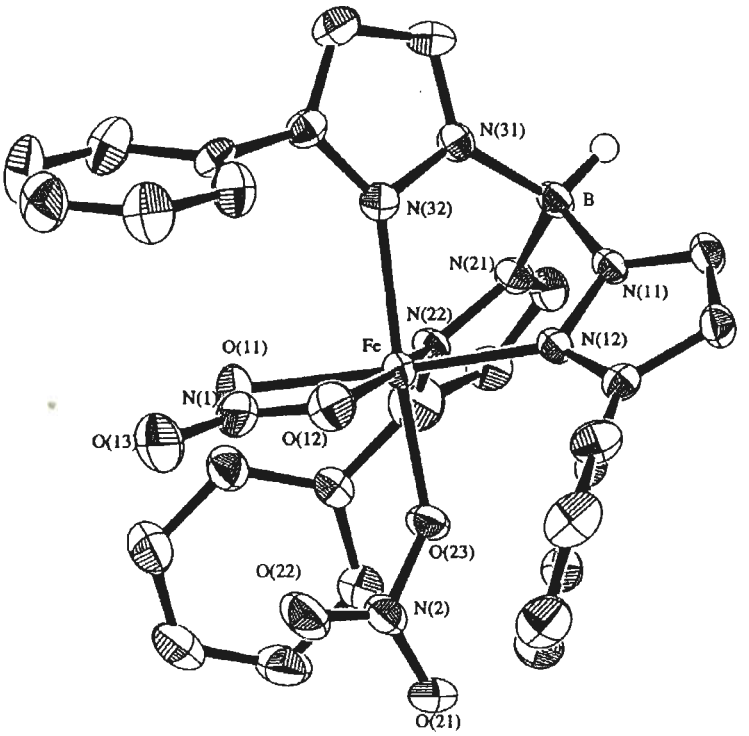

Fig. 1-11 Crystal structure of $[Tp^{Ph}Fe(NO_3)_2]$

Lukasiewicz et al. [46] reported the high-spin cobalt (II) complexes with homoscorpionate hydrotris(3-phenylpyrazolyl)borate $[Tp^{Ph}]$ and heteroscorpionate hydrobis(3-phenylpyrazolyl)(3-tert-butylpyrazolyl)borate $[HB(Pz^{Ph})_2(Pz^{t\text{-}Bu})]$ ligands. The former tripodal ligand provides intermediate steric hindrance to the central metal ion, which is able to adopt two additional donors from thiocyanate and neutral ligands like pyrazole [PzH] and methanol, or two oxygen donors from the lactate anion. Replacement of one of the three 3-phenyl substituents in Tp^{Ph} by tert-butyl produced a ligand of high steric hindrance which gave tetracoordinate cobalt complexes with thiocyanate or monodentate lactate. The complexes were studied by the ^1H NMR and two of them, $[Tp^{Ph}Co(NCS)(PzH)]$ and $[\{HB(Pz^{Ph})_2(Pz^{t\text{-}Bu})\}Co(NCS)]$ were characterized structurally by X-ray crystallography.

Kremer-Aach et al. [47] reported the synthesis and structure of blood-red colored bis(ligand) complex $[\eta^3\text{-}Tp^{Ph}Co(\eta^2\text{-}Tp^{Ph})]$ by the reaction of

cobalt (II) perchlorate with one equivalent each of potassium hydroxide and potassium hydrotris(3-phenylpyrazolyl)borate (Tp^{Ph}). As shown in Fig. 1-12, [η^3-Tp^{Ph}Co(η^2-Tp^{Ph})] contains a square Co-N(5) pyramid with an agostic BH-Co interaction of 2.17(2) Å. One Tp^{Ph} ligand acts tridentate and the other bidentate. They also suggested that the reaction of Tp^{Ph} with zinc and cobalt halides gave a series of heteroleptic halogeno complexes [Tp^{Ph}MX]. They also prepared the 2-aminobenzoate (anthranilate) complexes [Tp^{Ph}M(anthranilate)], M = Zn(II), Co(II) where the X-ray study suggested that anthranilate acts as a chelating oxygen ligand with Zn-O distances of 1.932(2) and 2.460(2) Å and the amino group was not involved in metal coordination. The reaction of the chloro complexes [Tp^{Ph}MCl] with sodium or potassium acetylacetonate gave zinc and cobalt complexes [(η^3-Tp^{Ph})M(η^2-acac)]. Both complexes were crystallized in the monoclinic system having space group $P2_1/c$, with Z = 4 and the structures were best described as slightly distorted trigonal bipyramids with the two axial positions occupied by one of the acetylacetonate oxygen and one of the tripodal N donor atoms.

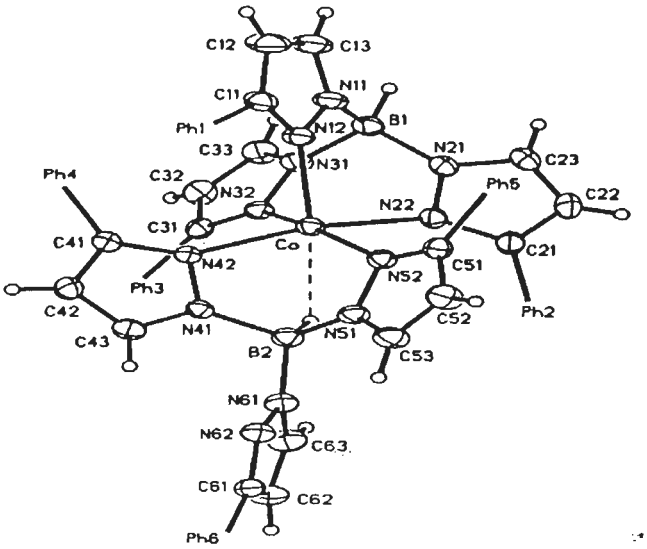

Fig. 1-12 Crystal structure of [Co(η^3-Tp^{Ph})(η^2-Tp^{Ph})]

Hydrotris(3-phenyl-5-methylpyrazolyl)borate [$HB(Pz^{Ph,Me})_3 = Tp^{Ph,Me}$]

This is similar to Tp^{Ph}, but the presence of the three 5-methyl groups offers steric protection to the B-H bond; moreover the nonbonding repulsions of the three 5-Me groups are likely to somewhat tighten the bite of the ligand at the metal end. Due to this fact the $[Tp^{Ph,Me}M(X)]$ derivatives show greater stability than their Tp^{Ph} analogs. It readily formed five coordinated species, such as $[Tp^{Ph,Me}CoCl(Pz^{Ph,Me}H)]$ (Fig. 1-13) [48]. The X-ray structure showed that the tris(pyrazolyl)borate ligand occupied one axial and two equatorial coordination sites, the remaining two sites being occupied by the 3-phenyl-5-methylpyrazole (axial) and an equatorial chloride anion. The ligands with aromatic substituents are less robust and show hydrolytic cleavage, with coordination of the corresponding pyrazoles $[Pz^{Ph,Me}H]$ in the resulting complexes.

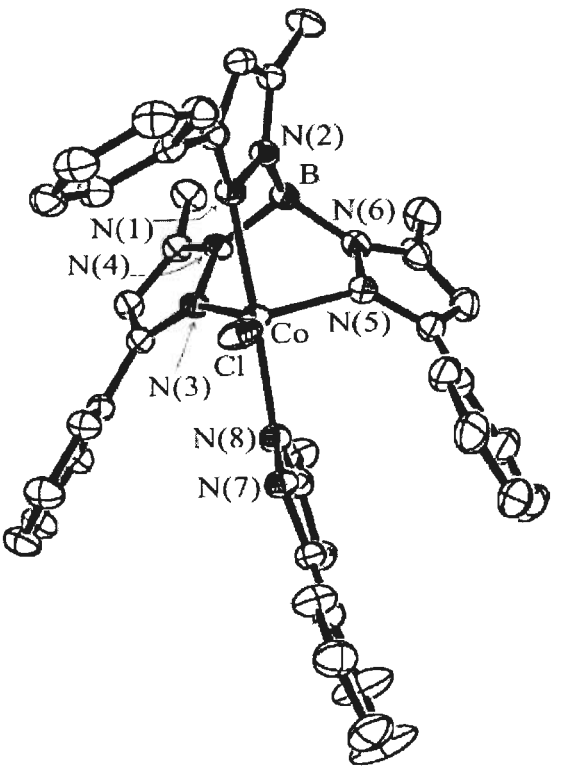

Fig. 1-13 Crystal structure of $[Tp^{Ph,Me}CoCl(Pz^{Ph,Me}H)]$

Uehara et al. [49] reported the formation of cationic tris-MeCN adducts of Tp^RM fragments, $[Tp^RM(NCMe)_3]OTf$ [Tp^R = hydrotrispyrazolylborato, R = 3-Ph-5-Me, 3,5-iPr_2 ; M = Ni (Fig. 1-14), Co] by chloride abstraction from the corresponding chloro complexes, Tp^RM–Cl with AgOTf in acetonitrile. The MeCN solvent molecules in these complexes were labile enough and readily converted to a variety of adducts, $[Tp^RM(L)_n]OTf$, via treatment with N- and P-donors [$NC(CH_2)_2CN$, *p*-NCC_6H_4CN, pyridine, *o*-bipy, *p*-bipy, $Ph_2P(CH_2)_mPPh_2$ (m = 2, 3)].

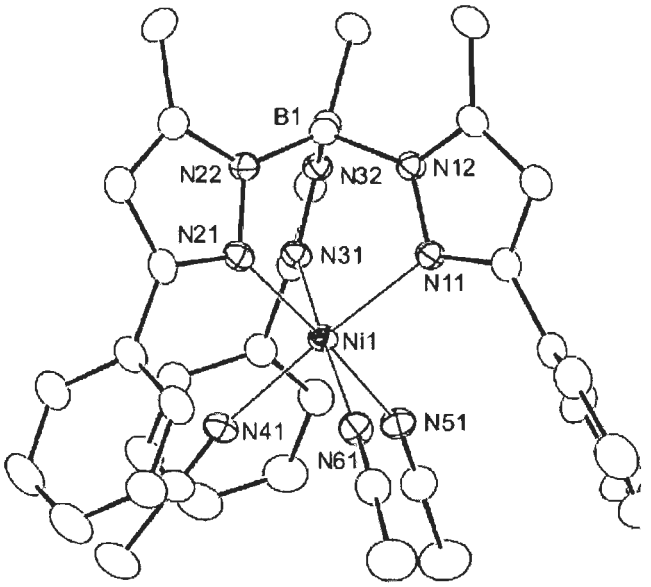

Fig. 1-14 Crystal structure of $[Tp^{Ph,Me}Ni(NCMe)_3]OTf$

Yakovenko et al. reported the formation of Ni(II), Co(II) and Mn(II) tris(3-phenyl-5-methylpyrazolyl)borate complexes with 2,6-di-tert-butyl-4-carboxy-phenol. They found that the oxidation of nickel and cobalt complexes resulted in the formation of coordinated phenoxyl radical and diphenoquinone (Fig. 1-15), whereas only quinone was formed in the case of Mn complex and free 2,6-di-tert-butyl-4-carboxy-phenol [50].

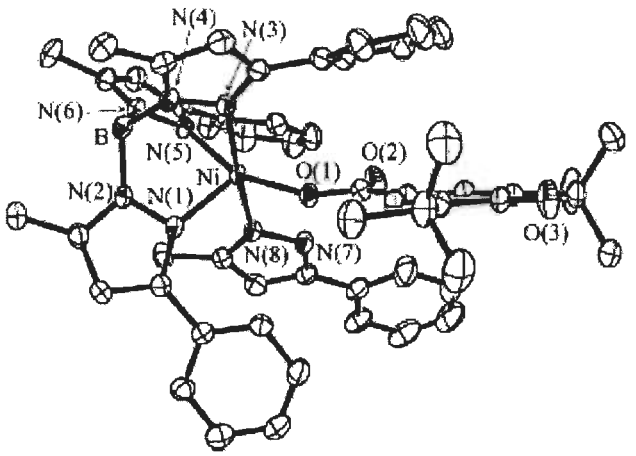

Fig. 1-15 Crystal structure of [$Tp^{Ph,Me}$Ni($Pz^{Ph,Me}$H)(2,6-di-tert-butyl-4-carboxy-phenol)]

Ruman et al. [51] reported the synthesis of cobalt hydrotris(3-phenyl-5-methylpyrazolyl)borate nitrato complex. The X-ray structure revealed that the central metal ion was coordinated to three nitrogen atoms of the $Tp^{Ph,Me}$ ligand, two oxygen atoms from nitrate and one additional oxygen from THF. They also synthesized hydrobis(3,5-dimethylpyrazolyl)(3,5-diphenylpyrazolyl)borate and hydrobis(3,5-diphenylpyrazolyl)(3,5-dimethylpyrazolyl)borate ligands and their high-spin cobalt (II) complexes.

Hydrotris(3,5-diphenylpyrazolyl)borate [$HB(Pz^{Ph2})_3 = Tp^{Ph2}$]

Mehn et al. [52] reported the synthesis of the mononuclear iron (II) α-keto carboxylate and carboxylate compounds of Tp^{Ph2} (Tp^{Ph2} = hydrotris(3,5-diphenylpyrazol-1-yl)borate) as models for the active sites of nonheme iron oxygenases. The structures of an aliphatic R-keto carboxylate complex, [$Tp^{Ph2}Fe^{II}(O_2CC(O)CH_3)$], [$Tp^{Ph2}Fe^{II}$(OBz)] (Fig. 1-16) and [$Tp^{Ph2}Fe^{II}$(OAc)($Pz^{Ph2}$H)] were determined by single-crystal X-ray diffraction. They found that both the R-keto carboxylate and the carboxylate compounds reacted with dioxygen resulting in the hydroxylation of a single ortho phenyl position of the Tp^{Ph2} ligand.

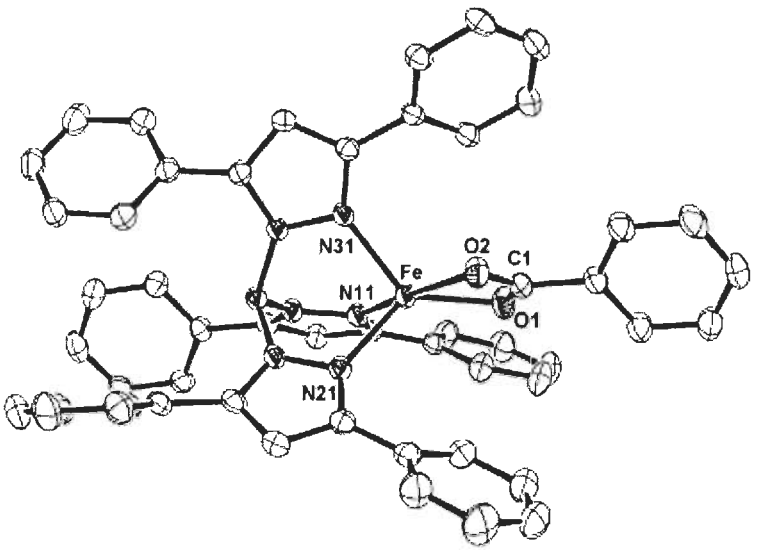

Fig. 1-16 Crystal structure of [$Tp^{Ph2}Fe^{II}$(OBz)]

Hegg et al. [53] also reported a mononuclear iron (II) α-keto carboxylate complex [Tp^{Ph2}Fe(BF)] by the reaction of $FeCl_2$, KTp^{Ph2} and the α-keto acid, sodium benzoylformate (BF) in an acetonitrile slurry. The crystal structure of [Tp^{Ph2}Fe(BF)] (Fig. 1-17) revealed a five-coordinate iron (II) center with a monoanionic, facecapping Tp^{Ph2} and a chelated benzoylformate.

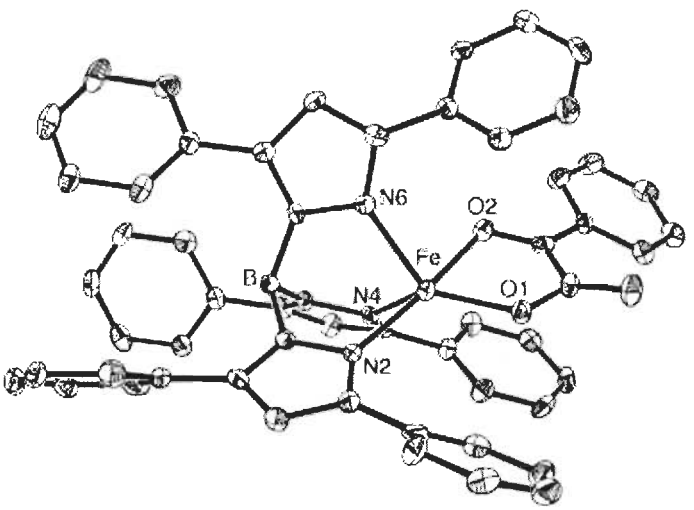

Fig. 1-17 Crystal structure of [Tp^{Ph2}Fe(BF)]

Hydrotris(3-tert-butylpyrazol-1-yl)borate [$HB(Pz^{tBu})_3 = Tp^{tBu}$]

The coordinative behavior reflected the severe screening of the metal in the $Tp^{tBu}M$ fragment, thus only four coordinate tetrahedral complexes of type $Tp^{tBu}MX$ were obtained (X=Cl, NCS, NCO, N_3) and no $(Tp^{tBu})_2M$ species could be obtained, in contrast to Tp and Tp^{Me2}. The structure of Tp^{tBu}CoNCS was established by X-ray crystallography (Fig. 1-18) [4].

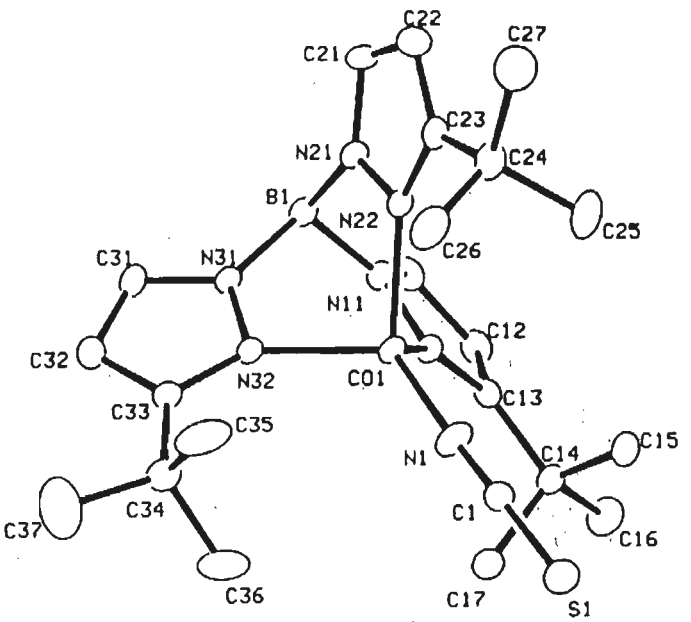

Fig. 1-18 Crystal structure of [Tp^{tBu}CoNCS]

Hydrotris(3-tert-butyl-5-methylpyrazolyl)borate [$HB(Pz^{tBu,Me})_3 = Tp^{tBu,Me}$]

It is also similar to Tp^{tBu}, with the difference that the presence of the 5-methyl groups offers steric protection to the B-H bond. Due to this fact, $Tp^{tBu,Me}MX$ derivatives showed greater stability than their Tp^{tBu} analogs. The X-ray structure of $Tp^{tBu,Me}$NiNCS (Fig. 1-19) was determined by Trofimenko and show the Ni was four coordinated [14]. The complex $[Tp^{tBu,Me}Cu]_2$ has a dimeric structure, similar to that of $[Tp^{tBu}Cu]_2$, while the structure of $Tp^{tBu,Me}$CuCl is different from that of Tp^{tBu}CuCl. The

other complexes reported with this ligand were tetrahedral $Tp^{tBu,Me}HgI$, $Tp^{tBu,Me}CdMe$ and the five coordinate $Tp^{tBu,Me}Cd(NO_3)$.

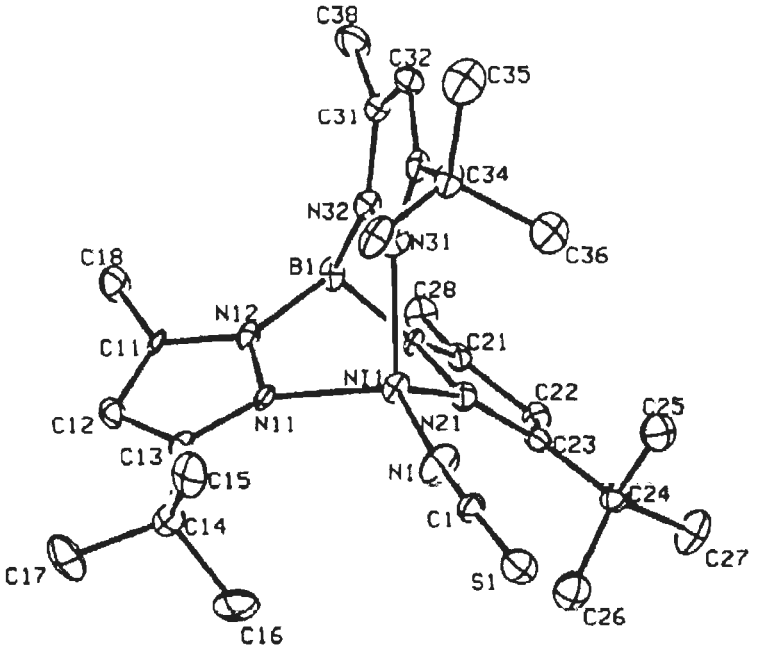

Fig. 1-19 Crystal structure of $[Tp^{tBu,Me}NiNCS]$

Santi et al. [54] prepared various 3,5-substituted tris(pyrazolyl)borate nickel (II) and palladium (II) complexes [tris(pyrazolyl)borate = tris(3,5-dimethylpyrazolyl)borate (Tp^{Me2}), tris(3-tert-butyl-5-methylpyrazolyl)borate ($Tp^{tBu,Me}$) or tris(3-cumyl-5-methyl pyrazolyl)borate ($Tp^{Cum,Me}$)] and characterized them in both the solid and solution state. They determined the crystal structures of [k^3-N,N',N''-$Tp^{tBu,Me}NiCl$] (Fig. 1-20) and [k^3-N,N',N''-$Tp^{Cum,Me}NiCl$(3-methyl-5-cumylpyrazole)] by X-ray diffraction analysis. They also tested the catalytic performance of all compounds in ethylene polymerisation. The nickel catalysts activated with methylaluminoxane (MAO) produce polyethylene with moderate to good activity, while the palladium compounds showed scarce activity.

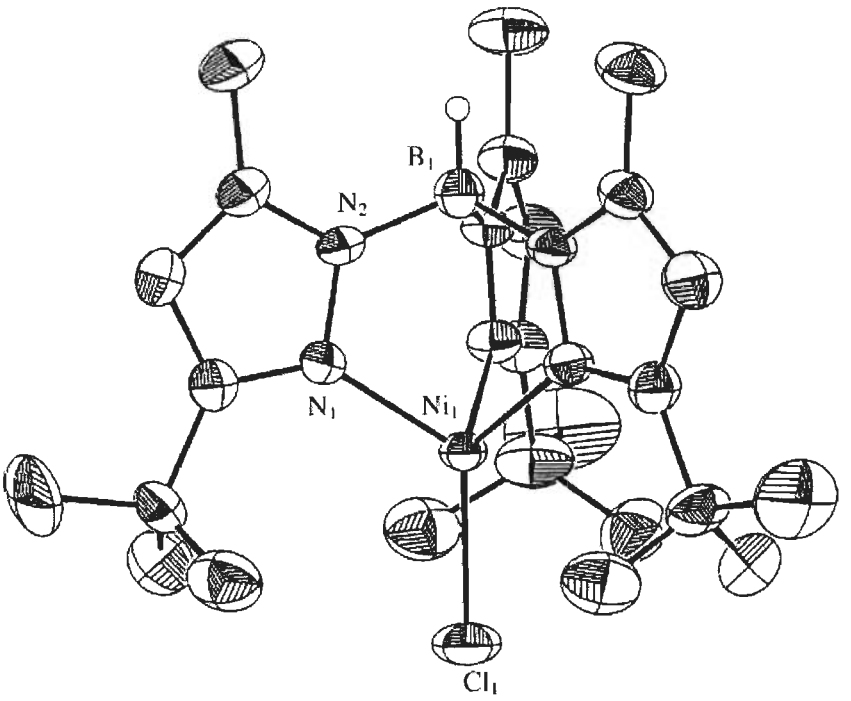

Fig. 1-20 Crystal structure of [k^3-N,N′,N″-$Tp^{tBu,Me}$NiCl]

Berquist et al. [55] studied the protonation of [$Tp^{tBu,Me}$Zn(OH)] by $(C_6F_5)_3B(OH_2)$ and structurally characterized by X-ray diffraction. The protonation studies resulted in a lengthening of the Zn-O bond by ca. 0.1 Å. The cobalt hydroxide complex [$Tp^{tBu,Me}$ Co(OH)] after similar protonation reaction resulted in a product, which was isostructural with the zinc complex. The aqua complexes [$Tp^{tBu,Me}M(OH)_2$][$HOB(C_6F_5)_3$] (M = Zn (Fig. 1-21), Co) exhibited a hydrogen bonding interaction between the metal aqua and boron hydroxide moieties, which may be viewed as analogous to that between the aqua ligand and Thr-199 at the active site of carbonic anhydrase. The cobalt hydroxide [$Tp^{tBu,Me}$Co(OH)] reacted with CO_2 and gave the bridging carbonate complex [($Tp^{tBu,Me}$)CoOH]$_2$(μ-η^1, η^2-CO_3) (Fig. 1-22).

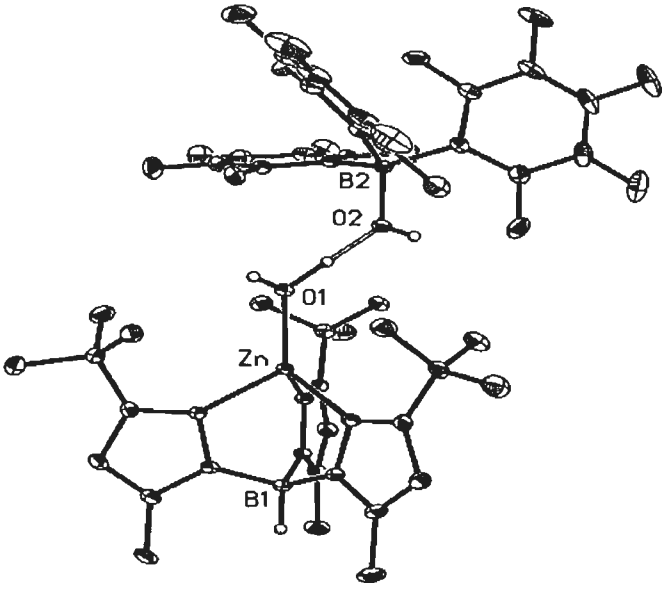

Fig. 1-21 Crystal structure of $[Tp^{tBu,Me}Zn(OH)_2][HOB(C_6F_5)_3]$

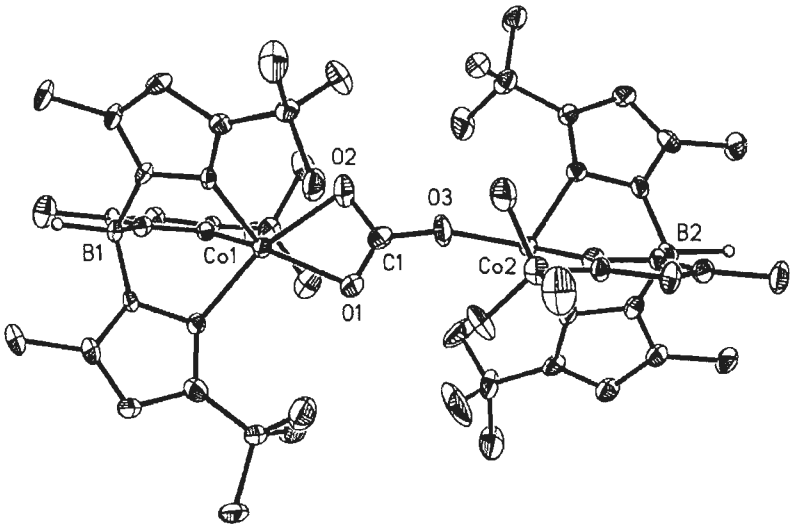

Fig. 1-22 Crystal structure of $[Tp^{tBu,Me}Co(OH)]_2(\mu\text{-}\eta^1, \eta^2\text{-}CO_3)$

Hydrotris(3-tert-butyl-5-isopropylpyrazolyl)borate [$HB(Pz^{tBu,iPr})_3 = Tp^{tBu,iPr}$]

Hikichi et al. [56] synthesized a series of monomeric ferrous complexes having acetate, hydroxide and benzoylformate ligands by using a hindered tripodal ligand, hydrotris(3-tert-butyl-5-isopropylpyrazol-1-yl)borate [$Tp^{tBu,iPr}$]. They carried out the reaction of $Tp^{tBu,iPr}$ with anhydrous $Fe(OAc)_2$ to get acetato complexes

[$Tp^{tBu,iPr}$Fe(OAc)] and [$Tp^{tBu,iPr}$Fe(OAc)($Pz^{tBu,iPr}$H)]. A hydroxo complex [$Tp^{tBu,iPr}$Fe(OH)] was also prepared by the treatment of above complexes with aqueous NaOH. They suggested that the geometry of Fe(II) in hydroxo complex was slightly distorted tetrahedron (Fig. 1-23).

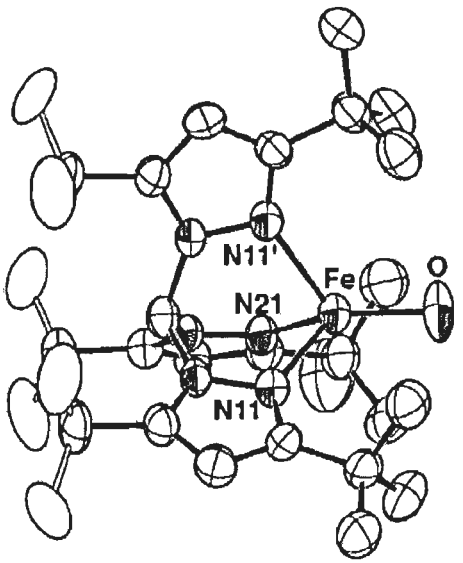

Fig. 1-23 Crystal structure of [$Tp^{tBu,iPr}$Fe(OH)]

Ogihara et al. [57] reported the synthesis of an Fe(II)–acetato and Fe(III)-dioxygen complexes with $Tp^{tBu,iPr}$ ligand. X-ray crystallography revealed that the acetato complex consists of the distorted square pyramidal Fe(II) center. They also found that in contrast to the Tp^{iPr2} complex, the highly hindered $Tp^{tBu,iPr}$ analog [$Tp^{tBu,iPr}$Fe(O_2CMe)] (Fig. 1-24) did not show affinity towards the σ-donating MeCN. Moreover, [$Tp^{tBu,iPr}$Fe(O_2CMe)] gave neither an O_2 adduct nor an oxidized complex (such as an Fe(III) acetato complex) upon O_2 exposure of solution of [$Tp^{tBu,iPr}$Fe(O_2CMe)] under any condition, although the decomposition of the $Tp^{tBu,iPr}$ ligand proceeded slowly.

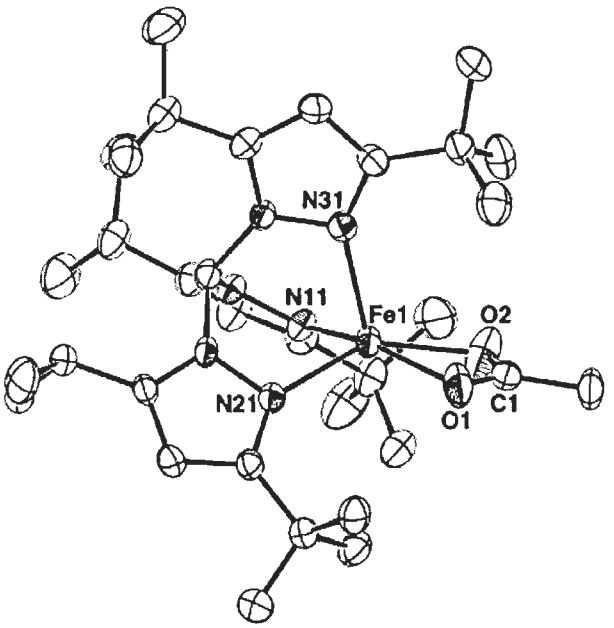

Fig. 1-24 Crystal structure of $[Tp^{tBu,iPr}Fe(O_2CMe)]$

Hydrotris(3-diphenylmethylpyrazolyl)borate [$HB(Pz^{CHPh2})_3 = Tp^{CHPh2}$]

Rheingold et al. [10] reported the synthesis of hydrotris(3-diphenylmethylpyrazolyl)borate, Tp^{CHPh2} and compared its coordination chemistry with that of Tp^{iPr}. They suggested that it was roughly similar to that of Tp^{iPr}, although there were indications that Tp^{CHPh2} provides a more open structure around the coordinated metal, permitting additional coordination by small ligands. They reported a variety of complexes, such as $[Tp^{CHPh2}M(X)]$ (M = Co, Ni, Zn; X = Cl, NCO, NCS), $[Tp^{CHPh2}Pd(\kappa^3$-methallyl)], $[Tp^{CHPh2}Co(acac)]$, $[Tp^{CHPh2}Co(scorpionate\ ligand)]$, $[Tp^{CHPh2}Tl]$, $[Tp^{CHPh2}Co(Cl)]$ (Fig. 1-25), $[Tp^{CHPh2}Co(NCS)(DMF)]$, $[Tp^{CHPh2}Ni\ (NCS)(DMF)_2]$, $[Tp^{CHPh2}Co(acac)]$ (Fig. 1-26), $[Tp^{CHPh2}Co(Bp^{Ph2})]$, $[Tp^{CHPh2}Co(Bp^{Ph})]$, $[Tp^{CHPh2}\ Co(Tp)]$ and $[(Tp^{CHPh2})_2Ni(C_2O_4)](H_2O)_2$ with this ligand.

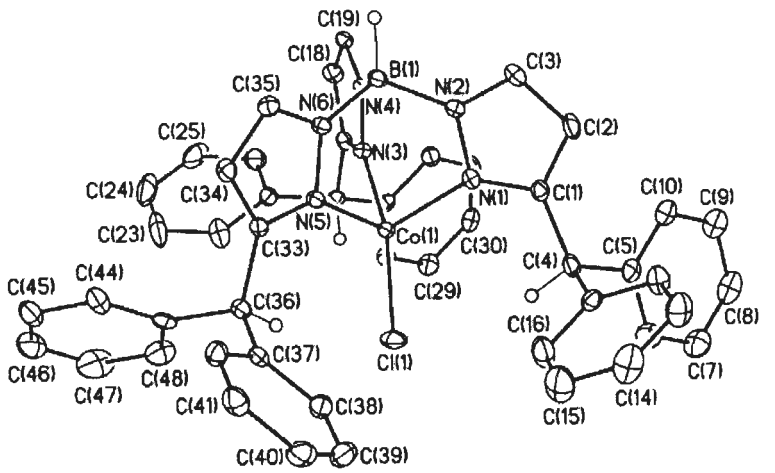

Fig. 1-25 Crystal structure of [Tp^{CHPh2}CoCl]

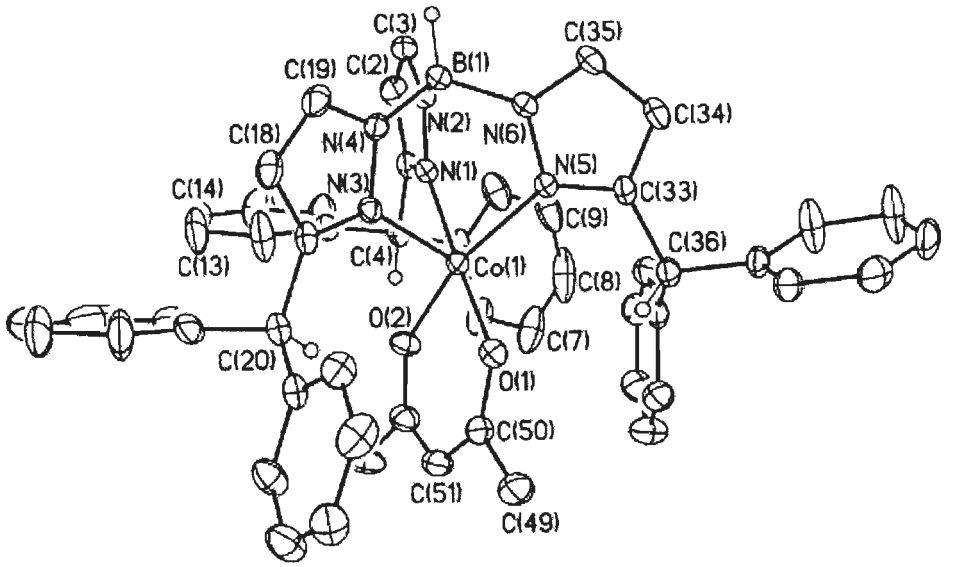

Fig. 1-26 Crystal structure of [Tp^{CHPh2}Co(acac)]

Hydrotris(3-(2-naphthyl)pyrazolyl)borate [$Tp^{\alpha Nt}$]

Rheingold et al. also reported the synthesis and characterization of two novel homoscoprionate ligands, containing a naphthyl substituent in the 3-position and bonded either through the 1-position [$Tp^{\alpha Nt}$], or through the 2-position, [$Tp^{\beta Nt}$] as the Tl salt. The $Tp^{\alpha Nt}$ ligand resembled other Tp^{Ar} ligands, where Ar is a para-substituted

phenyl group, although the 2-naphthyl substituent provided a substantially deeper pocket around the coordinated metal but retained rotational freedom. In contrast, rotation of the 1-naphthyl substituent in $Tp^{\alpha Nt}$ was restricted, which led to complexes with symmetry lower than those of the $Tp^{\beta Nt}$ ligand. The $[Tp^{\alpha Nt}Co(Tp)]$ (Fig. 1-27) and $[Tp^{\beta Nt}Co(Tp)]$ (Fig. 1-28) complexes were prepared by the reaction of $[Tp^{\alpha Nt}Co(Cl)]$ or $[Tp^{\beta Nt}Co(Cl)]$ and TlTp. The X-Ray crystallography suggested the octahedral coordination of cobalt (III) where the ligand coordinated in κ^3 fashion [11].

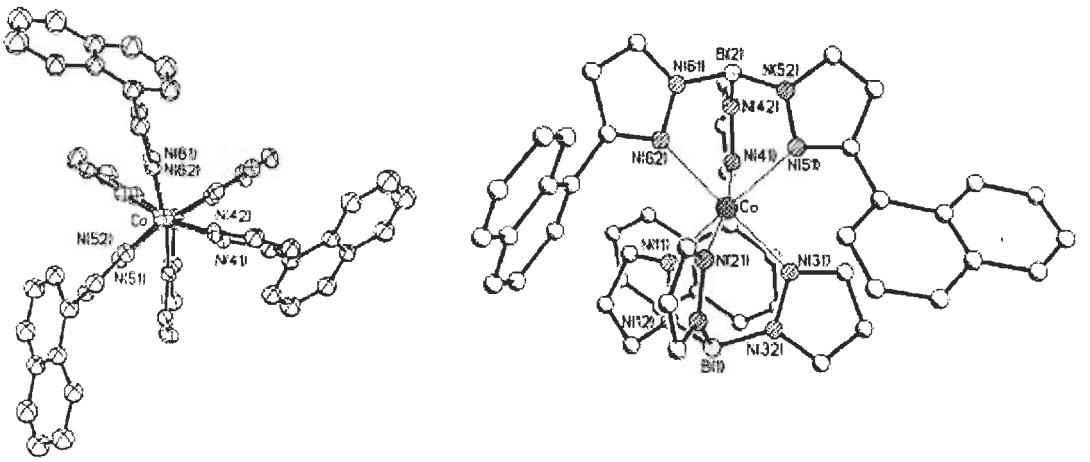

Fig. 1-27 Crystal structure of $[Tp^{\alpha Nt}Co(Tp)]$, viewed along the B-Co-B axis and side-on.

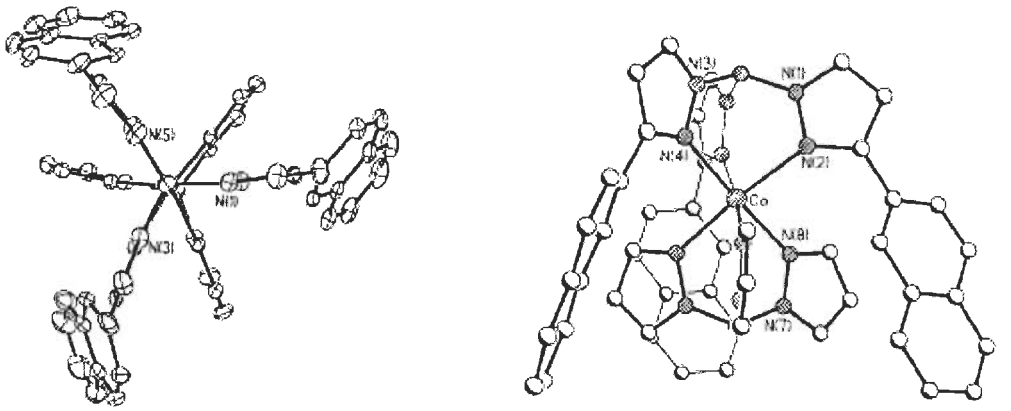

Fig. 1-28 Crystal structure of $[Tp^{\beta Nt}Co(Tp)]$, viewed along the B-Co-B axis and side-on.

Hydrotris(4-cyano-3-phenylpyrazolyl)borate [$HB(Pz^{Ph,4CN})_3 = Tp^{Ph,4CN}$]

Siemer et al. prepared the scorpionate ligands with cyano substituents in the 4-position of the pyrazole ring [13]. They suggested that besides from the strong electron-withdrawing properties of the cyano groups, these ligands also showed the possibility for the formation of coordination polymers through simultaneous coordination of metals at both the pyrazole and cyano N atoms [58]. Zhao et al. reported that the reaction of the $Tp^{Ph,4CN}$ with Co(II), Mn(II) and Fe(II) resulted in the isolation of crystals containing sandwich complexes in which the ligands were isomerized to produce the heterocyanoscorpionate hydrobis(4-cyano-3-phenylpyrazolyl)(4-cyano-5-phenyl- pyrazolyl)borate ($Tp^{Ph,4CN}$) [59].

Hydrotris(3-isopropyl-4-bromopyrazolyl)borate [$HB(Pz^{iPr,4Br})_3 = Tp^{iPr,4Br}$]

Brunker et al. described the synthesis of the 4-coordinate [$Tp^{iPr,4Br}M(Cl)$] complexes (where M = Fe, Mn) [60]. The single-crystal X-ray structures showed that the metal centers have distorted tetrahedral coordination (Fig. 1-29).

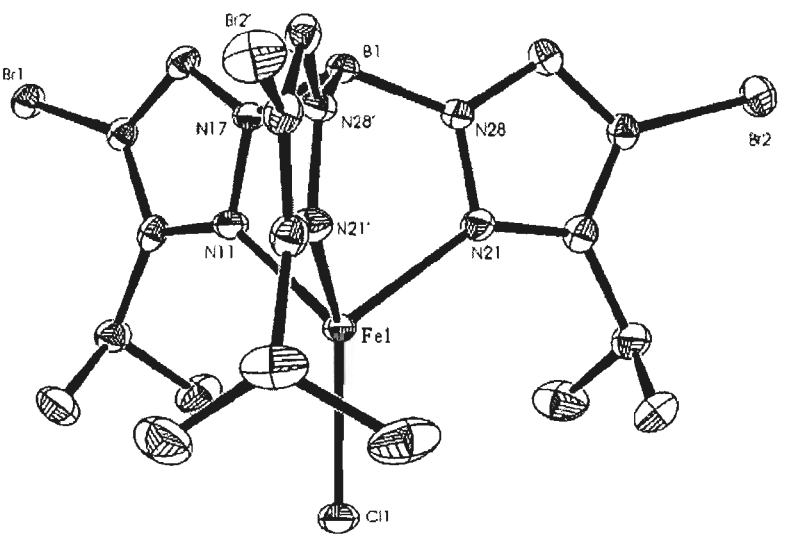

Fig. 1-29 Crystal structure of [$Tp^{iPr,4Br}Fe(Cl)$]

Analogous reaction of $CrCl_2(MeCN)_2$ with $TlTp^{iPr,4Br}$ gave $[Cr(\kappa^3\text{-}Tp^{iPr,4Br})(\kappa^2\text{-}Tp^{iPr,4Br})]$ (Fig. 1-30) as the initial product. It was found that the κ^3 ligand isomerized to hydro(3-isopropyl-4-bromopyrazolyl)$_2$(5-isopropyl-4-bromopyrazolyl)borate. This was labile in solution of pentane as it slowly converted to the 6-coordinate isomer $[Cr(\kappa^3\text{-}Tp^{iPr,4Br})_2]$. In $[Cr(\kappa^3\text{-}Tp^{iPr,4Br})_2]$ both ligands were isomerized and both $[Cr(\kappa^3\text{-}Tp^{iPr,4Br})(\kappa^2\text{-}Tp^{iPr,4Br})]$ and $[Cr(\kappa^3\text{-}Tp^{iPr,4Br})_2]$ displayed Jahn-Teller distorted structures as expected for high-spin d^4 configurations (Fig. 1-31).

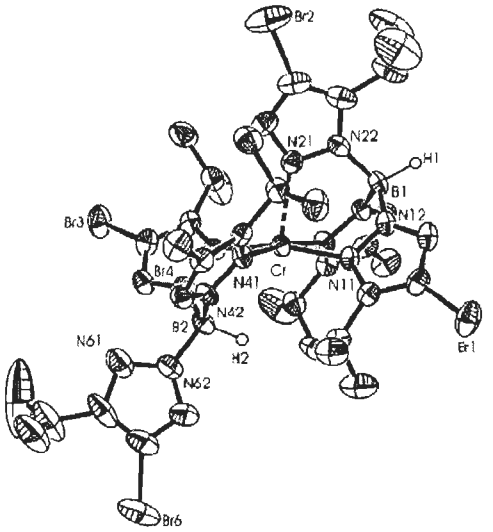

Fig. 1-30 Crystal structure of $[Cr(\kappa^3\text{-}Tp^{iPr,4Br})(\kappa^2\text{-}Tp^{iPr,4Br})]$

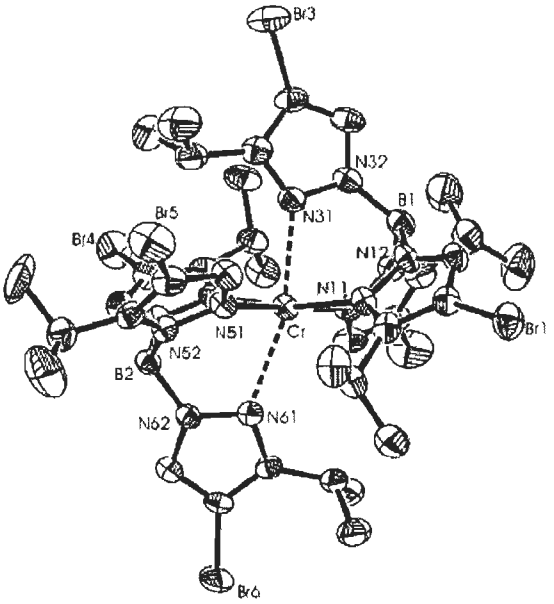

Fig. 1-31 Crystal structure of $[Cr(\kappa^3\text{-}Tp^{iPr,4Br})_2]$

Trofimenko et al. [14] also reported the spectroscopic analysis, coordination geometry and X-ray structures of nickel (II) compounds with sterically demanding tris(pyrazolyl) borate ligands i.e., hydrotris(3-isopropyl-4-bromopyrazolyl) borate [$Tp^{iPr,4Br}$] and hydrotris(3-tert-butyl-5-methylpyrazolyl) borate [$Tp^{tBu,Me}$] with azide or thiocyanate anions. They discussed crystal structures of bis[(μ-thiocyanato-N,S)(hydrotris(3-isopropyl-4-bromopyrazol-1-yl)borato)nickel (II)].3heptane (Fig. 1-32) and (thiocyanato-N)(hydrotris(3-tert-butyl-5-methylpyrazol-1-yl)borato) nickel (II).

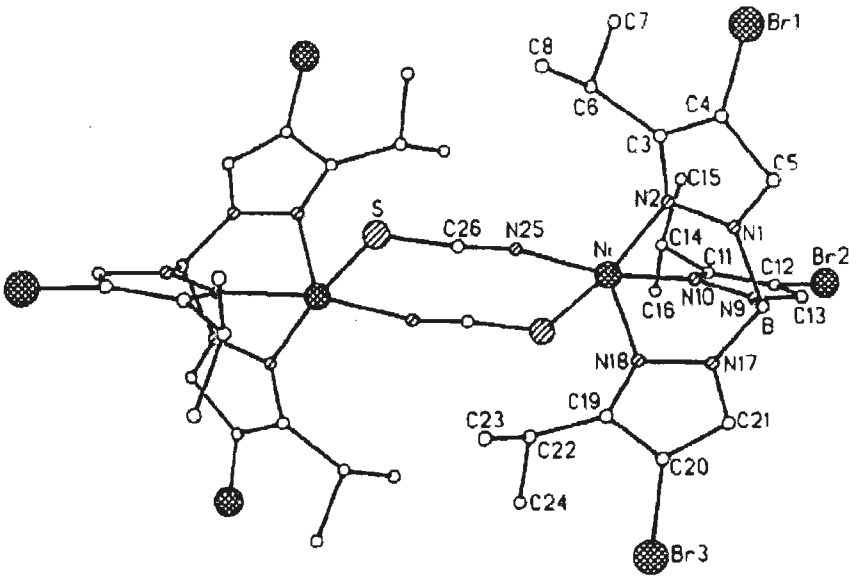

Fig. 1-32 Crystal structure of $[Tp^{iPr,4Br}Ni(\mu\text{-NCS-N,S})]_2.3C_7H_{16}$

Hydrotris(3-neopentylpyrazol-1-yl)borate [$HB(Pz^{Np})_3 = Tp^{Np}$]

Calabrese and Trofimenko reported the synthesis of hetroleptic $Tp^{Np}ML$ complexes like $Tp^{Np}CoTp$. They found that in tetrahedral $Tp^{Np}CoNCO$ (Fig. 1-33), the neopentyl group was oriented with the tert-butyl groups almost perpendicular to the pz plane, and all of them pointed either clockwise or counterclockwise, when viewed along the B-M axis [61]. They also established the structure of $[Tp^{Np}]_2Fe$, $[Tp^{Np}]_2Co$ and $[Tp^{Np}]_2Ni$ by X-ray crystallography and found that all the rearranged octahedral

complexes were isomorphous. In its effective steric blocking, the neopentyl 3-substituent was very similar to 3-isopropyl, so that the steric hindrance hierarchy for Tp^R ligands was R = H < 2-theinyl < Me < Ph < $^iPr \approx$ neopentyl < ^tBu.

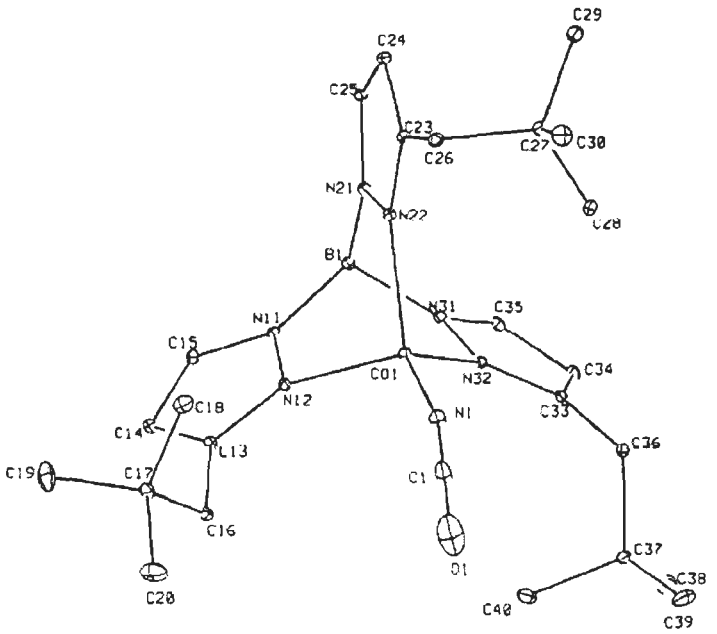

Fig. 1-33 Crystal structure of [Tp^{Np}Co(NCO)]

Hydrotris(3-mesitylpyrazol-1-yl)borate [$HB(Pz^{Ms})_3 = Tp^{Ms}$]

Rheingold et al. [22] synthesized two novel ligands, hydrotris(3-mesitylpyrazol-1-yl)borate $[HB(Pz^{3Ms})_3]^-$ (Tp^{Ms}) and its isomer hydrobis(3-mesitylpyrazol-l-yl)(5-mesitylpyrazol-l-yl)borate (Tp^{Ms*}) to form the complexes $Tp^{Ms}ZnX$, $Tp^{Ms*}MX$ (M = Zn, Cd; X = Cl, I, NCS), $Tp^{Ms}Pd(\eta^3$-methallyl), $Tp^{Ms*}Pd(\eta^3$-methallyl), $Tp^{Ms}Rh$-$(CO)_2$, $Tp^{Ms*}Rh(CO)_2$, $Tp^{Ms}Mo(CO)_2(\eta^3$-methallyal) and $Tp^{Ms'}Mo(CO)_2(\eta^3$-methallyl). Above 220 °C some of the Tp^{Ms*} complexes rearrange into their Tp^{Ms} analogs. Structures of $Tp^{Ms}Mo(CO)_2(\eta^3$-$CH_2CMeCH_2)$ (Fig. 1-34) and $Tp^{Ms*}ZnI$ were established by X-ray crystallography.

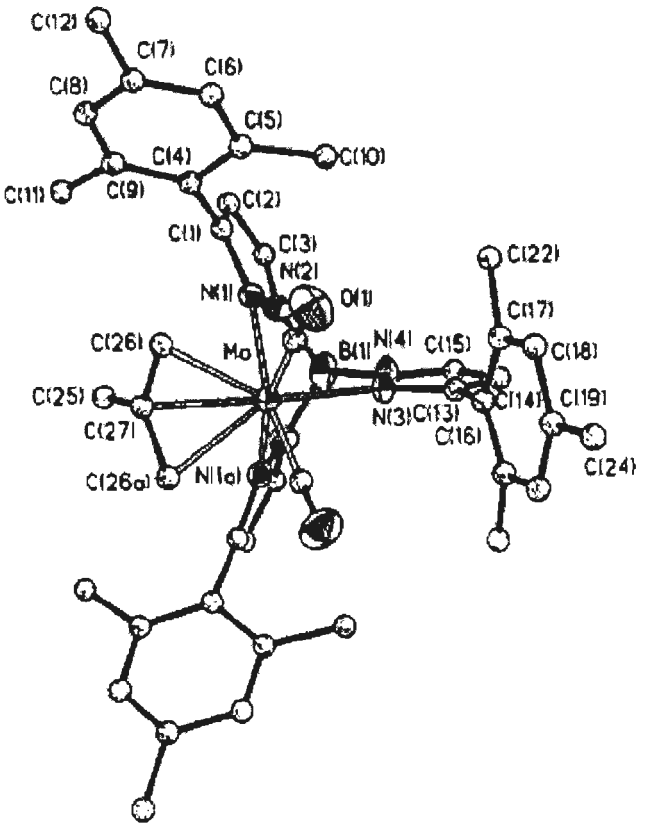

Fig. 1-34 Crystal structure of $Tp^{Ms}Mo(CO)_2(\eta^3\text{-}CH_2CMeCH_2)$

Kunrath et al. [62] reported that the reaction of TlTp′ {Tp′ = HB(3-mesitylpyrazolyl)$_3^-$ (Tp^{Ms}), HB(3-mesitylpyrazolyl)$_2$(5-mesitylpyrazolyl)$^-$ (Tp^{Ms*})} with $NiCl_2.6H_2O$ afforded $Tp^{Ms}NiCl$ and $Tp^{Ms*}NiCl$ in good yield. The compound $Tp^{Ms*}NiCl$ undergoes an isomerization process to form $[(Tp^{Ms**})NiCl]_2$ (Tp^{Ms**} = HB(5-mesitylpyrazolyl)$_2$(3-mesitylpyrazolyl)$^-$) in 68 % yield. They also found that the treatment of tris(pyrazolyl)borate nickel compounds $Tp^{Ms}NiCl$ (Fig. 1-35) and $Tp^{Ms*}NiCl$ with alkylaluminum co-catalyst such as methylalumoxane (MAO) and trimethylaluminum (TMA) in toluene generates active catalysts for ethylene oligomerization.

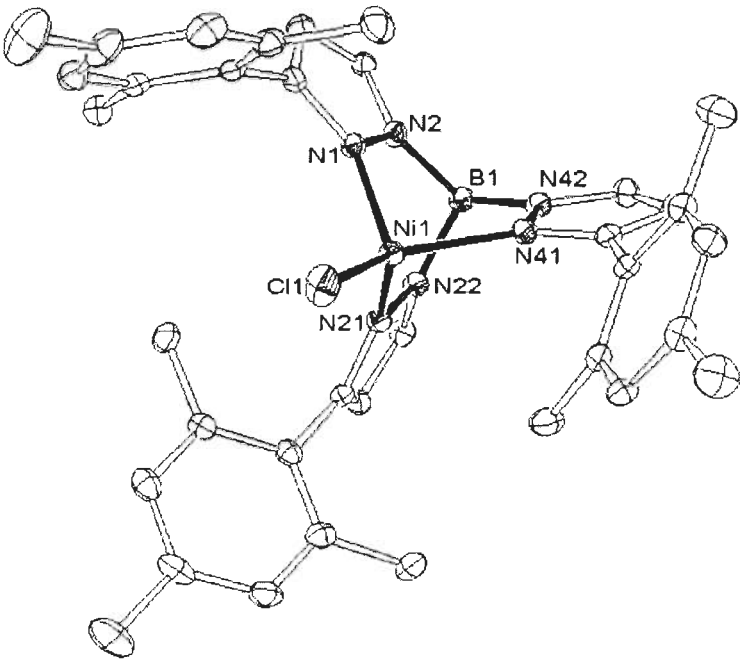

Fig. 1-35 Crystal structure of [Tp^{Ms}NiCl]

Hydrotris(3-(9-anthryl)pyrazol-1-yl)borate [$HB(Pz^{Ant})_3 = Tp^{Ant}$]

Han et al. reported the synthesis of Tp^{Ant}CoCl, and Tp^{Ant}CoNCS. Their X-ray structure (Fig. 1-36) showed that in all of them the anthryl group was almost orthogonal to the pz plane, but total orthogonality was prevented by nonbonding interaction of the 2, 3- and 6, 7-hydrogens. The anthryl groups provided extensive side shielding of the metal, but at the same time, permitted considerable frontal access [21].

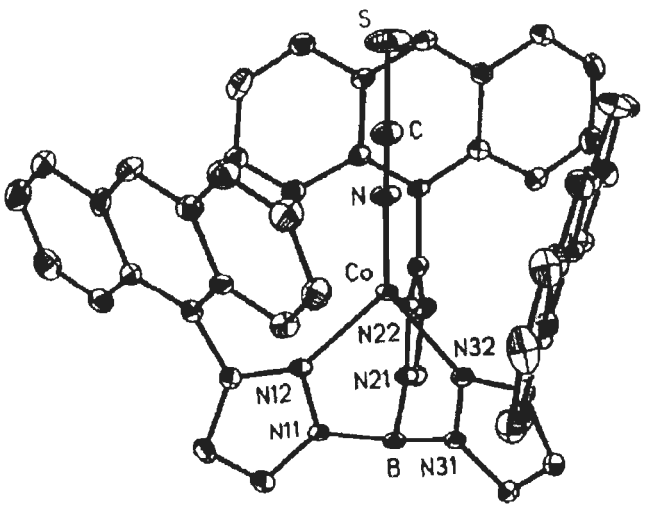

Fig. 1-36 Crystal structure of [Tp^{Ant}Co(NCS)]

Steric effects on hydrotris(pyrazolyl)borate play an important role in controlling the properties / chemical reactivity of resultant complexes. The advantageous characteristics of these ligands are as follows:

1. High solubility in non-coordinating solvents such as toluene and pentane.
2. High shielding effect of isopropyl groups to stabilize unusual coordinating structures.
3. Moderate steric hindrance to allow formation of dimeric complexes.
4. Strong electron donating property.

Owing to above properties, we have succeeded in preparing some iron (II), cobalt (II) and nickel (II) complexes with KTp / KTp^{Me2}, KTp^{iPr2} and $KTp^{Ph,Me}$ ligands. Some of them have been used for anion sensing in environmental and biological systems.

References

1. Trofimenko, S., "Boron-pyrazole chemistry", J. Am. Chem. Soc., **88**, 2445 (1966).

2. Trofimenko, S., "Boron-pyrazole chemistry II. Poly(1-pyrazolyl)borate", J. Am. Chem. Soc., **89**, 3170 (1967).

3. Trofimenko, S., "The coordination chemistry of pyrazole-derived ligands", Chem. Rev., **72**, 497 (1972).

4. Trofimenko, S., Calabrese, J. C. and Thompson, J. S., "Novel polypyrazolylborate ligands: Coordination control through 3-substituents of the pyrazole rings", Inorg. Chem., **26**, 1507 (1987).

5. Rheingold, A.L., Ostrander, R., Haggerty, B.S. and Trofimenko, S., "Homoscorpionate tris(pyrazolyl)borate ligands containing tethered 3-phenyl groups", Inorg. Chem., **33**, 3666 (1994).

6. Trofimenko, S., Calabrese, J.C., Domaille, P.J. and Thompson, J.S., "Steric effect in polypyrazolylborate ligands poly(3-isopropylpyrazolyl)borates: Ligands of intermediate steric requirements", Inorg. Chem., **28**, 1091 (1989).

7. Kitajima, N., Fujisawa, K., Fujimoto, C., Moro-oka, Y., Hashimoto, S., Kitagawa, T., Toriumi, K., Tatsumi, K. and Nakamura, A., "A new model for dioxygen binding in hemocyanin. Synthesis, characterization and molecular structure of the μ-η^2:η^2 peroxo dinuclear copper (II) complexes, $[Cu(HB(3,5\text{-}R_2pz)_3)]_2(O_2)$ (R = iPr and Ph)", J. Am. Chem. Soc., **114**, 1277 (1992).

8. Imai, S., Fujisawa, K., Kobayashi, T., Shirasawa, N., Fuju, H., Yoshimura, T., Kitajima, N. and Moro-oka, Y., "^{63}Cu NMR study of copper (I) carbonyl complexes with various hydrotris(pyrazolyl)borates: Correlation between ^{63}Cu chemical shifts and CO stretching vibrations", Inorg. Chem., **37**, 3066 (1998).

9. Hammes, B.S., Carrano, M.W. and Carrano, C.J., "New H-bond accepting tris(pyrazolyl)borates: stabilization of metal aquo species as models for the vicinal oxygen chelate enzyme superfamily", J. Chem. Soc., Dalton Trans., 1448 (2001).

10. Rheingold, A.L., Liable-Sands, L.M., Golen, J.A., Yap, G.P. and Trofimenko, S., "The coordination chemistry of the hydrotris(3-diphenylmethylpyrazol-1-yl)borate (Tp^{CHPh2}) ligand", J. Chem. Soc., Dalton Trans., 598 (2004).

11. Rheingold, A.L., Liable-Sands, L.M. and Trofimenko, S., "Hydrotris[3-(1-naphthylpyrazol-1-yl)]borate and hydrotris[3-(2-naphthylpyrazol-1-yl)]borate: Two novel homoscorpionate ligands of varying coordination behavior", Inorg. Chem., **40**, 6509 (2001).

12. Olmo, C.P., Böhmerle, K., Steinfeld, G. and Vahrenkamp, H., "New polar pyrazolylborate ligands and their basic zinc complex chemistry", Eur. J. Inorg. Chem., 3869 (2006).

13. Siemer, C.J., Goswami, N., Kahol, P.K., Stipdonk, M.J.V. and Eichhorn, D.M., "Dihydrobis(4-cyano-3-phenylpyrazol-1-yl)borate: Homoleptic mononuclear cobalt (II) and copper (II) complexes with a cyano-substituted scorpionate ligand", Inorg. Chem., **40**, 4081 (2001).

14. Trofimenko, S., Calabrese, J.C., Kochi, J.K., Wolowiece, S., Hulsbergen, R.B. and Reedijk, J., "Spectroscopic analysis, coordination geometry and X-ray structure of nickel (II) compounds with sterically demanding tris(pyrazolyl)borate ligands and azide or thiocyanate anions. Crystal and molecular structure of bis [(μ-thiocyanato-N,S)hydrotris(3-isopropyl-4-bromopyrazolyl)boratonickel (II)]–3-heptane and [(thiocyanato-N)hydrotris(3-tert-butyl-5-methylpyrazol-1-yl)boratonickel (II)]", Inorg. Chem., **31**, 3943 (1992).

15. Egan, J.W., Haggerty, B.S. Jr., Rheingold, A.L., Sendlinger, S.C. and Theopold, K. H., "Crystal structure of a side-on superoxo complex of abstraction by a reactive terminal oxo ligand", J. Am. Chem. Soc., **112**, 2445 (1990).

16. Cano, M., Heras, J.V., Jones, C.J., McCleverty, J.A. and Trofimenko, S., "Sterically induced rearrangements of the tripodal ligand $HB(^{i}PrMeC_3N_2H)_3$ in some molybdenum mononitrosyl derivatives", Polyhedron, **9**, 619 (1990).

17. Kitajima, N., "Synthetic approach to the structure and function of copper proteins", Adv. Inorg. Chem., **39**, 1 (1992).

18. Calabrese, J.C., Domaille, P.J., Trofimenko, S. and Long, G.J., "Hydrotris[3-(2'-thienyl)pyrazol-1-yl]borate: A ligand of remarkably low steric requirements", Inorg. Chem., **30**, 2795 (1991).

19. Ferguason, G., Jennings, M.C., Laor, F.J. and Shanahan, C., "Structure of hydrotris [3-(para-tolyl)pyrazolyl]boratothalium (I)", Acta. Cryst. C, **47**, 2079 (1991).

20. Libertini, E., Yoon, K. and Parkin, G., "The synthesis of $HB(3,5\text{-}(^{t}BuPh)_2pz)_3]^-$ [$^{t}BuPh$ = p-$C_6H_4{}^{t}Bu$], a new tris(pyrazolyl)hydroborato ligand: The crystal and molecular structure of $Tl\{\eta^3\text{-}HB[3,5\text{-}(^{t}BuPh)_2pz)_3]\}$", Polyhedron, **12**, 2539 (1993).

21. Han, R., Parkin, G. and Trofimenko, S., "The tris [3-(9-anthryl)pyrazol-1-yl]hydroborato ligand, [Tp^{Ant}]: Compositional disorder between a vacancy and a chain of three atoms", Polyhedron, **14**, 387 (1995).

22. Rheingold, A.L., White, C.B., and Trofimenko, S., "Hydrotris(3-mesitylpyrazol-1-y1)borate and hydrobis(3-mesitylpyrazol-1-yl)(5-mesitylpyrazol-1-y1)borate: symmetric and asymmetric ligands with rotationally restricted aryl substituents", Inorg. Chem., **32,** 3471 (1993).

23. Dias, H.V.R., "Chemistry of trifluoromethylated tris(pyrazolyl)borate: Synthesis and characterization of carbonyl and isonitrile adducts of silver (I)", J. Am. Chem. Soc., **117**, 11381 (1995).

24. Bergner, S., Wolmershauser, G., Kelm, H. and Thiel, W.R., "Hydrogen bonding in coordination compounds of 3(5)-(4-methoxyphenyl)pyrazole", Inorg. Chim. Acta, **361**, 2059 (2008).

25. Liu, C.-S., Zhang, H., Chen, R., Shi, X.-S., Bu, X.-H., and Yang, M., "Two new Co(II) and Ni(II) complexes with 3-(2-pyridyl)pyrazole-based ligand: Synthesis, crystal structures, and bioactivities", Chem. Pharm. Bull., **55**, 996 (2007).

26. Torralba, M.C., Cano, M., Campo, J.A., Heras, J.V., Pinilla, E. and Torres, M.R., "Chemistry of Rh(I) complexes based on mesogenic 3,5-disubstituted pyrazole ligands. X-ray crystal structures of 3,5-di(4-n-butoxyphenyl)pyrazole ($Pz^{bp2}H$)

and $[Rh(\mu\text{-}pz^{R2})(CO)_2]_2$ (R = $C_6H_4OC_nH_{2n+1}$, n = 10, 12) compounds. Part II", J. Organomet. Chem., **654**, 150 (2002).

27. Jones, L.F., Camm, K.D., Kilner, C.A. and Halcrow, M.A., "Novel hydrogen bond network topologies in complexes of the ditopic ligand 5-amino-3-(pyrid-2-yl)-1H-pyrazole", Cryst. Engg. Comm., **8**, 719 (2006).

28. Petrovic, A.F., Lukic, S.R., Petrovic, D.M., Iveges, E.Z. and Leovac, V.M., "Metal complexes with pyrazole-derived ligands IV. Thermal decomposition of cobalt (II) complexes with 3(5)-amino-4-acetyl-5(3)-methylpyrazole", J. Therm. Anal., **47**, 879 (1996).

29. Shebaldova, A.D. and Safronova, L.A., "Features of the complex formation of platinum (II), palladium (II) and cobalt (II) with 3,5-dimethyl-1-carbamidopyrazole", Russ. J. Coord. Chem., **21**, 465 (1995).

30. Saha, N. and Misra, A., "Synthesis, characterization and coordinating properties of a new benzimidazolylpyrazole: cobalt (II), nickel (II) and copper (II) complexes of 5-methyl-3-(2'-benzimidazolyl) pyrazole", J. Ind. Chem. Soc., **70**, 1035 (1993).

31. (a) Liu, X., Kilner, C.A. and Halcrow, M.A., "3(5)-tert-butylpyrazole is a ditopic receptor for zinc (II) halides", Chem. Comm., 704 (2002). (b) Renard, S.L., Franken, A., Kilner, C.A., Kennedy, J.D. and Halcrow, M.A., "Carbaborane salts of $[ZnCl(Pz^{tBu}H)_3]^+$, a host for inorganic anions ($Pz^{tBu}H$ = 5-tert-butylpyrazole)", New. J. Chem., **26**, 1634 (2002). (c) Nieto, S., Perez, J., Riera, V., Miguel, D. and Alvarez, C., "Cationic *fac*-tris(pyrazole) complexes as anion receptors", Chem. Comm., 546 (2005). (d) Renard, S.L., Sylvestre, I., Barrett, S.A., Kilner, C.A. and Halcrow, M.A., "Homoleptic zinc (II) complexes with first and second coordination shell of 5-tert-butylpyrazole", Inorg. Chem., **45**, 8711 (2006).

32. (a) Glenny, M.W., Blake, A.J., Wilson, C. and Schroder, M., "Anion effects in selective bifunctional metal salt extractants based on aza-thioether macrocycles: co-operative cation–anion binding", Dalton Trans., 1941 (2003). (b) Plieger, P.G., Tasker, P.A. and Galbraith, S.G., "Zwitterionic macrocyclic metal sulfate extractants containing 3-dialkylaminomethylsalicylaldimine units.", Dalton

Trans., 313 (2004). (c) Bondy, C.R., Gale, P.A. and Loeb, S.J., "Metal-organic anion receptors: Arranging urea hydrogen-bond donors to encapsulate sulfate ions", J. Am. Chem. Soc., **126**, 5030 (2004). (d) Harding, L.P., Jeffery, J., Rice, C.T.C.R. and Zeng, Z., "Anion control of ligand self-recognition in a triple helical array", Chem. Comm., 654 (2004). (e) Gunning, P., Benniston, A.C. and Peacock, R.D., "A modular ditopic crown-shielded phosphate ion-pair receptor", Chem. Comm., 2226 (2004). (f) Koskela, S.J.M., Fyles, T.M. and James, T.D., "A ditopic fluorescent sensor for potassium fluoride", Chem. Comm., 945 (2005). (g) Curiel, D. and Beer, P.D., "Anion directed synthesis of a hydrogensulfate selective luminescent rotaxane", Chem. Comm., 1909 (2005). (h) Vega, I.E., Gale, P.A., Light, M.E. and Loeb, S.J., "NH *vs* CH hydrogen bond formation in metal–organic anion receptors containing pyrrolylpyridine ligands", Chem. Comm., 4913 (2005). (i) Duckmanton, P.A., Blake, A.J. and Love, J.B., "Palladium and rhodium ureaphosphine complexes: Exploring structural and catalytic consequences of anion binding", Inorg. Chem., **44**, 7708 (2005). (j) Pask, C.M., Camm, K.D., Bullen, N.J., Carr, M.J., Clegg, W., Kilner, C.A. and Halcrow, M.A., "Two complexes of copper (II) salts with 5-amino-3-(pyrid-2-yl)-1H-pyrazole, the prototype for a new class of ditopic ligand", Dalton Trans., 662 (2006).

33. Beer, P.D. and Hayes, E.J., "Transition metal and organometallic anion complexation agents", Coord. Chem. Rev., **240**, 167 (2003).

34. Calabrese, J.C., Trofimenko, S. and Thompson, J.S., "A new class of poly(pyrazolyl)borate ligands", J. Chem. Soc., Chem. Comm., 1122 (1986).

35. Calabrese, J.C., Domaille, P.J., Thompson, J.S. and Trofimenko, S., "Steric effects in poly(pyrazolyl)borates: Mixed complexes MHB(3-isopropyl-4-bromo-pyrazolyl)$_3$)L", Inorg. Chem., **29**, 4429 (1990).

36. Calogero, S., Lobbia, G.G., Cecchi, P., Valle, G. and Fridel, J., "A Mössbauer study of some iron (II) and iron (III) poly(pyrazolyl)borates. The X-ray crystal structures of iron (II) bis[hydridotris(3-methyl-1H-pyrazol-1-yl)borate] and iron (III) bis[hydridotris(1H-pyrazol-1-yl)borate]tetrafluoroborate", Polyhedron, **13,** 87 (1994).

37. Mason, S.J., Hill, C.M., Murphy, V.J., O'Hare, D. and Watkin, D.J., "Synthesis, crystal structures and magnetic properties of salts containing bis[hydrotris(3,5-dimethyl-1-pyrazolyl)borate]iron (III)", J. Organomet. Chem., **485**, 165 (1995).

38. Sun, Y.-J., Cheng, P., Yan, S.-P., Jiang, Z.-H., Liao, D.-Z. and Shen, P.-W., "New half-sandwich nickel (II) complex with mono-hydrotris(3,5-dimethylpyrazolyl) borate ligand and nitrite", Inorg. Chem. Comm., **3**, 289 (2000).

39. Sun, Y.-J., Shen, W.-Z., Cheng, P., Yan, S.-P., Liao, D.-Z., Jiang, Z.-H. and Shen, P.-W., "Synthesis, structure and spectroscopic properties of novel half-sandwich nickel (II) complexes with less hindered hydrotris(pyrazolyl)borate ligand", Polyhedron, **23**, 211 (2004).

40. Sun, Y.-J., Shen, W.-Z., Cheng, P., Yan, S.-P., Liao, D.-Z., Jiang, Z.-H. and Shen, P.-W., "The first example of half-sandwich cobalt (III) complex with hydrotris(pyrazolyl)borate ligand", Inorg. Chem. Comm., **5**, 512 (2002).

41. Kitajima, N., Tamura, N., Amagai, H., Fukui, H., Moro-oka, Y., Mizutani, Y., Kitagawa, T., Mathur, R., Heerwegh, K., Reed, C.A., Randall, C.R., Que, L., Jr. and Tatsumi, K., "Monomeric carboxylate ferrous complexes as models for the dioxygen binding sites in non-heme iron proteins. The reversible formation and characterization of *p*-peroxo diferric complexes", J. Am. Chem. Soc., **116**, 9071 (1994).

42. Akita, M., Shirasawa, N., Hikichi, S. and Moro-oka, Y., "14e η^1-Hydrocarbyliron complexes supported by hydrotris(3,5-diisopropylpyrazolyl)borate: the allyl complex prefers a highly coordinatively unsaturated 14e η^1-structure to a 16e η^3-structure", Chem. Comm., 973 (1998).

43. Singh, U.P., Babbar, P. and Sharma, A.K., "Cobalt complexes bridge with a (μ-X)(μ-carboxylato) unit (X = OH, N_3): Synthesis and structural studies", Inorg. Chim. Acta, **358**, 271 (2005).

44. Fujisawa, K., Kakizaki, T., Miyashita, Y. and Okamoto, K.-I., "Structural and spectroscopic comparison of five-coordinate cobalt (II) and nickel (II) thiolato complexes with the related four-coordinate complexes", Inorg. Chim. Acta, **361**, 1134 (2008).

45. Siemer, C.J., Meece, F.A., Armstrong, W.H. and Eichhorn, D.M., "Iron, copper, and cobalt complexes of hydrotris(3-phenylpyrazolyl)borate and dihydrobis(3-phenylpyrazolyl)borate. Synthesis and X-ray crystallographic characterization", Polyhedron, **20**, 2637 (2001).

46. Lukasiewicz, M., Ciunik, Z. and Wolowiec, S., "Complexes of heteroscorpionate tris(pyrazolyl)borate anionic ligands Part I. The crystal structure and reactivity of thiocyanato[hydrobis(3-phenylpyrazolyl)(3-tert-butylpyrazolyl)borato]cobalt (II) complex", Polyhedron, **19**, 2119 (2000).

47. Kremer-Aach, A., Klaui, W., Bell, R., Strerath, A., Wunderlich, H. and Mootz, D., "Cobalt as a probe for zinc in metalloenzyme model compounds? A comparison of spectroscopic features and coordination geometry of four- and five-coordinate complexes. Crystal and molecular structures of [Co(η^3-Tp(Ph))(η^2-Tp(Ph))], [η^3-Tp(Ph))Zn(anthranilate)] and [(η^3-Tp(Ph))M(η^2-acac)] (Tp^{Ph} = Hydrotris(3-phenylpyrazol-1-yl)borate, acac = Pentane-2,4-dionate and M = Zn, Co)", Inorg. Chem., **36**, 1552 (1997).

48. Kolotilov, S.V., Addison, A.W., Trofimenko, S., Dougherty, W. and Pavlishchuk, V.V., "Efficient mechanochemical synthesis of tris(pyrazolylborate) complexes of manganese (II), cobalt (II) and nickel (II)", Inorg. Chem. Comm., **7**, 485 (2004).

49. Uehara, K., Hikichi, S. and Akita, M., "Highly labile cationic tris-acetonitrile complexes, [Tp^RM(NCMe)$_3$]OTf (M = Ni, Co; Tp^R: hydrotrispyrazolylborato, R = Ph, Me and iPr_2): versatile precursors for Tp^R-containing nickel and cobalt complexes", J. Chem. Soc., Dalton Trans., 3529 (2002).

50. Yakovenko, A.V., Kolotilov, S.V., Addison, A.W., Trofimenko, S., Yap, G.P.A., Lopushanskaya, V. and Pavlishchuk, V.V., "Ni(II), Co(II) and Mn(II) tris(pyrazolyl)borate complexes with 2,6-di-tert-butyl-4-carboxy-phenol: Formation of coordinated phenoxyl radical", Inorg. Chem. Comm., **8**, 932 (2005).

51. Ruman, T., Ciunik, Z., Goclan, A., Lukasiewicz, M. and Wolowiec, S., "Complexes of heteroscorpionate tris(pyrazolyl)borate anionic ligands. Part V. X-ray crystallographic studies of cobalt (II) complexes with hydrobis(3,5-dimethylpyrazolyl)(3,5-diphenylpyrazolyl)borate and hydrobis(3,5-diphenyl

pyrazolyl)(3,5-dimethylpyrazolyl)borate ligands", Polyhedron, **20**, 2965 (2001).

52. Mehn, M.P., Fujisawa, K., Hegg, E.L. and Que, L., Jr., "Oxygen activation by nonheme iron (II) complexes: α-keto carboxylate versus carboxylate", J. Am. Chem. Soc., **125**, 7828 (2003).

53. Hegg, E.L., Ho, R.Y.N. and Que, L., Jr., "Oxygen activation and arene hydroxylation by functional mimics of α-keto acid-dependent iron (II) dioxygenases", J. Am. Chem. Soc., **121**, 1972 (1999).

54. Santi, R., Romano, A.M., Sommazzi, A., Grande, M., Bianchini, C. and Mantovani, G., "Catalytic polymerisation of ethylene with tris(pyrazolyl)borate complexes of late transition metals", J. Mol. Catalysis A: Chem., **229**, 191 (2005).

55. Bergquist, C., Fillebeen, T., Morlok, M.M. and Parkin, G., "Protonation and reactivity towards carbon dioxide of the mononuclear tetrahedral zinc and cobalt hydroxide complexes, [$Tp^{But,Me}$ZnOH] and [$Tp^{But,Me}$CoOH]: Comparison of the reactivity of the metal hydroxide function in synthetic analogues of carbonic anhydrase", J. Am. Chem. Soc., **125,** 6189 (2003).

56. Hikichi, S., Ogihara, T., Fujisawa, K., Kitajima, N., Akita, M. and Moro-oka, Y., "Synthesis and characterization of the benzoylformato ferrous complexes with the hindered tris(pyrazolyl)borate ligand as a structural model for mononuclear non-heme iron enzymes", Inorg. Chem., **36**, 4539 (1997).

57. Ogihara, T., Hikichi, S., Akita, M., Uchida, T., Kitagawa, T. and Moro-oka, Y., "An approach to the O_2 activating mononuclear non-heme Fe enzymes: structural characterization of Fe(II)–acetato complex and formation of alkylperoxoiron (III) species with the highly hindered hydrotris(3-tert-butyl-5-isopropyl-1-pyrazolyl)borate", Inorg. Chim. Acta, **297**, 162 (2000).

58. Siemer, C.J., VanStipdonk, M.J., Kahol, P.K. and Eichhorn, D.M., "A coordination polymer from a cyanoscorpionate complex", Polyhedron, **23**, 235 (2004).

59. Zhao, N., Stipdonk, M.J.V., Bauer, C., Campana, C. and Eichhorn, D.M., "Sandwich compounds of cyanotris(pyrazolyl)borates: Complexation-induced ligand isomerization", Inorg. Chem., **46**, 8662 (2007).

60. Brunker, T.J., Hascall, T., Cowley, A.R., Rees, L.H. and O'Hare, D., "Variable coordination modes of hydrotris(3-isopropyl-4-bromopyrazolyl)borate (Tp′) in Fe(II), Mn(II), Cr(II), and Cr(III) complexes: Formation of MTp′Cl (M) Fe and Mn), structural isomerism in $CrTp'_2$, and the observation of Tp′-as an uncoordinated anion", Inorg. Chem., **40**, 3170 (2001).

61. Calabrese, J.C. and Trofimenko, S., "Hydrotris(3-neopentylpyrazol-1-yl) borates: A new type of sterically hindered poly(pyrazolyl)borate", Inorg. Chem., **31**, 4810 (1992).

62. Kunrath, F.A., de Souza, R.F., Casagrande, J.O.L., Brooks, N.R. and Young, J.V.G., "Highly selective nickel ethylene oligomerization catalysts based on sterically hindered tris(pyrazolyl)borate ligands", Organometallics, **22**, 4739 (2003).

Chapter 2

Synthesis and Characterization of Iron and some Mixed Ionic Complexes

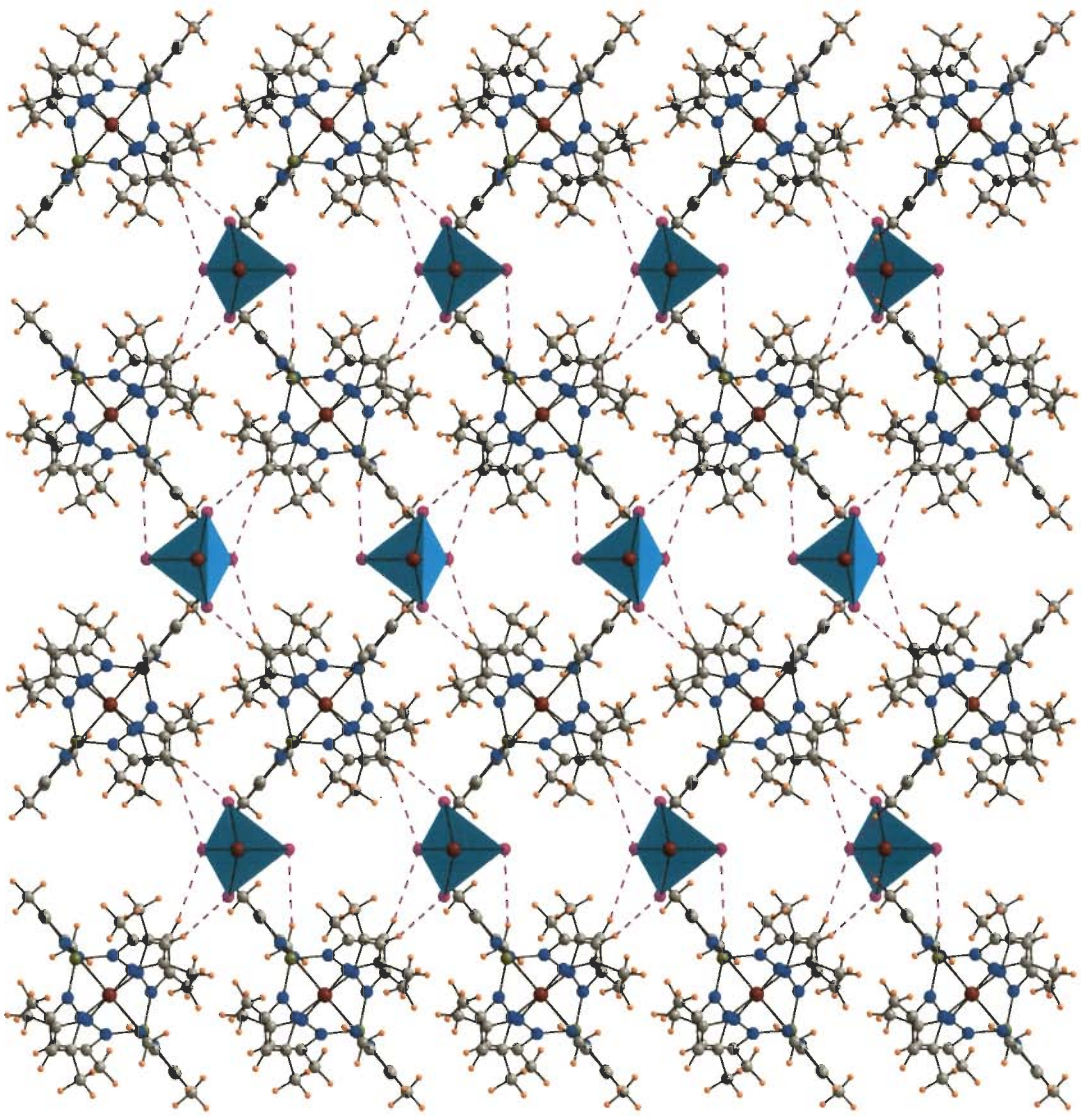

Iron is one of the essential elements for all living organisms, as it is involved in a wide variety of key physiological processes [1]. In case of humans, it is the most abundant metal with an iron content of 3 to 4 g present in healthy adult; excess or deficiency of iron is associated with serious diseased states of haemochromatosis and anaemia, respectively. In humans, the bulk of the iron is bound to haemoglobin in the red blood corpuscles (roughly 66%) and the rest is either bound to the muscle oxygen storage protein myoglobin (roughly 10%) or is stored by ferritin and the related protein haemosiderin (approximately 23%) mainly in liver, spleen and bone marrow. Iron (III) in free state is almost totally insoluble at physiological pH and for iron transport in the plasma, nature has devised a transporting protein, transferrin that moves the iron in ferric state from sites of absorption and storage to the sites of utilization and storage.

Iron metabolism in the body, requires the metal in both the ferrous [Fe(II)] and ferric [Fe(III)] states, but in nature, the presence of free ferrous iron, [Fe(II)], is potentially very dangerous as it can lead to the formation of the highly toxic ($OH^{\cdot}$) hydroxide radical by a Fenton-type reaction. Therefore, utilization of ferrous iron is required so that the metal can be encapsulated into macromolecules and its chemistry can be controlled. A prime example of this is the oxygen transporting protein, haemoglobin.

The iron atom is usually ligated by a protein, which is therefore called a metalloprotein. The most important factor determining the function of a metalloprotein is its active site structure [2], especially the ligand environment around iron is of crucial importance. The roles of metalloproteins are very diverse as some are involved in transport and / or storage and others in electron transfer / hydrolysis / catalysis a variety

of biologically important reactions. In general, the functions of iron ions in proteins are as follows:

(i) Dioxygen transport: One of the most important and probably best known processes involving iron is respiration. The uptake of dioxygen and transport to the muscles is a function almost exclusively performed by iron containing proteins [3]. Examples of this class of metalloproteins include myoglobin, hemoglobin and hemerythrin.

Myoglobin was one of the first protein structures solved using X-ray crystallographic methods [4]. Myoglobin is found in skeletal muscle cells and it not only stores oxygen, but also enhances its rate of diffusion through the cell. The structure contains the prosthetic haem group, a protoporphyrin ring with an iron atom at its centre, (Fig. 2-1). This iron atom reversibly binds an oxygen molecule and remains in the ferrous Fe(II) state in both the oxygenated and unliganded forms.

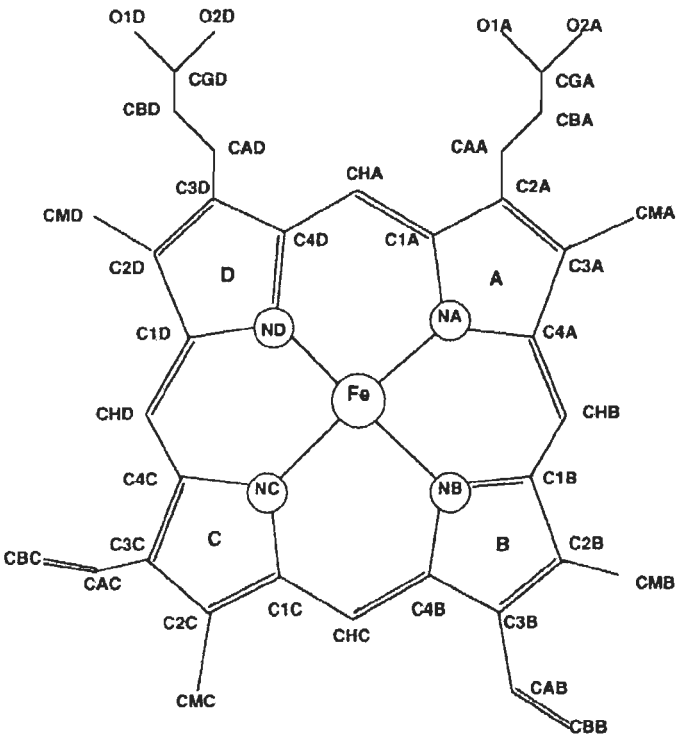

Fig. 2-1 The haem prosthetic group with the Brookhaven PDB numbering scheme.

The structure of oxy-myoglobin (Fig. 2-2) shows how the six helical units surround the haem group and the ferrous iron binds to the proximal histidine residue. The oxygen molecule is also shown bound to the metal. Haemoglobin, the carrier of oxygen in the blood, has been subjected to rigorous structural research, particularly by Perutz and his co-workers [5]. It is a tetramer of four globin subunits with an overall molecular weight of 65 kDa (Fig. 2-3). The subunits comprise two identical pairs, the subunits with 141 amino acids and the subunits with 146 residues, arranged in an approximate 222 symmetry. Haemerythrin is a non-haem oxygen-carrying protein utilized by several groups of marine invertebrate phyla and worms including the sipunculid worm.

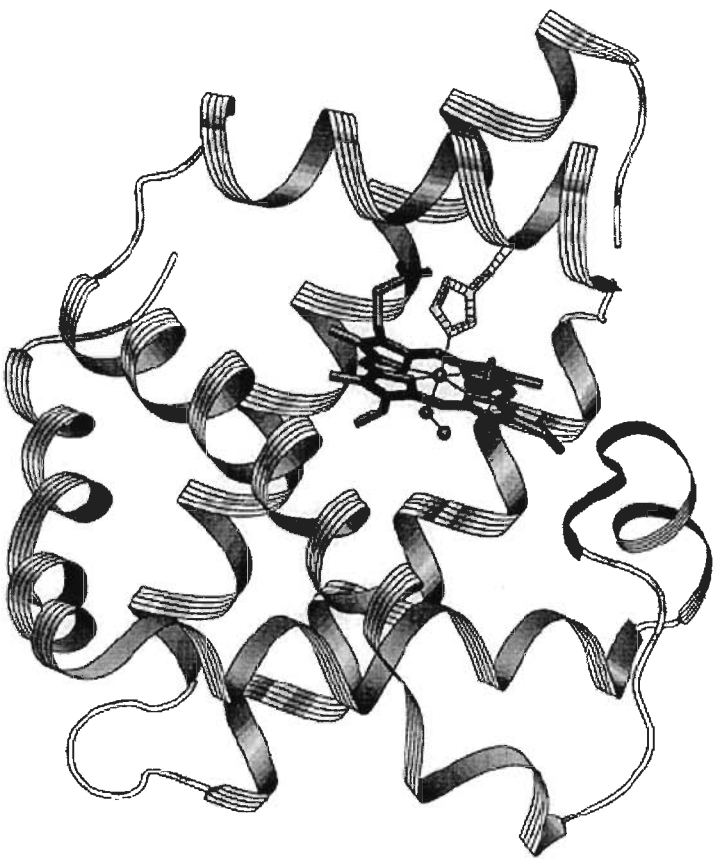

Fig. 2-2 The 'globin' fold.

Fig. 2-3 The overall organization of the haemoglobin molecule showing the four subunits.

(ii) Electron transfer: Many proteins need electrons to perform their function and these are supplied by electron transfer centers like iron-sulfur clusters [6] and the cytochromes, which contain iron porphyrin units in their active sites [7].

The iron–sulphur proteins are also found in a wide variety of organisms and are usually involved in electron transfer processes. These proteins contain one or more iron–sulphur centres, consisting of iron, inorganic sulphur and / or sulphur atoms from cysteine residues organized in a cluster. In size they can vary from around 50 residues (rubredoxin) to several hundred (nitrogenase) and the redox potentials also show a wide variation from −400 mV to +350 mV.

The cytochromes form a widespread family of proteins, first characterized spectroscopically in respiring mitochondria, but later found at other sites in the eukaryotic cells and in prokaryotes; they are haem containing proteins that act as electron carriers in different energy transducing systems.

(iii) Protection: A closely related class of metalloenzymes is the protective enzymes, which are involved in the detoxification of harmful compounds like superoxide and hydrogen peroxide. Although copper / zinc superoxide dismutases (SOD's) are the most studied, [8] but some manganese [9] and iron containing SOD's are also known [10]. X-ray structures have been elucidated for iron-dependent member of the superoxide dismutase family [10]. These enzymes catalyse a two-step disproportionation of the superoxide radical, e.g.

$$Fe(III) + O_2^- \rightarrow Fe(II) + O_2$$
$$Fe(II) + O_2^- + 2H^+ \rightarrow Fe(III) + H_2O_2$$

Catalases and peroxidases are heme containing proteins that are involved in H_2O_2 dismutation and reduction to H_2O, respectively [11].

(iv) Hydrolysis: These reactions are catalyzed by a class of metalloenzymes that in most cases is zinc dependent [12]. A few systems do not use zinc but another metal like iron. Examples of such hydrolytic enzymes are the purple acid phosphates (PAP), which are involved in the hydrolysis of phosphate esters [13].

(v) Oxidative and reductive transformations: The most important catalytic function of iron atoms in nature is mediation of redox transformations. Many iron containing metalloenzymes catalyze reactions that involve reduction or oxidation of a substrate. Examples of this subclass include isopenicillin N-synthase [14] which is involved in the biosynthesis of penicillins and the oxygenases like cytochrome P-450 and methane monooxygenase.

Iron containing oxidation enzymes can generally be divided in two classes: the oxidases, which act through electron transfer with concomitant reduction of O_2 to water and the oxygenases, which catalyze the reaction of O_2 with organic- or inorganic substrates [2, 15]. The latter category can again be subdivided into mono- and di-oxygenases. A monooxygenase incorporates one of the oxygen atoms from molecular oxygen into the substrate whereas the other oxygen is reduced to water. A dioxygenase incorporates both oxygen atoms from O_2 into the oxygenated product. Another subdivision can be made based on the ligands used to bind the metal ion. Higher organisms usually use a heme prosthetic group for this purpose. Enzymes that do not use a heme but instead bind the metal with ligands provided by the protein are called non-heme enzymes. This heme / non-heme division is also used for the model systems.

The most studied and best understood oxygen activating metalloenzymes are the cytochrome P-450's [11, 16]. This comprises a group of monooxygenases that can oxygenate a wide variety of substrates of great physiological importance. Some of the reactions catalyzed by cytochrome P-450 are key transformations in the metabolism of lipids or the biosynthesis of corticosteroids [17]. Substantial mechanistic insight has been obtained for a variety of oxidative transformations catalyzed by this enzyme, including the oxidation of unfunctionalized alkanes [18]. Because it is so well understood the oxygen activation pathway of cytochrome P-450 serves as a benchmark to which other systems are compared. Cytochrome P-450 is a heme iron protein that uses a protoporphyrin IX group to bind the iron (Fig. 2-4). The axial ligand, in this case a cysteinyl thiolate, was supplied by the protein backbone [19]. The same iron protoporphyrin IX group is also found in dioxygen transport proteins like hemoglobin and myoglobin, the only difference being the axial ligand, in this case a histidine [3b].

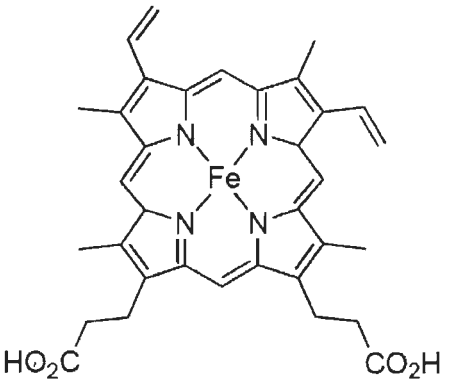

Fig. 2-4 An iron protoporphyrin IX complex

The proposed oxygen activation mechanism of cytochrome P-450 is summarized in scheme 2-1. First dioxygen is bound by the iron (II) center followed by one-electron reduction to give an iron (III) peroxo species. Heterolysis of the O-O bond gives a formally $Fe^{V}O$ species which is proposed to be the active species responsible for oxygenation of the substrate.

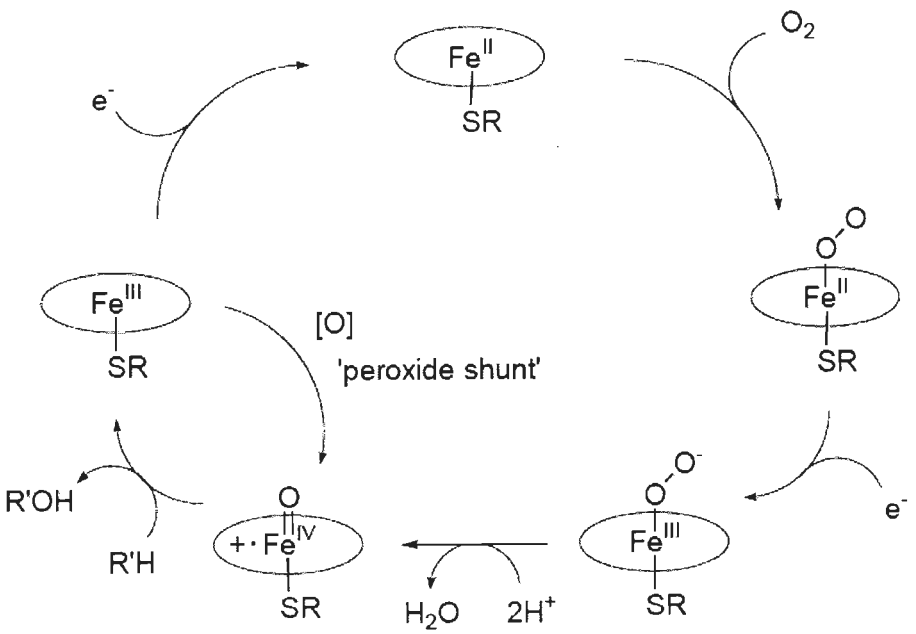

Scheme 2-1 Mechanism for O_2 activation by cytochrome P-450

This active species is actually thought to be an oxoiron (IV) porphyrin radical cation complex, characterized compound I of heme peroxidases [20]. Several

observations support the existence of this proposed high valent intermediate. First, using oxygen atom donors like peroxides, PhIO and NaOCl it is possible to generate species that give the same reactivity as in the O_2 system, a pathway known as the "peroxide shunt" [17]. Recently crystallographic evidence for all putative intermediates on the catalytic pathway, including a structure that appears to be the formally $Fe^{V}O$ intermediate, has been obtained for cytochrome P450cam [21].

Methane monooxygenase (MMO) is a remarkable enzyme that can catalyze the selective oxidation of methane to methanol using O_2 as the terminal oxidant [22]. It is found in methanotropic bacteria that use methane as their sole carbon source, like *Methylococcus capsulatus* (Bath) and *Methylosinus trichosporium*. It consists of 3 components, a hydroxylase (MMOH), which is responsible for the oxidation of methane, a reductase and a regulatory protein. These enzymes have structurally very similar active sites that consist of two iron atoms in a carboxylate-rich ligand environment. These iron atoms are often bridged by an oxo group and / or bidentate carboxylates. The structure of both the oxidized form of MMOH (MMOHox) and the reduced form (MMOHred) has been studied spectroscopically and by X-ray crystallography [23] (Fig. 2-5).

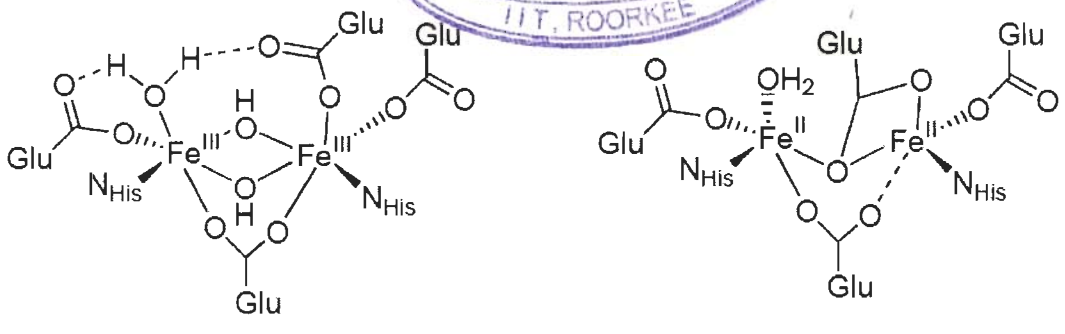

$MMOH_{ox}$ $MMOH_{red}$

Fig. 2-5 Active site structures of $MMOH_{ox}$ and $MMOH_{red}$

The catalytic cycle of MMOH goes through several discrete intermediates (Scheme 2-2). The best studied are the intermediates called P and Q. Mixing of MMOHred with O_2 gives intermediate P, which is proposed to be a μ-1,2-peroxo bridged diiron (III) species. P exhibits a weak visible absorption at 625-650 nm, associated with a peroxo-to-iron (III) charge transfer transition, for the MMOH isolated from *M. capsulatus*. Intermediate P converts to intermediate Q, which is believed to be the species responsible for methane hydroxylation [24, 25]. Based on Mössbauer spectroscopy compound Q was proposed to contain Fe^{IV}. Because of its diamagnetic ground state MMOH-Q was assigned as a diiron (IV) species.

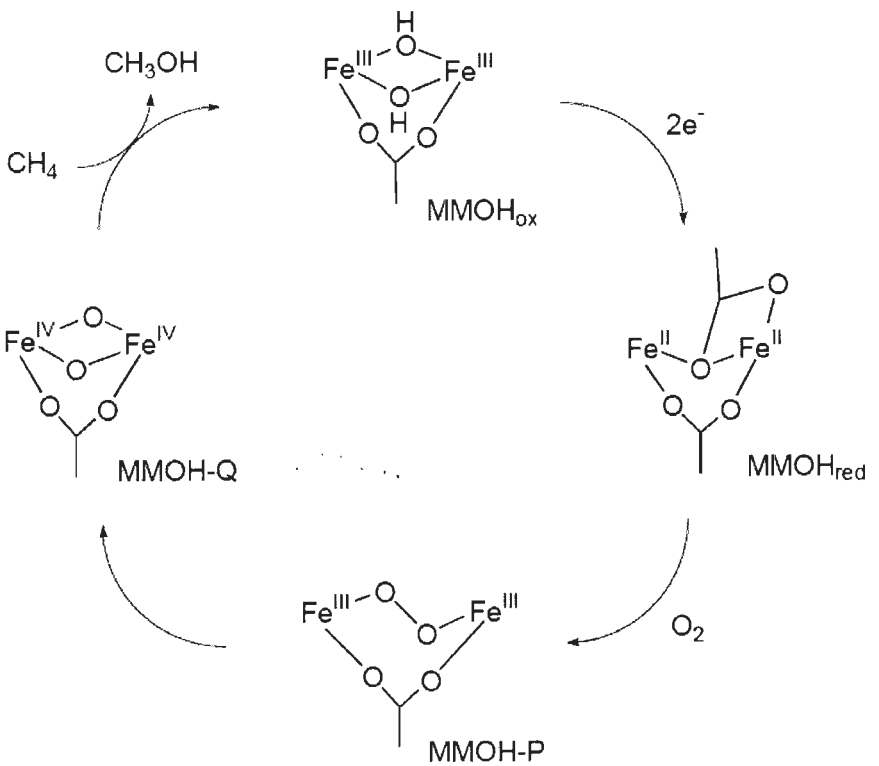

Scheme 2-2 Schematic representation of the catalytic cycle of MMOH.

Fungal nitric oxide reductase (cytochrome P450 nor) is a heme-containing enzyme, in which the iron-porphyrin complex is an active site of the enzyme. This

enzyme is involved in the fungal denitrification process and catalyzes the reduction of NO to N_2O.

$$2NO + NADH + H^+ \rightarrow N_2O + NAD^+ + H_2O$$

where NADH is an electron donor to the enzyme. The turnover number of this reaction is over 1,000 sec^{-1} at 10 °C, showing an effective NO diminishing system in cells [26]. The ferric-NO complex of P450 nor is extremely stable under anaerobic condition, in sharp contrast to other hemoproteins such as myoglobin (Mb) and hemoglobin (Hb), whose ferric-NO complexes are readily auto-reduced to the ferrous-NO complexes.

The active site structure of fungal NOR in Fe^{3+}-NO form is shown in Fig. 2-6. The Fe-NO bond length is 1.63 Å, and the Fe-N-O angle is 161° (a slightly bent configuration).

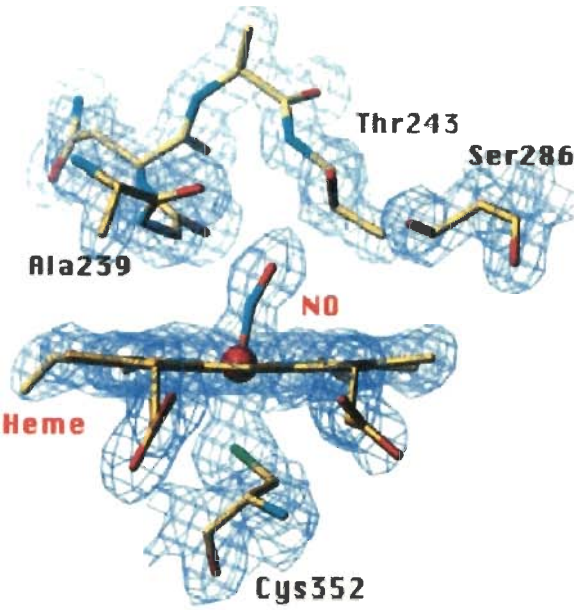

Fig. 2-6 Active site structure of fungal NOR in the ferric-NO state

The nitrogen atom of the iron-bound NO is positioned off the heme normal axis (a slightly tilt configuration) toward the porphyrin b-meso direction, as illustrated in Fig. 2-6, where the angle between the heme normal axis and the Fe-N line is 9°.

Temperature factors of the nitrogen and oxygen atoms are sufficiently low (12 and 13 $Å^2$, respectively), indicating that the bound NO is highly ordered in this complex. This observation also indicates that the crystal sustained no x-ray radiation damage during the diffraction measurement [27]. The Fe- S (Cys352) bond length is 2.31 Å. The iron is displaced only 0.03 Å from the heme plane toward the direction of the bound NO, but remains basically in the in-plane configuration.

A mechanism was also proposed for N_2O formation, which involves attack of another NO molecule to the electron rich Fe-NO unit in the intermediate, leading the N-O bond cleavage and the N-N bond formation (Fig. 2-7). For the intermediate formation, proton(s) should be delivered to the Fe-NO moiety from the solvent region through the hydrogen-bond network. So Cytochrome P450 nor catalyzes the reduction reaction of NO to N_2O, via the change of the spin state of the Fe-NO moiety, as shown in Fig.2-7.

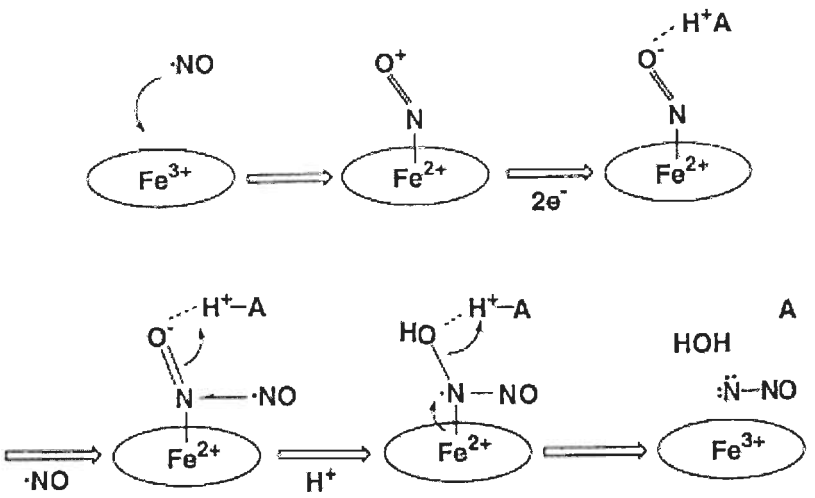

Fig. 2-7 The proposed mechanism for N_2O formation from the intermediate and NO

As we have seen that iron is the most prominent transition metal in biological systems and is known to play an active role in the catalytic cycles of many

metalloenzymes [1]. By far, the most common oxidation states of iron in proteins are the +2 and +3 states, though higher oxidation states (+4 and +5) are often proposed for specific intermediates in oxygen-activating enzymes and model systems [28-31] Because of these proposals, the chemistry of heme and non-heme iron in its high valent states is currently of intense interest.

Interest in high-oxidation-state iron chemistry derives from the potential intermediacy of such compounds during the function of many metalloenzymes and in other catalytic reactions [28, 32]. Low-molecular-weight model compounds have been synthetic targets for quite some time in an attempt to gain insight into both the spectroscopic features and reactivity patterns of these otherwise transient, yet important, species. Considerable attention has been devoted to the preparation of $Fe^{IV}O$ coordination compounds and many successful attempts have recently appeared [30]. Somewhat surprisingly, the chemistry of related high-valent, terminal iron nitrido compounds remains relatively underdeveloped. These compounds are of considerable interest due to their importance in both industrial [32] and biological [33] nitrogen fixation schemes and their potential to serve as efficient N-atom transfer agents.

The traditional synthetic approach to molecular iron nitrides has focused on the photooxidation of iron azido compounds (Scheme 2-3). Both the expulsion of the stable dinitrogen molecule and the ease with which the FeN_3 linkage can be assembled make this route attractive. It is often the case, however, that photochemical conversion of the azido compound to the desired nitrido species is accompanied by competing photoreduction, a process that initially generates the azine radical, which then quickly decomposes to dinitrogen.

Photooxidation – Targeted

$$L_nFe^{n+}{-}N_3 \xrightarrow{h\nu} L_nFe^{(n+2)+}{\equiv}N + N_2$$

Photoreduction – Unwanted

$$L_nFe^{n+}{-}N_3 \xrightarrow{h\nu} L_nFe^{(n-1)+} + 1.5\ N_2$$

Scheme 2-3 Photooxidation versus photoreduction of iron azido compounds

Adams et al. [34] prepared six-coordinate azido(pyridine)(tetraphenylporphinato) iron (III) complex, Fe(TPP)N_3py, and its structure was determined by diffraction techniques (Fig. 2-8). The nearly tetragonal geometry and bond distances of the coordination group were consistent with a low-spin ferric ion. This spin state was also confirmed by a temperature-dependent magnetic analysis by using the Faraday method over the temperature range from 77 to 297 K. The effective magnetic moments range from 2.09(1) μ_B at 77 K to 2.33(1) μ_B at 297 K and are characteristic of a low spin state with spin-orbit coupling. Equillibrium constants for the addition of pyridine, N-methylimidazole, and imidazole to Fe(TPP)N_3 in CH_2Cl_2 at 23 ± 1 °C were also determined from the visible spectra.

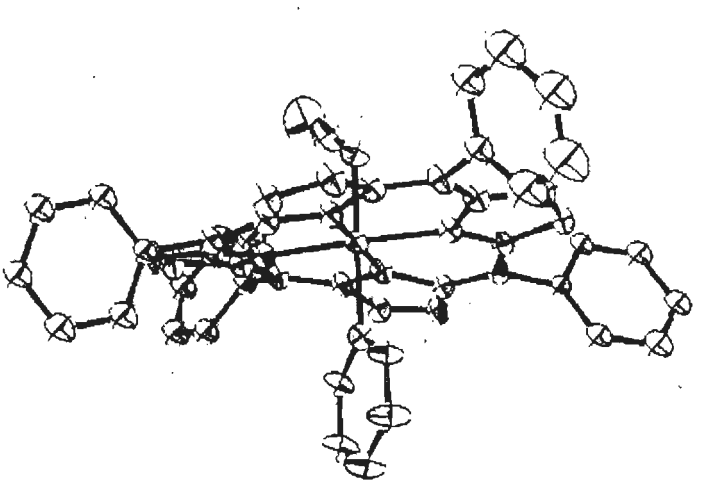

Fig. 2-8 Crystal structure of Fe(TPP)N_3py

From this azido compound, Wagner and Nakamoto [35] reported the first successful application of the photooxidation method to prepare iron nitrido complexes. Observation of substituted porphyrin (Por) iron nitrido compounds was achieved at 30 K by using resonance Raman spectroscopy, raising the temperature yielded relatively common -nitrido diiron compounds.

Zhang et al. [36] reported a structural study of the high-spin five-coordinate complex iron (III) tetraphenylporphyrin azide $Fe(TPP)N_3$ and its six-coordinate low-spin adducts with 1-methylimidazole (1-MeIm) and 1,2-dimethylimidazole (1,2-Me_2Im). The latter two complexes were studied in order to explore the structural effect of steric strain induced by the presence of the 2-methyl substituent and to determine to what extent, if any, the set of complexes Fe-(TPP)(l-MeIm)N_3 and Fe(TPP)(1,2-$Me_2$1m)N_3 mimic the structural differences observed in the vicinity of the metal in R-state HbO_2 and T-state HbO_2, respectively. All of these complexes were characterized by X-ray crystallography (Fig. 2-9). The porphyrin core in $Fe(TPP)N_3$ was domed with the iron displaced 0.46 Å, from the plane of the four pyrrole nitrogens (P_N). In Fe-(TPP)(l-MeIm)N_3 and Fe(TPP)(1,2-$Me_2$1m)N_3 the porphyrin core display approximate S_4 ruffling with the metal located nearly in the P_N plane. In going from Fe-(TPP)(l-MeIm)N_3 to Fe(TPP)(1,2-$Me_2$1m)N_3, there was essentially no change in the Fe-N_3 or Fe-N_P (pyrrole nitrogen) bond distances. From these results, a comparision to the structural features of the analogous picket fence complexes Fe(TPP)(RIm)O_2 (RIm = 1-MeIm and 2-MeIm) was discussed with reference to possible structural changes that accompany the T-HbO_2 to R-HbO_2 switch.

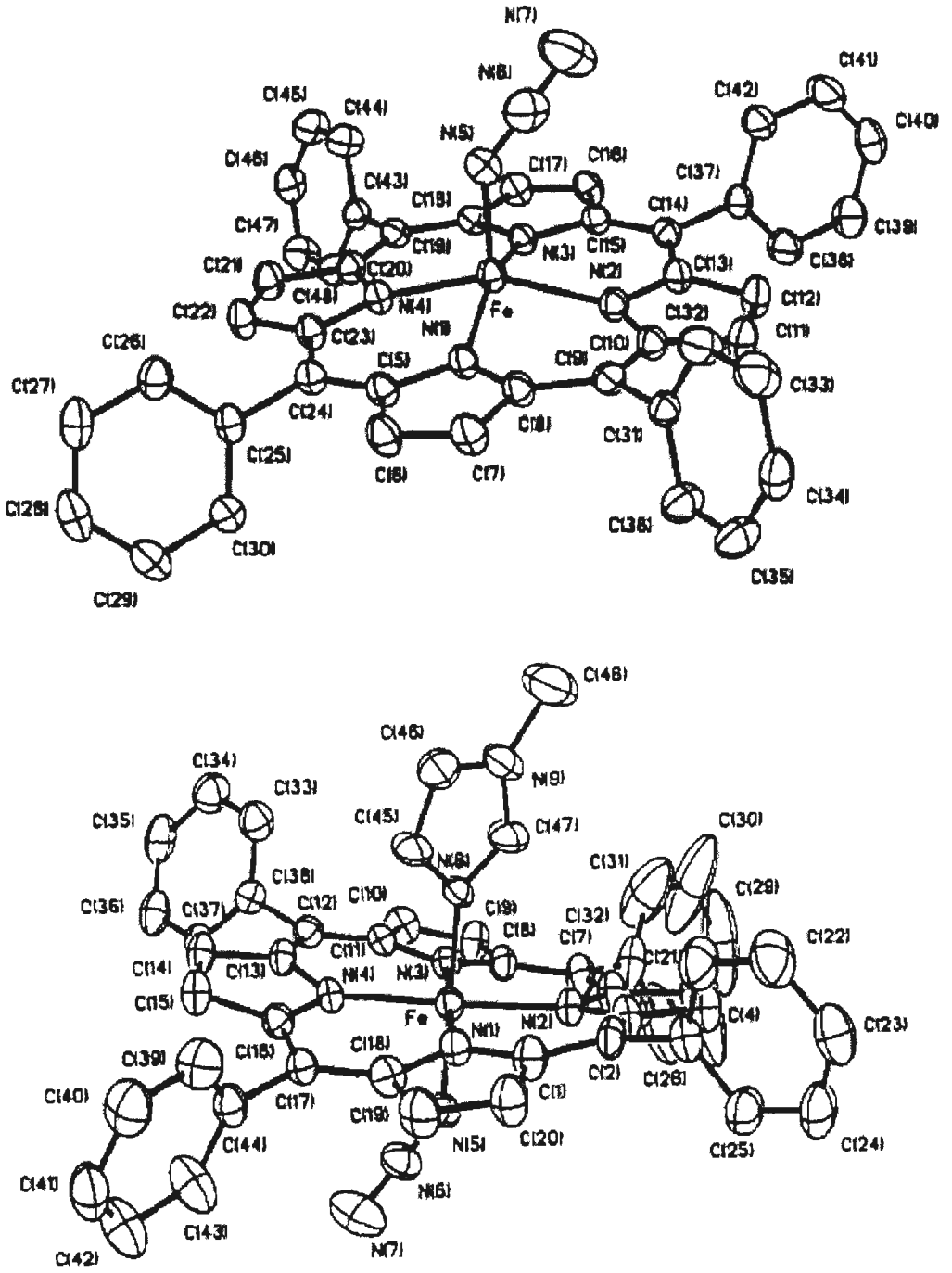

Fig. 2-9 Crystal structures of $Fe(TPP)N_3$ and Fe-(TPP)(1-MeIm)N_3

Fukui et al. [37] reported that the reaction of a binuclear iron (III) complex $(Et_4N)_2(Fe_2OCl_6)$ with $KHB(Pz)_3$ or $KHB(Pz^{Me2})_3$ gave the mononuclear iron complex $[LFeCl_3]^-$. They also described syntheses and crystal structures of $[Et_4N][HB(Pz)_3FeCl_3]$ (Fig. 2-10) and $[Et_4N][HB(Pz^{Me2})_3Fe(N_3)_3]$ complex (Fig. 2-11).

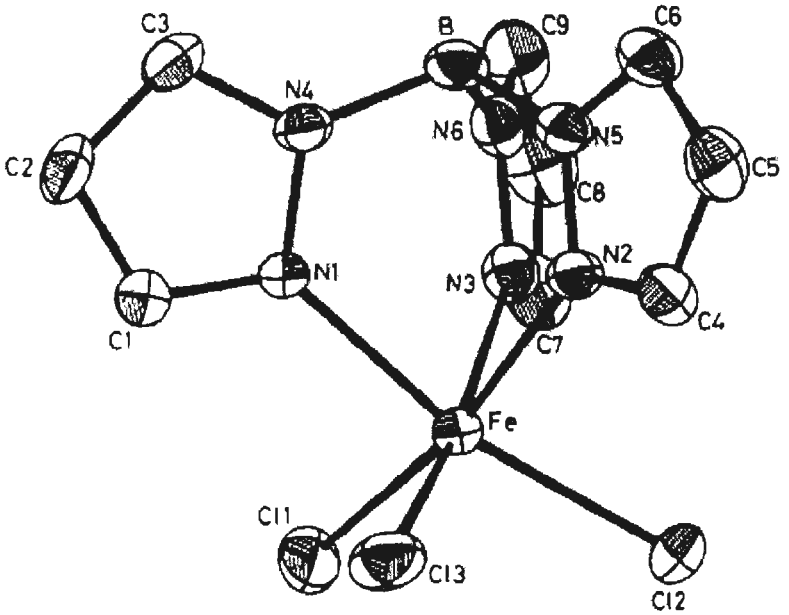

Fig. 2-10 Crystal structure of $[Et_4N]$ $[HB(Pz)_3FeCl_3]$

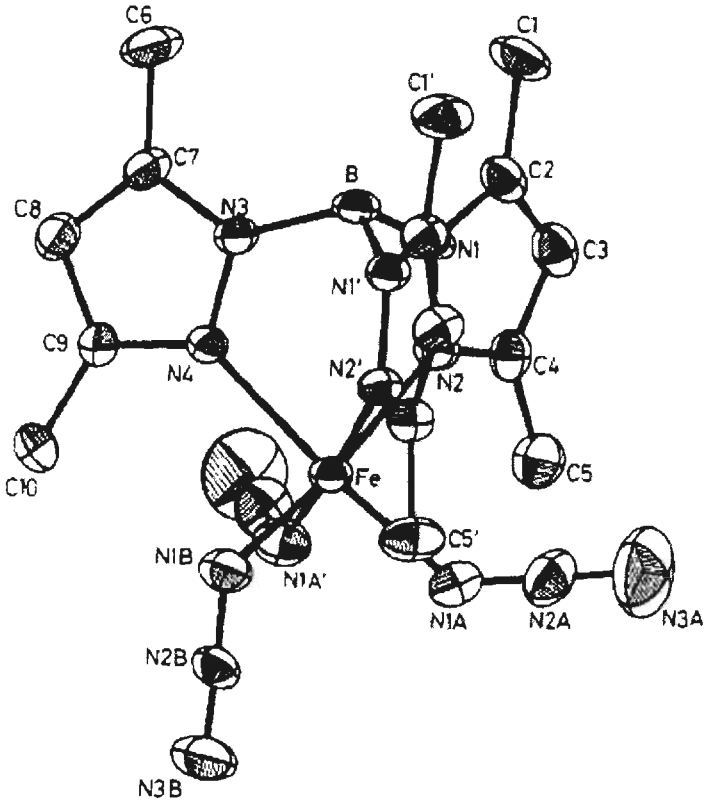

Fig. 2-11 Crystal structure of $[Et_4N][HB(Pz^{Me2})_3Fe(N_3)_3]$

Sellmann et al. [38] prepared some model compounds exhibiting structural and functional characteristics of the active sites of nitrogenases. The phosphine complexes [Fe(L)('N_HS_4')] (L = PMe_3, PMe_2, Ph, PBu_3, $PMePh_2$), the azido complexes (NEt_4)[Fe(N_3)('N_HS_4')] and [Fe('N_HS_4')].THF were investigated as potential precursors for the synthesis of the hypothetical N_2 complex [{Fe('N_HS_4')}$_\chi$(N_2)] (χ = 1 or 2). All these complexes were characterized by X-ray structure analyses. The phosphine complexes [Fe(PR_3)('N_HS_4')] have low-spin Fe(II) centers and chiral [Fe('N_HS_4')] cores. $PMePh_2$ was the bulkiest phosphine (cone angle 136°) which could be coordinated to the [Fe('N_HS_4')] fragment. The phosphine ligands were labile and rapidly substituted by CO but not by N_2. (NEt_4)[Fe(N_3)('N_HS_4')] (Fig. 2-12) was an Fe(II) high-spin complex exhibiting an achiral [Fe('N_HS_4')] core and long iron-donor distances analogous to other high-spin [Fe(L)('N_HS_4')] complexes. The azido ligand was labile and could neither oxidatively nor thermally be transformed into an N_2 ligand.

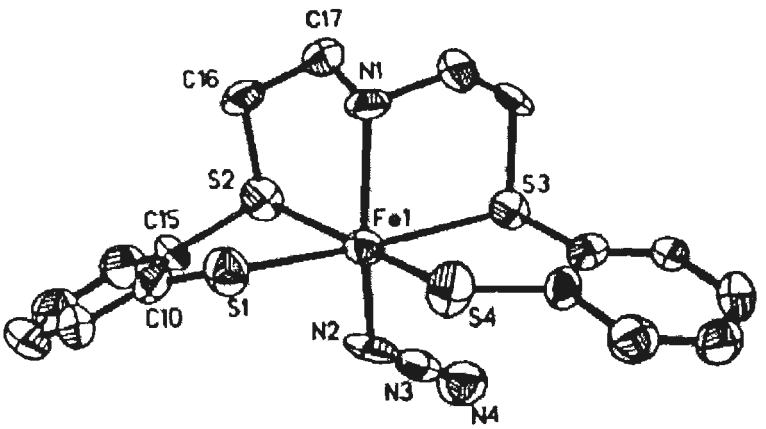

Fig. 2-12 Crystal structure of (NEt_4)[Fe(N_3)('N_HS_4')]

Field et al. [39] carried out a reaction of sodium azide with $FeH_2(dmpe)_2$ [dmpe = 1,2-bis(dimethylphosphino) ethane] in methanol solution to form $FeH(N_3)(dmpe)_2$ and finally a bis-azido complex, $Fe(N_3)_2(dmpe)_2$. The azide ligand was easily replaced

by terminal alkynes to form bisacetylide iron complexes. The X-ray crystal structure of $Fe(N_3)_2(dmpe)_2$ (Fig. 2-13) showed that the azide groups were mutually trans and that the N-N-N groups are essentially linear and tilted by approximately 132° with respect to the plane containing the Fe and four P atoms.

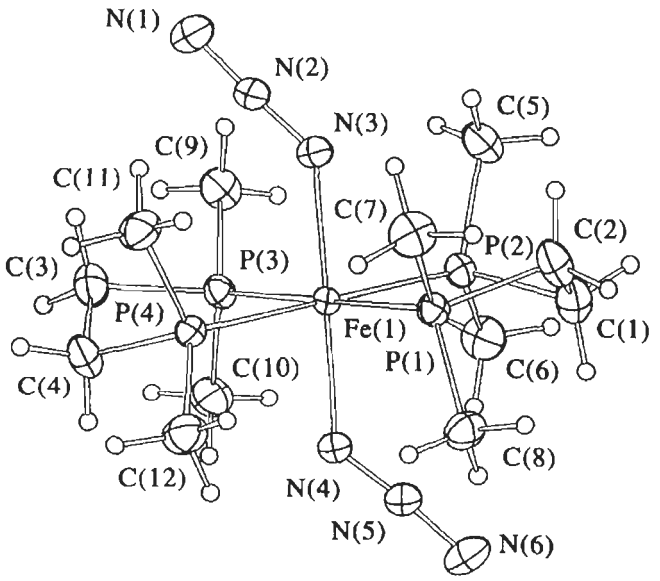

Fig. 2-13 Crystal structure of trans-$Fe(N_3)_2(dmpe)_2$

Ellison et al. [40] synthesized the complex anion bis(azido)(tetraphenyl-porphinato) ferrate (III) (Fig. 2-14) and characterized by variable temperature X-ray structure determinations, powder and single-crystal EPR, IR, Mössbauer spectroscopy, and magnetic susceptibility measurements. The synthesis utilized 18-crown-6 to solubilize sodium azide. All physical data for $[Na(18C6)(H_2O)_2]$-$[Fe(TPP)(N_3)_2]\cdot 2C_6H_5Cl$ were consistent with a thermal spin-equilibrium system: low spin ($S = {}^1/_2$) $\leftrightarrow$ high spin ($S = {}^5/_2$). Structural determinations at 130 and 293 K showed equatorial and axial Fe-N bond elongation at 293 K. $Fe\text{-}N_p$ = 1.9991(11) Å, $Fe\text{-}N_{az}$ = 1.9734(14) Å at 130 K, and $Fe\text{-}N_p$ = 2.010(4) Å, $Fe\text{-}N_{az}$ = 1.998(2) Å at 293 K. The asymmetric azide IR absorption bands at 2014 and 2036 cm^{-1} were assigned to

low- and high-spin species, respectively, and displayed temperature-dependent intensities.

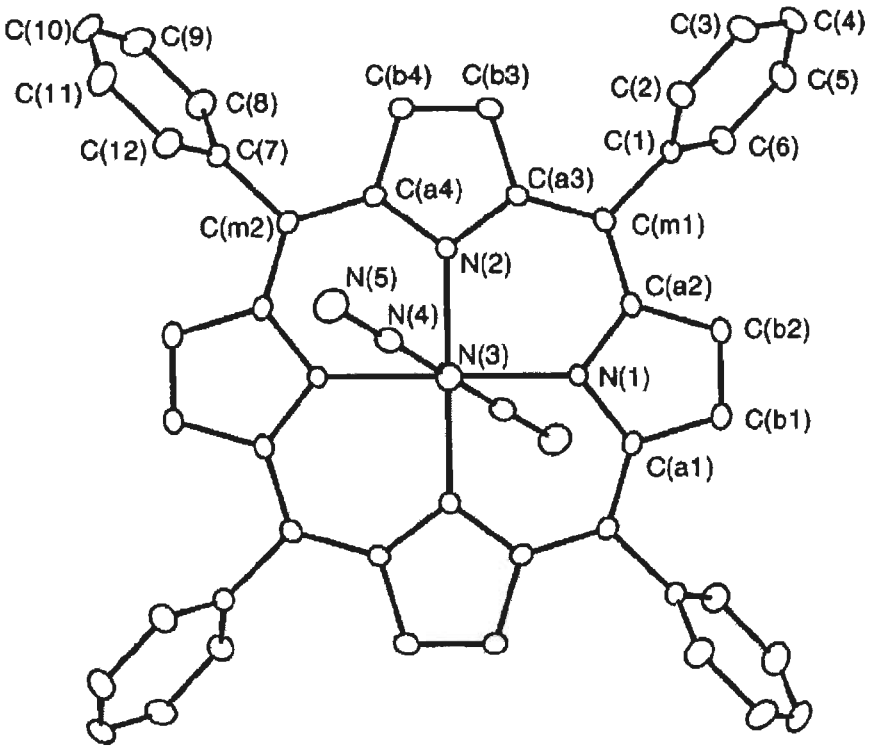

Fig. 2-14 Crystal structure of $[Fe(TPP)(N_3)_2]^-$

Zeller et al [41] reported the reactivity of calix[4]arene dialkyl- or -silylethers H_2R_2calix, R = Me, Bz, $SiMe_3$ (*p*-tert-butyl-calix[4]arene = H_4calix), towards the iron (III) complex $[FeCl(NSiMe_3)_2(thf)]$. The reactions of $[FeCl(NSiMe_3)_2(thf)]$ with H_2Me_2calix and H_2Bz_2calix afforded mononuclear iron (III) chloro compounds $[FeCl(R_2calix)]$ (R=Me) and (R=Bz). The calix[4]arene ether stabilized iron (III) chloro complexes are susceptible to nucleophilic substitution reactions, as exemplified by the reaction of $[FeCl(Me_2calix)]$ with sodium azide yielding an azido complex $[Fe(N_3)(Me_2calix)]$. The crystal structures have also been determined by X-ray diffraction (Fig. 2-15).

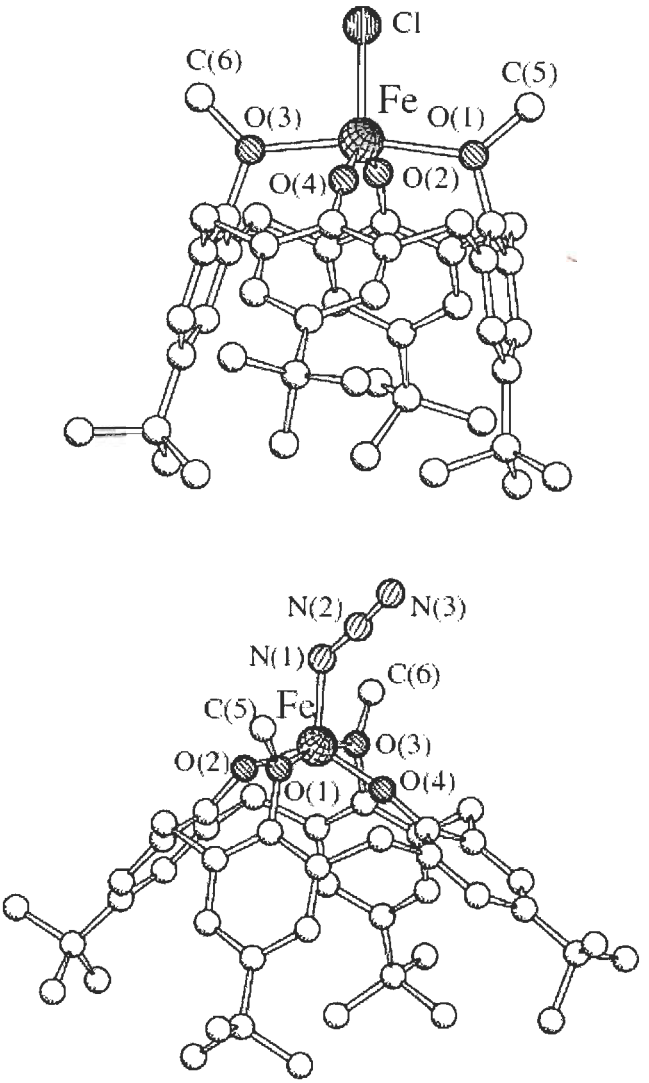

Fig. 2-15 Crystal structures of [FeCl(Me_2calix)] and [Fe(N_3)(Me_2calix)]

A problem encountered in the chemistry of heme complexes in their higher oxidation states is that the porphyrin ligand itself can also be oxidized forming a π radical. To avoid complications from redox- and spectroscopically active ligands, Wieghardt and some co-workers introduced saturated cyclam (1,4,8,11-tetraazacyclotetradecane) tetradentate chelates into iron nitrido chemistry.

Meyer et al. [42] reported the reaction of cis-[Fe^{III}(cyclam)Cl_2]Cl in acidic H_2O / CH_3OH or CH_3CN / H_2O mixtures with NaN_3 at 50 °C to get complex *trans*-

$[Fe^{III}(cyclam)(N_3)_2]ClO_4$ or the trans-$[Fe^{III}(cyclam)(N_3)_2]PF_6$ upon addition of $NaClO_4$ or $NaPF_6$, whereas at -18 °C the same reaction produced cis-$[Fe^{III}(cyclam)(N_3)_2](ClO_4)$ (cyclam = 1,4,8,11-tetraazacyclotetradecane). These complexes were characterized by variable-temperature magnetic susceptibility measurements, Mössbauer, X-band EPR spectroscopy and crystal structures of trans-$[Fe^{III}(cyclam)(N_3)_2]PF_6$ and cis-$[Fe^{III}(cyclam)(N_3)_2](ClO_4)$ were determined by single crystal X-ray crystallography (Fig. 2-16). Photolysis of low-spin trans-$[(cyclam)Fe(N_3)_2]^+$ in a frozen CH_3CN matrix at 4.2 K yielded 29 % of an iron(II) species generated by photoreduction and 54 % of the desired iron nitrido trans-$[(cyclam)Fe(N)(N_3)]^+$, as determined by Mössbauer and EPR spectroscopy (Scheme 2-4). Conditions for generating the terminal iron (V) nitrido are exquisitely sensitive. Performing the photolysis at higher temperatures yields a localized -nitrido diiron compound, $[(cyclam)(N_3)Fe^{IV}\text{-}N\text{-}Fe^{III}(N_3)(cyclam)]^{2+}$, a result of the combination of photooxidation and photoreduction products. Remarkably, isomeric, high-spin cis-$[(cyclam)Fe(N_3)_2]^+$ does not undergo photooxidation to yield the terminal iron nitrido. Irradiation again yielded a nitrido diiron complex arising from combination of both photooxidation and photoreduction products.

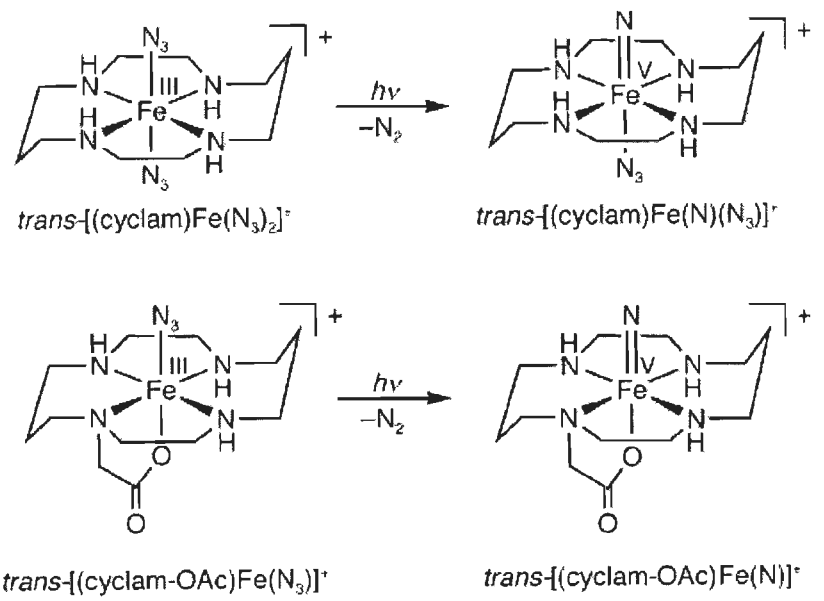

Scheme 2-4 Synthesis of iron (V) nitrido by photolysis of ferric azides

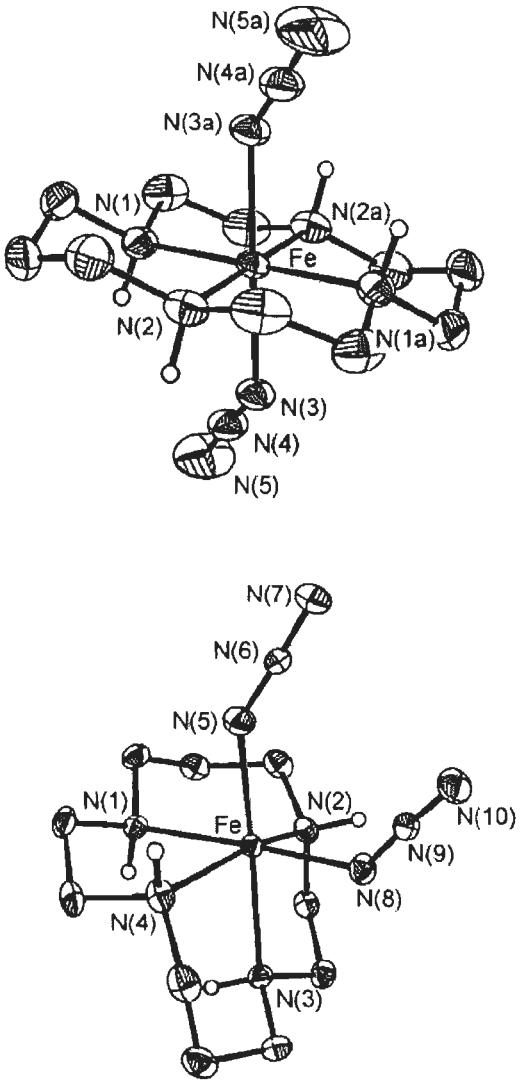

Fig. 2-16 Crystal structure of trans-$[Fe^{III}(cyclam)(N_3)_2]PF_6$ and cis $[Fe^{III}(cyclam)(N_3)_2](ClO_4)$

Koner et al. [43] synthesized a Fe(III)–azido complex with the formula $[Fe(cyclam)(N_3)_2]ClO_4$ (cyclam=1,4,8,11-tetraazacyclotetradecane) from the reaction of *cis*-$[Fe(cyclam)Cl_2]Cl$ with sodium azide in methanol. They also succeeded to get X-ray structure of $[Fe(cyclam)(N_3)_2]ClO_4$ (Fig. 2-17) that revealed that the Fe(III) atom possesses a tetragonally compressed octahedral geometry with a trans configuration of two azido ions. Variable-temperature (4.5–295 K) magnetic susceptibility measurements showed that the complex was low spin over the whole temperature

range. ^{57}Fe Mössbauer spectral measurements also suggested the same spin state of the Fe(III) ion.

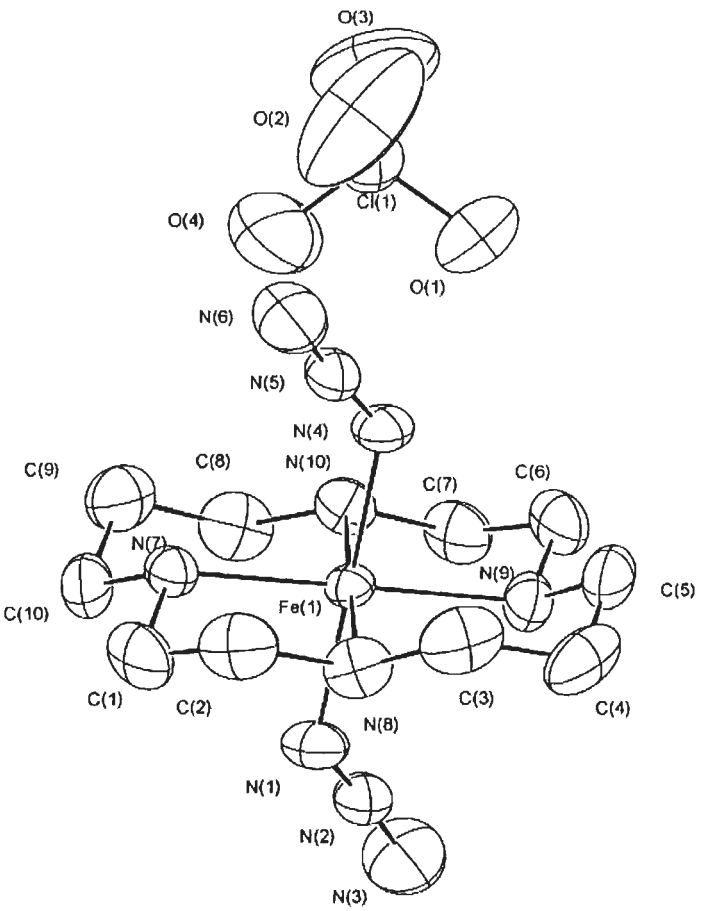

Fig. 2-17 Crystal structure of trans-[Fe^{III}(cyclam)$(N_3)_2$](ClO_4)

Justel et al. [44] reported the photolysis of [LFe^{III}(nadiol)(N_3)] in dry MeCN at 20 °C to produce red-brown crystals of the dinuclear symmetrical coordinated complex [{L(nadiol)Fe}$_2$(μ-N)] in 40 % yield (L = 1,4,7-trimethyl-1,4,7-triazacyclononane and nadiol^{2-} = naphthalene-2,3-diolate). One-electron oxidation of [{L(nadiol)Fe}$_2$(μ-N)] in dry CH_2Cl_2 with one equivalent of ferrocenium hexafluorophosphate generated blue crystals of [{L(nadiol)-Fe^{IV}}$_2$(μ-N)]PF_6. Photolysis of an equimolar MeCN solution of [L(Ph_2acac)$Fe^{III}$$(N_3)$]$ClO_4$ (Ph_2acac- is the monoanion 1,3-diphenylpropane-1,3-dionate) and [L(Cl_4-cat^{2-})$Fe^{III}$$(N_3)$] ($Cl_4$-$cat^{2-}$ = tetrachlorocatecholate dianion)

produced the asymmetrical coordinated species [L(Ph_2acac)-Fe^{III}-N-Fe^{IV}(Cl_4-cat)L]ClO_4 in 50 % yield. The (μ-oxo)diferric complexes [{L(acac)Fe^{III}}$_2$(μ-O)] $(ClO_4)_2$ (acac- = pentane-2,4-dionate) and [{L(nadiol)Fe^{III}}$_2$(μ-O)] were also prepared for comparison with other complexes. They also suggested from X-ray crystallography that complexes [{L(nadiol)Fe}$_2$(μ-N)] and [L(Ph_2acac)-Fe^{III}-N-Fe^{IV}(Cl_4-cat)L]ClO_4 contained mixed-valent [Fe^{IV}-(μ-N)Fe^{III}]$^{4+}$ cores, whereas [{L(nadiol)-Fe^{IV}}$_2$(μ-N)]PF_6 contained the linear, symmetrical [Fe^{IV}(μ-N)Fe^{IV}]$^{5+}$ core with an Fe^{IV}-N bond length of 1.694(1) Å. The electronic structure of these complexes was characterized by Mössbauer, EPR, resonance Raman (RR) and UV / vis spectroscopy, electrochemical and magnetic susceptibility measurements, and also by MO calculations. These studies revealed that [{L(acac)Fe^{III}}$_2$(μ-O)]$(ClO_4)_2$ and [{L(nadiol)Fe^{III}}$_2$(μ-O)] contain two equivalent high-spin Fe^{III} ions which exhibit the usual antiferromagnetic coupling of the [Fe^{III}(μ-O)Fe^{III}]$^{4+}$ core (J = -90 and -95 cm^{-1}) to a diamagnetic ground state. Similarly, [{L(nadiol)-Fe^{IV}}$_2$(μ-N)]PF_6 was diamagnetic even at room temperature and contain two equivalent Fe^{IV} ions, which were strongly antiferromagnetically coupled to yield an S = 0 ground state. However, complexes [{L(nadiol)Fe}$_2$(μ-N)] and [L(Ph_2acac)-Fe^{III}-N-Fe^{IV}(Cl_4-cat)L]ClO_4 displayed an S = 3/2 ground state and two nonequivalent, strongly antiferromagnetically coupled Fe sites with partially delocalized valencies.

Since these initial studies, second-generation versions of the cyclam ligand were introduced where an acetate group was appended to one of the nitrogen donors Grapperhaus et al. [45] carried out a reaction of the monoanionic, pentacoordinate ligand lithium 1,4,8,11-tetraazacyclotetradecane-1-acetate, Li(cyclamacetate), with $FeCl_3$, which yielded, [(cyclam-acetato)FeCl]PF_6 as a red microcrystalline solid upon addition of KPF_6. Addition of excess NaN_3 prior to addition of KPF_6 yielded the azide

derivative [(cyclam-acetato)FeN_3]PF_6 as orange microcrystals. The X-ray crystal structure of the azide derivative was determined as the tetraphenylborate salt i.e., [(cyclam-acetato)FeN_3]BPh_4 (Fig. 2-18). Photolysis of [(cyclam-acetato)FeN_3]PF_6 at 419 nm in frozen acetonitrile yielded a nearly colorless species in approximately 80 % conversion with an isomer shift δ = -0.04 mm s^{-1} and a quadrupole splitting ΔE_Q = -1.67 mm s^{-1} and spin-Hamiltonian analysis of the magnetic Mössbauer spectra was consistent with an Fe^V ion (d^3, S = 3/2). The proposed [(cyclam-acetato)Fe^V=N]$^+$ results from the photooxidation of [(cyclam-acetato)FeN_3]PF_6 via heterolytic N-N cleavage of coordinated azide (Scheme 2-4). Also photolysis of [(cyclam-acetato)FeN_3]PF_6 in acetonitrile solution at -35 °C (300 nm) or 20 °C (Hg immersion lamp) resulted primarily in photoreduction via hemolytic Fe-N_{azide} cleavage yielding Fe^{II} ($d,^6$ S = 0) with an isomer shift δ = 0.56 mm s^{-1} and quadrupole splitting ΔE_Q = 0.54 mm s^{-1} and a minor product containing high-valent iron was suggested by Mössbauer spectroscopy and was proposed to originate from [{(cyclam-acetato)Fe}$_2$(μ-N)]$^{2+}$ with a mixed-valent {Fe^{IV}(μ-N)Fe^{III}}$^{4+}$ S = 1/2 core.

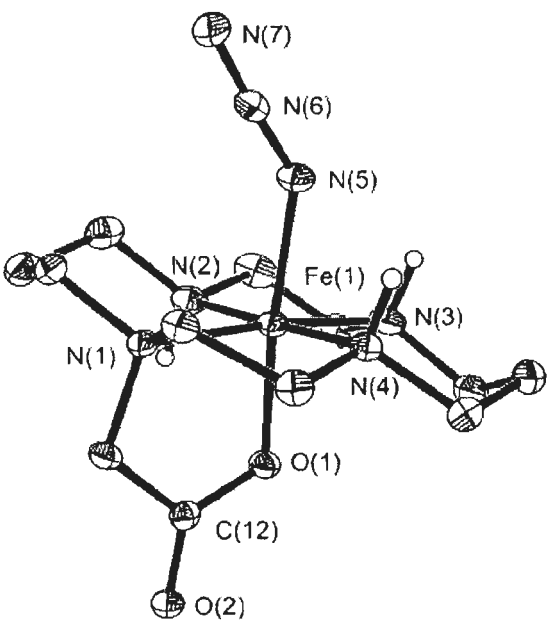

Fig. 2-18 Crystal structure of [[(cyclam-acetato)FeN_3]BPh_4

Aliaga-Alcalde et al. [46] carried out magnetic studies and Mössbauer spectroscopy in combination with DFT calculations to establish an S=1/2 ground state for and $[(\text{cyclam-acetato})\text{Fe(N)}]^+$ complex. Thus indicating a low-spin Fe^V d^3 ion S=1/2 and not S=3/2 as has been previously assumed. XAS and EXAFS data were also used to establish the FeN bond length to be approximately 1.60 Å. The results of this study indicated that the [Fe(V)-nitrido-cyclam-acetato]$^+$ complex is an unusual d^3 system with a nearly orbitally degenerate $S = {}^1/_2$ ground state. Although the calculations predicted fairly different Fe-N stretching frequencies for the $S = {}^1/_2$ and the competing $S = {}^3/_2$ ground states, a direct experimental determination of this important fingerprint quantity was missing. Petrenko et al. [47] applied synchrotron-based nuclear resonance vibrational scattering (NRVS) to characterize the Fe-N stretching frequency of an Fe(V)-nitrido complex and its Fe(III)-azide precursor. The NRVS data showed a new isolated band at 864 cm^{-1} in the Fe(V)-nitrido complex that is absent in the precursor. The NRVS spectra were fit and simulated using a DFT approach, and the new feature was unambiguously assigned to a Fe(V)-N stretch. The calculated Fe-N stretching frequency was too high by ~75 cm^{-1}.

Cyclam complexes were not the only examples of iron nitrides. Recently, Betley and Peters have reported the synthesis and characterization of a four-coordinate iron (IV) nitrido, $[\{PhB(P^{iPr})_3\}Fe^{IV}N]$ ($PhB(P^{iPr})_3$=$PhB(CH_2P^{iPr2})_3^-$) [48]. In this case, the supporting tridentate phosphine ligand was monoanionic by virtue of the apical borate, a feature known to have a profound impact on the electronic structure of the resulting metal complex. Notably, the synthesis of $[\{PhB(P^{iPr})_3\}Fe^{IV}N]$ was achieved under thermal rather than photochemical conditions by salt metathesis of $[\{PhB(P^{iPr})_3\}Fe^{II}Cl]$ with the N-atom transfer agent Li(dbabh) (dbabh=2,3:5,6-dibenzo-7-azabicyclo-[2.2.1]hepta-2,5-diene). The loss of anthracene from the intermediate iron

amide yielded the desired nitrido product (Scheme 2-5). DFT calculations on $[\{PhB(P^{iPr})_3\}Fe^{IV}N]$ established a $(xy)^2(x^2\text{-}y^2)^2(z^2)^0$ d-electron configuration with a large HOMO-LUMO gap (ca. 4 eV), consistent with the diamagnetic (S=0) ground state observed experimentally. In an argon atmosphere or when concentrated under vacuum, $[\{PhB(P^{iPr})_3\}Fe^{IV}N]$ was coupled to form the iron (I) dinitrogen complex $[\{\{PhB(P^{iPr})_3\}Fe^{I}\}_2(\mu_2\text{-}N_2)]$, which represented a unique example of a six-electron redox process mediated by two iron centers. It was also noteworthy that $[\{PhB(P^{iPr})_3\}Fe^{IV}N]$ could be treated with proton / electron equivalents to yield NH_3.

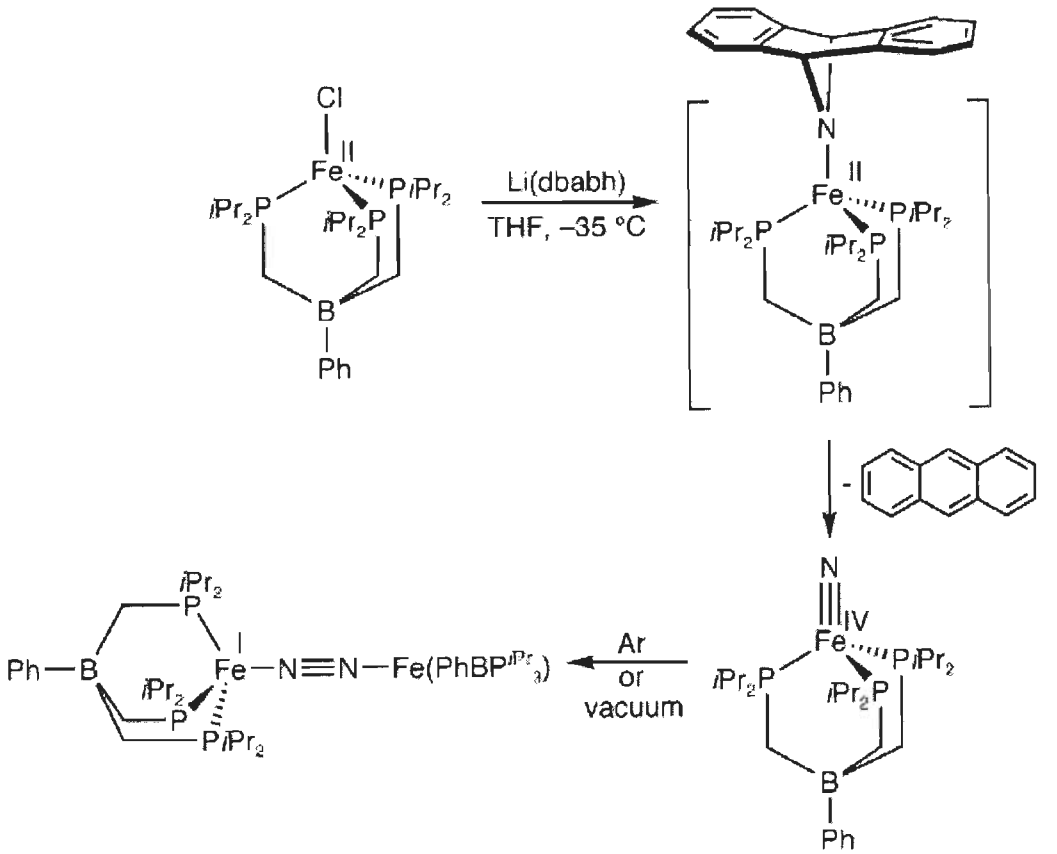

Scheme 2-5 Thermal synthesis of the iron (IV) nitrido complex, $[\{PhB(P^{iPr})_3\}Fe^{IV}N]$

Berry et al. [49] reported a subsequent variation of the acetato-substituted cyclam ligand. Replacing the amine hydrogen atoms with methyl groups yielded a high-spin, instead of a low-spin, ferric azido compound, $[(Me_3\text{-cyclam-OAc})Fe^{III}(N_3)]^+$

(Fig. 2-19). It was remarkable that N-alkylation of the cyclam-acetate ligand causes the resulting iron complex to be high spin at high temperatures because one may naively expect the electron-donating effects of the methyl groups to cause the N-methylated ligand to have stronger ligand field strength than cyclam acetate.

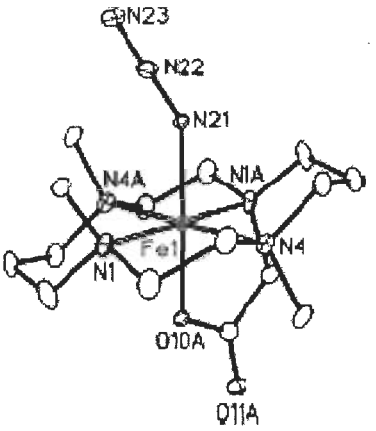

Fig. 2-19 Crystal structure of $[(Me_3\text{-cyclam-OAc})Fe^{III}(N_3)]^+$

Further, they [50] proved this fact by synthesis and characterization of their fluoro complexes i.e., $[(\text{cyclamacetate})FeF]PF_6$ and the corresponding N-methylated complex $[(\text{trimethylcyclamacetate})FeF]PF_6$. Magnetic susceptibility and spectroscopic data including electron paramagnetic resonance and Mössbauer spectra indicated that $[(\text{cyclamacetate})FeF]PF_6$ contained low-spin Fe^{III} (S = 1/2), while $[(\text{trimethylcyclam-acetate})FeF]PF_6$ was high spin (S = 5/2) (Fig. 2-20). The difference between their spin states was explained by combination of steric effects caused by the N-methyl groups, which compelled the Fe-N bond distances to be longer in $[(\text{trimethylcyclam-acetate})FeF]PF_6$ than they ordinarily would be, and also electronic effects, which caused the N-methylated ligand to be a weaker σ donor than its nonmethylated counterpart.

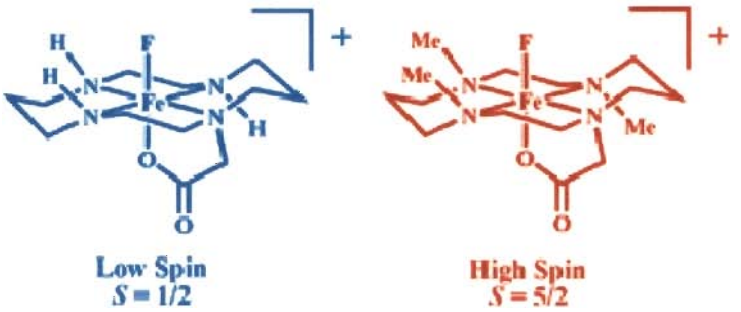

Fig. 2-20 Change in spin states by N-methylation in ligand

Berry et al. [51] also used this methyl substitution to produce a molecule that undergoes reversible one-electron oxidation to furnish a stable iron (IV) azido compound, $[(Me_3\text{-cyclam-OAc})Fe^{IV}(N_3)]^{2+}$ (Scheme 2-6).

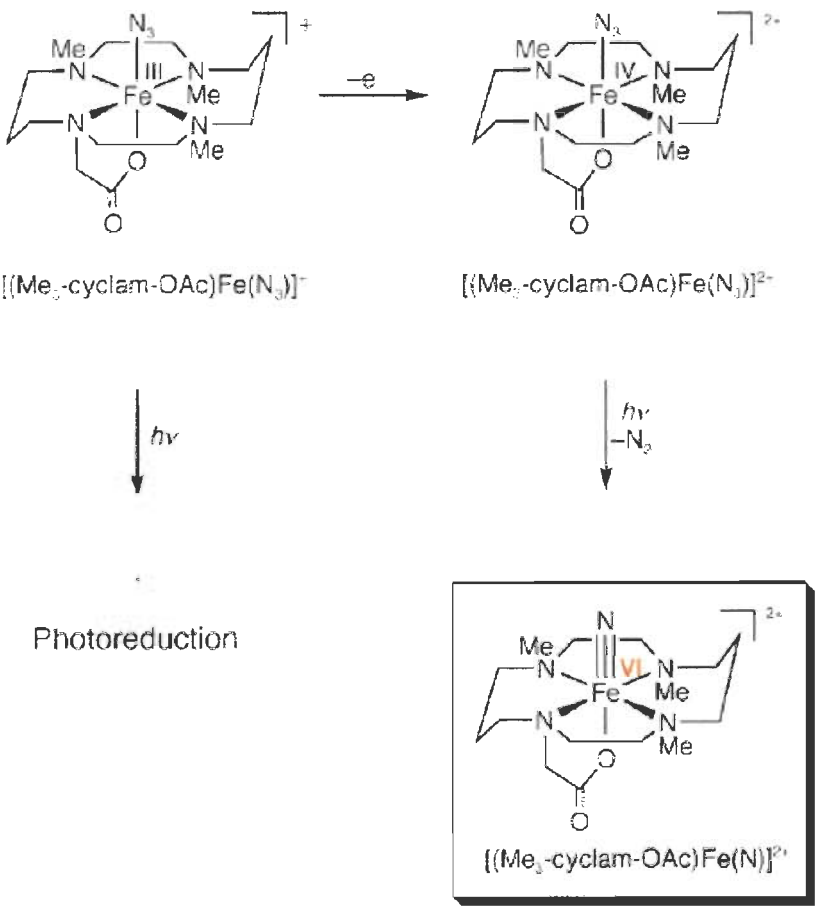

Scheme 2-6 Photolysis of an iron (IV) azide to yield an iron (VI) nitrido

The stability of the electrochemically generated iron (IV) azide allow photooxidation at 77 K with light of wavelength 650 nm to furnish a new major product with a zero-field Mössbauer isomer shift of δ = -0.29 mm s^{-1}. The low value of δ was as predicted for the +6 oxidation state, thus supporting assignment as the iron (VI) nitrido $[(Me_3\text{-cyclam-OAc})Fe^{VI}(N)]^{2+}$. Additional evidence for the formation of $[(Me_3\text{-cyclam-OAc})Fe^{VI}(N)]^{2+}$ was provided by XAS and EXAFS. In the X-ray absorption spectrum, an intense pre-edge peak was observed, which was consistent with a covalent iron-ligand multiple bond. Likewise, the EXAFS data yielded an FeN bond length of 1.57 Å, slightly contracted from the values measured for related iron (V) nitrides.

Song et al. [52] reported three new pentadentate, pendent arm macrocycles containing the 1,4,7-triazacyclononane-1,4-diacetate motif and their coordination chemistry with Fe(III). They prepared eight new octahedral Fe(III) complexes containing chloro, azido, or μ-oxo ligands, five of which have been characterized by X-ray crystallography (Fig. 2-21). Spectroscopic characterization of these octahedral Fe(III) complexes by UV / vis, IR, electrochemistry, EPR, magnetic susceptibility and zero-field Mössbauer measurements firmly established the high-spin state of the iron in all complexes. Electrochemistry studies of the azido-Fe(III) complexes show that they can be reversibly oxidized to the corresponding Fe(IV) species at -20 °C. Photolysis of one of the azido complexes was studied as a function of temperature (room temperature vs 77 K) and wavelength (480, 419, and 330 nm). Photoreduction to a high-spin Fe(II) species occurred under all conditions, which was proposed to be the dominant photochemical pathway generally available to high-spin ferric azido complexes.

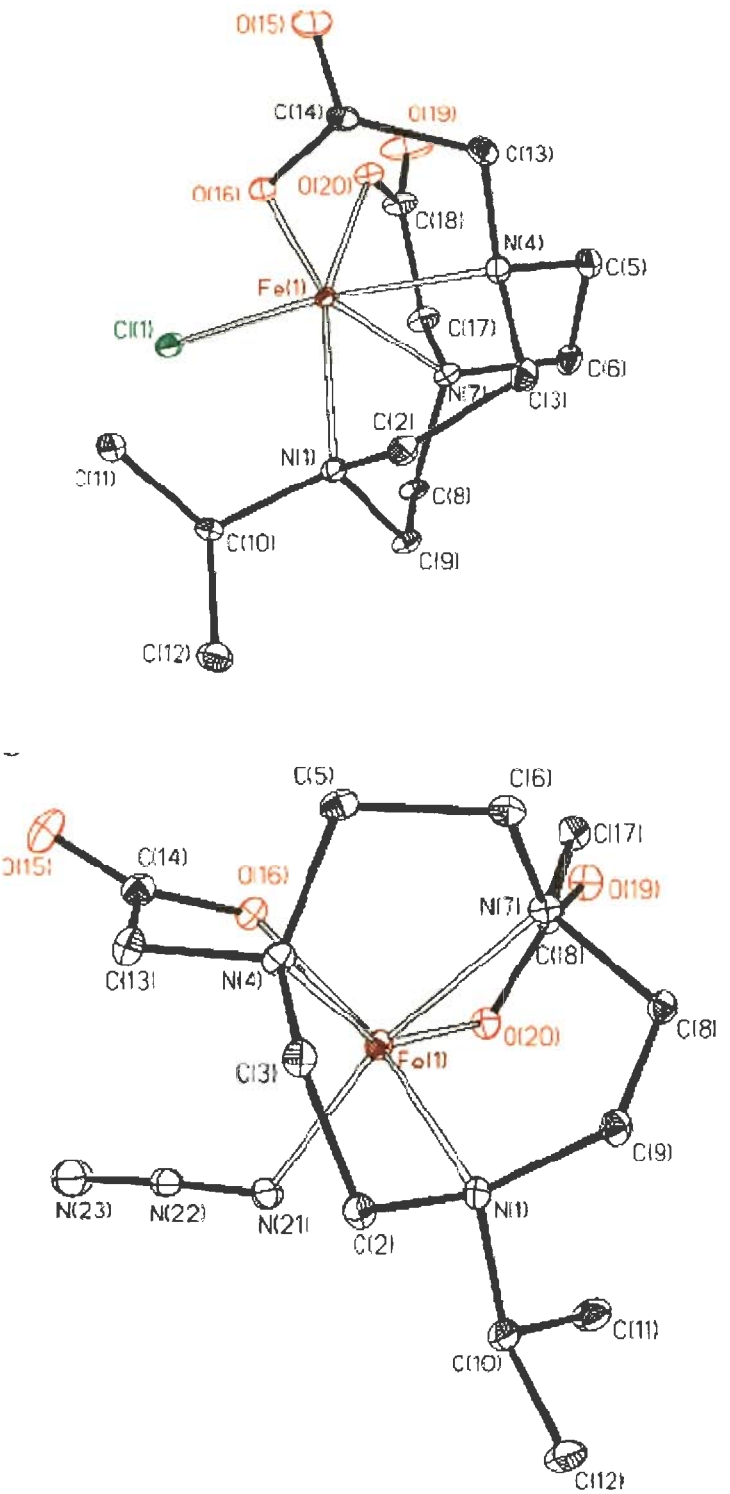

Fig. 2-21 Crystal structures of chloro and azido complexes of iron (III) 1,4,7-triazacyclononane-1,4-diacetate motif

Molecular assemblies consisting of cationic and anionic modules are of special interest for crystal engineering of molecular networks. The design of such assembly into ion-pair containing supramolecular systems where the cationic and anionic units interact through non-covalent hydrogen bonding and /or π-π interactions, ionic and van der Waals interactions is a challenging task in modern chemistry.

Chen et al. [53] reported a linear polymeric manganese (II) complex bridged by skew-skew bridging carboxylato groups. Crystal structure of catena-tris(betaine)manganese (II) tetrachloromanganate (II), $[Mn(Me_3NCH_2COO)_3]_n$. $nMnCl_4$ is given in Fig. 2-22.

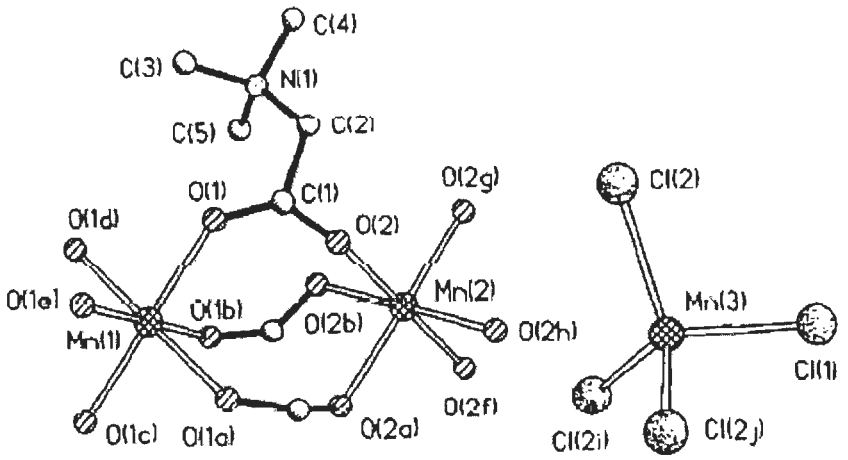

Fig. 2-22 Crystal structure of $[Mn(Me_3NCH_2COO)_3].MnCl_4$

Mudasir et al. [54] prepared two types of mixed-ligand complexes, i.e., $[M(phen)_2(dip)]^{2+}$ and $[M(phen)(dip)_2]^{2+}$ (M = iron(II) and nickel(II); phen = 1,10-phenanthroline and dip = 4,7-diphenyl-1,10-phenanthroline) from their related tris-complexes, $[M(phen)_3]^{2+}$ by ligand substitution and isolated by semi-preparative HPLC. In addition, they demonstrated that hypochromicity in the MLCT band and circular dichroism (CD) emerged in the UV / vis. region upon addition of CT(calf thymus)-DNA to the racemic complexes and indicated that the iron (II) mixed-ligand complexes interact with CT-DNA.

Yu et al. [55] synthesized the title compound $[Ni^{II}(phen)_3]_2[Cu_{10}H_2I_{16}]$ (phen = 1,10-phenanthroline, $C_{12}H_8N_2$) hydrothermally from a simple reaction of CuI–$NiCl_2 \cdot 6H_2O$–phen.H_2O–H_2O. X-ray analysis revealed that it consists of NiN_6^{2+} core cation and decanuclear iodocuprate (I) anion together with two dissociative H^+ ions (Fig. 2-23). In anionic unit, the discrete decanuclear iodocuprate (I) was formed by crystallographically independent five monovalent copper atoms and eight iodine atoms via an inversion center. The third-order non-linear optical property of $[Ni^{II}(phen)_3]_2[Cu_{10}H_2I_{16}]$ was also investigated and the compound exhibits the reverse saturable absorption and self-defocusing performance.

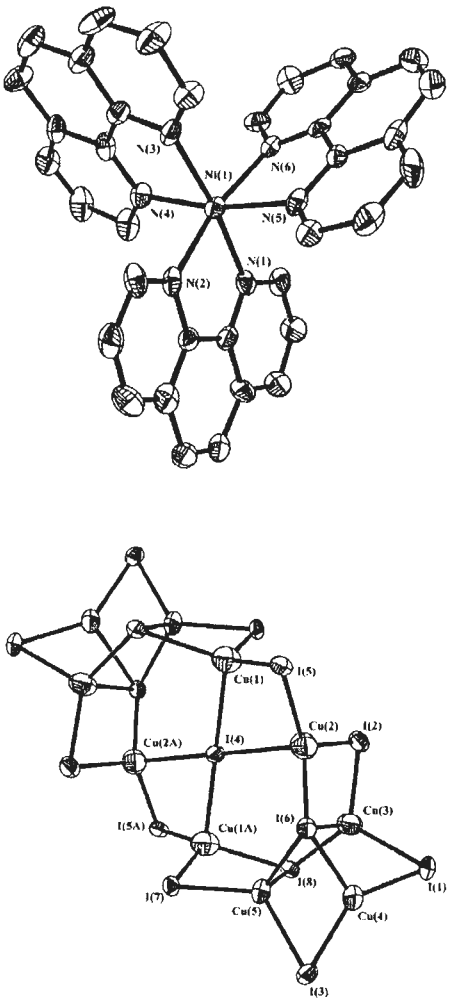

Fig. 2-23 Crystal structure of $[Ni^{II}(phen)_3]_2[Cu_{10}H_2I_{16}]$

Fritsky et al. [56] reported the formation of the molecular assemblies consisting of anionic and cationic molecules based on the tetradentate oxime and amide open-chain ligand CH_3–C(=NOH)–C(O)–NH–$(CH_2)_3$–NH–C(O)–C(=NOH)–CH_3 (PAP). All the structures contain the complex cations, complex anions $[M(PAP-3H)]^-$ and solvating water molecules, i.e., $[Ni(1,3\text{-n})_2(H_2O)_2][Ni(PAP-3H)]_2.4H_2O$ (Fig. 2-24), $[Ni(Im)_4(H_2O)_2][Ni(PAP-3H)]_2$ and $[Cu(Im)_4(H_2O)_2][Cu(PAP-3H)]_2.2H_2O$ (Im = imidazole; 1-3-pn = 1,3-diaminopropane). All of these compounds were synthesized by co-crystallisation of octahedral amine-containing cationic complex with oxime-containing anionic complexes in methanol solution.

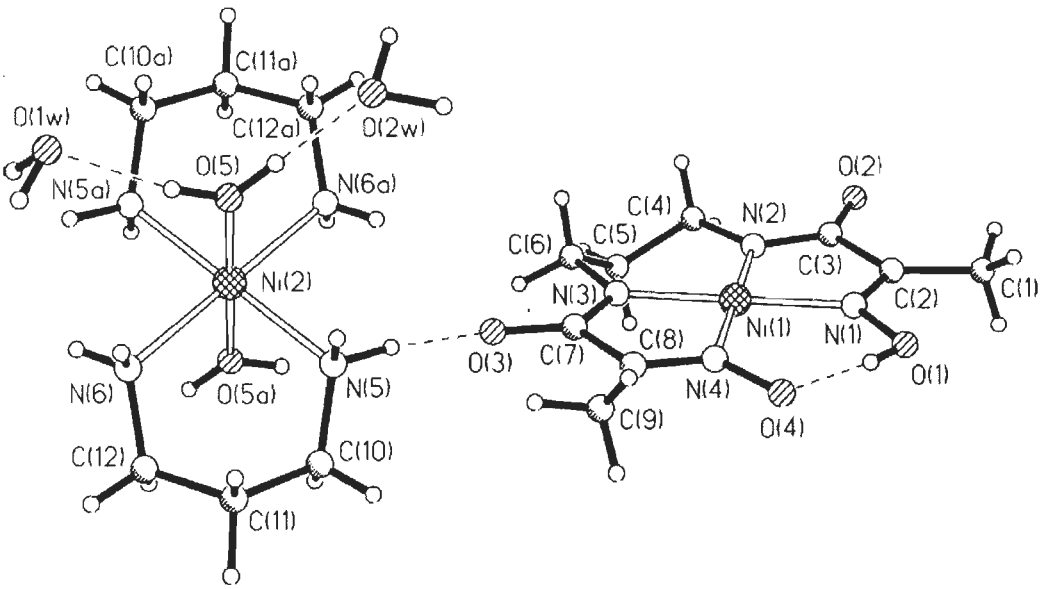

Fig. 2-24 Crystal structure of $[Ni(1,3\text{-pn})_2(H_2O)_2][Ni(PAP-3H)]_2.4H_2O$

Wang et al. [57] reported a novel mixed-valence complex $[Ni(phen)_3]_2[Ni(mnt)_2]_3 \cdot 2DMF$ (Fig. 2-25) by the combination of a cationic complex $[Ni(phen)_3]^{2+}$ and an anionic complex $[Ni(mnt)_2]^-$ (phen = 1,10′-phenathroline, mnt = 1,2-dicyanovinylene-1,2-dithiolato, DMF = *N,N*-dimethylformamide). Its crystal structure consists of two different types of $[Ni(mnt)_2]$ units, i.e., $[Ni(mnt)_2]^-$ and

$[Ni(mnt)_2]^{2-}$, the arrangement of the $[Ni(mnt)_2]$ anion was found to be quite different from segregated stack layers often found for $[Ni(mnt)_2]$-based compounds. Infrared and electronic spectra also confirmed the existence of both $[Ni(mnt)_2]^-$and $[Ni(mnt)_2]^{2-}$ units.

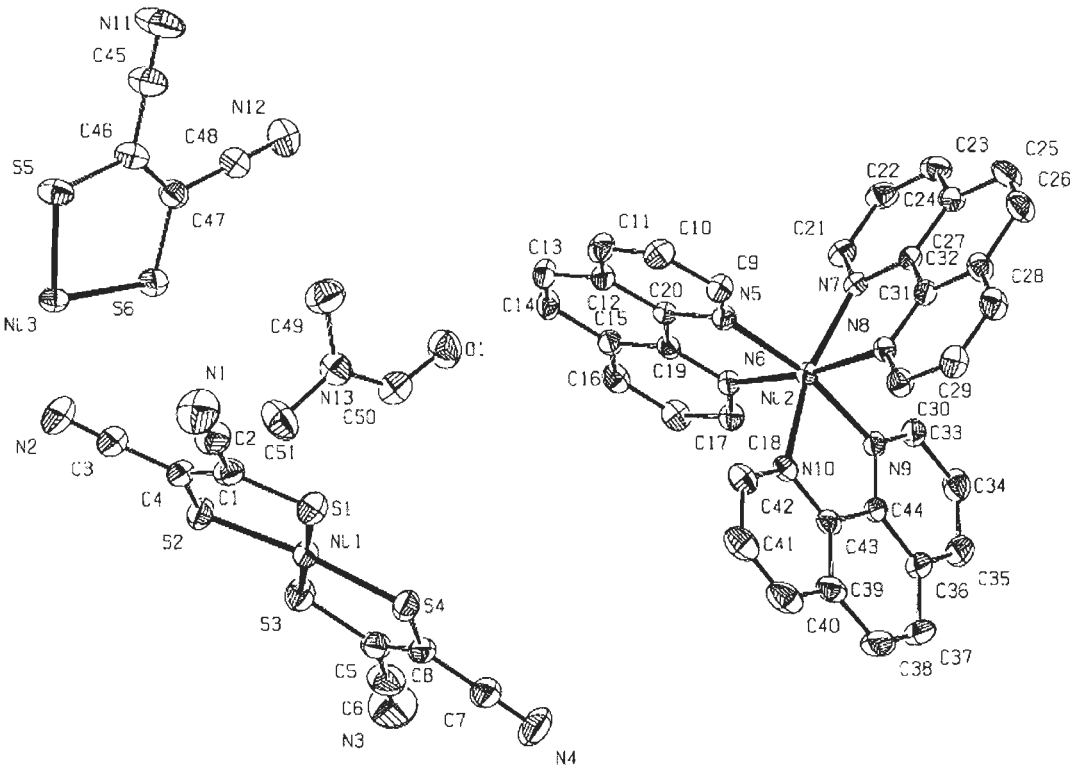

Fig. 2-25 Crystal structure of $[Ni(phen)_3]_2[Ni(mnt)_2]_3 \cdot 2DMF$

Dang et al. [58] synthesized a new ion–pair complex, 1-methyl-3-benzylbenzimidazolium bis(maleonitrile-dithiolato) nickelate (III) and characterized by elemental analysis, IR spectroscopy and X-ray crystallography (Fig. 2-26). In solid state, the $Ni(mnt)_2^-$ anions and $[MeBzBzim]^+$ cations were alternately stacked and formed a one-dimensional (1D) column through π–π interactions between the plane of $Ni(mnt)_2^-$ and the neighbored benzimidazole ring. The π–π interactions between adjacent cations and the weak interactions between adjacent anions further gave rise to

a three-dimensional supramolecular structure. The variable temperature magnetic susceptibilities investigation suggested that the π–π stacking interactions resulted in an antiferromagnetic exchange coupling between Ni(III) ions of the complex and the Neel temperature (TN) at 5.0 K was observed.

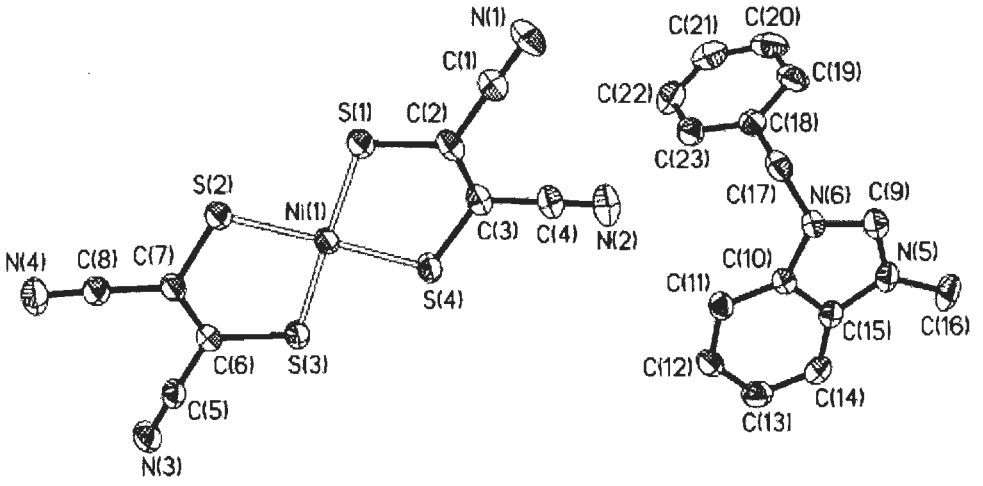

Fig. 2-26 Crystal structure of [MeBzBzim][Ni(mnt)$_2$]

Madhu and Das [59] reported the ion-pair complexes [Ni($C_9H_{22}N_6$)][Cu(mnt)$_2$], [Ni($C_9H_{22}N_6$)][Ni(mnt)$_2$], and [Ni($C_9H_{22}N_6$)][Pd(mnt)$_2$] (mnt^{2-} = 1,2-dicyanoethylenedithiolate, $C_9H_{22}N_6$ = 3,7-bis(2-aminoethyl)-1,3,5,7-tetraazabicyclo[3.3.1]nonane) and characterized by elemental analysis, IR, UV / vis, ^{1}H NMR spectroscopy, X-ray powder diffraction, electrochemical studies and unambiguously by single crystal X-ray crystallography (Fig. 2-27). The N–H···S-type hydrogen-bonding capabilities of the classical sulfur-containing complex anions $[M^{II}(mnt)_2]^{2-}$ (M = Cu, Ni and Pd) have been explored using amine groups containing the nickel complex cation $[Ni(C_9H_{22}N_6)]^{2+}$ in the ion-pair compounds. In the crystal, the cation interacted with two different anions through three N– H···S hydrogen bonds

and, likewise, the anion was hydrogen-bonded to two different cations through three hydrogen bonds, resulting in the formation of a chain-like arrangement.

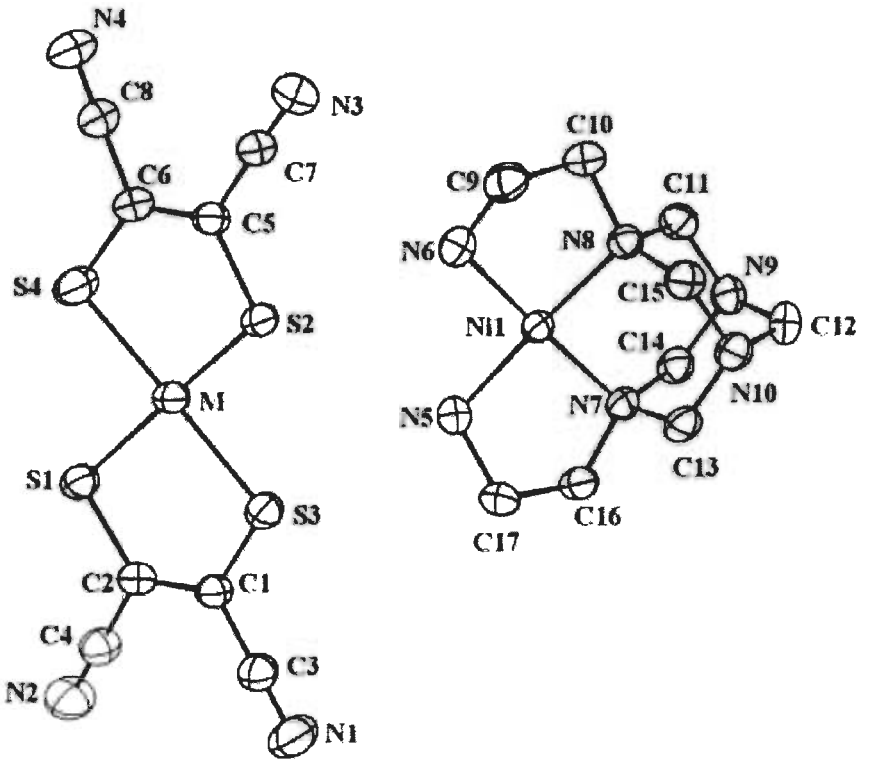

Fig. 2-27 Crystal structure of $[Ni(C_9H_{22}N_6)][M(mnt)_2]$; (M = Cu, Ni and Pd)

Pereira et al. [60] reported the salts of $[Fe^{III}(sal_2\text{-trien})]^+$ and $[Fe^{II}(phen)_3]^{2+}$ cations and $M[(dcbdt)_2]^-$ anions with M = Ni and Au (dcbdt = dicyanobenzenedithiolate) with formula $[Fe(sal_2\text{-trien})][M(dcbdt)_2]$ (Fig. 2-28) and $[Fe(phen)_3][M(dcbdt)_2]_2$ and characterized by single X-ray diffraction and magnetic measurements. None of these salts show a clear spin crossover behavior and their magnetic properties were due essentially to the cations in a high spin S = 5/2 and low spin states for the Fe^{III} and Fe^{II} salts respectively. The magnetic Ni sublattices in both compounds appear to have a negligible direct contribution to the magnetization but enhance the antiferromagnetic interactions in the cation sublattice.

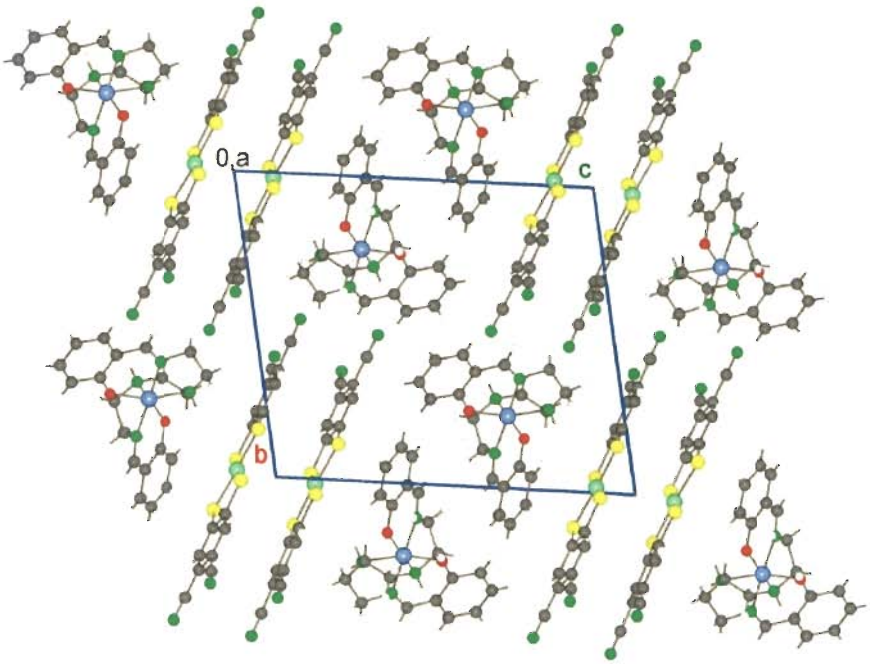

Fig. 2-28 Crystal structure of $[Fe(sal_2\text{-trien})][Ni(dcbdt)_2]$

Faulmann et al. [61] reported a new compound of formula $[Fe(qsal)_2][Ni(dmit)_2]$, structurally and magnetically characterised (qsalH = N-(8-quinolyl)salicylaldimine, $dmit^{2-}$ = 1,3-dithiol-2-thione-4,5-dithiolato). Mössbauer spectra clearly showed that the magnetic properties must be interpreted as an incomplete spin crossover of the iron (III) ions. They also compared its structural features and magnetic behaviour with those of $[Fe(qsal)_2]$ based complexes and more particularly $[Fe(qsal)_2][Ni(dmit)_2].2CH_3CN$ (Fig. 2-29).

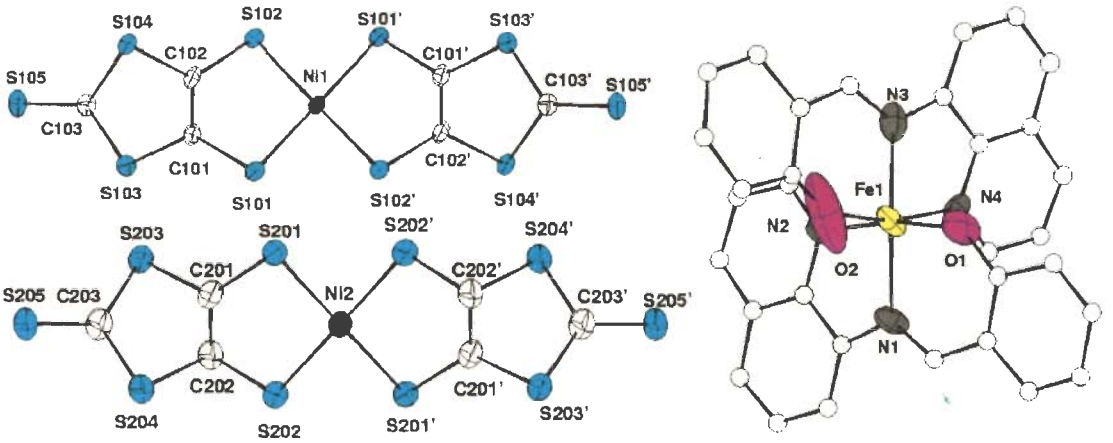

Fig. 2-29 Crystal structure of $[Fe(qsal)_2][Ni(dmit)_2]$

Shi et al. [62] reported the hydrothermal synthesis and structural characterization of a number of complex compounds containing the divalent tris(oxalato-O,O′)germanate anion, $[Ge(C_2O_4)_3]^{2-}$, or the neutral bis(oxalate-O,O′)germanium fragment, $[Ge(C_2O_4)_2]$, with transition-metal (M) cationic complexes of 1,10-phenanthroline (phen). $[M(phen)_3]$-$[Ge(C_2O_4)_3]$.xH2O (where M^{2+} = Cu^{2+} (Fig. 2-30) Fe^{2+}, Ni^{2+}, Co^{2+}), $[MGe\text{-}(phen)_2(\mu_2\text{-}OH)_2(C_2O_4)_2]$ (where M^{2+} = Cd^{2+} and Cu^{2+}). All compounds were characterized using EDS, SEM, vibrational spectroscopy (FT-IR and FT-Raman), thermogravimetry, and CHN elemental composition and their structure determined on the basis of single crystal X-ray diffraction studies. The crystal packing of the different chemical moieties for each series of compounds were discussed on the basis of the various intermolecular interactions present.

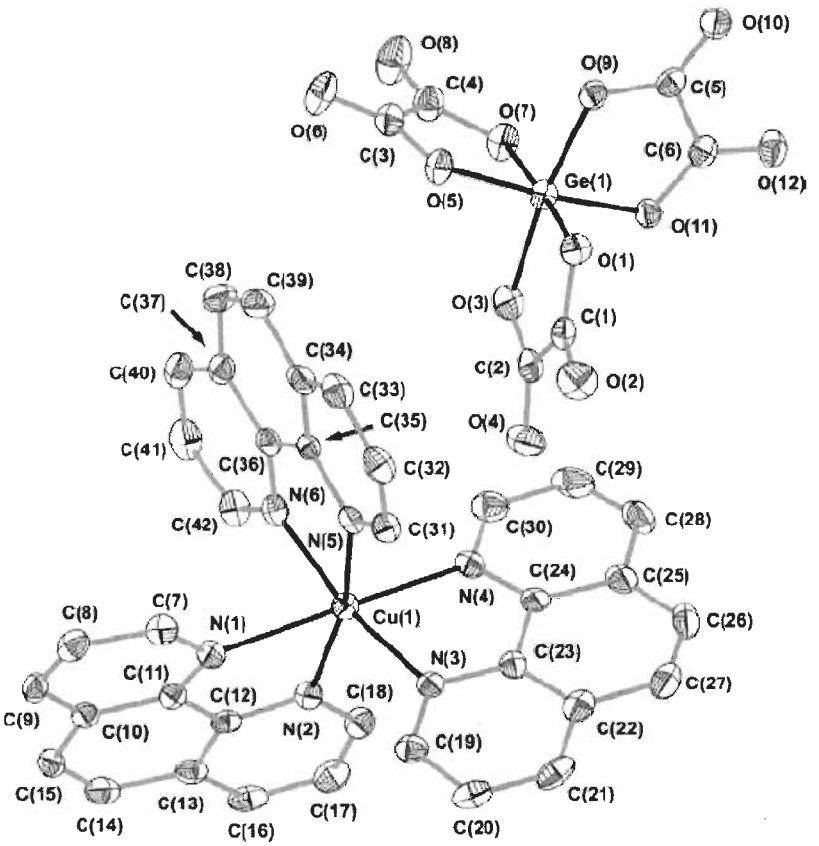

Fig. 2-30 Crystal structure of $[Cu(phen)_3][Ge(C_2O_4)_3]$

Sharma et al. [63] obtained single crystal of $[Co(phen)_3](IO_4)_3.2H_2O$ by dissolving the yellow coloured precipitated product (obtained by slowly mixing the separately dissolved tris(1,10-phenanthroline)-cobalt (III) chloride with sodium periodate in aqueous medium in 1:3 molar ratio) in hot water and allowed it to evaporate slowly at room temperature (Fig. 2-31). These complex salts were characterized by elemental analyses, spectroscopic studies (IR, UV / vis, ^{1}H and ^{13}C NMR), solubility product and conductance measurements. The six nitrogen atoms, originating from three 1,10-phenanthroline ligands (each bidentate) showed distorted octahedral geometry around the central Co(III) metal ion. Supramolecular hydrogen bonding networks between ionic groups [Co-phen$CH^{\delta+}$...$O^{\delta-}_{anion}$] by second sphere coordination besides electrostatic forces of attraction have been observed that stabilize crystal lattice. The structural studies suggest that $[Co(phen)_3]^{3+}$ was a potential anion receptor for the periodate ion, $(IO_4)^-$ in aqueous medium.

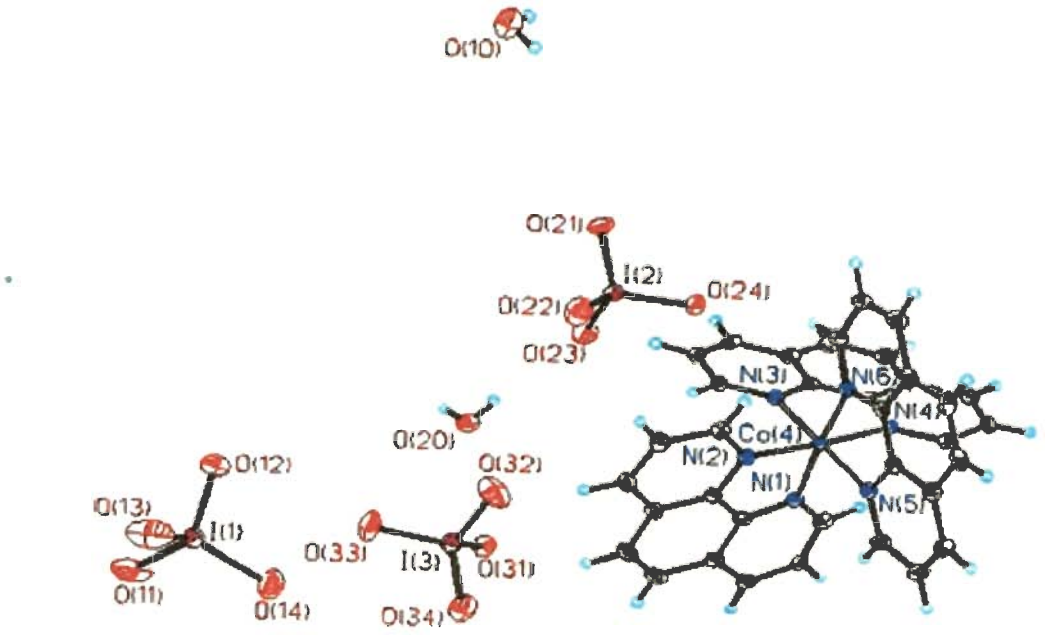

Fig. 2-31 Crystal structure of $[Co(phen)_3](IO_4)_3.2H_2O$

Results and Discussion

The potassium hydrotris(pyrazolyl)borate [KTp] **2a** and potassium hydrotris(3,5-dimethyl-1-pyrazolyl) borate [KTp^{Me2}] **2b** have been prepared by the modified method of Trofimenko et al. (Scheme 2-7) as described in chapter 5.

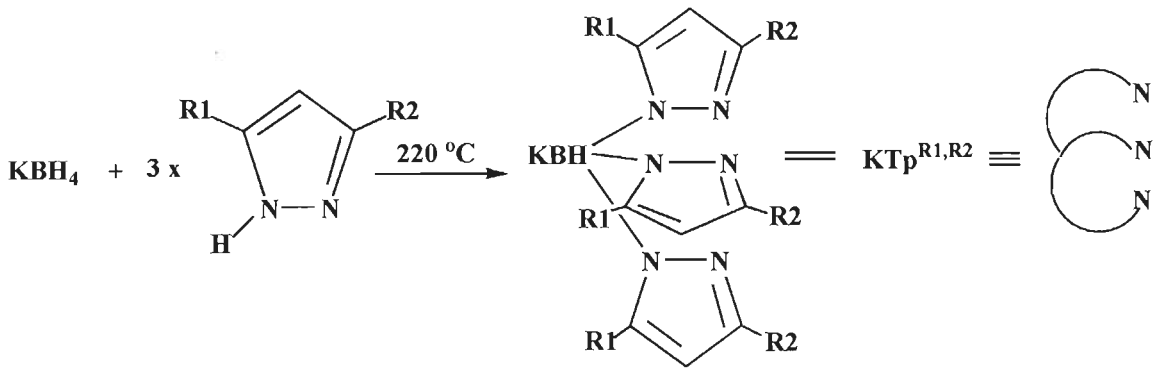

Scheme 2-7

The complexes **2c-2f** were prepared by the reaction of ferric chloride with KTp / KTp^{Me2} and potassium picolinate / sodium acetylacetonate in 1:1:1 ratio (Scheme 2-8).

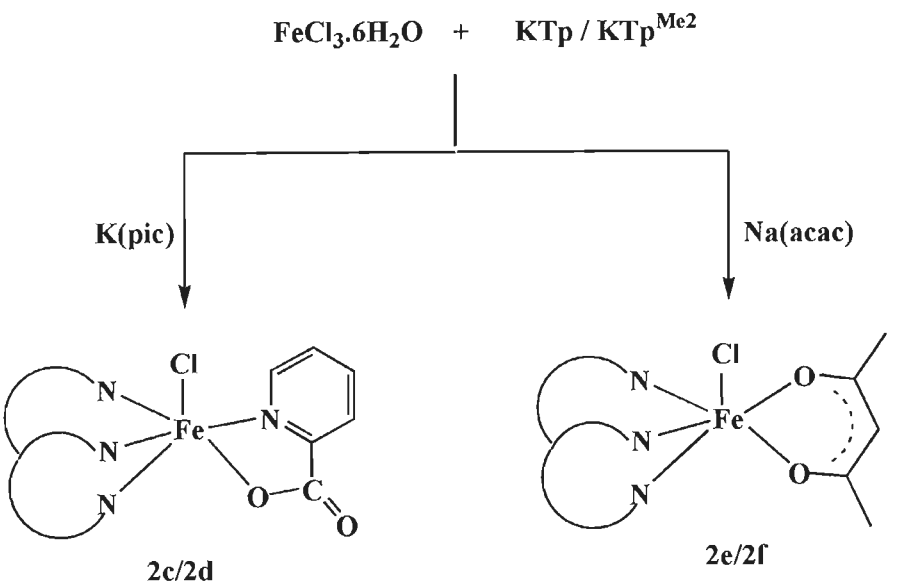

Scheme 2-8

Complexes **2c-2f** were showing B-H band in the range of 2496-2547 cm^{-1} suggesting binding of Tp / Tp^{Me2}. In the IR spectra of complexes **2c** and **2d**, the asymmetric mode ν_{as}(COO) of the free picolinate at 1726 cm^{-1} shows shifts to a lower wave-number on coordination (1642 and 1636 cm^{-1}) and the symmetric mode ν_s(COO) shows shifts to higher wave-number on coordination (1371 and 1378 cm^{-1}) as compared to the free picolinate (1342 cm^{-1}) showing that the ligand was bound to the iron through the carboxylate oxygen. Also, the vibrations related to the pyridine ring in the lower frequency region (752, 708, 518 cm^{-1}) were slightly shifted to higher wave-numbers (768, 721, 546 cm^{-1}) suggesting coordination through pyridine nitrogen [64]. The complex **2e** and **2f** also showed decrease in wave-number of the carbonyl stretching band of the acac ligand from 1710 to 1623 and 1618 cm^{-1} respectively, upon complexation with metal [65].

After preliminary characterization of complexes **2c-2f**, attempts were made to crystallize them. Unfortunately, we were able to crystallize only complex **2f** in acetonitrile at -20 °C. The crystal structure of complex **2f** has been shown in Fig. 2-32. The crystallographic data are summarized in Table 2-1 whereas the selected bond lengths and bond angles are given in Table 2-2. Compound **2f** crystallizes in the triclinic system with Z = 2. The complex is neutral and contains a terminal chloro ligand with octahedrally coordinated Fe(III). As shown in Fig. 2-32, the terminal chloro ligand is trans to one of the N atom of the pyrazole ring. The acac ligand is coordinated in bidentate fashion. The average Fe-N and Fe-O bond lengths are 2.134 and 1.985 Å, respectively. The chloro ligand is at a distance of 2.364(16) Å from Fe atom which is in the range of other reported trans-chloro complex [66]. Fig. 2-33 shows that two molecules were interacting with C-H...π interaction (2.813 Å) through C-H of pyrazole and π electrons of pyrazole ring of other molecule. Fig. 2-34 demonstrates the

intermolecular interaction between two independent molecules. Each molecule is intermolecularly connected through two type of weak interactions viz., C-H···O (2.533 Å) and C-H···Cl (2.864 Å). C-H···O interaction occurs between O atom of acac in one molecule with hydrogen atom of methyl group of 3,5-dimethylpyrazole in other molecule [67, 68] whereas the C-H···Cl interaction is due the interaction of Cl atom in one molecule with hydrogen atom of acac in other molecule. In order to know whether azide ion binds to the complex **2f**, potentiometric studies were carried out with ion-selective membrane method.

The effect of membrane composition and potential response towards azide ion

The sensitivity and performance of the ionophore $[Tp^{Me2}Fe(acac)Cl]$ **2f** significantly depends on the membrane composition and the nature of solvent mediator and the additive used. Thus, to optimize potentiometric performance of azide-selective electrode various PVC membranes based on **2f** were prepared and investigated. The influence of plasticizer type and concentration on the characteristics of azide ion-selective electrodes was investigated by using four plasticizers with different polarities including DBP, DOP, o-NPOE and BA (Table 2-3). It should be noted that the nature of plasticizer influences both the dielectric constant of the membrane and the mobility of the ionophore and its complex with N_3^- [69]. Among the four plasticizers, DOP gave the best performance with regard to working concentration range and slope for the N_3^- ion-selective electrode. It seems that DOP, as a low polarity compound provides more appropriate conditions for incorporation of highly lipophilic azide ion into the PVC membrane. Several membrane compositions were investigated by varying the proportions of PVC and DOP. Irrespective of ionophore concentration the slope was relatively larger when DOP / PVC weight ratio was approximately 2.0.

The effects of cationic additive concentrations in the membrane were investigated at several ionophore / additive weight ratios [70, 71]. Sensitivity of electrode response increases with increase in the **2f** content from 2 mg to 5 mg (sensor nos. 10 to 13). Further addition of ionophore (6 mg; sensor no. 14) will however, result in diminished response of the sensor. Better response characteristics, i.e., Nernstian response and improved selectivity were observed with an optimum ionophore / HTAB weight ratio of approximately 2.5. Based on results obtained on the optimization of the membrane composition (Table 2-3), the best response was observed with the membrane composed of **2f** / HTAB / DOP / PVC ratio of 5 / 2 / 190 / 100, (sensor no. 13) and this was selected for the preparation of polymeric membrane electrode for azide ion. It was found that for the best selected membrane (sensor no. 13) potential response was linear for N_3^- ions, over the concentration range of 6.3×10^{-7} to 1.0×10^{-2} M (Table 2-3) with a Nernstian slope of 59.4 mV decade^{-1} of N_3^- activity. The limit of detection was 3.8×10^{-7} M and reproducibility and stability of the electrode was evaluated by repeated calibration of the electrode in NaN_3 solutions. Repeated monitoring of potentials and calibration using the same electrode over several days gave good slope reproducibility; the standard deviation (S.D.) of slope was 0.2 mV decade^{-1} activity. A MES buffer solution pH 5.0 was used as the background electrolyte in the measurements.

Analytical Application

Because of the high selectivity and the very low detection limit of the constructed N_3^- sensor, it was applied for the monitoring of the azide ion concentration in various aqueous samples (black tea, green tea, orange juice and human urine).

Samples were directly injected after minimal sample preparation. The samples were diluted (1:10 with double distilled water) and filtered to remove particulates and treated by MES / NaOH buffer (pH 5.5) solution. Green tea and black tea were prepared by steeping a teabag in about 100 mL of hot reagent grade water for 10 min. After cooling, the infusion was diluted 10-fold with reagent grade water and filtered before injection. For spike recovery measurements, the tea was spiked with 10 mg L^{-1} sodium azide before dilution and filtration. Orange juice was diluted 10-fold with reagent grade water and filtered before injection. For spike recovery measurements, the orange juice was spiked with 10 mg L^{-1} sodium azide before dilution and filtration. Human urine was diluted 10-fold with reagent grade water and filtered before injection. For spike recovery measurements, the urine was spiked with 10 mg L^{-1} sodium azide before dilution and filtration.

For each sample, precision and recovery from interferences were measured by adding 1 mg L^{-1} azide into four samples; reagent water, black tea, green tea, orange juice and urine. Recovery of all samples was greater than 80 % and the precision varied from 2 to 8 % for all the samples. The results are shown in Table 2-4. Orange juice contains phosphate, sulfate, fluoride and fumarate but these compounds do not interfere with azide.

Hence, it was proved from above experiments that complex **2f** and other complexes of this type i.e., **2c-2e** can be used to prepare their corresponding azido complexes. The monoazide bonded iron complexes **2g-2j** were further synthesized by the reaction of complexes **2c-2f** with one equivalent of sodium azide in a mixture of acetonitrile and methanol (Scheme 2-9)

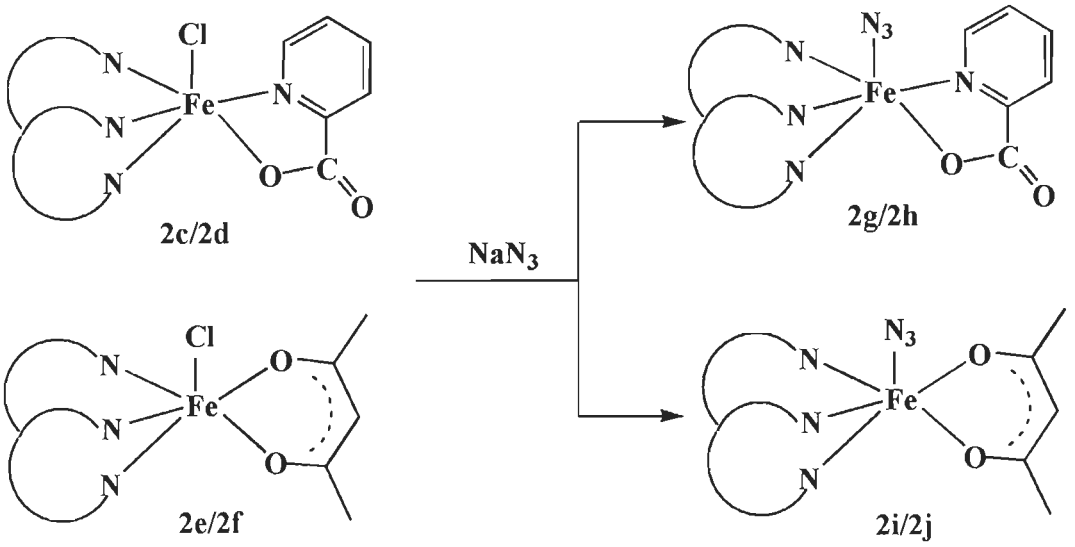

Scheme 2-9

In complexes **2g-2j**, an additional band at 2046-2058 cm^{-1} in the IR spectra confirmed the terminal binding of azide group [72]. All of these complexes were tried for crystallization with different techniques. But we succeeded in obtaining the crystal structure only of complex **2j** that is shown in Fig. 2-35. The crystallographic data are given in Table 2-5 whereas important bond lengths and bond angles are given in Table 2-6. The crystal structures of the Fe(III)-chloro and single azide bonded Fe(III)-azido complex appear to be similar except for the presence of N_3^- in **2j** instead of Cl^- anion at terminal position in **2f**. The structure contains the ferric ion having N4O2 coordination in a distorted octahedral environment. Each nitrogen atom of the Tp^{Me2} is unique in its coordination to iron; therefore, the Fe-N (Tp^{Me2}) distances in **2f** and **2j** were all slightly different, though all were around 2.135 ± 0.027 Å. The intermolecular interaction between two molecules of complex **2j** is shown in Fig. 2-36 where C-H···O interaction is clearly demonstrated between oxygen of acac in one molecule and hydrogen atom of CH_3 group at pyrazole ring in other molecule between 2.551-2.611 Å. Also C-H···N interaction of 2.583 Å between CH_3 of acac and nitrogen of

azide attached to iron center (Fig. 2-37) and C-H···π interaction of 2.790 Å between C-H of pyrazole and π electrons of pyrazole in other molecule (Fig. 2-38) were present as non-covalent interaction in complex **2j**.

To prepare di-azido complexes **2k** and **2l**, the reaction of ferric chloride, KTp / KTp^{Me2} and two equivalent of sodium azide was performed in the presence of pyrazole [PzH] and 3,5-dimethylpyrazole [$Pz^{Me2}H$] (Scheme 2-10).

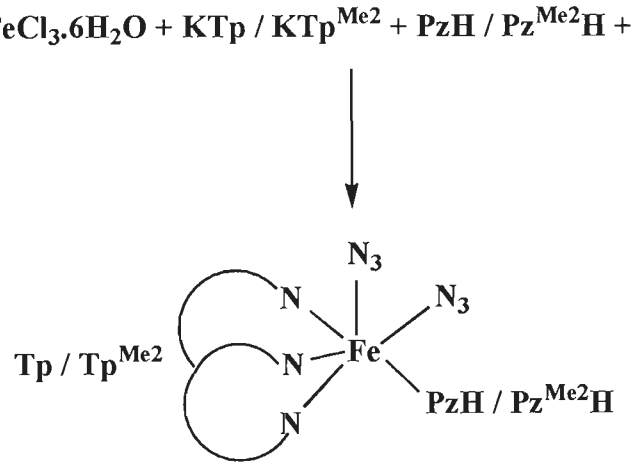

Scheme 2-10

In the IR spectra of complexes **2k** and **2l**, binding of Tp / Tp^{Me2} was confirmed as the B-H band was shifted to higher wave-number (2494 and 2547 cm^{-1}) as compared to free Tp / Tp^{Me2} (2411 and 2480 cm^{-1}). Also the peaks at 2046 and 2052 cm^{-1} clearly indicate the terminal binding of azide ion in complexes **2k** and **2l**. Efforts were also undertaken to crystallize them and we were able to get a single crystal structure of complex **2l** that is shown in Fig. 2-39. The crystallographic data are given in Table 2-7 whereas their important bond lengths and bond angles are given in Table 2-8. The complex **2l** has two azide bonded in cis fashion along with Tp^{Me2} and $Pz^{Me2}H$ in octahedral environment. The structure of complex **2l** (Fig. 2-39) is also similar to the

previous two complexes i.e., **2f** and **2j**. The only difference is that in place of acac, in compound **2l**, the coordination number six is completed by the nitrogen of $Pz^{Me2}H$ and one more azide group. The Fe-N bond distance of coordinated $Pz^{Me2}H$ is 2.142(12) Å, is smaller than the Fe-N bond distances of coordinated Tp^{Me2} (Table 2-8). Fe-N_3 bond lengths in **2j** and **2l** (about 1.990 Å) are typical for Fe(III) azido complexes [42, 52]. Fe-N bond length of both coordinated azide are 1.985(17) and 1.972(16) Å where as the bond angle N5-Fe-N6 is 89.6(6)°. The Fig. 2-40 shows the intermolecular C-H···N interaction (2.894-2.912 Å) between a nitrogen atom of coordinated azide group in one complex with hydrogen atom of CH_3 group located on ring of pyrazole in other complex [73]. Also, one dimensional chain was formed due to $CH_3 \cdots \pi$ interaction (2.801 Å) occurring between CH_3 of Tp^{Me2} and π electrons of Pz^{Me2} of Tp^{Me2} in other molecule as shown in Fig. 2-41. This complex **2l** was prepared by both reaction conditions i.e., at room temperature as well as on refluxing but in both cases, we got cis di-azido complex **2l**. It is important to mention here that the reaction of cis-$[Fe^{III}(cyclam)Cl_2]Cl$ with sodium azide [42] yielded the cis azide bonded system at -18 °C and trans azide bonded system at 50 °C. However, in the present case the product is always cis irrespective of the temperature of reaction medium. This may be due to the presence of methyl substituted pyrazolylborate as supporting ligand in place of cyclam. The compounds **2j** and **2l** are high-spin in nature like other reported compounds with 1,4,7-triazacyclononane-1,4-diacetate motif [52].

Electrochemistry and Photolysis Study

The electrochemistry of the azido-Fe(III) complexes **2j** and **2l** in acetonitrile have been studied by cyclic and square-wave voltammetry. The redox potentials were calculated with reference to the ferrocene / ferrocenium couple. The chloro complex **2f**

was also studied but only irreversible waves were observed. As can be seen in Fig. 2-42 and Fig. 2-43, the azido complexes showed two important electrochemical processes, a one-electron reduction at -623 and -768 mV and a one-electron oxidation at 1389 and 785 mV for **2j** and **2l** respectively which were fully irreversible. The reduction as well as oxidation potential of **2l** was lower than other high-spin azido complex reported in literature [45, 49].

On the basis of relatively smaller redox potential, the photolysis of the powder sample of **2l** (50.0 mg) was performed in liquid nitrogen frozen state with a Rayonet Photochemical Reactor (RPR-100) equipped with 480, 419 and 330 nm tubes in anticipation to form high valent iron-nitride compound. Samples for photolysis at 77 K were prepared via the previously described method [42] and photolysis was performed on a stirred suspension of a fine snow of **2l** in liquid nitrogen. Since the photolysis products of azido-manganese complexes have been shown to be wavelength-dependent [74], we performed the photochemistry of **2l** using both visible (480, 419 nm) and UV (330 nm) light. After photolysis of the azide complex for 6 h, the color of the snow became darker and a portion of the photolyzed snow was packed in a Mössbauer cup for analysis.

Mössbauer Measurements

The results of zero-field Mössbauer measurements of complex **2l** are listed in Table 2-9. Before photolysis, the isomer shift of complexes **2l** was 0.58 mm s^{-1} and quadrupole splitting was 0.62 mm s^{-1} (Fig. 2-44), which were typical for high-spin octahedral Fe(III) complexes and reflecting the high symmetry of the high-spin d^5 electron configuration [42]. The zerofield Mössbauer spectrum (80 K, Fig. 2-45) of

complex **2l** on photolysis showed new signal at isomer shift of 1.13 mm s^{-1} and quadrupole splitting of 3.51 mm s^{-1} indicating the formation of high-spin iron (II) compound upon photoreduction which accounts for 34 % of the spectral intensity. The signal for the presence of Fe(V) could not be observed in Mössbauer spectrum. The Mössbauer parameters of photoreduced product are comparable to those of similar high-spin Fe(II) compounds found in literature [42, 49]. The remaining 66 % of intensity is fitted to the Fe(III) high spin ($\delta = 0.49$ mm s^{-1}, $\Delta E_Q = 0.82$ mm s^{-1}), most likely as starting sample which could not be photolyzed. From the present result, it was concluded that the photolyzed product is Fe(II), not Fe(V) compound.

In another set of experiments, we reduced the complex **2l** electrochemically and tried to characterize the one electron reduced product. The Mössbauer study suggested that the reduced compound is high–spin Fe(II). The suitable crystal for X-ray data collection was obtained by cooling the acetonitrile solution at -20 ^{o}C in aerobic condition in presence of lithium chloride. The crystal structure of complex **2m** is shown in Fig. 2-46. The crystallographic data are given in Table 2-10 whereas their important bond lengths and bond angles are given in Table 2-11. The X-ray structure shows that the metal center is in three oxidation state and six coordinated with two Tp^{Me2}. The average Fe-N bond of coordinated Tp^{Me2} ligand is 1.957 Å well within the range of Fe-N bond distances of other Tp^{Me2} coordinated ligands [Ref. [37] of chapter 1]. Here, iron (II) centre is converted to Fe(III) due to aerial oxidation during crystallization and the additional charge on **2m** is balanced by presence of $FeCl_4^-$ in the lattice. Also, due to intermolecular interactions between chloride ions bonded to iron centre and hydrogen atoms present on Tp^{Me2}, the complex cation is linked to six complex anions (Fig. 2-47) and complex anions are linked to six complex cations (Fig. 2-48) with the

C-H···Cl interactions in the range of 2.839 to 2.967 Å. In three-dimensional packing these interactions play important role and join the layers of cations and anions as shown in Fig. 2-49. Such type of six coordinated bis chelated iron (III) complex with Tp^{Me2} has already been reported in literature [Ref. [37] of chapter 1] where $FeBr_4^-$ is present in lattice.

As reported in literature, when both cis- and trans-$[(cyclam)Fe(N_3)_2]^+$ were subjected to photolysis, only the trans isomer with low spin was photolyzed and gave trans-$[(cyclam)FeN(N_3)]^+$ species but no such species was observed with the high-spin cis isomer [42]. This further supported the hypothesis that only low spin Fe(III) azido undergo photolysis for the formation of iron (V) nitrido. The spin-states of the iron complexes are important for the generation of nitrido species in solution and not the nature of isomers. On the basis of present studies as well as similar studies with different ligands in literature, it may be suggested that if the azide bonded compound is of high-spin, it will undergo photo-reduction irrespective of the nature of isomer but if the complex is low-spin, most likely photo-oxidation will occur.

Complex **2m** was of ionic nature and showed different non-covalent interactions with interesting three-dimensional packing. Our interest arise in these cationic-anionic molecular assemblies containing different metal ions and efforts were made with 1,10-phenanthroline and N-tert-butyl-thioimidazole [$tm^{t\text{-}Bu}$] **2n** as supporting ligands. The ligand **2n** was synthesized by the method of Kister et al. as described in chapter 5 and characterized by different spectroscopic techniques including single crystal X-ray diffractometer. The crystal structure of ligand **2n** is shown in Fig. 2-50 although it was earlier reported in literature [75]. The crystallographic data are given in Table 2-12 whereas their important bond lengths and bond angles are given in Table 2-13. Also

there exist intermolecular N-H···S and C-H···S interactions of 2.416 Å and 2.893 Å, respectively as shown in Fig. 2-51.

$[Ni(phen)_3]Cl_2.2H_2O$ **2o** was synthesized by a reported method [76] as described in chapter 5. The preparation of $[Ni(phen)_2(tm^{t\text{-}Bu})Cl)]Cl$ **2r** has also been described in chapter 5. The reaction of $[Ni(phen)_3]Cl_2.2H_2O$ with $MnCl_2.4H_2O$ and a solution of $CoCl_2.6H_2O$ / $NiCl_2.6H_2O$ and **2n** led to the isolation of ion-pair complexes $[Ni(phen)_3][MnCl_4].2CH_3CN$ **2p**, $[Ni(phen)_3][Co(tm^{t\text{-}Bu})Cl_3]_2.2CH_3CN$ **2q** and $[Ni(phen)_3][Co(tm^{t\text{-}Bu})Cl_3]_2.2CH_3CN$ **2r** respectively, whereas the complex **2t** $[Ni(phen)_2(tm^{t\text{-}Bu})Cl)][Zn(tm^{t\text{-}Bu})Cl_3].2CH_3CN.CH_3OH$ was isolated from the reaction of $[Ni(phen)_2(tm^{t\text{-}Bu})Cl)]Cl$ **2s** and a solution of $ZnCl_2$ and $tm^{t\text{-}Bu}$ in a mixture of acetonitrile and methanol solvent. The equations are given below.

$$[Ni(phen)_3]Cl_2.2H_2O + MnCl_2.4H_2O \longrightarrow [Ni(phen)_3][MnCl_4]\ (2p) + 6H_2O$$

$$[Ni(phen)_3]Cl_2.2H_2O + 2CoCl_2.6H_2O + 2tm^{t\text{-}Bu} \longrightarrow [Ni(phen)_3][Co(tm^{t\text{-}Bu})Cl_3]_2\ (2q) + 14H_2O$$

$$[Ni(phen)_3]Cl_2.2H_2O + 2NiCl_2.6H_2O + 2tm^{t\text{-}Bu} \longrightarrow [Ni(phen)_3][Ni(tm^{t\text{-}Bu})Cl_3]_2\ (2r) + 14H_2O$$

$$[Ni(phen)_2(tm^{t\text{-}Bu})Cl]Cl\ (2s) + ZnCl_2 + tm^{t\text{-}Bu} \longrightarrow [Ni(phen)_2(tm^{t\text{-}Bu})Cl][Zn(tm^{t\text{-}Bu})Cl_3]\ (2t)$$

The crystalline complexes **2p**, **2q**, **2r** and **2t** gave satisfactory elemental analysis. These complexes were stable at room temperature but decomposed above 200 °C. In the IR spectrum of complexes **2o-2t**, ν(C=N) band of phenanthroline was exhibited in the range of 1618-1627 cm^{-1}. The free thioimidazole ligand showed C=S stretching band at 1117 cm^{-1} that shifted to lower side upon complexation, i.e., at 1089 cm^{-1} in **2q**, 1087 cm^{-1} in **2r**, 1082 cm^{-1} in **2s** and 1084 cm^{-1} in **2t** suggesting the coordination of ligand through sulphur atom.

Crystal structure of $[Ni(phen)_3]$ $[MnCl_4]$ (2p)

The complex **2p** is ionic in nature, comprises of one complex cation $[Ni(phen)_3]^{2+}$ and one complex anion $[MnCl_4]^{2-}$ along with two acetonitrile molecules in asymmetric unit. The crystal structure (Fig. 2-52) demonstrated that the metal centre in $[Ni(phen)_3]^{2+}$ is in octahedron environment, the equatorial plane of which is formed by the four nitrogen atoms and the axial positions are occupied by other two nitrogen atoms of phen with Ni-N bond distances range from 2.086(3) Å to 2.107(3) Å (Table 2-15). The crystallographic data are given in Table 2-14. The dihedral angles between the planes of the neighboring phen rings are 83.86°, 83.83° and 85.43°. The cis-angles in the octahedron are slightly deviated from the value of 90° and trans angle in axial position are an average of 170° (Table 2-15).

The $[MnCl_4]^{2-}$ anion shows average angle of 110.83°, slightly deviating from regular tetrahedron geometry. Manganese is coordinated by four chlorine atoms available in reaction mixture due to dissociation of $[Ni(phen)_3]Cl_2.2H_2O$ and form distorted tetrahedral geometry with different Mn-Cl bond distances. These Mn-Cl bond distances are in the range of 2.3566(13) to 2.3894(13) Å and are in good agreement with the literature value [53]. There are no intramolecular bonding interactions between the constituent atoms of the cation and anion but all the four chloride ions attached to the manganese centre are extensively involved in intermolecular hydrogen bonding with hydrogen atoms of phen moiety (Table 2-22). Due to the presence of several intermolecular interactions between chloride ions bonded to manganese centre and hydrogen atoms present on phen rings, the complex cation is linked to seven complex anions (Fig. 2-53) and complex anions are linked to seven complex cations (Fig. 2-54) through hydrogen bonds (intermolecular C-H···Cl bonds are in the range of 2.732(12) to

2.937(9) Å). In crystal packing of complex **2p**, hydrogen bonding interaction played an important role and the cationic-anionic layer along the b-axis formed alternatively (Fig. 2-55). These two layers are united by H-bonds as a result of the interaction of chlorine atoms from $[MnCl_4]^{2-}$ and hydrogen atoms present on phen moiety of $[Ni(phen)_3]^{2+}$. In **2p**, all the rings of coordinated 1,10-phenanthroline ligands are planar. The distance between Ni(II) and Mn(II) centre is of 8.832 Å which is too large for any kind of interactions between these centers.

Crystal structure of $[Ni(phen)_3][Co(tm^{t\text{-}Bu})Cl_3]_2$ (2q)

The single crystal X-ray studies of **2q** revealed that the complex is centrosymmetric, ionic in nature and is composed of one complex cation $[Ni(phen)_3]^{2+}$ and two complex anions $[Co(tm^{t\text{-}Bu})(Cl)_3]^-$ along with two acetonitrile molecules as solvent of crystallization in one asymmetric unit. The crystal structure of **2q** is shown in Fig. 2-56. The crystallographic data are given in Table 2-16 whereas their important bond lengths and bond angles are given in Table 2-17. The anionic complex $[Co(tm^{t\text{-}Bu})(Cl)_3]^-$ acts as a monomer and is significantly responsible for layered structure. The nickel centre in $[Ni(phen)_3]^{2+}$ (Fig. 2-56) is in octahedron environment as in complex **2p** with slight difference in dihedral angles between the planes of the neighboring phen rings that are 78.50°, 85.58° and 85.70°. The cis-angles in the octahedron (Table 2-17) are slightly deviated from the value of 90° and the average trans angle in axial position is 171.73°.

The equatorial plane of $[Co(tm^{t\text{-}Bu})(Cl)_3]^-$ shows distortions with the average angles of 111.28° which is slightly less from regular tetrahedron angle. Cobalt is coordinated by three chlorine atoms and one sulphur atom of $tm^{t\text{-}Bu}$ in distorted tetrahedral geometry. The Co-Cl bond distances are in the range of 2.2638(6) to

2.2836(7) Å which are larger than the reported distance in the literature [77-80]. The metal centre in this complex is 0.678 Å above the equatorial plane and the three chloride ions attached to the cobalt centre are extensively involved in intermolecular C-H···Cl hydrogen bonding. Due to the presence of several intermolecular non-covalent interactions between chloride ions bonded to cobalt centre and hydrogen atoms present on phenanthroline moiety, the complex cation is linked to six complex anions (Fig. 2-57) whereas the complex anion is linked to three complex cations and one complex anion (Fig. 2-58) (Table 2-22). Besides, C-H···Cl intermolecular interactions, complex anion also shows intramolecular N-H···Cl interaction (2.463 Å) between bonded chloride ion and hydrogen atom present on the nitrogen of thioimidazole ring and π-π stacking (3.528 Å) between two thioimdazole rings of the complex anion (Fig. 2-58). It is important to mention here that out of three bonded chloride ions, only one (Cl2) is involved in both intra as well as in intermolecular interactions (Fig. 2-58) whereas the other two chloride ions are involved only in intermolecular hydrogen bond formation. The two cationic layers are united with anionic layers by hydrogen bond formed between the chloride of $[Co(tm^{t\text{-}Bu})(Cl)_3]^-$ anion and the hydrogen atoms at the periphery of phenanthroline moiety in complex cation $[Ni(phen)_3]^{2+}$ (Fig. 2-59). Thus weak C-H···Cl hydrogen bonds and π-π stacking play prominent role in stabilization of the layered structure in complex **2q**. It is also significant that there is no π-π stacking between the phenanthroline moiety present in the lattice.

Crystal structure of $[Ni(phen)_3][Ni(tm^{t\text{-}Bu})Cl_3]_2$ (2r)

The complex **2r** is similar to complex **2q**, with only difference that it has both nickel centers. The crystal structure of complex **2r** is given in Fig. 2-60. The

crystallographic details are given in Table 2-18 and important bond lengths and angles are listed in Table 2-19. The complex is centrosymmetric, ionic in nature and comprises of one complex cation $[Ni(phen)_3]^{2+}$ and two complex anions $[Ni(tm^{t\text{-}Bu})(Cl)_3]^-$ in unit cell. The anionic complex $[Ni(tm^{t\text{-}Bu})(Cl)_3]^-$ acts as monomer and is mainly responsible for the layered structure. The metal centre in $[Ni(phen)_3]^{2+}$ (Fig. 2-60) is in octahedron environment, the equatorial plane of which is formed by the four nitrogen atoms and the axial positions are occupied by other two nitrogen atoms of phen with Ni-N bond distances in the range of 2.079(4) to 2.100(4) Å. The dihedral angles between the planes of the neighboring phen rings are 77.53°, 86.07° and 85.97°. The cis-angles in the octahedron (Table 2-19) are slightly deviated from the value of 90° and the trans angle of 170.54(15)° in axial position is nearly linear.

The equatorial plane of $[Ni(tm^{t\text{-}Bu})(Cl)_3]^-$ shows distortions with the average angles deviating from regular tetrahedron angles. Nickel is coordinated by three chlorine atoms and one sulphur atom of $tm^{t\text{-}Bu}$ in distorted tetrahedral geometry. The Ni-Cl bond distances are in the range of 2.251(15) to 2.275 (15) Å. The Ni(2)-Cl(2) bond distance is longer than Ni(2)-S(1), 2.305(6) Å. In this complex the two short bond distances (Ni(1)-Cl(3) and Ni(1)-Cl(1)) and two long bond distances (Ni(2)-S(1) and Ni(1)-Cl(2)) make the geometry distorted tetrahedral. The metal centre in this complex is 0.592 Å above the equatorial plane. The three chloride ions attached to the nickel centre are extensively involved in intermolecular hydrogen bonding.

Due to the presence of several intermolecular interactions between chloride ions bonded to nickel centre and hydrogen atoms present on phen rings, the complex cation is linked to six complex anions through hydrogen bonds (C-H···Cl) in the range of 2.714 to 2.943 Å (Fig. 2-61) whereas the complex anions are linked to four complex

cations (Fig. 2-62). Besides, C-H···Cl intermolecular interactions, complex anion also shows intramolecular N-H···Cl interaction (2.410 Å) between bonded chloride ion and hydrogen atom present on the nitrogen of thioimidazole ring and π-π stacking (3.517 Å) between two thioimdazole rings of the complex anion (Fig. 2-62). In crystal packing, hydrogen bond interactions play an important role and the cationic-anionic layer parallel to yz plane is formed. The two layers are united by H-bond in which chlorine atoms belong to the tetrahedral complex anion. $[Ni(phen)_3]^{2+}$ and $[Ni(tm^{t\text{-}Bu})(Cl)_3]^-$ interacted with each other by hydrogen bonding (Fig. 2-63).

Crystal structure of $[Ni(phen)_2(tm^{t\text{-}Bu})Cl]$ $[Zn(tm^{t\text{-}Bu})Cl_3]_2$ (2t)

The complex **2t** crystallizes in the monoclinic system with space group $P2_1/n$ and crystallographic details are given in Table 2-20 and the important bond lengths and bond angles are listed in Table 2-21. The crystal structure of complex **2t** is given in Fig. 2-64. It is ionic in nature and comprises of one complex cation $[Ni(phen)_2(tm^{t\text{-}Bu})Cl]^+$ and one complex anion $[Zn(tm^{t\text{-}Bu})Cl_3]^-$ along with two acetonitrile and one methanol molecule as solvent for crystallization in asymmetric unit. The Ni(II) in $[Ni(phen)_2(tm^{t\text{-}Bu})Cl]^+$ (Fig. 2-64) is in octahedral geometry where the equatorial plane is formed by the three nitrogen atoms of two phenanthroline and one sulphur atom from **2n**. The axial positions are occupied by another nitrogen atom of phen and chloride atom with an angle of 173.02(9)°. The Ni-N bond distances are in the range of 2.084(3)-2.117(3) Å whereas the Ni-S bond distance is 2.5601(10) Å which is well within the reported range in literature [81]. The Ni-Cl bond distance in **2t** is 2.4206(10) Å and the dihedral angle between the planes of the neighboring phen rings is 88.92°. The cis angles in the octahedron (Table 2-21) are slightly deviated from the value of 90° and trans angle in axial position is 173.02(9)°, which is slightly less than 180°.

The equatorial plane of $[Zn(tm^{t\text{-}Bu})Cl_3]^-$ shows distortions with the average angle (110.65°) slightly deviating from regular tetrahedral geometry and the zinc centre in this complex is 0.709 Å above the equatorial plane. Zinc (II) is coordinated by three chlorine atoms and one sulphur atom of **2n** leaving overall one negative charge on the unit. The Zn-Cl bond distances are in the range of 2.2462(12) to 2.2783(12) Å which is very close to Zn-Cl bond distance in other complexes [82]. The complex anion also exhibited intermolecular C-H···S bonding (2.970(1) Å) due to the interaction between coordinated sulphur atom and hydrogen atom of phenanthroline moiety and intramolecular N-H···Cl bonding (2.317(1) Å) between bonded chloride ions and N-H group of thioimidazole molecule, respectively (Fig. 2-66). The chloride ions present on both nickel (II) and zinc (II) metal ions are extensively involved in intermolecular hydrogen bonding (C-H···Cl) during complex cation to cation interactions and cation to complex anion $[Zn(tm^{t\text{-}Bu})Cl_3]^-$ interactions. Due to the presence of such type of non-covalent interactions in unit cell, each complex cation is linked to two complex cations and two complex anions as demonstrated in Fig. 2-65. The cationic unit also shows one intramolecular N-H···Cl interaction (2.286(1) Å) between the bonded chloride ion on nickel centre and hydrogen atom present on thioimidazole moiety but this interaction does not take part in crystal packing. In complex **2t**, the one anion unit has capability to interact with three complex cations and one complex anion with C-H···Cl hydrogen bonding interaction (Fig. 2-66) and both cation and anion serve as receptor as well as acceptor for each other. The presence of various non-covalent interactions resulted in interesting three dimensional packing view (Fig. 2-67) for complex **2t**.

Magnetic properties

The temperature dependence of the $\chi_M T$ product for complex **2p** is shown in Fig. 2-68. The room temperature value is 7.93 emu $mol^{-1}K$ that is inline with that

expected for the sum of the $\chi_M T$ of Ni(II) ion (S = 1, g = 2) and Mn(II) ion (S = 5/2, g = 2) in high spin state as they were magnetically isolated due to large separation of 8.832 Å. This distance is too large for any kind of interaction. Below 30 K, the $\chi_M T$ value slightly decreases which may be due to zero-field splitting and / or intermolecular magnetic coupling. The value of the $\chi_M T$ product is 9.14 emu $mol^{-1}K$ for **2q**, 3.09 emu $mol^{-1}K$ for **2r** and 2.63 emu $mol^{-1}K$ for **2t** (Table 2-23). The metal–metal separation in **2q**, **2r** and **2t** are 5.873 Å, 5.794 Å and 8.488 Å respectively. The $\chi_M T$ product of 9.14 emu $mol^{-1}K$ for **2q** can be attributed to the presence of one complex cation and two complex anion where all the metal centres {i.e., Ni(II) (S = 1) and two Co(II) (S = 3)} are in high-spin states (Fig. 2-69). This value agrees with the theoretical value (8.99 emu $mol^{-1}K$) for sum of the spin state of metals present in this complex. Fig. 2-70 shows the $\chi_M T$ product of 3.09 emu $mol^{-1}K$ for complex **2r** and it can be explained on the basis of the fact that both metal centers were nickel and two Ni(II) with S = 2 were in high spin state. This $\chi_M T$ product agrees with the theoretical value (2.97 emu $mol^{-1}K$) for sum of spin states of two nickel centers. In complex **2t**, the metal present in anionic component is zinc which is diamagnetic in nature. The experimental $\chi_M T$ value corresponds to Ni(II) with S = 1 only (Fig. 2-71). In magnetic measurements, we could not observe any interaction between metal ions present in ion-pair complexes but results show that these complexes were magnetically pure.

Thermal analysis

Thermo-gravimetric analyses (TGA) were carried out in air atmosphere in the temperature range of 25-700°C for complexes **2p**, **2q**, **2r** and **2t** with the heating rate of 10 °C min^{-1}. The TGA curve of the complex **2p** shows two well separated stages as shown in Fig. 2-72. The first weight loss of 9.85 % occurs in the temperature range of

100-200 °C, corresponds to the loss of acetonitrile molecules (calculated value 9.33 %). Subsequent distinct weight loss stage of 59.41 % in the temperature range of 200-460 °C, can be attributed to the loss of three phen molecules against the calculated value 61.52 %. The TGA curve of complex **2q** shows three well-separated weight loss stages (Fig. 2-73). The first weight loss of 6.46 % occurs in the temperature range of 100-200 °C, which corresponds to the loss of two acetonitrile molecules (calculated value 6.19 %). Second weight loss of 25.26 % was observed at a temperature range of 200-240 °C against the weight due to loss of two N-tert-butyl-2-thioimidazole molecules (calculated value 23.56 %). In the third stage, 42.05 % weight loss in the temperature range 240-435 °C corresponds to the loss of two phen molecules (calculated value 40.78 %). The TGA curve of complex **2r** also shows a similar pattern as complex **2q** (Fig. 2-74). The first weight loss of 6.32 % occurs in the temperature range of 100-200 °C, which corresponds to the loss of two acetonitrile molecules (calculated value 6.20 %). Second weight loss of 25.31 % was observed at a temperature range of 200-240 °C against the weight due to loss of two N-tert-butyl-2-thioimidazole molecules (calculated value 23.63 %). In the third stage, 41.94 % weight loss in the temperature range of 240-435 °C corresponds to the loss of two phen molecules (calculated value 41.02 %).The complex **2t** also exhibits three well-separated weight loss stages in its TGA curve (Fig. 2-75) i.e., first weight loss (observed 9.52 %, calculated 9.98 % from 100-200 °C) corresponds to the loss of solvent molecules present in lattice and the second weight loss (observed 32.21 %, calculated 29.94 % from 200-250 °C) corresponds to the loss of two N-tert-butyl-2-thioimidazole molecules from complex cation and anion. In the third stage, 32.65 % weight loss occurs in the temperature range of 250-415 °C due to loss of two coordinated phen molecules (calculated value 34.55 %) from the complex cation. Later, it can be

assumed that in all these complexes, both metal ions form their oxides as the TGA curve becomes constant at 700 °C. This study reflects that the thermal stability of **2p**, **2q** and **2t** are same because all these involve same extent of inter- as well as intramolecular interaction as demonstrated in their three dimensional packing view.

Cyclic voltammetry studies

The electrochemical behavior of the complexes was studied in DMSO / acetonitrile solvent. The cyclic voltammograms (CV) and differential pulse voltammograms (DPV) of complex **2p** recorded at a scan rate of 0.100 Vs^{-1} is shown in Fig. 2-76. The voltammograms of **2p** display three reduction peaks at -1.70, -1.38 and -1.07 V in DMSO solvent. These peaks can be assigned to the Ni(II) → Ni(0), Mn(II) → Mn(0) and Ni(II) → Ni(I) reduction process, respectively (Table 2-24). Fig. 2-77 shows the CV and DPV of complex **2q,** which exhibited two irreversible redox couple i.e., E_{pa}= 0.75 V and E_{pc}= -1.53 V for Ni(II) ↔ Ni(0); E_{pa}= 1.47 V and E_{pc}= -1.12 V for Co(II) ↔ Co(III) process respectively. In CV and DPV measurement of complex **2t** (Fig. 2-78), two reduction peaks (at -1.72 and -1.06 V) were observed and assigned due to the reduction of Ni(II) →Ni(0) and Ni(II) → Ni(I) respectively [83].

Summary

Four iron (III) complexes **2c-2f** with Tp / Tp^{Me2} and pic / acac as supporting ligand have been reported. One of these complexes, **2f** has been characterized by single crystal X-ray diffractometer and found that it has octahedral geometry having vacant side for azide binding. In order to establish, whether these type of complexes can be used to prepare corresponding azido complexes or not, the complex **2f** was used as an ionophore to prepare its membrane and potentiometric studies were carried out to check azide interaction. This azide selective sensor has also been used to determine azide ion

concentration in various aqueous samples (black tea, green tea, orange juice and human urine). After confirming selectivity of azide ion to **2f**, different mono-azido complexes (**2g-2j**) were also synthesized. Among them, complex **2j** has been structurally characterized and it shows terminal binding of azide ion. Two di-azido complexes **2k** and **2l** were also synthesized having Tp / Tp^{Me2}, PzH / $Pz^{Me2}H$. Crystal structure of complex **2l** shows that the two azides are in cis position along with Tp^{Me2} and $Pz^{Me2}H$. On the basis of relatively smaller redox potential of complex **2l** as compared to complex **2j**, the photolysis of complex **2l** was performed and it was observed that **2l** was photoreduced to iron (II) compounds, which was proved by Mössbauer studies. The complex **2l** was reduced electrochemically to give one electron reduced iron (II) product that was characterized and the crystal structure shows that the metal center is coordinated with two Tp^{Me2}. It was also concluded that if the azide bonded compound is of high-spin, it will undergo photo-reduction irrespective of the nature of isomer but if the complex is low-spin, most likely photo-oxidation will occur. Also, iron (II) has been oxidized to iron (III) due to aerial oxidation during crystallization and $FeCl_4^-$ was present in lattice. Some interesting ion-pair complexes **2p**, **2q**, **2r** and **2t** with different metal ions were also synthesized having 1,10-phenanthroline and **2n** as supporting ligands. The three dimensional packing view of these complexes demonstrated the presence of C-H···Cl hydrogen bonding interaction between cationic complexes like $[Ni(phen)_3]^{2+}$, $[Ni(phen)_2(tm^{t\text{-}Bu})Cl]^+$ (that has H-donor sites) and the anionic complexes like $[MnCl_4]^{2-}$, $[Co(tm^{t\text{-}Bu})Cl_3]^-$, $[Ni(tm^{t\text{-}Bu})Cl_3]^-$ and $[Zn(tm^{t\text{-}Bu})Cl_3]^-$ (which have Cl^- and sulphur a hydrogen bond acceptor sites). The existence of such intermolecular C-H···Cl and C-H···S bonding in these ion-pair complexes are also supported by IR, magnetic and thermal studies. Thus, we explored the utility of $[Ni(phen)_3]^{2+}$ as anion receptor for $[MnCl_4]^{2-}$ and thioimdazole coordinated complex anions.

Table 2-1 Crystal Data and Collection Details of [Tp ^{Me2}Fe(acac)Cl] (2f)

Emperical formula	$C_{22}H_{32}N_7O_2BClFe$
Formula weight	528.66
Crystal system	Triclinic
Space group	$P\bar{1}$
Lattice parameters	
a (Å)	8.090(5)
b (Å)	11.140(5)
c (Å)	15.090(5)
α (°)	104.170(5)
β (°)	93.000(5)
γ (°)	100.190(5)
Cell volume V (Å^3)	1291.2(11)
Z	2
D_{Calc} (g cm^{-3})	1.360
Data collection	
μ (Mo K_α) mm^{-1})	0.720
θ_{max} (°)	27.35
Reflections measured	5856
Independent reflections	3432
Number of parameters refined	320
R	0.0509
R_w	0.1472

Table 2-2 Selected Bond Distances (Å) and Bond Angles (°) for [Tp ^{Me2}Fe(acac)Cl] (2f)

Bond Distances			
Fe(1)-N(1)	2.131(4)	Fe(1)-O(1)	1.987(4)
Fe(1)-N(2)	2.107(4)	Fe(1)-O(2)	1.983(4)
Fe(1)-N(3)	2.164(4)	Fe(1)-Cl(1)	2.364(16)
Bond Angles			
N(1)-Fe(1)-N(2)	91.39(16)	N(1)-Fe(1)-N(3)	82.87(16)
N(1) -Fe(1)-O(1)	90.91(15)	N(1)-Fe(1)- O(2)	175.10(15)
N(1)-Fe(1)-Cl(1)	91.14(12)	N(2)-Fe(1)-N(3)	83.90(16)
N(2)-Fe(1)-O(1)	174.74(14)	N(2)-Fe(1)-O(2)	89.85(15)
N(2)-Fe(1)-Cl(1)	92.35(12)	N(3)-Fe(1)-O(1)	91.70(15)
N(3)-Fe(1)-O(2)	92.55(15)	N(3)-Fe(1)-Cl(1)	172.84(12)
O(1)-Fe(1)-O(2)	87.47(15)	O(1)-Fe(1)-Cl(1)	92.33(11)
O(2)-Fe(1)-Cl(1)	93.54(11)		

Table 2-3 Optimizations of membrane compositions and potential response towards azide ion

Sensor no.	Composition of membranes (amount in mg)				Slope ± 0.2 (mV decade^{-1} activity)	Working concentration range (M)	Detection limit (M)
	Ionophore **2f**	Additive (HTAB)	Plasticizer	PVC			
1.	4	2	190,DBP	100	55.1	3.8×10^{-5} - 1.0×10^{-2}	1.2×10^{-5}
2.	4	2	190,DOP	100	45.2	4.6×10^{-4} - 1.0×10^{-2}	2.5×10^{-4}
3.	4	2	190,BA	100	46.6	3.5×10^{-6} - 1.0×10^{-2}	1.8×10^{-6}
4.	4	2	190,NPOE	100	49.1	5.4×10^{-6} - 1.0×10^{-2}	2.7×10^{-6}
5.	-	2	190,DOP	100	4.6	-	-
6.	4	-	190,DOP	100	51.4	7.8×10^{-5} - 1.0×10^{-2}	3.0×10^{-5}
7.	4	2	-	200	44.2	4.8×10^{-4} - 1.0×10^{-2}	1.9×10^{-4}
8.	4	3	190,DOP	100	56.1	6.4×10^{-6} - 1.0×10^{-2}	2.3×10^{-6}
9.	4	4	190,DOP	100	62.0	7.1×10^{-6} - 1.0×10^{-2}	4.4×10^{-6}
10.	2	2	190,DOP	100	52.8	4.5×10^{-5} - 1.0×10^{-2}	2.1×10^{-5}
11.	3	2	190,DOP	100	54.7	2.8×10^{-6} - 1.0×10^{-2}	1.1×10^{-6}
12.	4	2	190,DOP	100	62.1	1.0×10^{-6} - 1.0×10^{-2}	8.9×10^{-7}
13.	5	2	190,DOP	100	59.4	6.3×10^{-7} - 1.0×10^{-2}	3.8×10^{-7}
14.	6	2	190,DOP	100	63.6	9.2×10^{-6} - 1.0×10^{-2}	6.4×10^{-6}
15.	5	2	220,DOP	100	61.7	7.2×10^{-6} - 1.0×10^{-2}	5.2×10^{-6}
16.	5	2	200,DOP	100	58.4	6.3×10^{-6} - 1.0×10^{-2}	4.0×10^{-6}
17.	5	2	180,DOP	100	56.4	1.2×10^{-6} - 1.0×10^{-2}	8.2×10^{-7}

Table 2-4 Determination of azide in different aqueous samples

Samples	Calculated by proposed sensor ($\mu g\ L^{-1}$)	Amount added ($mg\ L^{-1}$)	Recovery (%) (n=3)	Precision (RSD) (n=3)
Black Tea	140	1	91	5.4
Green Tea	68	1	104	1.9
Orange Juice	155	1	87	8.0
Urine	133	1	108	3.7

Table 2-5 Crystal Data and Collection Details of $[Tp^{Me2}Fe(acac)N_3]$ (2j)

Emperical formula	$C_{21}H_{31}N_9O_2BCl_2Fe$
Formula weight	579.11
Crystal system	Triclinic
Space group	$P\bar{1}$
Lattice parameters	
a (Å)	8.107(5)
b (Å)	11.738(5)
c (Å)	14.643(5)
α (°)	100.779(5)
β (°)	91.280(5)
γ (°)	98.175(5)
Cell volume V ($Å^3$)	1353.2(11)
Z	2
D_{Calc} ($g\ cm^{-3}$)	1.421
Data collection	
μ (Mo K_α) mm^{-1})	0.791
θ_{max} (°)	26.51
Reflections measured	5619
Independent reflections	2806
Number of parameters refined	337
R	0.0692
R_w	0.1762

Table 2-6 Selected Bond Distances (Å) and Bond Angles (°) for $[Tp^{Me2}Fe(acac)N_3]$ (2j)

Bond Distances			
Fe(1)-N(1)	2.131(5)	Fe(1)-N(2)	2.134(5)
Fe(1)-N(3)	2.122(5)	Fe(1)-N(4)	1.995(5)
Fe(1)-O(1)	1.988(4)	Fe(1)-O(2)	1.986(4)
Bond Angles			
N(1)-Fe(1)-N(2)	84.31(19)	N(1)-Fe(1)-N(3)	84.72(19)
N(1)-Fe(1)-N(4)	174.70(2)	N(1)-Fe(1)-O(1)	91.95(18)
N(1)-Fe(1)-O(2)	92.71(18)	N(2)-Fe(1)-N(3)	88.69(19)
N(2)-Fe(1)-N(4)	91.10(2)	N(2)-Fe(1)-O(1)	91.52(19)
N(2)-Fe(1)-O(2)	176.71(18)	N(3)-Fe(1)-N(4)	92.50(2)
N(3)-Fe(1)-O(1)	176.63(18)	N(3)-Fe(1)-O(2)	92.45(18)
N(4)-Fe(1)-O(1)	90.90(2)	N(4)-Fe(1)-O(2)	92.00(2)
O(1)-Fe(1)-O(2)	87.16(1)		

Table 2-7 Crystal Data and Collection Details of $[Tp^{Me2}Fe(Pz^{Me2}H)(N_3)_2]$ (2l)

Emperical formula	$C_{22}H_{32}N_{15}BFe$
Formula weight	573.29
Crystal system	Orthorhombic
Space group	Pbca
Lattice parameters	
a (Å)	19.946(5)
b (Å)	17.439(5)
c (Å)	15.807(5)
α (°)	90.00(5)
β (°)	90.00(5)
γ (°)	90.00(5)
Cell volume V ($Å^3$)	5498(3)
Z	8
D_{Calc} (g cm^{-3})	1.385
Data collection	
μ (Mo K_α) mm^{-1})	0.591
θ_{max} (°)	28.45
Reflections measured	6936
Independent reflections	5788
Number of parameters refined	227
R	0.0899
R_w	0.1879

Table 2-8 Selected Bond Distances (Å) and Bond Angles (°) for $[Tp^{Me2}Fe(Pz^{Me2}H)(N_3)_2]$ (2l)

Bond Distances			
Fe(1)-N(1)	2.137(12)	Fe(1)-N(2)	2.112(12)
Fe(1)-N(3)	2.171(12)	Fe(1)-N(4)	2.142(12)
Fe(1)-N(5)	1.985(17)	F e(1)-N(6)	1.972(16)
Bond Angles			
N(1)-Fe(1)-N(2)	85.4(5)	N(1)-Fe(1)-N(3)	83.6(4)
N(1)-Fe(1)-N(4)	170.0(5)	N(1)-Fe(1)-N(5)	94.1(5)
N(1)-Fe(1)-N(6)	95.4(5)	N(2)-Fe(1)-N(3)	86.5(5)
N(2)-Fe(1)-N(4)	87.0(5)	N(2)-Fe(1)-N(5)	178.6(5)
N(2)-Fe(1)-N(6)	91.6(5)	N(3)-Fe(1)-N(4)	89.6(5)
N(3)-Fe(1)-N(5)	92.2(5)	N(3)-Fe(1)-N(6)	177.9(6)
N(4)-Fe(1)-N(5)	93.5(5)	N(5)-Fe(1)-N(6)	89.6(6)

Table 2-9 Zero-Field Mössbauer Parameters for $[Tp^{Me2}Fe(Pz^{Me2}H)(N_3)_2]$ (2l)

Complex	δ, mm s^{-1}	ΔE_Q, mm s^{-1}
2l (before photolysis)	0.58	0.62
2l (after photolysis)	[a]0.49	0.82
	[b]1.13	3.51

[a] stands for Fe (III) species and [b] stands for Fe(II) species

Table 2-10 Crystal Data and Collection Details of $[(Tp^{Me2})_2Fe][FeCl_4]$ (2m)

Emperical formula	$C_{32}H_{45}N_{13}B_2Cl_4Fe_2$
Formula weight	886.93
Crystal system	Triclinic
Space group	$P\bar{1}$
Lattice parameters	
a (Å)	8.765(4)
b (Å)	10.489(5)
c (Å)	22.622(8)
α (°)	90.144(18)
β (°)	90.230(17)
γ (°)	93.027(18)
Cell volume V ($Å^3$)	2076.9(16)
Z	2
D_{Calc} (g cm^{-3})	1.418
Data collection	
μ (Mo K_α) mm^{-1})	0.997
θ_{max} (°)	28.25
Reflections measured	10272
Independent reflections	8080
Number of parameters refined	495
R	0.0997
R_w	0.2124

Table 2-11 Selected Bond Distances (Å) and Bond Angles (°) for $[(Tp^{Me2})_2Fe][FeCl_4]$ (2m)

Bond Distances			
Fe(1)-N(1)	1.965(6)	Fe(1)-N(1a)	1.965(6)
Fe(1)-N(3)	1.975(8)	Fe(1)-N(3a)	1.975(8)
Fe(1)-N(5)	1.931(7)	Fe(1)-N(5a)	1.931(7)
Fe(2)-Cl(1)	2.194(3)	Fe(2)-Cl(2)	2.197(3)
Fe(2)-Cl(3)	2.179(3)	Fe(2)-Cl(4)	2.206(3)
Bond Angles			
N(1)-Fe(1)-N(1a)	180.0(3)	N(1)-Fe(1)-N(3)	89.8(3)
N(1)-Fe(1)-N(3a)	90.2(3)	N(1a)-Fe(1)-N(3)	90.2(3)
N(1a)-Fe(1)-N(3a)	89.7(3)	N(1)-Fe(1)-N(5)	89.4(3)
N(1)-Fe(1)-N(5a)	90.6(3)	N(1a)-Fe(1)-N(5)	90.6(3)
N(1a)-Fe(1)-N(5a)	89.4(3)	N(3)-Fe(1)-N(3a)	180.0(3)
N(3)-Fe(1)-N(5)	89.4(3)	N(3)-Fe(1)-N(5a)	90.6(3)
N(3a)-Fe(1)-N(5)	90.6(3)	N(3a)-Fe(1)-N(5a)	89.4(3)
N(5)-Fe(1)-N(5a)	180.0(3)	Cl(1)-Fe(2)-Cl(2)	112.7(12)
Cl(1)-Fe(2)-Cl(3)	108.90(11)	Cl(1)-Fe(2)-Cl(4)	107.1(11)
Cl(2)-Fe(2)-Cl(3)	109.46(12)	Cl(2)-Fe(2)-Cl(4)	107.3(11)
Cl(3)-Fe(2)-Cl(4)	111.36(12)		

Table 2-12 Crystal Data and Collection Details of [$tm^{t\text{-}Bu}$] (2n)

Emperical formula	$C_7H_{12}N_2S$
Formula weight	156.26
Crystal system	Orthorhombic
Space group	Pbca
Lattice parameters	
a (Å)	10.138(2)
b (Å)	9.7439(19)
c (Å)	17.548(4)
α (°)	90.00
β (°)	90.00
γ (°)	90.00
Cell volume V ($Å^3$)	1733.5(6)
Z	8
D_{Calc} (g cm^{-3})	1.197
Data collection	
μ (Mo K_α) mm^{-1})	0.304
θ_{max} (°)	31.80
Reflections measured	2961
Independent reflections	1732
Number of parameters refined	98
R	0.0602
R_w	0.1436

Table 2-13 Selected Bond Distances (Å) and Bond Angles (°) for [$tm^{t\text{-}Bu}$] (2n)

Bond Distances			
C(1)-C(2)	1.498(3)	C(1)-C(3)	1.512(3)
C(1)-C(4)	1.499(4)	C(1)-N(1)	1.490(3)
C(5)-N(1)	1.371(3)	C(8)-N(1)	1.348(2)
C(6)-N(3)	1.354(3)	C(8)-N(3)	1.338(3)
C(8)-S(1)	1.6762(19)		
Bond Angles			
C(1)-C(2)-C(3)	108.2(2)	C(1)-C(3)-C(4)	109.6(2)
C(1)-C(2)-C(4)	112.1(2)	C(1)-C(2)-N(1)	108.3(2)
C(1)-C(3)-N(1)	109.4(2)	C(1)-C(4)-N(1)	109.21(18)
C(1)-C(5)-N(1)	108.67(18)	C(1)-C(8)-N(1)	126.90(17)
C(5)-C(8)-N(1)	109.4(2)	C(6)-C(8)-N(1)	111.04(18)

Table 2-14 Crystal Data and Collection Details of $[Ni(phen)_3][MnCl_4]$ (2p)

Emperical formula	$C_{40}H_{30}N_8Cl_4MnNi$
Formula weight	878.15
Crystal system	Triclinic
Space group	$P\bar{1}$
Lattice parameters	
a (Å)	9.872(2)
b (Å)	12.406(2)
c (Å)	16.986(3)
α (°)	80.298(8)
β (°)	85.098(8)
γ (°)	85.648(8)
Cell volume V ($Å^3$)	2039.1(6)
Z	2
D_{Calc} ($g\ cm^{-3}$)	1.430
Data collection	
μ (Mo K_α) mm^{-1})	1.073
θ_{max} (°)	29.79
Reflections measured	11411
Independent reflections	6798
Number of parameters refined	489
R	0.0588
R_w	0.1590

Table 2-15 Selected Bond Distances (Å) and Bond Angles (°) for $[Ni(phen)_3][MnCl_4]$ (2p)

Bond Distances			
Ni(1)-N(1)	2.089(3)	Ni(1)-N(2)	2.106(3)
Ni(1)-N(3)	2.107(3)	Ni(1)-N(4)	2.089(3)
Ni(1)-N(5)	2.086(3)	Ni(1)-N(6)	2.103(3)
Mn(2)-Cl(1)	2.3701(12)	Mn(2)-Cl(2)	2.3799(14)
Mn(2)-Cl(3)	2.3894(13)	Mn(2)-Cl(4)	2.3566(13)
Bond Angles			
N(1)-Ni(1)-N(2)	79.51(12)	N(1)-Ni(1)-N(3)	92.43(12)
N(1)-Ni(1)-N(4)	168.80(11)	N(1)-Ni(1)-N(5)	94.62(11)
N(1)-Ni(1)-N(6)	94.64(12)	N(2)-Ni(1)-N(3)	93.68(13)
N(2)-Ni(1)-N(4)	92.96(11)	N(2)-Ni(1)-N(5)	168.95(12)
N(2)-Ni(1)-N(6)	90.80(13)	N(3)-Ni(1)-N(4)	79.71(11)
N(3)-Ni(1)-N(5)	95.94(11)	N(3)-Ni(1)-N(6)	172.23(11)
N(4)-Ni(1)-N(5)	94.11(11)	N(4)-Ni(1)-N(6)	93.73(11)
N(5)-Ni(1)-N(6)	80.27(11)	Cl(1)-Mn(2)-Cl(2)	111.41(5)
Cl(1)-Mn(2)-Cl(3)	109.16(6)	Cl(1)-Mn(2)-Cl(4)	106.09(5)
Cl(2)-Mn(2)-Cl(3)	107.28(6)	Cl(2)-Mn(2)-Cl(4)	115.15(5)
Cl(3)-Mn(2)-Cl(4)	107.61(5)		

Table 2-16 Crystal Data and Collection Details of $[Ni(phen)_3][Co(tm^{t\text{-}Bu})Cl_3]_2$ (2q)

Emperical formula	$C_{54}H_{54}N_{12}S_2Cl_6Co_2Ni_2$
Formula weight	1324.48
Crystal system	Monoclinic
Space group	C2/c
Lattice parameters	
a (Å)	23.030(3)
b (Å)	15.383(2)
c (Å)	19.866(4)
α (°)	90.00
β (°)	123.469(5)
γ (°)	90.00
Cell volume V ($Å^3$)	5870.9(15)
Z	4
D_{Calc} ($g\ cm^{-3}$)	1.498
Data collection	
μ (Mo K_α) mm^{-1})	1.268
θ_{max} (°)	33.68
Reflections measured	11691
Independent reflections	6864
Number of parameters refined	356
R	0.0363
R_w	0.1064

Table 2-17 Selected Bond Distances (Å) and Bond Angles (°) for $[Ni(phen)_3][Co(tm^{t\text{-}Bu})Cl_3]_2$ (2q)

Bond Distances			
Ni(1)-N(1)	2.1044(15)	Ni(1)-N(2)	2.0785(15)
Ni(1)-N(3)	2.0936(14)	Co(1)-S(1)	2.3462(6)
Co(1)-Cl(1)	2.2700(6)	Co(1)-Cl(2)	2.2836(7)
Co(1)-Cl(3)	2.2638(6)		
Bond Angles			
N(1)-Ni(1)-N(2)	79.75(6)	N(1)-Ni(1)-N(2')	96.39(6)
N(1)-Ni(1)-N(3)	93.31(6)	N(1)-Ni(1)-N(3')	90.98(6)
N(1)-Ni(1)-N(1')	174.42(9)	N(1')-Ni(1)-N(2)	96.39(6)
N(1')-Ni(1)-N(2')	79.75(6)	N(1')-Ni(1)-N(3)	90.98(6)
N(1')-Ni(1)-N(3')	93.31(6)	N(2)-Ni1-N(2')	93.49(8)
N(2)-Ni(1)-N(3)	170.39(6)	N(2)-Ni(1)-N(3')	93.88(6)
N(2')-Ni(1)-N(3)	93.89(6)	N(2')-Ni(1)-N(3')	170.39(6)
N(3')-Ni(1)-N(3)	79.49(8)	S(1)-Co(1)-Cl(1)	96.43(2)
S(1)-Co(1)-Cl(2)	107.11(2)	S(1)-Co(1)-Cl(3)	120.95(2)
Cl(1)-Co(1)-Cl(2)	123.83(3)	Cl(1)-Co(1)-Cl(3)	106.66(2)
Cl(2)-Co(1)-Cl(3)	103.35(3)		

Table 2-18 Crystal Data and Collection Details of $[Ni(phen)_3][Ni(tm^{t\text{-}Bu})Cl_3]_2$ (2r)

Emperical formula	$C_{54}H_{54}N_{12}S_2Cl_6Ni_3$
Formula weight	1324.04
Crystal system	Monoclinic
Space group	C2/c
Lattice parameters	
a (Å)	22.8953(15)
b (Å)	15.2934(10)
c (Å)	19.9417(19)
α (°)	90.00
β (°)	123.543(3)
γ (°)	90.00
Cell volume V ($Å^3$)	5819.7(8)
Z	4
D_{Calc} (g cm^{-3})	1.511
Data collection	
μ (Mo K_α) mm^{-1})	1.356
θ_{max} (°)	23.50
Reflections measured	4570
Independent reflections	3346
Number of parameters refined	370
R	0.0504
R_w	0.1381

Table 2-19 Selected Bond Distances (Å) and Bond Angles (°) for $[Ni(phen)_3][Ni(tm^{t\text{-}Bu})Cl_3]_2$ (2r)

Bond Distances			
Ni(1)-N(1)	2.100(4)	Ni(1)-N(2)	2.096(4)
Ni(1)-N(3)	2.079(4)	Ni(2)-S(1)	2.3053(15)
Ni(2)-Cl(1)	2.2508(16)	Ni(2)-Cl(2)	2.2753(15)
Ni(2)-Cl(3)	2.2526(15)		
Bond Angles			
N(1)-Ni(1)-N(2)	90.94(15)	N(1)-Ni(1)-N(2')	93.72(15)
N(1)-Ni(1)-N(3)	96.28(16)	N(1)-Ni(1)-N(3')	79.52(16)
N(1)-Ni(1)-N(1')	173.9(2)	N(1')-Ni(1)-N(2)	90.94(15)
N(1')-Ni(1)-N(2')	93.72(15)	N(1')-Ni(1)-N(3)	79.52(16)
N(1')-Ni(1)-N(3')	96.28(16)	N(2)-Ni1-N(2')	80.0(2)
N(2)-Ni(1)-N(3)	93.40(15)	N(2)-Ni(1)-N(3')	170.53(15)
N(2')-Ni(1)-N(3)	170.53(15)	N(2')-Ni(1)-N(3')	93.40(15)
N(3')-Ni(1)-N(3)	93.9(2)	S(1)-Ni(2)-Cl(1)	118.26(6)
S(1)-Ni(2)-Cl(2)	107.47(5)	S(1)-Ni(2)-Cl(3)	94.21(6)
Cl(1)-Ni(2)-Cl(2)	100.47(6)	Cl(1)-Ni(2)-Cl(3)	104.92(6
Cl(2)-Ni(2)-Cl(3)	133.13(7)		

Table 2-20 Crystal Data and Collection Details of $[Ni(phen)_2(tm^{t\text{-}Bu})Cl)][Zn(tm^{t\text{-}Bu})Cl_3]$ (2t)

Emperical formula	$C_{43}H_{40}N_{10}OS_2Cl_4NiZn$
Formula weight	1042.87
Crystal system	Monoclinic
Space group	$P2_1/n$
Lattice parameters	
a (Å)	13.1861(2)
b (Å)	22.2517(4)
c (Å)	17.0737(3)
α (°)	90.00
β (°)	110.5130(10)
γ (°)	90.00
Cell volume V ($Å^3$)	4692(14)
Z	4
D_{Calc} (g cm^{-3})	1.476
Data collection	
μ (Mo K_α) mm^{-1})	1.275
θ_{max} (°)	26.26
Reflections measured	6936
Independent reflections	5788
Number of parameters refined	227
R	0.0899
R_w	0.1879

Table 2-21 Selected Bond Distances (Å) and Bond Angles (°) for $[Ni(phen)_2(tm^{t\text{-}Bu})Cl)][Zn(tm^{t\text{-}Bu})Cl_3]$ (2t)

Bond Distances			
Ni(1)-N(1)	2.084(3)	Ni(1)-N(2)	2.085(3)
Ni(1)-N(3)	2.117(3)	Ni(1)-N(4)	2.094(3)
Ni(1)-S(1)	2.5601(10)	Ni(1)-Cl(4)	2.4206(10)
Zn(1)-Cl(1)	2.2783(12)	Zn(1)-Cl(2)	2.2615(11)
Zn(1)-Cl(3)	2.2462(12)		
Bond Angles			
N(1)-Ni(1)-N(2)	80.02(12)	N(1)-Ni(1)-N(3)	92.99(12)
N(1)-Ni(1)-N(4)	171.50(13)	N(1)-Ni(1)-S(1)	93.58(9)
N(1)-Ni(1)-Cl(4)	92.99(9)	N(2)-Ni(1)-N(3)	89.86(12)
N(2)-Ni(1)-N(4)	96.12(12)	N(2)-Ni(1)-S(1)	80.12(8)
N(2)-Ni(1)-Cl(4)	173.02(9)	N(3)-Ni(1)-N(4)	79.37(13)
N(3)-Ni(1)-S(1)	166.89(9)	N(3)-Ni(1)-Cl(4)	90.42(9)
N(4)-Ni(1)-S(1)	93.21(9)	N(4)-Ni(1)-Cl(4)	90.79(9)
S(1)-Ni(1)-Cl(4)	100.55(4)	S(2)-Zn(1)-Cl(1)	110.36(4)
S(2)-Zn(1)-Cl(2)	110.18(4)	S(2)-Zn(1)-Cl(3)	104.26(4)

Table 2-22 Non-covalent interactions in complexes

Complex	D-H	H···A	D···A	D-H···A
$[Ni(phen)_3][MnCl_4]$ (2p)				
C(6)-H(6)···Cl(2)	0.93	2.937(9)	3.825(13)	160
C(20)-H(20)···Cl(3)	0.93	2.902(10)	3.673(13)	141
C(27)-H(27)···Cl(1)	0.93	2.869(14)	3.733(17)	155
C(24)-H(24)···Cl(1)	0.93	2.860(14)	3.531(18)	130
C(1)-H(1)···Cl(1)	0.93	2.732(12)	3.472(15)	137
C(10)-H(10)···Cl(4)	0.93	2.743(9)	3.539(10)	144
C(21)-H(21)···Cl(4)	0.93	2.802(12)	3.678(15)	157
$[Ni(phen)_3][Co(tm^{t\text{-}Bu})Cl_3]_2$ (2q)				
C(13)-H(13)···Cl(1)	0.93	2.840(11)	3.626(12)	143
C(15)-H(15)···Cl(2)	0.93	2.874(6)	3.774(8)	163
C(24)-H(24)···Cl(2)	0.93	2.923(5)	3.559(3)	127
C(11)-H(11)···Cl(3)	0.93	2.687(8)	3.534(10)	152
C(1)-H(1)···Cl(3)	0.93	2.983(13)	3.772(16)	144
C(21)-H(21A)···Cl(3)	0.96	2.914(4)	3.616(6)	131
C(16)-H(16)···Cl(3)	0.93	2.707(2)	3.616(6)	131
N(5)-H(5)···Cl(2)	0.83	2.463(24)	3.232(10)	154
$[Ni(phen)_3][Ni(tm^{t\text{-}Bu})Cl_3]_2$ (2r)				
C(5)-H(5B)···Cl(1)	0.96	2.906(8)	3.617(8)	131
C(8)-H(8)···Cl(1)	0.93	2.867(7)	3.642 (9)	141
C(10)-H(10)···Cl(3)	0.93	2.714(5)	3.557(8)	150
C(14)-H(14)···Cl(2)	0.93	2.897(3)	3.550(8)	128
C(16)-H(16)···Cl(2)	0.93	2.906(4)	3.813(8)	165
C(19)-H(19)···Cl(3)	0.93	2.943(8)	3.726(10)	142
N(5)-H(5)···Cl(2)	0.83	2.410(4)	3.176(8)	149
$[Ni(phen)_2(tm^{t\text{-}Bu})Cl)][Zn(tm^{tBu})Cl_3]$ (2t)				
C(11)-H(11)···Cl(1)	0.93	2.824(1)	3.711(5)	160
C(12)-H(12)···Cl(2)	0.93	2.723(2)	3.527(6)	145
C(3)-H(3)···Cl(2)	0.93	2.747(1)	3.656(6)	166
C(29)-H(29)···Cl(2)	0.93	2.733(1)	3.558(5)	148
C(26)-H(26)···Cl(4)	0.93	2.859(2)	3.735(5)	157
C(14)-H(14)···S(2)	0.93	2.970(1)	3.849(6)	158
N(6)-H(6)···Cl(1)	0.86	2.317(1)	3.148(4)	163
N(8)-H(7)···Cl(4)	0.86	2.286(1)	3.069(3)	151

Table 2-23 The $\chi_M T$ products for complexes

Complex	Metals spin state	$\chi_M T$ / emu mol^{-1} K (theortical)	$\chi_M T$ / emu mol^{-1} K (experimental)
$[Ni(phen)_3][MnCl_4]$ (2p)	Ni (S = 1) and Mn (S = 5/2)	7.81	7.93
$[Ni(phen)_3][Co(tm^{t\text{-}Bu})\ Cl_3]_2$ (2q)	Ni (S = 1) and Co (S = 3/2)	8.99	9.14
$[Ni(phen)_3][Ni(tm^{t\text{-}Bu})\ Cl_3]_2$ (2r)	Two Ni (S = 1)	2.97	3.09
$[Ni(phen)_2(tm^{t\text{-}Bu})Cl)]$ $[Zn(tm^{t\text{-}Bu})Cl_3]$ (2t)	Ni (S = 1) and Zn (S = 0)	2.45	2.63

Table 2-24 Electrochemical data for complexes

Complex	Solvent	E_{pa}	E_{pc}	Redox reaction
$[Ni(phen)_3][MnCl_4]$ (2p)	DMSO		-1.70	Ni(II) → Ni(0)
			-1.38	Mn(II) → Mn(0)
			-1.07	Ni(II) → Ni(I)
$[Ni(phen)_3][Co(tm^{t\text{-}Bu})Cl_3]_2$ (2q)	MeCN	0.75	-1.53	Ni(0) ↔ Ni(II)
		1.47	-1.12	Co(II) ↔ Co(III)
$[Ni(phen)_2(tm^{t\text{-}Bu})Cl)][Zn(tm^{t\text{-}Bu})Cl_3]$ (2t)	DMSO		-1.72	Ni(II) → Ni(0)
			-1.06	Ni(II) → Ni(I)

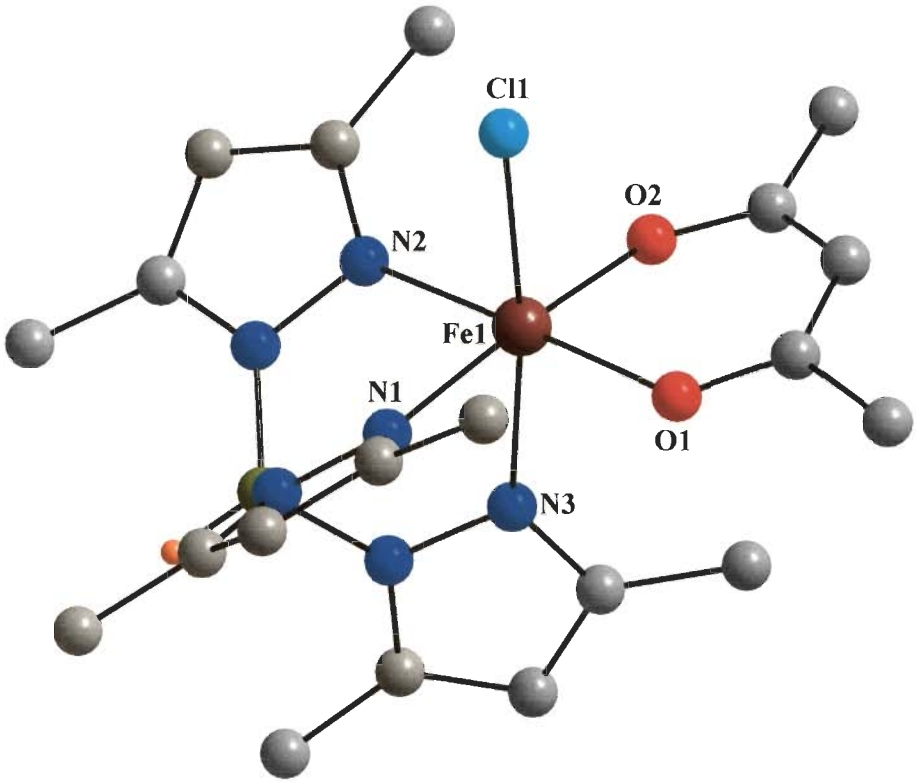

Fig. 2-32 Crystal structure of [Tp ^{Me2}Fe(acac)Cl] **2f**

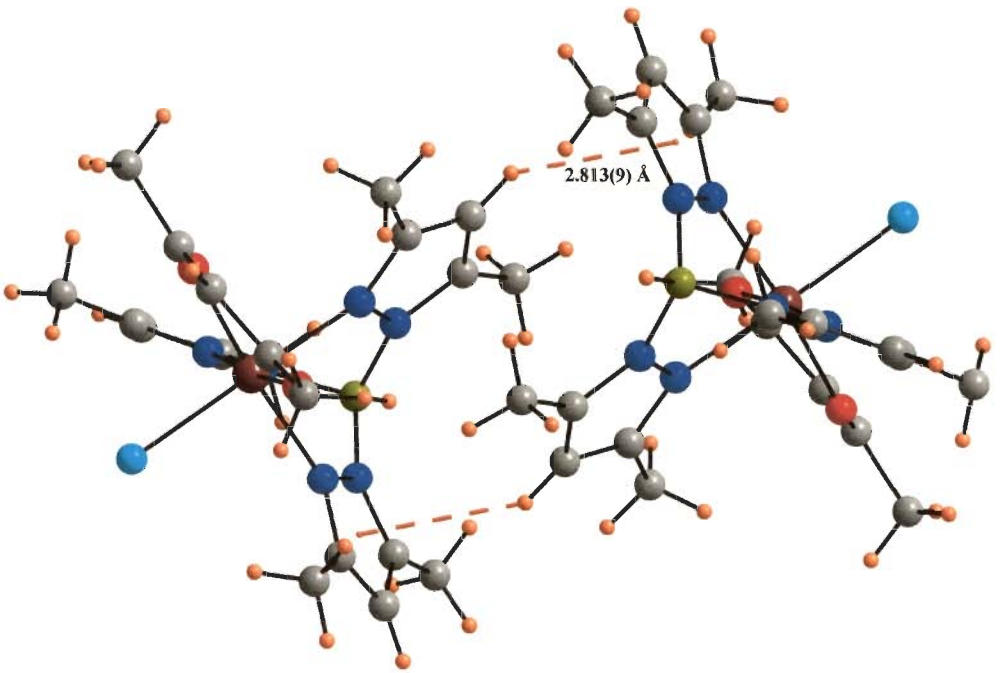

Fig. 2-33 Intermolecular C-H···π interactions present in complex **2f**

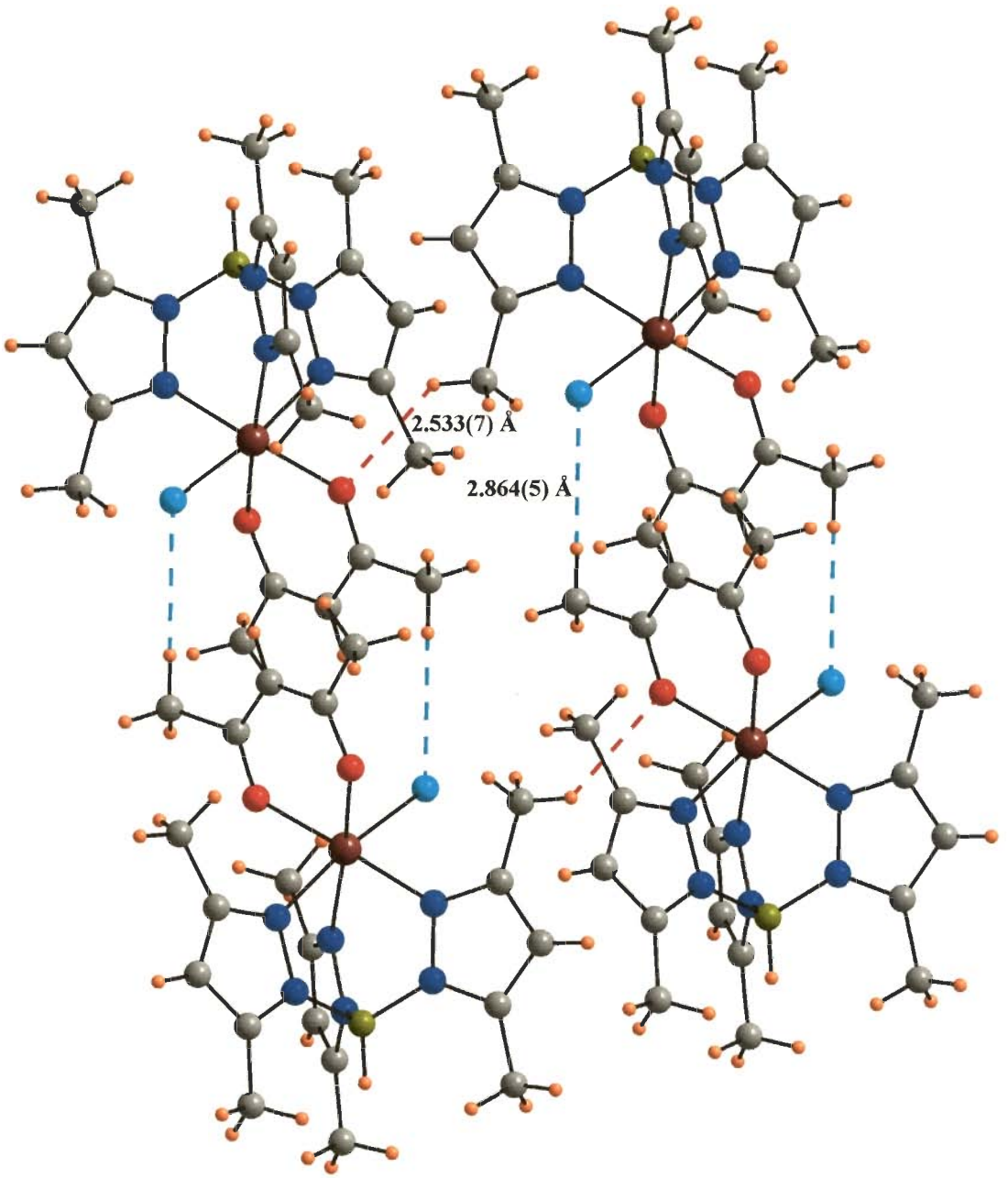

Fig. 2-34 Intermolecular C-H···O and C-H···Cl interactions present in complex **2f**

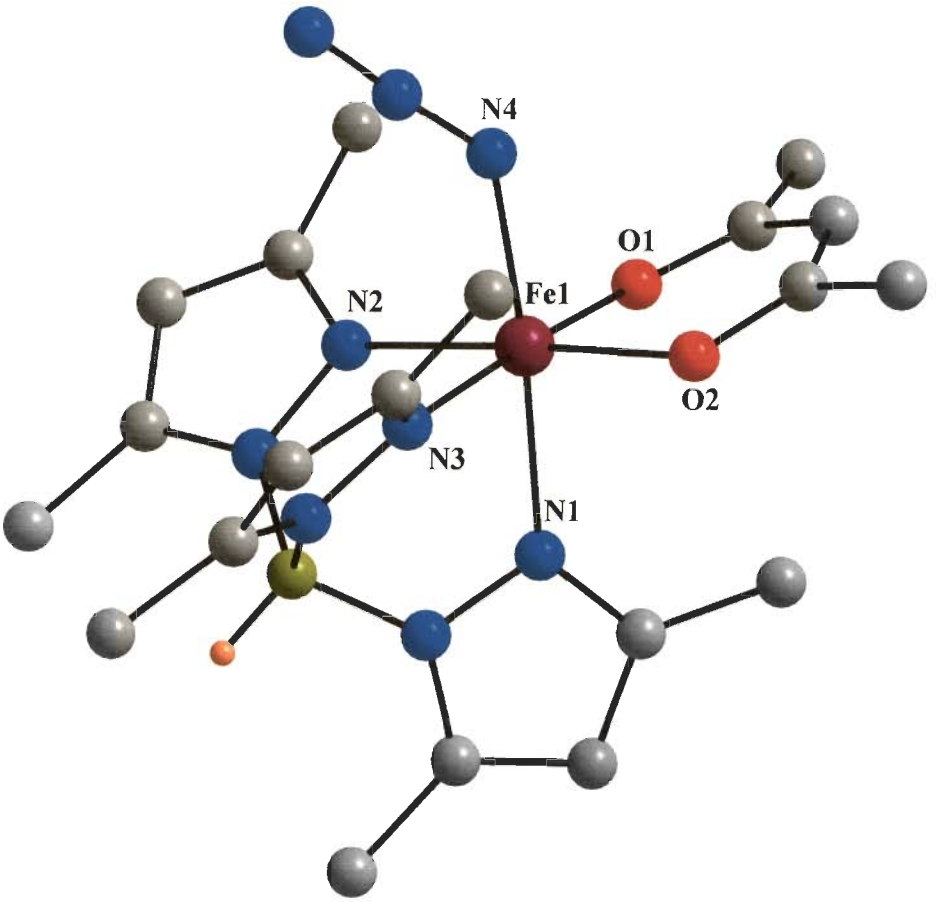

Fig. 2-35 Crystal structure of [Tp ^{Me2}Fe(acac)N_3] **2j**

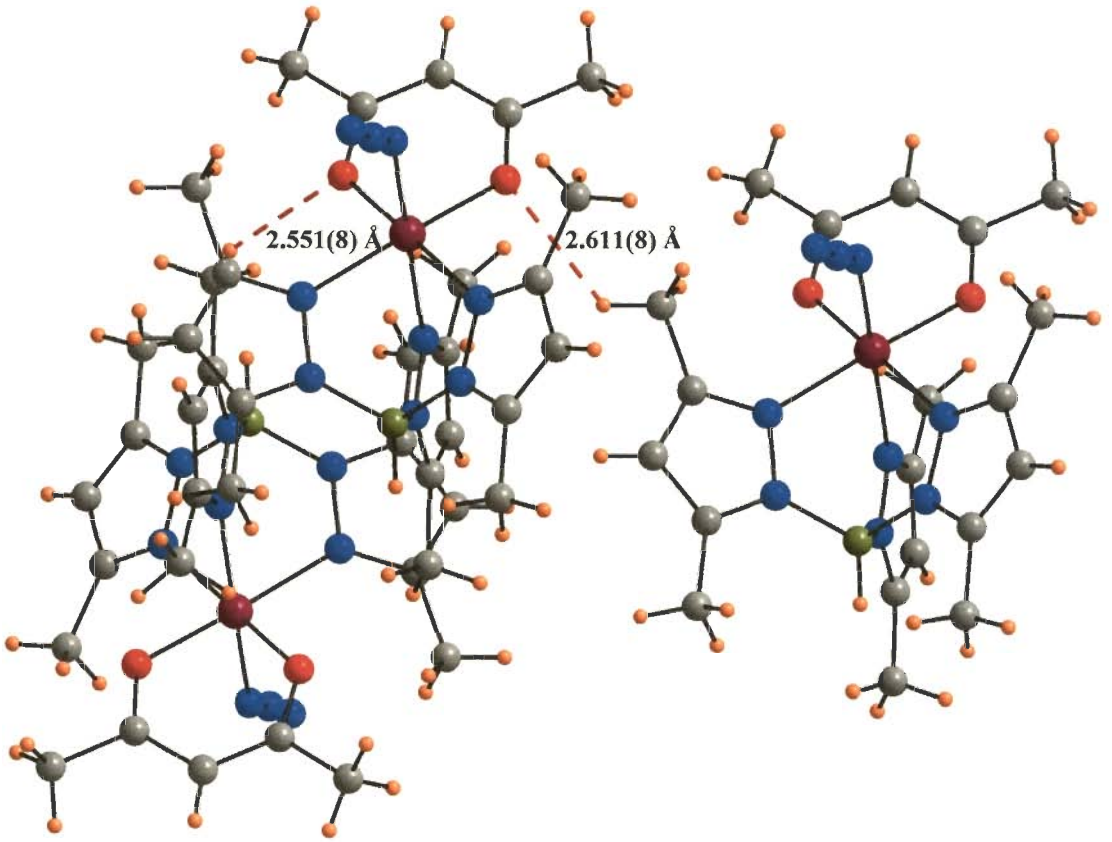

Fig. 2-36 Intermolecular C-H···O interactions present in complex **2j**

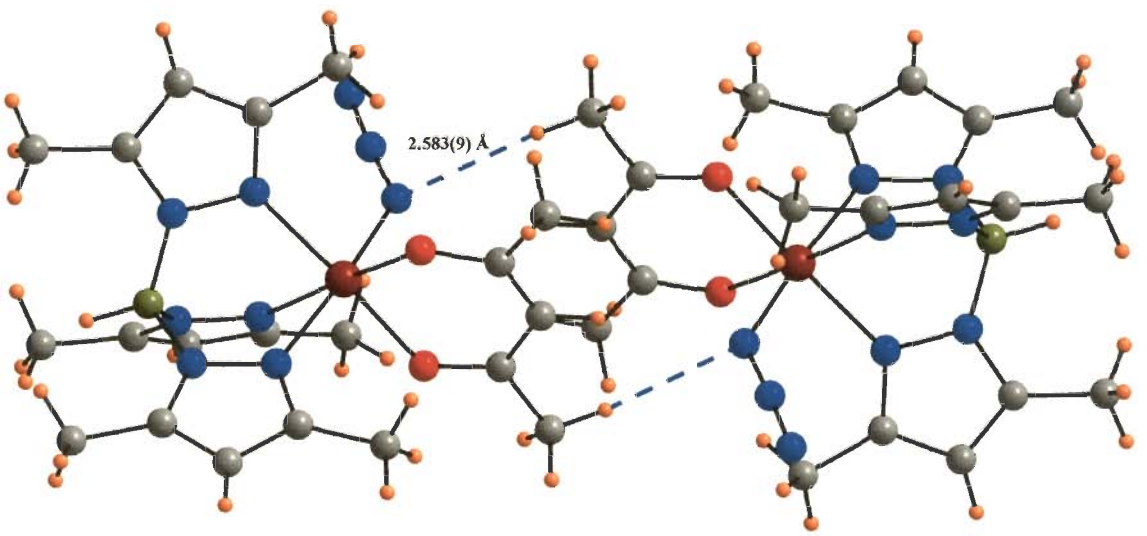

Fig. 2-37 Intermolecular C-H···N interactions present in complex **2j**

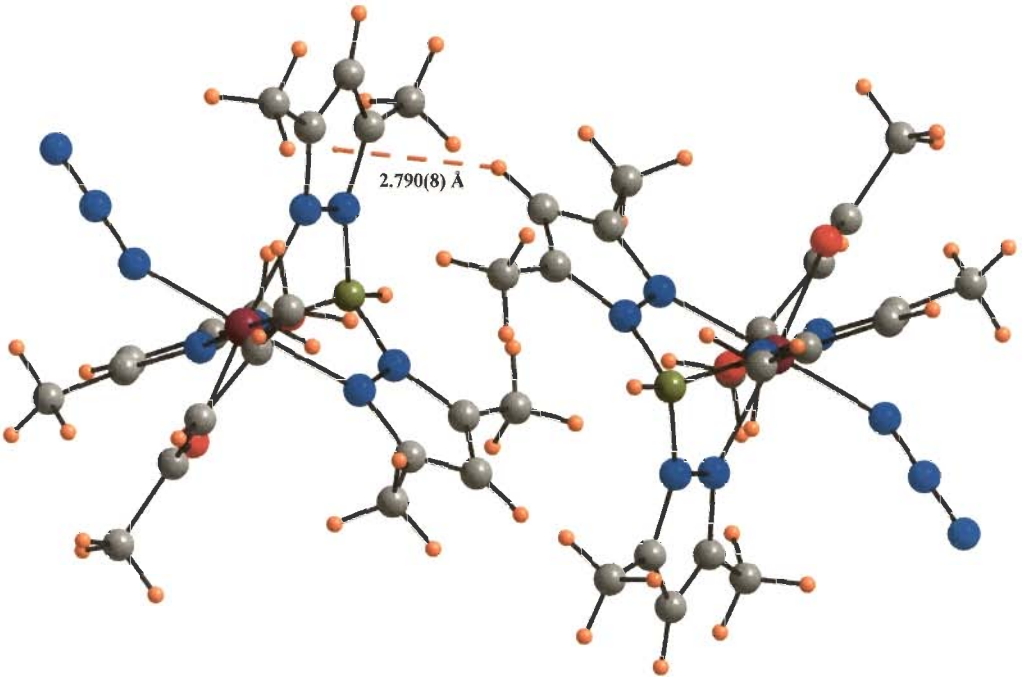

Fig. 2-38 Intermolecular C-H···π interactions present in complex **2j**

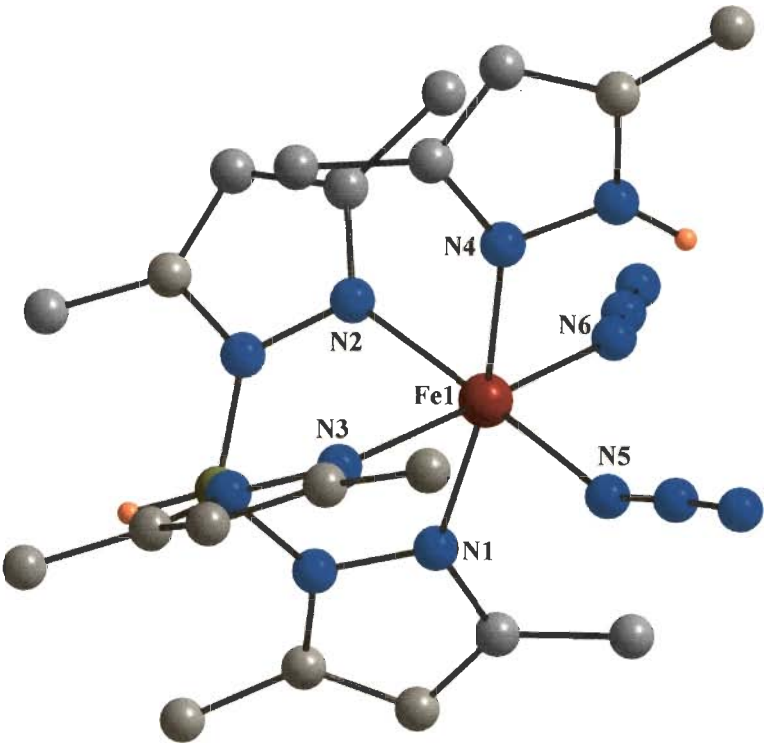

Fig. 2-39 Crystal structure of $[Tp^{Me2}Fe(Pz^{Me2}H)(N_3)_2]$ **2l**

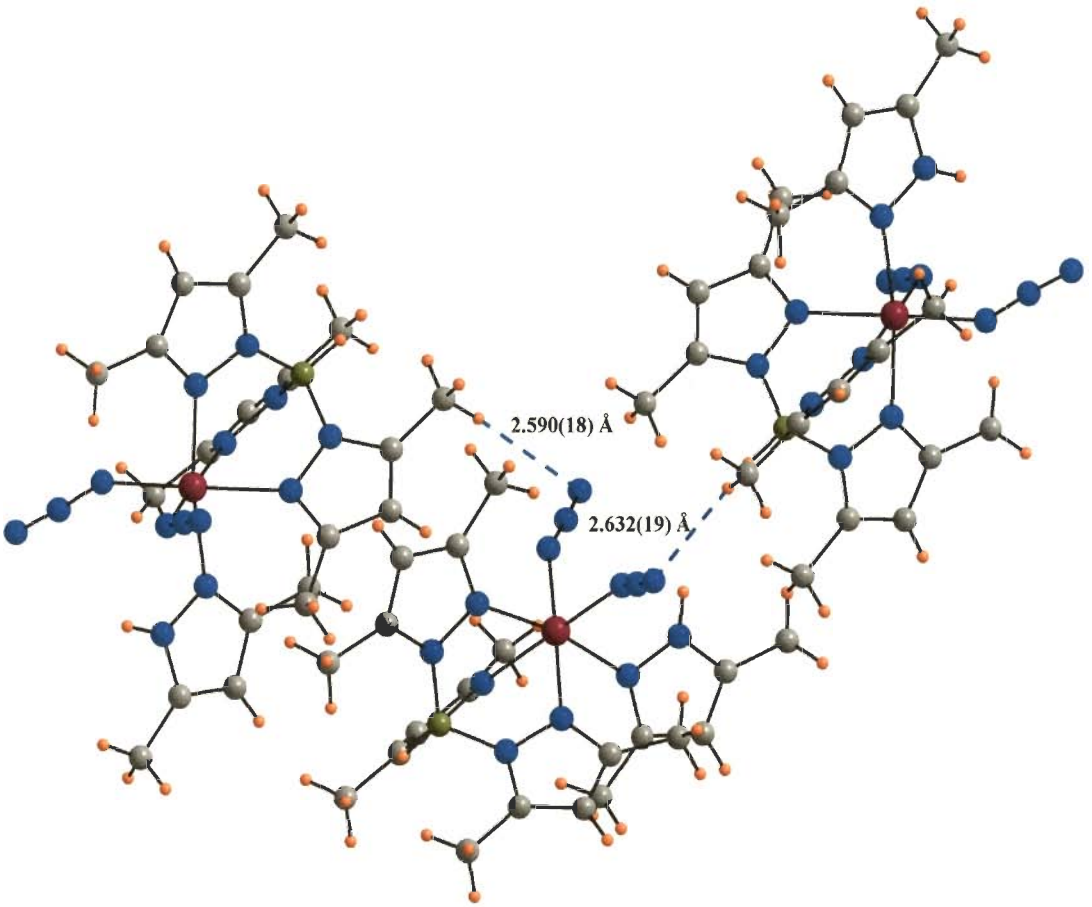

Fig. 2-40 Intermolecular C-H···N interactions present in complex **2l**

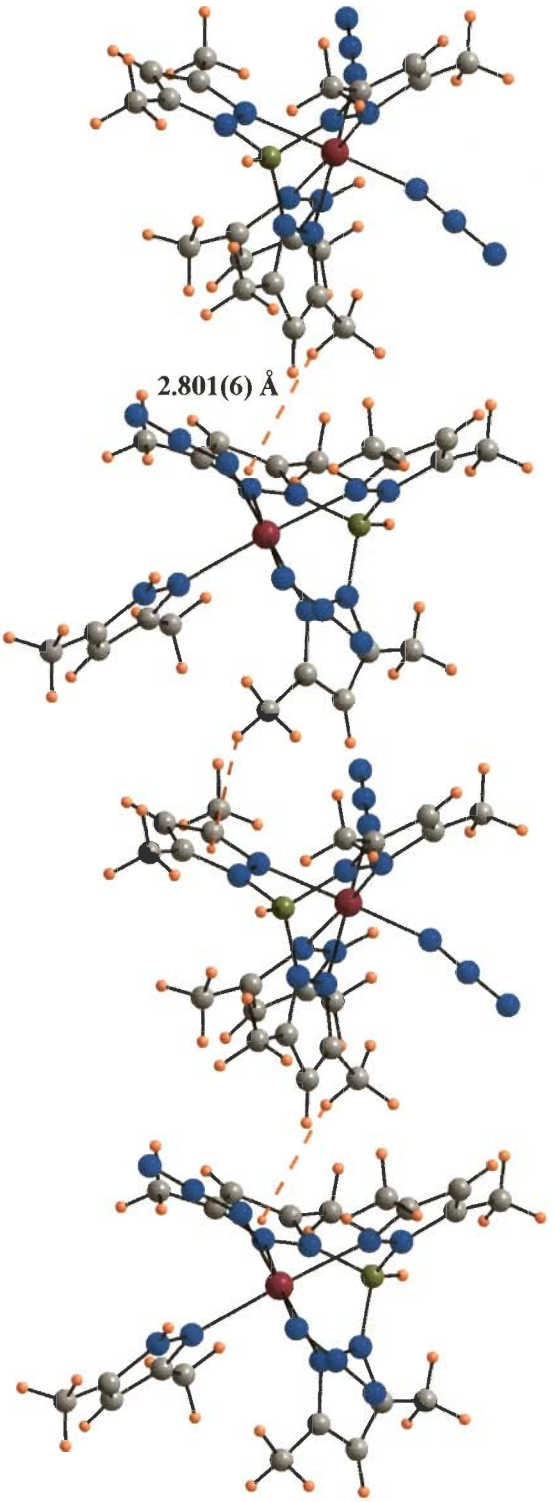

Fig. 2-41 One dimensional chain formed by C-H···π interactions in complex **2l**

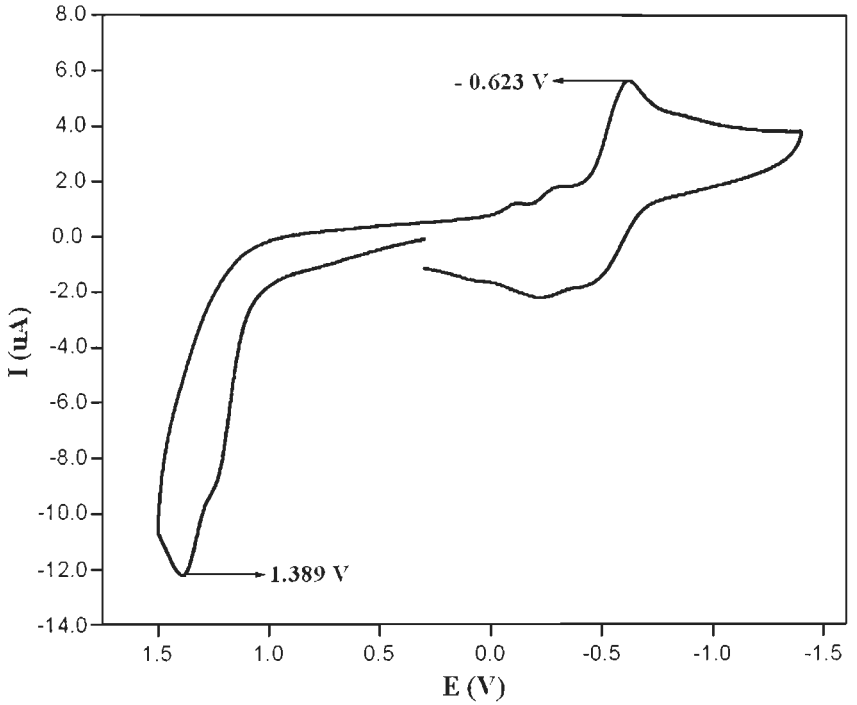

Fig. 2-42 Cyclic Voltammogram of **2j** in MeCN at room temperature (25 °C, 0.10 $[N(n\text{-}Bu)_4]PF_6$ supporting electrolyte; recorded at a scan rate of 0.20 V s^{-1} at a glassy carbon electrode

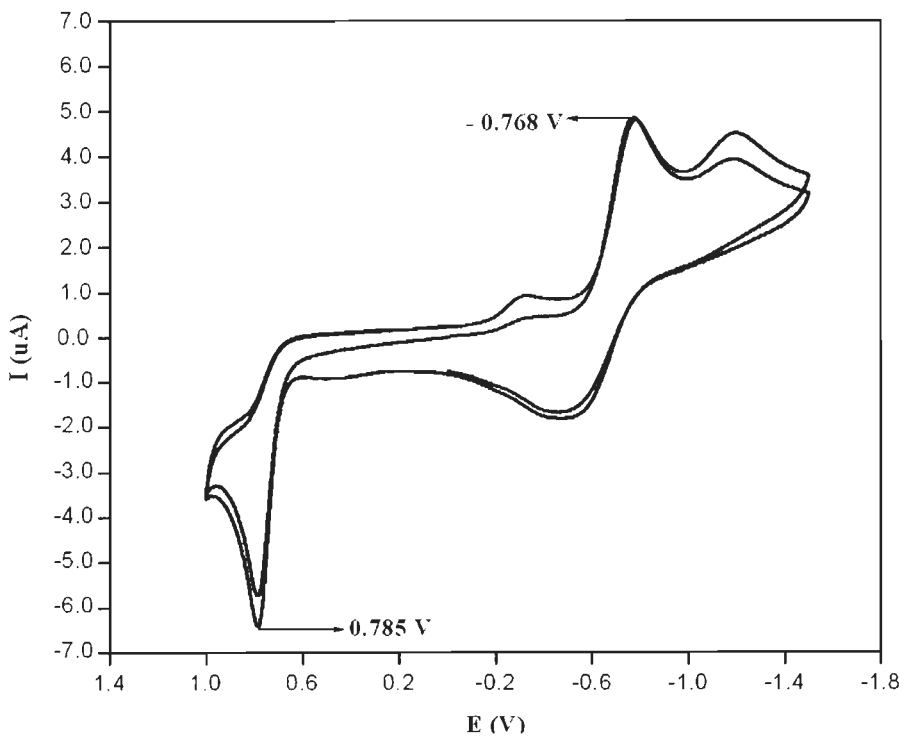

Fig. 2-43 Cyclic Voltammogram of **2l** in MeCN at room temperature (25 °C, 0.10 $[N(n\text{-}Bu)_4]PF_6$ supporting electrolyte; recorded at a scan rate of 0.20 V s^{-1} at a glassy carbon electrode

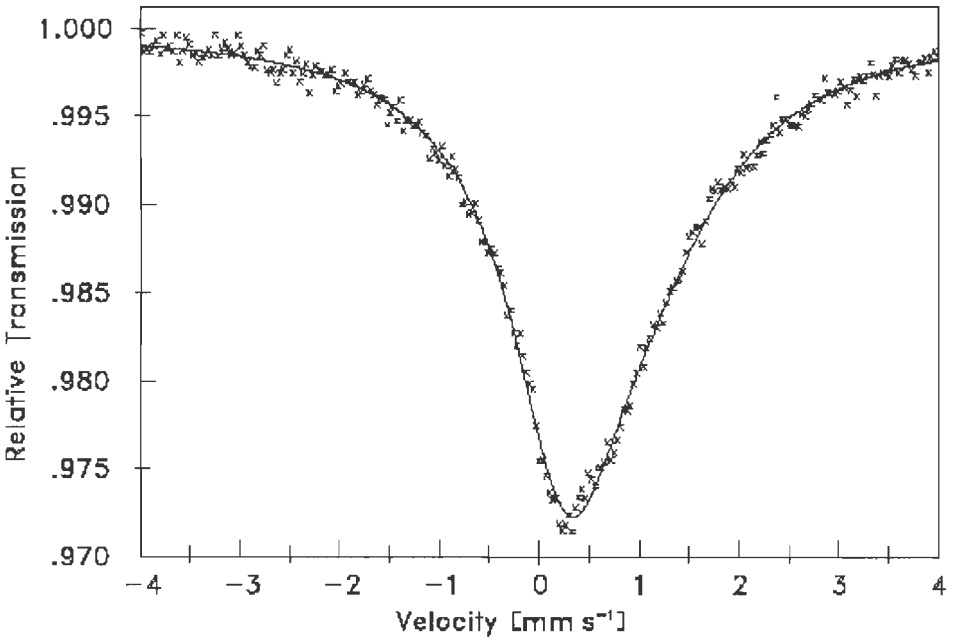

Fig. 2-44 Zero-field Mossbauer spectra measured at 80 K of **2l** before photolysis

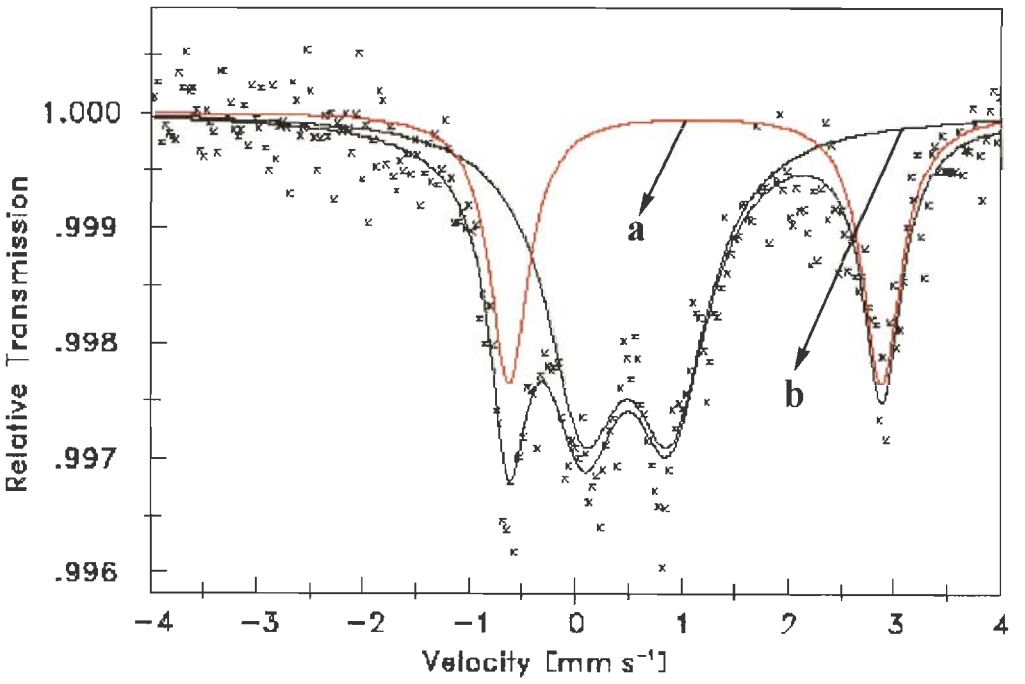

Fig. 2-45 Zero-field Mossbauer spectra measured at 80 K of **2l** after photolysis

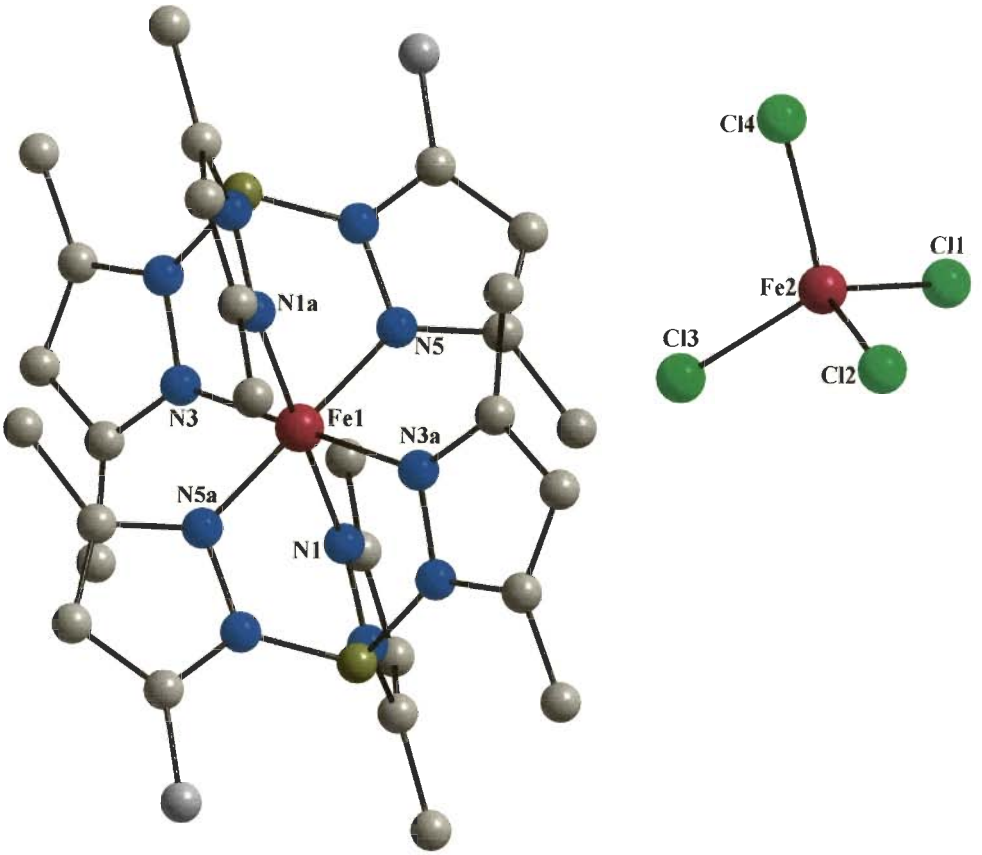

Fig. 2-46 Crystal structure of $[Tp^{Me2})_2Fe][FeCl_4]$ **2m**

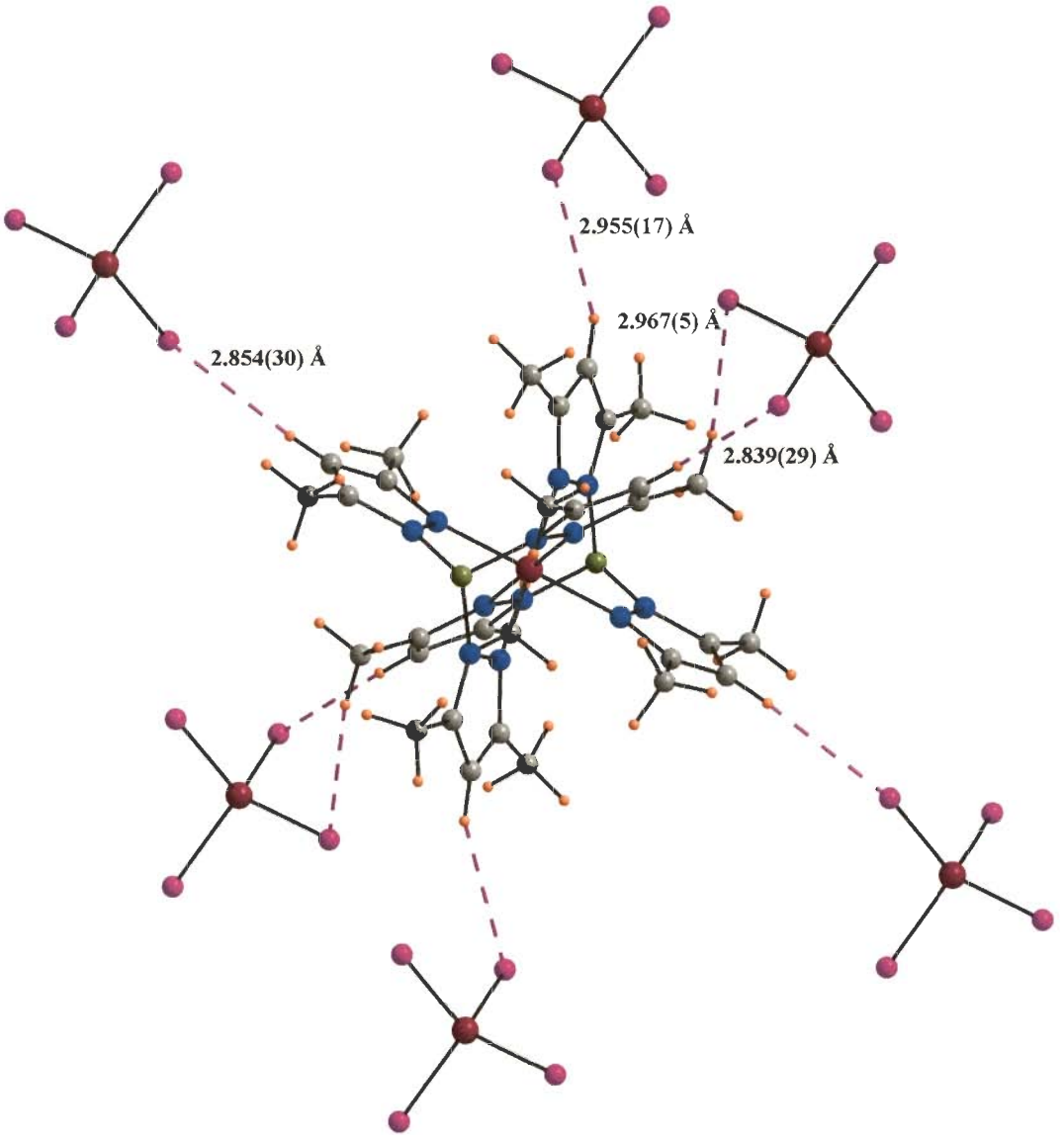

Fig. 2-47 Intermolecular C-H···Cl interactions shown by one cation molecule with anion molecules in complex **2m**

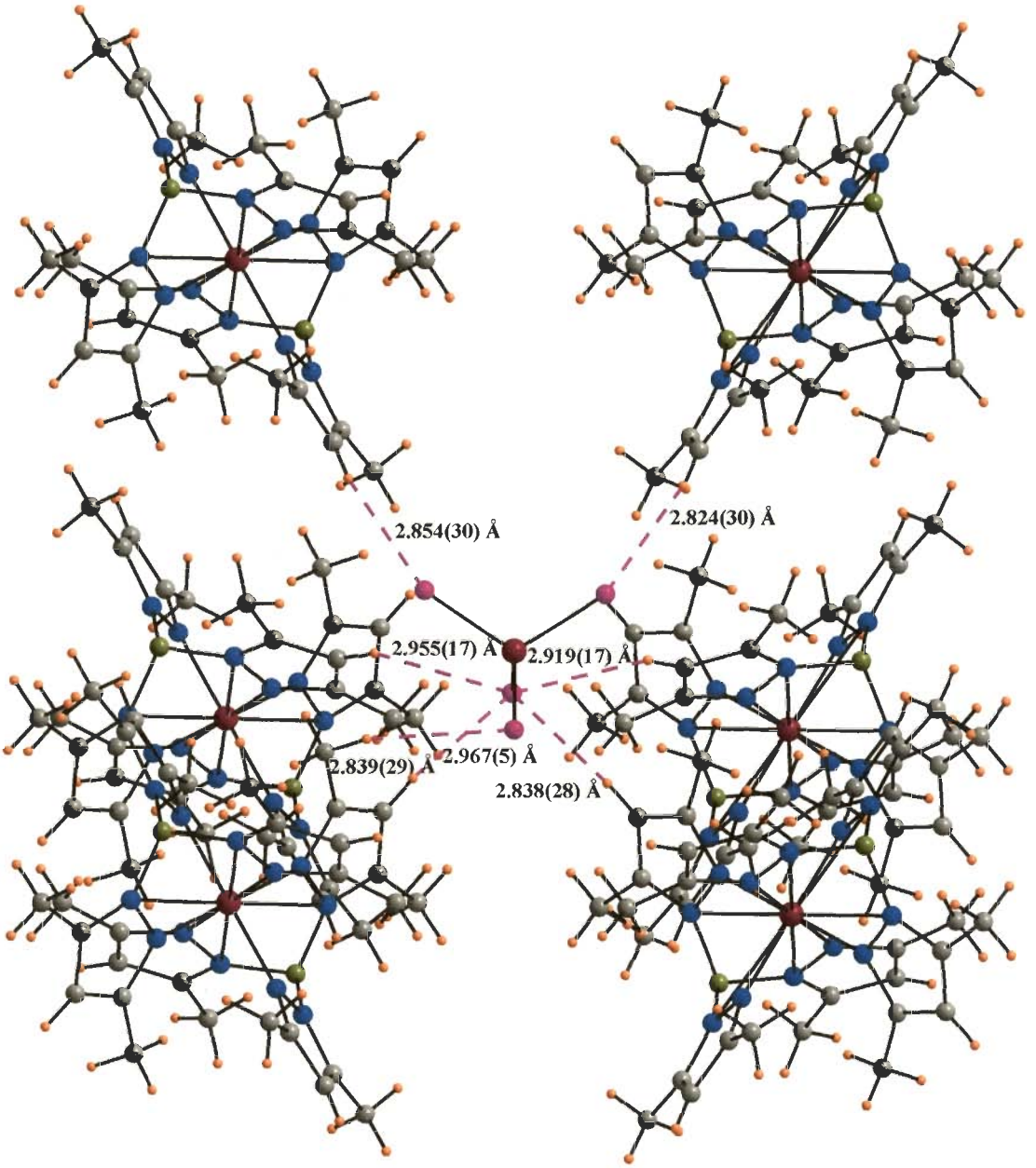

Fig. 2-48 Intermolecular C-H···Cl interactions shown by one anion molecule with cation molecules in complex **2m**

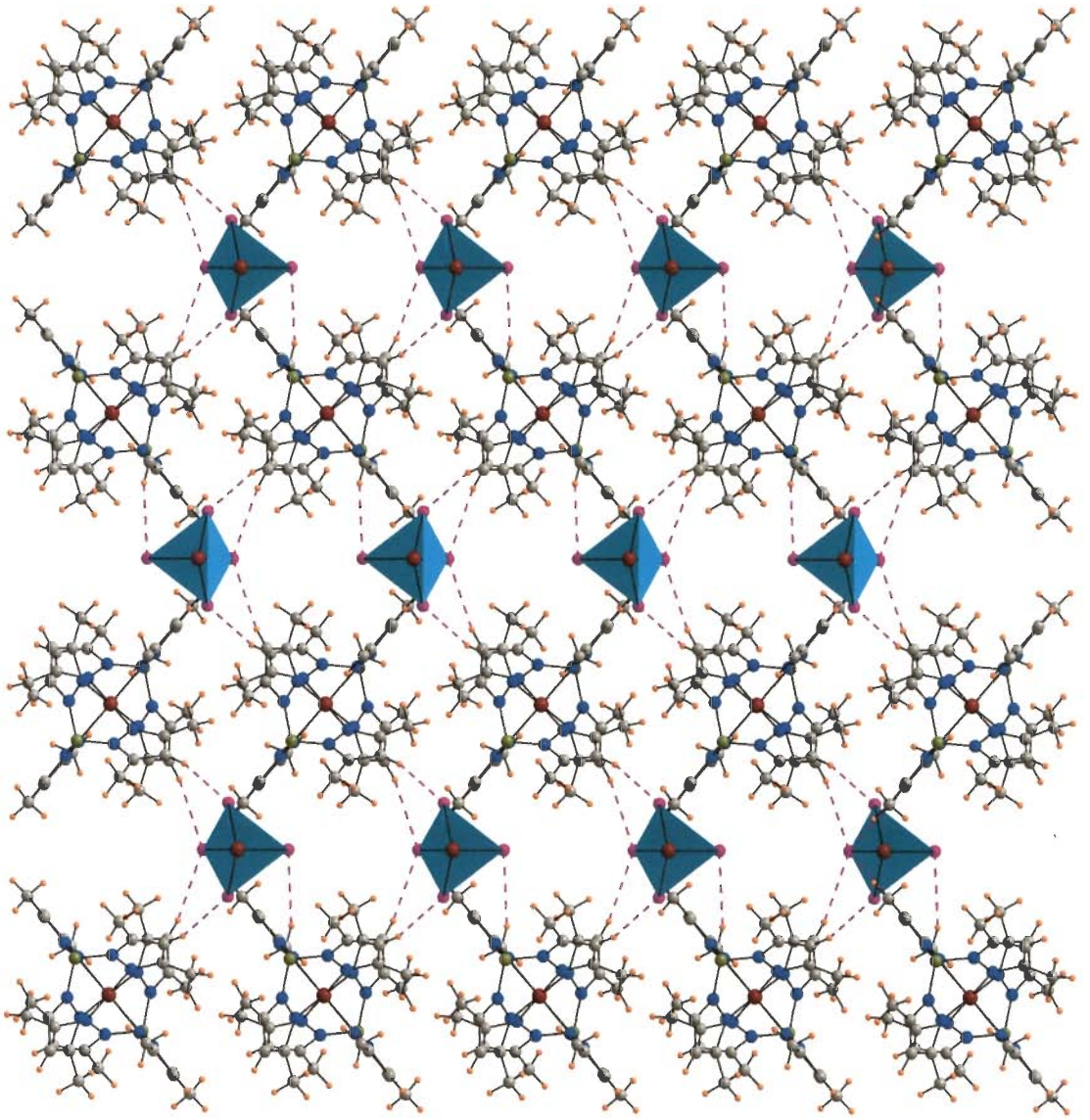

Fig. 2-49 Three-dimensional arrangement in complex **2m** due to C-H···Cl interactions

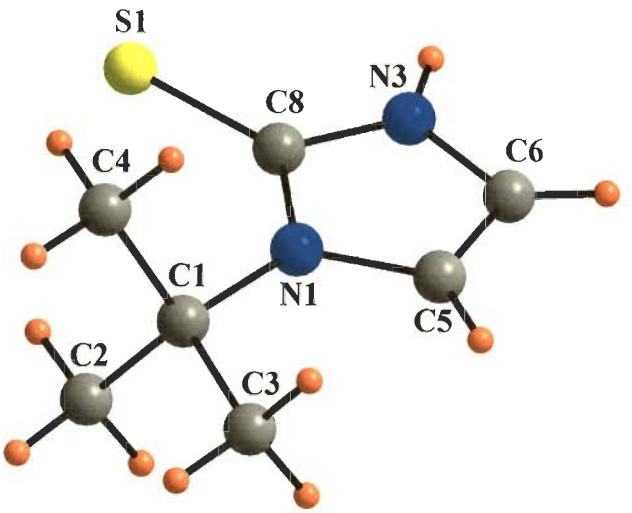

Fig. 2-50 Crystal structure of N-tert-butyl-2-thioimidazole [$tm^{t\text{-}Bu}$] **2n**

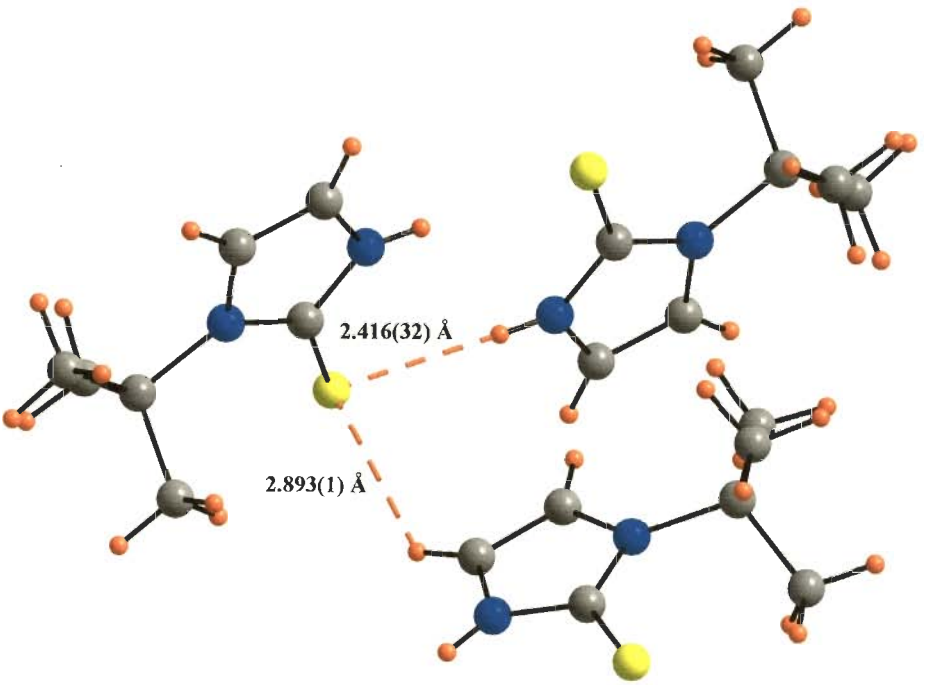

Fig. 2-51 Intermolecular C-H···S and N-H···S interactions present in **2n**

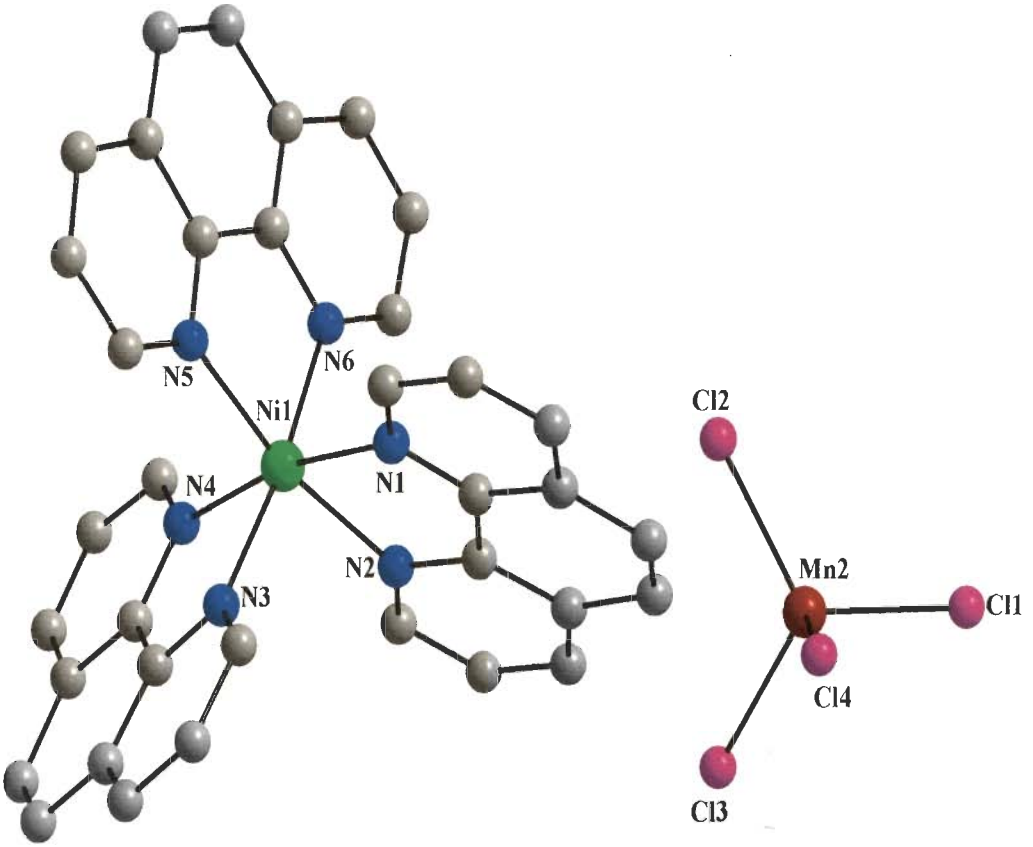

Fig. 2-52 Crystal structure of $[Ni(phen)_3]$ $[MnCl_4]$ **2p**

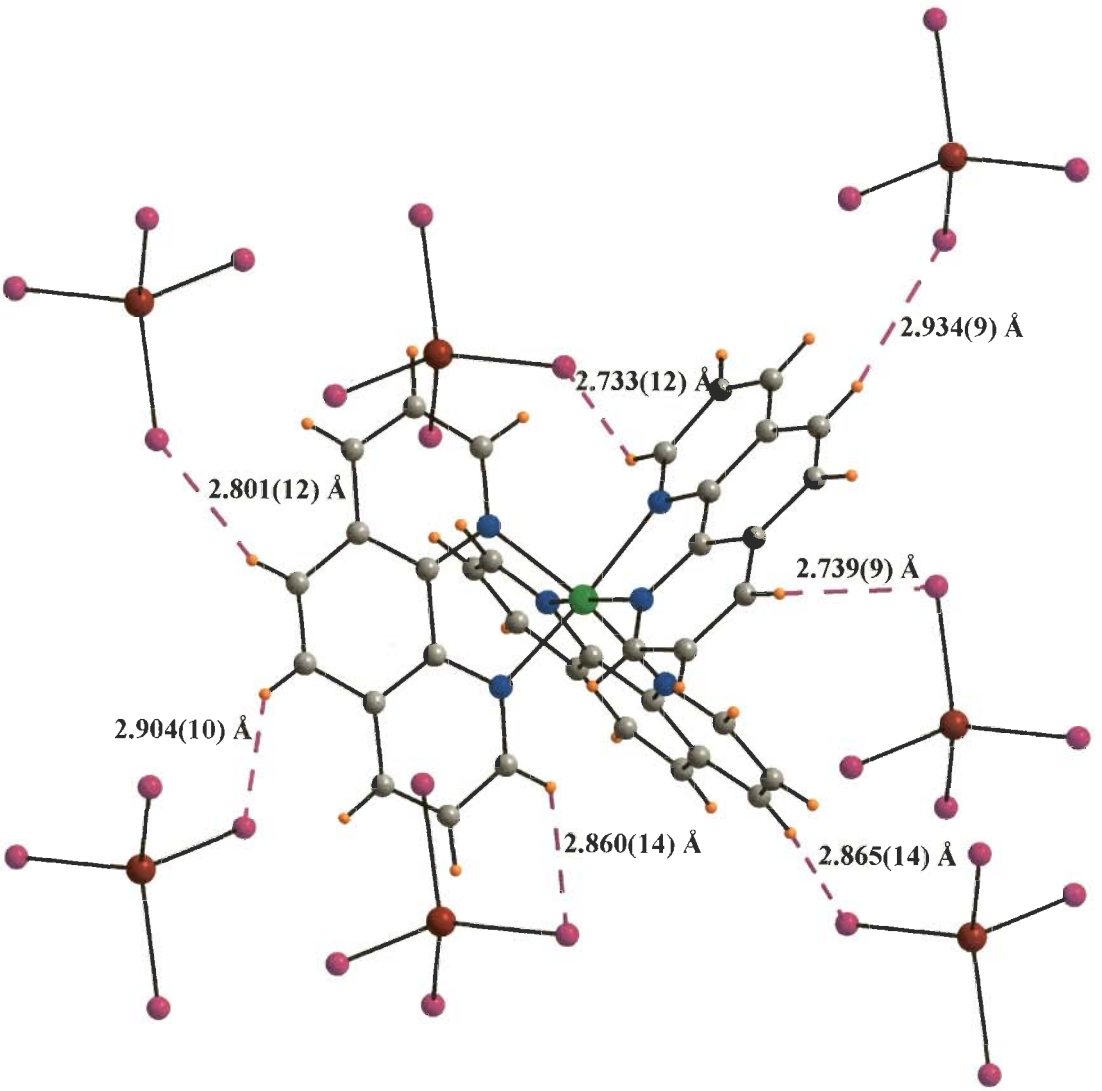

Fig. 2-53 Intermolecular C-H···Cl interactions shown by one cation molecule with anion molecules in complex **2p**

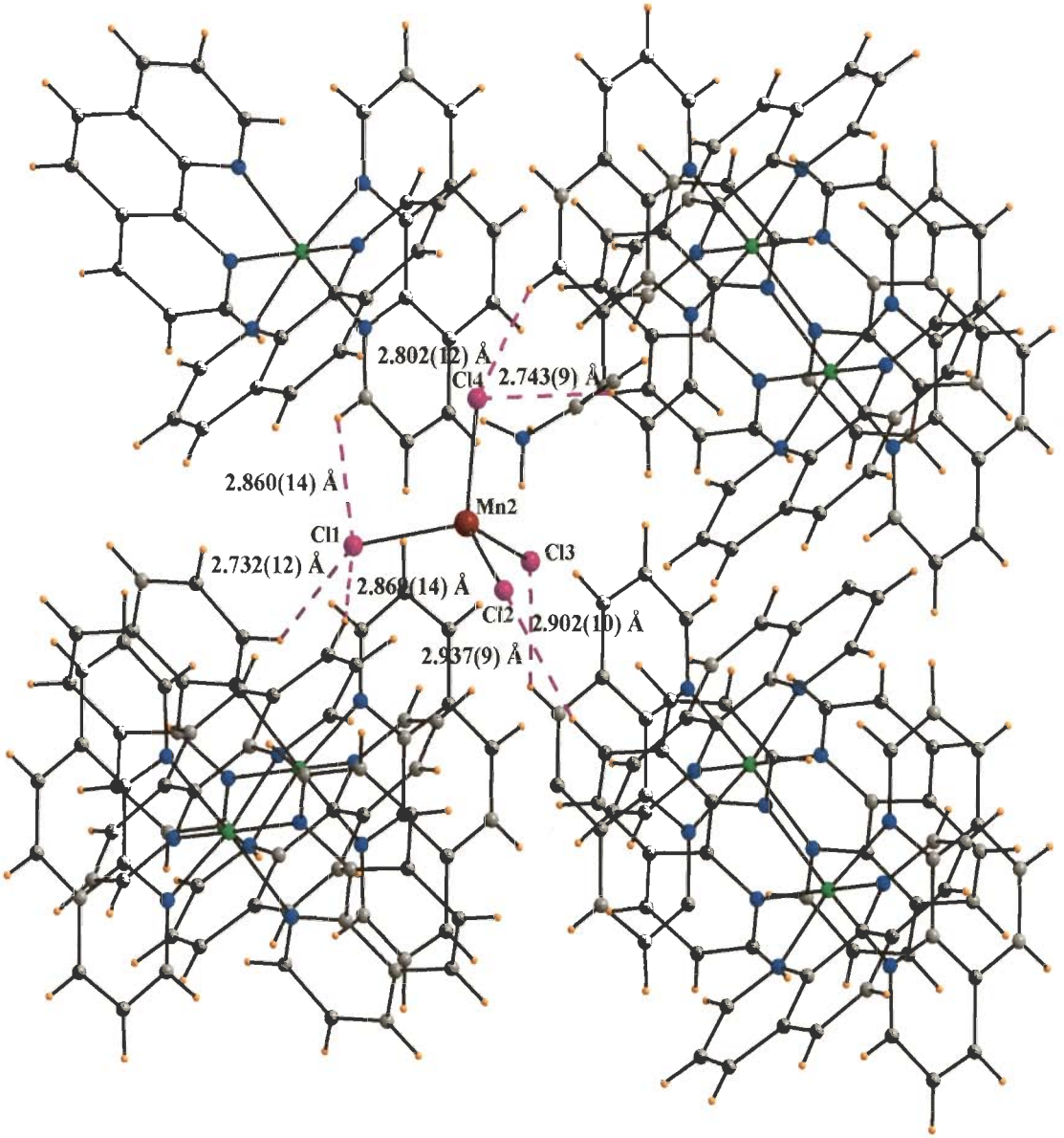

Fig. 2-54 Intermolecular C-H···Cl interactions shown by one anion molecule with cation molecules in complex **2p**

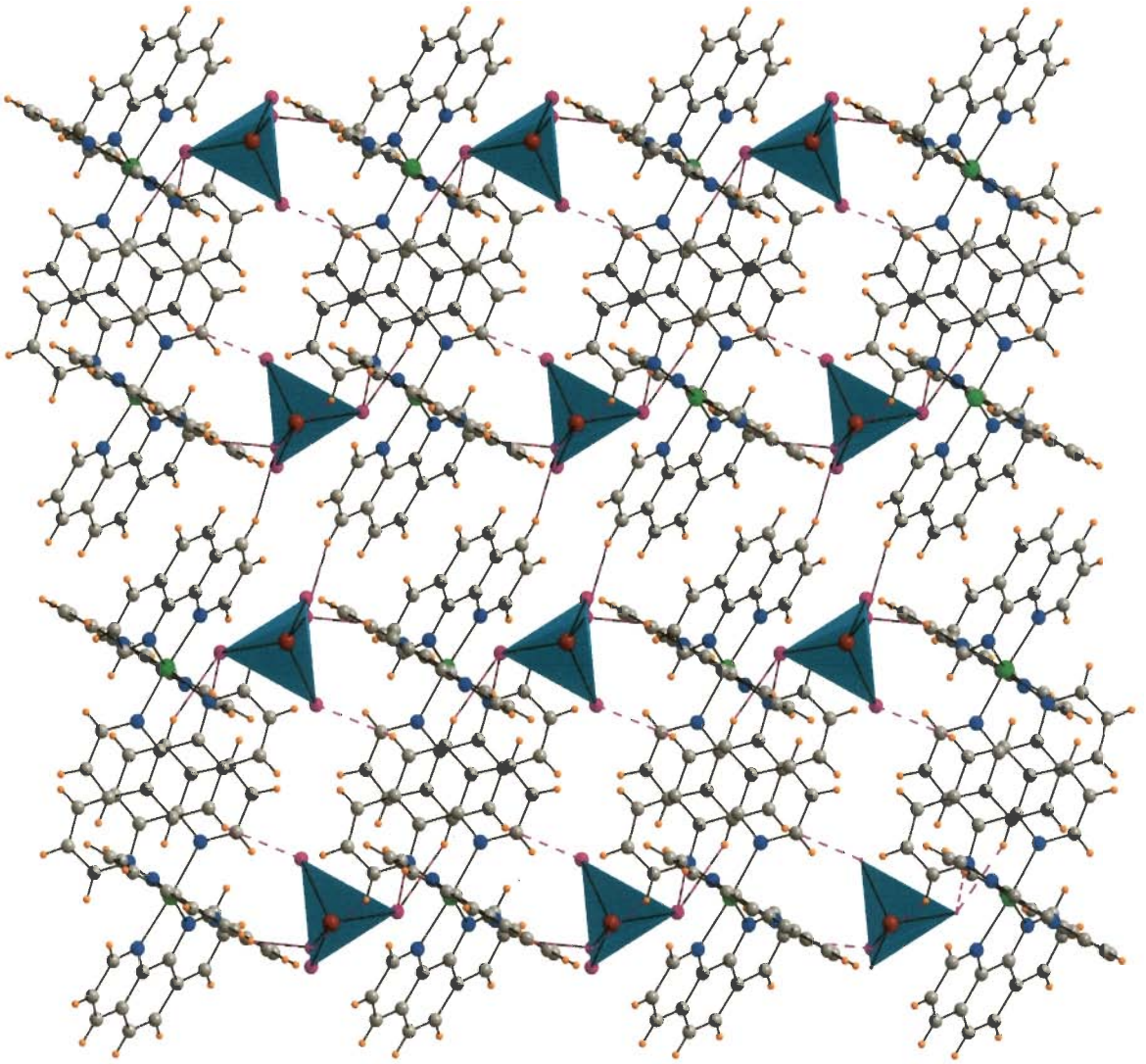

Fig. 2-55 Three-dimensional arrangement in complex **2p** due to C-H···Cl interactions

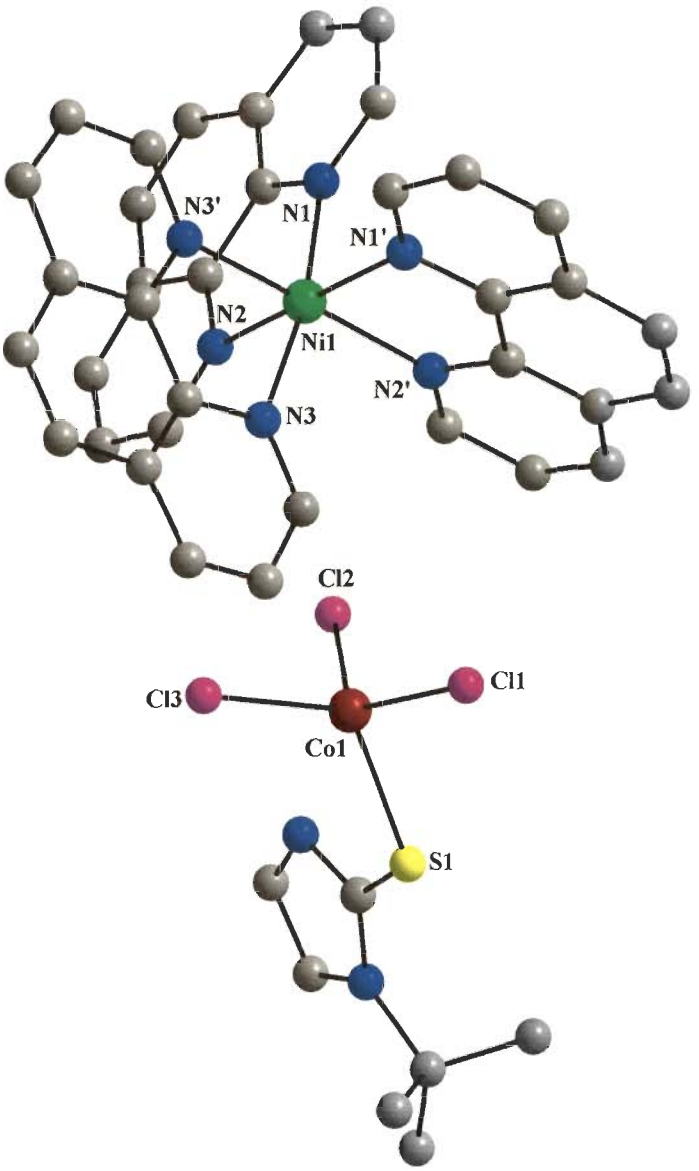

Fig. 2-56 Crystal structure of $[Ni(phen)_3]$ $[Co(tm^{t\text{-}Bu})Cl_3]_2$ **2q**

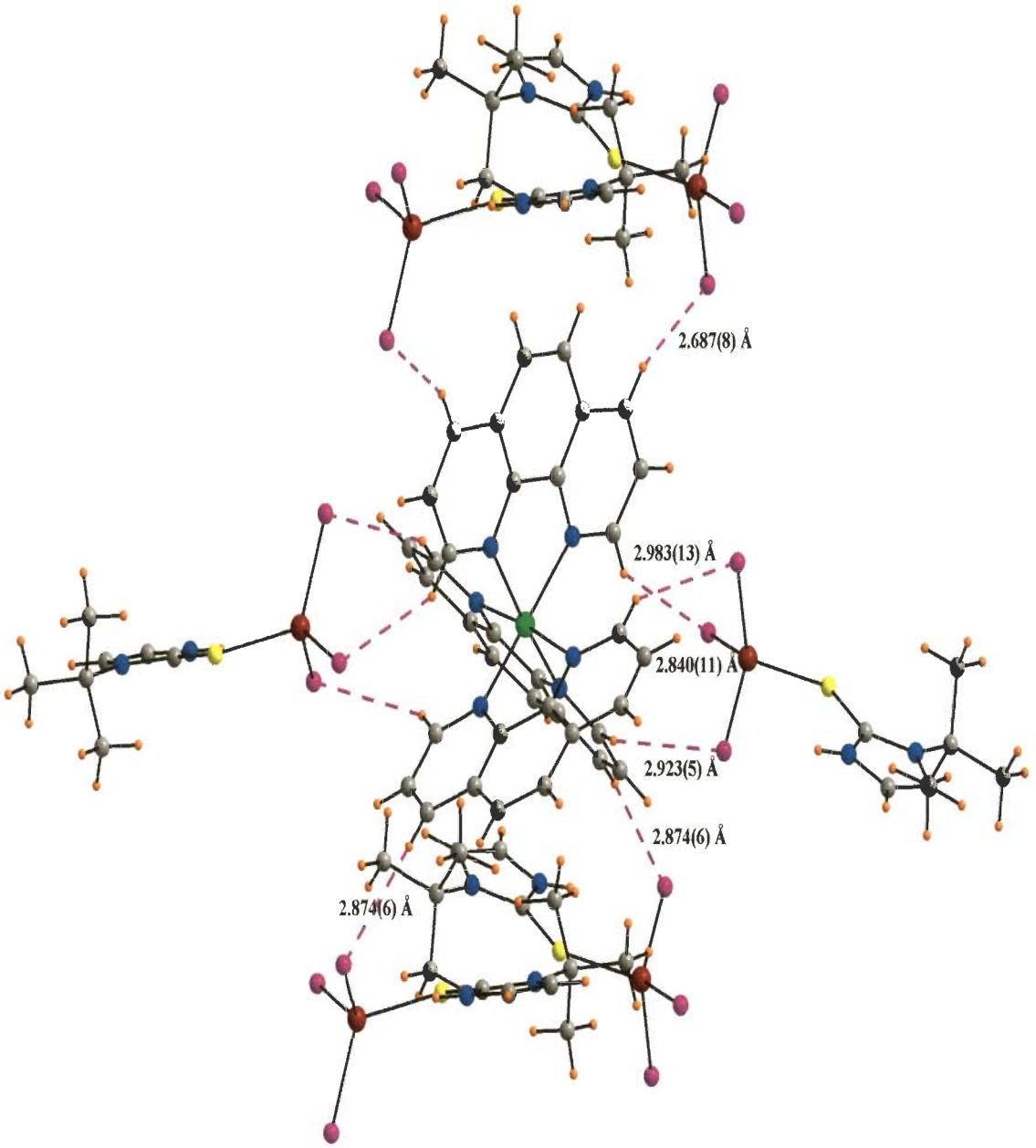

Fig. 2-57 Intermolecular C-H···Cl interactions shown by one cation molecule with anion molecules in complex **2q**

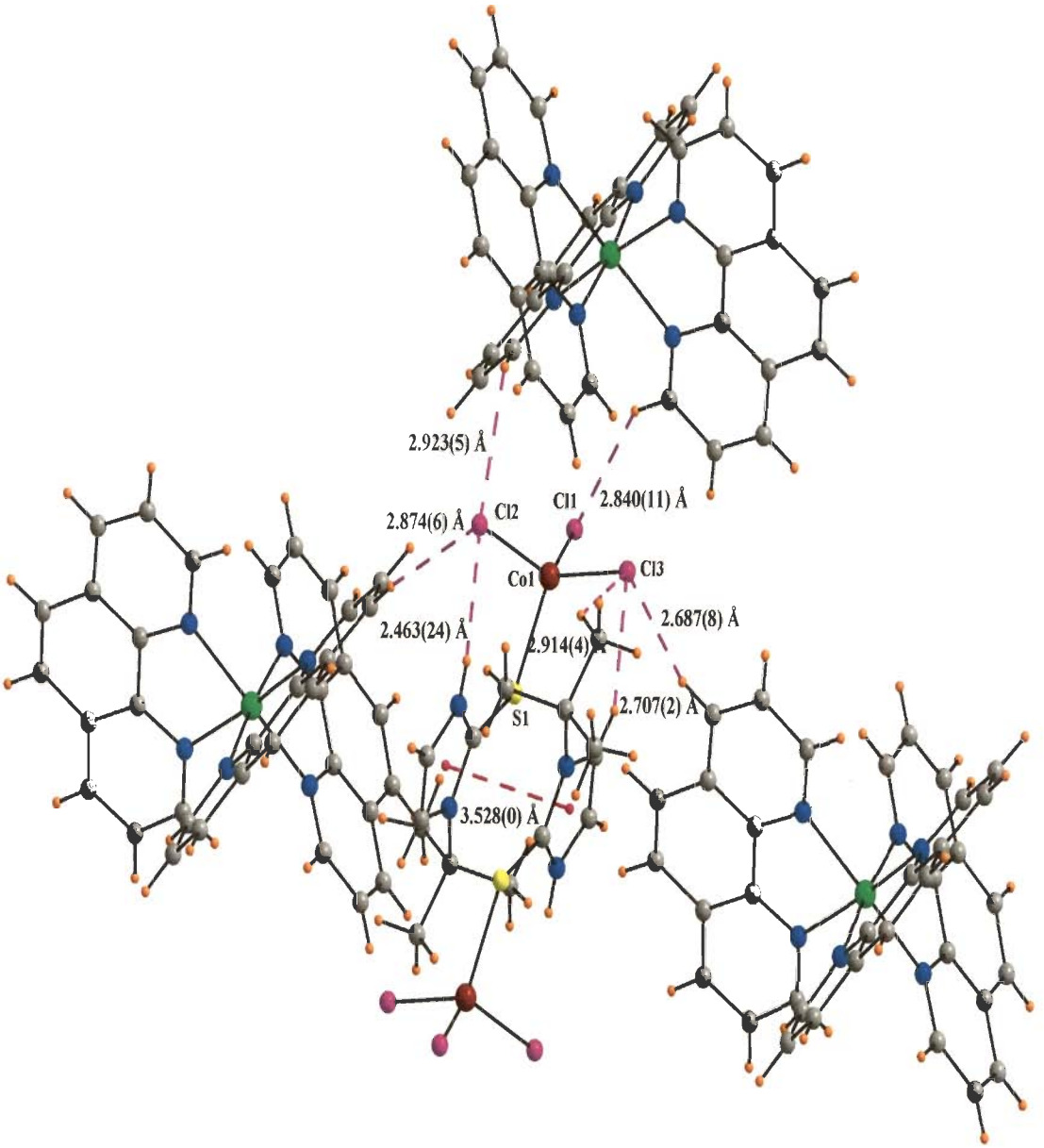

Fig. 2-58 Intermolecular C-H···Cl interactions shown by one anion molecule with cation molecules in complex **2q**

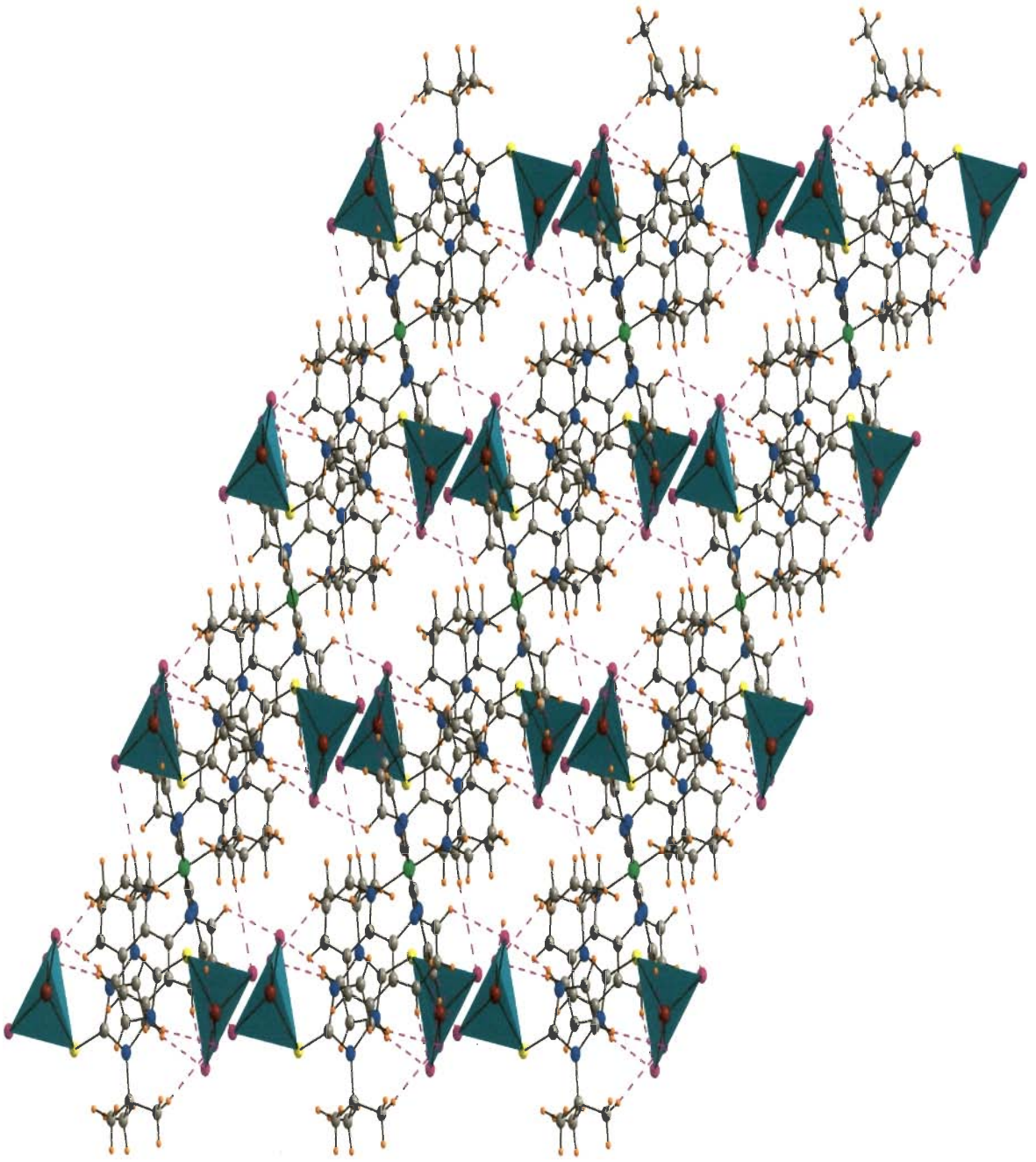

Fig. 2-59 Three-dimensional arrangement in complex **2q** due to C-H···Cl interactions

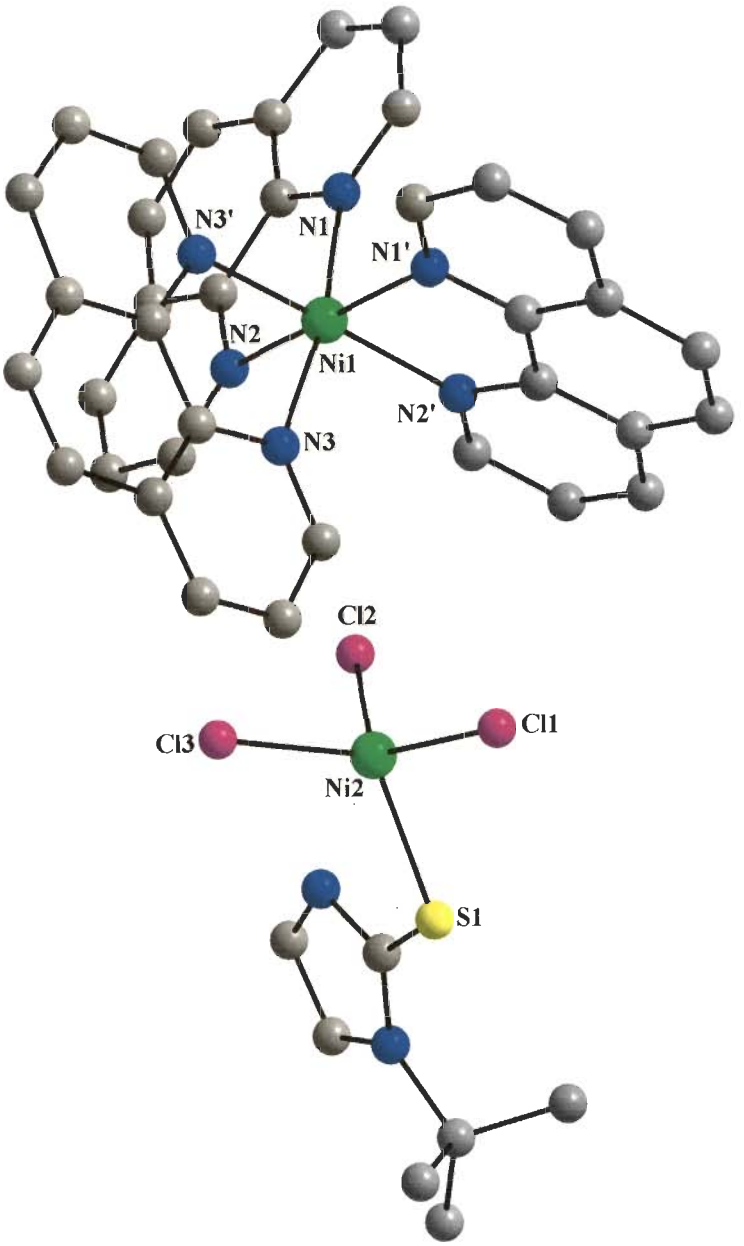

Fig. 2-60 Crystal structure of $[Ni(phen)_3]$ $[Ni(tm^{t\text{-}Bu})Cl_3]_2$ **2r**

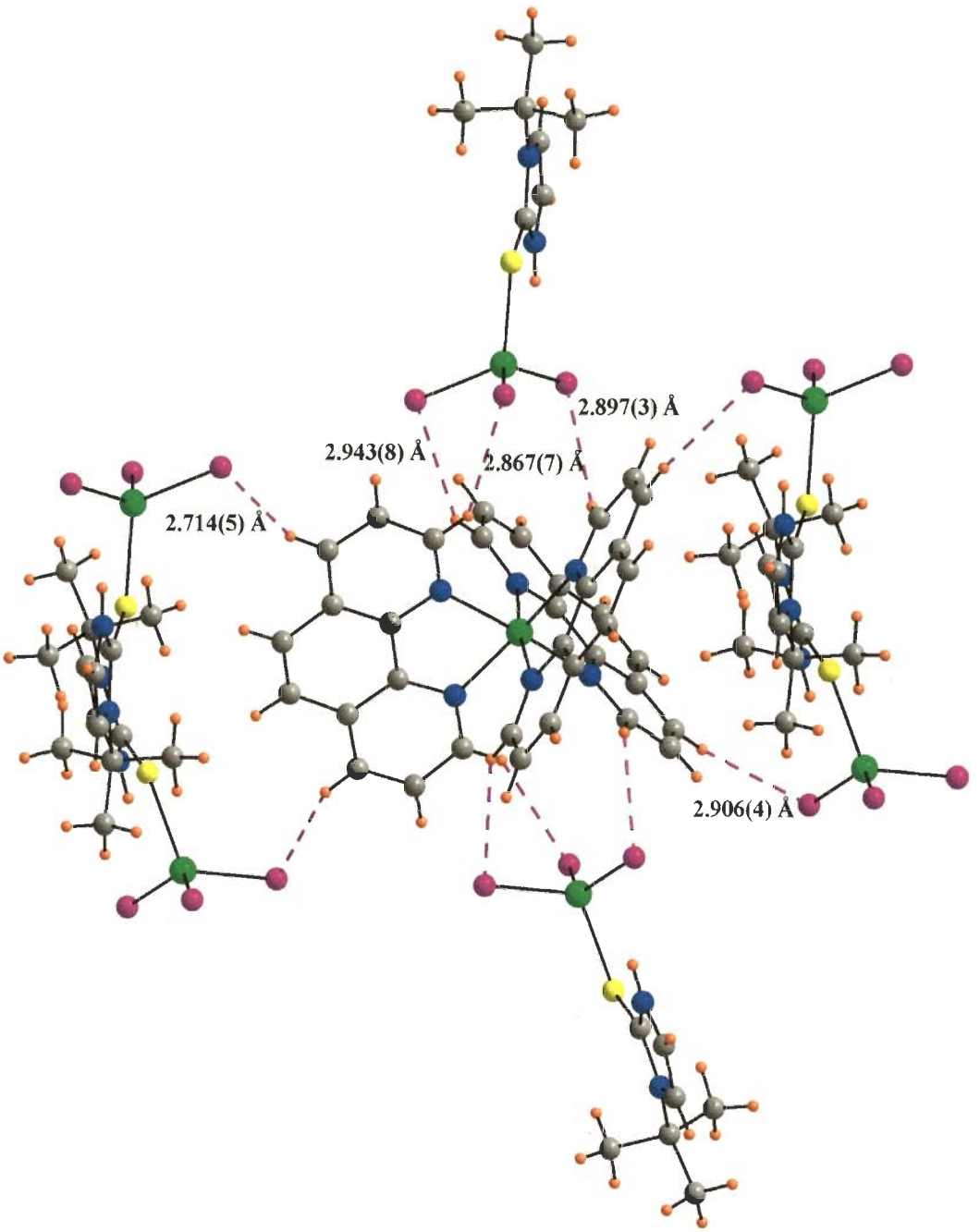

Fig. 2-61 Intermolecular C-H···Cl interactions shown by one cation molecule with anion molecules in complex **2r**

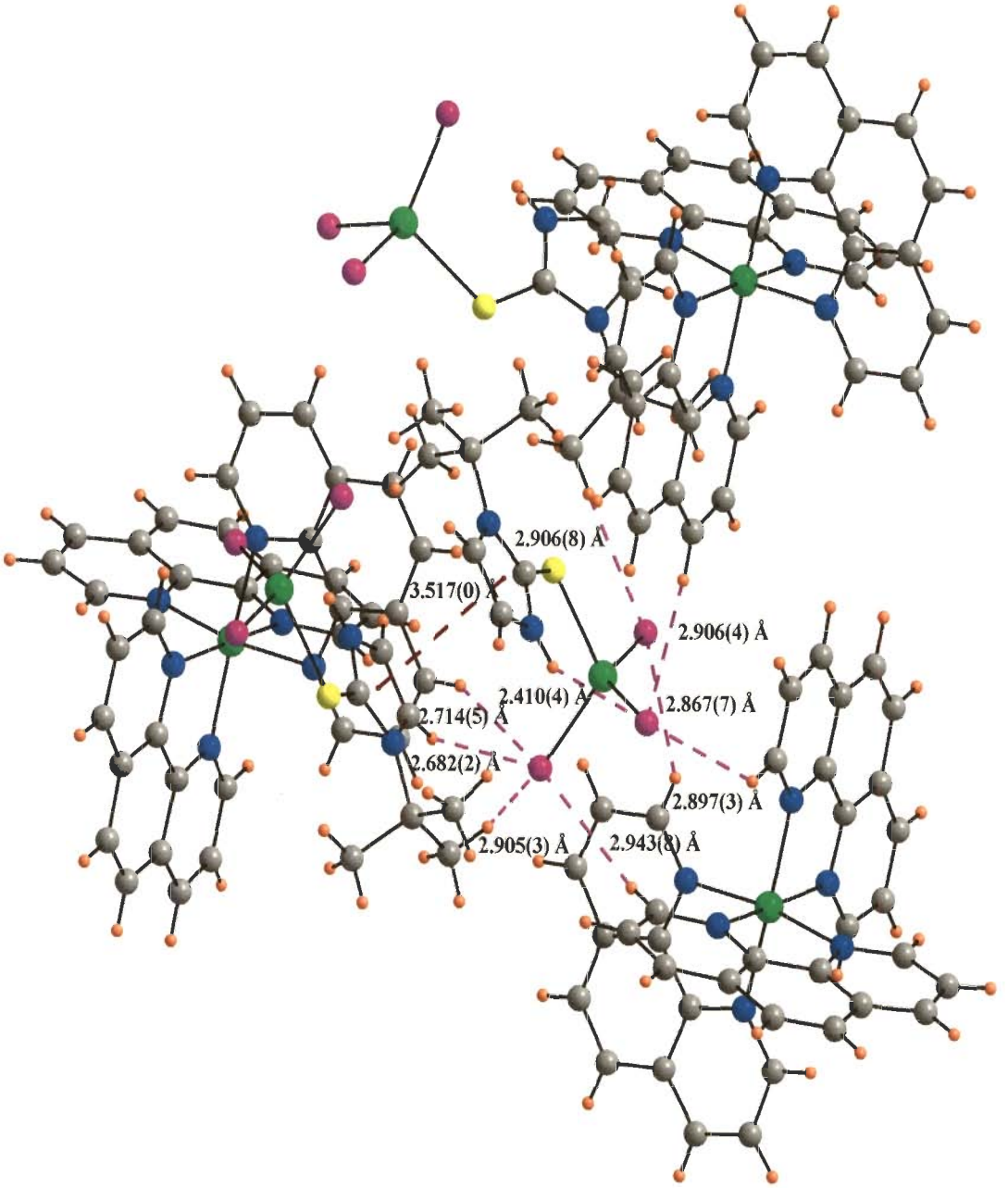

Fig. 2-62 Intermolecular C-H···Cl interactions shown by one anion molecule with cation molecules in complex **2r**

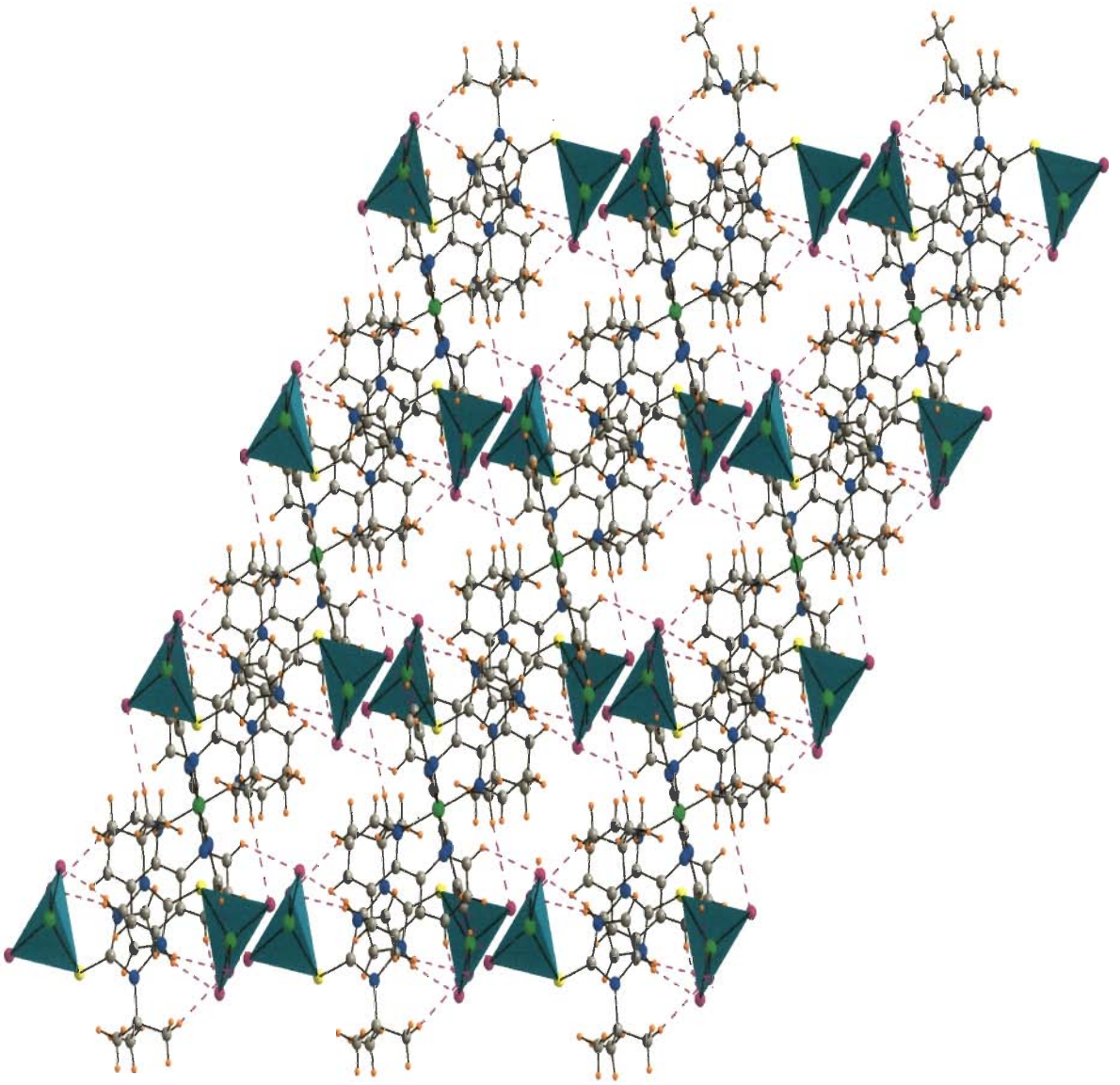

Fig. 2-63 Three-dimensional arrangement in complex **2r** due to C-H···Cl interactions

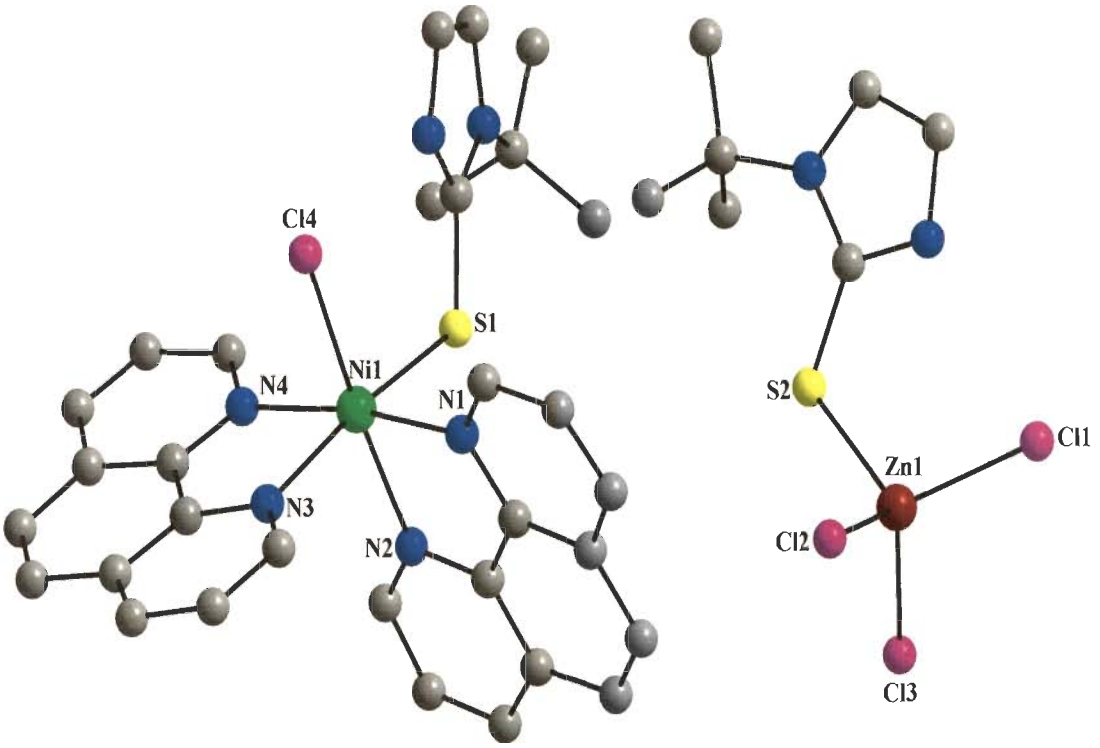

Fig. 2-64 Crystal structure of $[Ni(phen)_2(tm^{t\text{-}Bu})Cl)]$ $[Zn(tm^{t\text{-}Bu})Cl_3]$ **2t**

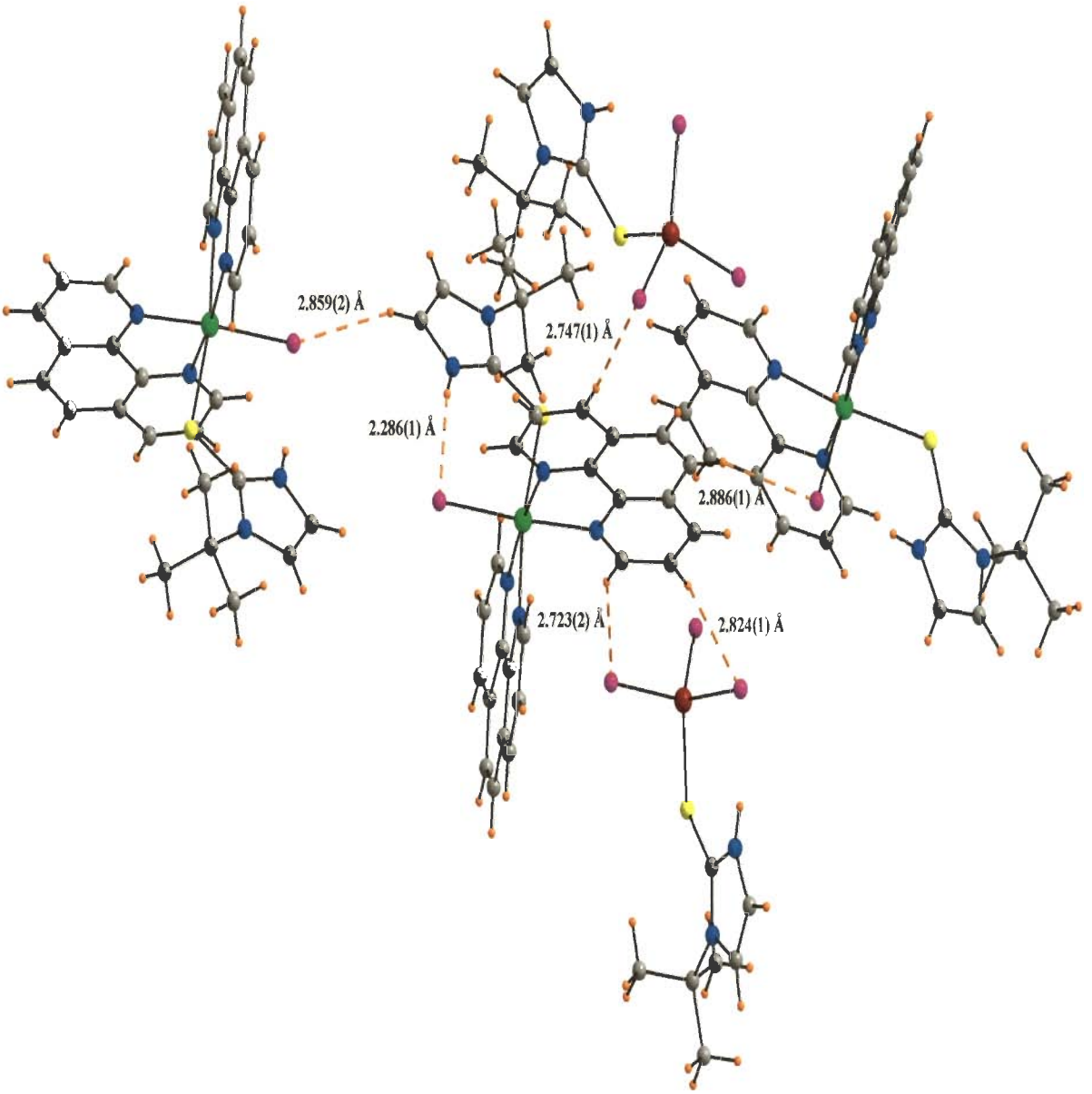

Fig. 2-65 Intermolecular C-H···Cl interactions shown by one cation molecule with anion molecules in complex **2t**

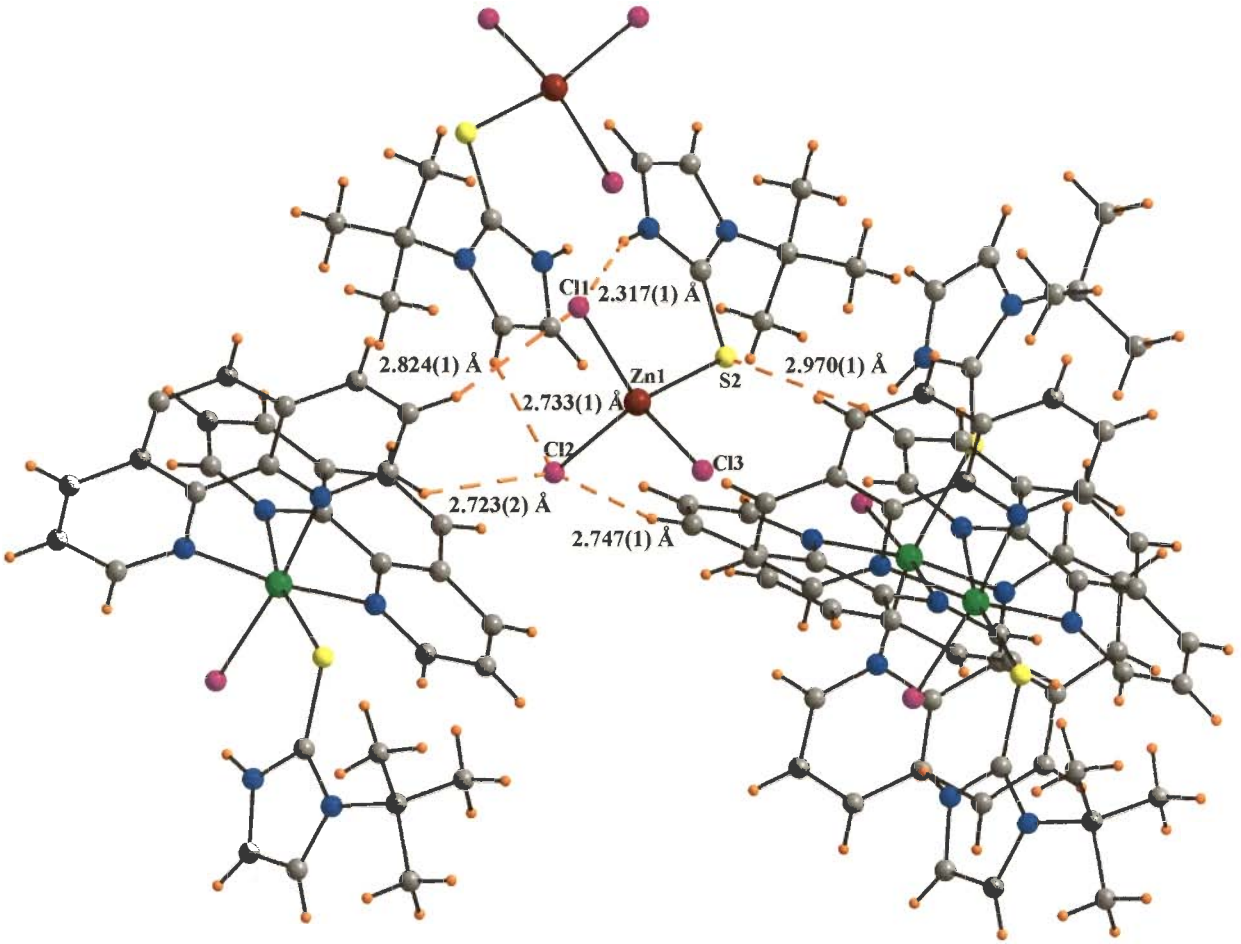

Fig. 2-66 Intermolecular C-H···Cl interactions shown by one anion molecule with cation molecules in complex **2t**

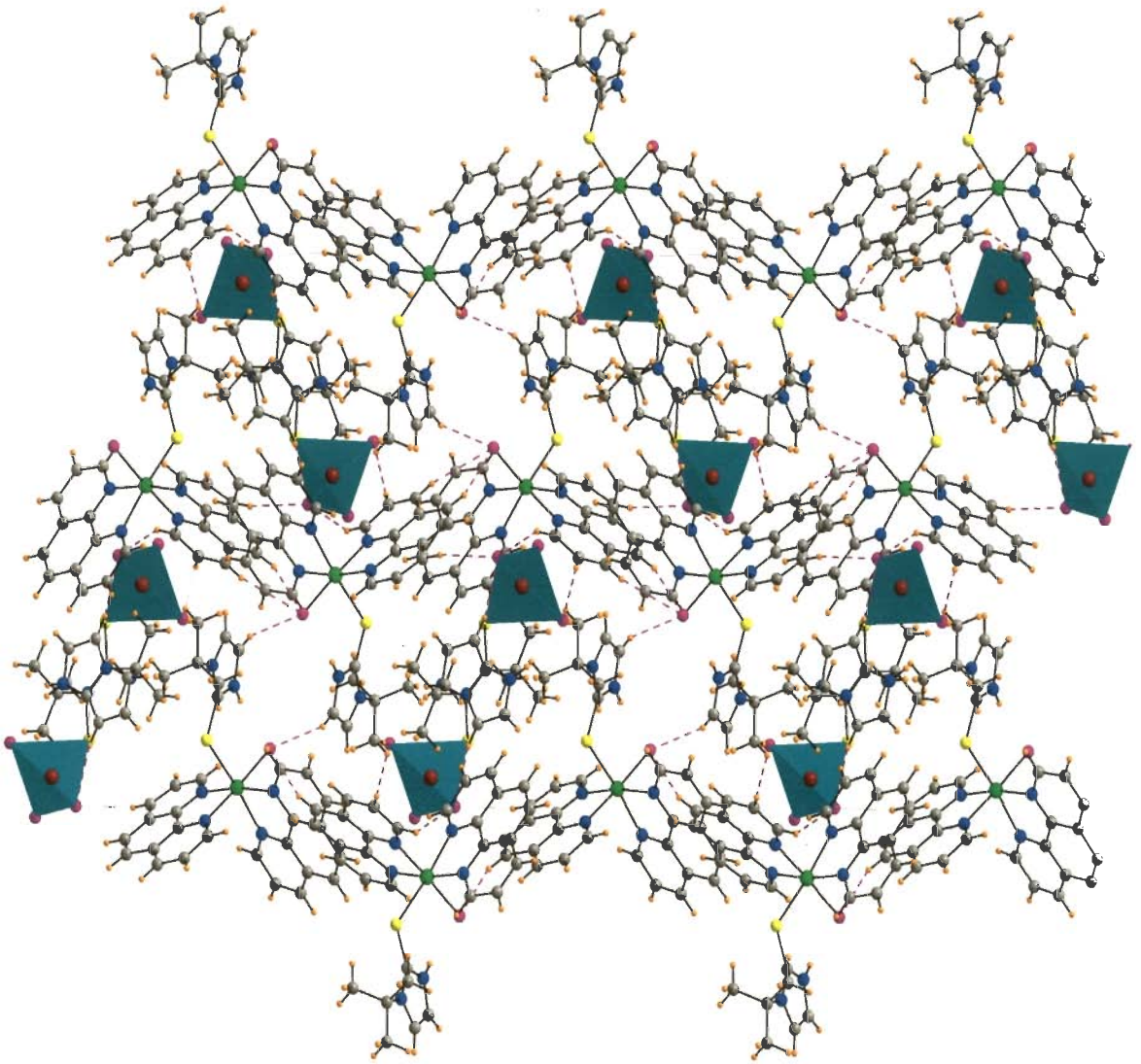

Fig. 2-67 Three-dimensional arrangement in complex **2t** due to C-H···Cl interactions

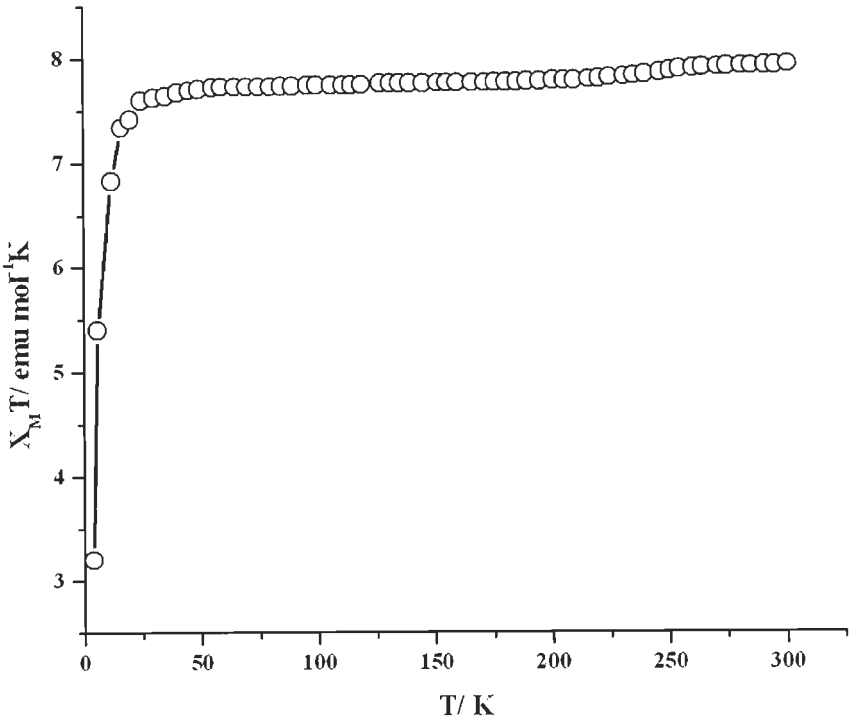

Fig. 2-68 Tempreature dependence of the $\chi_M T$ product for complex **2p**

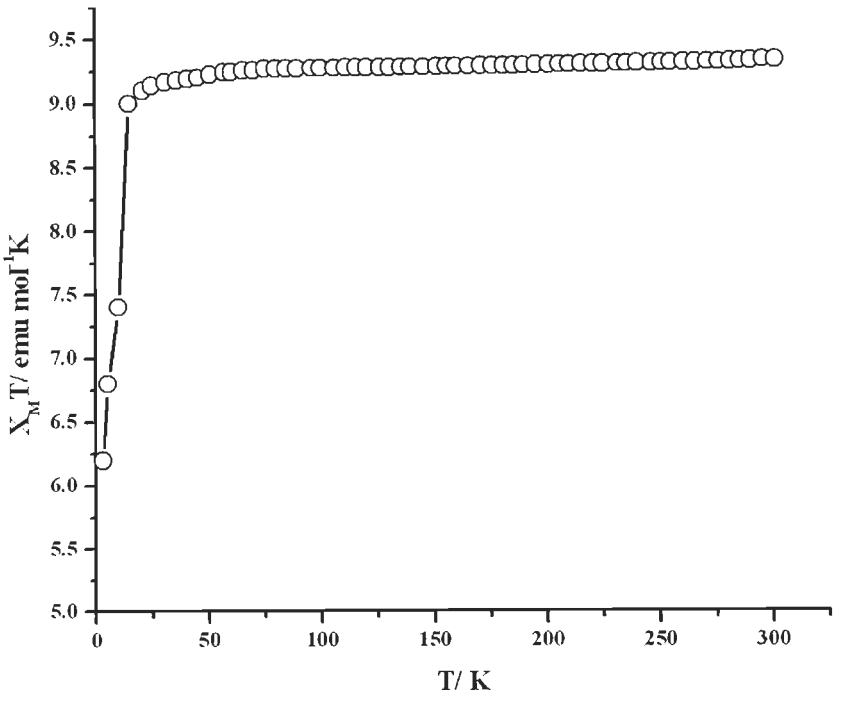

Fig. 2-69 Tempreature dependence of the $\chi_M T$ product for complex **2q**

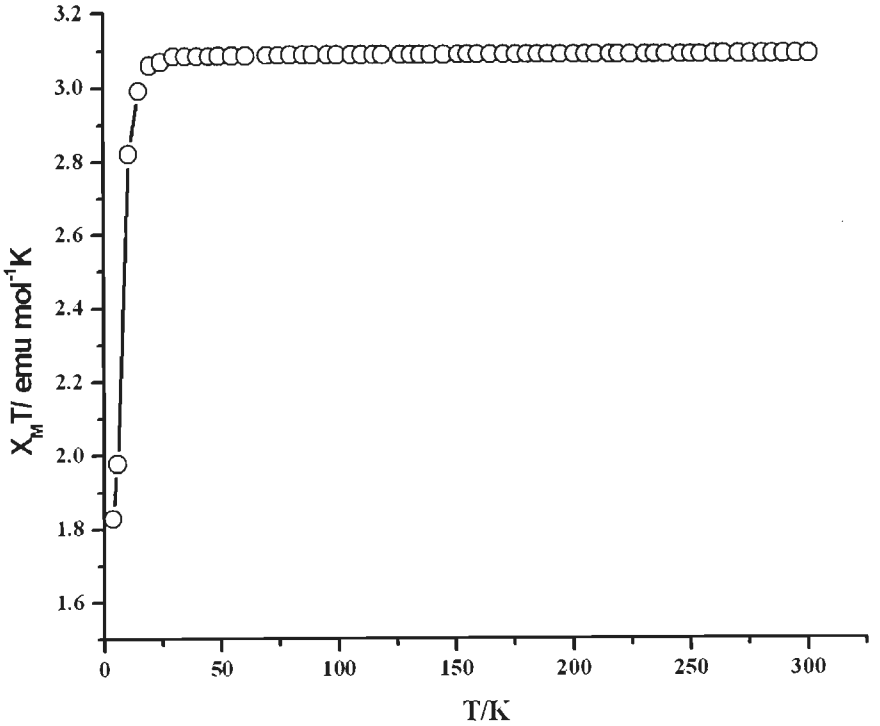

Fig. 2-70 Tempreature dependence of the $\chi_M T$ product for complex **2r**

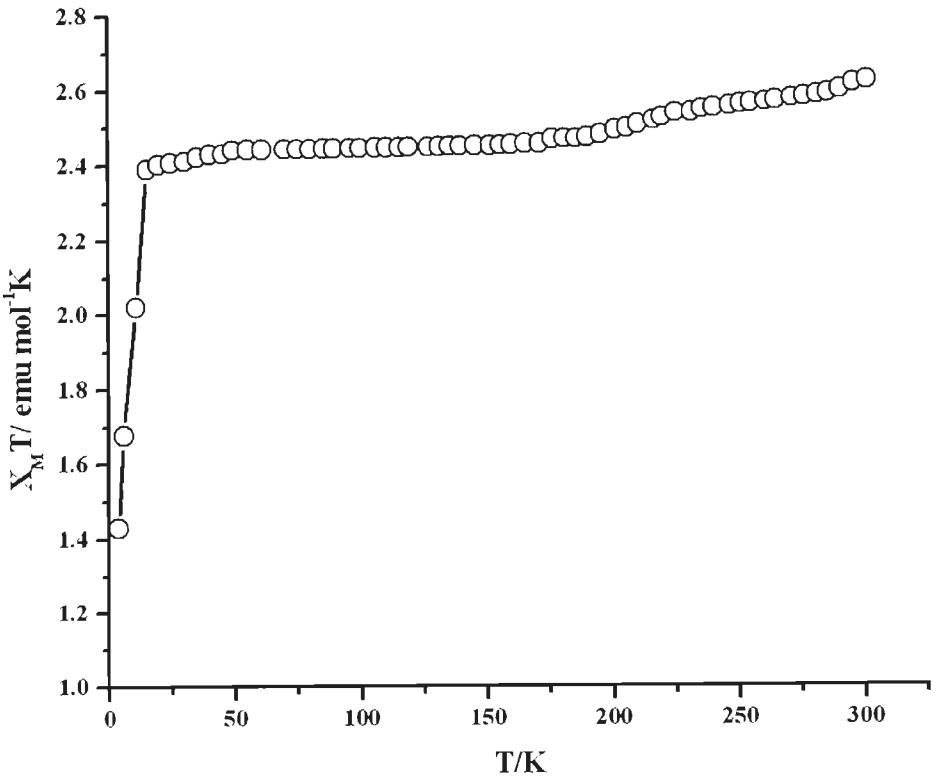

Fig. 2-71 Tempreature dependence of the $\chi_M T$ product for complex **2t**

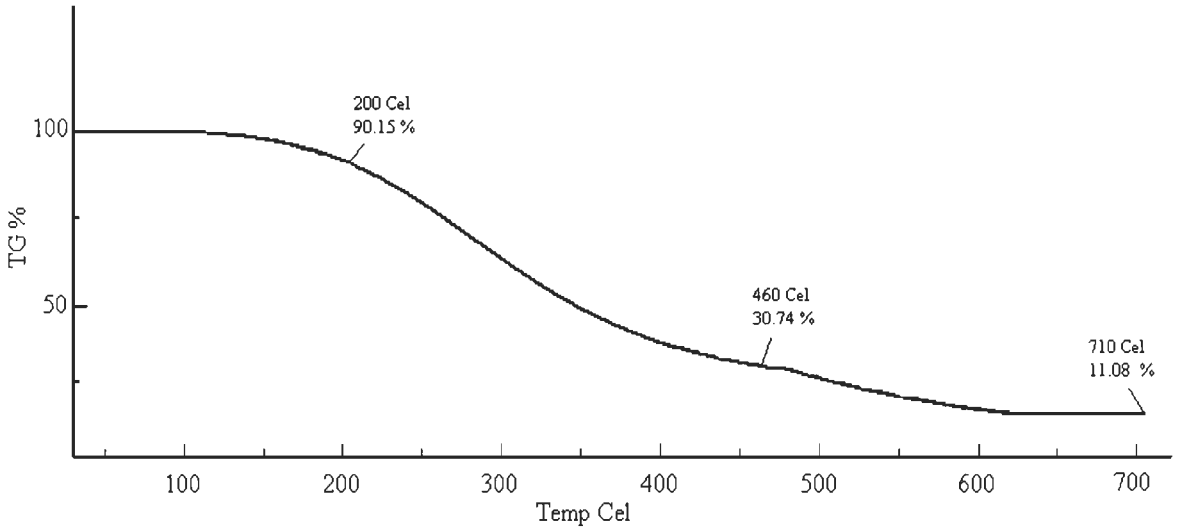

Fig. 2-72 TGA plot for complex **2p**

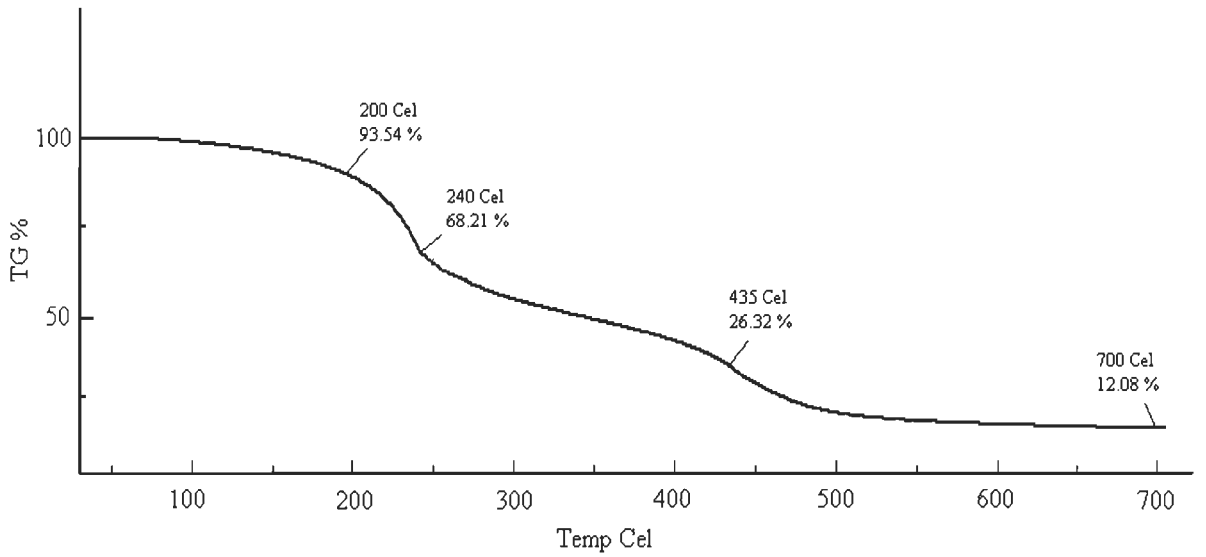

Fig. 2-73 TGA plot for complex **2q**

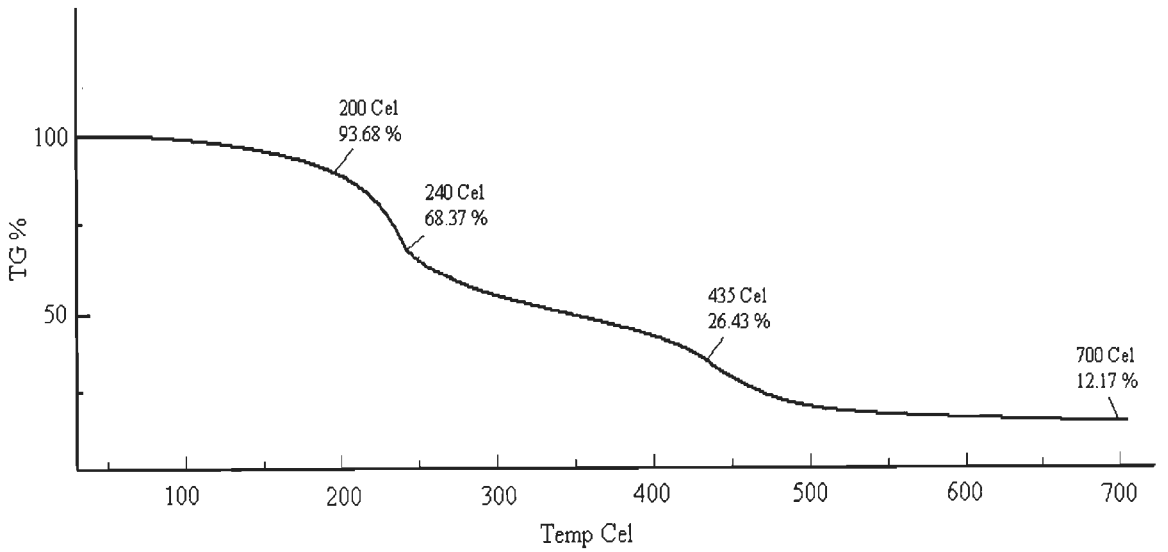

Fig. 2-74 TGA plot for complex **2r**

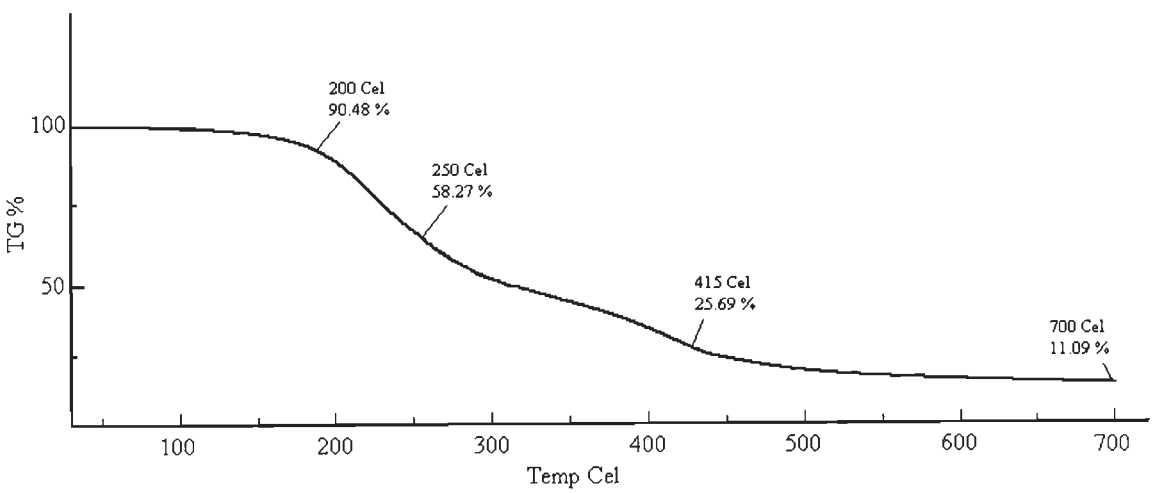

Fig. 2-75 TGA plot for complex **2t**

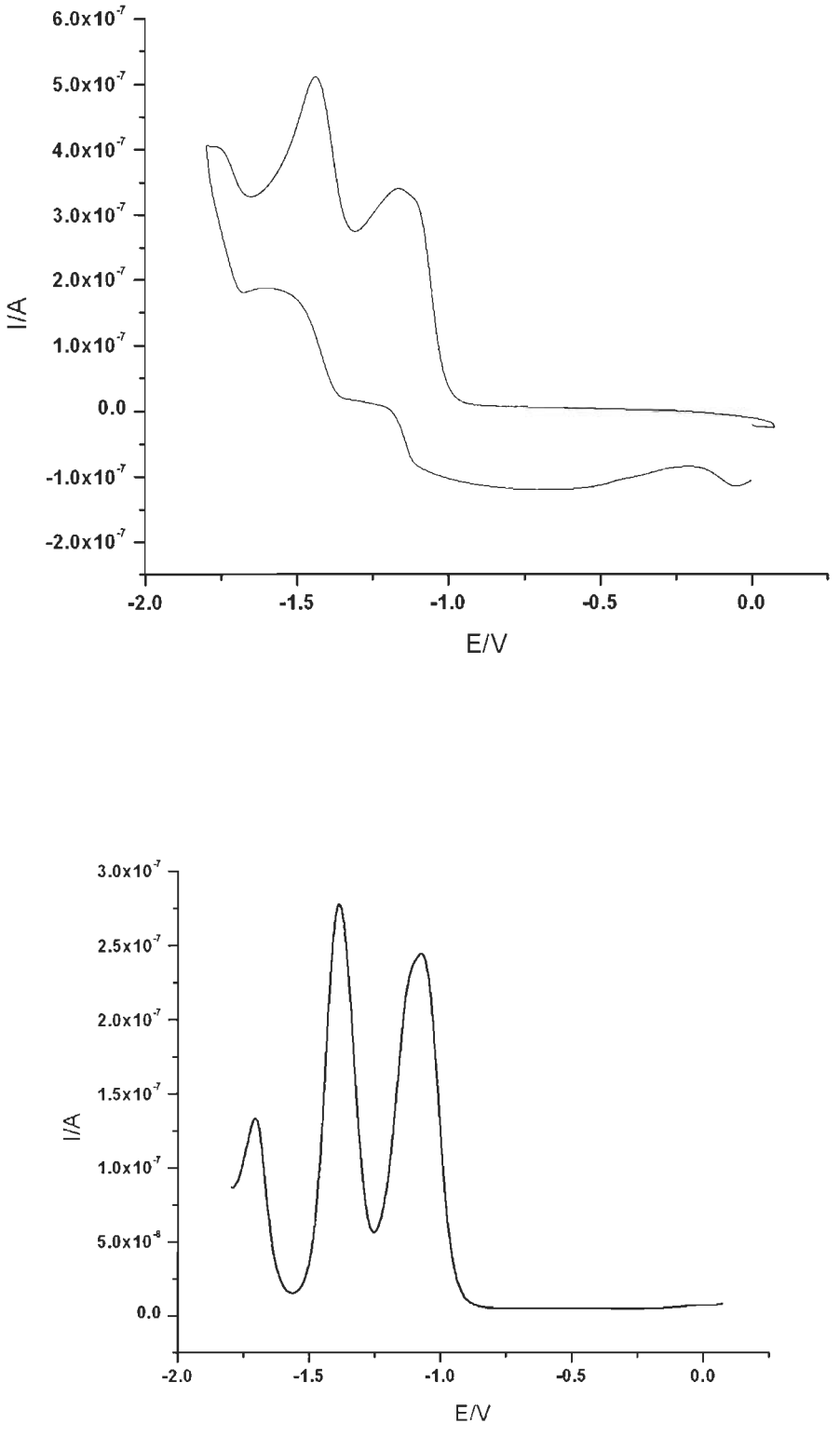

Fig. 2-76 Cyclic and differential pulse voltammograms of complex **2p** in 0.1 M TBAP/ DMSO electrolyte system at 0.1 V s^{-1} scan rate.

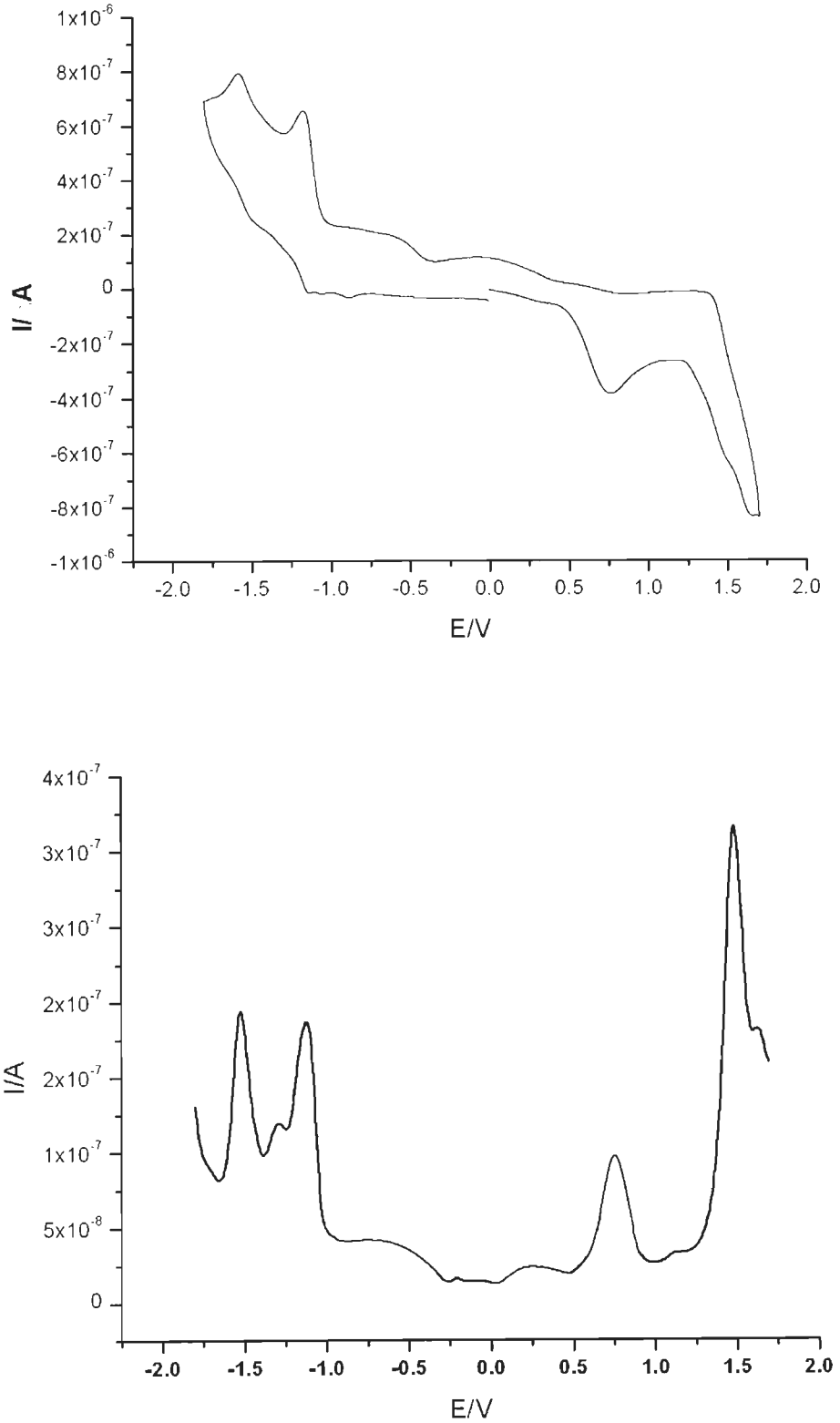

Fig. 2-77 Cyclic and differential pulse voltammograms of complex **2q** in 0.1 M TBAP/ acetonitrile electrolyte system at 0.1 V s^{-1} scan rate.

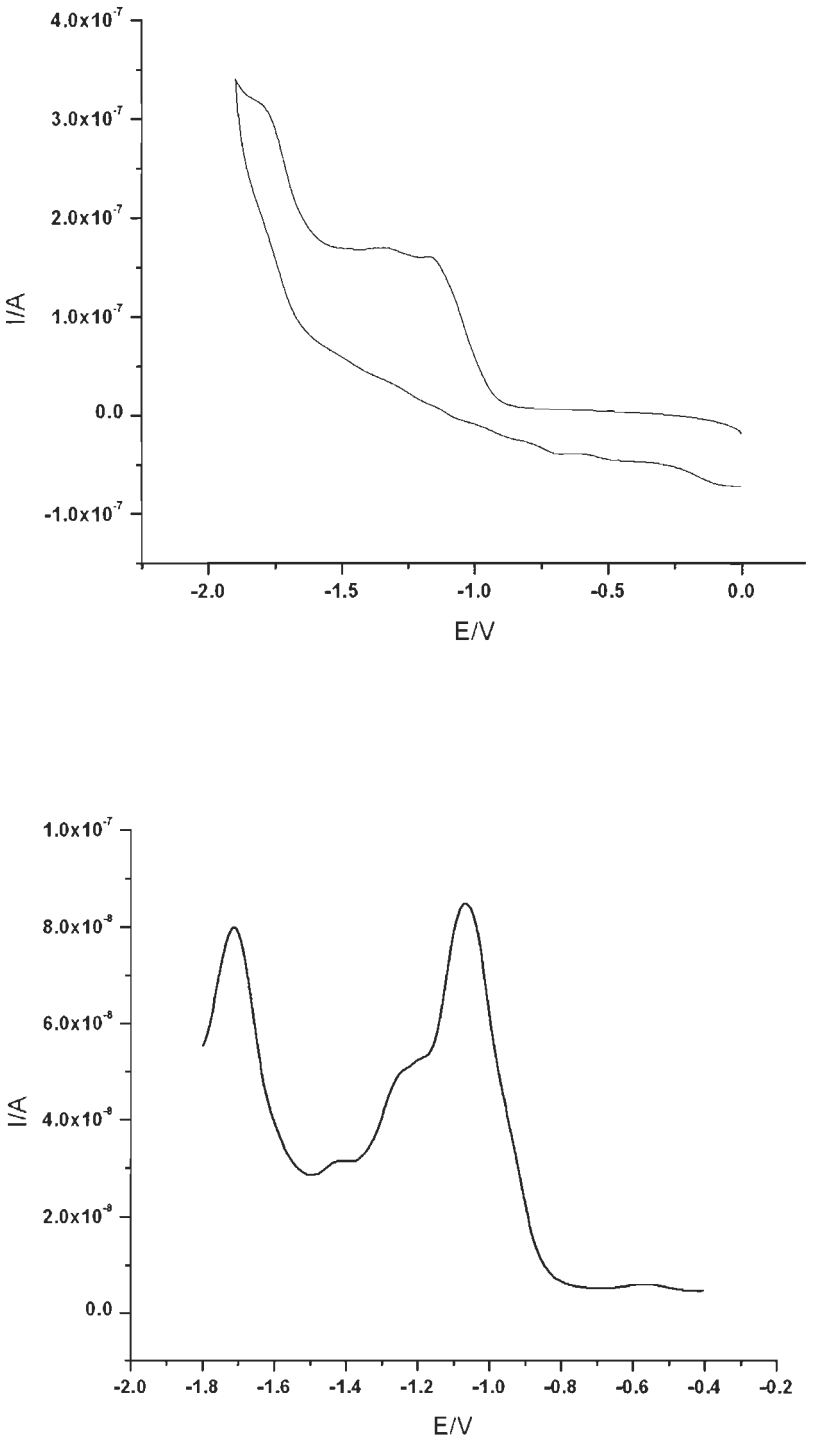

Fig. 2-78 Cyclic and differential pulse voltammograms of complex **2t** in 0.1 M TBAP/ DMSO electrolyte system at 0.1 V s^{-1} scan rate.

References

1. Lippard, S.J. and Berg, J.M., "In Principles of Bioinorganic Chemistry", University Science Books, Mill Valley, California, U.S.A., (1994).

2. Holm, R.H., Kennepohl, P. and Solomon, E.I., "Structural and functional aspects of metal sites in biology", Chem. Rev., **96**, 2239 (1996).

3. (a) Jameson, G.B. and Ibers, J.A., "In Bioinorganic Chemistry, University Science Books: Mill Valley, California, U.S.A., 167 (1994). (b) Traylor, T.G. and Traylor, P.S., "In Active Oxygen in Biochemistry", Blackie Academic and Professional, Chapman and Hall, Glasgow, U.K., 276 (1995).

4. (a) Kendrew, J.C., Bodo, G., Dintzis, H.M., Parrish, R.G., Wycoff, H. and Phillips, D.C., "3-Dimensional model of the myoglobin molecule obtained by X-ray analysis", Nature, **181**, 662 (1958). (b) Kendrew, J.C, Dickerson, R.E., Strandberg, B.E., Hart, R.G, Davies, D.R., Phillips, D.C. and Shore, V.C., "Structure of myoglobin-3-dimensional fourier synthesis at 2 Å resolution", Nature, **185**, 422 (1960).

5. (a) Perutz, M.F., Rossmann, M.G., Cullis, A.F., Muirhead, H., Will, G. and North, A.C.T., "Structure of haemoglobin. A three dimensional fourier synthesis at 5.5 Å resolution obtained by X-ray analysis", Nature, **185**, 416 (1960). (b) Perutz, M.F., Muirhead, H., Cox, J.M., Goaman, G.C., Mathews, F.S., McGandy, E.L. and Webb, L.E. "Three-dimensional fourier synthesis of horse oxyhemoglobin at 2.8 Å resolution I. X-ray analysis", Nature, **219**, 29 (1968). (c) Perutz, M.F., Muirhead, H., Cox, J.M. and Goaman, L.G.G., "Three-dimensional fourier synthesis of horse oxyhaemoglobin at 2.8 Å resolution: the atomic model", Nature, **219**, 131 (1968). (d) Fermi, G., Perutz, M.F., Shaanan, B. and Fourme, R., "The crystal structure of human deoxyhaemoglobin at 1.74 Å resolution", J. Mol. Biol., **175**, 159 (1984).

6. Holm, R., "Trinuclear cuboidal and heterometallic cubane-type iron-sulfur clusters: new structural and reactivity themes in chemistry and biology", Adv. Inorg. Chem., **38**, 1 (1992).

7. Gray, H.B. and Ellis, Jr. W.R., "In Bioinorganic Chemistry", University Science Books: Mill Valley, California, U.S.A., 315 (1994).

8. Bertini, I., Mangani, S. and Viezzoli, M.S., "Structure and properties of copper-zinc superoxide dismutases", Adv. Inorg. Chem., **45**, 127 (1998).

9. Wikaira, J. and Gorun, S.M., "In Bioinorganic Catalysis", Marcel Dekker, Inc.: New York, U.S.A., 355 (1999).

10. (a) Stoddard, B.L., Howell, P.L., Ringe, D. and Petsko, G.A., "The 2.1-Å resolution structure of iron superoxide dismutase from *Pseudomonas ovalis*", Biochemistry, **29**, 8885 (1990). (b) Solomon, E.I. and Zhang, Y., "The electronic structures of active sites in non-heme iron enzymes", Acc. Chem. Res., **25**, 343 (1992).

11. Mansuy, D. and Battioni, P., "In Bioinorganic Catalysis", Marcel Dekker, Inc.: New York, U.S.A., 323 (1999).

12. Bertini, I. and Luchinat, C., "In Bioinorganic Chemistry", University Science Books: Mill Valley, California, U.S.A., 37 (1994).

13. (a) Wilcox, D.E., "Binuclear metallohydrolases", Chem. Rev., **96**, 2435 (1996). (b) Vincent, J.B., Olivier-Lilley, G.L. and Averill, B.A, "Proteins containing oxo-bridged dinuclear iron centers: a bioinorganic perspective", Chem. Rev., **90**, 1447 (1990).

14. Baldwin, J.E. and Bradley, M., "Isopenicillin N synthase: Mechanistic studies", Chem. Rev., **90**, 1079 (1990).

15. Ho, R.Y.N, Liebman, J.F. and Valentine, J.S., "In Active Oxygen in Biochemistry", Blackie Academic and Professional, Chapman and Hall: Glasgow, U.K., 1 (1995).

16. Sono, M., Roach, M.P., Coulter, E.D. and Dawson, J.H., "Heme-containing oxygenases", Chem. Rev., **96**, 2841 (1996).

17. Valentine, J.S. "In Bioinorganic Chemistry", University Science Books: Mill Valley, California, U.S.A., 253 (1994).

18. (a) Groves, J.T., McClusky, G.A., White, R.E. and Coon, M.J., "Aliphatic hydroxylation by highly purified liver microsomal cytochrome P-450: Evidence for a carbon radical intermediate", Biochem. Biophys. Res. Comm., **81**, 154 (1978). (b) Hjelmeland, L.M., Aronow, L. and Trudell, J.R., "Intramolecular determination of primary kinetic isotope effects in hydroxylations catalyzed by cytochrome P-450", Biochem. Biophys. Res. Comm., **76**, 541 (1977).

19. (a) Poulos, T.L., Finzel, B.C., Gunsalus, I.C., Wagner, G.C. and Kraut, J., "2.6-Å crystal structure of Pseudomonas putida cytochrome P450", J. Biol. Chem., **260**, 16122 (1985). (b) Poulos, T.L., Finzel, B.C. and Howard, A., "Crystal structure of substrate-free *Pseudomonas putida* cytochrome P–450", J. Biochemistry, **25**, 5314 (1986). (c) Cupp-Vickery, J.R. and Poulos, T.L., "Structure of cytochrome P450eryF involved in erythromycin biosynthesis", Nature Struct. Biol., **2**, 144 (1995).

20. Dawson, J.H., "Probing structure-function relations in heme-containing oxygenases and peroxidases", Science, **240**, 433 (1988).

21. Schlichting, I., Berendzen, J., Chu, K., Stock, A.M., Maves, S.A., Benson, D.E., Sweet, R.M., Ringe, D., Petsko, G.A. and Sligar, S.G., "The catalytic pathway of cytochrome p450cam at atomic resolution", Science, **287**, 1615 (2000).

22. (a) Que, L., Jr., "In Bioinorganic Catalysis", Marcel Dekker, Inc.: New York, U.S.A., 269 (1999). (b) Wallar, B.J. and Lipscomb, J.D., "Dioxygen activation by enzymes containing binuclear non- heme iron clusters", Chem. Rev., **96**, 2625 (1996). (c) Feig, A.L. and Lippard, S.J., "Reactions of non-heme iron (III) centers with dioxygen in biology and chemistry", Chem. Rev., **94**, 759 (1994).

23. (a) Rosenzweig, A.C., Nordlund, P., Takahara, P.M., Frederick, C.A. and Lippard, S.J., "Geometry of the soluble methane monooxygenase catalytic diiron center in two oxidation states of special interest", Chem. Biol., **2**, 409 (1995). (b) Rosenzweig, A.C. and Lippard, S.J., "Determining the structure of a hydroxylase enzyme that catalyzes the conversion of methane to methanol in methanotrophic bacteria", Acc. Chem. Res., **27**, 229 (1994). (c) Fox, B.G., Hendrich, M.P., Surerus, K.K., Andersson, K.K., Froland, W.A., Lipscomb, J.D.,

and Münck, E., "Mössbauer, EPR and ENDOR studies of the hydroxylase and reductase components of methane monooxygenase from *Methylosinus Trichosporium OB3B*", J. Am. Chem. Soc., **115**, 3688 (1993). (d) Rosenzweig, A.C., Frederick, C.A., Lippard, S.J. and Nordlund, P., "Crystal structure of a bacterial non-haem iron hydroxylase that catalyses the biological oxidation of methane", Nature, **366**, 537 (1993). (e) DeWitt, J.G., Bentsen, J.G., Rosenzweig, A.C., Hedman, B., Green, J., Pilkington, S., Papaefthymiou, G.C., Dalton, H., Hodgson, K.L. and Lippard, S.J., "X-ray absorption, Mossbauer, and EPR studies of the dinuclear iron center in the hydroxylase component of methane monooxygenase", J. Am. Chem. Soc., **113**, 9219 (1991).

24. Liu, K.E., Valentine, A.M., Wang, D., Huynh, B.H., Edmondson, D.E., Salifoglou, A. and Lippard, S.J., "Kinetic and spectroscopic characterization of intermediates and component interactions in reactions of methane monooxygenase from *Methylococcus capsulatus* (Bath)", J. Am. Chem. Soc., **117**, 10174 (1995).

25. Lee, S.-K., Nesheim, J.C. and Lipscomb, J.D., "Transient intermediates of the methane monooxygenase catalytic cycle", J. Biol. Chem., **268**, 21569 (1993).

26. Nakahara, K., Tanimoto, T., Hatano, K., Usuda, K., and Shoun, H., "Cytochrome P-450 55 A1 (P-450dNIR) acts as nitric oxide reductase employing NADH as the direct electron donor", J. Biol. Chem., **268**, 8350 (1993).

27. Shiro, Y., Fujii, M., Iizuka, T., Adachi, S., Tsukamoto, K., Nakahara, K., and Shoun, H., "Spectroscopic and kinetic studies on reaction of cytochrome P450nor with ntric oxide: Implication for its NO reduction mechanism", J. Biol. Chem. **270**, 1617 (1995).

28. Merkx, M., Kopp, D.A., Sazinsky, M.H., Blazyk, J.L., Muller, J. and Lippard, S.J., "Dioxygen activation and methane hydroxylation by soluble methane monooxygenase: A tale of two irons and three proteins", Angew. Chem., Int. **40**, 2782 (2001).

29. Costas, M., Mehn, M.P., Jensen, M.P. and Que, L., Jr., "Oxygen activation at mononuclear non-heme iron: Enzymes, intermediates, and models," Chem. Rev., **104**, 939 (2004).

30. Bassan, A., Blomberg, M.R.A., Siegbahn, P.E.M. and Que, L., Jr., "Two faces of a biomimetic non-heme HO-Fe^{V}=O oxidant: Olefin epoxidation versus cis-dihydroxylation", Angew. Chem. Int., **44**, 2939 (2005).

31. Ghosh, A., "High-valent iron intermediates in biology", J. Inorg. Biochem., **100**, 419 (2006).

32. Ertl, G., "Heterogeneous catalysis on the atomic scale", Chem. Rec., **1**, 33 (2001).

33. Howard, J.B. and Rees, D.C., "Structural basis of biological nitrogen fixation", Chem. Rev., **96**, 2965 (1996).

34. Adams, K.M., Rasmussen, P.G., Scheidt, W.R. and Hatano, K., "Structure and properties of an unsymmetrically substituted six-coordinate iron (III) porphyrin", Inorg. Chem., **18**, 1892 (1979).

35. (a) Wagner, W.D. and Nakamoto, K., "Formation of nitridoiron (V) porphyrins detected by resonance raman spectroscopy", J. Am. Chem. Soc., **110**, 4044 (1988). (b) Wagner, W.D. and Nakamoto, K., "Resonance Raman spectra of nitridoiron (V) porphyrin intermediates produced by laser photolysis", J. Am. Chem. Soc., **111**, 1590 (1989).

36. Zhang, Y., Hallows, W.A., Ryan, W.J., Jones, J.G., Carpenter, G.B., and Sweigart, D.A., "Models for steric interactions in heme proteins. Structures of the five-coordinate complex iron (III) tetraphenylporphyrin azide and its six-coordinate 1:1 adducts with 1-methylimidazole and 1,2-dimethylimidazole", Inorg. Chem., **33**, 3306 (1994).

37. Fukui, H., Ito, M., Moro-oka, Y. and Kitajima, N., "Preparation and structure of mononuclear iron (III) complexes $[LFeCl_3]^-$ and $[LFe(N_3)_3]^-$ (L = Hydrotris(1-pyrazolyl)borate and Hydrotris(3,5-dimethyl-1-pyrazolyl)borate)", Inorg. Chem., **29**, 2968 (1990).

38. Sellmann, D., Hofmann, T. and Knoch, F., "Transition metal complexes with sulfur ligands. Phosphine and azido [Fe(L)('N_HS_4')] complexes; structural characterization of the key complex [Fe('N_HS_4')].THF (L = PMe_3, PBu_3, PMe_2Ph, $PMePh_2$, N_3^-; 'N_HS_4'$^{2-}$ = dianion of 2,2'-bis-(2-mercaptophenylthio) diethylamine)", Inorg. Chim. Acta, **224**, 61 (1994).

39. Field, L.D., George, A.V. and Pike, S.R., "Synthesis and reactions of azido complexes of iron", Polyhedron, **14**, 3133 (1995).

40. Ellison, M.K., Nasri, H., Xia, Y.-M., Marchon, J.-C., Schulz, C.E., Debrunner, P.G. and Scheidt, W.R., "Characterization of the bis(azido)(meso-tetraphenyl-porphinato)ferrate (III) anion. An unusual spin-equilibrium system", Inorg. Chem., **36**, 4804 (1997).

41. Zeller, J., Koenig, S. and Radius, U., "Synthesis and structural analysis of calix[4]arene-supported iron (III) complexes", Inorg. Chim. Acta, **357**, 1813 (2004).

42. Meyer, K., Bill, E., Mienert, B., Weyhermu1ller, T. and Wieghardt, K., "Photolysis of cis- and trans-$[Fe^{III}(cyclam)(N_3)_2]^+$ complexes: Spectroscopic characterization of a nitridoiron (V) species", J. Am. Chem. Soc., **121**, 4859 (1999).

43. Koner, S., Iijima, S., Mizutani, F., Harata, K., Watanabe, M., Nagasawa, A. and Sato, M., "Fe(III)–azido complex with tetragonally compressed octahedral FeN_6 geometry: Synthesis, spectroscopic and X-ray single crystal analysis of $[Fe(cyclam)(N_3)_2](ClO_4)$", Polyhedron, **18**, 2201 (1999).

44. Justel, T., Muller, M., Weyhermuller, T., Kressl, C., Bill, E., Hildebrandt, P., Lengen, M., Grodzicki, M., Trautwein, A.X., Nuber, B. and Wieghardt, K., "The molecular and electronic structure of symmetrically and asymmetrically coordinated, non-heme iron complexes containing $[Fe^{III}(\mu\text{-}N)Fe^{IV}]^{4+}$ (S = 3/2) and $[Fe^{IV}(\mu\text{-}N)Fe^{IV}]^{5+}$ (S = 0) cores", Chem. Eur. J., **5**, 793 (1999).

45. Grapperhaus, C.A., Mienert, B., Bill, E., Weyhermuller, T. and Wieghardt, K., "Mononuclear (nitrido)iron (V) and (oxo)iron (IV) complexes via photolysis of $[(cyclam\text{-}acetato)Fe^{III}(N_3)]^+$ and ozonolysis of $[(cyclam\ acetato)Fe^{III}(O_3SCF_3)]^+$ in water / acetone mixtures", Inorg. Chem., **39**, 5306 (2000).

46. Aliaga-Alcalde, N., DeBeer George, S., Mienert, B., Bill, E., Wieghardt, K. and Neese, F., "The geometric and electronic structure of $[(cyclam\text{-}acetato)FeN]^+$: A genuine iron (IV) species with ground state spin S=1/2", Angew. Chem., **117**, 2968 (2005).

47. Petrenko, T., DeBeer, G.S., Aliaga-Alcalde, N., Bill, E., Mienert, B., Xiao, Y., Guo, Y., Sturhahn, W., Cramer, S.P., Wieghardt, K. and Neese, F., "Characterization of a genuine iron (V)-nitrido species by nuclear resonant vibrational spectroscopy coupled to density functional calculations", J. Am. Chem. Soc., **129**, 11053 (2007).

48. Betley, T.A. and Peters, J.C., "A tetrahedrally coordinated $L_3Fe\text{-}N_x$ platform that accommodates terminal nitride ($Fe^{IV}\equiv N$) and dinitrogen ($Fe^{I}\text{-}N_2\text{-}Fe^{I}$) ligands", J. Am. Chem. Soc., **126**, 6252 (2004).

49. Berry, J.F., Bill, E., Bothe, E., Weyhermuller, T. and Wieghardt, K., "Octahedral non-heme non-oxo Fe(IV) species stabilized by a redox-innocent N-methylated cyclam-acetate ligand", J. Am. Chem. Soc., **127**, 11550 (2005).

50. Berry, J.F., Bill, E., Garcia-Serres, R., Neese, F., Weyhermu1ller, T. and Wieghardt, K., "Effect of N-methylation of macrocyclic amine ligands on the spin state of iron (III): A tale of two fluoro complexes", Inorg. Chem., **45**, 2027 (2006).

51. Berry, J.F., Bill, E., Bothe, E., DeBeer, S., George, Mienert, B., Neese, F. and Wieghardt, K., "An octahedral coordination complex of iron (VI)", Science, **312**, 1937 (2006).

52. Song, Y.-F., Berry, F., Bill, E., Bothe, E., Weyhermuller, T. and Wieghardt, K., "Iron complexes of new pentadentate ligands containing the 1,4,7-triazacyclononane-1,4-diacetate motif. Spectroscopic, electro-, and photochemical studies", Inorg. Chem., **46**, 6, (2007).

53. Chen, X.-M. and Mak, T.C.W., "A linear polymeric manganese (II) complex bridged by skew-skew bridging carboxylato groups. Crystal structure of *catena*-tris(betaine)manganese(II) tetrachloromanganate (II), $[Mn(Me_3NCH_2COO)_3]_n{\cdot}n$ $MnCl_4$", Inorg. Chim. Acta, **189**, 3 (1991).

54. Mudasir, N.Y. and Hidenari, I., "Iron (II) and nickel (II) mixed-ligand complexes containing 1,10-phenanthroline and 4,7-diphenyl-1,10-phenanthroline", Transition Met. Chem., **24**, 210 (1999).

55. Yu, J.-H., Jia, H.-B., Pan, L.-Y., Yang, Q.-X., Wang, T.-G., Xu, J.-Q., Cui, X.-B., Liu, Y.-J., Li, Y.-Z., Lu, C.-H. and Ma, T.-H., "Hydrothermal synthesis, crystal structure and third-order non-linear optical property of a discrete decanuclear iodocuprate (I) $[Cu^{I}_{10}H_2I_{16}]^{4-}$with $[Ni^{II}(phen)_3]^{2+}$ as a template", J. Solid State Chem., **175**, 152 (2003).

56. Fritsky, I.O., Swiaztek-Kozlowska, J., Dobosz, A., Sliva, T.Y. and Dudarenko, N.M., "Hydrogen bonded supramolecular structures of cationic and anionic module assemblies containing square-planar oximate complex anions", Inorg. Chim. Acta, **357**, 3746 (2004).

57. Wang, C., Peng, Z., Guo, W., Yunhong, Z. and Cheng, G., "A novel mixed-valence $Ni(mnt)_2$ salt: synthesis and crystal structure of $[Ni(phen)_3]_2[Ni(mnt)_2]_3{\cdot}2DMF$ (phen = 1,10-phenathroline, mnt = 1,2-dicyanovinylene-1,2-dithiolato, DMF = N,N-dimethylformamide)", J. Mol. Struct., **702**, 1 (2004).

58. Dang, D., Chunlin, N., Bai, Y., Tian, Z., Wen, L., Meng, Q. and Gao, S., "Synthesis, crystal structure and magnetic properties of a nickel (III) maleonitriledithiolate complex using1-methyl-3-benzylbenzimidazolium cation", J. Mol. Struct., **743**, 197 (2005).

59. Madhu, V. and Das, S.K., "N–H···S hydrogen bonds in a new family of ion-pair complexes between cationic nickel tetraazabicyclononane and anionic metal dithiolates: Synthesis, characterization and properties of $[Ni(C_9H_{22}N_6)][M(mnt)_2]$ (M^{II} = Cu, Ni, Pd)", Eur. J. Inorg. Chem., 1505 (2006).

60. Pereira, L.C.J., Gulamhussen, A.M., Dias, J.C., Santos, I.C. and Almeida, M., "Searching for switchable molecular conductors: Salts of $[M(dcbdt)_2]$ (M = Ni, Au) anions with $[Fe(sal_2\text{-trien})]^+$ and $[Fe(phen)_3]^{2+}$", Inorg. Chim. Acta, **360**, 3887 (2007).

61. Faulmann, C., Dorbes, S., Lampert, S., Jacob, K., Bonneval, B.G., Molnar, G., Bousseksou, A., Antonio, R.J. and Valade, L., "Crystal structure, magnetic properties and Mössbauer studies of $[Fe(qsal)_2][Ni(dmit)_2]$", Inorg. Chim. Acta, **360**, 3870 (2007).

62. Shi, F.N., Cunha-Silva, L., Hardie, M.J., Trindade, T., Paz, F.A.A. and Rocha, J. "Hetrodimetallic germanium (IV) complex structures with transition metals", Inorg. Chem., **46**, 6502 (2007).

63. Sharma, R.P., Singh, A., Brandao, P., Felix, V. and Venugopalan, P., "Second sphere coordination in anion binding: Synthesis, characterization and X-ray structure of tris(1,10-phenanthroline)cobalt (III) periodate dihydrate, $[Co(phen)_3](IO_4)_3.2H_2O$", J. Mol. Struct., (2008) in press.

64. Soares-Santos, P.C.R., Nogueira, H.I.S., Felix, V., Drew, M.G.B., Sa Ferreira, R.A., Carlos, L.D. and Trindade, T., "Synthesis and crystal structure of $[^nBu_4N][Er(pic)_4].5.5H_2O$: a new infrared emitter", Inorg. Chem. Comm., **6**, 1234 (2003).

65. Brasil, M.C., Benvenutti, E.V., Gregorio, J.R. and Gerbase, A.E., "Iron acetylacetonate complex anchored on silica xerogel polymer", React. Funct. Polymers, **63**, 135, (2005).

66. Mayilmurugan, R., Suresh, E. and Palaniandavar, M., "A new tripodal iron (III) monophenolate complex: Effects of ligand basicity, steric hindrance and solvent on regioselective extradiol cleavage", Inorg. Chem., **46**, 6038 (2007).

67. (a) Berkovitch-Yellin, Z. and Leiserowitz, L., "The role played by C-H···O and C-H···N interactions in determining molecular packing and conformation", Acta Cryst. B, **40**, 159 (1984). (b) Sarma, J.A.R.P. and Desiraju, G.R., "Crystal engineering via donor-acceptor interactions. X-ray crystal structure and solid state reactivity of the 1:1 complex 3,4-dimethoxycinnamic acid-2,4-dinitrocinnamic acid", Acc. Chem. Res., **19**, (1986) 222.

68. (a) Aakeroy, C.B., Evans, T.A., Seddon, K.R. and Palinko, I., "The C–H···Cl hydrogen bond: does it exist?", New J. Chem., **23**, 145 (1999). (b) Freytag, M. and Jones, P.G., "Hydrogen bonds C–H···Cl as a structure-determining factor in the gold (I) complex bis(3-bromopyridine)gold (I) dichloroaurate (I)", Chem. Comm., 277 (2000).

69. Bakker, E., Buhlmann, P. and Pretsch, E., "Carrier-based ion-selective electrodes and bulk optodes. General characteristics", Chem. Rev., **97**, 3083 (1997).

70. Schaller, U., Bakker, E., Spichiger, U.E. and Pretsch, E., "Ionic additives for ion-selective electrodes based on electrically charged carriers", Anal. Chem., **66**, 391 (1994).

71. Rosatzin, T., Bakker, E., Suzuki, K. and Simon, W., "Lipophilic and immobilized anionic additives in solvent polymeric membranes of cation-selective chemical sensors", Anal. Chim. Acta., **280**, 197 (1993).

72. Nakamoto, K., "Infrared and Raman Spectra of Inorganic and Coordination Compounds", third ed., Wiley–Interscience, New York, 278 (1978).

73. (a) Desiraju, G.R., "Hydrogen bridges in crystal engineering: interactions without borders", Acc. Chem. Res., **35**, 565 (2002). (b) Nangia, A., "Database research in crystal engineering", Cryst. Engg. Comm., **4**, 93 (2002). (c) Taylor, R. and Kennard, O., "Crystallographic evidence for the existence of C-H···O, C-H···N, and C-H···Cl hydrogen bonds", J. Am. Chem. Soc., **104**, 5063 (1982).

74. Meyer, K., Bendix, J., Metzler-Nolte, N., Weyhermuller, T. and Wieghardt, K., "Nitridomanganese (V)- and -(VI) complexes containing macrocyclic amine ligands", J. Am. Chem. Soc., **120**, 7260 (1998).

75. White, J.L., Tanski, J.M., Churchill, D.G., Rheingold, A.L. and Rabinovich, D., "Synthesis and structural characterization of 2-mercapto-1-tert-butylimidazole and its group 12 metal derivatives $(Hmim^{tBu})_2MBr_2$ (M = Zn, Cd, Hg)", J. Chem. Crystall., **33**, 437 (2003).

76. Inskeep, R.G., "Infrared spectra of metal complex ions below 600 cm^{-1}. Spectra of the tris complexes of 1,10-phenanthroline and 2,2'-bipyridine with the transition metals iron (II) through zinc (II)", J. Inorg. Nucl. Chem., **24,** 763 (1963).

77. Singh, A., Sharma, R.P., Brandao, P., Felix, V. and Venugopalan, P., "Second sphere coordination in anion binding: Synthesis, characterization of $[Co(phen)_2CO_3]X.\ nH_2O$ where X = *o*-nitrophenolate(onp), *p*-nitrophenolate (pnp), 2,4-dinitrophenolate(dnp), 2,4,6-trinitrophenolate(tnp) and single crystal X-ray structures of $[Co(phen)_2CO_3](onp).2H_2O$ and $[Co(phen)_2CO_3](dnp)\ 4.5\ H_2O$", J. Mol. Struct., (2008) in press.

78. Sharma, R.P., Sharma, R., Bala, R., Salas, J.M. and Quiros, M., "Second sphere coordination complexes via hydrogen bonding: Synthesis, spectroscopic characterisation of [trans-$Co(en)_2Cl_2$]CdX_4 (X=Br or I) and single crystal X-ray structure determination of [trans-$Co(en)_2Cl_2$]$CdBr_4$", J. Mol. Struct., **794**, 341 (2006).

79. Sharma, R.P., Sharma, R., Bala, R., Burrows, A.D., Mahon, M.F. and Cassar, K., "Second sphere coordination in anion binding: Syntheses, characterization and X-ray structures of [trans-$Co(en)_2(X)_2$]Y where X=Cl when Y= IO_4 or X=N_3 when Y=N_3", J. Mol. Struct., **794**, 173 (2006).

80. Sharma, R.P., Sharma, R., Bala, R. and Venugopalan, P., "Molecular recognition of pyramidal oxoanions using cationic cobaltammine: Synthesis, characterization, X-ray structure determination and packing of [trans-$Co(en)_2Cl_2$]ClO_3 and [trans-$Co(en)_2Cl_2$]BrO_3", J. Mol. Struct., **789**, 133 (2006).

81. Singh, U.P. and Aggarwal, V., "Hydrogen-bonding and π–π stacking interactions in tris(1,10-phenanthroline-κ^2N,N′)nickel (II) bis{[1-tert-butylimidazole-2(3H)-thione-κS]trichloridonickelate (II)} acetonitrile disolvate", Acta Cryst., **E64**, m935 (2008).

82. Maldonado-Rogado, M.A., Vinuelas-Zahinos, E., Luna-Giles, F. and Bernalte Garcia, A., "Nickel (II) and zinc (II) complexes with *N*-(5,6-dihydro-4H-1,3-thiazin-2-yl)-2-aminobenzimidazole (BzTz): Synthesis, spectral and structural characterization", Polyhedron, **26**, 3112 (2007).

83. (a) Hernandez, H.J.G., Pandiyan, T. and Bernes, S., "Mercaptoethanesulfonic acid (CoM imitator) interaction studies with nickel (II) complexes of pyridyl groups containing tetradentate ligands: Synthesis, structure, spectra and redox properties", Inorg. Chim. Acta, **359**, 1 (2006) (b) Sener, M.K., Koca, A., Gul, A. and Kocak, M.B., "Synthesis and electrochemical characterization of biphenyl-malonic ester substituted cobalt, copper and palladium phthalocyanines", Polyhedron, **26**, 1070 (2007) (c) Pui, A., Policar, C. and Mahy, J.-P., "Electronic and steric effects in cobalt Schiff bases complexes: Synthesis, characterization and catalytic activity of some cobalt (II) tetra-halogens-dimethyl salen complexes", Inorg. Chim. Acta, **360**, 2139 (2007).

Chapter 3

Synthesis and Structural Studies of Cobalt Complexes

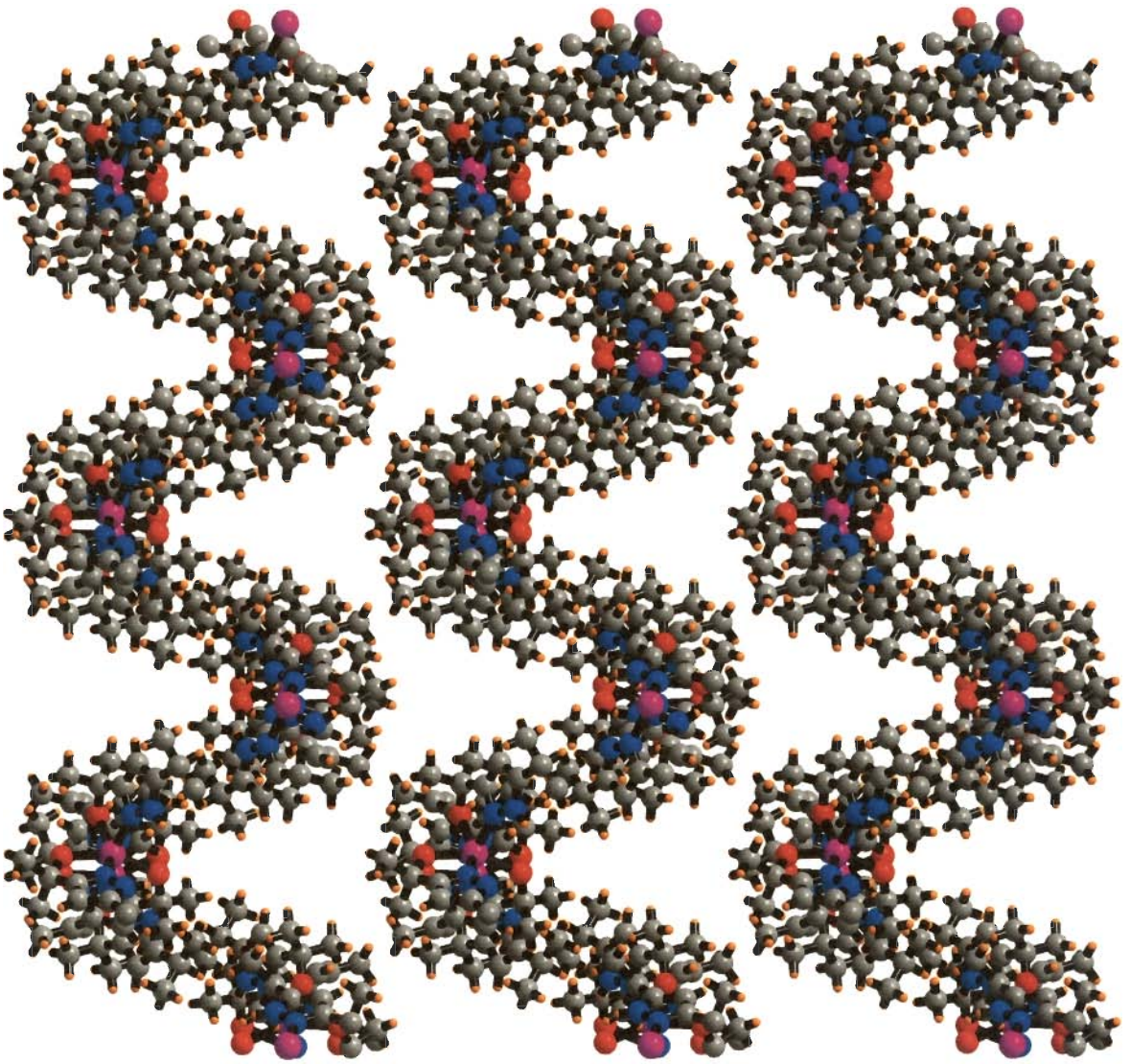

Organic synthesis involves transformation of functional groups or structural features exhibiting relatively high chemical reactivity. As a result, almost every class of organic compounds can now be used as a source of starting material for conversion to members of other classes which include complicated materials such as polymers, biomolecules etc. Alkanes or the saturated hydrocarbons, an important class of organic compounds, represent an exception to this generalization. Thus, C-H bonds are generally not viewed as functional groups in regards to organic synthesis. Out of thousands of reagents that are regularly used in synthetic organic methods, only a few are capable of carrying out selective chemistry on alkanes.

The reason for the difficulty in converting alkanes to more useful products is alluded to by their other name 'paraffin' meaning less affinity suggesting alkanes are relatively inert. The chemical inertness of alkanes arises due to the fact that the constituent atoms of alkanes are all held by strong and localized C-C and C-H bonds, such that the molecules have no empty orbitals of low energy or filled orbitals of high energy that can readily participate in a chemical reaction, as is the case with unsaturated hydrocarbons such as olefins and alkynes [1]. Therefore, the lack of reactivity of alkane C-H bonds is often attributed to their high bond energies (typically 90-100 kcal mol^{-1}) and very low acidity (difficult to measure directly but estimated to have $pK_a = 45\text{-}60$) and basicity [2].

Inspite of the fact that aliphatic C-H bonds are hard to break or transform, they are not completely inert. They do react at high temperatures, as seen in combustion but such reactions are not easily controllable and they usually result in thermodynamically stable but economically unattractive products i.e., carbon dioxide and water. At present the use of alkanes in combustion applications, utilizes their energy content but not their

potential to be used as efficient precursors for the fine synthesis of important and economically important chemicals. Cracking and thermal dehydrogenation of alkanes converts them into valuable olefins but these reactions require extreme conditions of high temperature and intensive energy. Alkanes have also been found to undergo a gas phase or solution phase reaction which involves exposure to reactive species such as super acids or free radicals but these species are usually expensive to make and also such processes pose a problem of relative unselectivity.

Aliphatic C-H bond activation or functionalization has great practical implications. Usually the preparation of a certain class of compounds requires that there should be some heteroatom or unsaturation in the carbon backbone of the starting material but this cannot be done in alkanes. In order to bring this conversion the reactive sites or functional groups are usually incorporated by means of multiple transformations but if the new functionality can be somehow introduced directly through transformation of C-H bonds, the same target molecule will be accessible in a single step by displacement of hydrogen atom. Moreover, the ability to selectively target a number of different C-H bonds in a complex substrate will permit direct access to multiple analogs from a common structural precursor. The C-H bond functionalization strategies if once successfully established will also be helpful in utilization of alkanes especially methane, which is the principal constituent of natural gas. In nature, several microorganisms are capable of performing functionalization of aliphatic C-H bonds continuously at ambient temperature and sometimes with great selectivity.

Table 3-1 Enzymes capable of oxidizing alkanes

Enzyme	Composition and cofactors	Example of host organism	Substrate range
Class I P450 (CYP153)	P450 oxygenase: P450 heme Ferredoxin: [2Fe-2S] Ferredoxin reductase: FAD, NADH	*Sphingomonas* sp.HXN-200, *Mycobacterium* sp.HXN-1500, *Acinetobacter* sp EB 104	C_4-C_{16}
Class II P450 (CYP52)	Microsomal oxygenase: P450 heme reductase: FAD, FMN, NADPH	*Candida maltosa, Candida tropicalis, Yarrowia lipolytica*	C_{10}-C_{16}
Class II P450 (CYP2E,CYP4B)	Microsomal oxygenase: P450 heme reductase: FAD, FMN, NADPH	Humans and rabbits	C_6-C_{10}
Integral membrane alkane hydroxylase	Membrane hydroxylase: dinuclear iron Rubredoxin iron: Rubredoxin reductase: FAD, NADH	*Acinetobacter, Alcanivorax, Burkholderia, Mycobacterium, Pseudomonas, Rhodococcus*	C_5-C_{16}
Soluble methane monooxygenase	$\alpha_2\beta_2\gamma_2$ structure Hydroxylase: dinuclear iron reductase [2Fe-2S] FAD, NADH Regulatory subunit	*Methylisinus trichosporium* OB3b, *Methylococcus capsulatus* (Bath)	C_1-C_{10}
Particulate methane monooxygenase	Putative $\alpha_2\beta_2\gamma_2$ structure	All known methanotrophs	C_1-C_5
Propane monooxygenase	Putative $\alpha_2\beta_2\gamma_2$ structure: NADH Regulatory subunit	*Gordonia sp.* TY-5	C_3 and C_{13}-C_{22}
Butane monooxygenase	$\alpha_2\beta_2\gamma_2$ structure Hydroxylase: dinuclear iron reductase [2Fe-2S] FAD, NADH Regulatory subunit	*Pseudomonas butanovora* ATCC 43655	C_2-C_8
Engineered P450 cam	P450 oxygenase: P450 heme putidaredoxin: [2Fe-2S] putidaredoxin reductase: FAD, NADH	*Pseudomonas putida* ATCC 29607	C_3-C_{10}
Engineered P450 BM-3	Single polypeptide FAD, FMN, NADPH	*Bacillus megaterium* ATCC 14581	C_3-C_8

Oxygenases are the oxidative enzymes that catalyze the selective oxidation of a wide range of organic compounds at physiological temperature and pressure. Oxidation of a wide range of linear alkanes to corresponding alcohols is catalyzed by a group of oxidative enzymes: multicomponent oxygenases, alkane hydoxylase and cytochrome P450 selectively. Different bacterial multicomponent monooxygenases catalyze the O_2 dependent hydroxylations of hydrocarbons. This family of enzymes includes methane / butane monooxygenases, four-component alkene / aromatic monooxygenases, phenol hydroxylases, alkene monooxygenases, hyperthermophilic toluene monooxygenases and tetrahydrofuran / propane monooxygenases. Different bacterial hydroxylases that are capable of being used in synthesis of fine chemicals using the whole cells are alkane monooxygenase, toluene monooxygenase, xylene monooxygenase, styrene monooxygenase and toluene dioxygenase. These enzymes are unique among diiron proteins for their ability to hydroxylate a variety of hydrocarbon substrates including alkanes, alkenes and aromatics depending on the microorganism which produces it, these enzymes carry out oxidation of a wide range of alkanes [3-5].

Cytochrome P450 is a monooxygenase enzyme which catalyzes the incorporation of molecular oxygen into alkane. It is a heme protein [6] and is found in certain yeast as well as bacteria. Cytochrome P450 present in certain strains of the yeast *Candida* is able to carry out ω-oxidation of alkanes (C-11 – C-16) to corresponding alcohols which in turn is converted to α,ω-dicarboxylic acids by other enzymes [7]. The natural activity of this enzyme when present in *Bacillus megaterium* is to catalyze the enantioselective hydroxylation of alkanes with chain lengths ranging from dodecane to octadecane. However, certain mutants have been found which have the ability to carry out direct, regioselective and enantioselective hydroxylation of a wider range of alkanes from propanes to octadecanes [8].

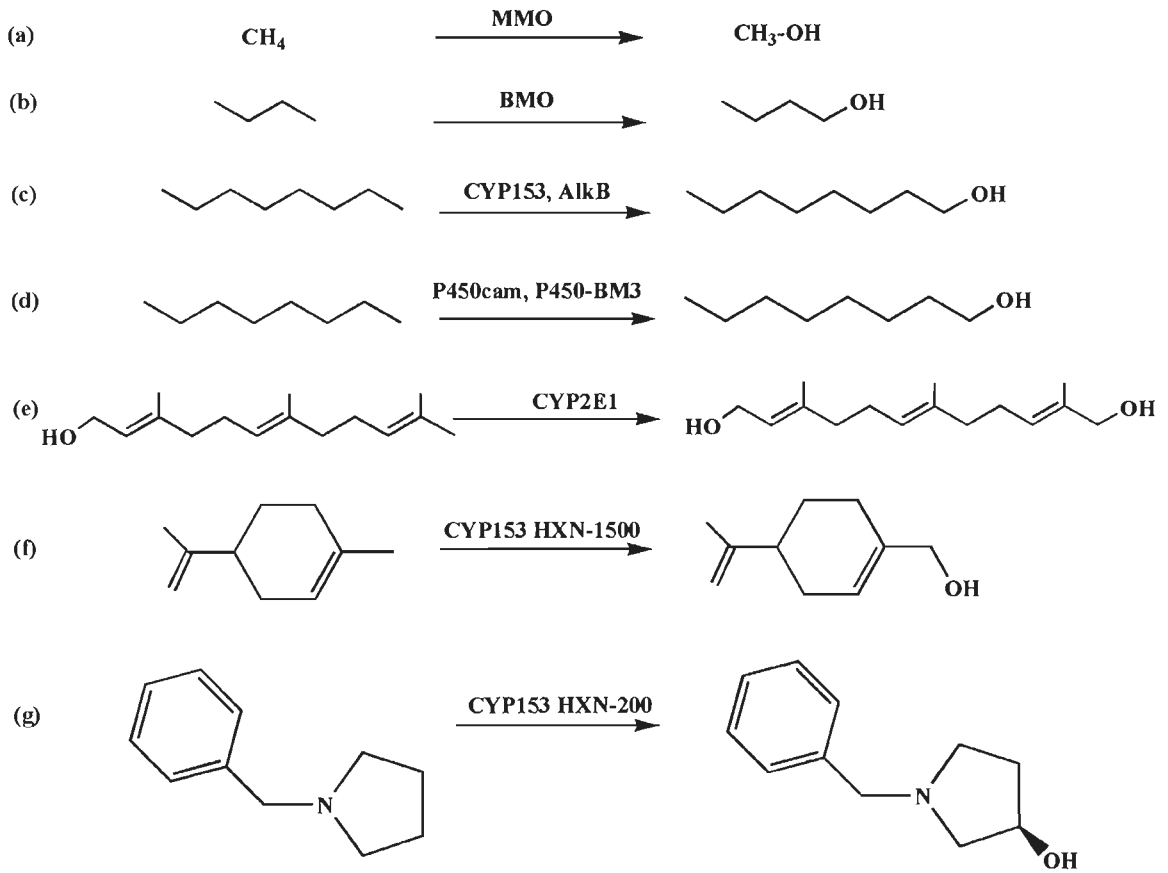

Scheme 3-1 Representative reactions catalyzed by alkane oxygenases

Despite the practical limitations involved, enzymatic transformations are widely studied, to understand the underlying reaction mechanism and to design synthetic catalysts that are capable of mimicking the function, efficiency and selectivity of their biological counterparts. A number of structural and functional mimics of these monooxygenases have been developed to oxidize C-H bonds.

Recently, some metal complexes have also been used in C-H activation of both aromatic and aliphatic compounds. Bharath et al. [9] carried out the reactions of low-spin complexes $[Co^{II}L_3][ClO_4]_2.H_2O$ [L = 2-(arylazo)pyridine, $(R)C_6H_4N{=}NC_5H_4N$ (R = H, *o*-Me / Cl, *m*-Me / Cl or *p*-Me / Cl] with *m*-chloroperbenzoic acid (*m*-$ClC_6H_4CO_3H$) in acetonitrile at room temperature and isolated a low-spin $[Co^{III}L_2']ClO_4.H_2O$ [L′ = *o*-$OC_6H_3(R)N{=}NC_5H_4N$]. In $[Co^{III}L_2']ClO_4.H_2O$, the *o*-carbon–hydrogen bond of the

pendant phenyl ring of both parent ligands L were selectively and spontaneously hydroxylated. During the transformation, the metal ion was oxidised from Co^{II} to Co^{III}. They also concluded that when one methyl or chloro group was present at the meta position of the pendant phenyl ring of L the reaction resulted in two isomeric complexes due to free rotation of the singly bonded meta-substituted phenyl ring with respect to the azo group.

Fujita et al. [10] reported the C-H bond activation by cobalt (I) macrocycles through rapid H / D exchange between macrocycle and acetonitrile solvent. Rapid (20-min $t_{1/2}$ at room temperature) proton exchange between the N-H groups of a cobalt (I) macrocycle and CD_3CN solvent occurred. The reaction was anomalously rapid for a "simple" proton transfer process and showed signal reactivity of the metal center toward C-H activation. They suggested that oxidative addition of the methyl group of CH_3CN to the Co(I) complex would result in the formation of the cobalt-carbon bond in the metallated $Co^{III}L(D)(CD_2CN)^+$ species and H / D exchange could occur via a sequence such as shown in Fig. 3-1.

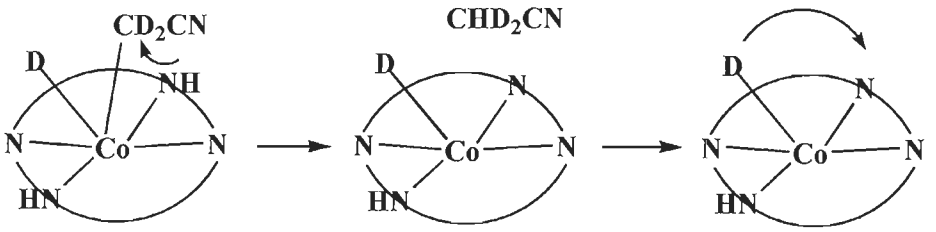

Fig. 3-1 Suggested mechanism for H / D exchange

Paneque et al. [11] reported that the reaction of thiophene with the rhodium compound $[Tp^*Rh(C_2H_4)(PMe_3)]$ (Tp^* = hydrotris-(3,5-dimethyl-1-pyrazolyl)borate) gave a mixture of the C-H and C-S activation products $[Tp^*Rh(H)(2\text{-}C_4H_3S)(PMe_3)]$ and $[Tp^*Rh(CHCHCHCHS)(PMe_3)]$ respectively. They also observed that PEt_3 derivative $[Tp^*Rh(C_2H_4)(PEt_3)]$ showed higher selectivity toward C-H activation.

Wiley et al. [12] reported that the reaction of methylene chloride solutions of the tris(1-pyrazolyl)borate (Tp) complexes $TpIr(PPh_3)$-(C_2H_4) or $TpIr(C_2H_4)_2$ with excess PPh_3 via activation of a pyrazole C-H bond formed equilibrium mixtures of $TpIr(PPh_3)(C_2H_4)$, $(N,C^5,N\text{-}Tp\text{-}H)Ir(PPh_3)_2H$ and free ethylene upon standing at room temperature. Complete conversion was accomplished by removing the displaced ethylene. They suggested that the protonation at the unbound nitrogen of the pyrazole ring afforded cationic complex $[(N,C^5,N\text{-}Tp)\text{-}HIr(PPh_3)_2]BF_4$ as the BF_4 salt. The structures of $TpIr(C_2H_4)_2$ and $[(N,C^5,N\text{-}Tp)\text{-}HIr(PPh_3)_2]BF_4$ (CH_3CN solvate) were verified by X-ray crystallography (Fig. 3-2).

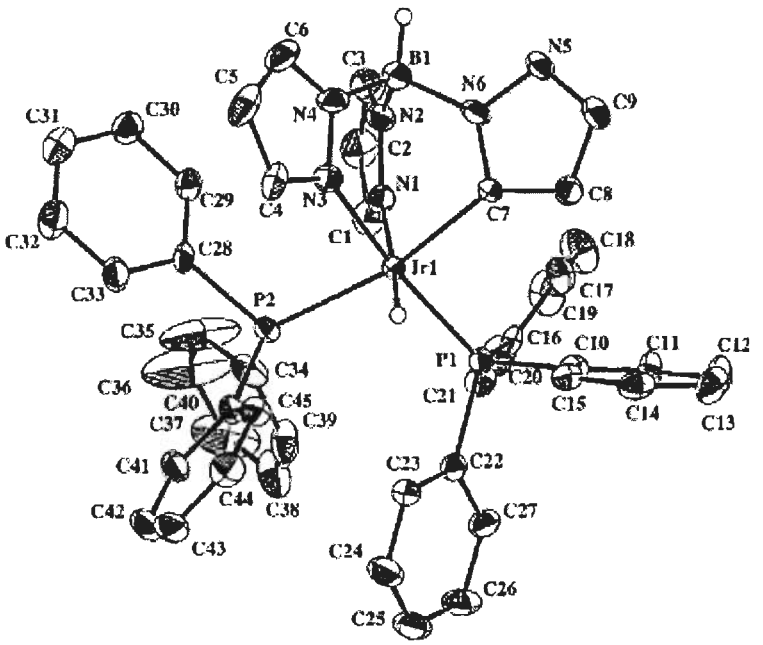

Fig. 3-2 Crystal structure of $[(N,C^5,N\text{-}Tp)\text{-}HIr(PPh_3)_2]BF_4$

Canty et al. [13] reported alkylpalladium complexes bearing the $[N\text{-}C(sp^3)\text{-}N]^-$ donor motif and two six-membered palladacycles were generated on activation of $C(sp^3)$-H bonds by palladium (II) acetate. Cyclopalladation of the new reagents 1,5-bis(pyridin-2-yl)pentane $[CH_2(CH_2CH_2py)_2]$, 1,5-bis(pyrazol-1-

yl)pentane [$CH_2(CH_2CH_2Pz)_2$] and 1,5-bis(N-methylimidazol-2-yl)pentane [$CH_2(CH_2CH_2mim)_2$], followed by reaction with lithium chloride afforded the palladium (II) complexes Pd{$CH(CH_2CH_2py)_2$-N,C,N'}Cl, Pd{$CH(CH_2CH_2Pz)_2$-N,C,N'}Cl (Fig. 3-3) and Pd{$CH(CH_2CH_2mim)_2$-N,C,N'}Cl respectively. Also abstraction of chloride from Pd{$CH(CH_2CH_2Pz)_2$-N,C,N'}Cl with $AgBF_4$ in acetone generated the cationic acetone complex [Pd{$CH(CH_2CH_2Pz)_2$-N,C,N'}($OCMe_2$)][BF_4]. X-ray crystal structures of Pd{$CH(CH_2CH_2py)_2$-N,C,N'}Cl, Pd{$CH(CH_2CH_2Pz)_2$-N,C,N'}Cl and [Pd{$CH(CH_2CH_2Pz)_2$-N,C,N'}($OCMe_2$)][BF_4] revealed tridentate [N-$C(sp^3)$-N']$^-$ intramolecular coordination of the ligands.

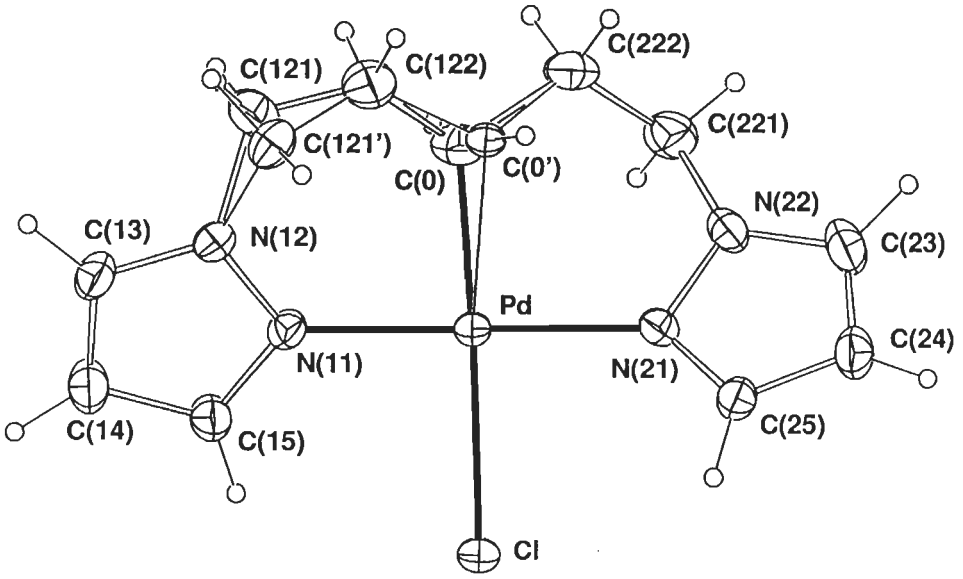

Fig. 3-3 Crystal structure of Pd{$CH(CH_2CH_2Pz)_2$-N,C,N'}Cl

Chantson et al. [14] synthesized platinum (II) hydride complexes of the type trans-[PtH(1-azolyl)(PEt_3)$_2$], by the reactions of [$Pt(PEt_3)_4$] with various azoles (where azoles = indole, imidazole, benzimidazole, pyrazole and indazole) through oxidative insertion of the metal centre into the N–H bonds of the respective azoles. It was found that pyrrole was much less reactive. Complexes trans-[PtH(R)(PEt_3)$_2$], where R = 2-furyl, 2-benzoxazolyl and 2-benzothiazol were prepared via C–H bond activation. Their

efforts towards benzothiazole insertion into the C–S bond and analogous C–H activation products with 1-methylpyrrole and dibenzofuran were not successful. They concluded that activation of the relatively weaker N–H bonds occurs more readily than at C–S or C–H bonds.

Kitajima et al. [15] reported the oxidative conversion of a (di-μ-hydroxo)manganese (II,II) complex $[Mn(HB(3,5\text{-}Pz^{iPr2})_3]_2$-(OH), to the corresponding (di-μ-oxo)manganese (III,III) complex with $KMnO_4$. However, when $[Mn(HB(3,5\text{-}Pz^{iPr2})_3]_2$-(OH) was aerobically oxidized, formation of C-H bond oxygenated product (Fig. 3-4) was observed. The resultant complex had a dinuclear structure in which the two manganese ions were solely bridged with an oxo ligand.

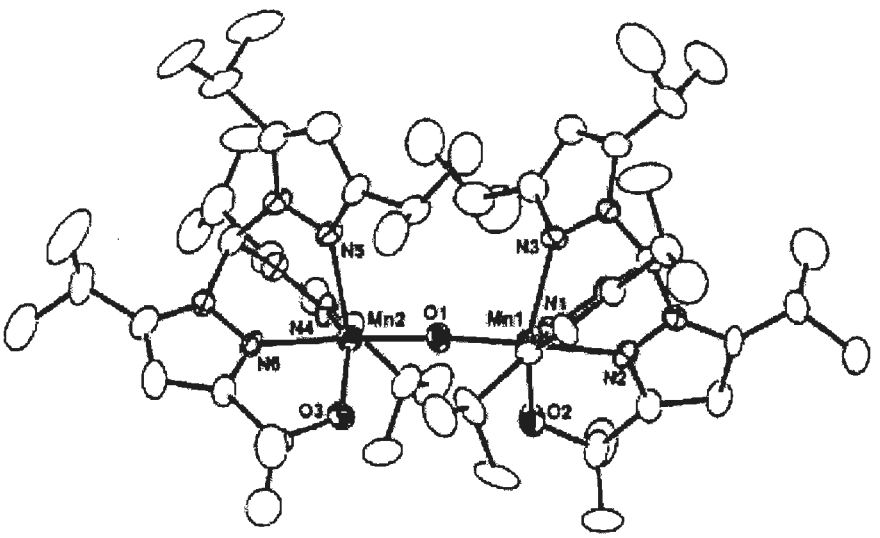

Fig. 3-4 Crystal structure of C-H bond oxidized product

Liu et al. [16] reported the half-sandwich cobalt (III) and rhodium (III) complexes with pyridine-2-thiolato ligands Cp*Co(PyS)I and Cp*Rh(PyS)Cl [Cp* = pentamethyl cyclopentadienyl, PyS = pyridine-2-thiolate] by the reactions of lithium pyridine-2-thiolate (PySLi) with $Cp^*Co(CO)I_2$ and $[Cp^*RhCl_2]_2$ respectively, in high yield. Complexes Cp*Co(PyS)I and Cp*Rh(PyS)Cl reacted with monodentate

$LiSC_2(H)B_{10}H_{10}$ to give $Cp^*Co(PyS)[SC_2\text{-}(H)B_{10}H_{10}]$ and $Cp^*Rh(PyS)[SC_2(H)B_{10}H_{10}]$ respectively. Reactions of $Cp^*Co(PyS)I$ and $Cp^*Rh(PyS)Cl$ with $Li_2S_2C_2B_{10}H_{10}$ resulted in C-H activation of a methyl group of the Cp* of the cobalt complex to give $[(C_5Me_4CH_2SC_5H_4N)Co(S_2C_2\text{-}B_{10}H_{10})]$ (Fig. 3-5) but no such activation of a methyl group of the Cp* of the rhodium complex occurred.

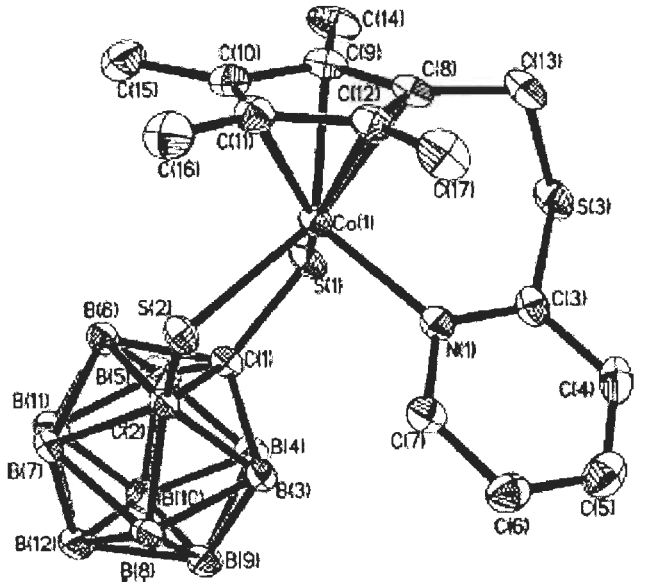

Fig. 3-5 Crystal structure of $[(C_5Me_4CH_2SC_5H_4N)Co(S_2C_2\text{-}B_{10}H_{10})]$

Hu et al. [17] reported the reactions between H_2dc3 and $Co(acac)_3$ both in the presence and absence of base. They found that in the presence of base, a complex with an intramolecular Co-C bond, $Co(dc3\text{-}C\text{-}(8))(H_2O)$ (Fig. 3-6) was formed, presumably through heterolytic C-H bond activation. An X-ray crystallographic study demonstrated the presence of a Co-C bond and the diazacyclooctane (daco) subunit adopted the chair-boat conformation with respect to the metal. However, they were unable to cleave this bond in presence of a strong acid. In absence of base, the reaction of $Co(acac)_3$ with H_2dc3 resulted in C-N cleavage of the ligand and the formation of a complex of dioxocyclam, Co(dc)(acac).

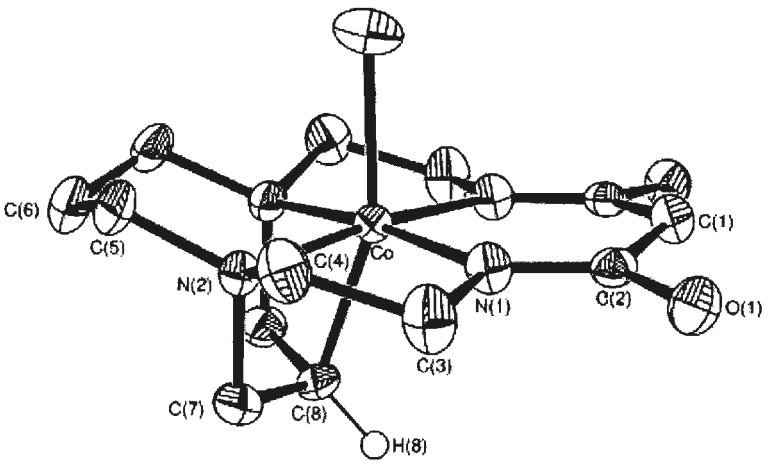

Fig. 3-6 Crystal structure of $[(C_5Me_4CH_2SC_5H_4N)Co(S_2C_2\text{-}B_{10}H_{10})]$

Zhou et al. [18] described the reaction of 1,4-bis(2-pyridylmethyl)-1,4-diazacyclononane (dmpdacn) ligand with a N_4C donor set deprotonates at CH_2 γ to an amine under extraordinarily mild conditions (pH 7) and behaved as a pentadentate ligand to Co(III) as the $[Co(dmpdacn\text{-}C)(OH_2)]^{2+}$ complex (Fig. 3-7).

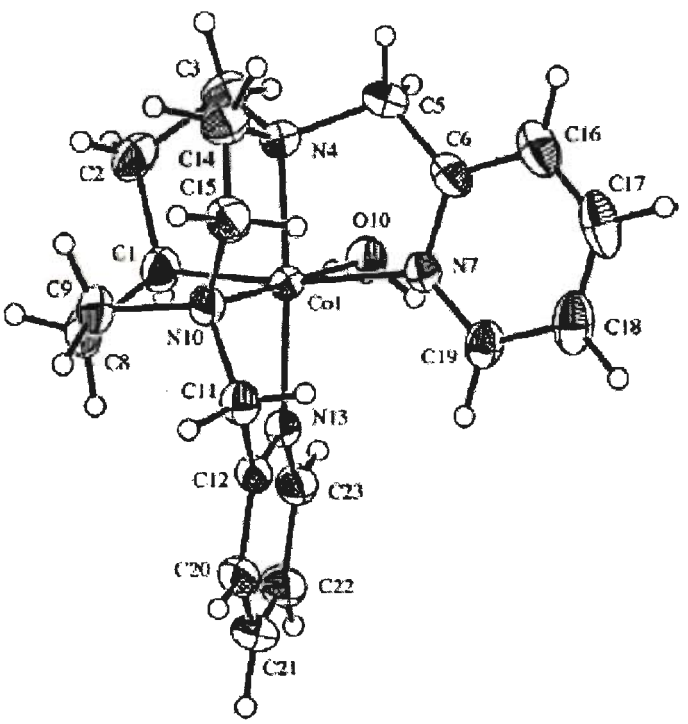

Fig. 3-7 Crystal structure of $[Co(dmpdacn\text{-}C)(OH_2)]^{2+}$ complex

They also reported an alternative synthesis from Co(II)dmpdacn and air and isolated the same C-bonded complex along with a novel hydroxylated Co(III) complex $[Co(dmpdacnOH\text{-}O)Cl]^{2+}$. Here, the carbanion was oxidized, a C- to O-bonded rearrangement took place and the bound aqua group was replaced by Cl^-.

Shay et al. [19] prepared [$Tp^{tBu,Me}$-Co=NAd] compound (Fig. 3-8) by the reaction of one equivalent of adamantyl azide (AdN_3) and THF solution of [$Tp^{tBu,Me}Co(N_2)$]. They found that the similar reaction of [$Tp^{tBu,Me}Co(N_2)$] with tert-butyl azide ($tBuN_3$) yielded a mixture of [$Tp^{tBu,Me}$Co=NtBu] and [$Tp^{tBu,Me}CoN_3$]. Both imido complexes were also structurally characterized by X-ray diffraction. The facile transformation of these complexes by a C-H activation demonstrated the inherent reactivity of compounds of this nature.

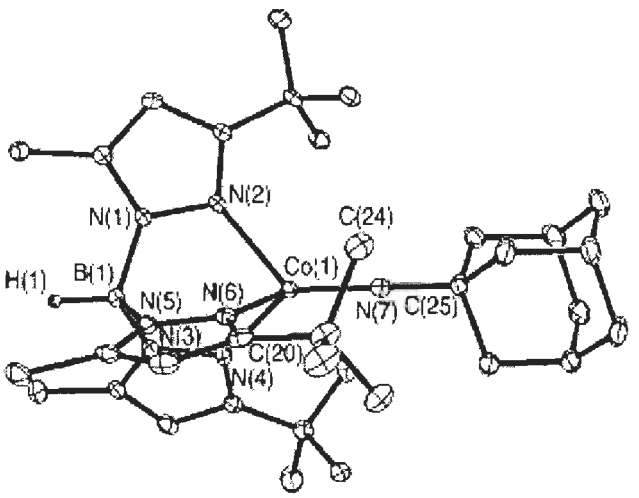

Fig. 3-8 Crystal structure of [$Tp^{tBu,Me}$-Co=NAd] complex

Leung et al. [20] reported a chiral self-assembled supramolecular M_4L_6 assembly as suitable host for a series of reactive monocationic half-sandwich iridium guests that are capable of activating C-H bonds. They found that upon encapsulation, selective C-H bond activation of organic substrates occurred. Purwoko et al. [21]

investigated the intermolecular C-H bond activation by photochemistry of $HB(Pz^{Me2})_3Rh(CO)_2$ (Pz^{Me2} = 3,5-dimethylpyrazolyl) in various alkane solutions at 293 K. The spectral results revealed that the photochemistry was exceptionally clean and that the reagent complex could be completely converted to the corresponding $HB(Pz^{Me2})_3Rh(CO)(R)H$ photoproduct at each of the irradiation wavelengths.

Wayland et al. [22] studied the kinetic and mechanistic aspects for the reaction of rhodium porphyrins in activating methane and toluene. The two rhodium complexes (tetramesitylporphyrinato)rhodium (II) monomer and (tetraxylylporphyrinato)rhodium (II) dimer were reacted with the benzene solution of methane to give equal quantities of hydride and methyl derivatives of the rhodium complexes. The reactions were studied using ^1H NMR. Some metalloporphyrins were also designed and studied for carrying out the oxidation of alkanes [23-25]. Lavrushko et al. [26] for the first time demonstrated the possibility of activating methane and its homologs with Pt salts. According to their studies the addition of alkanes including methane to a mixture of H_2PtCl_6 and Na_2PtCl_4 led to the generation of both alkyl halides and alcohols. In an attempt to deduce the mechanism with the help of proton NMR and chemical analysis they found that a complex of Pt(IV) containing a CH_3-Pt is formed, which was isolated from the solution as an adduct of Ph_3P.

Janowicz et al. [27] reported direct C-H bond activation in completely saturated hydrocarbons with organotransition-metal systems. They prepared a dihydridoiridium (III) complex, $(Me_5C_5)(Me_3P)Ir(H)_2$ by treatment of $[(Me_5C_5)IrCl_2]_2$ with trimethylphosphine followed by lithium triethylborohydride. This iridium complex on irradiation in benzene solution gave (η^5-

pentamethylcyclopentadienyl)(trimethylphosphine)hydridophenyliridium (III) complex, while on irradiation in cyclohexane solution, gave (η^5-pentamethylcyclopentadienyl) (trimethylphosphine)hydridocyclohexyliridium (III) complex and neopentane solution separately led to the formation of (η^5-pentamethylcyclopentadienyl)(trimethylphosphine) hydridoneopentyliridium (III) complex. The structures of these products were studied and confirmed by NMR spectroscopic studies. The NMR data suggested that the hydridoalkyliridium complexes formed are the intermolecular C-H activation products.

Sen et al. [28] studied the activation of different substrates including light alkanes (ethane, propane) in presence of species of platinum i.e., K_2PtCl_4 and Pt / O_2 in aqueous medium. They found that inactivated C-H bonds were activated by Pt(II) species while the C-H bonds adjacent to an oxygen atom were activated by metallic Pt.

Backlund et al. [29] reported the Ru complexes of 3-hydroxy-2-methyl-4-thiopyrone (thiomaltol or Htma) and 3-hydroxy-2-methyl-4H-thiopyran-4-thione (dithiomaltol or Httma). The complexes $[Ru(bpy)_2(tma)]^+$ and $[Ru(bpy)_2(ttma)]^+$ were able to undergo unexpected C-H bond activation upon oxidation. Oxidation of $[Ru(bpy)_2(ttma)]^+$ with different peroxidants and C-H bond activation at its pendant methyl group gave an air-stable aldehyde $[Ru(bpy)_2(ttma\text{-}aldehyde)]^+$ through the formation of an intermediate oxidation product $[Ru(bpy)_2(ttma\text{-}alcohol)]^+$. Oxidation with different peroxidants i.e., oxone, *m*-chloroperbenzoic acid, urea hydrogen peroxide and 2,6-dicarboxypyridinium chlorochromate gave similar yield of around 15 % while yield of the aldehyde was found to be slightly higher with 2-iodoxybenzenoic acid and $Na_2Ir(IV)Cl_6$. The structure of the aldehyde $[Ru(bpy)_2(ttma\text{-}aldehyde)]^+$ (Fig. 3-9) was confirmed by X-ray crystallography.

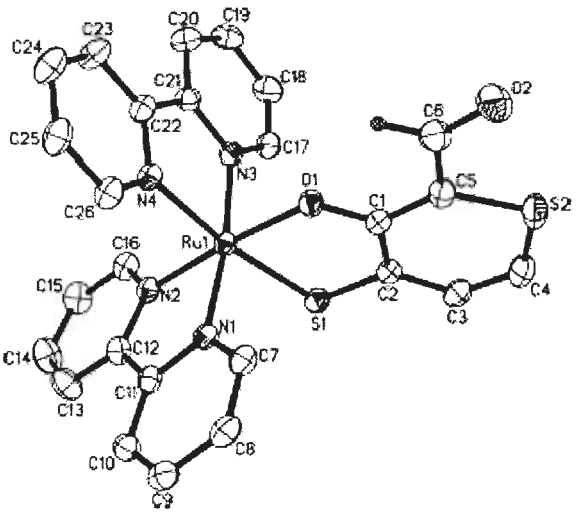

Fig. 3-9 Crystal structure of $[Ru(bpy)_2(ttma\text{-}aldehyde)]^+$ complex

Ito et al. [30] demonstrated that heating a mixture 3,5-dimethyl-R-Phebox (Phebox = bis(oxazolinylphenyl)) ligand, $RhCl_3(H_2O)_3$ and $NaHCO_3$ at 50 °C for 3 h in a methanolic solution gave a rhodium complex (3,5-dimethyl-dimethylPhebox)$RhCl_2(H_2O)$ (Fig. 3-10) with a yield of 84 %. The production of this rhodium complex involved aliphatic C-H bond activation. The rhodium complex (3,5-dimethyl-dimethylPhebox)$RhCl_2(H_2O)$ acted as a catalyst for asymmetric conjugate reduction of α,β-unsaturated carbonyl compounds and the asymmetric reductive aldol reaction of acralytes and aldehydes. Similarly, they prepared iridium complex (3,5-dimethyl-dimethylPhebox)$IrCl_2(H_2O)$ by the C–H bond activation in a reaction that involved heating a mixture consisting 3,5-dimethyl-R-Phebox (Phebox = bis(oxazolinylphenyl)) ligand, $H_2IrCl_6(H_2O)_6$ and $NaHCO_3$ in a methanolic solution at 50 °C for 3 h. This complex was also capable of catalyzing asymmetric conjugate reduction of α,β-unsaturated carbonyl compounds and the asymmetric reductive aldol reaction of acralytes and aldehydes. The structures of the two complexes were determined with the help of X- ray diffraction method.

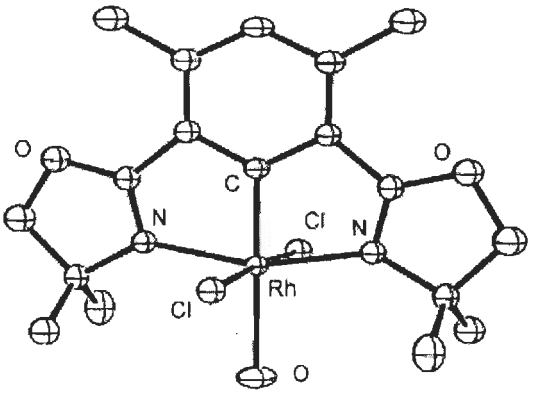

Fig. 3-10 Crystal structure of (3,5-dimethyl-dimethylPhebox)$RhCl_2(H_2O)$ complex

Sakakura et al. [31] reported a catalytic system for the carbonylation of hydrocarbons including alkanes to produce aldehydes via C-H bond activation steps. They showed that the rhodium complex $RhCl(CO)(PR_3)_2$ on irradiation catalyzed the carbonylation of hydrocarbons including alkanes at ambient temperature under an atmospheric pressure of CO to yield aldehydes. However, the use of other complexes of Co, Ir and Ru resulted in much lower catalytic activites. Bolig et al. [32] reported highly selective activation and functionalization of sp^3 C-H bond with the help of a cobalt complex $[(Cp)Co(VTMS)_2]$ (VTMS = vinyltrimethyl silane). 1-(dimethyl(vinyl)silyl)azepane and 1-(dimethyl(vinyl)silyl)azocane) were transformed to seven- and eight- membered N-protected enamines in a reaction catalyzed by this cobalt complex.

Cho et al. [33] described the oxidation of a methyl group in a complex of Ni using H_2O_2 to give a ligand based carboxylate group and an alkoxide as the final product. The reaction of $[Ni_2(OH)_2(Me_2\text{-tpa})_2]^{2+}$ (Me_2-tpa = bis(6-methyl-2-pyridylmethyl)(2-pyridylmethyl)amine with H_2O_2 led to the oxidation of a methylene group on the Me_2-tpa ligand to give an N-dealkylated ligand and oxidation of a methyl

group to afford a ligand-based carboxylate and an alkoxide as the final oxidation products. A series of sequential reaction intermediates produced in the oxidation pathways: a bis(μ-oxo) dinickel (III) ($[Ni_2(O)_2(Me_2\text{-tpa})_2]^{2+}$), a bis(μ-superoxo)dinickel (II) ($[Ni_2(O_2)_2(Me_2\text{-tpa})_2]^{2+}$), a (μ-hydroxo)(μ-alkylperoxo)dinickel (II) ($[Ni_2(OH)(Me_2\text{-tpa})(Me\text{-tpa-}CH_2OO)]^{2+}$), and a bis(μ-alkylperoxo)dinickel (II) ($[Ni_2(Me\text{-tpa-}CH_2OO)_2]^{2+}$) were isolated and characterized by various physicochemical measurements including X-ray crystallography and their oxidation pathways were investigated.

Hikichi et al. [34] reported oxidation of an aliphatic C-H bond in an isopropyl chain of the ligand in a Co complex to an alkoxo ligand using H_2O_2 as an oxidizing agent. A dinuclear Co(II)-μ-peroxo complex, $\{Co[HB(3,5\text{-}Pz^{iPr2})_3]\}_2(\mu\text{-}O_2)$, was yielded by reaction of the bis(μ-hydroxo)-Co(II)complex, $\{Co(OH)[HB(3,5\text{-}Pz^{iPr2})_3]\}_2$, with an equimolar amount of H_2O_2. Spontaneous decomposition of the μ-peroxo complex $\{Co(OH)[HB(3,5\text{-}Pz^{iPr2})_3]\}_2$ yielded a mono-oxygenated μ-alkoxo-μ-hydroxo complex, $Co_2(\mu\text{-}OH)[HB(\mu\text{-}3\text{-}OCMe_2\text{-}5\text{-}Pz^{iPr})(3,5\text{-}Pz^{iPr2})_2][HB(3,5\text{-}Pz^{iPr2})_3]$, in which one of the six 3-isopropyl methine carbon atoms was oxygenated and the resulting alkoxo ligand bridges the two Co(II) centers. In contrast, decomposition of $\{Co[HB(3,5\text{-}Pz^{iPr2})_3]\}_2(\mu\text{-}O_2)$ in the presence of an excess amount of H_2O_2 resulted in further oxygenation to give a mixture of the dinuclear Co(II)-bis(μ-alkoxo) complex, $\{Co[HB(\mu\text{-}3\text{-}OCMe_2\text{-}5\text{-}Pz^{iPr2})(3,5\text{-}Pz^{iPr2})_2]\}_2$, and the mononuclear Co(II)-hydroxo alcohol complex, $Co(OH)[HB(3\text{-}Me_2COH\text{-}5\text{-}Pz^{iPr2})(3\text{-}Me_2COH\text{-}5\text{-}Pz^{iPr2})_2]$ (Fig 3-11). In the bis(μ-alkoxo) complex $\{Co[HB(\mu\text{-}3\text{-}OCMe_2\text{-}5\text{-}Pz^{iPr})(3,5\text{-}Pz^{iPr2})_2]\}_2$, one of the three 3-isopropyl groups in each ligand was functionalized to give the alkoxide group,

which bridges the two metal centers. In the mononuclear hydroxo alcohol complex $Co(OH)[HB(3\text{-}Me_2COH\text{-}5\text{-}Pz^{iPr})(3\text{-}Me_2COH\text{-}5\text{-}Pz^{iPr2})_2]$, all of the three 3-isopropyl groups were oxygenated. The Co(II) center was coordinated by the resulting alcohol ligand as well as an hydroxide. Reaction of $\{Co(OH)[HB(3,5\text{-}Pz^{iPr2})_3]\}_2$ with 2 equivalents of ROOH (R = ^{t}Bu and $PhMe_2C$) at low temperature yielded a thermally unstable blue alkylperoxo compound. The $HB(3\text{-}^t Bu\text{-}5\text{-}Pz^{iPr})_3$ derivative, $Co(OOCMe_2\text{-}Ph)[HB(3\text{-}^t Bu\text{-}5\text{-}Pz^{iPr})_3]$, characterized successfully by X-ray crystallography contains the tetrahedral Co center.

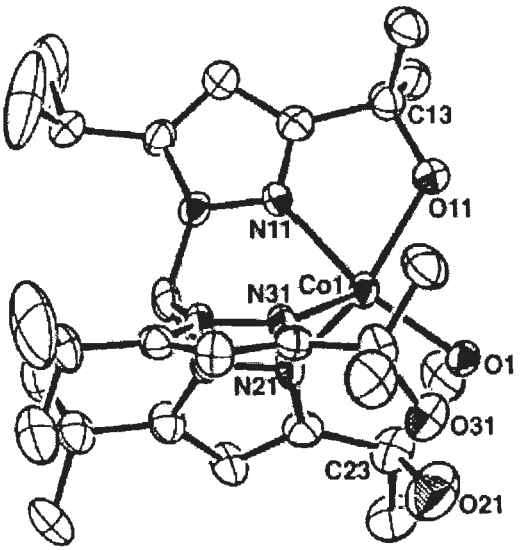

Fig. 3-11 Crystal structure of $Co(OH)[HB(3\text{-}Me_2COH\text{-}5\text{-}Pz^{iPr})(3\text{-}Me_2COH\text{-}5\text{-}Pz^{iPr})_2]$

The present chapter reports the synthesis and characterization of cobalt complexes with hydrotris(3,5-diisopropyl-1-pyrazolyl)borate [Tp^{iPr}], 3,5-diisopropyl pyrazole [$Pz^{iPr}H$] and N-tert-butyl-2-thioimidazole [tm^{tBu}] as supporting ligands. Also, efforts were made to oxidize C-H bond of methine present on isopropyl pyrazole and characterization of product by X-ray crystallography.

Results and Discussion

The 3,5-diisopropylpyrazole, ($Pz^{iPr2}H$) **3a** and potassium hydrotris(3,5-diisopropyl-1-pyrazolyl)borate (KTp^{iPr2}) **3b** have been prepared by the modified method of Kitajima et al. (Scheme 3-2) as described in chapter 5.

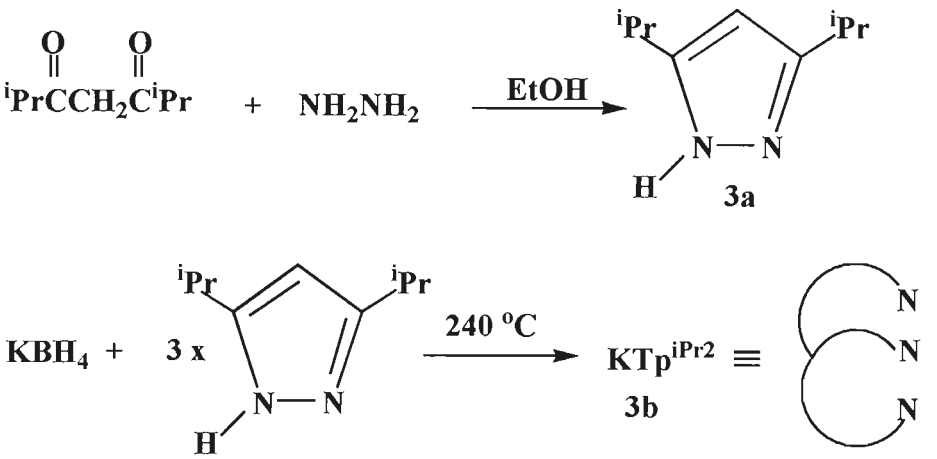

Scheme 3-2

The complex $[Tp^{iPr2}Co(NO_3)]$ **3c** was used as starting material for the preparation of benzoate complexes and was prepared by literature reported method (Scheme 3-3) [Ref. [43] of chapter 1]. Attempts were made to prepare the oxygen sensitive cobalt (II) compound so that the oxidation / oxygenation studies could be performed. The reaction of complex **3c** with sodium fluoro / chloro-benzoate in acetonitrile-toluene solution resulted in the formation of five coordinated [$Tp^{iPr2}Co$(*p*-X-OBz)] (X = F for **3d** and Cl for **3e**) (Scheme 3-3), whose IR data clearly indicated that the benzoate group was coordinated in bidentate manner as the separation between the ν_{as} and ν_s stretching vibration is less than 200 cm^{-1} [35]. The complexes **3d** and **3e** also show B-H stretching vibration in the range of 2532 and 2536 cm^{-1} respectively.

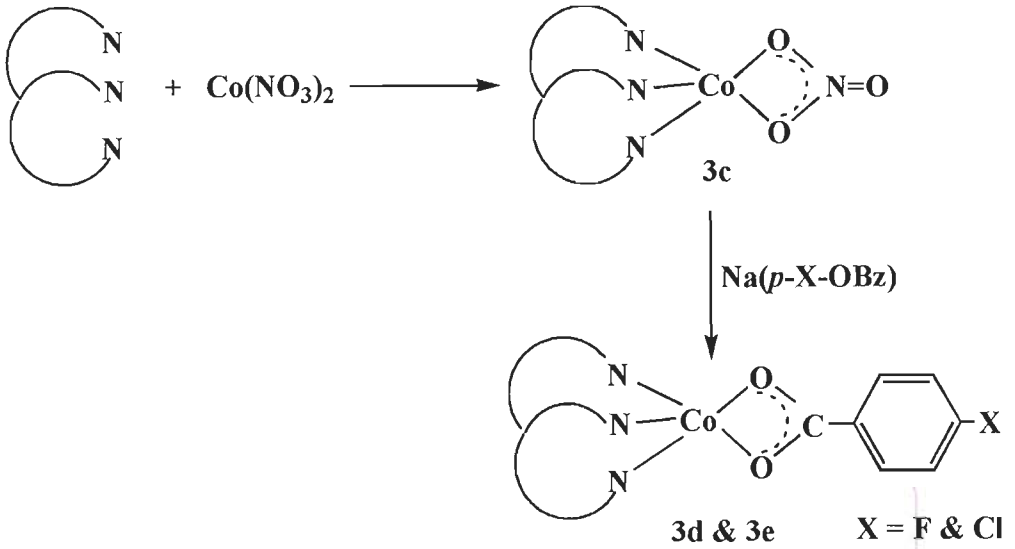

Scheme 3-3

The suitable crystal for X-ray data collection was obtained by slow cooling of the acetonitrile-dichloromethane solution of **3d** at -20 °C. The crystallographic data of **3d** is listed in Table 3-2 and important bond lengths and bond angles are given in Table 3-3. As can be seen in Fig. 3-12, the metal center of **3d** was in five coordination atmosphere, coordinated with three nitrogen atom from Tp^{iPr2} ligand and two oxygen atoms from the fluorobenzoate. The Co-O and Co-N bond lengths (Table 3-3) were similar to the literature reported value [Ref. [43] of chapter 1]. On the basis of X-ray data, it may be presumed that the geometry around metal center should be square pyramidal. It was also observed that adjacent molecules interacted with one C-H···π interaction i.e., 2.745 Å {C-H of fluorobenzoate ring and π-electrons of Pz^{iPr2} from Tp^{iPr2}} and two CH_3···π interactions i.e., 2.563 Å {CH_3 of Tp^{iPr2} and π-electrons of fluorobenzoate ring} and 2.762 Å {CH_3 of Tp^{iPr2} and π-electrons of Pz^{iPr2} from Tp^{iPr2}} [36] as shown in Fig. 3-13.

As per our effort towards the oxygen activation by transition metal complexes, toluene solution of **3d** and **3e** were exposed to dioxygen at room temperature but no color change was observed even after cooling the solution at -50 °C. Since the complex **3d** was five coordinate, coordinatively unsaturated, it was thought that it could be oxidized by suitable oxidizing agents. Thus H_2O_2 was added to the solution of complexes **3d** and **3e** in presence of $Pz^{iPr2}H$ and a color change was observed from blue to purple. This can be attributed to the oxidation of C-H bond present on isopropyl group along with metal center (Scheme 3-4).

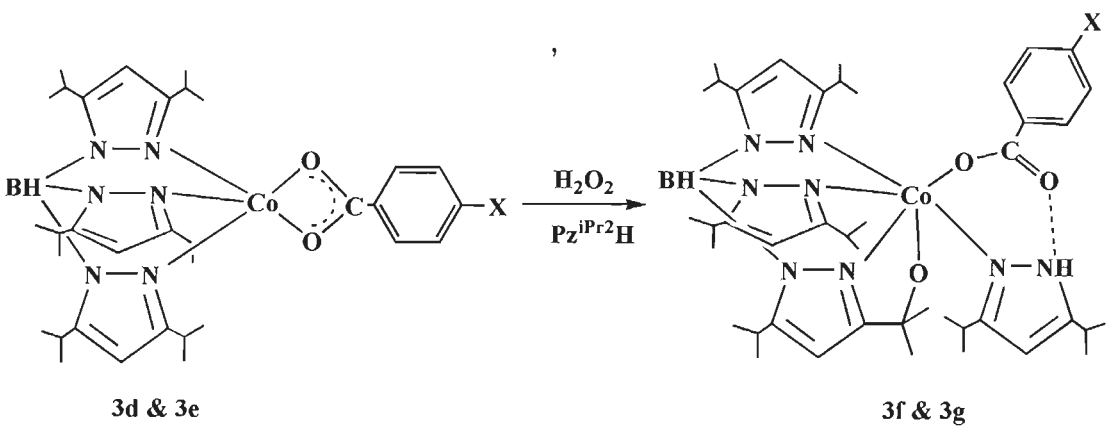

3d & 3e **3f & 3g**

Scheme 3-4

In complex **3f** and **3g**, the presence of N-H band at 3354 and 3362 cm^{-1} and B-H band at 2541 and 2537 cm^{-1} confirmed the binding of these ligands to the metal center. Also the separation between the ν_{as} and ν_s stretching vibration of carboxylate group was more than 200 cm^{-1} suggesting monodentate behavior of benzoate [35]. Room temperature magnetic moment values correspond to diamagnetic nature of complexes **3f** and **3g** suggesting the presence of low-spin cobalt (III) center. Suitable single crystal of complex **3f** for X-ray data collection was obtained by slow cooling of acetonitrile solution at -20 °C. The complex **3f** crystallizes in the triclinic system with space

group $P\bar{1}$. The crystallographic data is given in Table 3-4 whereas the important bond lengths and bond angles are given in Table 3-5. The crystal structure of complex **3f** is shown in Fig. 3-14. To our surprise, during the oxidation of **3d** with H_2O_2, in presence of one equivalent of free 3,5-diisopropylpyrazole, the monooxygenated intramolecular hydrogen bonded cobalt (II) complex **3f** was obtained. In complex **3f**, one of the six methine groups in the isopropyl substituents of Tp^{iPr2} distal to the metal center was oxidized along with metal and resulted in the six coordinated intramolecular hydrogen bonded fluorobenzoate complex. As shown in Fig. 3-14, the coordination behavior of fluorobenzoate changed form bidentate to monodentate. The Co1-O1 bond distance of the coordinated oxygen was 1.951(8) Å whereas the Co1-O2 bond distance was 3.474 Å. The long distance of Co1-O2 bond indicated that this oxygen was not involved in coordination with metal center. The cobalt–nitrogen bond distances of coordinated Tp^{iPr2} were in the range of 1.851(8)-2.010(9) Å which were shorter than metal-nitrogen bond distances in **3d** and were well in the range of reported value for cobalt (III)–nitrogen bond [37]. The nonbonded oxygen atom of fluorobenzoate formed intramolecular hydrogen bond with NH group of 3,5-$Pz^{iPr2}H$. The existence of hydrogen bonding in complex **3f** has been established as the location of hydrogen atom in crystal structure with bond distance of N8-Ha, 0.861 Å; O2-Ha, 1.921 Å. The bond distance between nitrogen of free pyrazole and the non-bonded oxygen atom of fluorobenzoate was 2.752 Å (N8-O2). These distances were well within the range of hydrogen bonding as reported in literature for other metal complexes [38, 39]. The formation of monooxygenated cobalt (III) complex was not unusual in the oxidation chemistry of Tp^{ipr2} coordinated cobalt (II) compound as reported by Hikichi et al. [34].

They have reported the extensive studies on aliphatic C-H oxygenation by Co(II)-peroxo species and demonstrated the formation of binuclear mono-oxygenated, di-oxygenated and mononuclear fully oxygenated Co(II) complex. In all these complexes, the metal center is five coordinated and no hydrogen bonding exists. In present mono-oxygenated Co(III) complex **3f**, the metal center is six coordinate and intramolecular hydrogen bonding exists having Co(III) as metal center. To our knowledge this was the first example of monooxygenated Co(III) six coordinate complex with intramolecular hydrogen bonding.

After confirming the C-H bond oxygenation in hydrotris(3,5-diisopropyl-1-pyrazolyl)borate [Tp^{iPr2}] system in presence of H_2O_2 and 3,5-diisopropylpyrazole, [$Pz^{iPr2}H$], the oxygenation reactions were also performed only on $Pz^{iPr2}H$ ligand in presence of different substituted benzoates using H_2O_2 as oxidant.

The reaction mixture of cobalt chloride, 3,5-diisopropylpyrazole and sodium fluoro / chloro-benzoate in absence of H_2O_2 resulted in binuclear compound [(3,5-$Pz^{iPr2}H)_2Co_2(\mu$-3,5-$Pz^{iPr2}H)_2$(*p*-X-OBz)$_2$] (X = F for **3h** and Cl for **3i**) (Scheme 3-5). The presence of NH band at 3367 and 3374 cm^{-1} in IR spectra of complexes **3h** and **3i** confirmed the binding of $Pz^{iPr}H$. Also the separation between ν_{as}(COO) and ν_s(COO) in both complexes were more than 200 cm^{-1} suggesting monodentate behavior of benzoates. The suitable crystal for X-ray data collection was obtained by slow cooling of the acetonitrile solution of **3h** at -20 °C. The crystal structure of complex **3h** is shown in Fig. 3-15. The crystallographic data of **3h** are listed in Table 3-6 and important bond lengths and bond angles are given in Table 3-7.

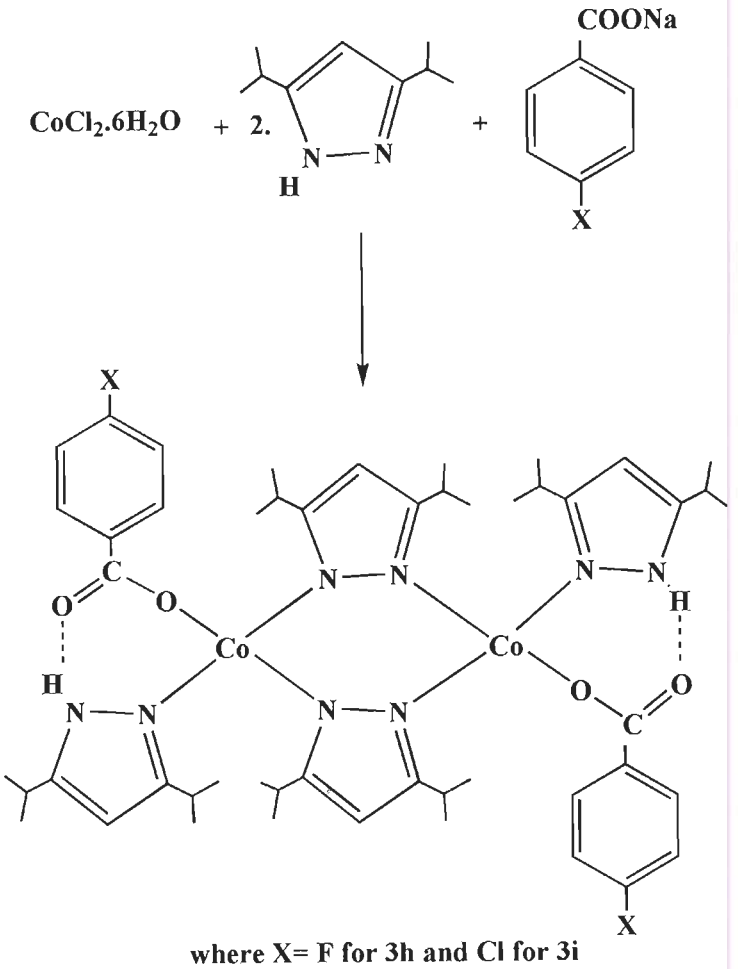

where X= F for 3h and Cl for 3i

Scheme 3-5

The crystal structure of complex **3h** representing a di(μ-pyrazolato) dicobalt complex with both terminal and bridging pyrazoles along with hydrogen bonded benzoates. The cobalt-nitrogen bond distances for terminally coordinated pyrazoles were slightly longer than the bridging ones (Fig. 3-15). Both fluorobenzoate groups were coordinated unidentately with cobalt centre and the non bonded oxygen atoms form hydrogen bonding with $Pz^{iPr2}H$. The nitrogen-oxygen bond distance (N6-O2) of 2.723 Å, (N6-H6a; 0.860 Å, O2-H6a; 1.947 Å) clearly demonstrated the presence of hydrogen bonding in this complex. The Co-Co separation in this complex was 3.603 Å which was longer than the Co-Co separation in binuclear cobalt complexes having

Tp^{iPr2} ligand [34, 40] but shorter than the recently reported similar binuclear cobalt (II) complex with Co-Co distance of 3.629 Å [41]. This complex seems to be an unusual binuclear complex in which each cobalt (II) atom was electron deficient (15 electrons) and was in a distorted tetrahedral environment.

When methanolic solution of fluoro-benzoate and few drops of H_2O_2 (30 %) was added in dichloromethane solution of cobalt chloride and 3,5-diisopropylpyrazole at – 40 °C, the color of the complex changed from blue to pink. Similar reactions were also carried out with different *p*-X-benzoates (X = F for **3j**, Cl for **3k**, CH_3 for **3l**, NO_2 for **3m**, CN for **3n**, CHO for **3o**) to see the effect of substituents on crystal packing (Scheme 3-6).

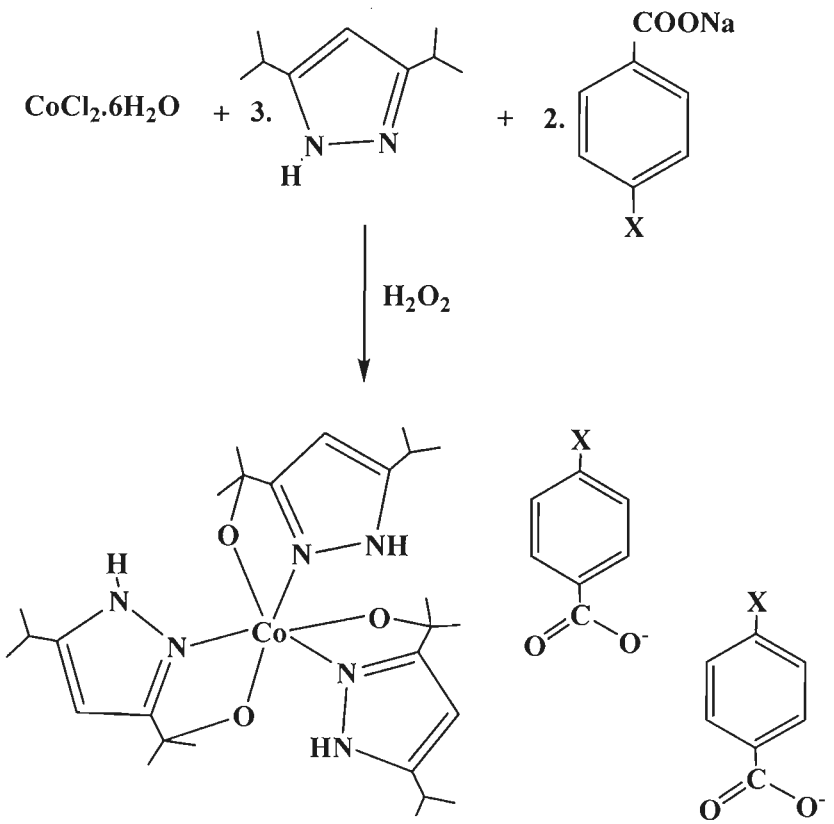

where X= F for 3j, Cl for 3k, CH_3 for 3l, NO_2 for 3m, CN for 3n, CHO for 3o

Scheme 3-6

All of these complexes have been characterized by elemental, IR and magnetic susceptibility measurements. They were found to be diamagnetic in nature. The suitable pink color crystals of **3j, 3k, 3l** and **3n** for X-ray data collections were obtained in acetonitrile at -20 °C. They crystallize in centrosymmetric $P2_1/c$ group with one molecule of the cobalt complex and two *p*-X-benzoate (X = F for **3j**, Cl for **3k**, CH_3 for **3l**, CN for **3n**) anions in the asymmetric unit. Thus cobalt complex acted as host molecule and benzoates occupied their positions as guest molecules. The crystal structure of complexes **3j, 3k, 3l** and **3n** are shown in Fig. 3-16, 3-23, 3-28 and 3-33 respectively. The crystallographic data is given in Table 3-8, 3-10, 3-12 and 3-14 whereas the important bond lengths and bond angles are given in Table 3-9, 3-11, 3-13 and 3-15. The X-ray structures demonstrated that the metal center was six coordinated with N3O3 donor atoms in octahedral arrangement in all complexes having formula $[Co(3\text{-}OCMe_2\text{-}5\text{-}Pz^{iPr}H)_3].(p\text{-}X\text{-}OBz)_2$ (where X = F for **3j**, Cl for **3k**, CH_3 for **3l**, CN for **3n**). The three of six methine groups of 3,5-diisopropylpyrazole were oxygenated by cleavage of H_2O_2 through free radical mechanism and coordinated the cobalt center as in monooxygenases [34]. In this reaction, along with the oxidation of methine groups, metal center also oxidized from cobalt (II) to cobalt (III). The two cobalt complexes were interacting with C-H···π interactions and building a three-dimensional architecture having vacant space for guest molecules (benzoates). The shape and size of vacant space was different for different benzoates and it mainly depends upon extent of CH_3···π interactions. It was observed that small CH_3···π interactions caused spiral packing view whereas long CH_3···π interactions caused rectangular view [36]. In complexes **3j**, **3k** and **3l,** the distance of CH_3···π interactions were in the range of 2.713 to 2.866 Å (Fig. 3-17, 3-24 and 3-29) and host molecules were forming spiral packing

having triangular void spaces for guest molecules as can be seen in Fig. 3-18, 3-25 and 3-30. A space fill model of host and host-guest framework for complex **3j** was also drawn to see the exact shape of cavity (Fig. 3-19 and 3-22) and was found to be triangular. The guests (benzoates) molecules were also interacting with host molecule through C-H···O interactions as can be seen in the Fig. 3-20, 3-26 and 3-31 [36] and in complexes **3j** and **3k**, additional C-H···F and C-H···Cl interactions were also observed [42]. Due to these interactions benzoate molecules were sited in triangular voids and forming host-guest supramolecular architecture as shown in Fig. 3-21, 3-27 and 3-32 (Table 3-16).

It was really surprising that in case of *p*-cyanobenzoate as guest molecule, shape of cavity changed from spiral to rectangular. This change can be explained on the basis of $CH_3\cdots\pi$ interactions occurring between host molecules. As in complex **3n**, the distance of $CH_3\cdots\pi$ interactions was 3.055 Å (Fig. 3-34) as compared to other complexes **3j-3l** (2.713 to 2.866 Å), that elongate the two host molecules to form rectangular shaped packing (Fig. 3-35) and can be easily seen in space fill model (Fig. 3-36). Further, host and guest molecules were interacting through four C-H···O interactions as shown in Fig. 3-37 (Table 3-16). In three-dimensional framework, rectangular voids were filled with *p*-cyanobenzoate molecules with these non-covalent interactions (Fig. 3-38 and 3-39).

Thermal analysis

Thermo-gravimetric analyses (TGA) were carried out in air atmosphere in temperature range of 25-700 °C for complexes **3j-3o** with the heating rate of 10 °C min^{-1}. The TGA curve of these complexes was almost same and showed one sharp weight loss (Fig. 3-40 to 3-45). This sharp weight loss can be attributed to

removal of guest molecules (para-substituted benzoates) from host-guest complex at that temperature. The calculated and experimental values for that loss are given in Table 3-17. Later, it can be assumed that in all these complexes, cobalt ions form their oxides as the TGA curve becomes constant at 700 °C.

Further to check the host-guest interaction in solution state, we prepared host complex $[Co(3\text{-}OCMe_2\text{-}5\text{-}Pz^{iPr}H)_3]$ (**3p**) and used sandwich membrane method to determine formation constant for different benzoates. The sandwich membrane was prepared as described in chapter 5 and membrane composition was optimized as follows.

Optimization of membrane composition

The composition of membrane with different plasticizers and additive, performing best is given along with their characteristics in Table 3-18. Among the four different plasticizers (NPOE, DBP, BA, TBA) used, NPOE was the most effective solvent mediator in preparing the benzoate selective membrane electrode. The amount of ionophore (**3p**) was also found to affect the response of membrane electrode (Table 3-18). The sensitivity of the electrode response increased with increase in the ionophore content upto the value of 4 mg, further addition of ionophore however diminished the response of the electrode, which may be due to some inhomogenities and possible saturation of the membrane. The presence of 3 mg of HTAB as a cationic additive improved the sensitivity of benzoate sensor considerably (no. 6). As can be seen from Table 3-18, that the membrane having composition PVC : NPOE : **3p** : HTAB as 150 : 330 : 4 : 3 (w / w) exhibited the best results with a Nernstian slope and a limit of detection of 3.2×10^{-6} M. The electrode showed a linear response to the concentration of benzoate ion in the range of 3.6×10^{-6} - 1.0×10^{-1} M. The slope of the

calibration graph was 59.2 ± 0.2 mV per decade of activity. The membrane sensor prepared could be used for at least 10 weeks without any divergence in potentials. The response time of the electrode was determined by measuring the time required to achieve a 96 % of the steady potential. The static response time thus obtained was 20 s over the entire concentration range.

Determination of formation constant

Formation constant of the ion–ionophore complex within the membrane phase is a very important parameter that dictates the practical selectivity of the ionophore [43]. To determination of formation constant, sandwich membrane was prepared in which two membrane segments are fused together, with only one containing the ionophore, to give a concentration-polarized sandwich membrane. A membrane potential measurement of this transient condition reveals the ion activity ratio at both interfaces that could be translated into the apparent binding constants of the ion-ionophore complex. In this method complex formation constants are obtained by neglecting ion pairing. As reported, the membrane potential E_M is determined by substracting the cell potential for a membrane without ionophore from that for the sandwich membrane. The formation constant is then calculated from the following equation:

$$\beta_{IL_n} = \left(L_T - \frac{nR_T}{Z_I} \right)^{-n} \exp\left(\frac{E_M z_I F}{RT} \right)$$

where, L_T is the total concentration of ionophore in the membrane segment; R_T is the concentration of lipophilic ionic site additives; n is the ion–ionophore complex stoichiometry and R, T and F are the gas constant, the absolute temperature and the Faraday constant. The ion I carries a charge of z_I.

The determined formation constants (log β_{IL_n}) for the examined complexes were recorded in Table 3-19. The elapsed time between sandwich fusion and exposure to electrolyte was typically <1 min. The potential was recorded as the mean of the last minute of a 5 min measurement period in the appropriate salt solution. The potential of such sandwich membranes remains free of diffusion-induced potential drifts for about 20 min. Standard deviations were obtained based on the measurements of sets of at least three replicate membrane disks that were made from the same parent membrane. The formation constant clearly indicates that it was high for electron donating benzoate than electron withdrawing benzoate anions. The formation constant of the ions was in the following order: *p*-F-OBz > *p*-Cl-OBz > *p*-CH_3-OBz > *p*-NO_2-OBz > *p*-CN-OBz > *p*-CHO-OBz. All benzoates showed significant values confirming their interactions with host cobalt complex in solution state.

In another set of experiment, some cobalt complexes having N-tert-butyl-2-thioimidazole ligand were also prepared and change in structure due to the effect of reaction time was discussed. Figueroa et al. [44] recently reported the formation of compound with disulphide bond in catalytic reaction of N-tert-butyl-2-thioimidazole and its metal complexes. In present study, we used N-tert-butyl-2-thioimidazole which in solution converted to disulphide without any catalyst and coordinated to cobalt center through nitrogen atoms. It implied that the formation of disulphide can be achieved in solution without using any catalyst. With this background, we started the preparation of **3q** where the reaction of cobalt chloride hexahydrate and N-tert-butyl-2-thioimidazole for 2 h resulted in the formation of complex **3q** but the same reaction in the same stoichiometric ratio for 8 h resulted in the formation of product **3r** with an entirely different structure (Scheme 3-7).

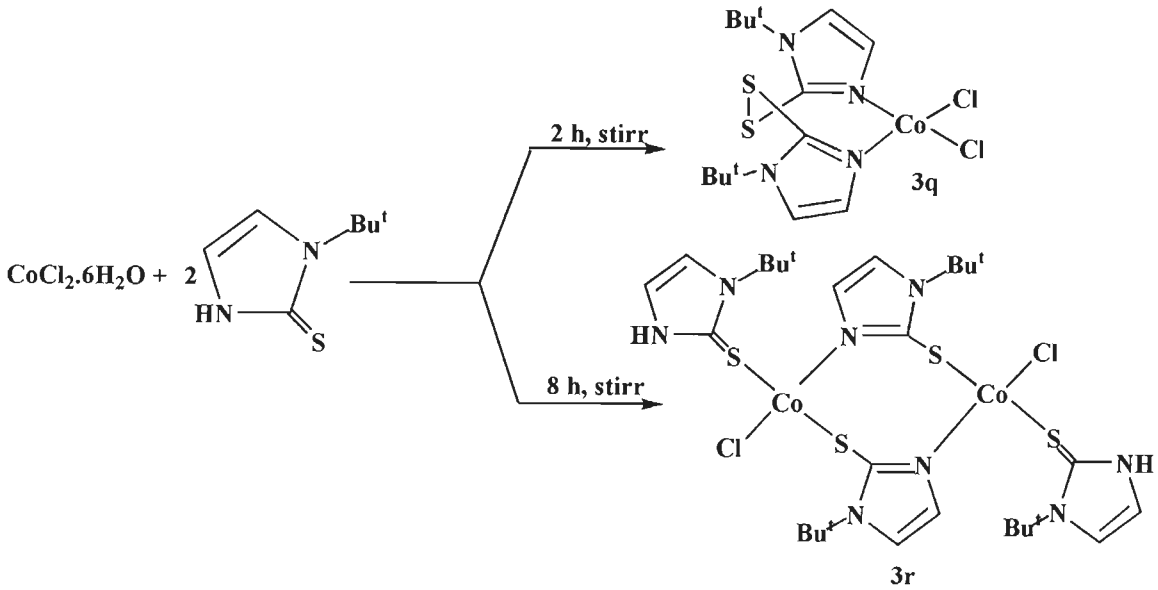

Scheme 3-7

This is an interesting example of time dependent product formation with different structures and reflects the idea that time period of reaction plays an important role in deciding the fate of reaction product. The complex **3q** crystallizes in the orthorhombic system (P 21 21 21 space group) whereas the complex **3r** crystallizes in the monoclinic system ($P2_1/c$ space group). The crystal structure of **3q** is shown in Fig. 3-46 where the cobalt centre was four coordinated with two nitrogen atoms from N-tert-butyl-2-thioimidazole and two chloride ions. The crystallographic data of **3q** is listed in Table 3-20 and important bond lengths and bond angles are given in Table 3-21. The cobalt - nitrogen bond distances are Co(1)-N(1) 2.034(9) Å, Co(1)-N(2), 2.016(9) Å. These are well within the range of nitrogen containing coordinated ligands with cobalt center [45]. The cobalt-chloride bond distances are 2.239(3) Å {Co(1)-Cl(1)} and 2.237(3) Å {Co(1)-Cl(2)} which are almost same and fall well within the reported range [46]. The coordination of these ligands gives tetrahedral geometry to the metal centre in complex **3q**. Interestingly the sulphur atom of ligand did not coordinate with the metal center but the formation of S-S bond occurs between

two molecule of ligands with S-S and S-C bond distances of 2.050(4) and 1.777(10) Å which were typical of single bonds [47]. In fact there is one example of zinc complex where the complex was not obtained by using the disulphide $(mim^{Me})_2$ as a reagent; rather than, $[k^2\text{-}(mim^{Me})_2]ZnCl_2$ was only isolated as a side product in 4 % yield resulting from adventitious oxidation of methimidazole $(mim^{Me})_2$ during the reaction with $ZnCl_2$ over a period of several months at 0 °C [48]. The chloride ion shows intermolecular C-H···Cl interaction between hydrogen atoms of tert-butyl group and coordinated chloride ion during packing in unit cell which is along the a-axis (Fig. 3-47). The other non-covalent interactions like C-H···π and CH_3···π exists in complex **3q** as shown in Fig. 3-48.

When the reaction in scheme 3-7 was performed for 8 h, a thioimidazole bridged binuclear complex was obtained where four N-tert-butyl-2-thioimidazole were coordinated to both cobalt centers. Out of four ligands, two ligands were behaving as bidentate, binding to the metal centers through nitrogen as well as sulphur atoms, whereas the other two ligands were coordinated through sulphur atoms only. The crystal structure of complex **3r** is shown in Fig. 3-49. The crystallographic data of **3r** is listed in Table 3-22 and important bond lengths and bond angles are given in Table 3-23. Like in complex **3q**, here also, each metal center was four coordinated with distorted tetrahedral geometry. The most striking feature of this complex was that N-tert-butyl-2-thioimidazole coordinated through both nitrogen and sulphur atoms whereas in complex **3q**, it coordinates through only nitrogen atom. The metal-sulphur distances were clearly different for both the bridging as well as the terminal metal–sulphur bonds i.e., Co(1)-S(1), 2.3366(11) (terminal); Co(1)-S(2), 2.3006(10) (bridging) and in the range of reported values [49]. The cobalt-nitrogen bond distances

with both metal centers were same (1.997(3) Å). The larger terminal cobalt-sulphur bond distances in complex **3r**, make the geometry distorted tetrahedral. The crystal packing of complex **3r** shows the presence of C-H···Cl and C-H···S intermolecular interaction between hydrogen atoms of tert-butyl group and chloride / sulphur atoms respectively (Fig. 3-50). Due to the presence of C-H···S non-covalent interactions between two molecules, the formation of one dimensional chain along the b-axis occurs in complex **3r** as shown in Fig. 3-51.

Summary

The reaction of $[Tp^{iPr2}Co(NO_3)]$ **3c** with sodium fluoro / chlorobenzoate gave five coordinate complex $[Tp^{iPr2}Co(p\text{-X-OBz})]$ **3d** and **3e**. The complex $[Tp^{iPr2}Co(p\text{-F-OBz})]$ **3d** was characterized from X-ray studies and confirmed that it was coordinatively unsaturated with three nitrogen atoms from Tp^{iPr2} ligand and two oxygen atoms from fluorobenzoate. Further **3d** was oxidized with 30 % H_2O_2 in presence of free pyrazole. The oxidized product **3f** has unique structure, the cobalt was oxidized in +3 oxidation state and one of the six methine carbon atom in the isopropyl groups of Tp^{iPr2} ligand was oxygenated and form Co-O bond with metal center. The coordination behavior of fluorobenzoate changed from bidentate to monodentate and unbonded oxygen atom of fluorobenzote forms intramolecluar hydrogen bond with NH fragment of the coordinated $Pz^{iPr2}H$ giving six coordination number to the cobalt center.

When the reaction of cobalt chloride, 3,5-diisopropyl pyrazole and para-substituted benzoates were performed in absence of H_2O_2, a binuclear pyrazole bridged moiety i.e., **3h** and **3i** were formed whereas similar reactants in presence of H_2O_2 produce host-guest type complexes i.e., **3j-3o**. In these complexes, the methine C-H bond of $Pz^{iPr2}H$ was oxidized and form octahedral cobalt complex having N3O3

coordination environment, acting as host and two benzoate anions were sited as guest molecules. Also, on changing electron donating group (F, Cl, CH_3) from electron withdrawing group (NO_2, CN, CHO) at para position of benzoate, three-dimensional packing of host molecule changed and shape of the cavity also changed from triangular to rectangular voids. To our knowledge, this is the first example where a cobalt complex of 3,5-disisopropylpyrazole after oxygenation of methine C-H gave different void space for encapsulation of different benzoate anions. Formation constant studies also confirmed the interaction of host and guest molecules in solution state.

We have also prepared two new cobalt (II) complexes and demonstrated the role of reaction time. For less reaction time, monomeric product was obtained and for longer reaction time with the same reactants dimeric product was obtained and the coordination site of ligands completely changed from nitrogen to sulphur. The nature of the ligand was monodentate in complex **3q** and the sulphur atoms were involved in the formation of disulphide bond. But the same ligand behaved as bidentate in complex **3r**. Hence, we may suggest that time of reaction is one of the important factor in determining the structure of the product and coordination mode of the ligands as revealed by present study.

Table 3-2 Crystal Data and Collection Details of [Tp^{iPr2}Co(*p*-F-OBz)] (3d)

Empirical formula	$C_{34}H_{50}N_6O_2FBCo$
Formula weight	663.54
Crystal system	Triclinic
Space group	$P\bar{1}$
Lattice parameters	
a (Å)	9.260(5)
b (Å)	15.260(5)
c (Å)	24.850(5)
α (°)	90.360(5)
β (°)	95.020(5)
γ (°)	90.910(5)
Cell volume V ($Å^3$)	3498(2)
Z	4
D_{Calc} (g cm^{-3})	1.260
Data collection	
μ (Mo K_α) mm^{-1})	
θ_{max} (°)	25.5
Reflections measured	13030
Independent reflections	6829
Number of parameters refined	819
R	0.0461
R_w	0.1022

Table 3-3 Selected Bond Distances (Å) and Bond Angles (°) for $[Tp^{iPr2}Co(p\text{-F-OBz})]$ (3d)

Bond Distances			
Co(1)–N(1)	2.049(9)	Co(1)–N(3)	2.057(8)
Co(1)–N(5)	2.088(9)	Co(1)–O(1)	2.179(7)
Co(1)–O(2)	2.050(7)		
Bond Angles			
N(1)–Co(1)–N(3)	87.6(4)	N(1)–Co(1)–N(5)	89.5(4)
N(3)–Co(1)–N(5)	91.9(4)	N(1)–Co(1)–O(1)	103.2(4)
N(1)–Co(1)–O(2)	154.6(4)	N(3)–Co(1)–O(1)	111.3(4)
N(3)–Co(1)–O(2)	116.3(4)	N(5)–Co(1)–O(1)	153.7(4)
N(5)–Co(1)–O(2)	97.8(4)	O(1)–Co(1)–O(2)	61.5(3)

Table 3-4 Crystal Data and Collection Details of [{HB(μ-3-OCMe$_2$-5-Pz^{iPr})(Pz^{iPr2})$_2$}Co(Pz^{iPr2}H)(*p*-F-OBz)] (3f)

Empirical formula	$C_{43}H_{65}N_8O_3FBCo$
Formula weight	1787.52
Crystal system	Triclinic
Space group	$P\bar{1}$
Lattice parameters	
a (Å)	14.026(5)
b (Å)	18.810(5)
c (Å)	21.645(5)
α (°)	98.232(5)
β (°)	95.002(5)
γ (°)	103.018(5)
Cell volume V (Å^3)	5464(3)
Z	2
D_{Calc} (g cm^{-3})	1.086
Data collection	
μ (Mo K_α) mm^{-1})	
θ_{max} (°)	25.81
Reflections measured	21050
Independent reflections	5128
Number of parameters refined	1058
R	0.0838
R_w	0.2192

Table 3-5 Selected Bond Distances (Å) and Bond Angles (°) for [{HB(μ-3-OCMe$_2$-5-Pz^{iPr})(Pz^{iPr2})$_2$}Co(Pz^{iPr2}H)(p-F-OBz)] (3f)

Bond Distances			
Co(1)-N(1)	1.984(9)	Co(1)-N(3)	2.010(9)
Co(1)-N(5)	1.851(8)	Co(1)-N(7)	1.985(10)
Co(1)-O(1)	1.951(8)		
Bond Angles			
N(1)-Co(1)-N(3)	87.9(4)	N(1)-Co(1)-N(7)	173.4(5)
N(5)-Co(1)-N(1)	84.0(4)	N(5)-Co(1)-N(3)	96.2(5)
N(5)-Co(1)-N(7)	90.4(4)	N(7)-Co(1)-N(3)	89.2(4)
N(5)-Co(1)-O(1)	171.6(3)	N(5)-Co(1)-O(3)	81.7(4)
O(1)-Co(1)-N(1)	89.4(4)	O(1)-Co(1)-N(3)	88.7(4)
O(1)-Co(1)-N(7)	96.4(4)	O(3)-Co(1)-N(1)	94.1(4)
O(3)-Co(1)-N(3)	176.9(3)	O(3)-Co(1)-N(7)	88.5(4)
O(3)-Co(1)-O(1)	93.7(3)		

Table 3-6 Crystal Data and Collection Details of $[(Pz^{iPr2}H)_2Co_2(\mu\text{-}Pz^{iPr2})_2(p\text{-}F\text{-}OBz)_2]$ (3h)

Empirical formula	$C_{50}H_{70}N_8O_4F_2Co_2$
Formula weight	1003.00
Crystal system	Triclinic
Space group	$P\bar{1}$
Lattice parameters	
a (Å)	10.2068(10)
b (Å)	11.3445(5)
c (Å)	13.6915(6)
α (°)	110.032(2)
β (°)	107.068(2)
γ (°)	94.366(2)
Cell volume V ($Å^3$)	1396.02(16)
Z	1
D_{Calc} (g cm^{-3})	1.193
Data collection	
μ (Mo K_α) (cm^{-1})	0.647
θ_{max} (°)	27.19
Reflections measured	6217
Independent reflections	3894
Number of parameters refined	298
R	0.0455
R_w	0.1392

Table 3-7 Selected Bond Distances (Å) and Bond Angles (°) for $[(Pz^{iPr2}H)_2Co_2(\mu\text{-}Pz^{iPr2})_2(p\text{-}F\text{-}OBz)_2]$ (3h)

Bond Distances			
Co(1)-N(1)	1.986(2)	Co(1)-N(2)	1.989(2)
Co(1)-N(5)	2.007(2)	Co(1)-O(1)	1.9363(19)
Bond Angles			
N(1)-Co(1)-N(2)	111.73(9)	N(1)-Co(1)-N(5)	106.88(9)
N(2)-Co(1)-N(5)	106.29(9)	N(1)-Co(1)-O(1)	109.43(9)
N(2)-Co(1)-O(1)	107.71(9)	N(5)-Co(1)-O(1)	114.83(9)

Table 3-8 Crystal Data and Collection Details of [Co(3-OCMe$_2$-5-Pz^{iPr}H)$_3$]. 2(*p*-F-OBz) (3j)

Empirical formula	$C_{41}H_{52}N_6O_7F_2Co$
Formula weight	837.82
Crystal system	Monoclinic
Space group	$P2_1/c$
Lattice parameters	
a (Å)	16.630(4)
b (Å)	14.597(4)
c (Å)	19.966(5)
α (°)	90.00
β (°)	111.094(7)
γ (°)	90.00
Cell volume V (Å^3)	4522(2)
Z	4
D_{Calc} (g cm^{-3})	1.231
Data collection	
μ (Mo K_α) (cm^{-1})	0.439
θ_{max} (°)	22.69
Reflections measured	6045
Independent reflections	4771
Number of parameters refined	525
R	0.0596
R_w	0.1494

Table 3-9 Selected Bond Distances (Å) and Bond Angles (°) for [Co(3-OCMe$_2$-5-Pz^{iPr}H)$_3$]. 2(*p*-F-OBz) (3j)

Bond Distances			
Co(1)-N(1)	2.069(4)	Co(1)-N(2)	2.082(4)
Co(1)-N(3)	2.084(4)	Co(1)-O(1)	2.160(3)
Co(1)-O(2)	2.200(3)	Co(1)-O(3)	2.157(3)
Bond Angles			
N(1)-Co(1)-N(2)	107.49(15)	N(1)-Co(1)-N(3)	153.06(15)
N(2)-Co(1)-N(3)	94.57(14)	N(1)-Co(1)-O(1)	73.70(13)
N(1)-Co(1)-O(2)	90.07(14)	N(1)-Co(1)-O(3)	94.90(13)
N(2)-Co(1)-O(1)	93.86(13)	N(2)-Co(1)-O(2)	72.57(12)
N(2)-Co(1)-O(3)	145.03(13)	N(3)-Co(1)-O(1)	89.90(13)
N(3)-Co(1)-O(2)	111.65(14)	N(3)-Co(1)-O(3)	73.95(12)
O(1)-Co(1)-O(2)	154.95(12)	O(1)-Co(1)-O(3)	118.49(11)
O(2)-Co(1)-O(3)	81.10(11)		

Table 3-10 Crystal Data and Collection Details of [Co(3-OCMe$_2$-5-Pz^{iPr}H)$_3$]. 2(*p*-Cl-OBz) (3k)

Empirical formula	$C_{41}H_{52}N_6O_7Cl_2Co$
Formula weight	870.72
Crystal system	Monoclinic
Space group	$P2_1/c$
Lattice parameters	
a (Å)	16.695(11)
b (Å)	14.776(10)
c (Å)	20.042(13)
α (°)	90.00
β (°)	110.44(2)
γ (°)	90.00
Cell volume V (Å^3)	4633(5)
Z	4
D_{Calc} (g cm^{-3})	1.248
Data collection	
μ (Mo K_α) (cm^{-1})	0.537
θ_{max} (°)	24.27
Reflections measured	7506
Independent reflections	4254
Number of parameters refined	521
R	0.0661
R_w	0.1763

Table 3-11 Selected Bond Distances (Å) and Bond Angles (°) for [Co(3-OCMe$_2$-5-Pz^{iPr}H)$_3$]. 2(*p*-Cl-OBz) (3k)

Bond Distances			
Co(1)-N(1)	2.102(4)	Co(1)-N(2)	2.089(4)
Co(1)-N(3)	2.113(4)	Co(1)-O(1)	2.204(4)
Co(1)-O(2)	2.140(4)	Co(1)-O(3)	2.170(4)
Bond Angles			
N(1)-Co(1)-N(2)	107.12(18)	N(1)-Co(1)-N(3)	93.85(17)
N(2)-Co(1)-N(3)	153.91(17)	N(1)-Co(1)-O(1)	72.64(15)
N(1)-Co(1)-O(2)	95.54(16)	N(1)-Co(1)-O(3)	144.76(15)
N(2)-Co(1)-O(1)	90.99(16)	N(2)-Co(1)-O(2)	74.15(16)
N(2)-Co(1)-O(3)	96.02(16)	N(3)-Co(1)-O(1)	110.37(16)
N(3)-Co(1)-O(2)	88.82(16)	N(3)-Co(1)-O(3)	73.72(16)
O(1)-Co(1)-O(2)	157.70(14)	O(1)-Co(1)-O(3)	80.92(13)
O(2)-Co(1)-O(3)	116.51(14)		

Table 3-12 Crystal Data and Collection Details of [Co(3-OCMe$_2$-5-Pz^{iPr}H)$_3$]. 2(*p*-CH$_3$-OBz) (3l)

Empirical formula	$C_{43}H_{59}N_6O_7Co$
Formula weight	830.89
Crystal system	Monoclinic
Space group	$P2_1/c$
Lattice parameters	
a (Å)	16.9077(16)
b (Å)	14.4924(12)
c (Å)	20.0743(17)
α (°)	90.00
β (°)	109.969(5)
γ (°)	90.00
Cell volume V (Å^3)	4623.1(7)
Z	4
D_{Calc} (g cm^{-3})	1.194
Data collection	
μ (Mo K_α) (cm^{-1})	0.423
θ_{max} (°)	22.83
Reflections measured	6182
Independent reflections	4035
Number of parameters refined	528
R	0.0788
R_w	0.2204

Table 3-13 Selected Bond Distances (Å) and Bond Angles (°) for [Co(3-OCMe$_2$-5-Pz^{iPr}H)$_3$]. 2(*p*-CH$_3$-OBz) (3l)

Bond Distances			
Co(1)-N(1)	2.076(5)	Co(1)-N(2)	2.072(5)
Co(1)-N(3)	2.089(5)	Co(1)-O(1)	2.128(4)
Co(1)-O(2)	2.150(4)	Co(1)-O(3)	2.177(4)
Bond Angles			
N(1)-Co(1)-N(2)	154.2(2)	N(1)-Co(1)-N(3)	107.8(2)
N(2)-Co(1)-N(3)	93.2(2)	N(1)-Co(1)-O(1)	73.7(2)
N(1)-Co(1)-O(2)	95.41(19)	N(1)-Co(1)-O(3)	90.8(2)
N(2)-Co(1)-O(1)	89.89(19)	N(2)-Co(1)-O(2)	73.86(19)
N(2)-Co(1)-O(3)	110.2(2)	N(3)-Co(1)-O(1)	95.3(2)
N(3)-Co(1)-O(2)	145.17(19)	N(3)-Co(1)-O(3)	72.75(18)
O(1)-Co(1)-O(2)	116.41(18)	O(1)-Co(1)-O(3)	156.73(17)
O(2)-Co(1)-O(3)	81.53(16)		

Table 3-14 Crystal Data and Collection Details of [Co(3-OCMe$_2$-5-Pz^{iPr}H)$_3$]. 2(*p*-CN-OBz) (3n)

Empirical formula	$C_{43}H_{51}N_8O_7Co$
Formula weight	850.85
Crystal system	Monoclinic
Space group	$P2_1/c$
Lattice parameters	
a (Å)	14.846(6)
b (Å)	30.365(11)
c (Å)	10.515(5)
α (°)	90.00
β (°)	103.81(2)
γ (°)	90.00
Cell volume V (Å^3)	4603(3)
Z	4
D_{Calc} (g cm^{-3})	1.228
Data collection	
μ (Mo K_α) (cm^{-1})	0.428
θ_{max} (°)	18.65
Reflections measured	3452
Independent reflections	2132
Number of parameters refined	542
R	0.0724
R_w	0.1763

Table 3-15 Selected Bond Distances (Å) and Bond Angles (°) for [Co(3-OCMe$_2$-5-Pz^{iPr}H)$_3$]. 2(*p*-CN-OBz) (3n)

Bond Distances			
Co(1)-N(1)	2.093(9)	Co(1)-N(2)	2.080(8)
Co(1)-N(3)	2.116(10)	Co(1)-O(1)	2.128(8)
Co(1)-O(2)	2.102(7)	Co(1)-O(3)	2.218(6)
Bond Angles			
N(1)-Co(1)-N(2)	147.4(3)	N(1)-Co(1)-N(3)	93.8(4)
N(2)-Co(1)-N(3)	114.5(3)	N(1)-Co(1)-O(1)	74.0(4)
N(1)-Co(1)-O(2)	90.1(3)	N(1)-Co(1)-O(3)	118.0(3)
N(2)-Co(1)-O(1)	90.5(3)	N(2)-Co(1)-O(2)	74.0(3)
N(2)-Co(1)-O(3)	86.9(3)	N(3)-Co(1)-O(1)	143.0(3)
N(3)-Co(1)-O(2)	91.5(3)	N(3)-Co(1)-O(3)	73.3(3)
O(1)-Co(1)-O(2)	122.6(3)	O(1)-Co(1)-O(3)	81.8(3)
O(2)-Co(1)-O(3)	148.3(3)		

Table 3-16 Non-covalent interactions in complexes

[Co(3-OCMe$_2$-5-Pz^{iPr}H)$_3$]. 2(*p*-F-OBz) (3j)	D-H	H···A	D···A	D-H···A
C(1)-H(1B)···π(pz^{iPr2})	0.96	2.713(1)	3.567(8)	148
C(8)-H(8C)···F(1)	0.96	2.513(8)	3.407(12)	155
C(10)-H(10B)···O(5)	0.96	2.549(5)	3.296(11)	135
C(12)-H(12C)···O(4)	0.96	2.583(4)	3.369(15)	139
[Co(3-OCMe$_2$-5-Pz^{iPr}H)$_3$]. 2(*p*-Cl-OBz) (3k)				
C(3)-H(3C)···π(pz^{iPr2})	0.96	2.748(1)	3.563(8)	143
C(26)-H(26C)···Cl(2)	0.96	2.848(8)	3.407(12)	155
C(8)-H(8A)···O(7)	0.96	2.616(5)	3.335(10)	132
C(44)-H(44B)···O(4)	0.96	2.707(6)	3.265(14)	118
[Co(3-OCMe$_2$-5-Pz^{iPr}H)$_3$]. 2(*p*-CH$_3$-OBz) (3l)				
C(19)-H(19C)···π(pz^{iPr2})	0.96	2.866(2)	3.667(3)	141
C(25)-H(25A)···O(4)	0.96	2.651(6)	3.298(12)	125
C(16)-H(16B)···O(7)	0.96	2.689(8)	3.381(17)	130
[Co(3-OCMe$_2$-5-Pz^{iPr}H)$_3$]. 2(*p*-CN-OBz) (3n)				
C(20)-H(20C)···π(pz^{iPr2})	0.96	3.055(25)	3.905(41)	148
C(18)-H(18C)···O(5)	0.96	2.524(12)	3.468(20)	168
C(1)-H(1C)···O(6)	0.96	2.665(30)	3.390(3)	133
C(17)-H(17C)···O(5)	0.96	2.687(30)	3.366(32)	128
C(41)-H(41)···O(6)	0.93	2.495(9)	3.386(15)	161

Table 3-17 Temperature range for removal of guest molecules in complexes

Complex	Weight loss (calculated %)	Weight loss (experimental %)	Temperature range (°C)	Removal of molecules
3j	32.25	31.34	180-200	Two *p*-fluorobenzoate
3k	34.75	33.83	175-200	Two *p*-chlorobenzoate
3l	31.52	30.82	165-190	Two *p*-methylbenzoate
3m	36.28	35.29	180-205	Two *p*-nitrobenzoate
3n	33.34	32.21	185-195	Two *p*-cyanobenzoate
3o	33.76	32.96	165-195	Two *p*-formylbenzoate

Table 3-18 Optimized membrane compositions and their potentiometric response as benzoate ion-selective electrodes.

Membrane no.	Composition of membrane (mg)				Slope (± 0.2) mV / decade activity	Working concentration range (M)
	PVC	Plasticizer	Ionophore **3p**	HTAB		
1.	150	277 (NPOE)	1	-	32.7	7.9×10^{-4}-1.0×10^{-1}
2.	150	301 (NPOE)	1	2	48.7	1.5×10^{-4} - 1.0×10^{-1}
3.	150	343 (NPOE)	3	3	52.0	8.7×10^{-6} - 1.0×10^{-1}
4.	150	346 (DBP)	5	3	49.2	3.2×10^{-5} - 1.0×10^{-1}
5.	150	333 (DBP)	5	3	37.1	1.9×10^{-4} - 1.0×10^{-1}
6.	150	330 (NPOE)	4	3	59.2	3.6×10^{-6} - 1.0×10^{-1}
7.	150	310 (BA)	5	3	43.2	8.6×10^{-4} - 1.0×10^{-1}
8.	150	339 (BA)	5	3	48.7	2.5×10^{-5} - 1.0×10^{-1}
9.	150	348 (TBP)	5	3	50.1	7.8×10^{-4} - 1.0×10^{-1}
10.	150	348 (NPOE)	7	3	68.7	8.9×10^{-5} - 1.0×10^{-1}

Table 3-19 Formation constant values for different substituted benzoate anions.

Anions	Formation constant ($\log \beta_{ILn}$)* ± SD
p-F-OBz	5.45 ± 0.2
p-Cl-OBz	5.32 ± 0.3
p-CH_3-OBz	4.27 ± 0.3
p-NO_2-OBz	4.02 ± 0.2
p-CN-OBz	3.82 ± 0.4
p-CHO-OBz	3.73 ± 0.3

* *Mean value ± standard deviation (three measurements)*

Table 3-20 Crystal Data and Collection Details of $[_{\kappa}^{2}(tm^{t\text{-}Bu})_2CoCl_2]$ (3q)

Empirical formula	$C_{14}H_{22}N_4Cl_2S_2Co$
Formula weight	440.33
Crystal system	Orthorhombic
Space group	P 21 21 21
Lattice parameters	
a (Å)	8.195(6)
b (Å)	13.778(10)
c (Å)	17.354(11)
α (°)	90.00
β (°)	90.00
γ (°)	90.00
Cell volume V ($Å^3$)	1960(2)
Z	4
D_{Calc} (g cm^{-3})	1.492
Data collection	
μ (Mo K_α) mm^{-1})	1.364
θ_{max} (°)	26.50
Reflections measured	2325
Independent reflections	1582
Number of parameters refined	215
R	0.0460
R_w	0.1219

Table 3-21 Selected Bond Distances (Å) and Bond Angles (°) for $[_k^2(tm^{t\text{-}Bu})_2CoCl_2]$ (3q)

Bond Distances			
Co(1)-N(1)	2.034(9)	Co(1)-N(2)	2.016(9)
Co(1)-Cl(1)	2.239(3)	Co(1)-Cl(2)	2.237(3)
Bond Angles			
N(1)-Co(1)-N(2)	106.7(3)	N(1)-Co(1)-Cl(1)	114.1(3)
N(1)-Co(1)-Cl(2)	106.3(3)	N(2)-Co(1)-Cl(1)	112.9(3)
N(2)-Co(1)-Cl(2)	107.1(3)	Cl(1)-Co(1)-Cl(2)	109.42(14)

Table 3-22 Crystal Data and Collection Details of $[(tm^{t\text{-}Bu})_2Co(\mu\text{-}tm^{t\text{-}Bu})_2Cl_2]$ (3r)

Empirical formula	$C_{32}H_{52}N_{10}S_4Cl_2Co_2$
Formula weight	893.88
Crystal system	Monoclinic
Space group	$P2_1/c$
Lattice parameters	
a (Å)	10.0699(7)
b (Å)	11.1810(7)
c (Å)	18.1558(12)
α (°)	90.00
β (°)	95.322(4)
γ (°)	90.00
Cell volume V ($Å^3$)	2035.4(2)
Z	2
D_{Calc} (g cm^{-3})	1.459
Data collection	
μ (Mo K_α) mm^{-1})	1.189
θ_{max} (°)	33.57
Reflections measured	8044
Independent reflections	4968
Number of parameters refined	237
R	0.0629
R_w	0.2040

Table 3-23 Selected Bond Distances (Å) and Bond Angles (°) for $[(tm^{t\text{-}Bu})_2Co(\mu\text{-}tm^{t\text{-}Bu})_2Cl_2]$ (3r)

Bond Distances			
Co(1)-N(1)	1.997(3)	Co(1)-Cl(1)	2.3006(10)
Co(1)-S(1)	2.3366(11)	Co(1)-S(2)	2.3001(10)
Bond Angles			
N(1)-Co(1)-S(1)	111.91(9)	N(1)-Co(1)-S(2)	115.24(9)
N(1)-Co(1)-Cl(1)	101.62(9)	S(2)-Co(1)-S(1)	110.45(4)
S(1)-Co(1)-Cl(1)	112.70(4)	S(2)-Co(1)-Cl(1)	104.42(4)

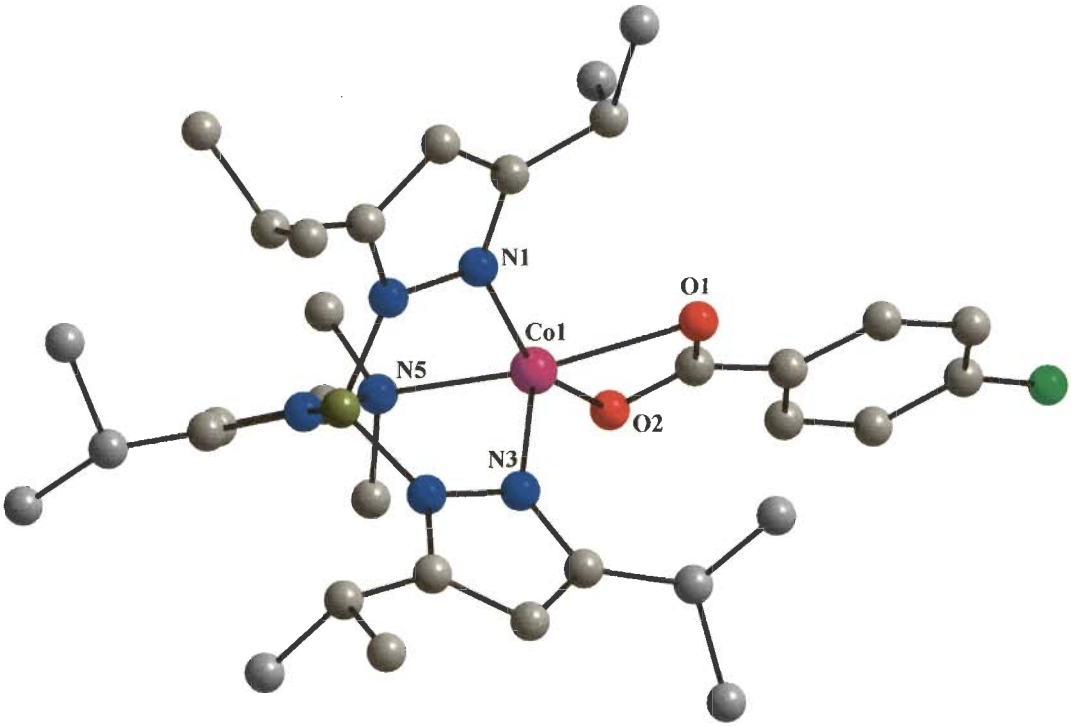

Fig. 3-12 Crystal structure of [Tp^{iPr2}Co(*p*-F-OBz)] (**3d**)

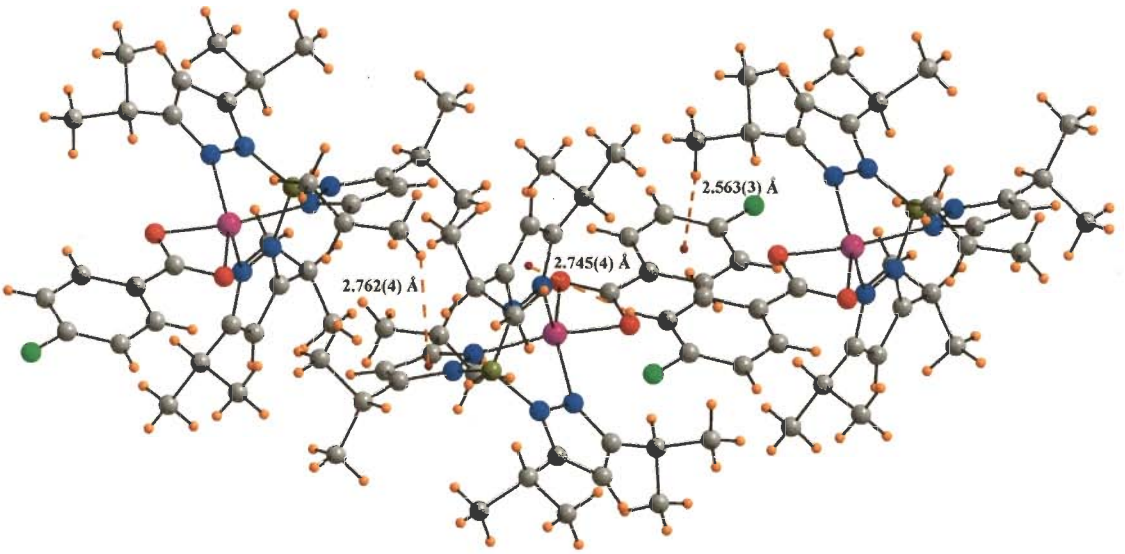

Fig. 3-13 Intermolecular C-H···π and CH_3···π interactions in complex **3d**

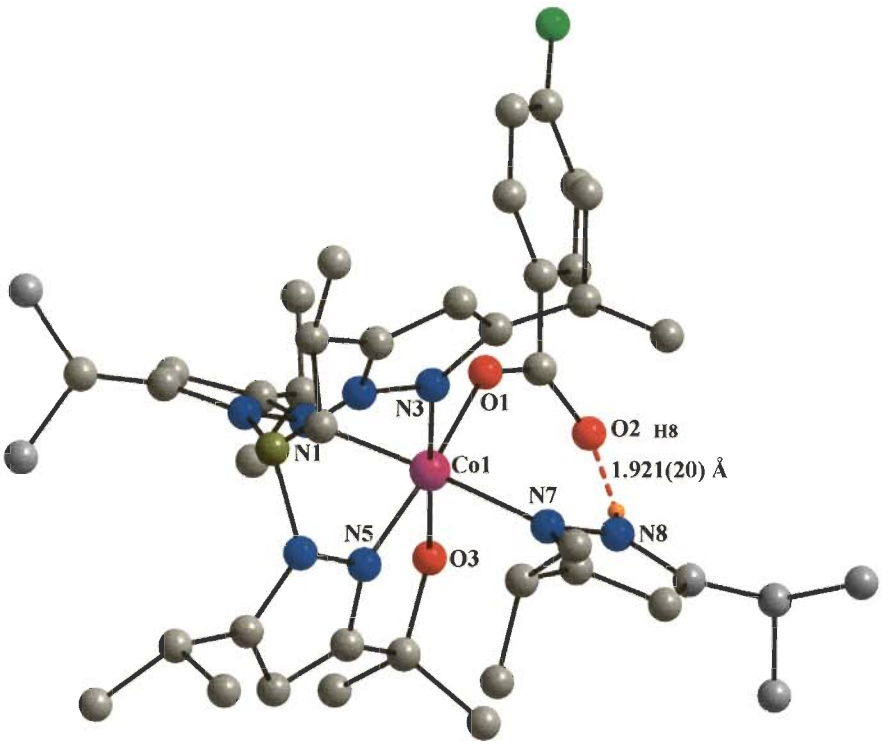

Fig. 3-14 Crystal structure of [Co(*p*-F-OBz){HB(3-OCMe$_2$-5-Pz^{iPr})(3,5-Pz^{iPr2})$_2$}(3,5-Pz^{iPr2}H)] **(3f)**

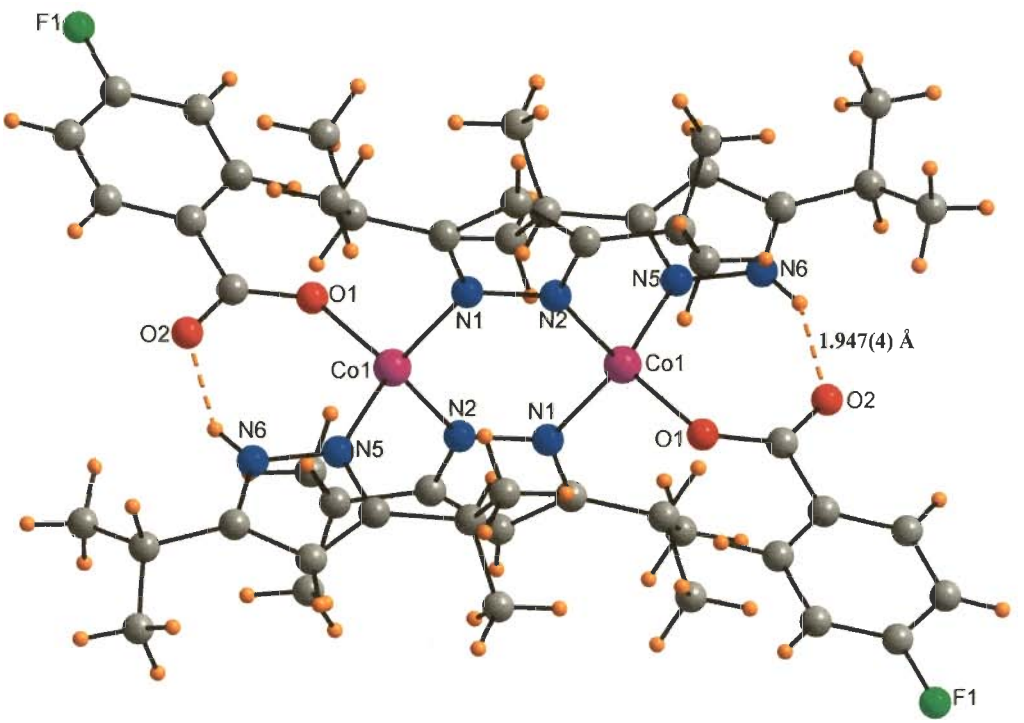

Fig. 3-15 Crystal structure of [(3,5-Pz^{iPr2}H)$_2$Co$_2$(μ-3,5-Pz^{iPr2})$_2$(*p*-F-OBz)$_2$] **(3h)**

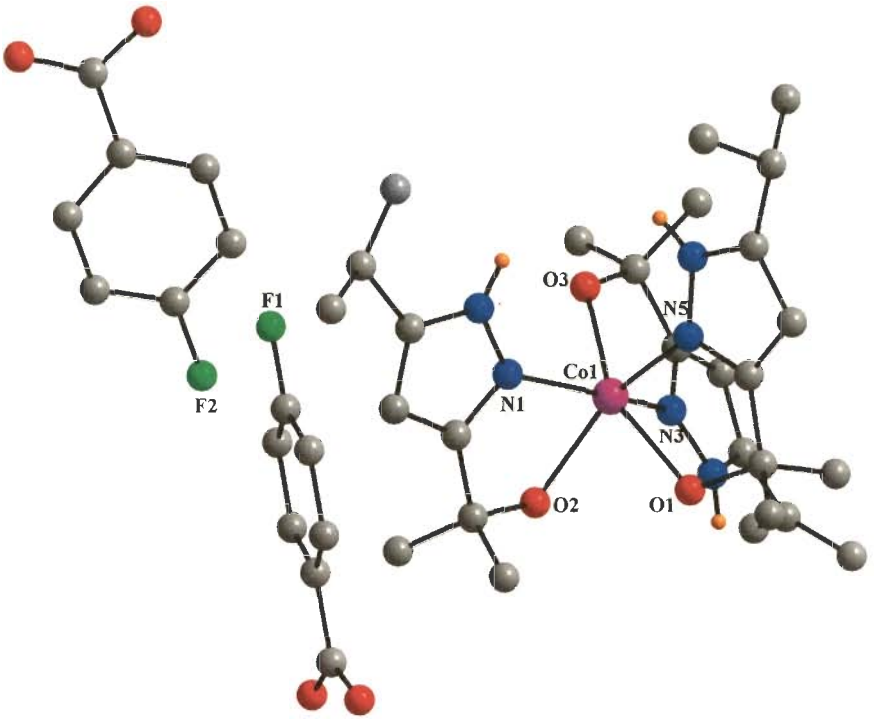

Fig. 3-16 Crystal structure of [Co(3-OCMe$_2$-5-Pz^{iPr}H)$_3$]. 2(*p*-F-OBz) (**3j**)

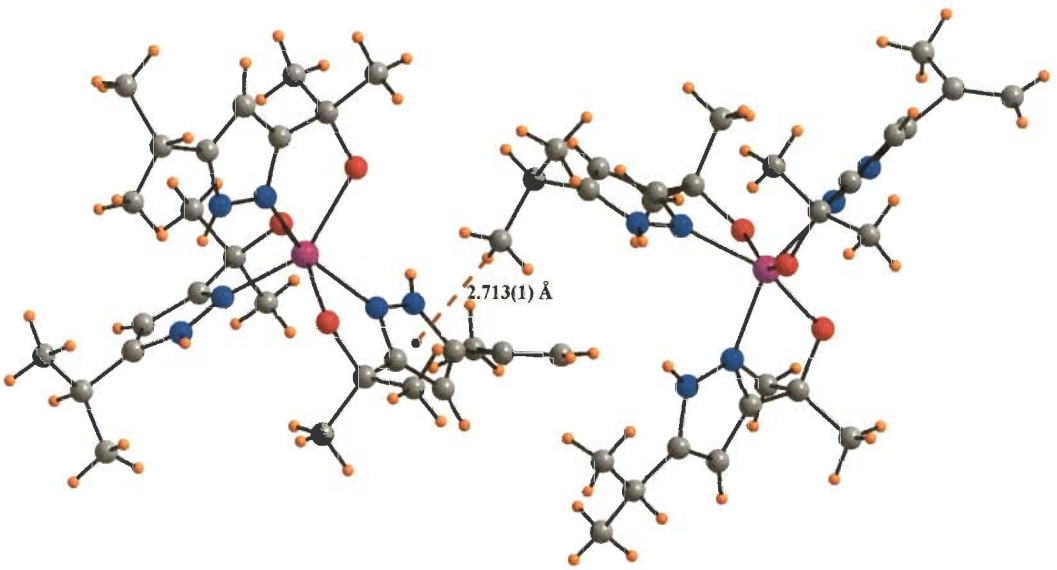

Fig. 3-17 Intermolecular $CH_3\cdots\pi$ interactions between host molecules present in complex **3j**

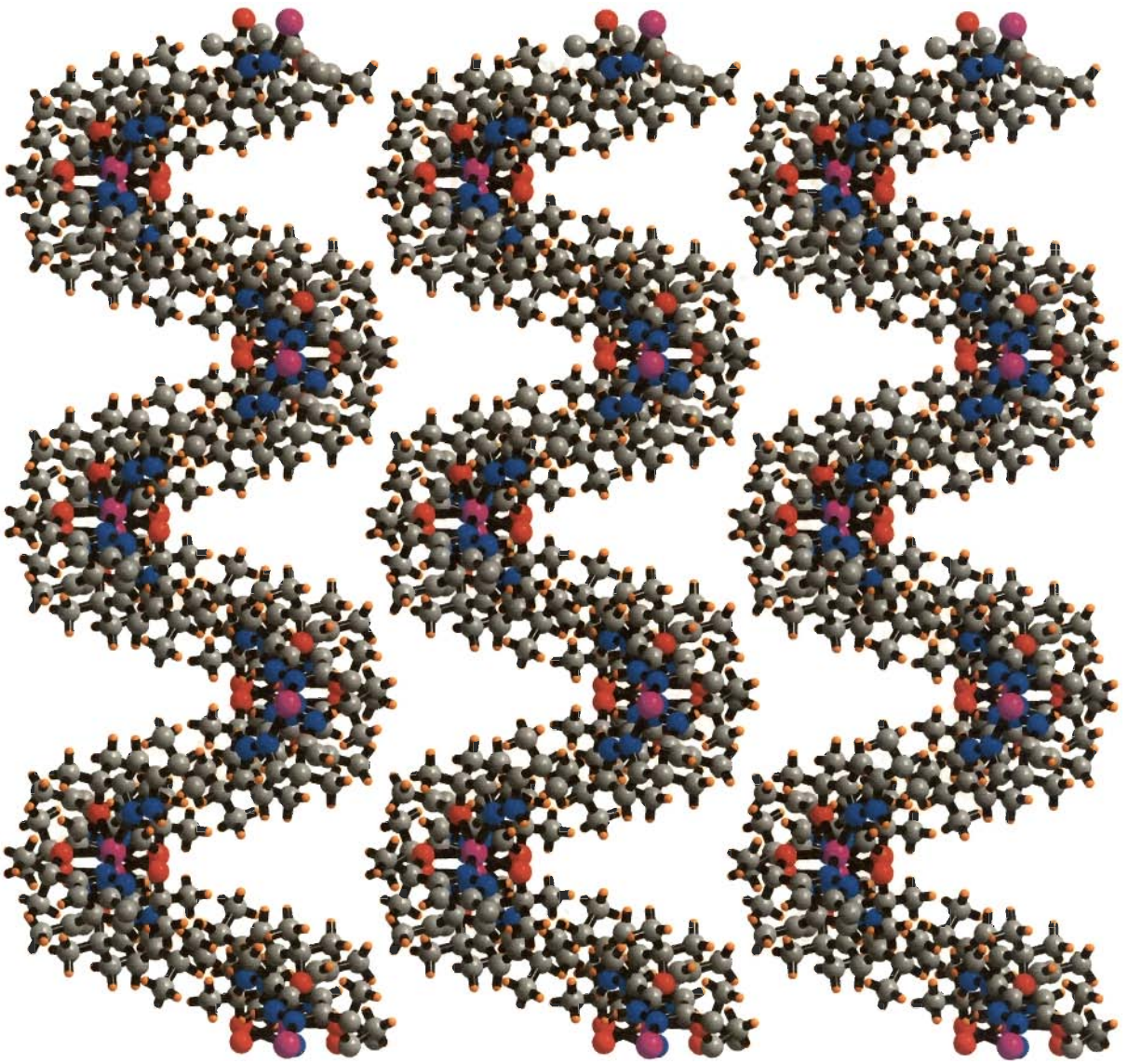

Fig. 3-18 Three-dimensional spiral packing observed in complex **3j** due to $CH_3\cdots\pi$ interactions between host molecules (cobalt complexes).

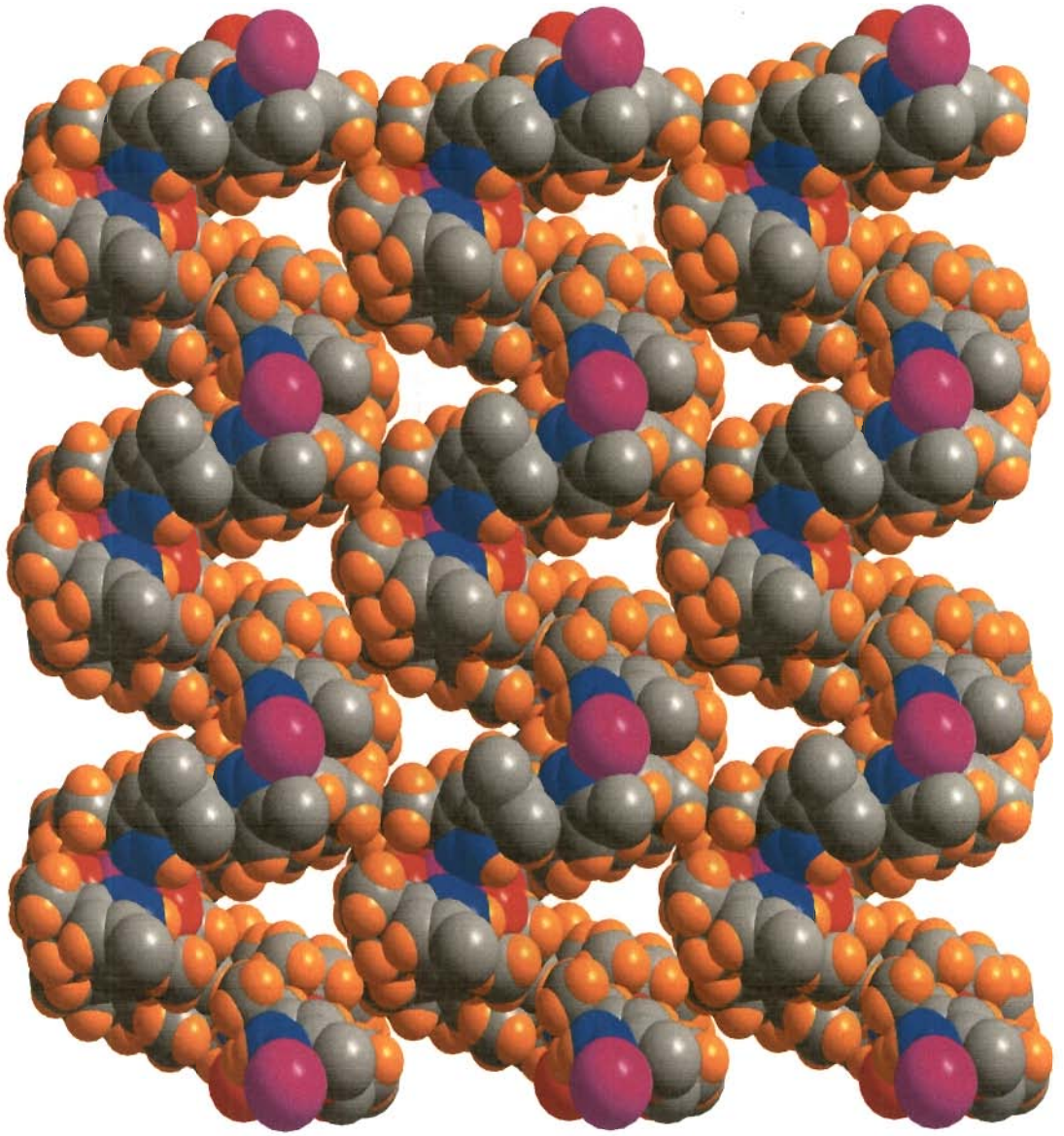

Fig. 3-19 Three-dimensional spiral packing (space-fill model) observed in complex **3j** due to $CH_3 \cdots \pi$ interactions between host molecules. Guest molecules will be present in the triangular void space.

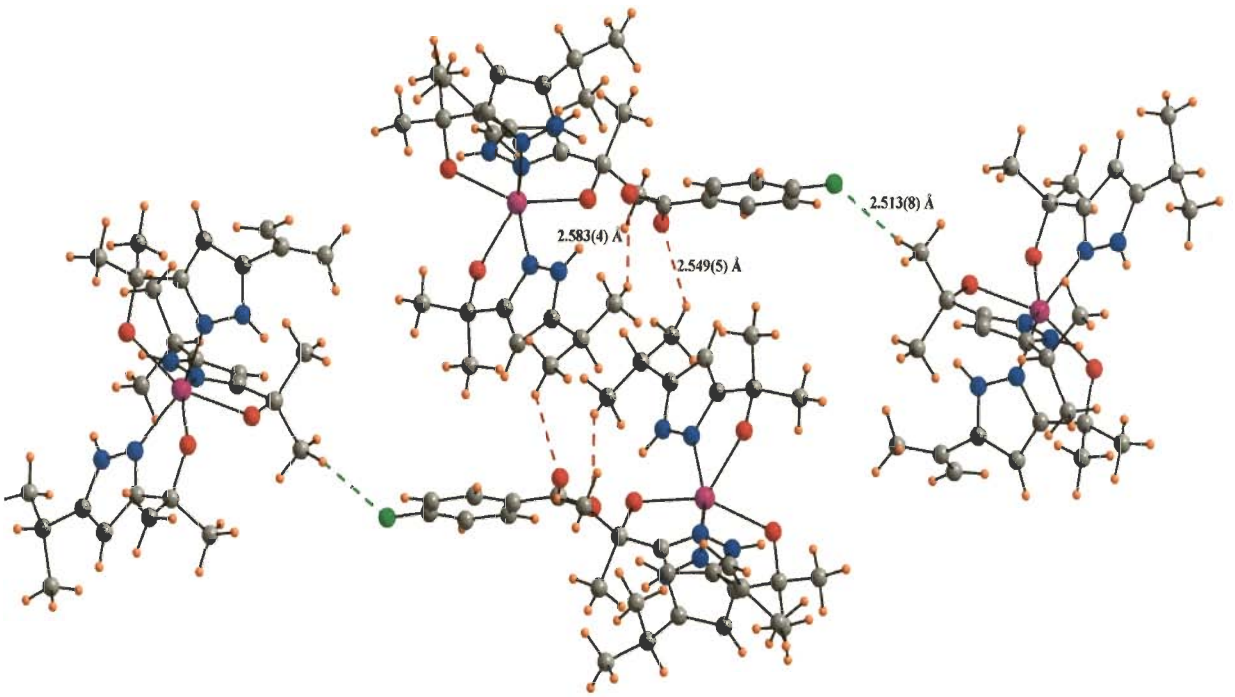

Fig. 3-20 The C-H…O and C-H…F interactions observed between host and guest molecules in complex **3j**

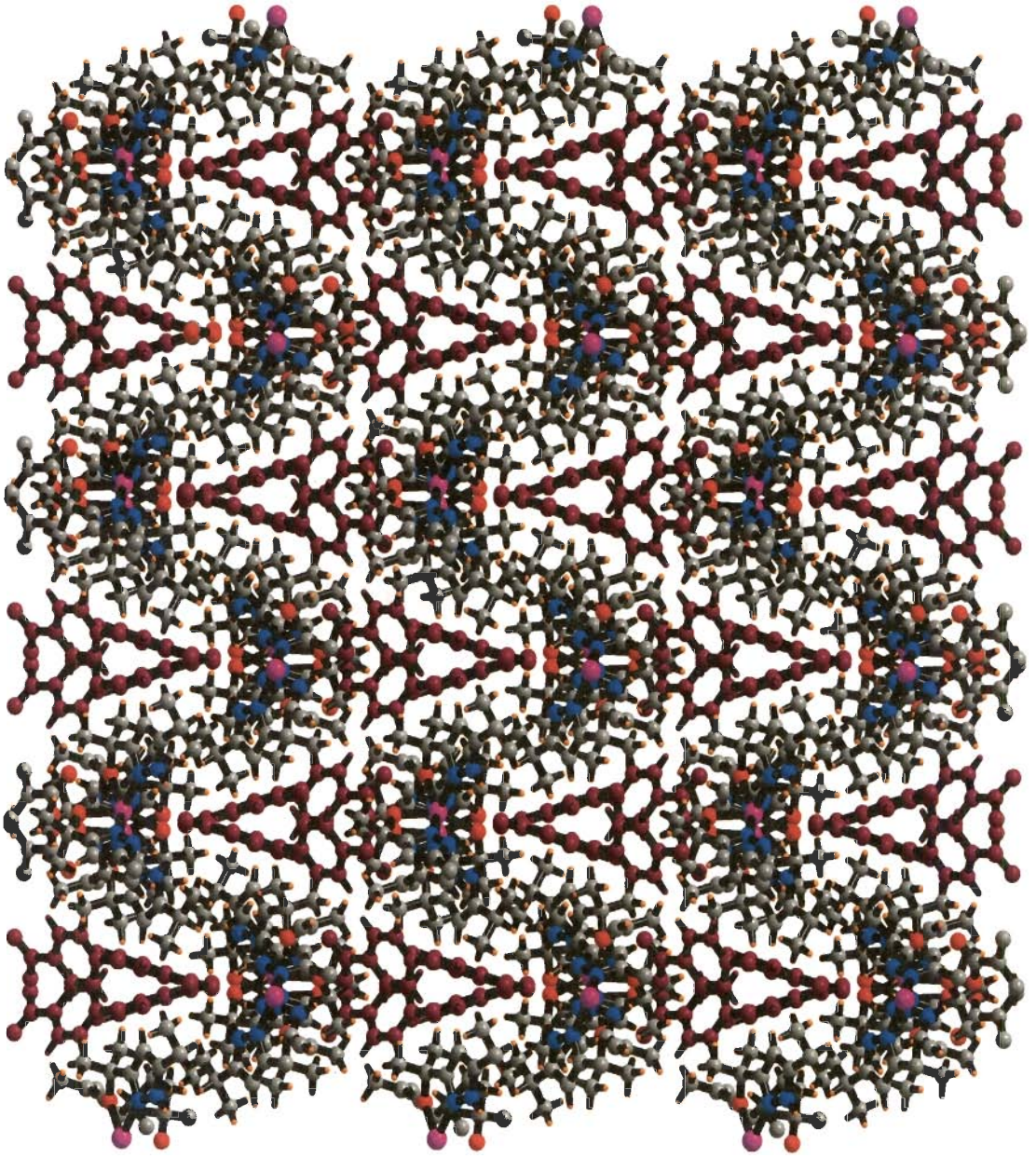

Fig. 3-21 Three-dimensional packing due to non-covalent interactions present in complex **3j**. Triangular voids were occupied by guest (p-fluorobenzoate anions) molecules.

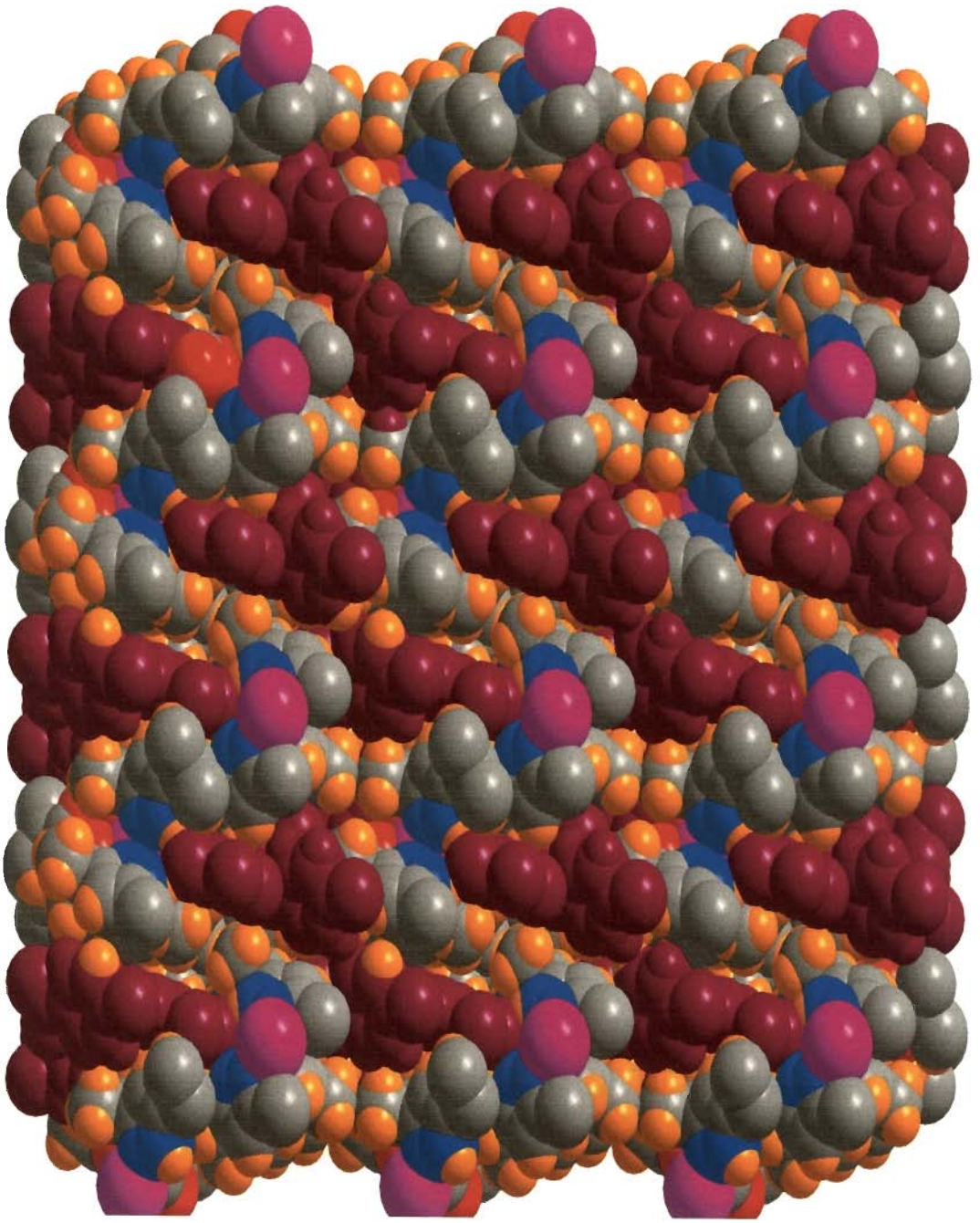

Fig. 3-22 Three-dimensional packing (space-fill model) due to non-covalent interactions present in complex **3j**. Triangular voids were occupied by guest (*p*-fluorobenzoate anions) molecules (cherry colored).

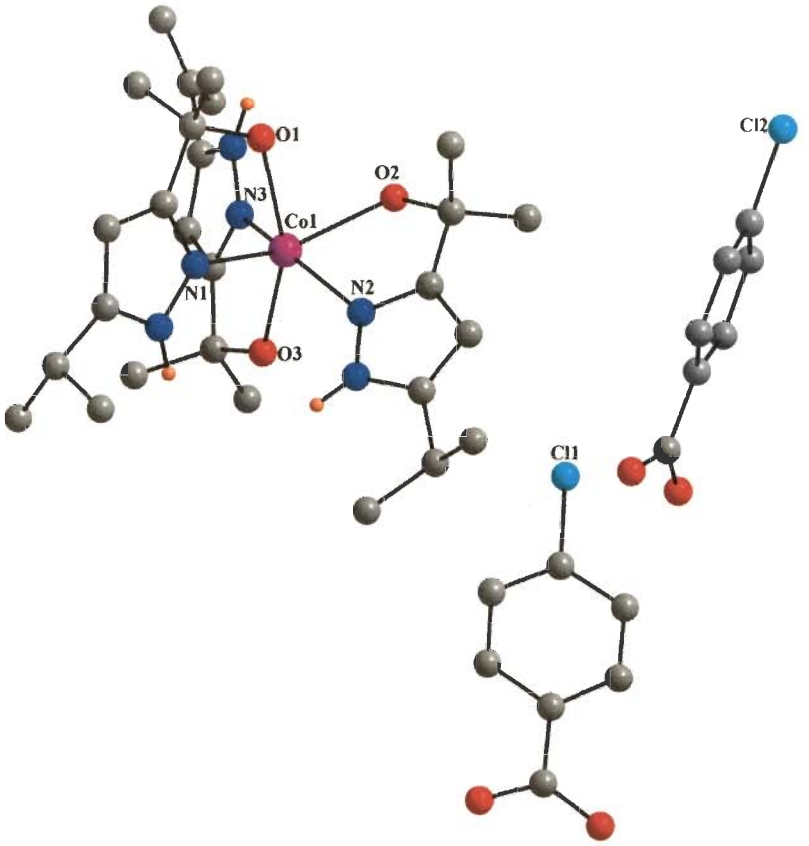

Fig. 3-23 Crystal structure of [Co(3-OCMe$_2$-5-Pz^{iPr}H)$_3$]. 2(Cl-OBz) (**3k**)

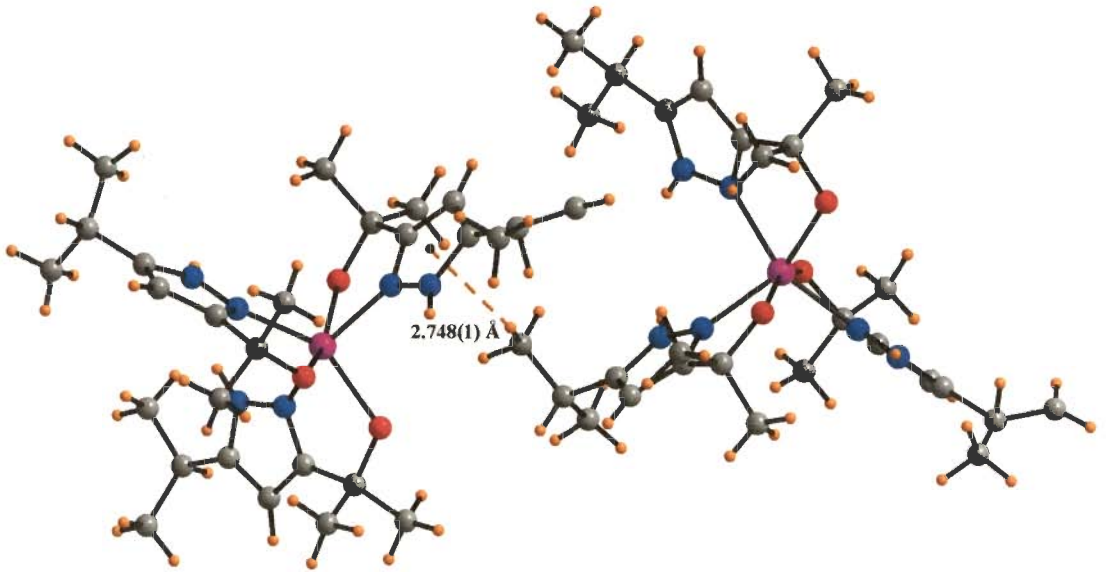

Fig. 3-24 Intermolecular $CH_3\cdots\pi$ interactions between host molecules present in complex **3k**

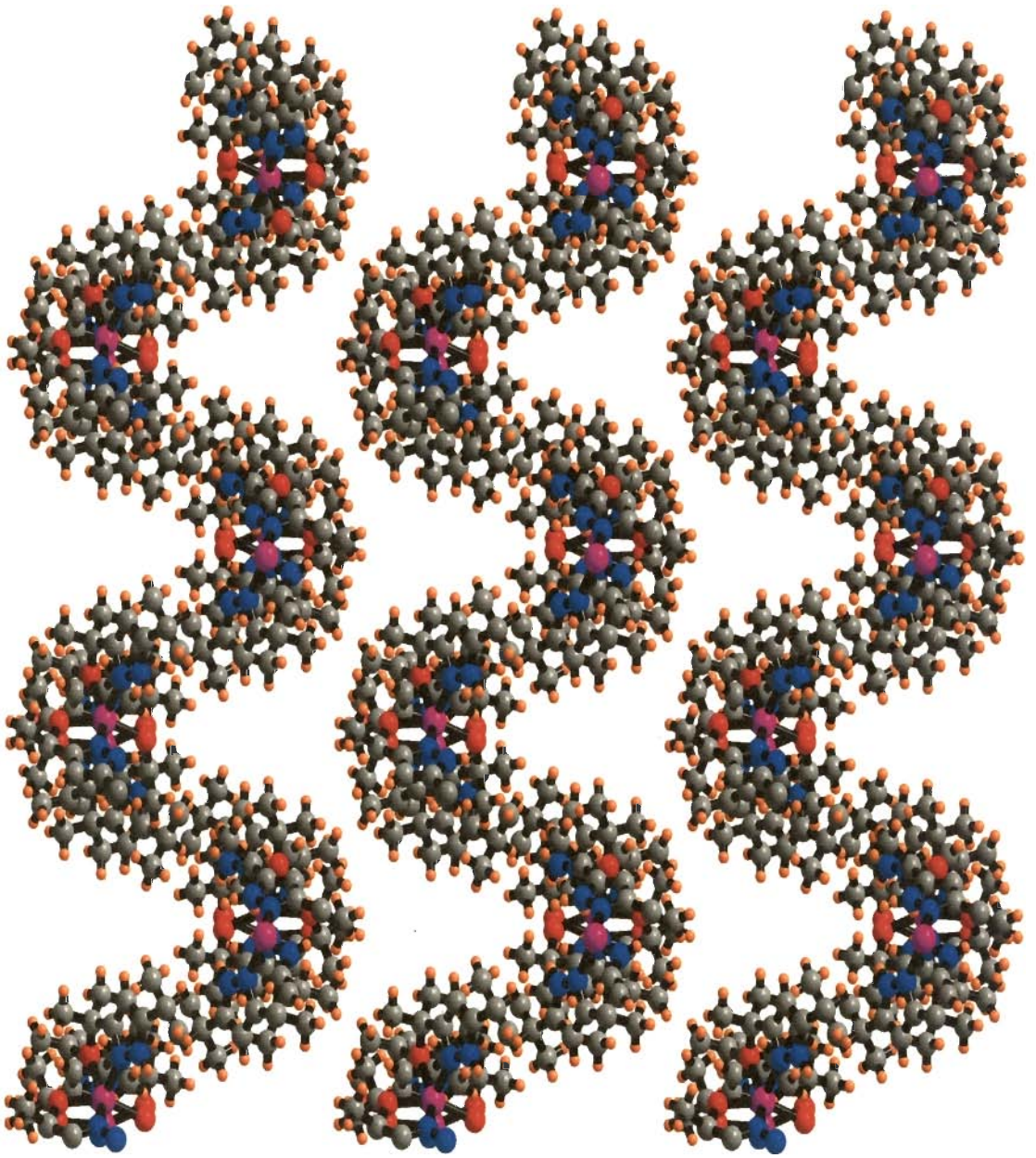

Fig. 3-25 Three-dimensional spiral packing observed in complex **3k** due to $CH_3\cdots\pi$ interactions between host molecules (cobalt complexes).

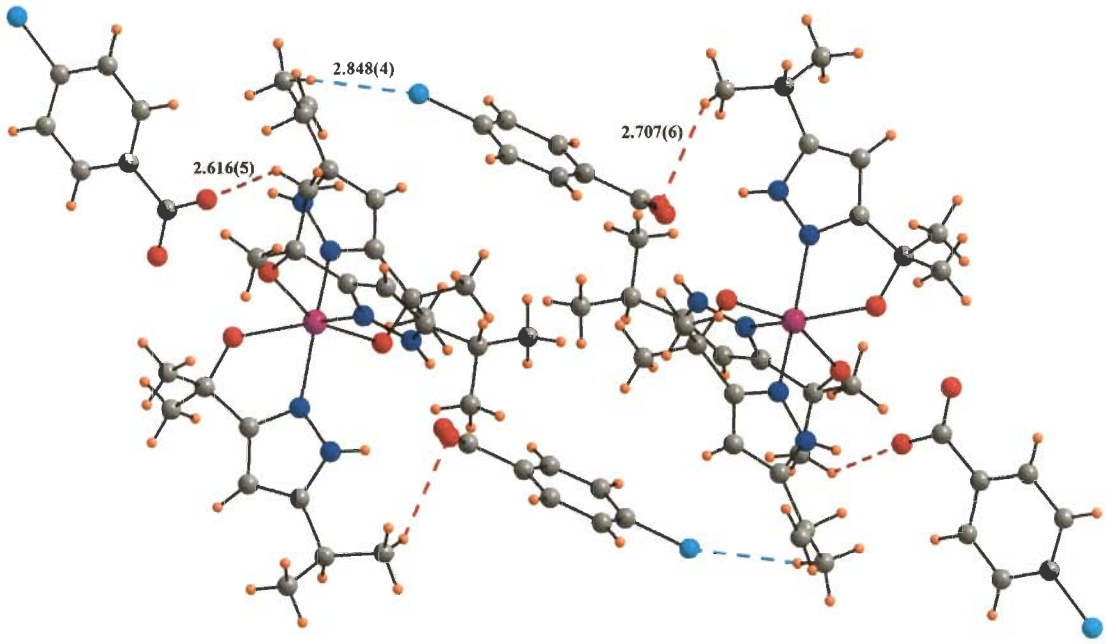

Fig. 3-26 The C-H···O and C-H···Cl interactions observed between host and guest molecules in complex **3k**

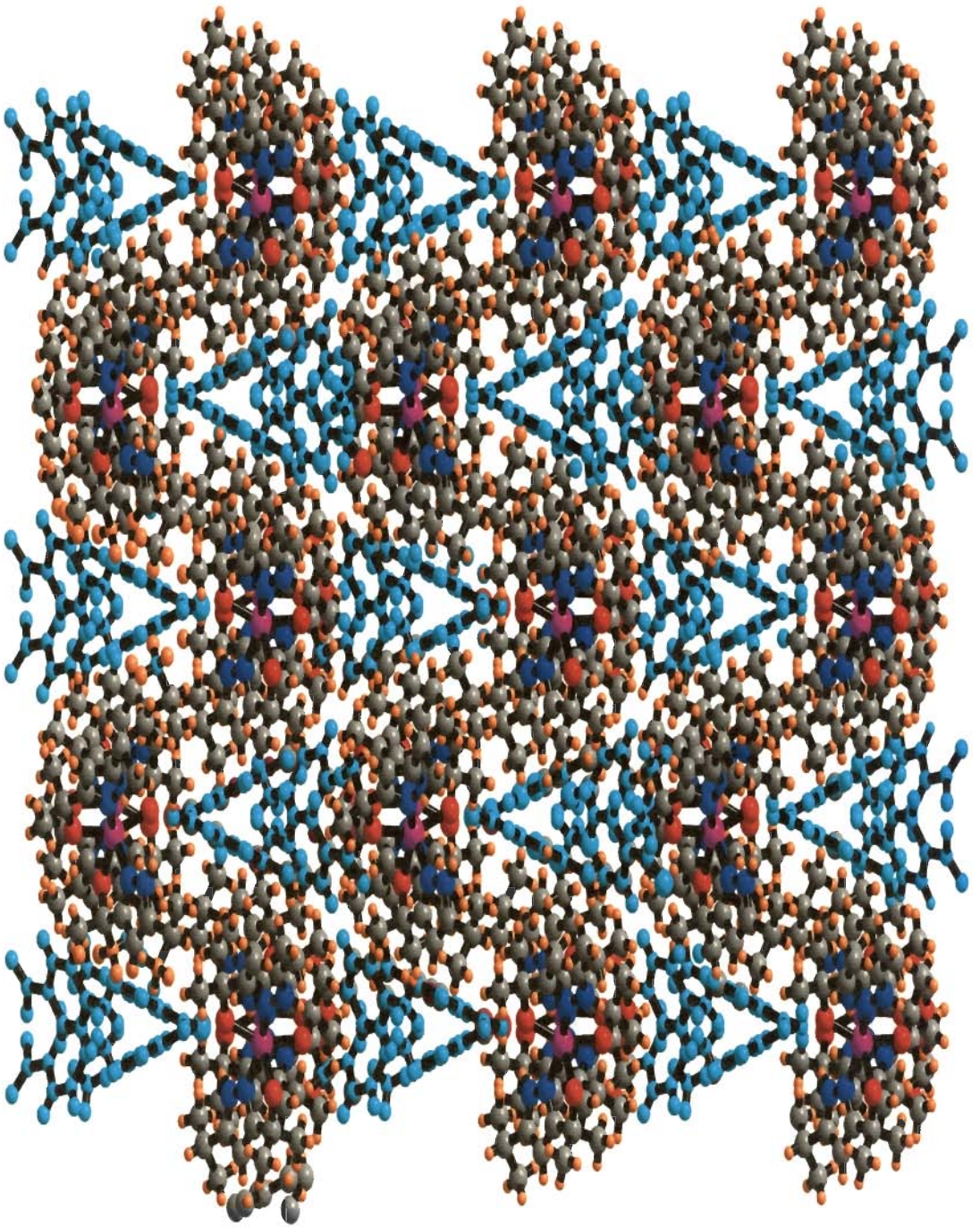

Fig. 3-27 Three-dimensional packing due to non-covalent interactions present in complex **3k**. Triangular voids were occupied by guest (*p*-chlorobenzoate anions) molecules

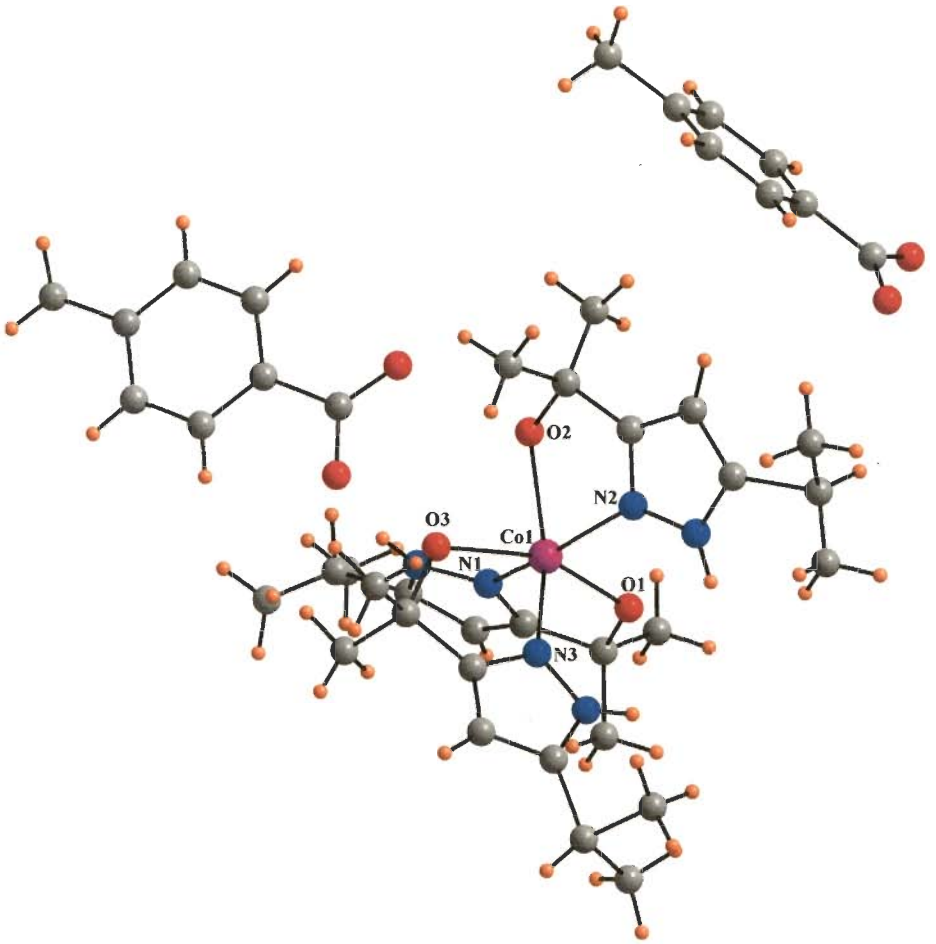

Fig. 3-28 Crystal structure of [Co(3-$OCMe_2$-5-$Pz^{iPr}H)_3$]. 2(CH_3-OBz) (**3l**)

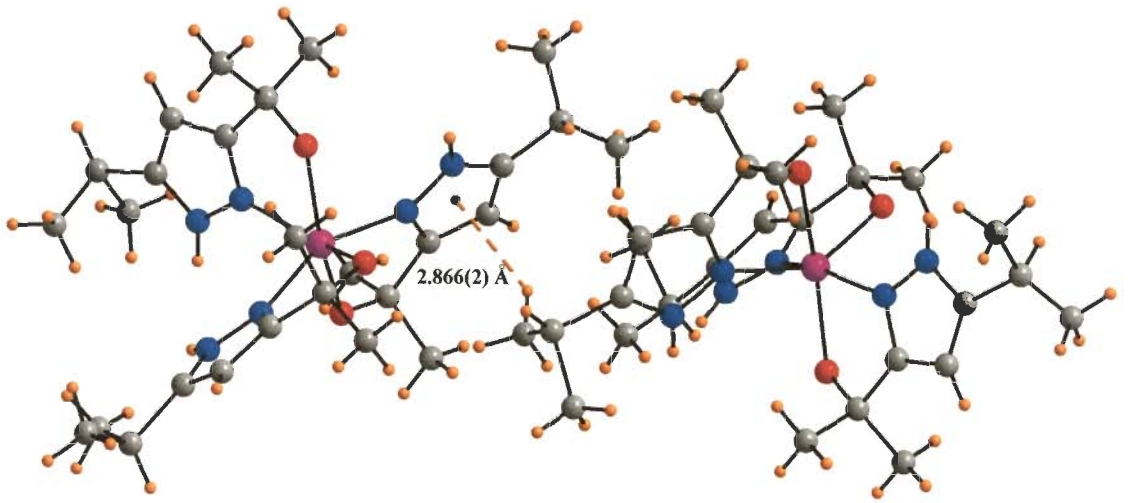

Fig. 3-29 Intermolecular $CH_3\cdots\pi$ interactions between host molecules present in complex **3l**

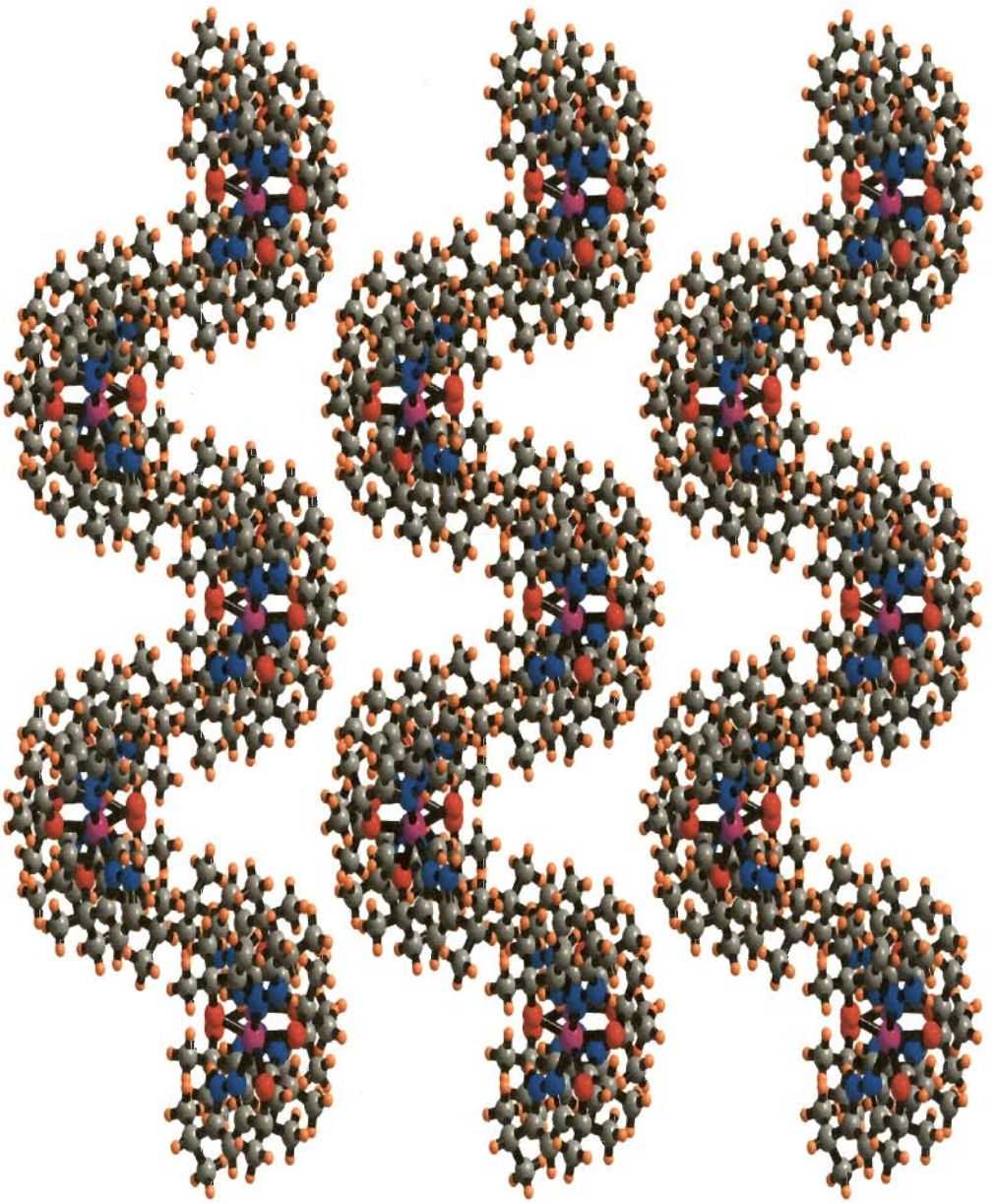

Fig. 3-30 Three-dimensional spiral packing observed in complex **3l** due to $CH_3 \cdots \pi$ interactions between host molecules (cobalt complexes).

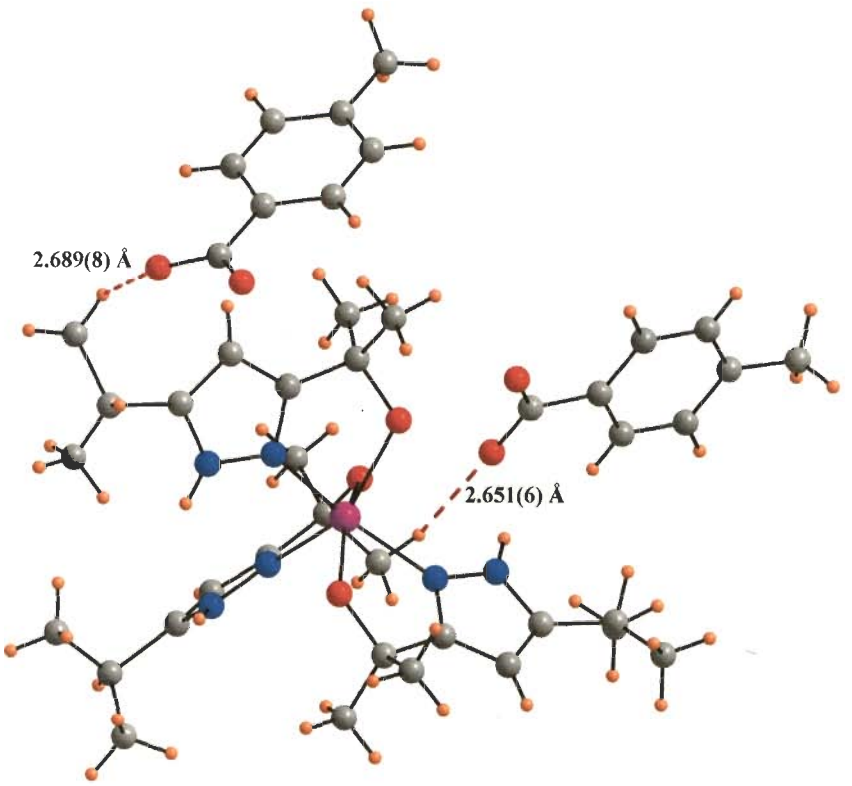

Fig. 3-31 The C-H···O interactions observed between host and guest molecules in complex **3l**

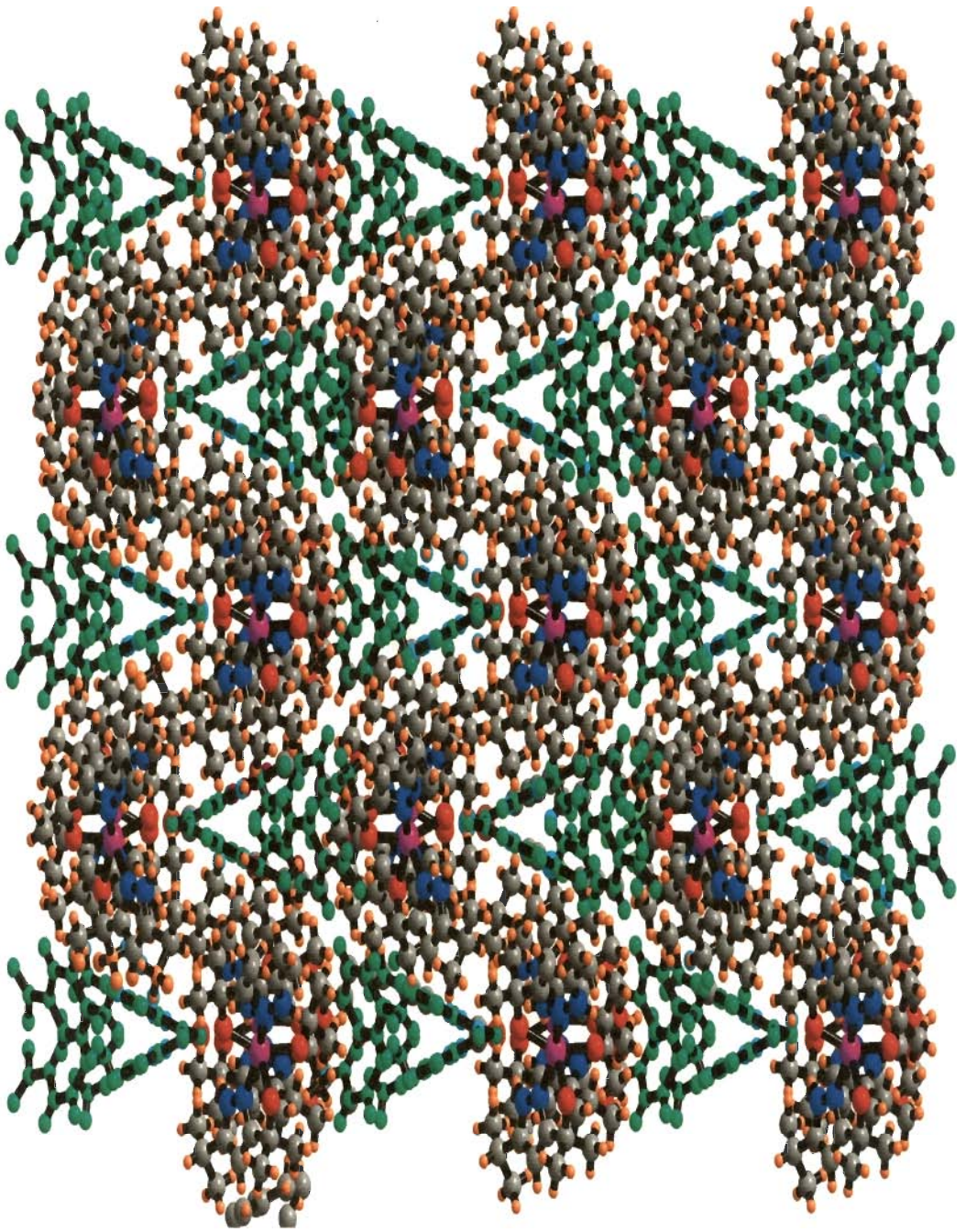

Fig. 3-32 Three-dimensional packing due to non-covalent interactions present in complex **3l**. Triangular voids were occupied by guest (*p*-methylbenzoate anions) molecules

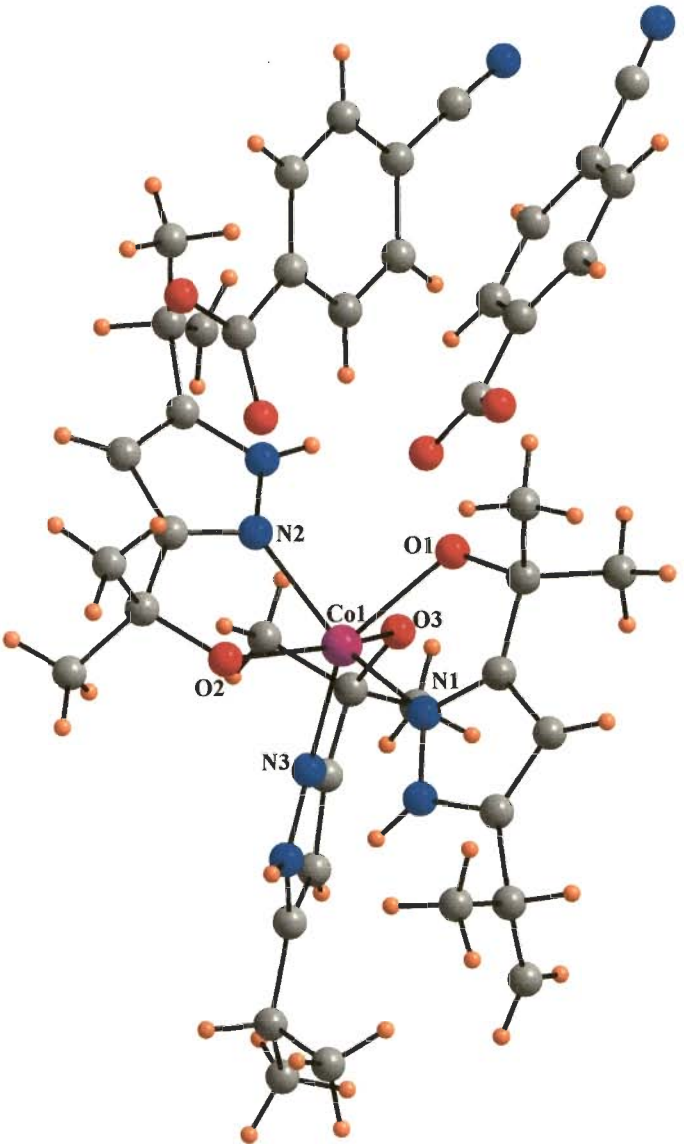

Fig. 3-33 Crystal structure of [Co(3-OCMe$_2$-5-Pz^{iPr}H)$_3$]. 2(CN-OBz) (**3n**)

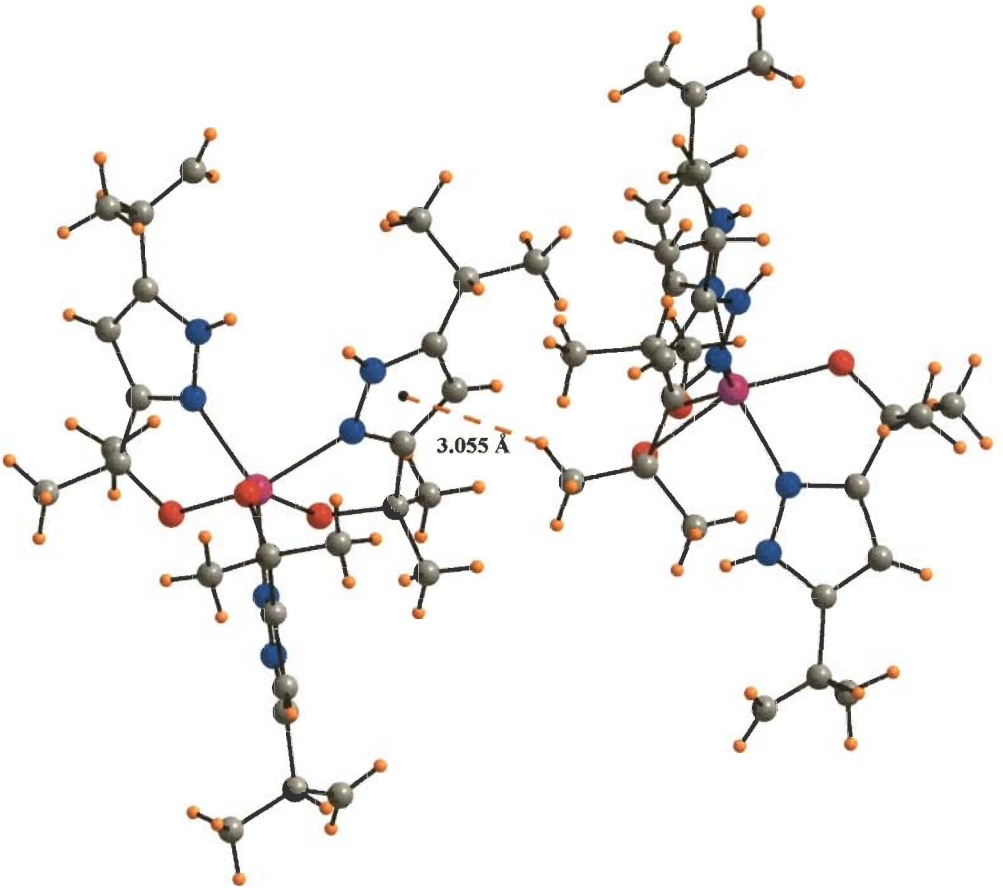

Fig. 3-34 Intermolecular $CH_3\cdots\pi$ interactions between host molecules present in complex **3n**

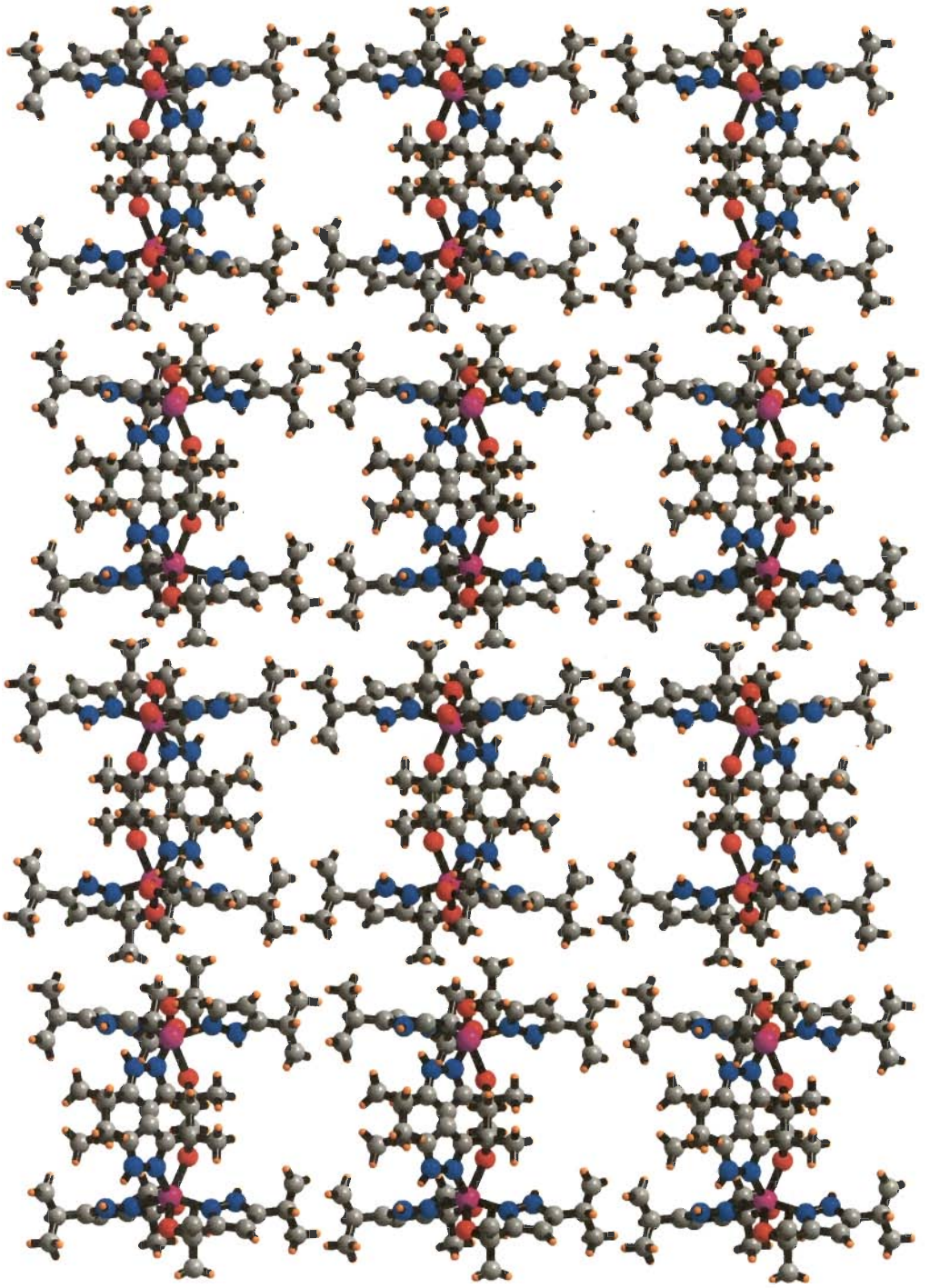

Fig. 3-35 Three-dimensional spiral packing observed in complex **3n** due to $CH_3 \cdots \pi$ interactions between host molecules (cobalt complexes). Rectangular voids were formed for guest molecules.

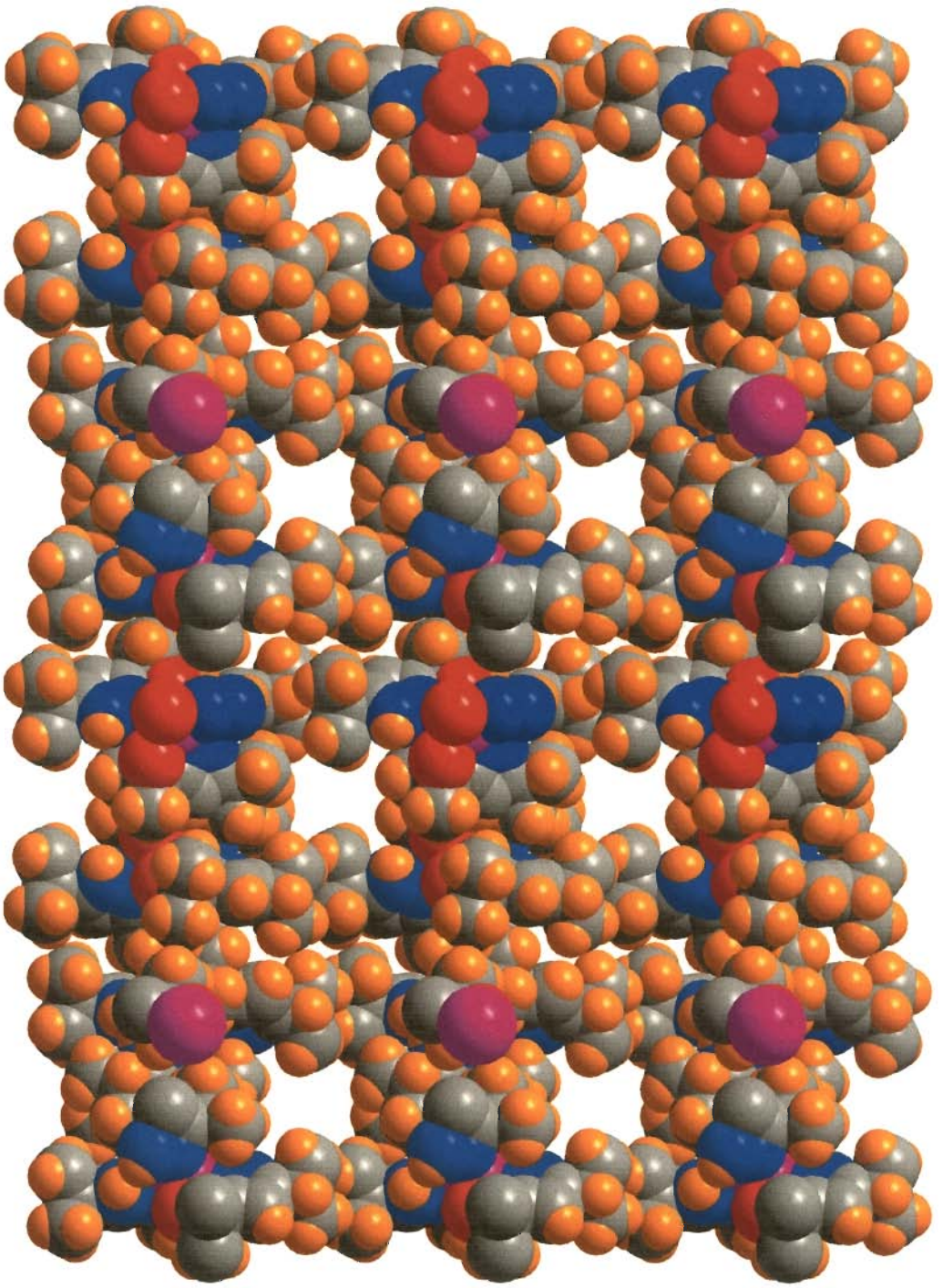

Fig. 3-36 Three-dimensional spiral packing (space-fill model) observed in complex **3n** due to $CH_3 \cdots \pi$ interactions between host molecules (cobalt complexes). Rectangular voids were formed for guest molecules.

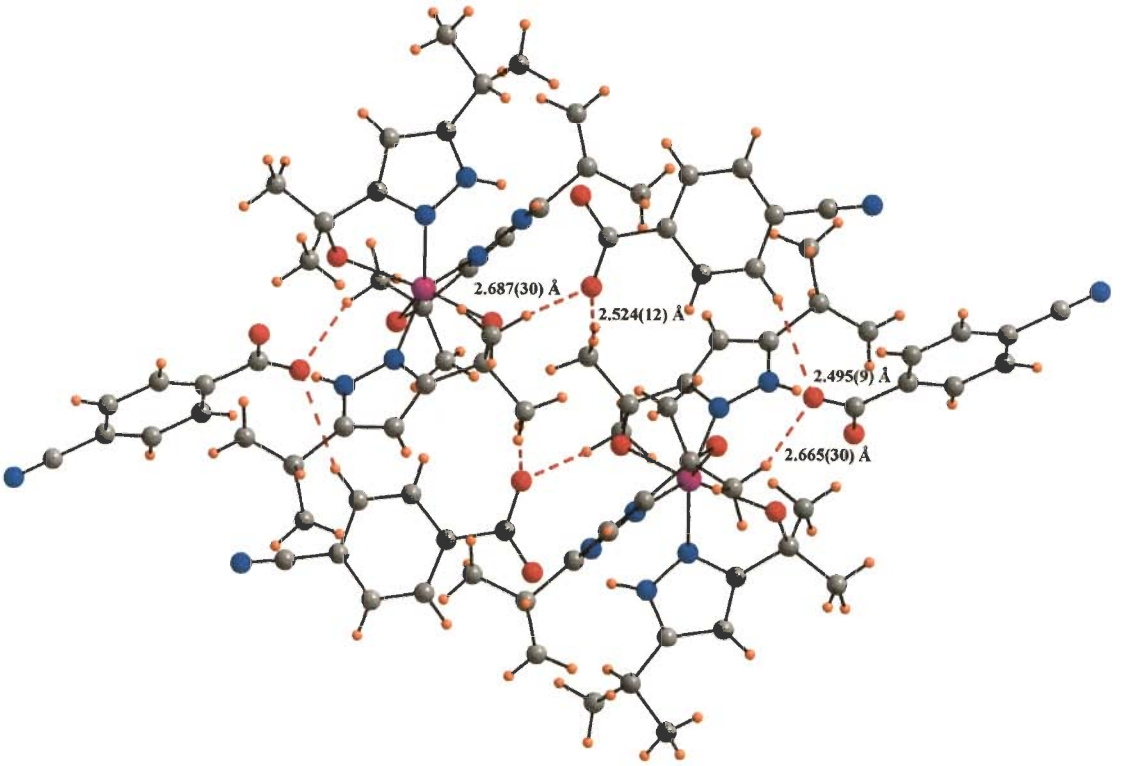

Fig. 3-37 The C-H···O interactions observed between host and guest molecules in complex **3n**

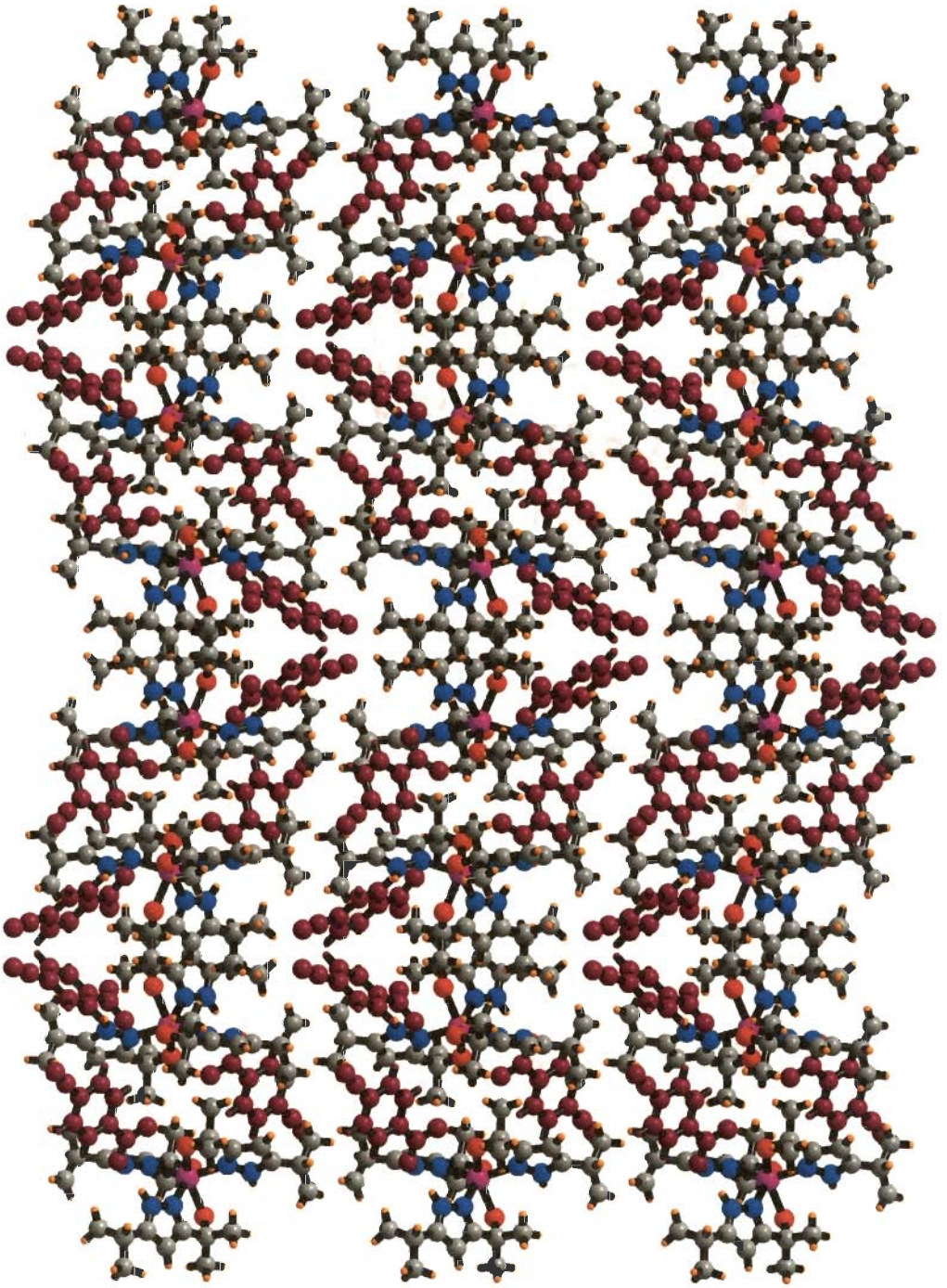

Fig. 3-38 Three-dimensional packing due to non-covalent interactions present in complex **3n**. Rectangular voids were occupied by guest (*p*-cyanobenzoate anions) molecules (cherry colored)

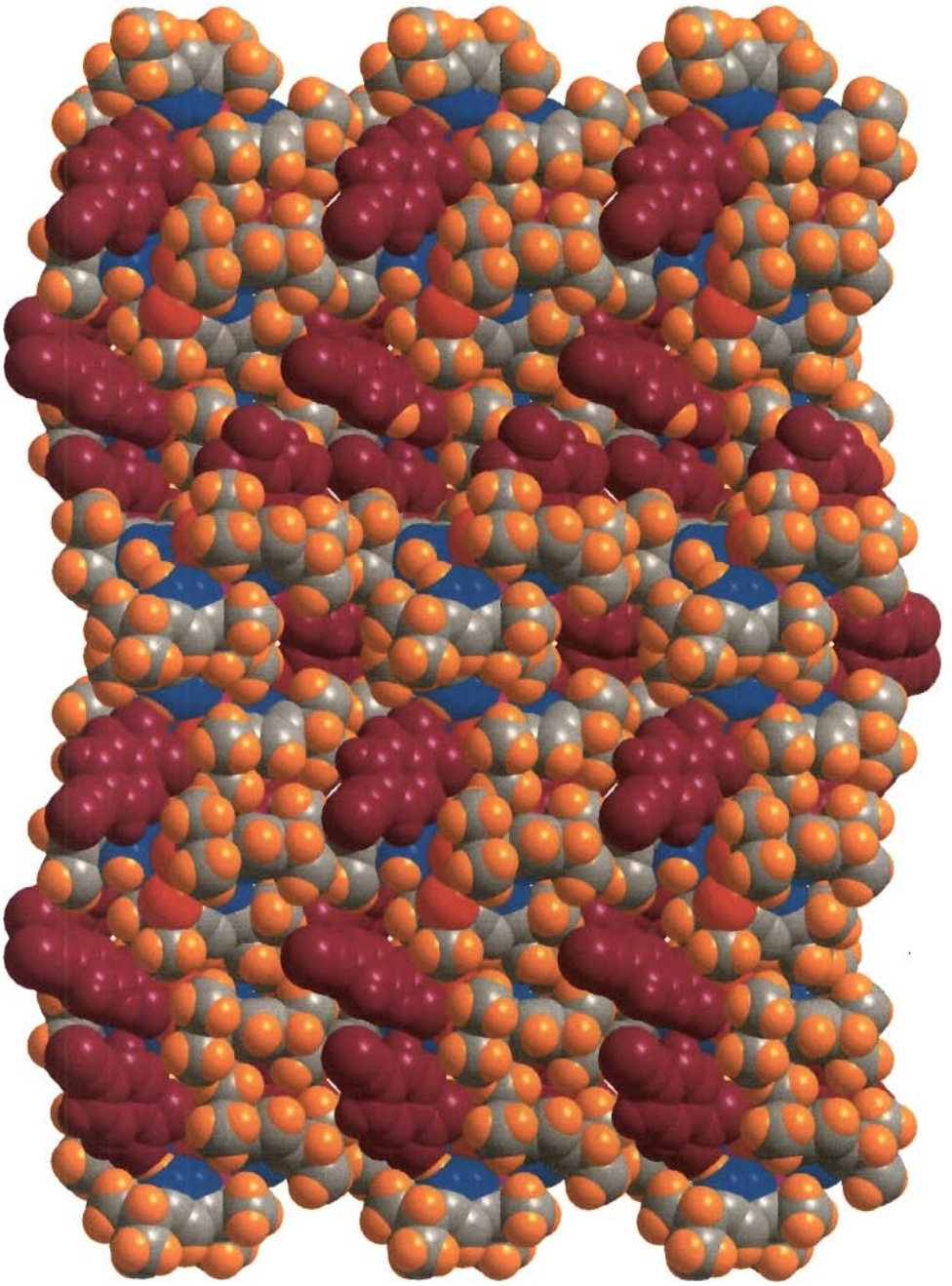

Fig. 3-39 Three-dimensional packing (space-fill model) due to non-covalent interactions present in complex **3n**. Rectangular voids were occupied by guest (*p*-cyanobenzoate anions) molecules (cherry colored).

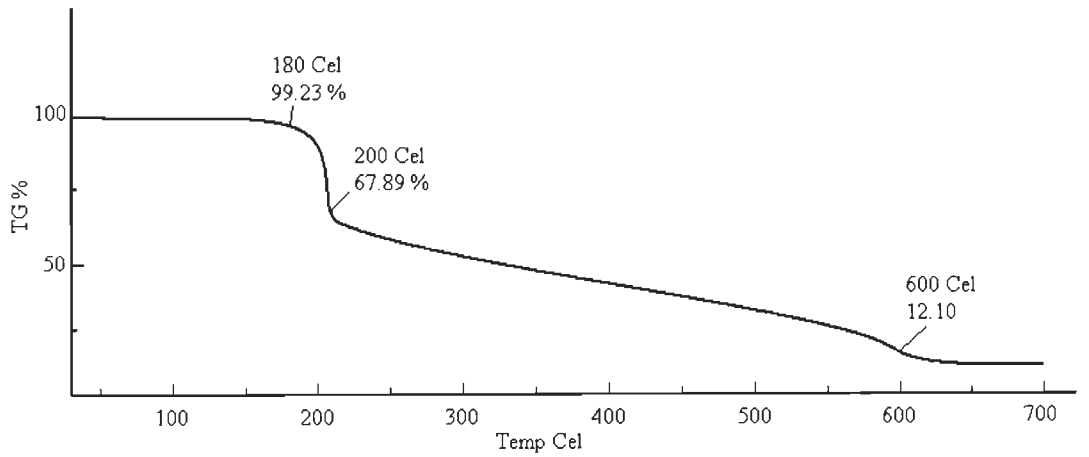

Fig. 3-40 TGA plot for complex **3j**

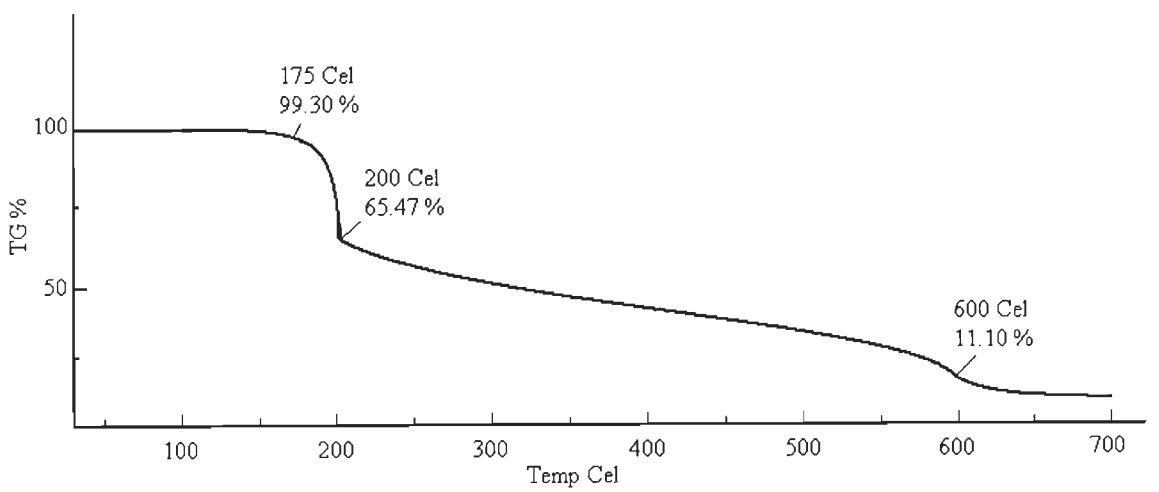

Fig. 3-41 TGA plot for complex **3k**

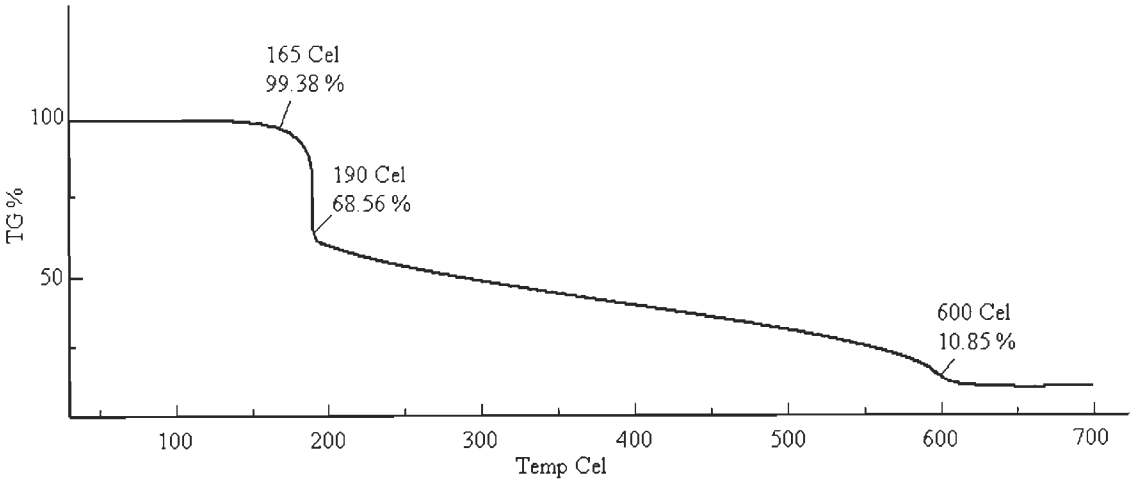

Fig. 3-42 TGA plot for complex **3l**

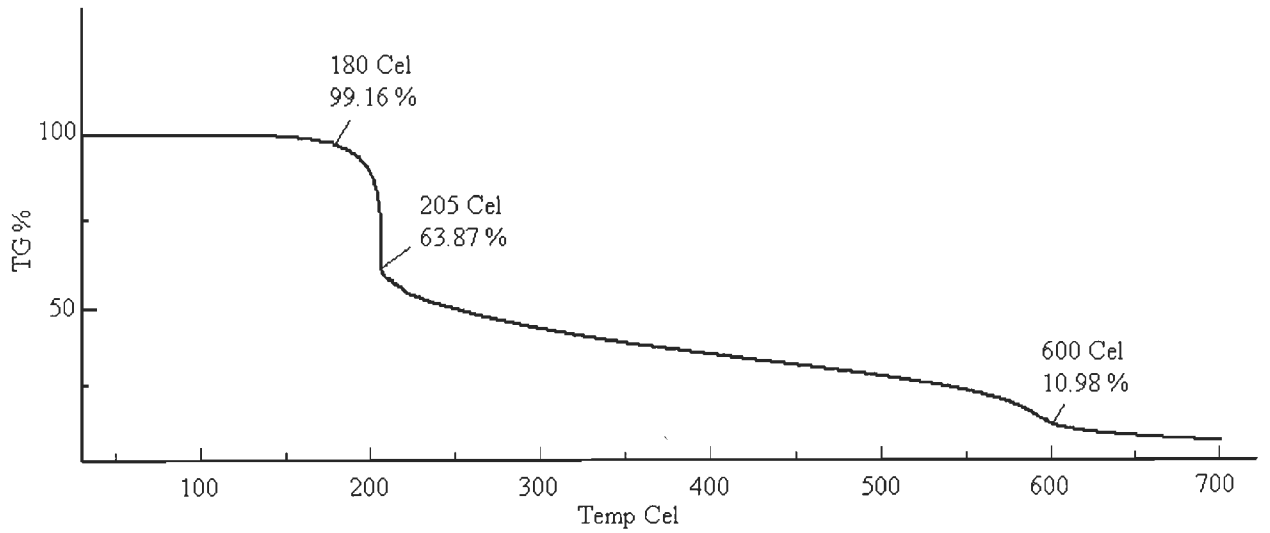

Fig. 3-43 TGA plot for complex **3m**

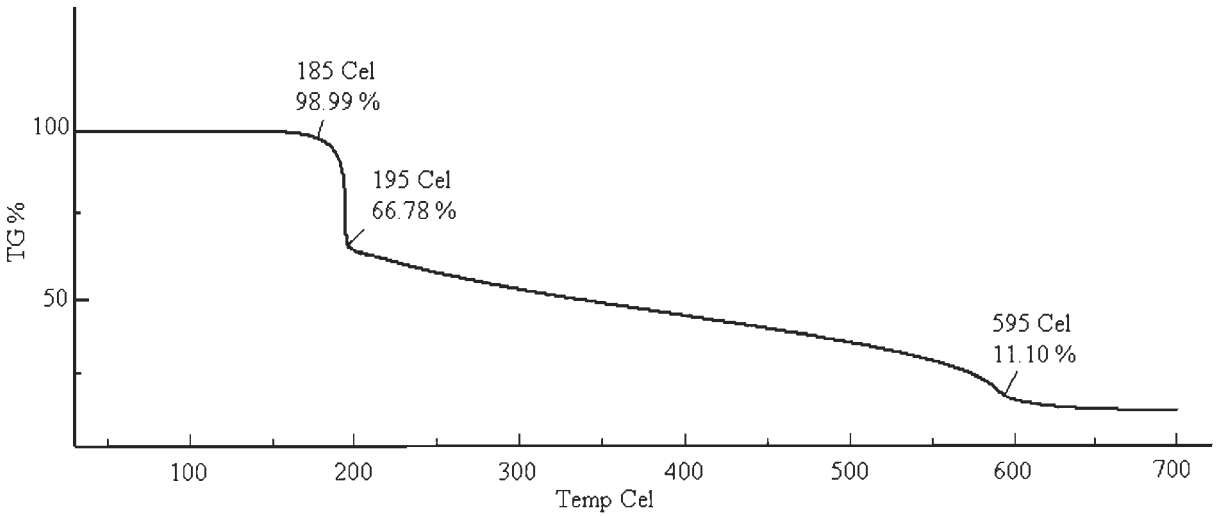

Fig. 3-44 TGA plot for complex **3n**

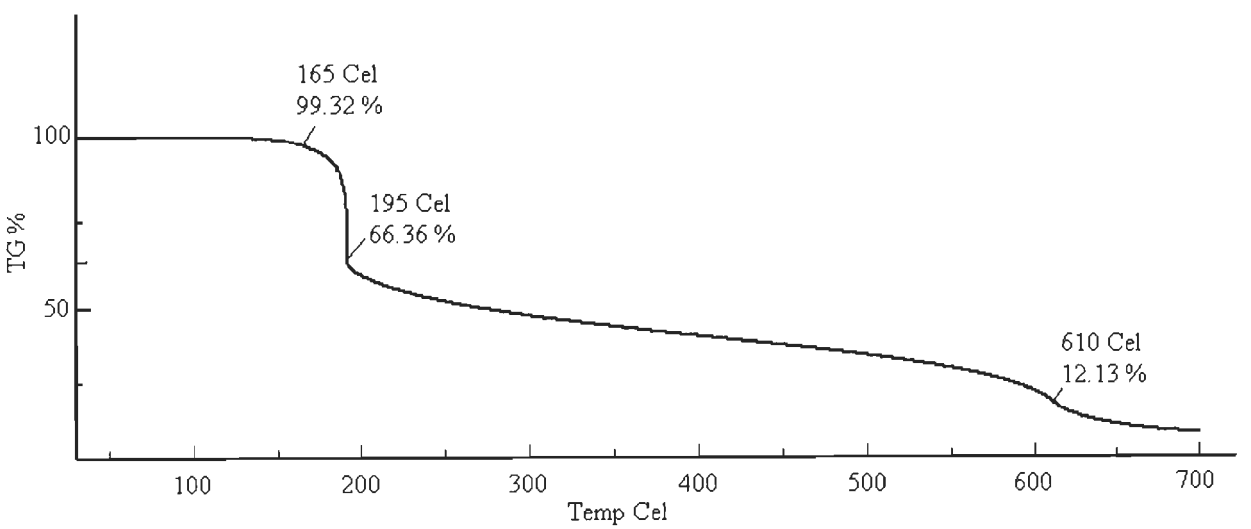

Fig. 3-45 TGA plot for complex **3o**

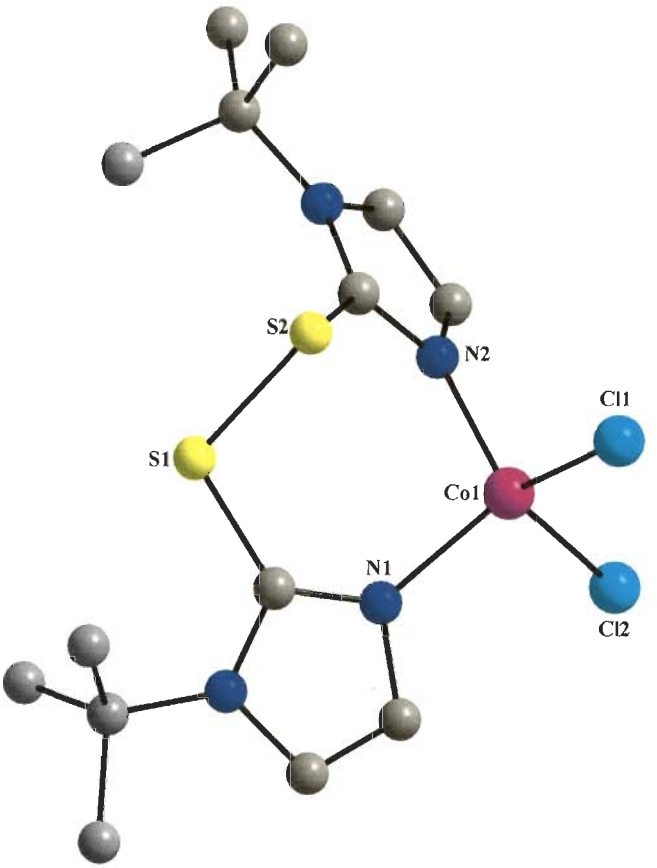

Fig. 3-46 Crystal structure of $[_k^2(tm^{t\text{-}Bu})_2CoCl_2]$ (**3q**)

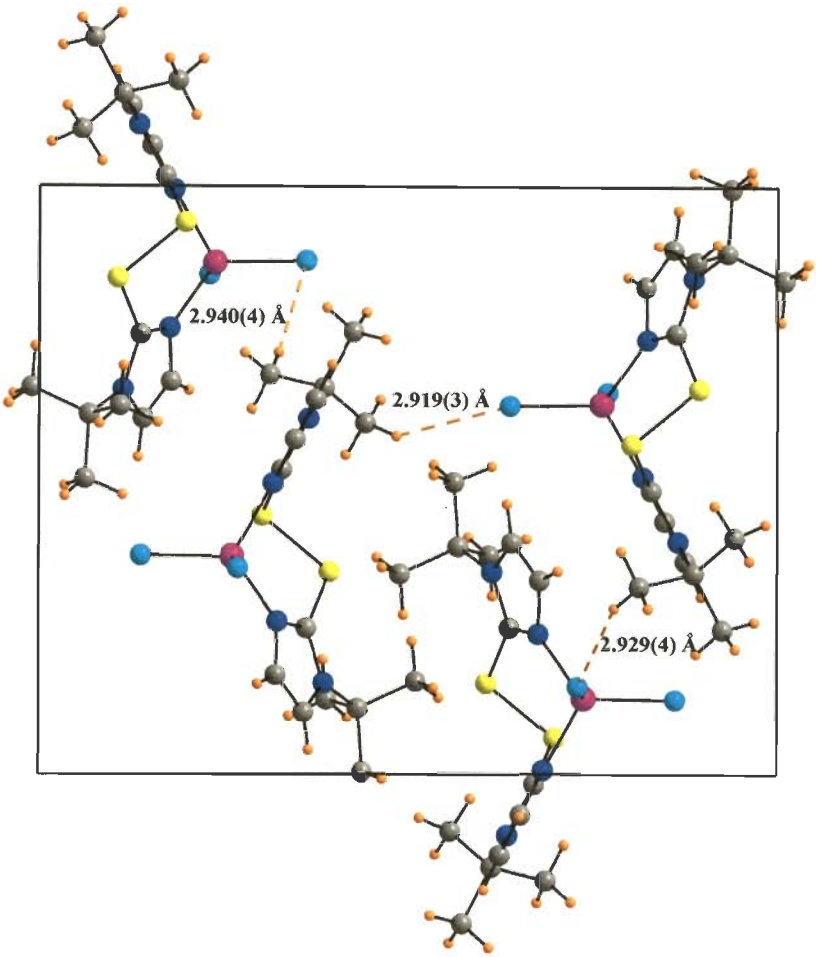

Fig. 3-47 Intermolecular C-H···Cl interaction in unit cell packing of complex **3q** along the a-axis

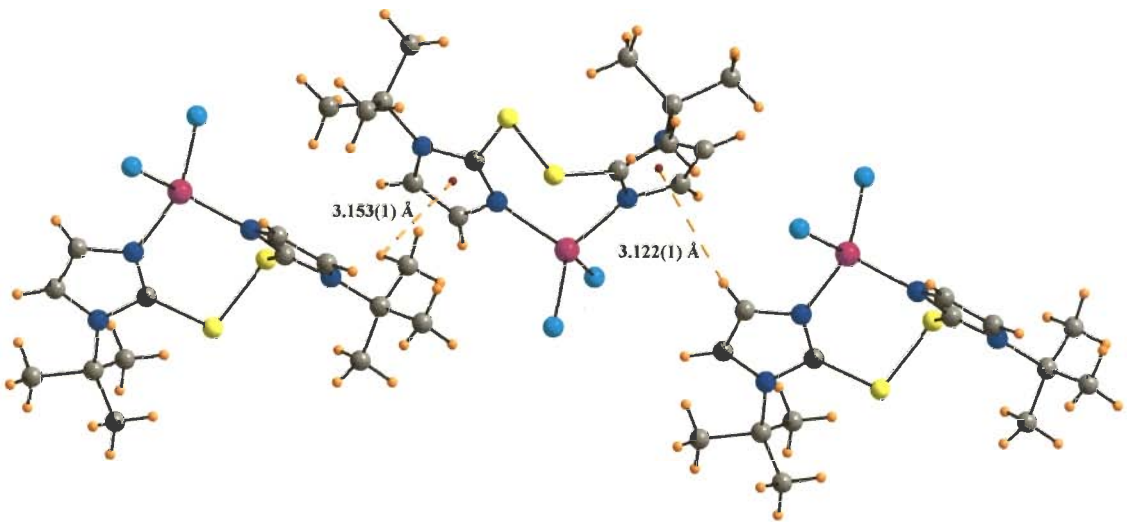

Fig. 3-48 Intermolecular CH···π and CH_3···π interactions present in complex **3q**

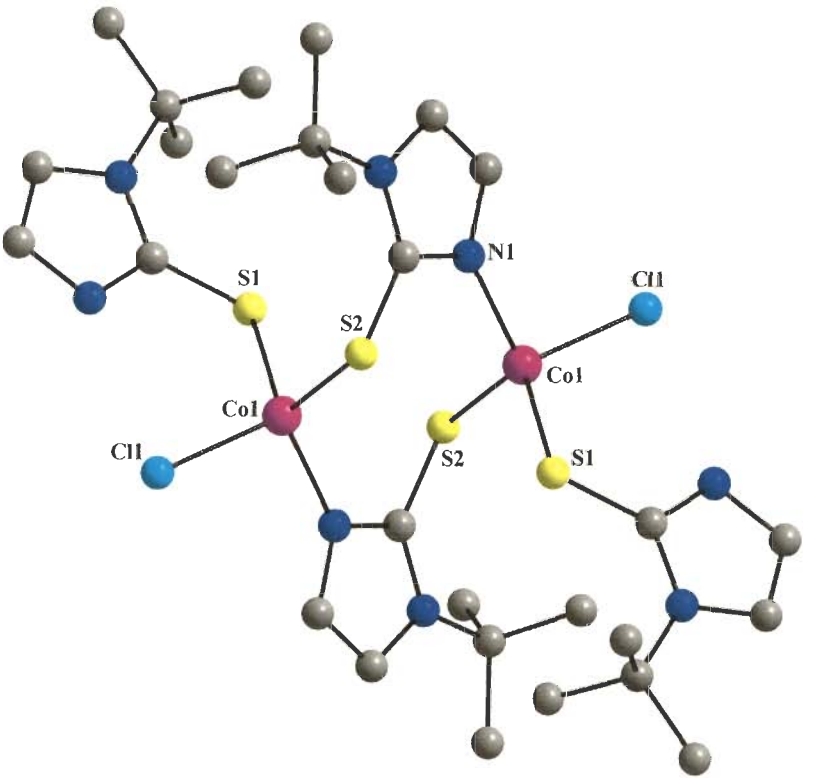

Fig. 3-49 Crystal structure of $[(tm^{t\text{-}Bu})_2Co(\mu\text{-}tm^{t\text{-}Bu})_2Cl_2]$ (**3r**)

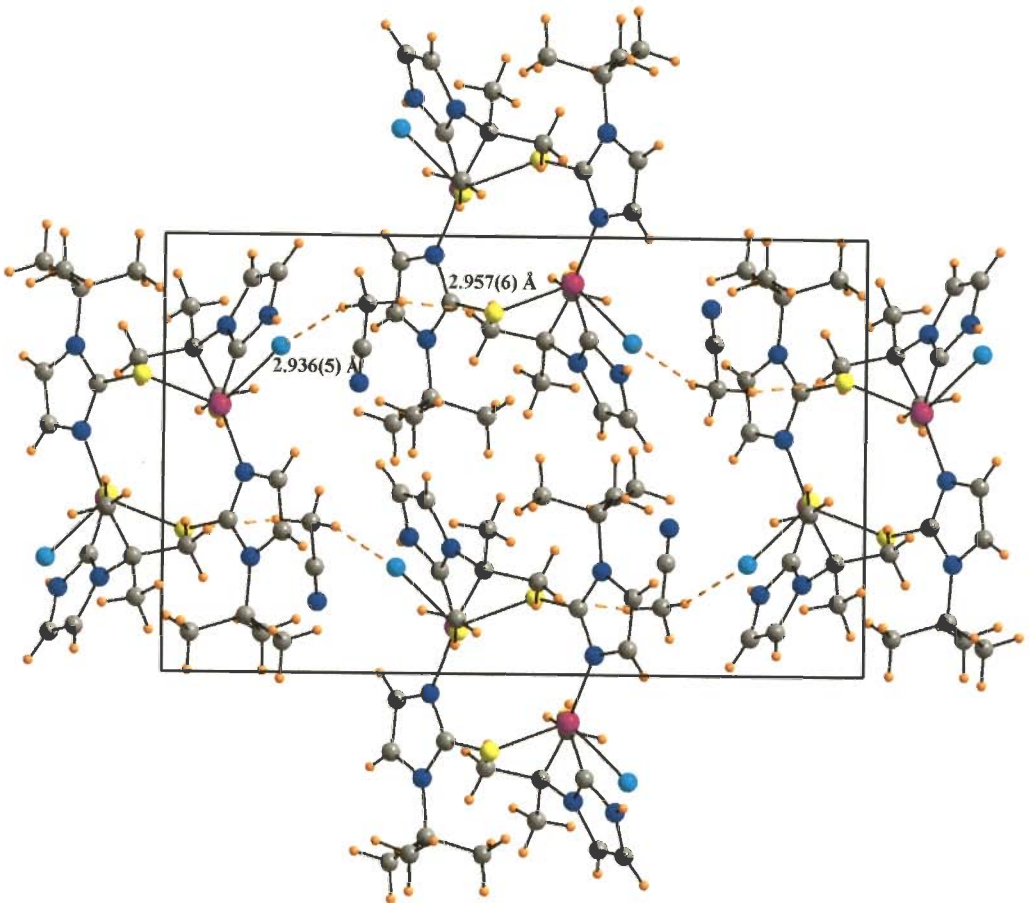

Fig. 3-50 Intermolecular C-H···Cl interaction in unit cell packing of complex **3r** along the a-axis

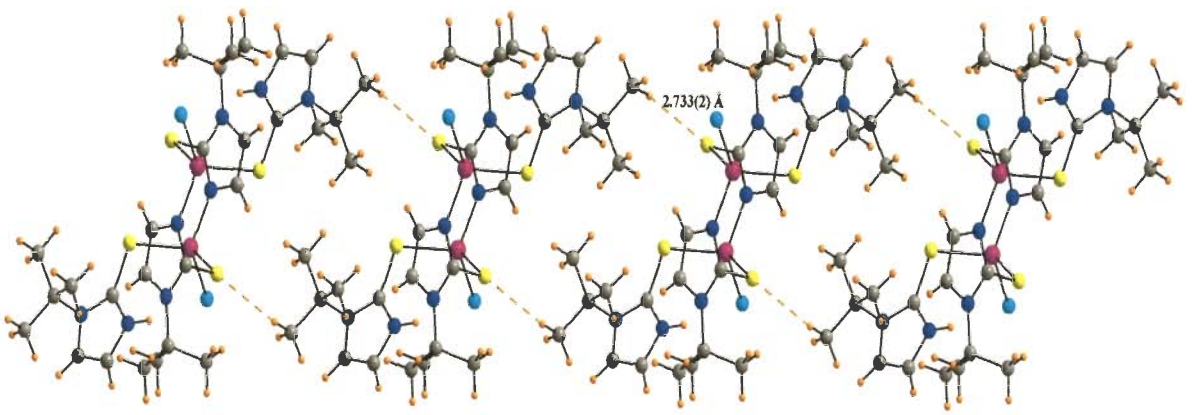

Fig. 3-51 Intermolecular CH···S interactions present in complex **3r**

References

1. Labinger, J.A. and Bercaw, J.E., "Understanding and exploiting C-H bond activation", Nature, **417**, 507 (2002).

2. Arndtsen, B.A., Bergman, R.G., Mobley, T.A. and Peterson, T.H., "Selective intermolecular carbon-hydrogen bond activation by synthetic metal complexes in homogeneous solution", Acc. Chem. Res., **28**, 154 (1995).

3. Marcela, A. and Torres, E., "Enzymatic activation of alkanes: constraints and prospectives", Appl. Cata. A: Gen, **272**, 1 (2004).

4. Notomista, E., Lahm, A., Di, D.A. and Tramontano, A., "Evolution of bacterial and archeal multicomponent monooxygenases", J. Mol. Evol., **56**, 435 (2003).

5. Duetz, W.A., van Beilen, J.B. and Witholt, B., "Using proteins in their natural environment: potential and limitations of microbial whole-cell hydroxylations in applied biocatalysis", Curr. Opin. Biotech., **12**, 419 (2001).

6. Stevenson, J.A., Westlake, A.C.G., Whittock, C. and Wong, L.L., "The catalytic oxidation of linear and branched alkanes by cytochrome P450cam", J. Am. Chem. Soc., **118**, 12846 (1996).

7. Hill, F.F., Venn, I. and Lukas, K.L., " Studies on the formation of long chain dicarboxylic acids from pure n- alkanes by a mutant of *Candida tropicalis*", Appl. Microbiol. Biotechnol., **24**, 168 (1986).

8. Peters, M.W., Meinhold, P., Glieder, A. and Arnold, F.H., "Regio- and enantio selective alkane hydroxylation with engineered cytochromes P450 BM-3", J. Am. Chem. Soc., **125**, 13442 (2003).

9. Bharath, A., Santra, B.K., Munshi, P. and Lahiri, G.K., "Cobalt-mediated selective C-H bond activation. Direct aromatic hydroxylation in the complexes $[Co^{III}\{o\text{-}OC_6H_3(R)N{=}NC_5H_4N\}_2]ClO_4.H_2O$ (R = H, *o*-Me / Cl, *m*-Me / Cl or *p*-Me / Cl). Synthesis, spectroscopic and redox properties", J. Chem. Soc., Dalton Trans., 2643 (1998).

10. Fujita, E. and Creutz, C., "C-H bond activation by cobalt (I) macrocycles: Rapid H / D exchange between macrocycle and acetonitrile solvent", Inorg. Chem., **33**, 1729 (1994).

11. Paneque, M., Taboada, S. and Carmona, E., "C-H and C-S activation of thiophene by rhodium complexes: Influence of the ancillary ligands on the thermodynamic stability of the products", Organometallics, **15**, 2678 (1996).

12. Wiley, J.S., Jr., Oldham, W.J. and Heinekey, D.M., "Carbon-hydrogen bond activation in hydridotris(pyrazolyl)borate complexes of iridium", Organometallics, **19**, 1670 (2000).

13. Canty, A.J., Patel, J., Skelton, B.W. and White, A.H., "C-H activation at the 3-position of pentane chains to form $[N\text{-}C(sp^3)\text{-}N]^-$ complexes incorporating six-membered pallada(II)cyclic rings and pyridine, pyrazole and N-methylimidazole donor groups. Structural studies and comparison with $[N\text{-}C(sp^2)\text{-}N]^-$ complexes", J. Organomet. Chem., **607**, 194 (2000).

14. Chantson, J.T. and Lotz, S., "C–H and N–H activation by Pt(0) in N- and O-heteroaromatic compounds", J. Organomet. Chem., **689**, 1315 (2004).

15. Kitajima, N., Osawa, M., Tanaka, M. and Moro-oka, Y., "A novel dioxygenase type oxygen insertion. C-H bond oxygenation of isopropyl groups in a dimanganese complex with molecular oxygen", J. Am. Chem. Soc., **113**, 8952 (1991).

16. Liu, S., Wang, H., Zhang, P.-C., Weng, L.-H. and Hou, X.-F., "Synthesis and structure of half-sandwich pyridine-2-thiolato cobalt (III) and rhodium (III) complexes and their reactivity toward monodentate or bidentate 1,2-dicarba-closo-dodecaborane thiolate ligands", Organometallics, **27**, 713 (2008).

17. Hu, C., Chin, R.M., Nguyen, T.D., Nguyen, K.T. and Wagenknecht, P.S., "Chemistry of constrained dioxocyclam ligands with Co(III): Unusual examples of C-H and C-N bond cleavage", Inorg. Chem., **42**, 7602 (2003).

18. Zhou, X., Day, A.I., Edwards, A.J., Willis, A.C. and Jackson, W.G., "Facile C-H bond activation: Synthesis of the N_4C donor set pentadentate ligand 1,4-Bis(2-pyridylmethyl)-1,4-diazacyclononane (dmpdacn) and a structural study of its alkyl-cobalt (III) complex $[Co(dmpdacn\text{-}C)(OH_2)](ClO_4).H_2O$ and its hydroxylated derivative $[Co(dmpdacnOH\text{-}O)Cl](ClO_4).C_3H_6O$", Inorg. Chem., **44**, 452 (2005).

19. Shay, D.T., Yap, G.P.A., Zakharov, L.N., Rheingold, A.L. and Theopold, K.H., "Intramolecular C-H activation by an open-shell cobalt (III) imido complex", Angew. Chem. Int. Ed., **44**, 1508 (2005).

20. Leung, D.H., Bergman, R.G. and Raymond, K.N., "Scope and mechanism of the C-H bond activation reactivity within a supramolecular host by an iridium guest: A stepwise ion pair guest dissociation mechanism", J. Am. Chem. Soc., **128**, 9781 (2006).

21. Purwoko, A.A. and Lees, A.J., "Photochemical C-H bond activation reactivity of $HB(Pz^{Me2})_3Rh(CO)_2$ (Pz^{Me2} = 3,5-dimethylpyrazolyl) in alkane solutions", Inorg. Chem., **35**, 675 (1996).

22. Wayland, B.B., Ba, S. and Sherry, A.E., "Activation of methane and toluene by rhodium porphyrin complexes", J. Am. Chem. Soc., **113**, 5305 (1991).

23. Sakuri, H., Hataya, Y., Goromaru, T. and Matsuura, H., "A model system for drug metabolism in isolated hepatocytes; oxidation of cyclohexene by metalloporphyrin complexes", J. Mol. Cata., **29**, 153 (1985).

24. Ostovic, D. and Bruice, T.C., "Mechanism of alkene epoxidation by iron, chromium and manganese higher valent oxo-metalloporphyrins", Acc. Chem. Res., **28**, 154 (1995).

25. Harvey, J.D. and Ziegler, C.J., "The metal complexes of N-confused porphyrin as heme model compounds", J Inorg. Biochem., **100**, 869 (2006).

26. Lavrushko, V.V., Lermontov, S.A. and Shilov, A.E., "Formation of methyl platinum complex in the reaction of methane with chloroplatinic acid", React. Kinet. Catal. Lett., **15**, 269 (1980).

27. Janowicz, A.H. and Bergman, R.G., "C-H activation in completely saturated hydrocarbons: direct observation of M + R-H M(R)(H)", J. Am. Chem. Soc., **104**, 352 (1982).

28. Sen, A., Lin, M., Kao, L.C. and Huston, A.C., "C-H activation in aqueous medium. The diverse roles of platinum (II) and metallic platinum in the catalytic and stoichiometric oxidative functionalization of organic substrates including alkanes", J. Am. Chem. Soc., **114**, 6385 (1992).

29. Backlund, M., Ziller, J. and Farmer, P.J., "Unexpected C-H activation of Ru(II)-dithiomaltol complxes upon oxidation", Inorg. Chem., **20**, 1000 (2007).

30. Ito, J.-I., Shiomi, T. and Nishiyama, H., "Efficient preparation of new-rhodium- and iridium-[bis(oxazolinyl)-3,5-dimethylphenyl] complexes by C-H bond activation: Applications in asymmetric synthesis", Adv. Synth. Catal., **348**, 1235 (2006).

31. Sakakura, T., Sodeyama, T., Sasaki, K., Wada, K. and Tanaka, M., "Carbonylation of hydrocarbons via C-H activation catalyzed by $RhCl(CO)(PMe_3)_2$ under irradiation", J. Am. Chem. Soc., **112**, 7221 (1990).

32. Bolig, A.D. and Brookhart, M., "Activation of sp^3 C-H bond with cobalt (I): catalytic synthesis of enamines", J. Am. Chem. Soc., **129**, 14544 (2007).

33. Cho, J., Furutachi, H., Fujinami, S., Tosha, T., Ohtsu, H., Ikeda, O., Suzuki, A., Nomura, M., Uruga, T., Tanida, H., Kawai, T., Tanaka, K., Kitagawa, T. and Suzuki, M., "Sequential reaction intermediates in aliphatic C-H bond functionalization initiated by a bis(μ-oxo)dinickel (III) complex", Inorg. Chem., **45**, 2873 (2006).

34. Hikichi, S., Komatsuzaki, H., Akita, M. and Moro-oka, Y., "Aliphatic C-H bond oxygenation by the $Co^{II}OOX$ species with the hindered hydrotris(pyrazolyl) borate ligand (X = Co(II), alkyl, H)", J. Am. Chem. Soc., **120**, 4699 (1998).

35. Nakamoto, K., "Infrared and Raman spectra of inorganic and coordination compounds", Wiley, New York, p. 236 (1986).

36. Mestrovic, E. and Kaitner, B., "A Supramolecular structure of bis(1,3-diphenyl-1, 3-propanedionato-O,O′)(1,10-phenanthroline-N,N′)cobalt (II) based on C-H···O, C-H···π and π···π interactions", J. Chem. Crystall., **36**, 599 (2006).

37. Vojinovic, L.S., Leovac, V.M., Novakovic, S.B., Bogdanovic, G.A., Csanadi, J.J. and Cesljevic, V.I., "Transition metal complexes with Girard reagent-based ligands, Part I: Synthesis and crystal structure of the first cobalt (III) complexes with Schiff base derivative of Girard reagent", Inorg. Chem. Comm., **7**, 1264 (2004).

38. Kitajima, N., Osawa, M., Tarmura, N., Moro-oka, Y., Hirano, T., Hirobe, M. and Nagano, T., "Monomeric (benzoato)manganese (II) complexes as manganese superoxide dismutase mimics", Inorg. Chem., **32**, 1879 (1993).

39. Singh, U.P., Sharma, A.K., Tyagi, P., Upreti, S. and Singh, R.K., "Mononuclear manganese carboxylate complexes: Synthesis and structural studies", Polyhedron, **25**, 3628 (2006).

40. Kitajima, N., Hikichi, S., Tanaka, M. and Moro-oka, Y., "Fixation of atmospheric carbon dioxide by a series of hydroxo complexes of divalent metal ions and the implication for the catalytic role of metal ion in carbonic anhydrase. Synthesis, characterization, and molecular structure of $[LM(OH)]_n$ (n = 1 or 2) and $LM(\mu\text{-}CO_3)ML$ (M(II) = Mn, Fe, Co, Ni, Cu, Zn; L = $HB(3,5\text{-}Pz^{iPr2})_3$)", J. Am. Chem. Soc., **115**, 5496 (1993).

41. Denisova, T.O. and Nefedov, S.E., "Synthesis, structure, and protonation of an unusual electron-deficient complex $Co_2(\mu\text{-}Pz^{Me2})_2(OOCCMe_3)_2(Pz^{Me2}H)_2$ ($Pz^{Me2}H$ is 3,5-dimethylpyrazole) with bridging pyrazolate ligands", Russ. Chem. Bull., **52**, 775 (2003).

42. Balamurugan, V., Hundal, M.S. and Mukherjee, R., "First systematic investigation of C-H···Cl hydrogen bonding using inorganic supramolecular synthons: Lamellar, stitched stair-case, linked-ladder and helical structures", Chem. Eur. J., **10**, 1683 (2004).

43. Mi, Y. and Bakker, E., "Determination of complex formation constants of lipophilic neutral ionophores in solvent polymeric membranes with segmented sandwich membranes", Anal. Chem., **71**, 5279 (1999).

44. Figueroa, J.S., Yurkerwich, K., Melnick, J., Buccella, D. and Parkin, G., "Applications of bis(1-R-imidazol-2-yl)disulfides and diselenides as ligands for main-group and transition metals: κ^2-(N,N) Coordination, S-S bond cleavage, and S-S / E-E (E = S, Se) bond metathesis reactions", Inorg. Chem., **46**, 9234 (2007).

45. Vinuelas-Zahinos, E., Maldonado-Rogado, M.A., Luna-Giles, F. and Barros-Garcia, F.J., "Coordination behaviour of schiff base 2-acetyl-2-thiazoline hydrazone (ATH) towards cobalt (II), nickel (II) and copper (II)", Polyhedron, **27**, 879 (2008).

46. Beloglazkina, E.K., Majouga, A.G., Romashkina, R.B., Moiseeva, A.A. and Zyk, N.V., "The preparation, crystal structure and electrochemistry of (5*Z*,5′*Z*)-2,2′-(alkane-α,ω-diylsulfanyldiyl)bis(5-(3-pyridylmethylene)-3,5-dihydro-4*H*-imidazol-4-ones) and their complexes with cobalt (II) chloride", Polyhedron, **26**, 797 (2007).

47. Allen, F.H. and Kennard, O., "3D-search and research using the Cambridge crystallographic database", Chem. Des. Autom. News, **8,** 31 (1993).

48. Matsunaga, Y., Fujisawa, K., Amir, N., Miyashita, Y. and Okamoto, K., "Dichloro[bis(1-methylimidazole-2)disulfide]zinc (II)", Appl. Organomet. Chem., **19,** 208 (2005).

49. Liu, H.-L., Mao, H.-Y., Xu, C., Zhang, H.-Y., Hou, H.-W., Wu, Q., Zhu, Y., Ye, B.-X. and Yuan, L.-J., "Four novel sulfur-rich complexes: syntheses, crystal structures of three nickel (II) and one cobalt (II) complex with derivatives of Lawesson's Reagent", Polyhedron, **23**, 1799 (2004).

Chapter 4

Synthesis and Structural Studies of Nickel Complexes

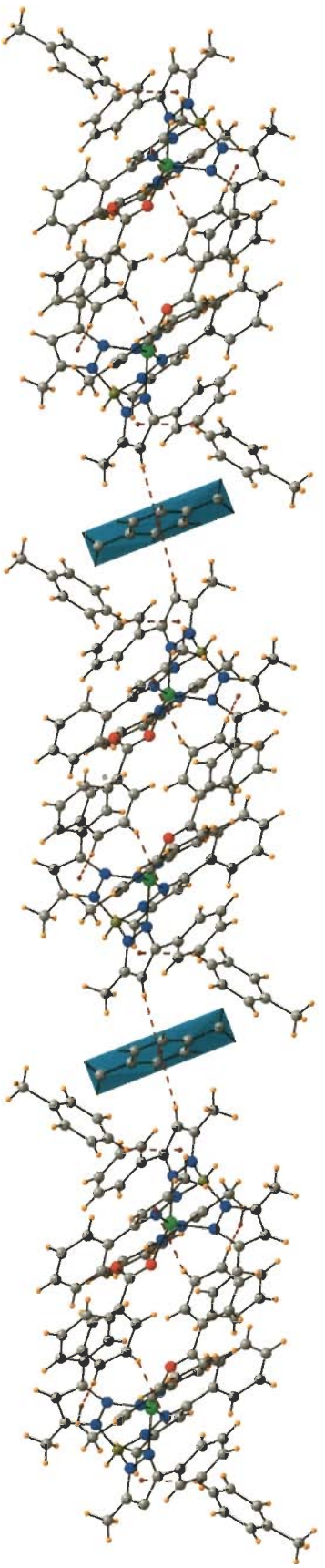

For a long time, Nickel was the only element of the "late" 3d transition metals for which a biological role could not be definitely established. The reasons for this oversight were manifold: nickel ions do not exhibit a very characteristic absorbance in the presence of physiologically relevant ligands and it is often only one of the several components of complex enzymes, which may otherwise contain several coenzymes as well as additional inorganic material. Later, it was found that nickel is an essential nutrient for selected microorganisms where it participates in a variety of cellular processes. Many microbes are capable of sensing cellular nickel ion concentrations and taking up this nutrient via nickel-specific permeases or ATP-binding cassette-type transport systems. The metal ion is specifically incorporated into nickel-dependent enzymes, often via complex assembly processes requiring accessory proteins and additional non-protein components, in some cases accompanied by nucleotide triphosphate hydrolysis. For instance, nickel centers remained undetected for a long time due to their frequent association with Fe / S clusters. However, applying more sensitive detection methods viz. atomic absorption or emission spectroscopy (AAS or AES), magnetic measuring (SQUID) or EPR spectroscopy using ^{61}Ni enriched material, has led to the establishment of some nickel containing enzymes of plants and microorganisms and partly their characterization.

Low concentrations of nickel (0.015 mg kg^{-1}) in the diet resulted in decreased weight gain in growing rats in comparison with nickel supplemented control animals. Nickel deficiency appeared to decrease the absorption of iron by rats, with resultant development of anemia, and also caused 29-82 % decrease in the activity of dehydrogenase enzymes and 45 % decrease in the activity of enzymes of amino acid metabolism in liver. In both liver and serum of nickel deficient rats, the concentration

of glucose and glycogen were decreased by 90 % [1]. In female goats and minipigs, nickel deficiency caused decrease conception rates after artificial insemination. The offspring from these nickel deficient dams had reduced birth weight and weight gain during suckling when compared to nickel-supplemented controls animals.

Only in the late 1960s, nickel began to be considered as a necessary component for the growth of some anaerobic bacteria. In 1975 the metal was reported to occur in plant urease and also the first documentation of nickel activity on a molecular level [2] was provided. To date, many nickel-containing enzymes viz., urease, methyl coenzyme M reductase, NiFe-hydrogenase, carbon monoxide dehydrogenase, acetyl-CoA decarbonylase / synthase, superoxide dismutase, some glyoxylases, acireductone dioxygenase and methylenediurease are known. Eight of these enzymes have been structurally characterized except methylenediurease, revealing distinct metallocenter environments in each case [3]. The urease enzyme from bacteria and plant contains 5- or 6- coordinate Ni(II) bound to N, O-ligands, both the hydrogenases of many bacteria and the CO dehydrogenase of anaerobic bacteria contain Ni which is mainly coordinated by sulphur ligands. The methyl-coenzymes M reductase of methanogenic bacteria features a nickel tetrapyrrole complex as the prosthetic group, the coenzyme F430. Another tetrapyrrole complex with an unspecified function, the nickel containing tunichlorin was isolated from a tunicate species [4]. The Ni environment within each protein is different, however the Ni centers are believed to reside within the active sites of all these enzymes and to be intimately involved in there catalytic cycles [5]. Several aspects of the chemistry of these biological Ni ions are unusual in the context of the known coordination chemistry of nickel, some of these enzymes are known to contain redox-active nickel centres that can cycle between +3, +2, and / or +1 oxidation states,

in thiolate-rich or tetrapyrrole ligand environments that were not previously thought to favor metal-centered redox processes in the Ni complexes. The details about some nickel- containing proteins are given below.

Urease is a metalloenzyme that catalyzes the hydrolysis of urea to ammonia and carbamate, which spontaneously decomposes to yield carbonic acid and another molecule of ammonia (Scheme 4-1).

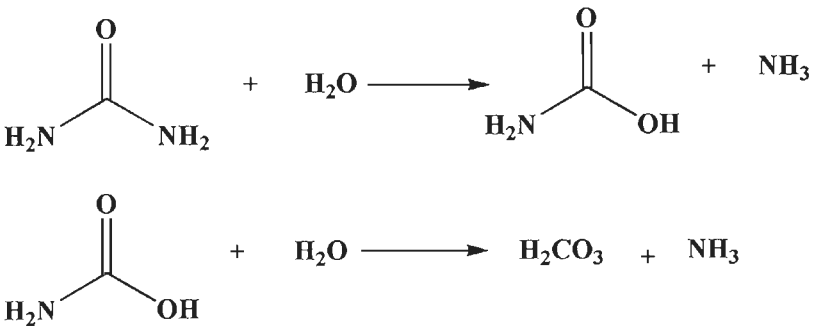

Scheme 4-1

This hydrolysis has not been observed without the enzyme, so the rate enhancement produced by urease is $>10^{14}$. The mechanism is likely to involve the two-nickel ions present in the urease active site, as well as amino acid residues, possibly acting as general acids and bases. The observed pH profile of activity is bell-shaped with two pKa's: a lower pKa of 6.5 and higher pKa of 9.0, indicating that the protonation state of two groups effect urease activity. Based on crystallographic and kinetic studies of the urease from *Klebsiella aerogenes* [6], it was proposed that the residue His 219, along with the first Ni ion, binds the urea oxygen, positioning the urea molecule and polarizing the carbonyl. The second nickel without the aid of general base stabilizes a hydroxide ion, which attacks the carbon of urea. One of the amide nitrogens of urea is protonated by the general acid His 320 and ammonia is eliminated. This key histidine act as an acid and must be in its protonated form for activity, even though it

has been assigned a pKa of 6.5 which is lower than the optimum pH for the enzyme. Thus, the active protonation state of urease is reverse-protonated, meaning that a group with a lower pKa must be protonated and a group with a higher pKa must be deprotonated for activity. The higher pKa of 9.0 has been interpreted as being due to the metal-bound hydroxide, which must be deprotonated for activity.

Further, the 2.2 Å resolution X-ray crystal structure of *Klebsiella aerogenes* urease revealed a trimer of trimers containing three di-Ni active sites [7]. The two Ni ions are located 3.5 Å apart and bridged by a carbamate formed by reaction of the activating CO_2 with Lys 217. The active site has two coupled Ni(II) ions, Ni-1 is coordinated by two N(His$^{\alpha 246}$, His$^{\alpha 272}$) and one O (O of carbamyrated Lys$^{\alpha 217}$), and Ni-2 is coordinated by two N (His$^{\alpha 134}$, His $^{\alpha 136}$) and three O (Asp $^{\alpha 360}$, water and carbamyrated Lys $^{\alpha 217}$).

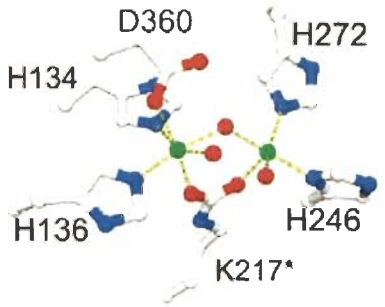

Fig. 4-1 Active site structure of Urease (Color code: C, light grey; N, blue; O, red; Ni, green)

The holoenzyme of jackbeans urease consists of six equivalent subunits; each subunit (91 kDa) contains two close but apparently different nickel ions [8]. EXAFS measurements suggests the presence of only nitrogen and oxygen ligands in the first coordination spheres and recommended the coordination numbers of five and / or six in agreement with the magnetic and absorption spectroscopic studies. Measurements of

the magnetic susceptibility point to an equilibrium between high spin and low spin forms, which would be typical for five coordinate or disordered six coordinate Ni(II) ion due to small and variable energy difference between dz^2 and dx^2-y^2 orbitals. On the basis of model studies, the proposed reaction mechanism involves an electrophilic attack of one of the nickel centers on the carbonyl oxygen atom and a nucleophilic attack of a nickel hydroxo species on the carbonyl carbon center. Similar mechanistical hypothesis exists for the function of Zn-containing hydrolytic enzymes where protons often function as the electrophilic species. On the basis of comparisons with dinuclear Ni complexes containing bridging carboxylate [9, 10-13] or carbonate ligands, [14, 15] or by employment of molecular models, the bridging intermediate in the proposed urease hydrolysis mechanism is thought to possess a Ni···Ni separation of approximately 3.4, 4.2 or 6.0 Å depending upon the Ni-O-C angle, the presence of carboxylate or imidazolate bridge between the Ni ions in this species would require a Ni…Ni distance of < 4.0 and 5.3 Å, respectively.

Methyl-CoM reductase is the key enzyme in the energy metabolism of strictly anaerobic archaea called methanogens [16]. Methyl-CoM reductase has a molecular mass of about 300 kDa and is composed of three different types of subunits α, β, γ arranged as a hexamer of $(\alpha\beta\gamma)_2$ composition. The multi subunit complex contains two molecule of Ni-porphinoid coenzyme F430, coenzyme M (mercaptoethane sulfonate) and coenzyme B (mercapto heptanothreonine phosphate). The enzyme catalyzes the final reaction of the methanogenic pathway by reducing methyl-CoM to methane with coenzyme B as electron donor forming the heterodisulphide CoM-S-S-CoB [17]. The crystal structure of methyl-CoM reductase from *Methanobacterium thermoautoropium* has been determined to 1.45 Å resolutions. The overall structure is characterized by a

series of α helices. The active site and the binding site of the coenzymes are formed by subunit α, α', β and γ indicating that the entire hexamer is required for enzymatic activity.

The coenzyme F_{430} is anchored to the protein matrix mainly by hydrogen bonds between carboxylate groups of the tetrapyrrole ring and main chain amide groups of residues from subunits α, α', β and γ. The Ni atom is axially coordinated to the side chain amide oxygen atom of Gln α'147. Coenzyme M and B and their active sites are located on the other side of the Ni-porphinoid plane. The binding of coenzyme B shields the active sites from bulk solvent by locking a channel leading from the protein surface to the active site.

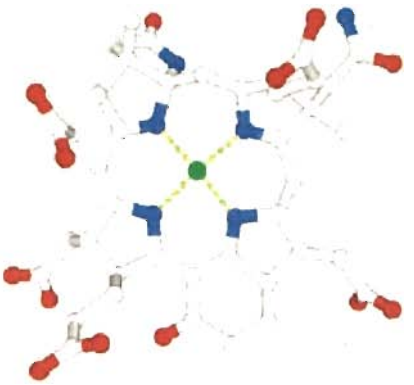

Fig. 4-2 Active site structure of Methyl-CoM reductase (Color code: C, light grey; N, blue; O, red; Ni, green)

Nickel-Iron hydrogenase is an enzyme, which catalyzes the oxidation and reduction of molecular hydrogen. Two types of hydrogenase, iron and nickel-iron hydrogenases have been found in the sulphate-reducing bacteria. The three dimensional structure of the nickel-iron hydrogenase from *Desulfovibrio gigas* at 2.85 Å can be seen in Fig. 4-3, showing the location, coordination and geometry of the metal center in the heterodimer [18]. In contrast to the Fe hydrogenases, the nickel enzyme possesses a

variety of compositions, molecular weights, activation behavior and redox potentials [19]. Some of the nickel hydrogenases contain selenium, likely in the form of selenocysteine, some contain flavin (FMN or FAD), and all contain iron-sulfur centers, but in amounts ranging from 4 to 14 iron atoms per Ni atom. Among the different Ni hydrogenases, there is a proper pattern of protein composition, to which many, but not all, seem to confirm (especially those enzymes originating from purple eubacteria). There are two protein subunits of approximate molecular masses 30 and 60 kDa, with the nickel probably residing in the latter subunit. The hydrogenase of the sulphate-reducing bacterium *Desulfovibrio gigas* is among the best investigated. This hydrogenase contains a single unit Ni, two Fe_2S_4 clusters, and one Fe_3S_4 cluster. EPR signals attributable to mononuclear nickel have been used in numerous investigations for the role of Ni in hydrogenases.

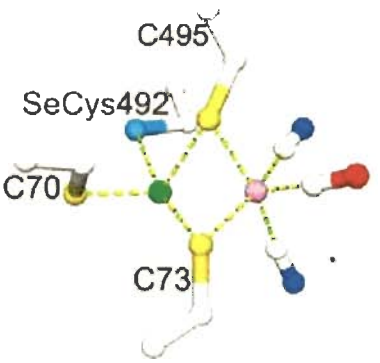

Fig. 4-3 Active site structure of Ni-Fe Hydrogenase (Color code: C, light grey; N, blue; O, red; Ni, green; Fe, pink; S, yellow; Se, light blue)

Carbon monoxide dehydrogenases (CODHs) catalyze the reversible oxidation of carbon monoxide to carbon dioxide in a variety of anaerobic microorganisms [20-22].

$$CO + H_2O \rightleftharpoons CO_2 + 2e^- + 2H^+$$

Crystal structures are known for homodimeric CODHs from *Carboxythermus hydrogenoformans* [23] and *R. rubrum* [24]. Both structures reveal the presence of a [4Fe-4S] center (site D) bridging the subunits and likely serving as the site of electron transfer to an external electron carrier protein. Two [4Fe-4S] centers (sites B and B′) are positioned appropriately to function as conduits for electrons to site D from Ni-Fe-S centers located in the opposite subunit (sites C′ and C).

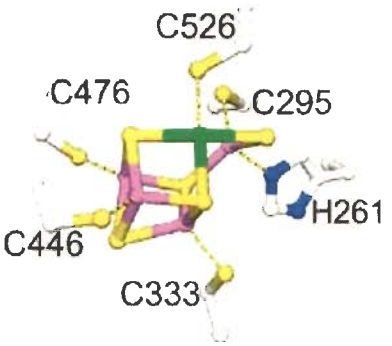

Fig. 4-4 Active site structure of carbon monoxide dehydrogenases (CODHs) (Color code: C, light grey; N, blue; Ni, green; Fe, pink; S, yellow)

The precise structure of the C site differs in the two proteins (or may vary depending on how the proteins are isolated), but appears to be comprised of a [1Ni-3Fe-4S] center fused with a mononuclear Fe site. An additional bridging sulfide is found in the 1.6 Å structure of the *C. hydrogenoformans* enzyme, whereas the 2.8 Å structure of the *R. rubrum* enzyme shows no bridging sulfide, but has an additional bonding interaction between the Ni-coordinated cysteine and the unique Fe along with a possible CO molecule bound to the Ni.

Acetyl-coenzyme A decarbonylase / synthase (ACDS)

In addition to the independent CODH enzymes described above, CODH activity also occurs as one of two distinct Ni-dependent activities associated with ACDS that

are found in selected methanogenic, sulfate reducing, and acetogenic microorganisms [20-22]. ACDS functions to decompose the acetyl group into separate one-carbon units in some cells [25, 26 and references therein] or to catalyze acetate synthesis from one-carbon precursors in others [20, 27, 28], but all of these enzymes are capable of the reversible reactions.

$$\mathbf{CH_3C(O)\text{-}S\text{-}CoA + Co(I)\text{-}FeSP \rightleftharpoons CH_3\text{-}Co(III)\text{-}FeSP + CO + CoA}$$

In acetate-degrading organisms, such as *Methanosarcina barkeri* or *Methanosarcina thermophila*, the reaction proceeds to the right at one Ni-containing active site with acetyl-CoA being split into CoA, a methyl group that becomes bound to a corrinoid-iron-sulfur protein (abbreviated Co(I)- FeSP), and CO. The CO molecule then is oxidized to CO_2 at a second Ni-containing active site. The corrinoid-bound methyl group is sequentially transferred to a reduced pterin analogue (tetrahydrosarcinapterin or tetrahydromethanopterin) and coenzyme M, eventually forming methane after being reduced using the electrons available from equation. Biochemical evidence suggests a molecular tunnel connects the CODH active site and the acetyl-CoA-binding site (i.e., the C- and A-clusters, respectively, present in distinct subunits of the *M. thermoacetica* enzyme) and allows for direct transfer of CO [29, 30].

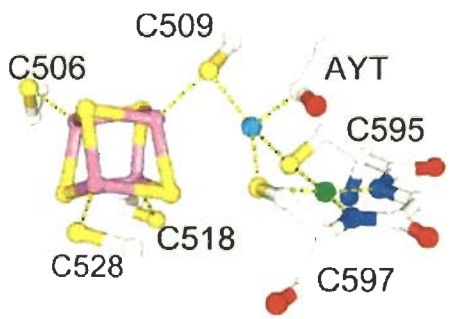

Fig. 4-5 Active site structure of Acetyl-coenzyme A decarbonylase / synthase (ACDS) (Color code: C, light grey; N, blue; O, red; Ni, green; Fe, pink; S,yellow; Cu, cyan)

According to X-ray crystallography, A-cluster possesses a typical [4Fe-4S] cluster bridged to Ni; however, the ligands to Ni and the identity of the bridge were unanticipated. Ni is bound in a Cys-Gly-Cys motif, with two thiolate ligands and two peptide backbone amide interactions making up the four-coordinate planar geometry. According to published structure [31, 32], a four-coordinate copper atom connects the Ni to the [4Fe-4S] cluster. This Cu(I) shares one thiol ligand with a cubane iron atom and shares both thiols that bind the Ni. An unidentified fourth ligand (labeled AYT in the figure) may be an acetyl group or CO occupying two different geometries.

Superoxide dismutases (SODs) are metalloenzymes involved in the protection of cells from oxidative damage arising from superoxide radical, or reactive oxygen species produced from superoxide.

$$2O_2^{\cdot -} + 2H^+ \xrightarrow{SOD} O_2 + H_2O_2$$

Superoxide radicals generated by a single-electron transfer to dioxygen, produced in large amounts in respiration and photosynthesis, during an immune response by phagocytosis, etc. [33, 34]. SODs play an important protective role in aerobes which encounter toxic $O_2^{\cdot -}$ radicals during their metabolism. The presence of SOD in the intracellular environment reduces oxidative stress and plays a key role in moderating the aging process. SOD is therefore used as an antioxidative therapeutic agent. Other medical applications involve treatment of arthritis and prevention of side effects of cancer treatment and injury to transplanted organs during surgery. To date, three independent SOD classes are known, based on their cofactor metal ion: Cu- and Zn-dependent SODs (CuZnSODs), SODs that use Fe or Mn, or either of the two (FeSODs, MnSODs, or Fe / MnSODs), and Ni-dependent enzymes (NiSODs). While CuZnSODs are the most abundant superoxide scavengers in nature, found in all

eucaryotes and many procaryotes, [35] the recently discovered NiSOD class is confined to *Steptomyces* soil bacteria [36-38] and cyanobacteria [39].

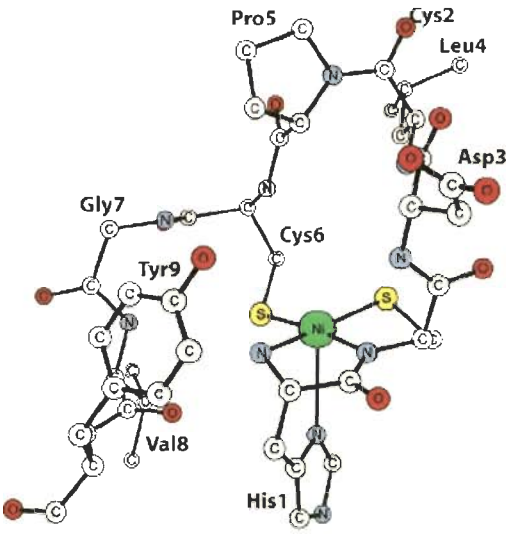

Fig. 4-6 Active site structure of Ni-SOD from *Streptomyces seoulensis*

The amino acid sequence of the NiSOD deduced from the nucleotide sequence of the structure gene sodN from *Streptomyces seoulensis* has been reported, which has no homology with other SODs [39]. X-ray crystallographic structure determinations [40-42] reveal a homohexameric NiSOD, possessing a three-fold symmetry axis. Composed of a four helix bundle in the all-antiparallel topology, the monomer subunit is a quite small 117 amino acid protein. The residues of the N-terminal loop form the metal-coordinating "Ni-hook" which is disordered in the absence of a bound metal ion [43]. Conserved between the known NiSODs, the Ni-hook His1-Cys2-X-X-Pro5-Cys6-Gly7-X-Tyr9 motif was proposed as a diagnostic 15 of this enzyme class. The amine of N-terminal His1, the deprotonated backbone amide of Cys2, and the thiolates of Cys2 and Cys6 form a square planar framework of the Ni coordination sphere. This N_2S_2 ligand field with the metal incorporation into the backbone nitrogens and thiolate

sulfurs is reminiscent of nickel coordination. The proposed two step redox mechanism of NiSOD for superoxide inhibition is given below [44]:

$$\text{Ni(III)-N}_{\text{His1}} + 2O_2^{\cdot-} + 2H^+ \longrightarrow \text{Ni(II)} + \text{H-N}_{\text{His1}}^+ + O_2$$

$$\text{Ni(II)} + \text{Ni(III)-N}_{\text{His1}} + 2O_2^{\cdot-} + H^+ \longrightarrow \text{Ni(III)-N}_{\text{His1}} + H_2O_2$$

Like SOD, **Glyoxylase (Glx)** is another enzyme involved in cellular protection; however, in this case the toxic species is methylglyoxal rather than a reactive oxygen species. Several enzymatic processes produce methylglyoxal including a minor side reaction of triosephosphate isomerase when using its normal substrates dihydroxyacetone phosphate and glyceraldehyde. Because these glycolysis intermediates and triosephosphate isomerase are so abundant in cells, significant amounts of methylglyoxal are generated and react to form covalent adducts of DNA and proteins. One mechanism to remove this reactive compound involves the two-component glyoxylase system, illustrated in scheme 4-2. Glutathione (G-SH) reacts with methylglyoxal in a non-enzymatic reaction to form the hemithioacetal substrate of glyoxylase I (Glx I). This enzyme carries out an isomerization reaction resulting in formation of S-D-lactoylglutathione. The product of Glx I is the substrate for glyoxylase II (Glx II) that hydrolyzes it to form lactate (Scheme 4-2).

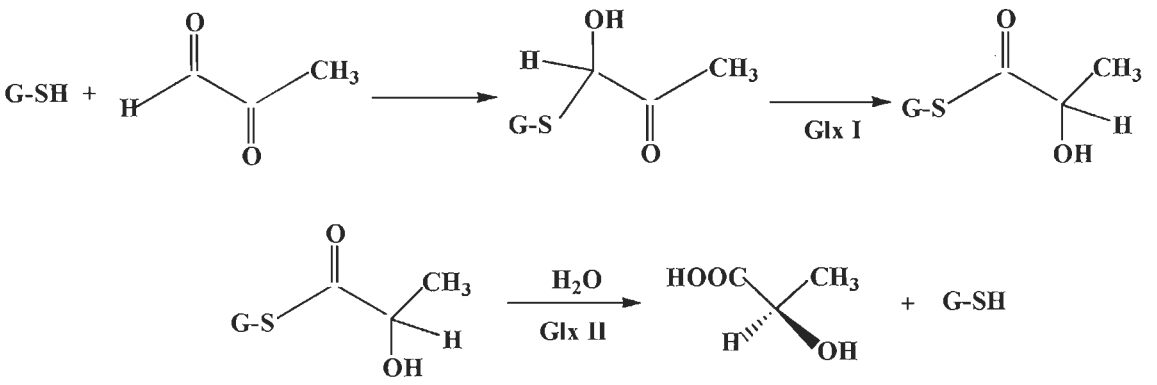

Scheme 4-2

Glx I from yeast and humans is well characterized and known to be a Zn-dependent enzyme. Surprisingly, the *E. coli* enzyme has a preference for Ni despite a high degree of sequence identity to the other enzymes [45]. The crystal structures of the active Ni enzyme and active Co- and Cd-substituted *E. coli* proteins each show octahedral metal coordination, analogous to the situation for Zn in the human enzyme, whereas the inactive Zn-containing *E. coli* protein has a five-coordinate metal site [46]. X-ray absorption studies of enzyme-product and enzyme-inhibitor complexes [47] provide evidence consistent with an enzyme mechanism involving proton transfers between substrate and metal coordinated solvent molecules, rather than direct coordination of substrate to the metal. On the basis of detailed sequence comparison of metal-binding residues, several pathogenic microorganisms including *Y. pestis* also are likely to possess Ni-dependent Glx I species [48].

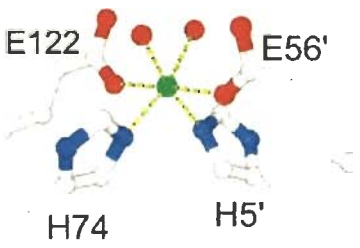

Fig. 4-7 Active site of *E. coli* glyoxylase with two bound water molecules. (Color code: C, light grey; N, blue; O, red; Ni, green)

Acireductone dioxygenases (ARDs) are enzymes found associated with the methionine salvage pathway (MSP) in species ranging from bacteria to mammals. Two ARD enzymes having the same amino acid sequence (polypeptide chain) but which differ in the active site metal present (Fe(II) or Ni(II)) have been identified in *Klebsiella*

ATCC 8724 [49]. Interestingly these enzymes catalyze the oxidation of 1, 2- dihydroxy-3-keto-5-(methylthio) pentene to give different products (Scheme 4-3).

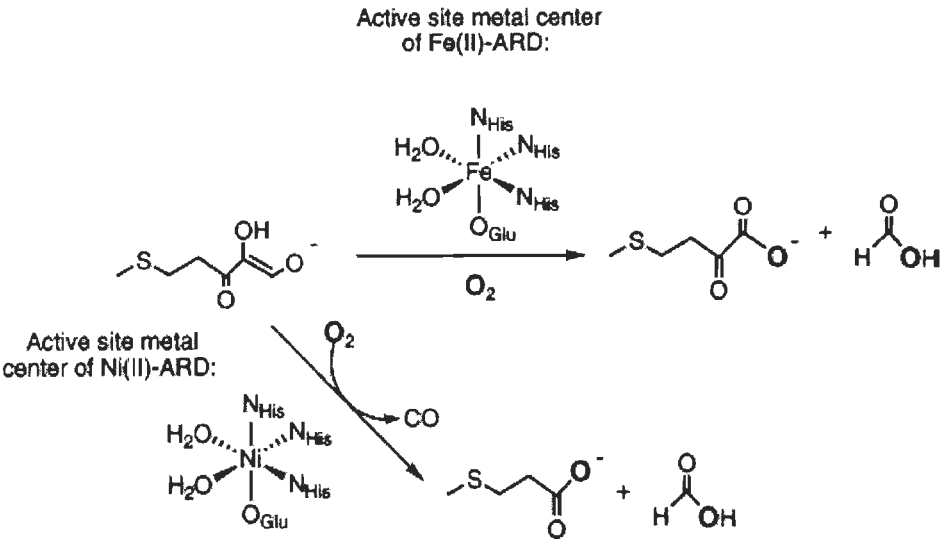

Scheme 4-3

The X-ray crystal structure of Ni(II)-ARD from *Klebsiella ATCC 8724* has been recently reported [50] and the ligand environment of the nickel center has also been confirmed previously by X-ray absorption spectroscopy (XAS) [51] as well as by NMR and conserved domain homology modeling methods [52, 53]. It was also found that Ni^{2+}-bound Ni-ARD catalyzes an off-pathway shunt from the methionine salvage pathway leading to the production of formate, methylthiopropionate and carbon monoxide, while the Fe^{2+}-bound Fe-ARD catalyzes the on-pathway formation of methionine precursor 2-keto-4-methylthiobutyrate and formate. Furthermore, both Ni- and Fe-containing forms of the enzyme, bind their respective metals with pseudo-octahedral geometry and both may lose a histidine ligand upon binding of substrate under anaerobic conditions.

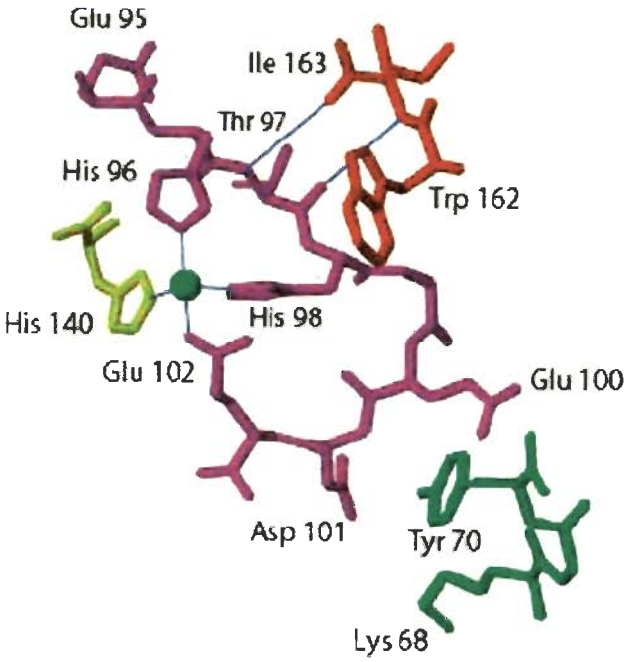

Fig. 4-8 Active site of the Ni-ARD from *Klebsiella ATCC 8724*

Methylenediurease is a Ni-dependent enzyme. Methyleneureas, or ureaforms, are condensation products of urea plus formaldehyde [general formula H_2N-(CO-NH-CH_2-NH)$_n$-CO-NH_2] and are used as slow-release fertilizers [54]. An enzyme capable of degrading methylenediurea (i.e., n = 1 in the above formula) was isolated from a *Burkholderia* species and shown to possess stoichiometric amounts of bound Ni. Methylenediurease contains two subunits, the largest of which (according to DNA accession number AY194235) is clearly related to urease and includes residues corresponding to all of the ligands of the urease dinuclear Ni active site. Further studies are required to characterize the structural basis for the unique specificity and to define the mechanism of this enzyme.

Also a large number of enzymes are dependent on a divalent lewis acid ion such as Ca, Mg, Fe or Zn. These metal ions are often readily removed by a chelating agent such as EDTA or bpy and many of the resultant apoenzymes have been reconstituted

with non-native cations. The fact that the Ni enzymes thus obtained often retain complete or partial activity demonstrates that Ni^{2+} can indeed carry out the roles proposed for it in urease, namely polarization of a C=O bond and activation of a coordinated water molecule towards deprotonation. The best characterized of these synthetic Ni proteins is Ni-carboxypeptidase A (Ni-CPA), whose native enzyme catalyzes the hydrolysis of peptide amide bonds and contain the five coordinated center within the active site, the carboxylate ligand being asymmetrically bound [55].

Ni-CPA shows *ca.* 50% of the activity of the native enzyme toward amide hydrolysis. A single crystal X-ray structure determination of Ni-CPA showed that Ni complex exhibits a more regular square pyramidal geometry compared with the native Zn site. Carboxylate inhibitors binds directly to the Ni^{2+} ion in Ni-CPA, the precise role played by metal ions in hydrolysis of amide by CPA is still unclear [56, 57]. In contrast to the above results, Ni substituted carbonic anhydrase shows greatly reduced activity for CO_2 hydration.

A common structural feature found in most of above proteins is the presence of one or more carboxylate groups in the active site. The coordination chemistry of metal carboxylato species is also an attractive subject from the bioinorganic standpoint as the carboxylate group of glutamate, lysinate and aspartate works as supporting ligand for the metal center in various metalloproteins and behave as monodentate or bidentate depending on the requirement of the active site [58]. It was also well known that the carboxylate anion involves in hydrogen bonding which plays an important role in biological systems and is a gateway to molecular organization [59] and also for crystal engineering [60]. The structurally characterized nickel-carboxylate complexes are limited in literature, some are described below.

Santana et al. [61] reported five-coordinate nickel (II) carboxylate complexes of the type $[Ni(mcN_3)(A)](PF_6)$ [mcN_3 = 2,4,4-trimethyl-1,5,9-triazacyclododec-1-ene(Me_3-mcN_3) or 2,4,4,9-tetramethyl-1,5,9-triazacyclododec-1-ene (Me_4-mcN_3)] by reacting the hydroxo complexes $[Ni_2(mcN_3)_2(\mu\text{-}OH)_2]_2(PF_6)_2$ with the corresponding carboxylic acid [HA = benzoic (Hbz), salicylic (Hsal) or acetylsalicylic (Hacsal) acid]. They also succeeded in determining the crystal structures of $[Ni(Me_4\text{-}mcN_3)(bz)](PF_6)$ (Fig. 4-9), $[Ni(Me_4\text{-}mcN_3)(sal)](PF_6)$ and $[Ni(Me_4\text{-}mcN_3)(acsal)](PF_6)$.

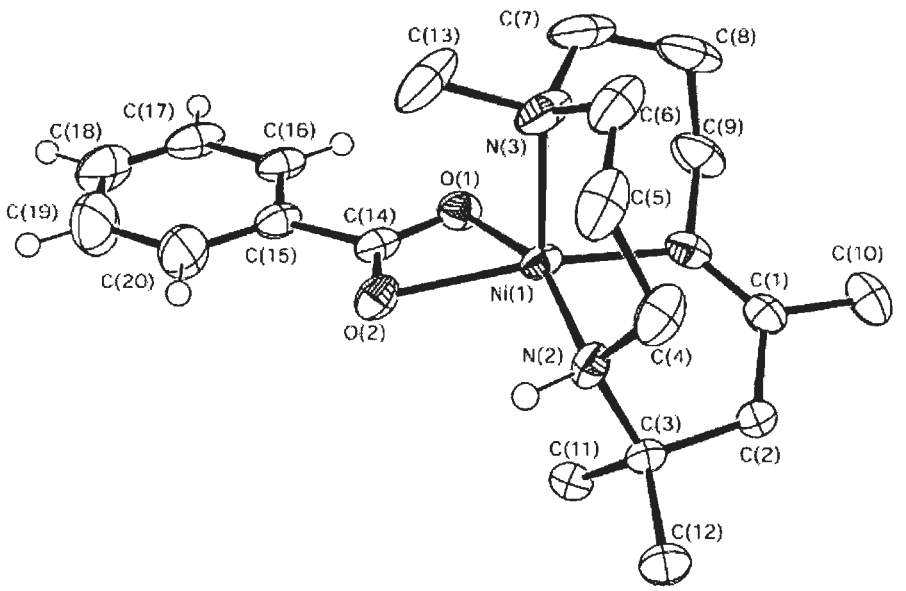

Fig. 4-9 Crystal structure of $[Ni(Me_4\text{-}mcN_3)(bz)](PF_6)$

Further, they synthesized substituted-benzoate complexes of nickel (II) of the types bidentate $[Ni(mcN_3)(bz)](PF_6)$ and monodentate $[Ni(mcN_3)(bz)(H_2O)](PF_6)$ by acid-base reaction between the hydroxo complexes $[Ni(mcN_3)(\mu\text{-}OH)]_2(PF_6)_2$ (mcN_3 = 2,4,4-trimethyl-1,5,9-triazacyclododec-1-ene (Me_3-mcN_3) or its 9-methyl derivative (Me_4-mcN_3)) and the corresponding benzoic acid [62]. These paramagnetic nickel (II) complexes were characterized in solution by NMR spectroscopy and showed the influence of the substituents on the hyperfine shift patterns for substituted-benzoate complexes.

Li et al. [63] prepared two new metal complexes, $[Co(Mamba)_2]$ and $[Ni(Mamba)_2]$, by the treatment of the tridentate ligand N-(2-methylpyridine)-2-aminomethyl benzoic acid (HMamba) with the respective metal salts $Co(ClO_4)_2$ and $Ni(C_2H_3O_2)_2$ in the presence of sodium hydroxide. The structure of the complexes were octahedral with each metal center chelated to two ligands through the amine nitrogen atom, the pyridine nitrogen atom and benzoic acid oxygen atom of each $Mamba^-$ (Fig. 4-10).

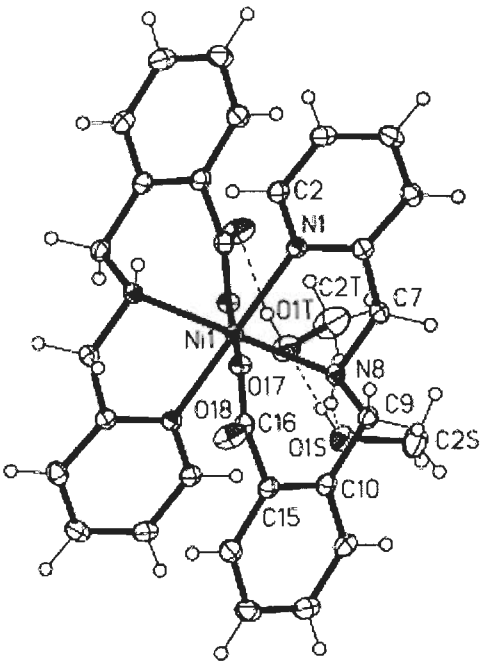

Fig. 4-10 Crystal structure of $[Ni(Mamba)_2]$

Hammes et al. [64] reported six new Ni(II) complexes of the "heteroscorpionate" ligand (3-tert-butyl-2-hydroxy-5-methylphenyl)bis(3,5-dimethylpyrazolyl)methane, L1OH. These complexes include: tetracoordinate [Ni(L1O)Cl]; pentacoordinate [Ni(L1O)(acac)] and [Ni(L1O)(OAc)] (Fig. 4-11) and hexacoordinate [Ni(L1O)(acac)(Pz)], [Ni(L1O)(OAc)(MeOH)] and $[Ni(L1O)_2]$. These second generation of heteroscorpionate ligand supports a tetrahedral environment for Ni(II) but is not a

tetrahedral enforcer. Thus the tetra- and pentacoordinate species readily added additional ligands to produce 5- and 6-coordinate complexes.

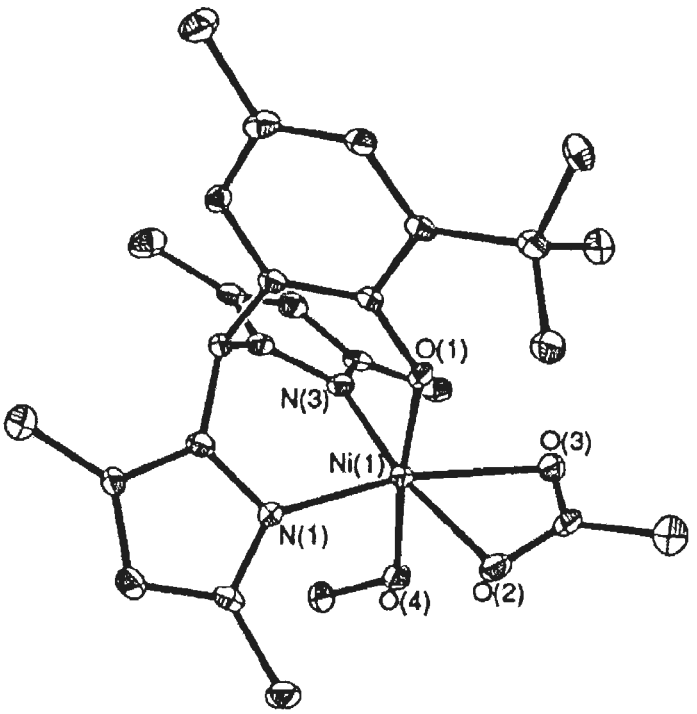

Fig. 4-11 Crystal structure of [Ni(L1O)(OAc)(MeOH)]

Eremenko et al. [65] carried out reaction of pyridine with nine-nuclear cluster $Ni_9(HOOCCMe_3)_4(\mu_4\text{-}OH)_3(\mu_3\text{-}OH)_3(OOCCMe_3)_{12}$ resulting in the binuclear species $Py_4Ni_2(OOCCMe_3)_2(\mu\text{-}OOCCMe_3)_2(\mu\text{-}OH_2)$. Thermolysis of $Py_4Ni_2(OOCCMe_3)_2(\mu\text{-}OOCCMe_3)_2(\mu\text{-}OH_2)$ at 100-140 °C in toluene or xylene leads to the complex $Py_2Ni_2(HOOCCMe_3)_2(OOCCMe_3)_2(\mu\text{-}OOCCMe_3)_2(\mu\text{-}OH_2)$. By reacting $Ni_9(HOOCCMe_3)_4(\mu_4\text{-}OH)_3(\mu_3\text{-}OH)_3(OOCCMe_3)_{12}$ with Dipy, complex $Dipy_2Ni_2(OOCCMe_3)_2(\mu\text{-}OOCCMe_3)_2(\mu\text{-}OH_2)$ was prepared. Thermolysis of solid $Dipy_2Ni_2(OOCCMe_3)_2(\mu\text{-}OOCCMe_3)_2(\mu\text{-}OH_2)$ at 170 °C in vacuo gave mononuclear complex $DipyNi(OOCCMe_3)_2$ [Fig. 4-12]. Hetero-ligand complex $DipyNi(NH_2Ph)(OOCCMe_3)_2$ was also obtained upon the reaction of $PhNH_2$ with complex $Dipy_2Ni_2(OOCCMe_3)_2(\mu\text{-}OOCCMe_3)_2(\mu\text{-}OH_2)$ at 20 °C in benzene or

MeCN and reaction of $Ni_9(HOOCCMe_3)_4(\mu_4\text{-}OH)_3(\mu_3\text{-}OH)_3(OOCCMe_3)_{12}$ with α, α', α''-tripyridyl leads to the formation of the monomeric $TerpyNi(OOCCMe_3)_2$. These complexes were characterized with X-ray data and magnetic properties.

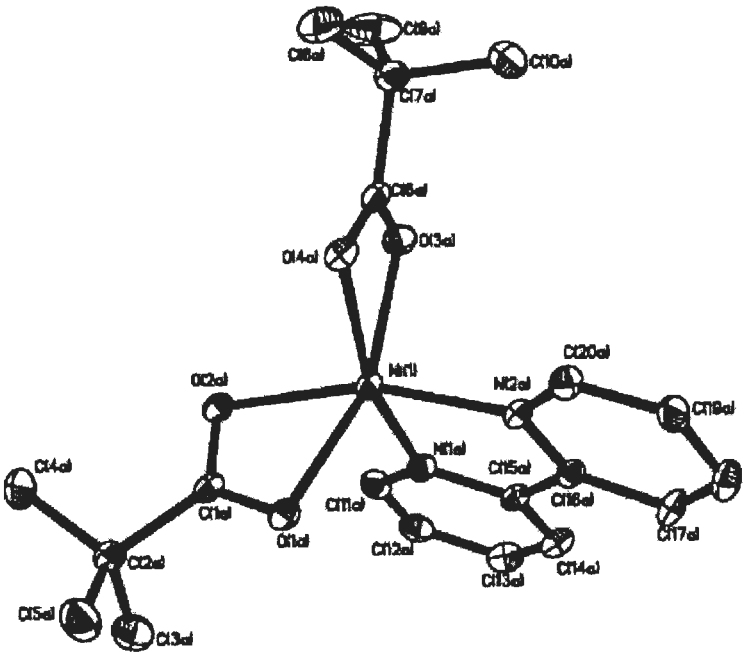

Fig. 4-12 Crystal structure of $DipyNi(OOCCMe_3)_2$

Szajna-Fuller et al. [66] synthesized a series of Ni(II) carboxylate complexes, supported by a chelate ligand having either secondary hydrophobic phenyl groups (6-Ph_2TPA, N,N-bis((6-phenyl-2-pyridyl)methyl)-N-((2-pyridyl)methyl)amine) or hydrogen bond donors (bnpapa, N,N-bis((6-neopentylamino-2-pyridyl)methyl)-N-((2-pyridyl)methyl)amine). X-ray crystallographic studies of [(6-Ph_2TPA)$Ni(O_2C(CH_2)_2SCH_3)]ClO_4$ and [(6-Ph_2TPA)$Ni(O_2$- $CCH_2SCH_3)]ClO_4$ proved that each complex contains a distorted octahedral Ni(II) center and a bidentate carboxylate ligand. Recrystallization of dry powdered samples of above complexes from wet organic solvents yielded a second series of crystalline Ni(II) carboxylate complexes having a coordinated monodentate carboxylate ligand [(6-

$Ph_2TPA)Ni(H_2O)(O_2CPh)]ClO_4$, $[(6\text{-}Ph_2TPA)Ni(H_2O)(O_2C(CH_2)2SCH_3)]ClO_4$, $[(6\text{-}Ph_2TPA)Ni(H_2O)(O_2CCH_2SCH_3)]ClO_4$ which were stabilized by a hydrogen-bonding interaction with a Ni(II)-bound water molecule. The mononuclear Ni(II) carboxylate complexes $[(bnpapa)Ni(O_2CPh)]ClO_4$ (Fig. 4-13), $[(bnpapa)Ni(O_2C(CH_2)2SCH_3)]ClO_4$, $[(bnpapa)Ni(O_2CCH_2SCH_3)]ClO_4$ and $[(bnpapa)Ni(O_2CH)]ClO_4$ were also isolated and characterized. From combined results, they also proposed a pathway for carboxylate product release from the active site Ni(II) center in acireductone dioxygenase.

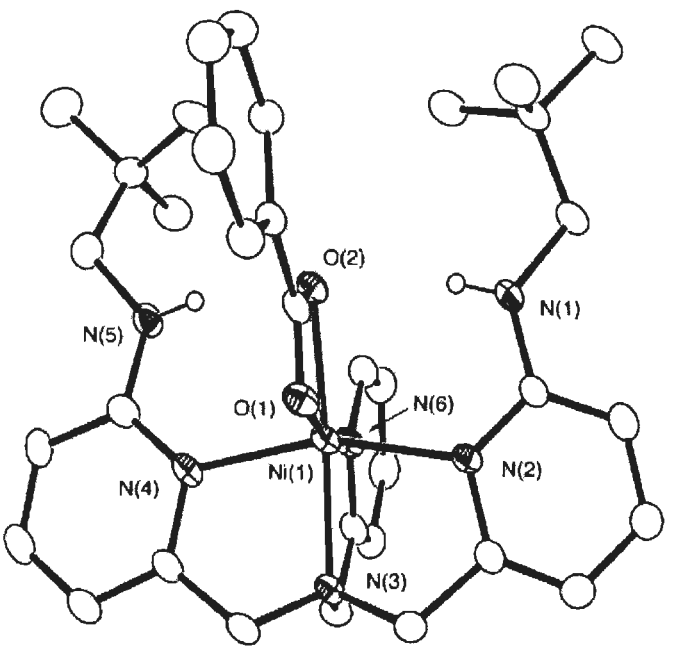

Fig. 4-13 Crystal structure of $[(bnpapa)Ni(O_2CPh)]ClO_4$

Further, this group reported a series of cis-β-keto-enolate Ni(II) complexes supported by the 6-Ph_2TPA ligand ($[(6\text{-}Ph_2TPA)Ni(PhC(O)CHC(O)Ph)]ClO_4$, $[(6\text{-}Ph_2TPA)Ni(CH_3C\text{-}(O)CHC(O)CH_3)]ClO_4$ and $[(6\text{-}Ph_2TPA)Ni(PhC(O)CHC(O)C(O)Ph)$ (Fig. 4-14) and characterized by different spectroscopic techniques including single crystal X-ray diffraction [67]. All of these complexes were unreactive toward O_2. They also discussed these complexes in terms of relevance to Ni(II)-containing acireductone

dioxygenase enzymes, as well as in the context of recently reported cofactor-free, quercetin and β-diketone dioxygenases.

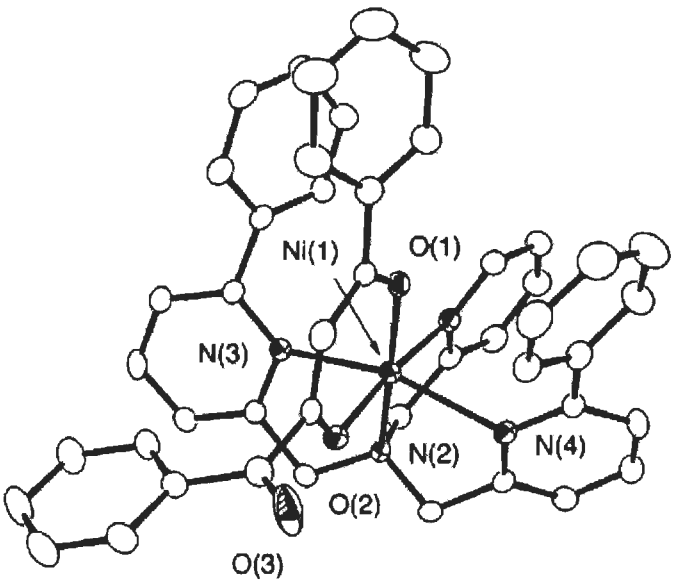

Fig. 4-14 Crystal structure of [(6-Ph_2TPA)Ni(PhC(O)CHC(O)C(O)Ph)]

Carlsson et al. [68] synthesized two new carboxylate-containing polydentate ligands, 2,6-bis[N-(N-(carboxylmethyl)-N-((1 methylimidazol)methyl) amine)methyl]-4-methylphenolate (BCIMP) and 2-(N-isopropyl-N-((1-aminomethyl)-4-methylphenol (ICIMP). They used these ligands to prepare model complexes for the active site of the dinuclear nickel enzyme urease, viz. $[Ni_2(BCIMP)Ac_2]^-$ (Fig. 4-15), $[Ni_2(BCIMP)\text{-}(Ph_2Ac)_2]^-$, $[Ni_2(ICIMP)(Ph_2Ac)_2]$, $[Ni_4(ICIMP)_2(Ph_2Ac)_2][ClO_4]_2$, $[Ni_4(ICIMP)_2(Ph_2Ac)_2(DMF)_2][ClO_4]_2$ and $[Ni_4(ICIMP)_2(Ph_2Ac)_2(urea)(H_2O)][ClO_4]_2$, where the latter complex contains urea coordinated in a unidentate fashion through the carbonyl oxygen. The $N_2O\text{-}N_2O_2$ donor set of ICIMP provided a good framework for the preparation of urease models, but in some cases tetranuclear nickel complexes were formed due to coordination of the carboxylate moiety of one dinickel-ICIMP unit to one or both of the nickel of a second Ni_2 unit. Reactivity and kinetics studies of

$[Ni_2(BCIMP)\text{-}(Ph_2Ac)_2]^-$ and $[Ni_4(ICIMP)_2(Ph_2Ac)_2][ClO_4]_2$ showed that these model complexes catalyzed the hydrolysis of 2-hydroxypropyl p-nitrophenyl phosphate (HPNP) at basic pH.

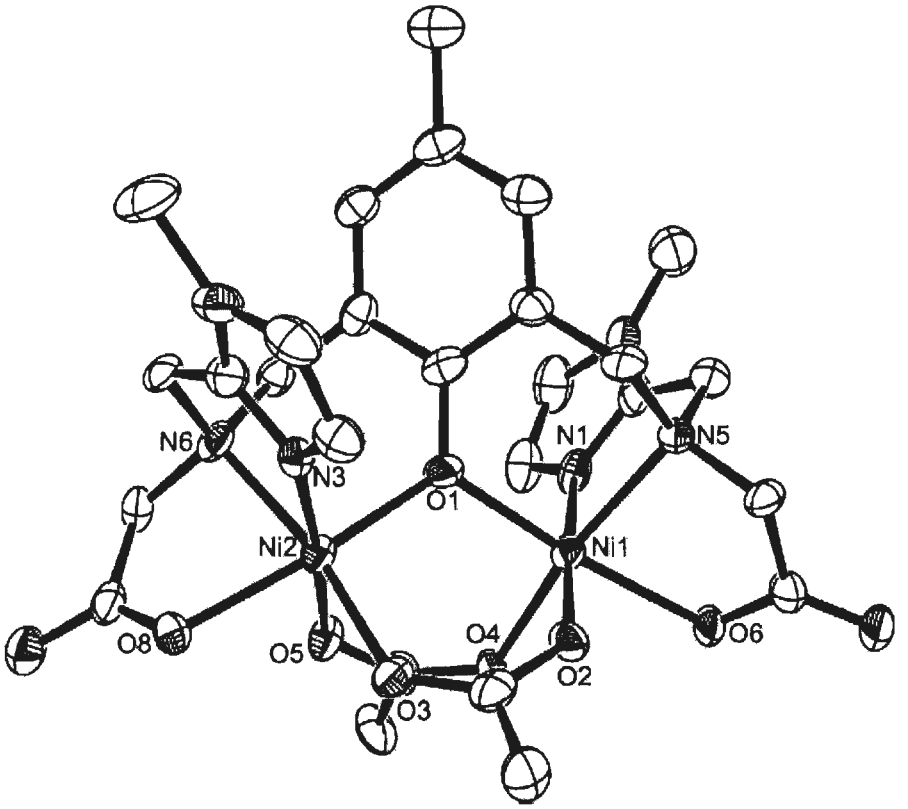

Fig. 4-15 Crystal structure of $[Ni_2(BCIMP)Ac_2]^-$

Yamaguchi et al. [69] demonstrated that the RCO_2^--bridged dinickel complexes $[Ni_2(Me_4\text{-tpdp})(CH_3CO_2)(ClO_4)(CH_3\text{-}OH)]^+$ and $[Ni_2(Me_4\text{-tpdp})(CH_3CO_2)(urea)]^{2+}$ (Fig. 1-16) where Me_4-Htpdp = N,N,N',N'-tetrakis{(6-methyl-2-pyridyl)methyl}-1,3-diaminopropan-2-ol) catalyzed the ethanolysis of urea. The X-ray crystal structure of the μ-acetato Ni(II) complexes revealed that one of the two Ni ions is capable of binding urea and the another one activated ethanol by coordination. The structures and catalytic reactions of the dinickel model complexes showed a striking resemblance to those of the dinickel site in urease.

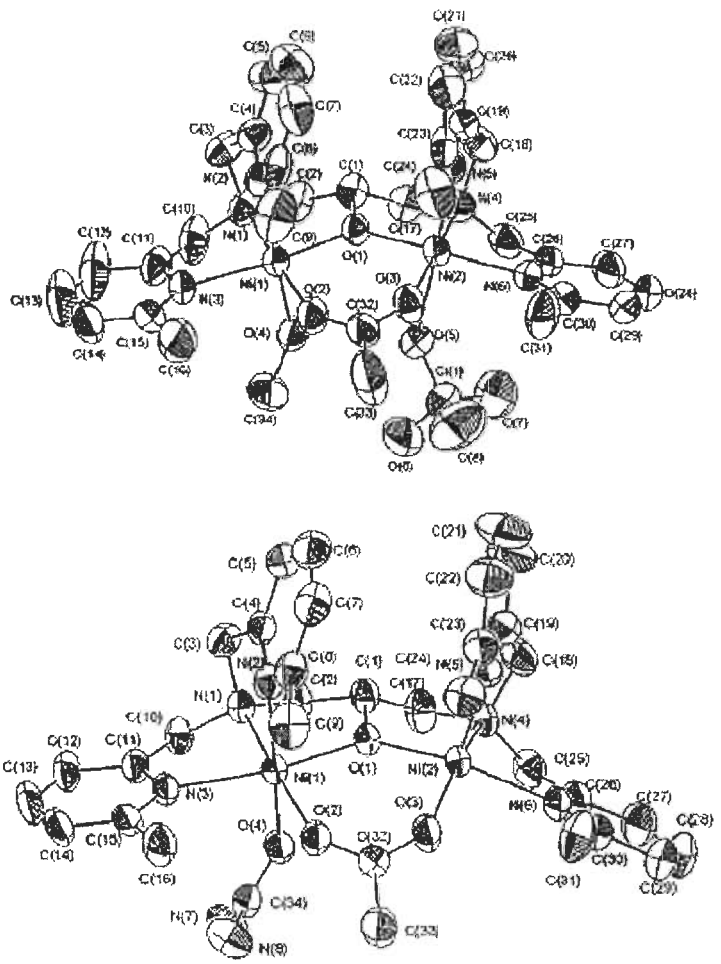

Fig. 4-16 Crystal structures of $[Ni_2(Me_4\text{-tpdp})(CH_3CO_2)(ClO_4)(CH_3\text{-}OH)]^+$ and $[Ni_2(Me_4\text{-tpdp})(CH_3CO_2)(urea)]^{2+}$

Rochon et al. [70] carried out the reactions of several divalent transition metals with 1,2,4,5 benzenetetra-carboxylate ions in aqueous solution. Mn(II), Co(II) and Ni(II) produced ionic products of formula $[M(H_2O)_6][C_6H_2(COO)_2(COOH)_2]$ that were characterized by crystallographic methods. The metal atom and two O atoms (from two aqua ligands) are located on a two-fold axis, while the other four aqua ligands are located in general positions. The anions contain an inversion center. The two hydrogens on the carboxylic functions formed intramolecular H bonds with the carboxylate groups. With the Ni salt, a dinuclear species, containing a bridging benzenetetracarboxylato ligand was synthesized and characterized by X-ray diffraction.

The compound $Ni(H_2O)_5(m\text{-}C_6H_2(COO)_4)Ni(H_2O)_5 \cdot 6H_2O$ (Fig. 4-17) contains an inversion center in the center of the phenyl ring. The crystal was stabilized by a very elaborate H-bonding system forming a H-bonded three-dimensional network.

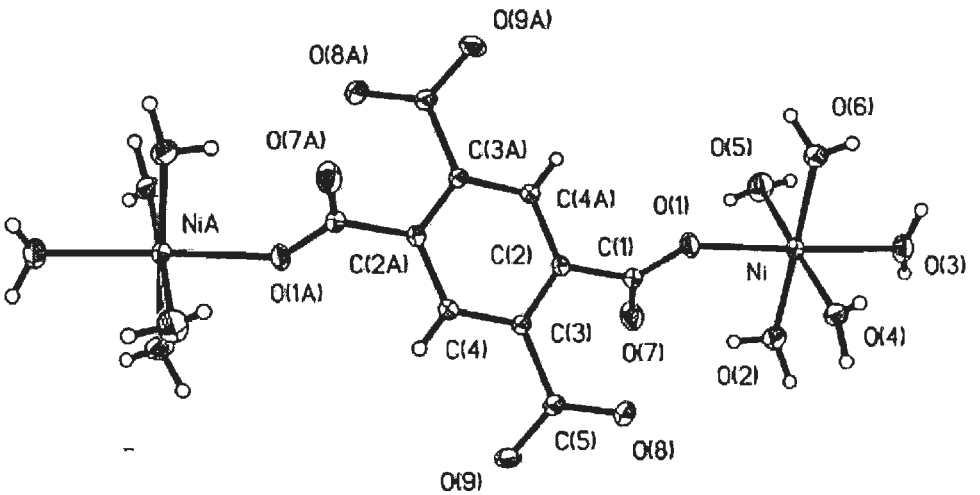

Fig. 4-17 Crystal structure of $Ni(H_2O)_5(m\text{-}C_6H_2(COO)_4)Ni(H_2O)_5$

Ivanikova et al. [71] reported nickel (II) complexes with the general formula $[Ni(L^1)_2(L^2)_2(H_2O)_2]$, where L^1 = 2-methylimidazole (Meiz), 1,2-dimethylimidazole (Me_2iz), iso-quinoline (iqu) and 4-furopyridine (fupy), L^2 = formate and acetate. The structures of four complexes $[Ni(Meiz)_2(HCOO)_2(H_2O)_2]$, $[Ni(Me_2iz)_2(HCOO)_2(H_2O)_2]$, $[Ni(iqu)_2(CH_3COO)_2(H_2O)_2]$ and $[Ni(fupy)_2(CH_3COO)_2(H_2O)_2]$ were determined by X-ray diffraction methods (Fig. 4-18). The chromophore of these compounds, $[NiO_2O_2'N_2]$ was formed by four oxygen atoms and two nitrogen atoms. In complex $[Ni(Meiz)_2(HCOO)_2(H_2O)_2]$, the formation of a three-dimensional network was supplemented by N–H···O, hydrogen bonds from the coordinated oxygen atom to the secondary nitrogen atom of an imidazole molecule from another unit. Rest of these structures were formed two-dimensional networks which consist of individual molecules linked together by O–H···O hydrogen bonds from carboxylate groups to aqua ligands. All complexes show magnetic behavior typical for zero-field splitting systems.

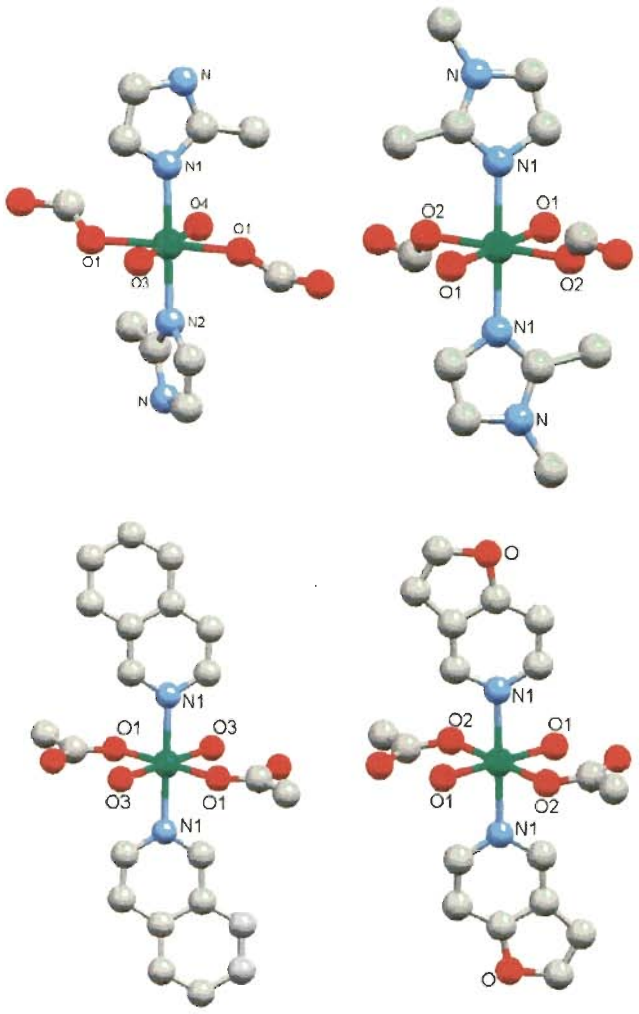

Fig. 4-18 Crystal structure of $[Ni(Meiz)_2(HCOO)_2(H_2O)_2]$, $[Ni(Me_2iz)_2(HCOO)_2(H_2O)_2]$, $[Ni(iqu)_2(CH_3COO)_2(H_2O)_2]$ and $[Ni(fupy)_2(CH_3COO)_2(H_2O)_2]$

Hong et al. [72] synthesized and characterized two binuclear compounds $[Ni_2(pmdtn)_2(tp)(H_2O)_2](ClO_4)_2(H_2O)_4$ and $[Ni_2(pmdtn)_2(tp)(N_3)](H_2O)_4$ (Fig. 4-19) by using the multibinding terephthalate (= tp) dianion and the tridentate capping ligand N,N,N',N',N''-pentamethyldiethyltriamine (= pmdtn). The crystal structures of both complexes showed distorted octahedral geometries around the Ni(II) centers linked by the tp bridges in a bisbidentate fashion. The intradimer distance of Ni···Ni through the tp ligand for both complexes were 10.731 and 10.800 Å, respectively. The magnetic data revealed weak antiferromagnetic interactions transmitted by the tp bridge with $J = -0.18\ cm^{-1}$ and $0.02\ cm^{-1}$, which was explained by the structural parameters.

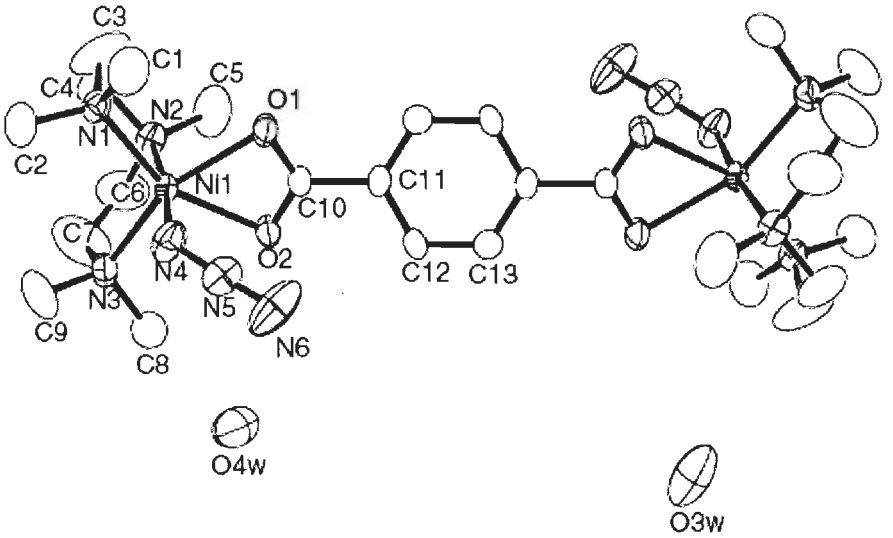

Fig. 4-19 Crystal structure of $[Ni_2(pmdtn)_2(tp)(N_3)](H_2O)_4$

Fan et al. [73] reported one-dimensional (1D) coordination polymer, $[Ni^{II}(imbz)_2(H_2O)_2]_n$ (Fig. 4-20) (imbz = 4'-(imidazol-1-ylmethyl)benzoate anion) by treatment of $Ni(CH_3COO)_2.4H_2O$ with piperidinium salt of 4'-(imidazol-1-ylmethyl)benzoic acid and characterized it by X-ray crystallography. The thermogravimetric analysis (TGA) and magnetic property of compound $[Ni^{II}(imbz)_2(H_2O)_2]_n$ were also reported.

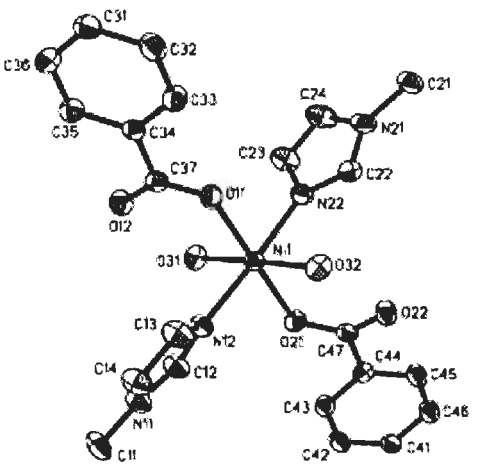

Fig. 4-20 Crystal structure of $[Ni^{II}(imbz)_2(H_2O)_2]_n$

Baruah et al. [74] reported a ring opening reaction of pyromellitic dianhydride by methanol to prepare first row transition metal dicarboxylate complexes. The reactions of different first row transition metal salts with pyromellitic dianhydride in the presence of nitrogen donating bidentate ligands such as 1,10-phenanthroline and 2,2′-bipyridine gave different compositions depending on the ligand and the metal salts used. They also suggested that the reaction of nickel (II) acetate with pyromellitic dianhydride in the presence of 1,10-phenanthroline resulted in the formation of a carboxylato bridged nickel (II) metallacycle through the ring opening reaction of pyromellitic dianhydride (PAH) at the 1 and 3-positions, whereas a mononuclear tetra-aqua 2,2′-bipyridine nickel (II) complex is formed in a similar reaction of nickel (II) acetate through ring opening at the 1,4-position of PAH.

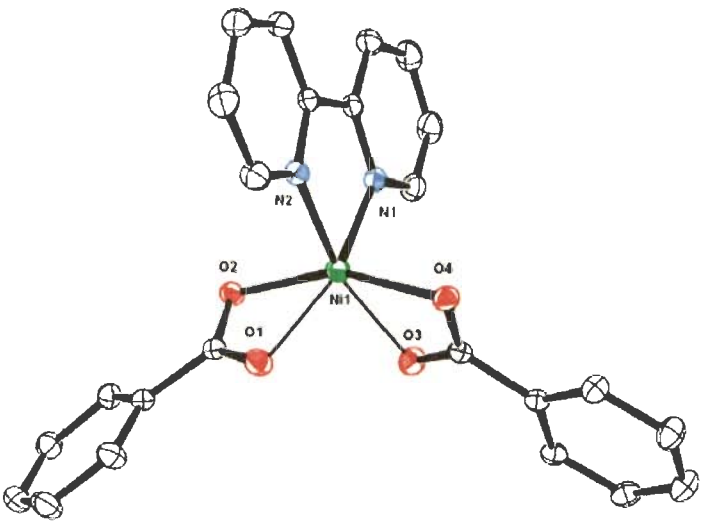

Fig. 4-21 Crystal structure of (2,2′-bipyridyl)dibenzoato nickel(II)

Mononuclear cobalt (II) dicarboxylate complexes were formed from the ring opening reaction of pyromellitic dianhydride in methanol in the presence of the nitrogen donor ligands 1,10-phenanthroline or 2,2′- bipyridine. Copper (II) chloride on

reaction with PAH and 2,2′-bipyridine gave a mononuclear complex via ring opening at the 1 and 4- positions; having chlorides inside and outside the coordination sphere but the reaction of copper (II) acetate gave dinuclear copper complexes having a monodentate carboxylato bridge arising from the carboxylato groups at the 1 and 4-positions on the aromatic ring. All the complexes were characterized by X-ray crystallography.

Choi et al. [75] reported that the reactions of $[Ni(L)]Cl_2.2H_2O$ (L = 3,14-dimethyl-2,6,13,17 tetraazatricyclo[14,4,$0^{1.18}$,$0^{7.12}$]docosane) with isophthalic acid (H_2isoph) and 1,3,5-cyclohexanetricarboxylic acid (H_3chtc) gave 1D nickel (II) complexes, $\{[Ni(L)(isoph)].3H_2O\}_n$ (Fig. 4-22) and $\{[Ni(L)(Hchtc)].H_2O\}_n$.

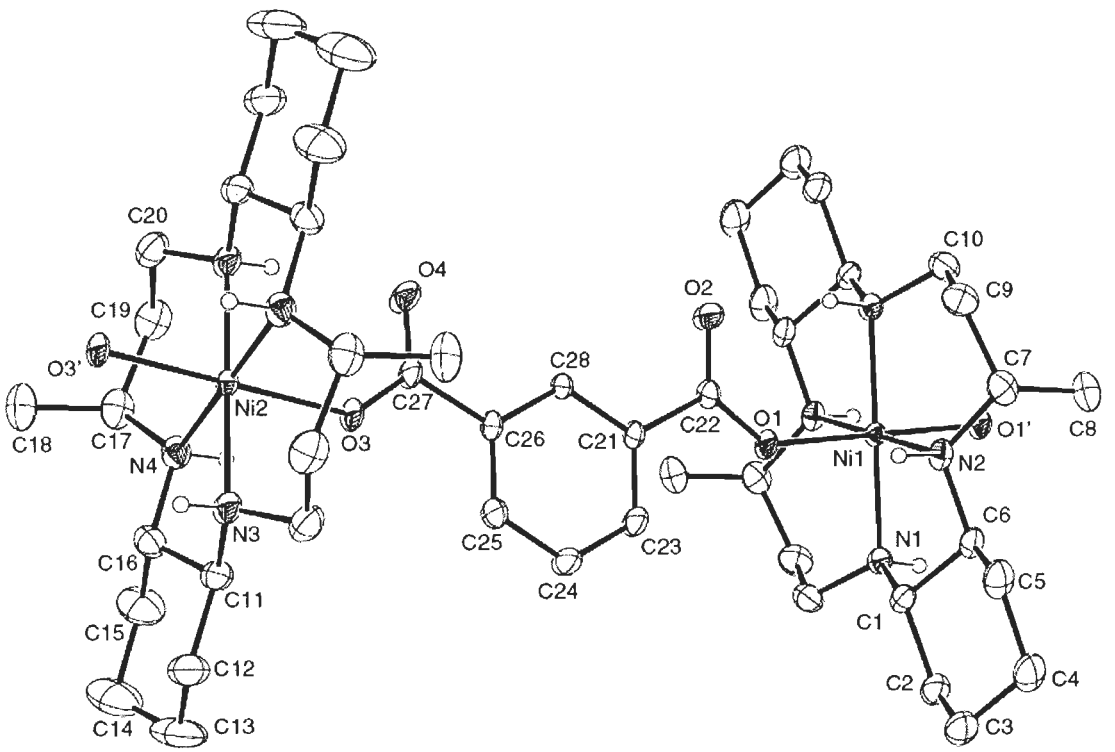

Fig. 4-22 Crystal structure of $\{[Ni(L)(isoph)].3H_2O\}_n$

The structures were characterized by X-ray crystallography, spectroscopic and magnetic susceptibility. The crystal structures of the 1D chain compounds showed an elongated distorted octahedron about each nickel (II) ion. The magnetic behavior of two compounds exhibits weak intrachain antiferromagnetic interaction with J values of -0.93 cm^{-1} and -1.28 cm^{-1} respectively.

Sileo et al. [76] reported the synthesis and the crystal structures of three metal (II) derivatives of lutidinic acid (lutidinic acid = 2,4-pyridinedicarboxylic acid = $H_2$2,4-pydc). $Zn(2,4\text{-pydc})(H_2O)_4]\cdot H_2O$ and $[Ni(H_2O)_6][Ni(2,4\text{-pydc})_2(H_2O)_2]$ (Fig. 4-23). The Zn and Ni ions were hexacoordinated and the lutidinate group was almost planar binding the metal through an oxygen atom from the 2-carboxylate group. All compounds presented a dangling uncoordinated 4-carboxylate group.

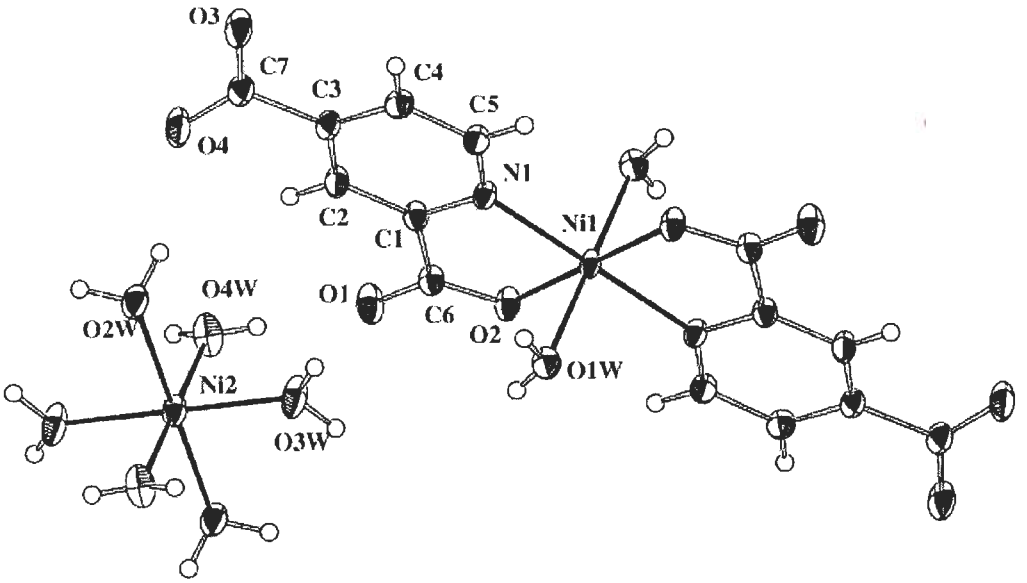

Fig. 4-23 Crystal structure of $[Ni(H_2O)_6][Ni(2,4\text{-pydc})_2(H_2O)_2]$

Maslejova et al. [77] synthesized the nickel (II) complexes of formula $[Ni(iz)_6]X_2$, (where iz = imidazole and X = formate, chloroacetate and 2-chloropropionate anions) and characterized by spectroscopic methods and magnetic measurements. The crystal structure of $[Ni(iz)_6](HCOO)_2$, $[Ni(iz)_6](ClCH_2COO)_2$ and

$[Ni(iz)_6](CH_3ClCHCOO)_2$ was determined by X-ray diffraction method. The structure of the all complexes exhibited a three-dimensional network consisting of $[Ni(iz)_6]^{2+}$ cations interlinked by formate, chloroacetate and 2-chloropropionate anions through three different N–H···O bonds, in which all the N–H imidazole units, as well as all the carboxylate O atoms, took part. The Ni atom was in a nearly octahedral environment formed by the tertiary nitrogen atom of the imidazole moieties. An analogous complex $[Ni(Meiz)_6]Cl_2.2H_2O$ showed a two-dimensional hydrogen-bond network in which only four ligands took part along with Cl^- and H_2O units. The distortion of Ni(II) coordination polyhedron rises in the order of 1 (negative) < 2 < 3 (positive) < 4. The magnetism of complexes exhibited a zero-field splitting D, the magnitude of which correlates with the distortion degree of the coordination polyhedra.

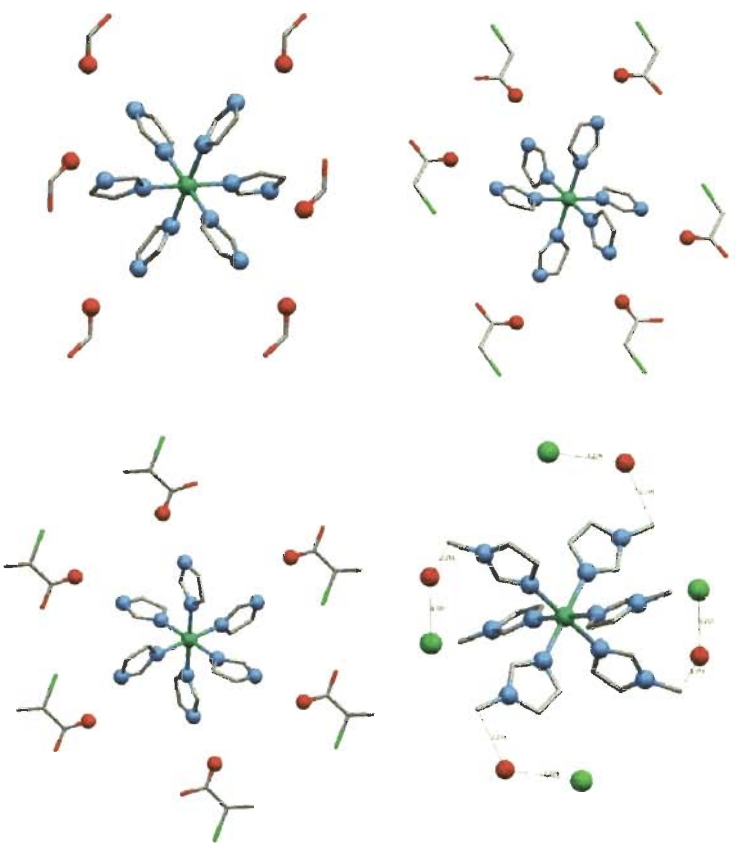

Fig. 4-24 Crystal structure of the complex $[Ni(iz)_6]^{2+}$ cations and the critical hydrogen bonds with formate, chloroacetate, 2-chloropropionate, water and chloride anions in complexes

Huang et al. [78] reported two new complexes $[Ni(pydc)(H_2O)_2]_n$ and $[Ni_2(pydc)_2(H_2O)_5]_n$ (H_2pydc = 2,4-pyridine dicarboxylic acid) by hydrothermal synthetic method and characterized by single crystal X-ray analysis. In $[Ni(pydc)(H_2O)_2]_n$ (Fig. 4-25) six-coordinate Ni(II) ions were coordinated by pydc ligands and formed 2-D layer structures; while in $[Ni_2(pydc)_2(H_2O)_5]_n$ six-coordinate Ni(II) ions were only connected into 1-D zigzag chains constructed by dinuclear nickel units. Variable temperature magnetic susceptibility studies showed that both compounds may display antiferromagnetic coupling between paramagnetic metal centers mediated by bridging carboxylate groups.

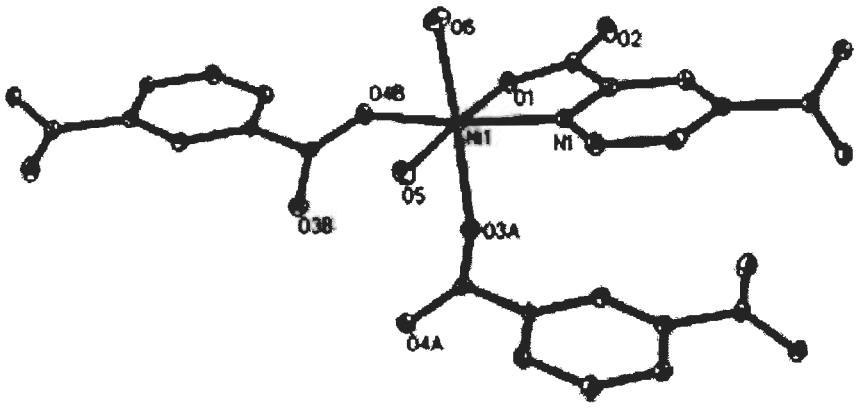

Fig. 4-25 Crystal structure of $[Ni(pydc)(H_2O)_2]_n$

Wang et al. [79] reported several membrane-coated carbon rod anion-selective electrodes (CCRISE) by incorporating metal complex of bis(diphenylphosphino) propane (BDPPP) in a plasticized PVC film and their response characteristics were studied. Highly sensitive sensors were obtained with detection limit of 10^{-5} M for benzoate ions.

Webber et al. [80] prepared the transition metal-directed self-assembly of dithiocarbamate ligand functionalised upper and lower rim calix[4]arenes to afford

novel dimeric bimetallic bis(calix[4]arene) species (Fig. 4-26), which were characterized by a combination of analytical methods including X-ray crystallography. An exception was a zinc (II) dithiocarbamate upper rim calix[4]arene assembly which was monomeric in nature. Electrochemical investigations revealed that the bimetallic copper (II) bis(calix[4]arene) systems can electrochemically sense dihydrogen phosphate, acetate and benzoate anions via significant cathodic perturbations of the respective copper (II) / (III) dithiocarbamate oxidation wave.

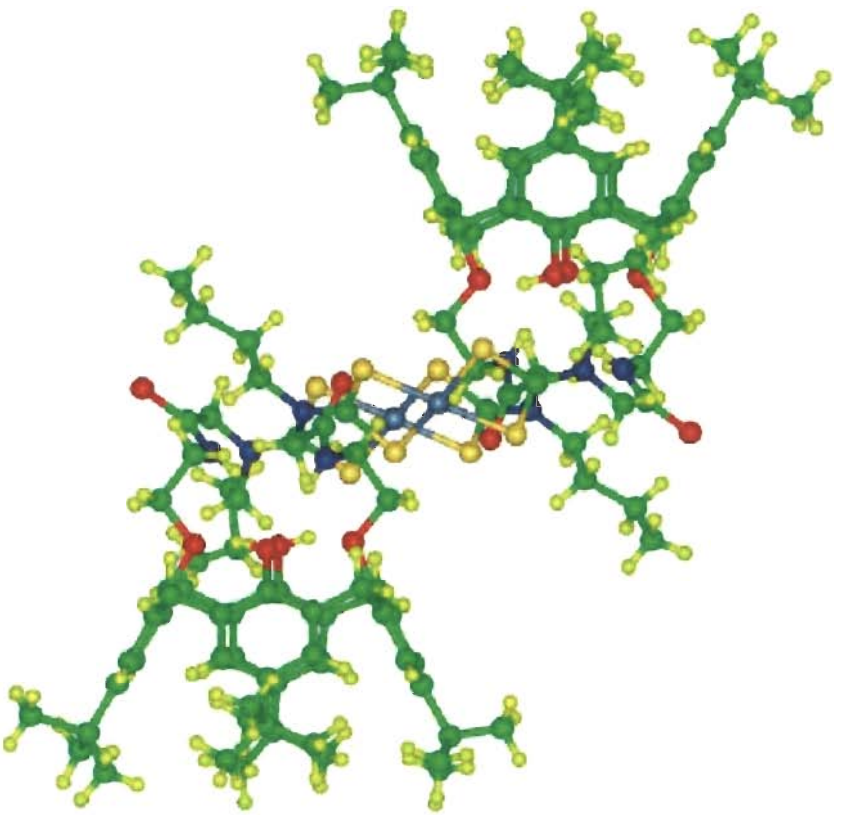

Fig. 4-26 Crystal structure of bimetallic nickel (II) bis(calix[4]arene) (color code Carbon, green; hydrogen, yellow; oxygen, red; nitrogen, blue; sulfur, light yellow; nickel, light blue)

Segui et al. [81] used polyamines, octyl-[2-(2-octylamino-ethylamino)-ethyl]-amine (L1) and octyl-{2-[2-(2-octylamino-ethylamino)-ethylamino]-ethyl}-amine (L2),

as anion ionophores in PVC-based membrane ion-selective electrodes. Different electrodes were prepared containing L1, or L2, and o-nitrophenyl octyl ether (NPOE) or bis(2-ethylhexyl)sebacate (DOS) as plasticizers. Electrodes containing L1 and L2 with NPOE (E1 and E2, respectively) showed a Nernstian response for thiocyanate with a good response time. They also determined the selectivity coefficients for different anions with respect to thiocyanate anion. The electrode was also used to determine concentration of thiocyanate in biological samples.

Behzad et al. [82] prepared a potentiometric thiocyanate-selective sensor based on Cu(II) bis(benzoylacetone)propylenediimine complex as a new neutral carrier for a thiocyanate-selective electrode. The response mechanism was discussed in view of the UV spectroscopy technique. The sensor displayed a near Nernstian slope of - 57.4 ± 0.5 mV per decade. The working concentration range of the electrode was 8.0×10^{-7} - 1.0×10^{-1} M with a detection limit of 7.4×10^{-7} M. The proposed electrode was successfully applied to direct determination of thiocyanate in the presence of other anions in biological and waste water samples.

Singh et al. [83] reported a potentiometric thiocyanate-selective sensor based on the zinc-tris(N-tert-butyl-2-thioimidazolyl)hydroborate complex [$Tt^{t\text{-}Bu}$-Zn]. They studied the effect of various plasticizers viz., *o*-nitrophenyloctyl ether (*o*-NPOE), dioctylphthalate (DOP), dibutylphthalate (DBP), benzylacetate (BA), and anion excluder, hexadecyltrimethylammonium bromide (HTAB), with $Tt^{t\text{-}Bu}$-Zn complex in poly (vinyl chloride) (PVC). The best performance was obtained with a membrane composition of DOP : PVC : $Tt^{t\text{-}Bu}$-Zn : HTAB percent ratio (w / w) of 60 : 33 : 5 : 2. The sensor exhibited significantly enhanced selectivity toward thiocyanate ions over

the concentration range of 6.3×10^{-7} to 1.0×10^{-2} M with a low detection limit of 3.16×10^{-7} M and a Nernstian slope of 59.4 ± 1.1 mV decade^{-1}. They also investigated the influence of the membrane composition, pH, and possible interfering anions on the response properties of the electrode and applied the proposed sensor for direct determination of thiocyanate within physiological fluids and environmental samples.

Prasad et al. [84] synthesized iron (III) and cobalt (III) complexes of 2,3,7,8,12,13,17,18-octakis(benzylthio)-5,10,15,20-tetraazaporphyrin, (OBTAP) and incorporated them into PVC matrix as ionophores to fabricate anion selective membrane electrodes that exhibit selective potentiometric response to azide and nitrite ions, respectively. The membrane of $[Fe(OBTAP)]^+$ with a composition of 6 : 190 : 200 ($[Fe(OBTAP)]^+$: DBP : PVC) (w / w), and of $[Co(OBTAP)]^+$ with a composition of 10 : 148 : 200 ($[Co(OBTAP)]^+$:DOP : PVC) (w / w), (where DBP = dibutylphthalate and DOP = dioctylphthalate) gave the best performance.

Hassan et al. [85] reported novel poly(vinyl chloride) matrix membrane electrodes for the azide ion used for manual and flow injection determination of soluble and insoluble metal azides. These electrodes incorporated iron (II) and nickel (II) bathophenanthroline–azide ion-pair complexes as ion exchangers and 2-nitrophenyl phenyl ether as a plasticizing solvent mediator. The electrodes exhibited (i) near-Nernstian response for 1×10^{-1} to 3.5×10^{-5} M N_3^- with an anionic slope of 56–57 mV decade^{-1} of concentration; (ii) a wide working range of pH (6–12); (iii) a fast response time (<40 s); (iv) long-term stability (>1 month); and (v) reasonable selectivity for N_3^- over many common anions. Methods for measuring the solubility products of some sparingly soluble metal azides and for monitoring the concentration level of azide in primer mixtures were also described.

The present chapter deals with the synthesis and characterization of some mononuclear nickel complexes with pyrazolylborate / pyrazolylborate and benzoates / thiocyanate / azide as well as with N-tert-butyl-2-thioimidazole ligand. One of the nickel complexes i.e., **4e** has been used as ionophore for determination of benzoate, thiocyanate and azide ions in environmental and biological samples.

Results and Discussion

The 3-phenyl-5-methylpyrazole ($Pz^{Ph,Me}H$) **4a** and potassium hydrotris(3-phenyl-5-methyl-1-pyrazolyl)borate $KTp^{Ph,Me}$ **4b** have been prepared by the modified method of Vahrenkamp et al. (Scheme 4-4) as described in chapter 5.

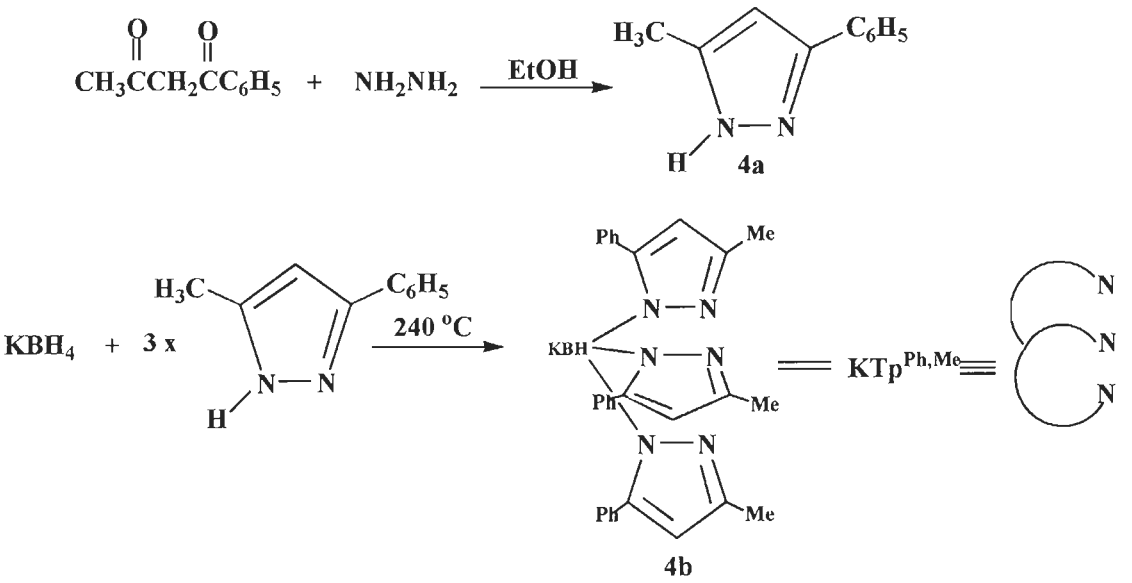

Scheme 4-4

When $NiCl_2.6H_2O$ was allowed to react with $KTp^{Ph,Me}$ **4b** / KTp **2a**, bis chelated $[(Tp^{Ph,Me})_2Ni]$ **4c** and $[(Tp)_2Ni]$ **4d** were formed suggesting no effect of substituents on metal center (Scheme 4-5). The complex **4c** and **4d** showed B-H band at 2546 cm^{-1} and 2492 cm^{-1} in the IR spectra suggesting the formation of the complex.

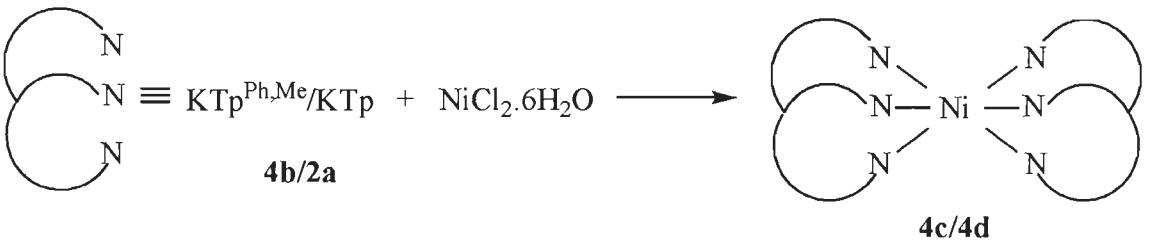

Scheme 4-5

Complex **4c** crystallizes in the monoclinic system with centosymmetric space group C2/c. The crystallographic data is given in Table 4-1 whereas the important bond lengths and bond angles are given in Table 4-2. The crystal structure of complex **4c** is shown in Fig. 4-27. The different intermolecular CH_3-π interactions are in the range of 2.782(3) to 2.910(11) (Fig. 4-28). Complex **4c** contains a mononuclear metal centre where nickel is in six coordination number, bonded by six nitrogen atoms from two $Tp^{Ph,Me}$ ligands. The two nickel-nitrogen bond distances are almost same i.e., Ni(1)-N(1) 2.146(3), Ni(1)-N(3) 2.153(3) Å whereas the Ni(1)-N(6) is slightly elongated with the distance of 2.230(3) Å.

The compound **4d,** a bis–chelated species was prepared by the reaction of nickel (II) chloride and Tp. It crystallizes in the monoclinic system with space group $P2_1/n$ and details of data collection are given in Table 4-3. As can be seen from the crystal structure of **3** (Fig. 4-29), nickel center is coordinated with six nitrogen atoms from two hydrotris(pyrazol-1-yl)borate ligands, forming NiN6 system with distorted octahedral geometry having average angle of 88.56°. The Ni-N bond distances of coordinated Tp ligands are in the range of 2.0799(6) to 2.0980(6) Å (Table 4-4), which are usual for Ni bonded Tp complexes [86]. During unit cell packing, two molecules are connected with each other through C-H···π intermolecular interaction of 2.895(3) Å between C-H of pyrazole and π electron of pyrazole ring as shown in Fig. 4-30.

When $NiCl_2.6H_2O$ was allowed to react with $KTp^{Ph,Me}$ **4b** in presence of $Pz^{Ph,Me}H$ **4a** having a reactant ratio of 1:1, the reaction resulted in the formation of five coordinate nickel complex $[Tp^{Ph,Me}Ni(Cl)Pz^{Ph,Me}H]$ **4e** (Scheme 4-6).

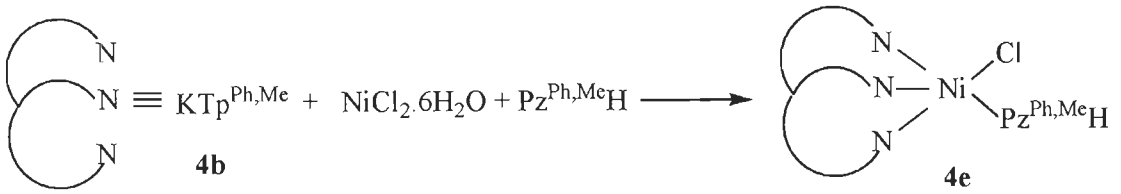

Scheme 4-6

The compound **4e** crystallizes in the monoclinic system with space group $P2_1/c$ and its crystal structure is shown in Fig. 4-31. The metal centre is coordinated by three nitrogen atoms from $Tp^{Ph,Me}$, one nitrogen atom from $Pz^{Ph,Me}H$ and by one chloride ion. The details of data collection as well as selected bond lengths and bond angles are given in Table 4-5 and Table 4-6, respectively. The nickel centre in this complex is five coordinate with nickel–nitrogen bond distances in the range of 2.045(2) – 2.1474(19) Å which is usual for nickel bonded Tp complexes [86, 87]. The metal-nitrogen bond distance of coordinated $Pz^{Ph,Me}H$ is greater than the Ni-N bond distances of Tp (Table 4-6). The Ni-Cl bond distance of 2.306(7) Å is also in the range of reported complexes [88] and shows its covalent character. The Fig. 4-32 shows the presence of C-H···π interaction (2.922(0) Å) between C-H group of phenyl ring present on $Tp^{Ph,Me}$ and π electrons of pyrazole ring from $Tp^{Ph,Me}$, thus forming a zig-zag chain along c-axis.

The complex **4e** has been used as an ionophore to prepare its polymeric membrane as a sensor for benzoate / thiocyanate / azide anions. After optimizing the membrane compositions for these anions, their formation constants were also calculated to check their interactions in solution state. Further, the proposed membranes were also used in various biological and environmental samples.

Optimization of benzoate membrane compositions

The composition of membrane with different plasticizers and additive, performing best is given along with their characteristics in Table 4-7. Among the four different plasticizers (NPOE, DBP, BA, TBA), the NPOE was the most effective solvent mediator in preparing the benzoate selective membrane electrode. It is important to mention here that the nature of the plasticizers influence both the dielectric constant of the membrane as well as the mobility of ionophore and its complex.

The amount of ionophore **4e** was also found to affect the response of membrane electrode (Table 4-7). The sensitivity of the electrode response increased with increase in the ionophore content till the value of 5 mg, further, addition of ionophore will however resulted in diminished the response of the electrode, which may be due to some inhomogenities and possible saturation of the membrane [89]. The presence of 3 mg of HTAB as a cationic additive improved the sensitivity of benzoate sensor considerably (No. 4). As can be seen from Table 4-7 that the membrane having composition PVC : NPOE : **4e** : HTAB as 150 : 345 : 5 : 3 (w / w) exhibits the best results with Nernstian slope and limit of detection of 1.4×10^{-6} M. This sensor no. 4 having the above composition gave response to benzoate ions over a wide concentration range (1.0×10^{-1} - 2.2×10^{-6} M).

The optimum equilibration time for the membrane electrode in the presence of 1.0×10^{-1} M Na(OBz) solution was three days and it generated stable potentials in contact with benzoate solution. The electrode showed a linear response to the concentration of benzoate ion in the range of 2.2×10^{-6} - 1.0×10^{-1} (Fig. 4-33). The slope of the calibration graph was 59.2 ± 0.2 mV per decade. The limit of detection, as determined from the intersection of the two extrapolated segments of calibration graph

was 1.4×10^{-6} M. The membrane sensor prepared could be used for at least 12 weeks without any divergence in potentials. The response time of the electrode was determined by measuring the time required to achieve a 90 % of the steady potential. The static response time thus obtained was 20 s over the entire concentration range.

Determination of formation constant for different para-substituted benzoate anions

To determine the binding capacity of different substituted benzoate anions, various sandwich-membrane electrodes were prepared and their formation constant was calculated. The determined formation constants ($\log \beta_{ILn}$) for different benzoates were recorded in Table 4-8, where benzoate shows a higher value than its para-substituted analogues. Although all examined benzoates were showing significant interaction in the following order OBz > *p*-F-OBz > *p*-Cl-OBz > *p*-OMe-OBz > *p*-OH-OBz > *p*-NH_2-OBz > *p*-CH_3-OBz > *p*-NO_2-OBz.

Analytical application of benzoate-selective sensor

The proposed sensor can be applied for the monitoring of the benzoate concentration in various diet soda, soya sauce and lemon juice samples, because of the high selectivity and the very low detection limit of the constructed benzoate sensor. The water samples were centrifuged (2000 rpm) for 10 min and a 1 mL aliquot of the supernatant was diluted with water. Carbonated samples were degassed in an ultrasonic bath prior to dilution. All samples were diluted with deionized water in the ratio of 1:100 prior to analysis, except the diet soda that was diluted in the ratio of 1:20. In order to verify the accuracy and precision of the analytical procedure, recovery studies were carried out by spiking selected samples of each matrix with standards. The sample solutions obtained were analyzed by proposed membrane sensor and the results

obtained by triplicate measurement are compiled in Table 4-9. The results showed that the recovery for all samples was greater than 90 % thereby reflecting the utility of the proposed sensors.

Optimization of thiocyanate and azide membranes compositions

Potential of the membranes of [$Tp^{Ph,Me}$Ni(Cl)$Pz^{Ph,Me}$H] ionophore (**4e**) were also investigated as a function of thiocyanate and azide ion activity in the range 1.0×10^{-8} to 1.0×10^{-2} M and the results obtained were compiled in Tables 4-10 and 4-11. The electrodes with no carrier (containing PVC, plasticizer and HTAB) displayed insignificant sensitivity towards both the anions. The influence of plasticizer on the response characteristics of the thiocyanate and azide electrodes was investigated by using four plasticizers of different polarities including DBP, *o*-NPOE, AP and TBP. The sensor nos. 3 and 16 having membranes without plasticizer exhibited a narrow working concentration range of 10^{-4} to 10^{-2} M with a sub Nernstian slope. Improvement in sensors performance was observed by the addition of plasticizer. Among the several membranes tested for each of the carriers, the membranes incorporating DBP and TBP showed better potentiometric responses, i.e., higher sensitivity and wider linearity of the calibration plots (sensor nos. 12 and 23). It seems that since these plasticizers have low polarity and a relatively high mobility, with respect to *o*-NPOE and AP, they provide appropriate conditions for incorporation of thiocyanate and azide ion into the membranes prior to its coordination with the nickel atom in the complexes.

The addition of lipophilic cationic additive in anion selective membranes is necessary to introduce permselectivity. The influence and concentration of the membrane additives was also investigated by incorporating HTAB into the membranes. The potentiometric sensitivity of the **4e** based membranes for both anions were greatly improved in the presence of HTAB as a lipophilic cationic additive, compared to the

membranes with no additive at all. Previous studies have shown that there is an optimal concentration of lipophilic ionic additives in the membranes and that gives the best electrode performance. The effect of HTAB concentration in the membrane was investigated at several additive / ionophore mole ratios. The sensors with HTAB / ionophore mole ratios of ~ 0.55 for both the carriers exhibited maximum sensitivity over a wide range of thiocyanate and azide concentration.

Among the different membrane compositions, membranes with composition (w / w, %) 7(**4e**) / 2(HTAB) / 31(PVC) / 60(DBP) and 6(**4e**) / 4(HTAB) / 31(PVC) / 59(TBP) showed highest sensitivity and widest linear range for thiocyanate and azide anions respectively and were selected as the optimum composition for further studies. Thiocyanate sensors (sensor no. 12, Table 4-9) exhibit the maximum working concentration range of 5.3×10^{-7} to 1.0×10^{-2} M with a slope of 59.2 mVdecade^{-1} of activity and detection limit of 1.8×10^{-7} M, while azide sensor (Sensor no. 23, Table 4-10) reveal working concentration range of 8.1×10^{-6} to 1.0×10^{-2} M with Nernstian slope of 59.3 mVdecade^{-1} of activity and detection limit of 5.2×10^{-6} M (Fig. 4-34).

Determination of formation constant for different anions

The determined formation constants (log $\beta_{\mathrm{IL}n}$) for different anions were recorded in Table 4-12. A careful analysis of the data in Table 4-12 revealed that thiocyanate and azide ion, both have significant anion-binding characteristics but thiocyanate was slightly at higher side.

Analytical applications of thiocyanate-selective sensor

Urine and saliva samples containing different thiocyanate concentrations were collected from smoker and non-smoker patients, and same samples were assayed multiple times. Samples were treated by MES / NaOH buffer (pH 5.5) solution, while

the river water sample was used directly by adjusting pH 5.5 by dilute HCl solution. All samples were analyzed in five replicate using the proposed electrode and the results were compared with those obtained by a standard colorimetric method. The results given in Table 4-13, show that the amount of thiocyanate ion evaluated with the help of the electrode are in good agreement with those obtained by the standard colorimetric method, thereby reflecting the utility of the proposed sensors.

Analytical applications of azide-selective sensor

Azide selective sensor was applied for the monitoring of the azide ion concentration in various aqueous samples (black tea and orange juice). Samples were directly injected after minimal sample preparation. The samples were diluted (1:10 with double distilled water) and filtered to remove particulates and treated by MES / NaOH buffer (pH 5.5) solution. Black tea was prepared by steeping a teabag in about 100 mL of hot reagent grade water for 10 min. After cooling, the infusion was diluted 10-fold with reagent grade water and filtered before injection. For spike recovery measurements, the tea was spiked with 10 mg L^{-1} sodium azide before dilution and filtration. Orange juice was diluted 10-fold with reagent grade water and filtered before injection. For spike recovery measurements, the orange juice was spiked with 10 mg L^{-1} sodium azide before dilution and filtration. Human urine was diluted 10-fold with reagent grade water and filtered before injection. For spike recovery measurements, the urine was spiked with 10 mg L^{-1} sodium azide before dilution and filtration.

For each sample, precision and recovery from interferences were measured by adding 1 mg L^{-1} azide; reagent water, black tea, orange juice and urine. Recovery for all samples was greater than 80 %. Precision varied from 2 to 8 % for all the samples. The results are shown in Table 4-14. Orange juice contains phosphate, sulfate, fluoride and fumarate but these compounds do not interfere with azide.

Solid state studies

After confirming the interactions of compound **4e** with benzoates / thiocyanate / azide in solution, attempts were made to synthesize and characterize these complexes by different spectroscopic techniques including X-ray crystallography.

The compounds **4f-4o** were synthesized by the reaction of **4e** with sodium *p*-X-benzoates (X = H, F, Cl, NO_2, Me, OMe, OH, CHO, CN, NH_2) (Scheme 4-7). In complex **4e**, the metal centre is coordinated by three nitrogen atoms from $Tp^{Ph,Me}$, one nitrogen atom from $Pz^{Ph,Me}H$ and by one chloride ion whereas in complexes **4f-4n**, the fifth site is occupied by only one oxygen atom of coordinated benzoate group resulted in the formation of five coordinated system. In **4o**, *p*-amino-benzoate replaced the $Pz^{Ph,Me}H$ and bonded in bidentate fashion. Complex **4p** and **4q** were also synthesized by the reaction of **4e** with NaN_3 and KSCN respectively (Scheme 4-7).

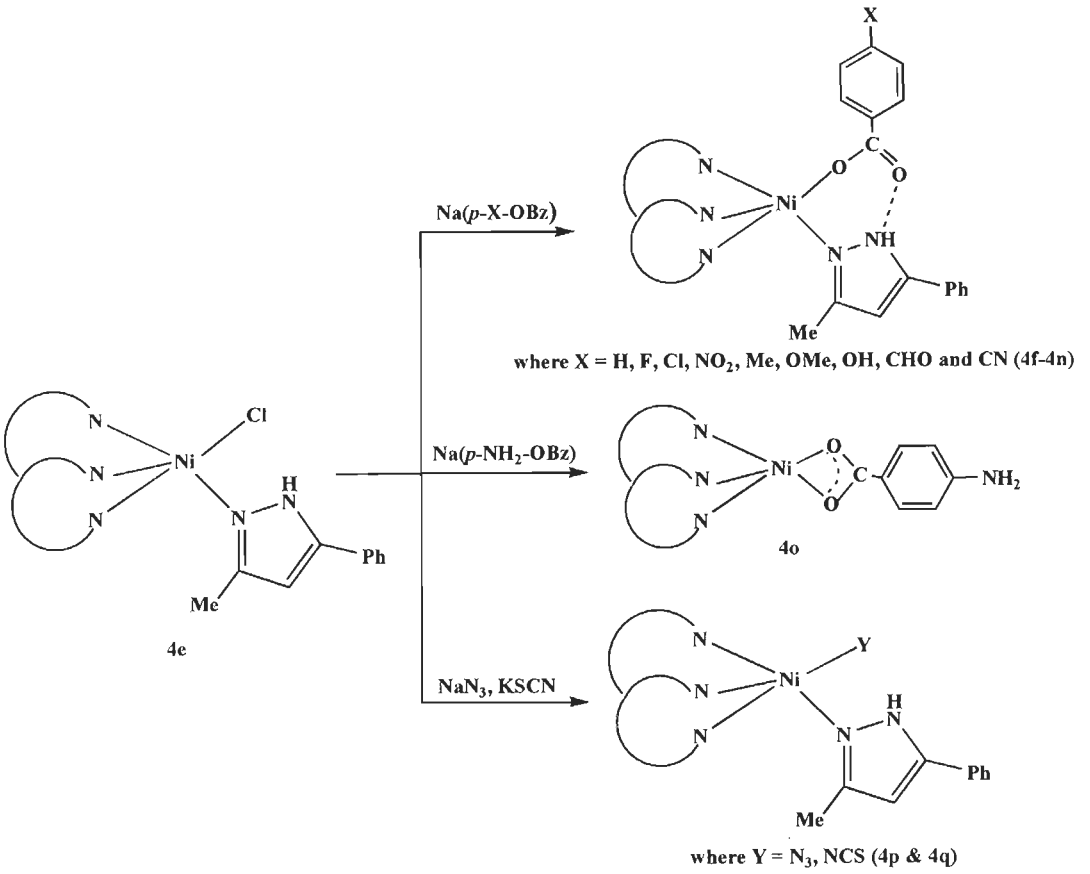

Scheme 4-7

The complex **4r** was synthesized by the reaction of hexahydrate nickel (II) chloride and N-tert-butyl-2-thioimidazole and **4s** was synthesized by the reaction of hexahydrate nickel (II) nitrate, N-tert-butyl-2-thioimidazole and 3-phenyl-5-methyl pyrazole. These complexes were characterized by elemental analysis, infrared, UV / vis spectra, magnetic susceptibility and single crystal X-ray crystallography.

$$NiCl_2.6H_2O + 2.tm^{t\text{-}Bu} \longrightarrow [Ni(tm^{t\text{-}Bu})_2Cl_2]\ (4r)$$

$$Ni(NO_3)_2.6H_2O + 2.Pz^{Ph,Me}H + tm^{t\text{-}Bu} \longrightarrow [Ni(Pz^{Ph,Me}H)_2(tm^{t\text{-}Bu})(NO_3)_2]\ (4s)$$

Scheme 4-8

Infrared spectral studies

The complexes **4f-4q** showed B-H stretching vibration in the range of 2513-2546 cm^{-1}. In addition, the complexes **4f-4n** showed IR bands in the range of 1589-1606 cm^{-1} and 1373-1404 cm^{-1} due to asymmetric (ν_{as}) and symmetric (ν_s) stretching vibrations of carboxylate group, respectively. The separation between the ν_{as} and ν_s stretching vibration is more than 200 cm^{-1} and is consistent with monodentate coordination behavior of benzoate. In complex **4o**, the separation between these two vibrations is 174 cm^{-1} (less than 200 cm^{-1}) suggesting the bidentate coordination behavior of *p*-amino-benzoate. In complex **4p**, the presence of ν(N=N) band at 2075 cm^{-1} is in accordance with terminal coordination mode of azide. The C=N stretching frequency of thiocyanates are generally lower in the N-bonded complexes (near and below 2050 cm^{-1}) than the S-bonded complexes (near 2110 cm^{-1}) [90]. Appearance of a single strong band at 2058 cm^{-1} of ν(C=N) suggested that the thiocyanate is bonded through nitrogen atom in complex **4q**. The complexes **4r** and **4s** showed C=S stretching vibration at 1089 and 1095 cm^{-1} suggesting binding to metal center. The complex **4s** also showed $\nu_{as}(NO_3)$ and $\nu_s(NO_3)$ at 1532 and 1262 cm^{-1}, indicating the coordination of nitrate ions.

Crystallographic studies

Crystal structure of [$Tp^{Ph,Me}$Ni(p-X-OBz)$Pz^{Ph,Me}$H] (X = H for **4f**, F for **4g**, Cl for **4h**, Me for **4j**, CHO for **4m**, CN for **4n,** NH_2 for **4o**)

The complexes **4f**, **4g**, **4h**, **4j**, **4m** crystallize in the triclinic system with space group $P\bar{1}$, **4n** crystallizes in the monoclinic system with space group $P\bar{1}$ whereas **4o** crystallizes in the tetragonal system with space group $I4_1/a$. The detailed crystallographic data for complexes **4f**, **4g**, **4h**, **4j**, **4m, 4n** and **4o** are given in Table 4-15, 4-17, 4-19, 4-21, 4-23, 4-25 and 4-27 whereas the important bond lengths and bond angles are given in Table 4-16, 4-18, 4-20, 4-22, 4-24, 4-26 and 4-28. The crystal structure of complex **4f** is shown in Fig. 4-35 as hydrogen bonded benzoate complex and other complexes **4g**, **4h**, **4j**, **4m** and **4n** are shown in Fig. 4-39, Fig. 4-43, Fig. 4-45, Fig. 4-47 and Fig. 4-51, repectively. In these complexes, the nickel centre is five coordinated with three nitrogen atoms from $Tp^{Ph,Me}$ ligand, one nitrogen atom from $Pz^{Ph,Me}H$ and one oxygen atom from benzoate ligand. The distance between metal centre and bonded oxygen atom of the benzoate molecule are almost same in all above complexes and lie within the range of 1.983(2)-2.026(3) Å as reported in literature [86, 87]. The distance between non-bonded oxygen atom and metal centre is too large for coordination and shows slight variation from complex to complex (Table 4-29). The non-bonded oxygen atom in these complexes is involved in hydrogen bonding with hydrogen atom lying on the nitrogen of $Pz^{Ph,Me}H$ coordinated at apical position to the nickel ion. The existence of hydrogen bonds in these complexes is clearly established on the basis of the location of the hydrogen with mean bond distances of Ha-O2, 1.904(36) Å and Ha-N8, 0.802(37) Å for **4f**; 1.792(4) Å and 0.899(2) Å for **4g**; 1.689(35) Å and 0.995(33) Å for **4h**; 1.861(4) Å and 0.859(4) Å for **4j**; 1.871(5) Å,

0.860(5) Å for **4m**; 1.870(6) Å and 0.860(5) Å for **4n**. The presence of a hydrogen bond also affects the appearance of the ν(NH) band in the IR spectra of the complexes as the $Pz^{Ph,Me}H$ gives the band at 3180 cm^{-1}. The short distances of the carbonyl oxygen (O2) of the benzoate anions from the nitrogen of neutral pyrazole (N8) (O2-N8 bond, 2.689(4) Å for **4f;** 2.672(5) Å for **4g**; 2.666(8) Å for **4h**; 2.672(6) Å for **4j**; 2.683(7) Å for **4m**; 2.711(1) Å for **4n**) also suggest the presence of hydrogen bonding in these complexes. Similar to complex **4e**, in these complexes also, Ni-N bond distances of coordinated $Tp^{Ph,Me}$ and $Pz^{Ph,Me}H$ ligands are in the range of 2.027(3) - 2.112(3) Å which is very similar to the Ni-N bond distances in other reported Ni(II) complexes with Tp [86, 87]. The non-bonded oxygen atom of benzoate in complexes **4f, 4g, 4j** and **4m** show intermolecular C-H···O interaction in the range of 2.630-2.703 Å with the hydrogen atom lying on phenyl ring of $Tp^{Ph,Me}$ (Fig. 4-36, 4-40, 4-46 and 4-48). Also, in complexes **4f**, **4g** and **4m,** C-H···π interactions were observed in the range of 2.686–2.973 Å with involvement of hydrogen atoms of benzoate as well as of toluene molecule and the π electrons of all three pyrazole rings of $Tp^{Ph,Me}$ [91] (Fig. 4-37, 4-41 & 4-49) (Table 4-34). In these complexes, the two molecules of each complex further interacted through toluene {with C-H···π interactions (2.710-2.966 Å)} and formed one dimensional chain as shown in Figure 4-39, 4-43 and 4-51. The complexes **4h, 4j and 4n** also show different type of non covalent interactions as shown in Fig. 4-44, 4-46 and 4-52. The crystal structure of complex **4o** is shown in Fig. 4-53. The amino-benzoate is behaving as bidentate ligand, yet one of the bonded oxygen atom is involved in C-H···O intermolecular interaction with hydrogen atom of phenyl ring present on $Tp^{Ph,Me}$ and both hydrogen atoms of amino group are involved in N-H···π interactions with phenyl group of $Tp^{Ph,Me}$ as well as of benzoate as shown in Fig. 4-54.

This complex also shows $CH_3\cdots\pi$ and C-H$\cdots\pi$ interactions through one of the pyrazole ring of $Tp^{Ph,Me}$ in the range of 3.001-3.057 Å (Fig. 4-55).

Crystal structure of $[Tp^{Ph,Me}Ni(X)Pz^{Ph,Me}H]$ (X=N_3 for **4p**, SCN for **4q**)

The compound **4p** and **4q** crystallize in the triclinic system with space group $P\bar{1}$. Their crystallographic data are given in Table 4-30 and Table 4-32 whereas their important bond lengths and bond angles are given in Table 4-31 and Table 4-33. The crystal structure of complex **4p** is shown in Fig. 4-56 and different intermolecular C-H$\cdots\pi$ (2.822-2.889 Å) and C-H$\cdots$N (2.822 Å) interactions are present in crystal lattice (Fig. 4-57). The crystal structure of **4p** contains a mononuclear five coordinated nickel center having three nitrogen atoms from $Tp^{Ph,Me}$, one nitrogen atom from $Pz^{Ph,Me}H$ and one nitrogen atom from terminally coordinated azide anion in end-on fashion. All the nickel-nitrogen bond distances are in the range of 2.005(3)-2.113(3) Å showing covalent character with nickel centre. The Ni-N bond distance of terminal azide (2.005(3) Å) is smaller than Ni-N bond distance present in bridged azide complexes [92]. Fig. 4-58 shows the crystal structure of the complex **4q**. In this complex also, the nickel is five coordinated with same coordination environment as in **4p** except the fifth site in this complex is occupied by the nitrogen atom of thiocyanate group which is coordinated in a monodentate fashion. Fig. 4-59 shows the presence of intermolecular CH$\cdots\pi$ interactions (2.788-3.022 Å) in complex **4q**.

Crystal structure of $[(tm^{t\text{-}Bu})_2NiCl_2]$ (4r)

The complex **4r** crystallizes in the monoclinic system with centrosymmetric space group C2/c. The crystallographic data is given in Table 4-35 whereas the important bond lengths and bond angles are given in Table 4-36. The crystal structure

of complex **4r** is shown in Fig. 4-60 and unit cell packing in Fig. 4-61 with intermolecular $CH_3\cdots\pi$ interactions of 2.952 Å between one CH_3 of tert-butyl group on thioimidazole and π-electrons of thioimidazole ring and intramolecular N-H···Cl of 2.507 Å between hydrogen atom present on nitrogen of thioimidazole and chloride bonded to metal center. The Fig. 4-62 shows the formation of a zig-zag chain along the x-axis due to the presence of non-covalent C-H···Cl interaction (2.804 Å) between two independent molecules in one chain. Complex **4r** contains a mononuclear metal centre where nickel is four coordinated and bonded by two sulphur atoms from $tm^{t\text{-}Bu}$ and two chloride ions. The nickel-sulphur and nickel-chloride bond distances are 2.2898(3) Å and 2.2485(5) Å respectively, which are in the range of reported literature [Ref. [44] of chapter 3]. The geometry around the nickel centre is distorted tetrahedral with an average bond angle of 115.48°.

Crystal structure of $[(tm^{t\text{-}Bu})Ni(Pz^{Ph,Me}H)_2(NO_3)_2]$ (4s)

The compound **4s** crystallizes in the triclinic system with space group $P\bar{1}$ and its crystal structure is shown in Fig. 4-63. The crystallographic data is given in Table 4-37 whereas the important bond lengths and bond angles are given in Table 4-38. The nickel centre is six coordinate with two nitrogen atoms from $Pz^{Ph,Me}H$, one sulphur atom from $tm^{t\text{-}Bu}$, two oxygen atoms from one nitrate and one oxygen atom from other nitrate molecule. Thus it is N2SO3 system with distorted octahedral geometry. Interestingly both nitrates behave in asymmetric fashion, Ni-O bond length (2.1449(14) Å) in monodentate nitrate coordination is larger than Ni-O bond lengths [2.1069(15) and 2.1327(15) Å] in bidentate nitrate coordination and even the Ni(1)-O(4) bond distance of 3.559 Å is too large for coordination of nitrate through both oxygen atoms confirming their hetero binding nature to the metal center. The Ni-S bond distance of 2.3930(5) Å is also large to form a covalent bond thus forming

coordinate bond with nickel [93]. The Ni-N bond distances (2.0408 Å) in this complex are well within the reported range [86]. Complex **4s** is also stabilized by presence of two intramolecular N-H···O interactions {one from interaction between hydrogen atom present on nitrogen of pyrazole ring and non-bonded oxygen atom of monodentately coordinated nitrate ion (1.994 Å) and other from the interaction between hydrogen atom present on nitrogen of thioimidazole ring and bonded oxygen atom of monodentately coordinated nitrate ion (1.954 Å) and one N-H···S intramolecular interaction (2.606 Å) between hydrogen atom present on nitrogen of pyrazole ring and sulphur atom of thioimdazole (Fig. 4-64). The various C-H···π and C-H···O intermolecular interactions between molecules are also present as demonstrated in Fig. 4-65, Fig. 4-66 and Table 4-39 [91]. The bonded and non-bonded oxygen atoms of nitrate group result in the formation of different types of intra- as well as intermolecular interaction (14 different interactions) with interesting packing structure. It is important to mention here that metal complexes with sulphur containing pyrazolylborate are reported in literature [94-98] but nickel complex with both pyrazole and thioimidazole in same compound is not available.

Summary

We have reported the formation of complexes **4c** and **4d** by the reaction of potassium hydrotris(3-phenyl-5-methyl-1-pyrazolyl)borate and potassium hydrotris(pyrazol-1-yl)borate with $NiCl_2.6H_2O$. Also, the same reaction in presence of 3-phenyl-5-methyl-pyrazole resulted in five coordinated nickel complex $[Tp^{Ph,Me}Ni(Cl)Pz^{Ph,Me}H]$ (**4e**), which was used for various purposes. The investigations on polymeric membranes of ionophore (**4e**) have shown that they act as benzoate, thiocyanate and azide selective sensors. The considerably high values of formation constant for benzoate / thiocyanate / azide anions calculated by sandwich PVC

membranes confirms that these anions bind strongly with complex **4e** in solution. However, the thiocyanate selective sensor was compared to azide anion sensor and comparison of data revealed that thiocyanate sensor was superior to the azide sensor. The formation constant studies in solution tempted us to prepare several hydrogen bonded mononuclear nickel benzoate complexes for structural studies. The results demonstrated that in all benzoate complexes except **4o**, the benzoate behaves as monodentate and unbonded oxygen atom of the same is involved in hydrogen bonding with the N-H of $Pz^{Ph,Me}H$. The compounds **4p** and **4q** were also characterized by their crystal structures and were established to be bonded as monodentate through nitrogen atom of azide and thiocyanate anion. These complexes were also show various intra / intermolecular interactions in the crystal lattice. The proposed benzoate selective sensor was also applied successfully for the trace level determination of benzoate in diet soda, soya sauce and lemon juice. The thiocyanate sensor was also applied successfully for thiocyanate determination in human urine, saliva and river water while azide selective sensor was used to determine azide content in aqueous black tea and orange juice samples. We also prepared other two nickel complexes having thioimidazole and pyrazole / thioimidazole, respectively. Due to different binding sites of thioimidazole and pyrazole, these complexes have different molecular structure. The complex **4r** is in the tetrahedral environment and shows a zig-zag chain formation mainly due to the presence of C-H···Cl interaction between bonded chloride and hydrogen atom present on thioimidazole ring. Complex **4s** is an example of compound having bidentate and monodentate nitrate existing on a single metal center. Due to the presence of two nitrates, complex **4s** showed various inter and intramolecular interactions in a crystal packing but no chain formation was observed in this complex.

Table 4-1 Crystal Data and Collection Details of [$(Tp^{Ph,Me})_2Ni$] (4c)

Emperical formula	$C_{60}H_{56}N_{12}B_2Ni$
Formula weight	1025.48
Crystal system	Monoclinic
Space group	C2/c
Lattice parameters	
a (Å)	17.926(5)
b (Å)	13.713(4)
c (Å)	21.974(5)
α (°)	90.000
β (°)	111.638(6)
γ (°)	90.000
Cell volume V ($Å^3$)	5021(2)
Z	4
D_{Calc} ($g\ cm^{-3}$)	1.354
Data collection	
μ (Mo K_α) (cm^{-1})	0.442
θ_{max} (°)	29.24
Reflections measured	5209
Independent reflections	4918
Number of parameters refined	345
R	0.0780
R_w	0.1960

Table 4-2 Selected Bond Distances (Å) and Bond Angles (°) for $[(Tp^{Ph,Me})_2Ni]$ (4c)

Bond Distances			
Ni(1)-N(1)	2.146(3)	Ni(1)-N(3)	2.153(3)
Ni(1)-N(6)	2.230(3)		
Bond Angles			
N(1)-Ni(1)-N(1a)	96.57(18)	N(1)-Ni(1)-N(3)	89.98(13)
N(1)-Ni(1)-N(3a)	169.49 (12)	N(1)-Ni(1)-N(6)	91.68(13)
N(1)-Ni(1)-N(6)	82.44(13)	N(3)-Ni(1)-N(3a)	84.75(18)
N(3)-Ni(1)-N(6)	89.99(13)	N(3a)-Ni(1)-N(6)	97.33(13)
N(6)-Ni(1)-N(6a)	171.18(18)		

Table 4-3 Crystal Data and Collection Details of $[(Tp)_2Ni]$ (4d)

Emperical formula	$C_{18}H_{20}B_2N_{12}Ni$
Formula weight	484.77
Crystal system	Monoclinic
Space group	$P2_1/n$
Lattice parameters	
a (Å)	9.7041(6)
b (Å)	17.2931(10)
c (Å)	13.0241(8)
α (°)	90.000
β (°)	97.392(3)
γ (°)	90.000
Cell volume V ($Å^3$)	2167.5(2)
Z	4
D_{Calc} (g cm^{-3})	1.486
Data collection	
μ (Mo K_α) (cm^{-1})	0.930
θ_{max} (°)	48.77
Reflections measured	76656
Independent reflections	21406
Number of parameters refined	306
R	0.0328
R_w	0.0978

Table 4-4 Selected Bond Distances (Å) and Bond Angles (°) for $[(Tp)_2Ni]$ (4d)

Bond Distances			
Ni(1)-N(1)	2.0980(6)	Ni(1)-N(2)	2.0812(6)
Ni(1)-N(3)	2.0844(6)	Ni(1)-N(4)	2.0799(6)
Ni(1)-N(5)	2.0839(6)	Ni(1)-N(6)	2.0923(6)
Bond Angles			
N(1)-Ni(1)-N(2)	87.60(2)	N(1)-Ni(1)-N(3)	86.69(2)
N(1)-Ni(1)-N(4)	94.08(2)	N(1)-Ni(1)-N(5)	91.11(2)
N(1)-Ni(1)-N(6)	177.90(2)	N(2)-Ni(1)-N(3)	86.03(2)
N(2)-Ni(1)-N(4)	93.09(2)	N(2)-Ni(1)-N(5)	178.63(2)
N(2)-Ni(1)-N(6)	94.33(2)	N(3)-Ni(1)-N(4)	178.81(2)
N(3)-Ni(1)-N(5)	94.36(2)	N(3)-Ni(1)-N(6)	92.62(2)
N(4)-Ni(1)-N(5)	86.54(2)	N(4)-Ni(1)-N(6)	86.65(2)
N(5)-Ni(1)-N(6)	86.97(2)		

Table 4-5 Crystal Data and Collection Details of [NiTp^{Ph,Me}(Pz^{Ph,Me}H)Cl] (4e)

Emperical formula	$C_{60}H_{56}N_{12}B_2Ni$
Formula weight	1025.48
Crystal system	Monoclinic
Space group	C 2/c
Lattice parameters	
a (Å)	17.926(5)
b (Å)	13.713(4)
c (Å)	21.974(5)
α (°)	90.000
β (°)	111.638(6)
γ (°)	90.000
Cell volume V (Å^3)	5021(2)
Z	4
D_{Calc} (g cm^{-3})	1.354
Data collection	
μ (Mo K_α) (cm^{-1})	0.442
θ_{max} (°)	29.24
Reflections measured	5209
Independent reflections	4918
Number of parameters refined	345
R	0.0780
R_w	0.1960

Table 4-6 Selected Bond Distances (Å) and Bond Angles (°) for $[NiTp^{Ph,Me}(Pz^{Ph,Me}H)Cl]$ (4e)

Bond Distances			
Ni(1)-N(1)	2.1474(19)	Ni(1)-N(4)	2.045(2)
Ni(1)-N(5)	2.0504(19)	Ni(1)-N(7)	2.1249(19)
Ni(1)-Cl(1)	2.3060(7)		
Bond Angles			
N(1)-Ni(1)-N(4)	90.37(8)	N(1)-Ni(1)-N(5)	84.66(7)
N(1)-Ni(1)-N(7)	178.03(7)	N(1)-Ni(1)-Cl(1)	91.10(5)
N(4)-Ni(1)-N(5)	94.24(8)	N(4)-Ni(1)-N(7)	90.63(8)
N(4)-Ni(1)-Cl(1)	119.73(6)	N(5)-Ni(1)-N(7)	93.57(7)
N(5)-Ni(1)-Cl(1)	145.83(6)	N(7)-Ni(1)-Cl(1)	89.88(5)

Table 4-7 Optimized membrane compositions and their potentiometric response as benzoate ion-selective electrodes.

Membrane No.	Composition of membrane (mg)				Slope	Linear range (M)
	PVC	Plasticizer	Ionophore 4e	HTAB	mV decade^{-1} (± 0.5)	
1.	150	277 (NPOE)	1	-	32.7	7.9×10^{-4} - 1.0×10^{-1}
2.	150	301 (NPOE)	1	2	48.7	1.5×10^{-4} - 1.0×10^{-1}
3.	150	343 (NPOE)	3	3	52.0	8.7×10^{-6} - 1.0×10^{-1}
4.	150	345 (NPOE)	5	3	59.2	2.2×10^{-6} - 1.0×10^{-1}
5.	150	333 (DBP)	5	3	37.1	1.9×10^{-4} - 1.0×10^{-1}
6.	150	346 (DBP)	5	3	49.2	3.2×10^{-5} - 1.0×10^{-1}
7.	150	310 (BA)	5	3	43.2	8.6×10^{-4} - 1.0×10^{-1}
8.	150	339 (BA)	5	3	48.7	2.5×10^{-5} - 1.0×10^{-1}
9.	150	348 (TBP)	5	3	50.1	7.8×10^{-4} - 1.0×10^{-1}
10.	150	348 (NPOE)	7	3	68.7	8.9×10^{-5} - 1.0×10^{-1}

Table 4-8 Formation constant values for different para-substituted benzoate anions with ionophore 4e.

Anions	Formation constant ($\log \beta_{ILn}$)* ± SD
OBz	5.87 ± 0.2
p-F-OBz	5.63 ± 0.5
p-Cl-OBz	5.41 ± 0.4
p-OMe-OBz	5.34 ± 0.5
p-OH-OBz	5.21 ± 0.4
p-NH_2-OBz	5.06 ± 0.5
p-CH_3-OBz	4.93 ± 0.3
p-NO_2-OBz	4.37 ± 1.2
p-CN-OBz	4.24 ± 0.5
p-CHO-OBz	4.18 ± 0.8

**Mean value ± standard deviation (three measurements)*

Table 4-9 Determination of benzoate in different aqueous samples using complex 4e as membrane sensor

Samples	Calculated by proposed sensor ($mg\ L^{-1}$)	Amount added ($mg\ L^{-1}$)	Recovery (%) (n=3)
Diet Soda	192	10	92.6
Soy Sauce	516	10	94.5
Lemon Juice	482	10	98.5

Table 4-10 Optimized membrane compositions and their potentiometric response as thiocyanate sensors.

Sensor no.	Composition (w / w, %)				Slope ($mV\ decade^{-1}$ of activity)	Linear Range (M)
	Ionophore **4e**	HTAB	Plasticizer	PVC		
1	0	3	64, DBP	33	N.M.	N.M.
2	6	0	62, DBP	32	52.8	7.5×10^{-5} to 1.0×10^{-2}
3	6	3	0	91	47.5	6.3×10^{-4} to 1.0×10^{-2}
4	6	3	60, *o*-NPOE	31	65.3	7.8×10^{-5} to 1.0×10^{-2}
5	6	3	60, AP	31	62.0	5.6×10^{-5} to 1.0×10^{-2}
6	6	3	60, TBP	31	61.4	1.2×10^{-5} to 1.0×10^{-2}
7	6	3	60, DBP	31	60.2	7.9×10^{-7} to 1.0×10^{-2}
8	6	2	60, DBP	32	59.6	7.4×10^{-7} to 1.0×10^{-2}
9	6	1	61, DBP	32	57.8	8.4×10^{-6} to 1.0×10^{-2}
10	6	4	59, DBP	31	62.3	5.7×10^{-6} to 1.0×10^{-2}
11	5	2	61, DBP	32	58.4	3.5×10^{-6} to 1.0×10^{-2}
12	7	2	60, DBP	31	59.2	5.3×10^{-7} to 1.0×10^{-2}
13	8	2	59, DBP	31	59.8	8.2×10^{-7} to 1.0×10^{-2}

Table 4-11 Optimized membrane compositions and their potentiometric response as azide sensors.

Sensor no.	Composition (w / w, %)				Slope (mV decade^{-1} of activity)	Linear Range (M)
	Ionophore **4e**	HTAB	Plasticizer	PVC		
14	0	3	64, DBP	33	N. M.	N. M.
15	6	0	62, DBP	32	62.4	2.4×10^{-4} to 1.0×10^{-2}
16	6	3	0	91	47.8	7.7×10^{-4} to 1.0×10^{-2}
17	6	3	60, *o*-NPOE	31	69.2	6.7×10^{-5} to 1.0×10^{-2}
18	6	3	60, AP	31	67.5	2.8×10^{-5} to 1.0×10^{-2}
19	6	3	60, TBP	31	58.0	9.4×10^{-5} to 1.0×10^{-2}
20	6	3	60, TBP	31	59.0	1.1×10^{-5} to 1.0×10^{-2}
21	6	2	60, TBP	32	57.2	5.2×10^{-5} to 1.0×10^{-2}
22	6	1	61, TBP	32	55.3	5.5×10^{-5} to 1.0×10^{-2}
23	6	4	59, TBP	31	59.3	8.1×10^{-6} to 1.0×10^{-2}
24	5	2	61, TBP	32	58.4	9.8×10^{-6} to 1.0×10^{-2}
25	7	2	60, TBP	31	58.8	8.4×10^{-5} to 1.0×10^{-2}
26	8	2	59, TBP	31	58.9	2.8×10^{-5} to 1.0×10^{-2}

Table 4-12 Formation constant values of various ions selective membrane based on $[Tp^{Ph,Me}Ni(Cl)Pz^{Ph,Me}H]$ 4e ionophore.

Interfering ions	Formation constant ($\log \beta_{ILn}$)* ± SD
N_3^-	6.41 ± 0.3
SCN^-	7.16 ± 0.2
ClO_4^-	3.95 ± 0.2
CN^-	4.62 ± 0.4
NO_2^-	1.65 ± 0.5
NO_3^-	1.84 ± 0.3
OAc^-	2.15 ± 0.2
$H_2PO_4^-$	2.58 ± 1.2
CO_3^{2-}	2.14 ± 0.5
SO_4^{2-}	1.14 ± 0.8
OH^-	2.12 ± 0.2

**Mean value ± standard deviation (three measurements)*

Table 4-13 Determination of thiocyanate in saliva, urine and river water samples.

Thiocyanate amount ($\mu g\ mL^{-1}$)[b]	Samples				
	Saliva (smoker)	Saliva (non -smoker)	Urine (smoker)	Urine (non - smoker)	River water
Proposed thiocyanate sensor	20.2 ± 0.54	5.5 ± 0.40	7.8 ± 0.61	1.8 ± 0.24	0.95
Colorimetric method	20.5 ± 0.54	5.6 ± 0.40	7.5 ± 0.61	1.6 ± 0.24	0.98

[b] *Mean value ± standard deviation (five measurements)*

Table 4-14 Determination of azide in different aqueous samples

Samples	Calculated by proposed sensor ($\mu g\ L^{-1}$)	Amount added ($mg\ L^{-1}$)	Recovery (%) (n=3)	Precision (RSD) (n=3)
Black Tea	140	1	91	5.4
Orange Juice	155	1	87	8.0

Table 4-15 Crystal Data and Collection Details of [NiTp^{Ph,Me}(Pz^{Ph,Me}H)(OBz)] (4f)

Emperical formula	$C_{115}H_{110}N_{16}O_4B_2Ni_2$
Formula weight	1919.19
Crystal system	Triclinic
Space group	$P\bar{1}$
Lattice parameters	
a (Å)	12.4267(9)
b (Å)	12.8452(10)
c (Å)	16.1978(12)
α (°)	76.512(2)
β (°)	84.087(3)
γ (°)	85.361(3)
Cell volume V (Å^3)	2496.5(3)
Z	1
D_{Calc} (g cm^{-3})	1.277
Data collection	
μ (Mo K_α) (cm^{-1})	0.441
θ_{max} (°)	35.67
Reflections measured	23112
Independent reflections	13962
Number of parameters refined	633
R	0.0475
R_w	0.1319

Table 4-16 Selected Bond Distances (Å) and Bond Angles (°) for $[NiTp^{Ph,Me}(Pz^{Ph,Me}H)(OBz)]$ (4f)

Bond Distances			
Ni(1)-N(1)	2.102(2)	Ni(1)-N(2)	2.046(2)
Ni(1)-N(3)	2.045(2)	Ni(1)-N(4)	2.069(2)
Ni(1)-O(1)	1.9934(17)		
Bond Angles			
N(1)-Ni(1)-N(2)	83.68(8)	N(1)-Ni(1)-N(3)	90.35(8)
N(1)-Ni(1)-N(4)	172.16(8)	N(1)-Ni(1)-O(1)	88.59(8)
N(2)-Ni(1)-N(3)	94.83(8)	N(2)-Ni(1)-N(4)	89.56(8)
N(2)-Ni(1)-O(1)	158.65(8)	N(1)-Ni(1)-N(4)	172.19(6)
N(1)-Ni(1)-O(1)	88.59(8)	N(4)-Ni(1)-O(1)	96.38(8)

Table 4-17 Crystal Data and Collection Details of $[NiTp^{Ph,Me}(Pz^{Ph,Me}H)(p\text{-F-OBz})]$ (4g)

Emperical formula	$C_{115}H_{108}N_{16}O_4F_2B_2Ni_2$
Formula weight	1955.17
Crystal system	Triclinic
Space group	$P\bar{1}$
Lattice parameters	
a (Å)	12.4269(9)
b (Å)	12.8270(9)
c (Å)	16.3643(12)
α (°)	76.248(4)
β (°)	83.789(4)
γ (°)	84.482(4)
Cell volume V ($Å^3$)	2512.1(3)
Z	1
D_{Calc} (g cm^{-3})	1.292
Data collection	
μ (Mo K_α) (cm^{-1})	0.441
θ_{max} (°)	25.50
Reflections measured	9357
Independent reflections	6613
Number of parameters refined	648
R	0.0398
R_w	0.1131

Table 4-18 Selected Bond Distances (Å) and Bond Angles (°) for [NiTp^{Ph,Me}(Pz^{Ph,Me}H)(*p*-F-OBz)] (4g)

Bond Distances			
Ni(1)-N(1)	2.098(2)	Ni(1)-N(2)	2.052(2)
Ni(1)-N(3)	2.043(2)	Ni(1)-N(4)	2.068(2)
Ni(1)-O(1)	2.0025(18)		
Bond Angles			
N(1)-Ni(1)-N(2)	84.29(8)	N(1)-Ni(1)-N(3)	90.24(8)
N(1)-Ni(1)-N(4)	172.20(8)	N(1)-Ni(1)-O(1)	88.16(8)
N(2)-Ni(1)-N(3)	95.11(8)	N(2)-Ni(1)-N(4)	88.85(8)
N(2)-Ni(1)-O(1)	158.51(8)	N(3)-Ni(1)-N(4)	94.08(8)
N(3)-Ni(1)-O(1)	105.03(8)	N(4)-Ni(1)-O(1)	96.98(8)

Table 4-19 Crystal Data and Collection Details of $[NiTp^{Ph,Me}(Pz^{Ph,Me}H)(p\text{-Cl-OBz})]$ (4h)

Emperical formula	$C_{54}H_{50}N_8O_2BClNi$
Formula weight	947.97
Crystal system	Triclinic
Space group	$P\bar{1}$
Lattice parameters	
a (Å)	11.2449(9)
b (Å)	14.5984(11)
c (Å)	15.8697(13)
α (°)	116.012(3)
β (°)	94.100(4)
γ (°)	90.265(4)
Cell volume V ($Å^3$)	2333.4(3)
Z	2
D_{Calc} (g cm^{-3})	1.349
Data collection	
μ (Mo K_α) (cm^{-1})	0.525
θ_{max} (°)	25.46
Reflections measured	8408
Independent reflections	5948
Number of parameters refined	617
R	0.0530
R_w	0.1382

Table 4-20 Selected Bond Distances (Å) and Bond Angles (°) for $[NiTp^{Ph,Me}(Pz^{Ph,Me}H)(p\text{-Cl-OBz})]$ (4h)

Bond Distances			
Ni(1)-N(1)	2.112(3)	Ni(1)-N(2)	2.045(3)
Ni(1)-N(3)	2.027(3)	Ni(1)-N(4)	2.063(3)
Ni(1)-O(1)	1.983(2)		
Bond Angles			
N(1)-Ni(1)-N(2)	84.08(12)	N(1)-Ni(1)-N(3)	91.57(12)
N(1)-Ni(1)-N(4)	172.60(12)	N(1)-Ni(1)-O(1)	88.32(11)
N(2)-Ni(1)-N(3)	94.67(12)	N(2)-Ni(1)-N(4)	91.31(12)
N(2)-Ni(1)-O(1)	160.84(11)	N(3)-Ni(1)-N(4)	94.58(12)
N(3)-Ni(1)-O(1)	103.11(11)	N(4)-Ni(1)-O(1)	94.29(11)

Table 4-21 Crystal Data and Collection Details of [NiTp^{Ph,Me}(Pz^{Ph,Me}H)(*p*-Me-OBz)] (4j)

Emperical formula	$C_{74}H_{68}N_{14}O_5B_2Ni$
Formula weight	927.55
Crystal system	Triclinic
Space group	$P\bar{1}$
Lattice parameters	
a (Å)	12.4106(10)
b (Å)	15.2244(13)
c (Å)	15.5054(13)
α (°)	64.385(2)
β (°)	75.449(3)
γ (°)	75.849(3)
Cell volume V (Å^3)	2525.8(4)
Z	2
D_{Calc} (g cm^{-3})	1.220
Data collection	
μ (Mo K_α) (cm^{-1})	0.433
θ_{max} (°)	25.73
Reflections measured	9628
Independent reflections	6352
Number of parameters refined	649
R	0.0657
R_w	0.2041

Table 4-22 Selected Bond Distances (Å) and Bond Angles (°) for $[NiTp^{Ph,Me}(Pz^{Ph,Me}H)(p\text{-Me-OBz})]$ (4j)

Bond Distances			
Ni(1)-N(1)	2.094(4)	Ni(1)-N(2)	2.058(4)
Ni(1)-N(3)	2.041(4)	Ni(1)-N(4)	2.073(4)
Ni(1)-O(1)	2.026(3)		
Bond Angles			
N(1)-Ni(1)-N(2)	84.23(15)	N(1)-Ni(1)-N(3)	89.87(15)
N(1)-Ni(1)-N(4)	172.27(15)	N(1)-Ni(1)-O(1)	89.10(15)
N(2)-Ni(1)-N(3)	94.33(15)	N(2)-Ni(1)-N(4)	88.65(15)
N(2)-Ni(1)-O(1)	157.52(15)	N(3)-Ni(1)-N(4)	93.68(16)
N(3)-Ni(1)-O(1)	107.13(16)	N(4)-Ni(1)-O(1)	96.39(14)

Table 4-23 Crystal Data and Collection Details of $[NiTp^{Ph,Me}(Pz^{Ph,Me}H)(p\text{-CHO-OBz})]$ (4m)

Emperical formula	$C_{117}H_{110}N_{16}O_6B_2Ni_2$
Formula weight	1975.21
Crystal system	Triclinic
Space group	$P\bar{1}$
Lattice parameters	
a (Å)	12.5167(7)
b (Å)	13.0506(7)
c (Å)	16.3573(8)
α (°)	74.497(3)
β (°)	85.790(3)
γ (°)	87.199(4)
Cell volume V ($Å^3$)	2566.6(2)
Z	1
D_{Calc} (g cm^{-3})	1.278
Data collection	
μ (Mo K_α) (cm^{-1})	0.432
θ_{max} (°)	25.66
Reflections measured	9720
Independent reflections	6166
Number of parameters refined	647
R	0.0397
R_w	0.1114

Table 4-24 Selected Bond Distances (Å) and Bond Angles (°) for [NiTp^{Ph,Me}(Pz^{Ph,Me}H)(*p*-CHO-OBz)] (4m)

Bond Distances			
Ni(1)-N(1)	2.032(4)	Ni(1)-N(2)	2.095(4)
Ni(1)-N(3)	2.050(4)	Ni(1)-N(4)	2.065(5)
Ni(1)-O(1)	1.996(4)		
Bond Angles			
N(1)-Ni(1)-N(2)	89.54(18)	N(1)-Ni(1)-N(3)	95.58(19)
N(1)-Ni(1)-N(4)	93.99(19)	N(1)-Ni(1)-O(1)	105.10(17)
N(2)-Ni(1)-N(3)	84.88(18)	N(2)-Ni(1)-N(4)	173.83(16)
N(2)-Ni(1)-O(1)	87.70(17)	N(3)-Ni(1)-N(4)	89.75(18)
N(3)-Ni(1)-O(1)	157.96(16)	N(4)-Ni(1)-O(1)	96.23(18)

Table 4-25 Crystal Data and Collection Details of $[NiTp^{Ph,Me}(Pz^{Ph,Me}H)(p\text{-CN-OBz})]$ (4n)

Emperical formula	$C_{59}H_{55}N_9O_2BNi$
Formula weight	991.62
Crystal system	Monoclinic
Space group	$P\bar{1}$
Lattice parameters	
a (Å)	11.5531(10)
b (Å)	13.9645(14)
c (Å)	15.7561(16)
α (°)	85.863(7)
β (°)	90.00
γ (°)	90.00
Cell volume V ($Å^3$)	2535.4(4)
Z	2
D_{Calc} (g cm^{-3})	1.299
Data collection	
μ (Mo K_α) (cm^{-1})	0.436
θ_{max} (°)	26.50
Reflections measured	10523
Independent reflections	6351
Number of parameters refined	877
R	0.0747
R_w	0.1453

Table 4-26 Selected Bond Distances (Å) and Bond Angles (°) for $[NiTp^{Ph,Me}(Pz^{Ph,Me}H)(CN\text{-}OBz)]$ (4n)

Bond Distances			
Ni(1)-N(1)	2.090(5)	Ni(1)-N(2)	2.050(5)
Ni(1)-N(3)	2.033(5)	Ni(1)-N(4)	2.052(5)
Ni(1)-O(1)	2.009(4)		
Bond Angles			
N(1)-Ni(1)-N(2)	85.78(19)	N(1)-Ni(1)-N(3)	88.64(18)
N(1)-Ni(1)-N(4)	174.3(2)	N(1)-Ni(1)-O(1)	88.78(18)
N(2)-Ni(1)-N(3)	94.5(2)	N(2)-Ni(1)-N(4)	89.6(2)
N(2)-Ni(1)-O(1)	158.48(18)	N(3)-Ni(1)-N(4)	95.05(19)
N(3)-Ni(1)-O(1)	106.17(19)	N(4)-Ni(1)-O(1)	94.32(18)

Table 4-27 Crystal Data and Collection Details of [NiTp^{Ph,Me}(*p*-NH_2-OBz)] (4o)

Emperical formula	$C_{74}H_{68}N_{14}O_5B_2Ni_2$
Formula weight	1372.42
Crystal system	Tetragonal
Space group	I 41/a
Lattice parameters	
a (Å)	34.3925(16)
b (Å)	34.3925(16)
c (Å)	11.4755(12)
α (°)	90.00
β (°)	90.00
γ (°)	90.00
Cell volume V (Å^3)	13573.7(17)
Z	8
D_{Calc} (g cm^{-3})	1.343
Data collection	
μ (Mo K_α) (cm^{-1})	0.618
θ_{max} (°)	25.40
Reflections measured	6240
Independent reflections	4365
Number of parameters refined	436
R	0.0577
R_w	0.1504

Table 4-28 Selected Bond Distances (Å) and Bond Angles (°) for [NiTp^{Ph,Me}(*p*-NH$_2$-OBz)] (4o)

Bond Distances			
Ni(1)-N(1)	2.031(13)	Ni(1)-N(2)	2.014(14)
Ni(1)-N(3)	2.067(14)	Ni(1)-O(1)	2.046(9)
Ni(1)-O(1)	2.077(9)		
Bond Angles			
N(1)-Ni(1)-N(2)	91.2(6)	N(1)-Ni(1)-N(3)	92.2(5)
N(1)-Ni(1)-O(1)	98.6(5)	N(1)-Ni(1)-O(2)	163.5(5)
N(2)-Ni(1)-N(3)	93.1(6)	N(2)-Ni(1)-O(1)	118.6(5)
N(2)-Ni(1)-O(2)	97.5(5)	N(3)-Ni(1)-O(1)	146.0(5)
N(3)-Ni(1)-O(2)	101.3(5)	O(1)-Ni(1)-O(2)	64.9(4)

Table 4-29 Distance (Å) between non-bonded oxygen atom and metal centre

Complexes		(Å)
4f	Ni(1)-O(2)	3.386
4g	Ni(1)-O(2)	3.291
4h	Ni(1)-O(2)	3.503
4j	Ni(1)-O(2)	3.326
4m	Ni(1)-O(2)	3.316
4n	Ni(1)-O(2)	3.578

Table 4-30 Crystal Data and Collection Details of [$Tp^{Ph,Me}Ni(N_3)Pz^{Ph,Me}H$] (4p)

Emperical formula	$C_{82}H_{79}N_{23}B_2Ni_2$
Formula weight	1525.68
Crystal system	Triclinic
Space group	$P\bar{1}$
Lattice parameters	
a (Å)	11.3684(19)
b (Å)	12.344(2)
c (Å)	14.252(2)
α (°)	86.878(10)
β (°)	89.953(10)
γ (°)	72.004(9)
Cell volume V ($Å^3$)	1899.1(5)
Z	1
D_{Calc} (g cm^{-3})	1.334
Data collection	
μ (Mo K_α) (cm^{-1})	0.558
θ_{max} (°)	27.80
Reflections measured	8804
Independent reflections	6509
Number of parameters refined	516
R	0.0496
R_w	0.1227

Table 4-31 Selected Bond Distances (Å) and Bond Angles (°) for $[Tp^{Ph,Me}Ni(N_3)Pz^{Ph,Me}H]$ (4p)

Bond Distances			
Ni(1)-N(1)	2.088(3)	Ni(1)-N(3)	2.013(3)
Ni(1)-N(5)	2.042(3)	Ni(1)-N(7)	2.113(3)
Ni(1)-N(9)	2.005(3)		
Bond Angles			
N(1)-Ni(1)-N(3)	90.74(10)	N(1)-Ni(1)-N(5)	90.43(10)
N(1)-Ni(1)-N(7)	174.19(10)	N(1)-Ni(1)-N(9)	86.00(11)
N(3)-Ni(1)-N(5)	95.38(11)	N(3)-Ni(1)-N(7)	90.08(10)
N(3)-Ni(1)-N(9)	116.34(12)	N(5)-Ni(1)-N(7)	83.77(10)
N(5)-Ni(1)-N(9)	148.09(12)	N(7)-Ni(1)-N(9)	98.77(11)

Table 4-32 Crystal Data and Collection Details of [$Tp^{Ph,Me}Ni(SCN)Pz^{Ph,Me}H$] (4q)

Emperical formula	$C_{41}H_{38}N_9BSNi$
Formula weight	758.37
Crystal system	Triclinic
Space group	$P\bar{1}$
Lattice parameters	
a (Å)	11.707(4)
b (Å)	11.806(4)
c (Å)	15.481(6)
α (°)	83.07(2)
β (°)	80.76(2)
γ (°)	64.931(19)
Cell volume V ($Å^3$)	1909.7(12)
Z	2
D_{Calc} (g cm^{-3})	1.319
Data collection	
μ (Mo K_α) (cm^{-1})	0.605
θ_{max} (°)	25.55
Reflections measured	7141
Independent reflections	4046
Number of parameters refined	490
R	0.0758
R_w	0.1793

Table 4-33 Selected Bond Distances (Å) and Bond Angles (°) for $[Tp^{Ph,Me}Ni(SCN)Pz^{Ph,Me}H]$ (4q)

Bond Distances			
Ni(1)-N(1)	2.122(8)	Ni(1)-N(3)	2.030(9)
Ni(1)-N(5)	2.032(9)	Ni(1)-N(8)	2.101(9)
Ni(1)-N(11)	2.007(13)		
Bond Angles			
N(1)-Ni(1)-N(3)	89.4(3)	N(1)-Ni(1)-N(5)	87.0(4)
N(1)-Ni(1)-N(8)	176.8(3)	N(1)-Ni(1)-N(11)	92.1(4)
N(3)-Ni(1)-N(5)	95.8(4)	N(3)-Ni(1)-N(8)	92.6(4)
N(3)-Ni(1)-N(11)	118.4(5)	N(5)-Ni(1)-N(8)	90.4(4)
N(5)-Ni(1)-N(11)	145.8(5)	N(8)-Ni(1)-N(11)	89.2(4)

Table 4-34 Non-covalent interactions present in complexes

Complexes	D-H	H···A	D···A	D-H···A
[NiTp^{Ph,Me}(Pz^{Ph,Me}H)(OBz)] (4f)				
C(18)-H(18)···O(2)	0.93	2.630(4)	3.412(6)	142
C(46)-H(46)···π (pz^{Ph,Me} of Tp^{Ph,Me})	0.93	2.973(2)	3.573(5)	124
C(45)-H(45)···π (pz^{Ph,Me} of Tp^{Ph,Me})	0.93	2.833(5)	3.554(7)	135
C(52)-H(52)···π (pz^{Ph,Me} of Tp^{Ph,Me})	0.93	2.811(4)	3.585(5)	141
C(33)-H(33)···π (Toluene)	0.93	2.710(3)	3.623(5)	167
[NiTp^{Ph,Me}(Pz^{Ph,Me}H)(*p*-F-OBz)] (4g)				
C(8)-H(8)···O(2)	0.93	2.703(5)	3.494(8)	143
C(46)-H(46)···π (pz^{Ph,Me} of Tp^{Ph,Me})	0.93	2.865(4)	3.566(7)	133
C(45)-F(1)···π (pz^{Ph,Me} of Tp^{Ph,Me})	1.36	3.292(8)	3.993(9)	111
C(51)-H(51)···π (pz^{Ph,Me} of Tp^{Ph,Me})	0.93	2.803(4)	3.558(7)	143
C(3)-H(3)···π (Toluene)	0.93	2.773(5)	3.688(5)	168
[NiTp^{Ph,Me}(Pz^{Ph,Me}H)(*p*-Cl-OBz)] (4h)				
C(1)-H(1C)···π(Ph of Cl-OBz)	0.96	2.956(7)	3.582(8)	124
C(7)-H(7)···π(Ph of Tp^{Ph,Me})	0.93	3.032(6)	3.525(7)	115
C(13)-H(13)···π(Ph of Tp^{Ph,Me})	0.93	2.976(5)	3.812(8)	150
[NiTp^{Ph,Me}(Pz^{Ph,Me}H)(*p*-Me-OBz)] (4j)				
C(47)-H(47C)···π(pz^{Ph,Me} of Tp^{Ph,Me})	0.96	2.781(6)	3.399(10)	123
C(47)-H(47B)···π(pz^{Ph,Me} of Tp^{Ph,Me})	0.96	2.712(5)	3.644(8)	164
C(28)-H(28)··· O(2)	0.93	2.670(6)	3.448(10)	142
[NiTp^{Ph,Me}(Pz^{Ph,Me}H)(*p*-CHO-OBz)] (4m)				
C(28)-H(28)···O(2)	0.93	2.658(5)	3.425(10)	140
C(7)-H(7)···O(3)	0.93	2.679(6)	3.366(10)	131
C(48)-H(48)···π(pz^{Ph,Me} of Tp^{Ph,Me})	0.93	2.708(6)	3.400(9)	132
C(48)-H(48)···π(pz^{Ph,Me} of Tp^{Ph,Me})	0.93	2.944(4)	3.602(9)	129
C(50)-H(50)···π(pz^{Ph,Me} of Tp^{Ph,Me})	0.93	2.686(4)	3.474(5)	143
C(23)-H(23)···π(Toluene)	0.93	2.835(4)	3.755(9)	170

[NiTp^{Ph,Me}(Pz^{Ph,Me}H)(CN-OBz)] (4n)				
C(1)-H(1A)···π(pz^{Ph,Me} of Tp^{Ph,Me})	0.96	3.069(8)	3.564(12)	114
C(44)-H(44)···π(pz^{Ph,Me} of Tp^{Ph,Me})	0.93	2.975(3)	3.479(9)	116
[NiTp^{Ph,Me}(*p*-NH$_2$-OBz)] (4o)				
N(7)-H(7A)···π(Ph of NH$_2$-OBz)	0.86	2.602(0)	3.356(10)	147
N(7)-H(7B)···π(pz^{Ph,Me} of Tp^{Ph,Me})	0.86	2.807(0)	3.621(9)	159
C(17)-H(17)··· O(2)	0.93	2.533(10)	3.209(23)	130
C(1)-H(1C)···π(pz^{Ph,Me} of Tp^{Ph,Me})	0.96	3.001(0)	3.753(14)	136
C(35)-H(35)···π(pz^{Ph,Me} of Tp^{Ph,Me})	0.93	3.057(0)	3.779(20)	136
[Tp^{Ph,Me}Ni(N$_3$)Pz^{Ph,Me}H] (4p)				
C(19)-H(19)···π(Ph of Pz^{Ph,Me}H)	0.93	2.822(12)	3.519(15)	133
C(11)-H(11C)···π(Ph of Pz^{Ph,Me}H)	0.96	2.829(11)	3.502(15)	128
C(33)-H(33)···π(pz^{Ph,Me} of Tp^{Ph,Me})	0.96	2.889(18)	3.698(20)	146
C(18)-H(18)···N(11)	0.93	2.822(16)	3.567(21)	138
[Tp^{Ph,Me}Ni(SCN)Pz^{Ph,Me}H] (4q)				
C(17)-H(17)···π(Ph of Tp^{Ph,Me})	0.93	2.976(20)	3.795(35)	148
C(3)-H(3)···π(Ph of Pz^{Ph,Me}H)	0.93	2.998(31)	3.776(50)	142
C(13)-H(13)···π(Ph of Pz^{Ph,Me}H)	0.93	2.788(23)	3.550(3)	140
C(1)-H(1A)···π(Ph of Pz^{Ph,Me}H)	0.93	3.022(31)	3.810(42)	140

Table 4-35 Crystal Data and Collection Details of $Ni(tm^{t\text{-}Bu})_2Cl_2$ (4r)

Emperical formula	$C_{14}H_{24}N_4S_2Cl_2Ni$
Formula weight	442.10
Crystal system	Monoclinic
Space group	C2/c
Lattice parameters	
a (Å)	16.949(2)
b (Å)	8.6647(10)
c (Å)	15.461(3)
α (°)	90
β (°)	117.662(4)
γ (°)	90.00
Cell volume V ($Å^3$)	2011.1(5)
Z	4
D_{Calc} (g cm^{-3})	1.460
Data collection	
μ (Mo K_α) (cm^{-1})	1.441
θ_{max} (°)	37.31
Reflections measured	23809
Independent reflections	5212
Number of parameters refined	112
R	0.0293
R_w	0.0523

Table 4-36 Selected Bond Distances (Å) and Bond Angles (°) for $Ni(tm^{t\text{-}Bu})_2Cl_2$ (4r)

Bond Distances			
Ni(1)-Cl(2)	2.2485(5)	Ni(1)-S(1)	2.2898(3)
Ni(1)-Cl(2')	2.2486(4)	Ni(1)-S(1')	2.2898(3)
Bond Angles			
Cl(2)-Ni(1)-Cl(2')	135.422(17)	Cl(2)-Ni(1)-S(1')	108.820(11)
Cl(2)-Ni(1)-S(1)	96.817(12)	Cl(2')-Ni(1)-S(1)	108.816(11)
Cl(2')-Ni(1)-S(1')	96.819(12)	S(1)-Ni(1)-S(1')	108.856(17)
Cl(2)-Ni(1)-Cl(2')	135.422(17)	Cl(2)-Ni(1)-S(1')	108.820(11)
Cl(2)-Ni(1)-S(1)	96.817(12)	Cl(2')-Ni(1)-S(1)	108.816(11)

Table 4-37 Crystal Data and Collection Details of $Ni(pz^{Ph,Me})_2(tm^{t\text{-}Bu})(NO_3)_2$ (4s)

Emperical formula	$C_{27}H_{32}N_8O_6SNi$
Formula weight	655.37
Crystal system	Triclinic
Space group	P-1
Lattice parameters	
a (Å)	9.9775(7)
b (Å)	11.2254(8)
c (Å)	14.8068(10)
α (°)	75.401(4)
β (°)	87.422(4)
γ (°)	74.874(4)
Cell volume V ($Å^3$)	1548.86(19)
Z	2
D_{Calc} (g cm^{-3})	1.405
Data collection	
μ (Mo K_α) (cm^{-1})	0.746
θ_{max} (°)	33.24
Reflections measured	30449
Independent reflections	11894
Number of parameters refined	393
R	0.0416
R_w	0.1125

Table 4-38 Selected Bond Distances (Å) and Bond Angles (°) for $Ni(pz^{Ph,Me})_2(tm^{t\text{-}Bu})(NO_3)_2$ (4s)

Bond Distances			
Ni(1)-N(1)	2.0180(16)	Ni(1)-N(2)	2.0637(16)
Ni(1)-O(1)	2.1449(14)	Ni(1)-O(2)	2.1069(15)
Ni(1)-O(3)	2.1327(15)	Ni(1)-S(1)	2.3930(5)
Bond Angles			
N(1)-Ni(1)-N(2)	94.73(7)	N(1)-Ni(1)-O(1)	89.01(6)
N(1)-Ni(1)-O(2)	99.10(6)	N(1)-Ni(1)-O(3)	160.15(6)
N(1)-Ni(1)-S(1)	101.37(5)	N(2)-Ni(1)-O(1)	173.82(6)
N(2)-Ni(1)-O(2)	88.50(6)	N(2)-Ni(1)-O(3)	88.36(6)
N(2)-Ni(1)-S(1)	92.33(5)	O(1)-Ni(1)-O(2)	86.05(6)
O(1)-Ni(1)-O(3)	86.47(6)	O(2)-Ni(1)-O(3)	61.33(6)
O(1)-Ni(1)-S(1)	91.74(4)	O(2)-Ni(1)-S(1)	159.37(4)
O(3)-Ni(1)-S(1)	98.09(4)		

Table 4-39 Non-covalent interactions present in complexes

Complexes	D-H	H···A	D···A	D-H···A
$Ni(tm^{t\text{-}Bu})_2Cl_2$ (4r)				
N(2)-H(11)···Cl(2)	0.86	2.507(4)	3.316	156
C(3)-H(3)···Cl(2)	0.93	2.804(2)	3.424(4)	125
C(6)-H(6C)···π ($tm^{t\text{-}Bu}$)	0.96	2.952(2)	7.734(3)	104
$Ni(pz^{Ph,Me})_2(tm^{t\text{-}Bu})(NO_3)_2$ (4s)				
N(3)-H(2) ··· O(4)	0.86	1.994(4)	2.824	162
N(8)-H(24) ··· O(1)	0.86	1.954(6)	2.740	151
N(4)-H(4) ··· S(1)	0.86	2.606(4)	3.149	122
C(1)-H(1B)··· O(6)	0.96	2.328(4)	3.236(4)	158
C(26)-H(26C)··· O(1)	0.96	2.551(4)	3.235(7)	128
C(28)-H(28C)··· O(5)	0.96	2.625(3)	3.576(4)	171
C(28)-H(28B)··· O(5)	0.96	2.667(5)	3.601(6)	164
C(30)-H(23)··· O(3)	0.93	2.688(8)	3.316(9)	126
C(17)-H(17)··· O(4)	0.93	2.666(5)	3.483(8)	147
C(17)-H(17)··· O(2)	0.93	2.524(3)	3.236(5)	134
C(19)-H(19)··· O(6)	0.93	2.574(4)	3.363(6)	143
C(28)-H(28A)···π (pz of $pz^{Ph,Me}$)	0.96	2.846(6)	3.770(8)	162
C(13)-H(13)···π (Ph of $pz^{Ph,Me}$)	0.93	2.823(6)	3.681(7)	154
C(6)-H(6)···π (Ph of $pz^{Ph,Me}$)	0.93	2.968(5)	3.776(7)	146

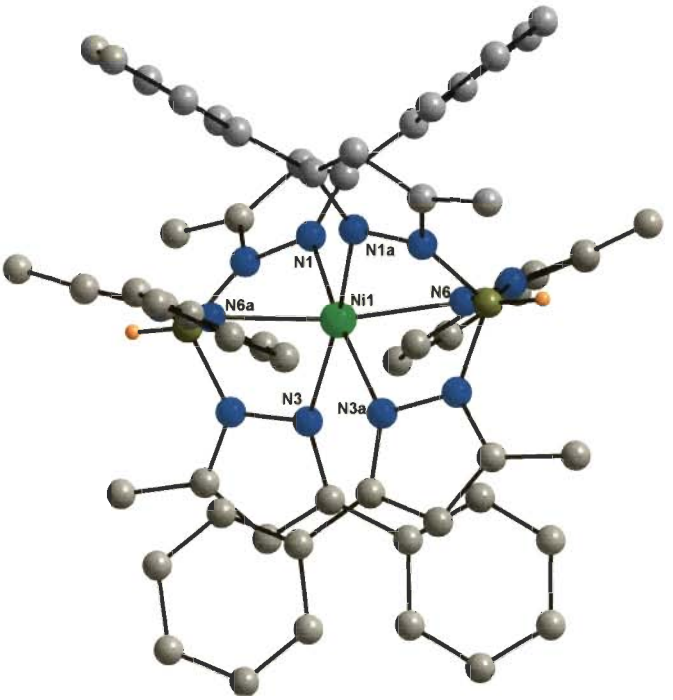

Fig. 4-27 Crystal structure of $[(Tp^{Ph,Me})_2Ni]$ **4c**

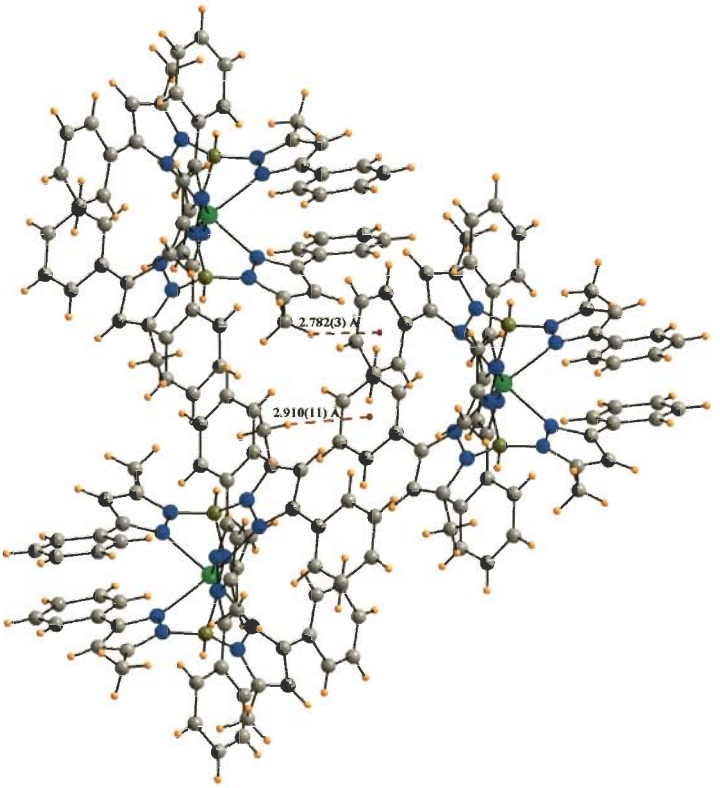

Fig. 4-28 Intermolecular $CH_3\cdots\pi$ interactions in complex $[(Tp^{Ph,Me})_2Ni]$ **4c**

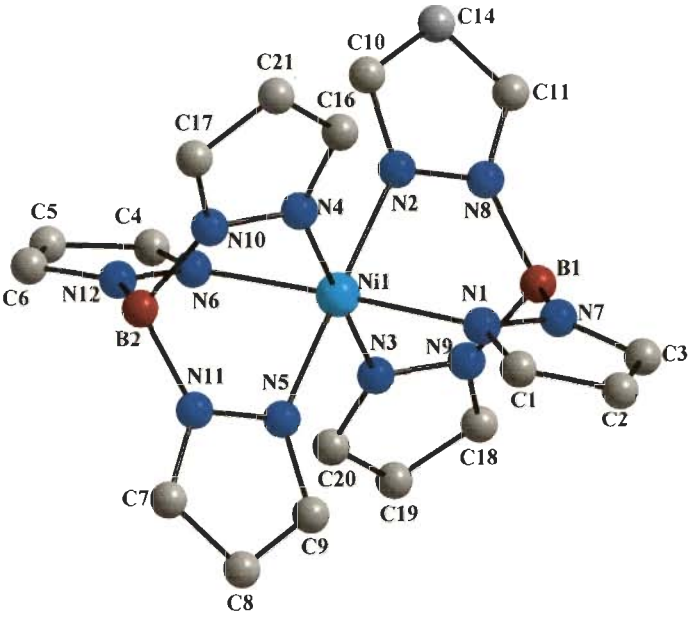

Fig. 4-29 Crystal structure of $[(Tp)_2Ni]$ **4d**

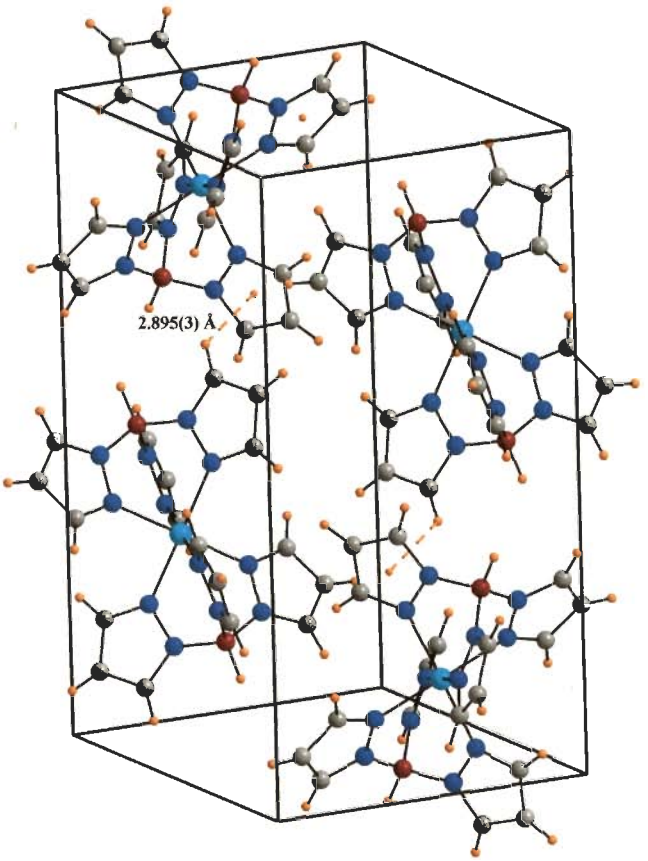

Fig. 4-30 Intermolecular CH···π interactions in complex **4d**

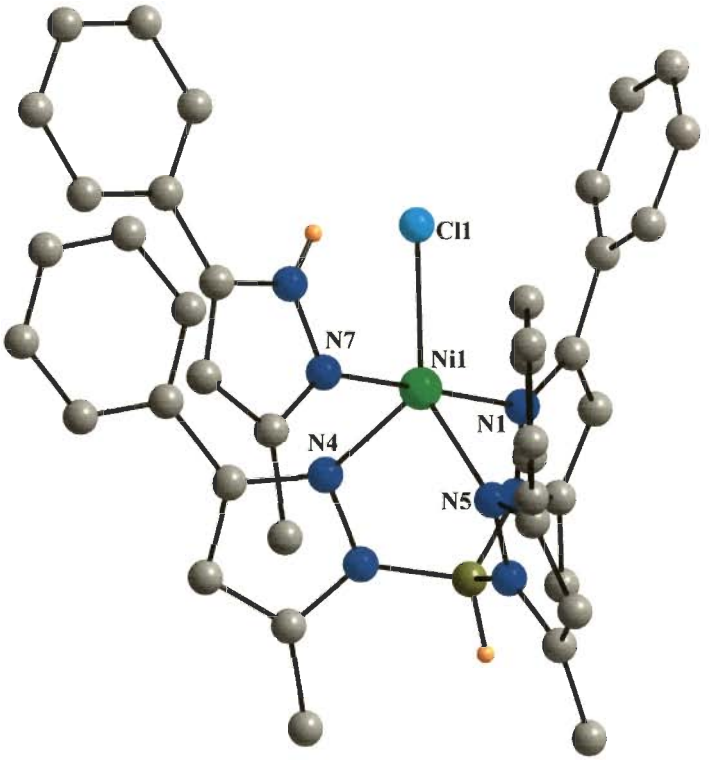

Fig. 4-31 Crystal structure of $[Tp^{Ph,Me}Ni(Cl)Pz^{Ph,Me}H]$ **4e**

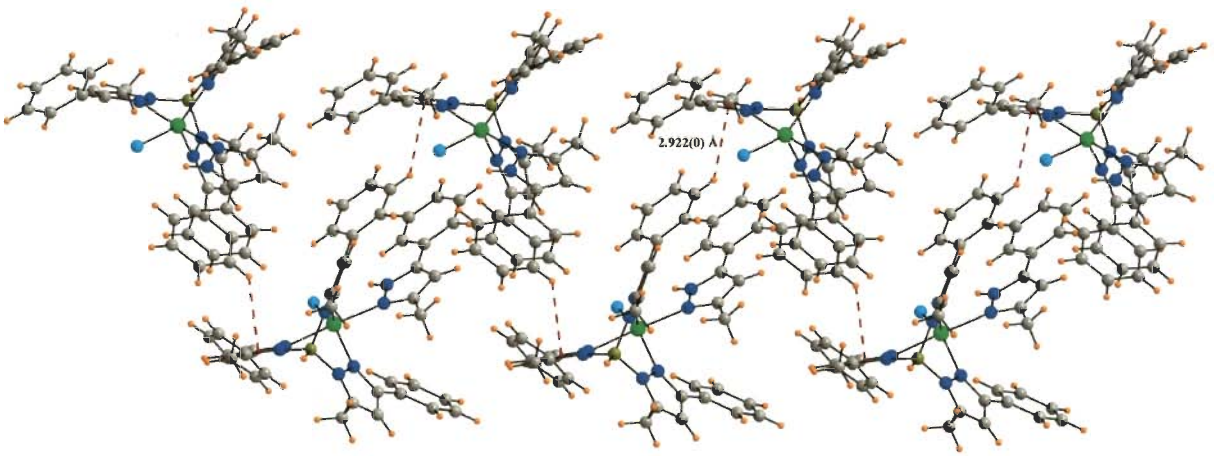

Fig. 4-32 One dimensional zig-zag chain of complex **4e** due to C-H···π interactions.

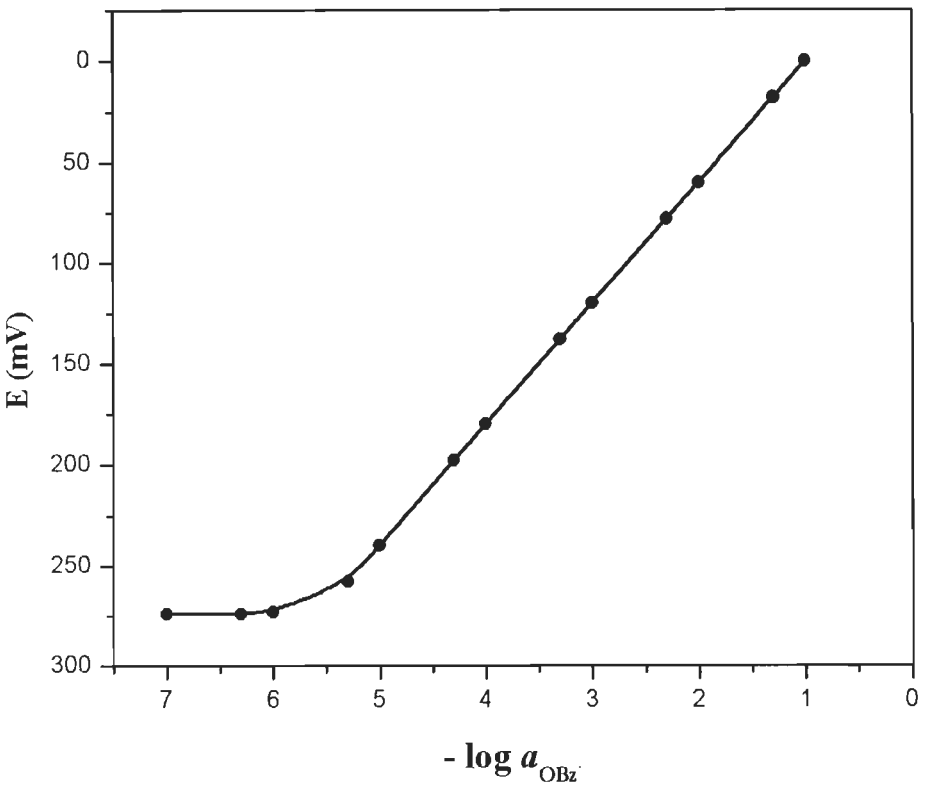

Fig. 4-33 Calibration plot for the proposed benzoate ion selective sensor

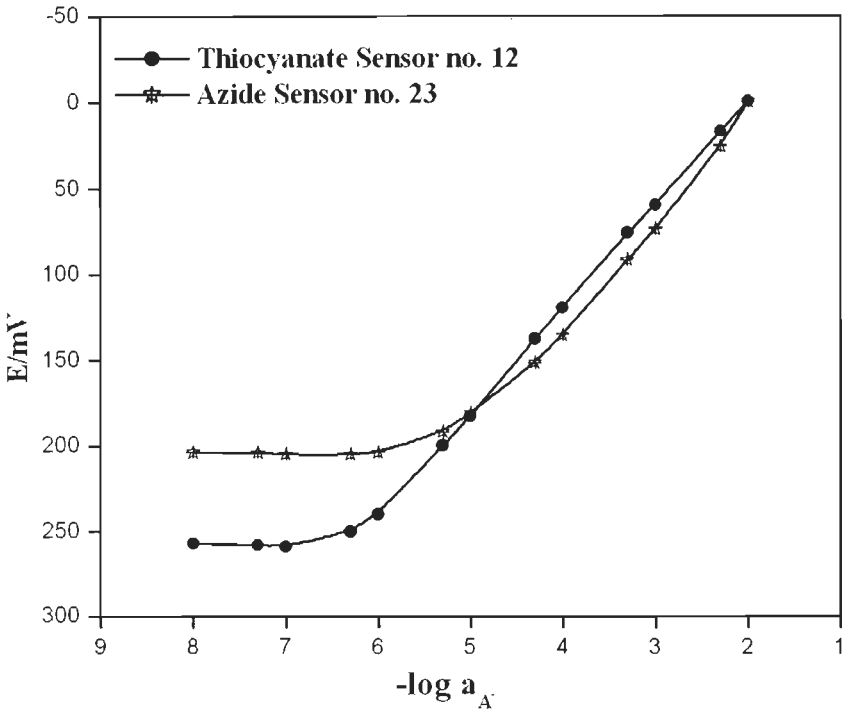

Fig. 4-34 Calibration plots for the proposed thiocyanate and azide ion selective sensors.

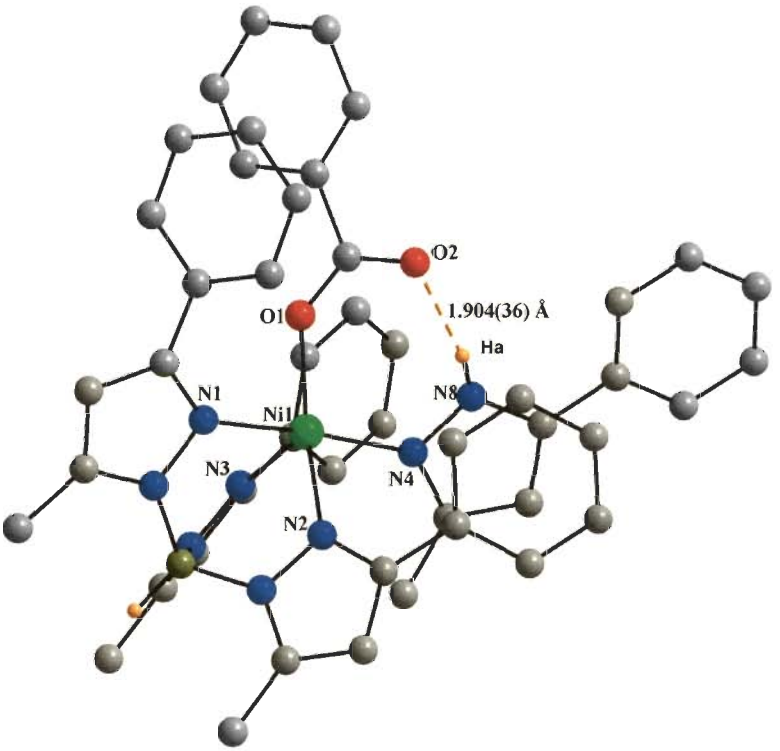

Fig. 4-35 Crystal structure of [$Tp^{Ph,Me}$Ni(OBz)$Pz^{Ph,Me}$H] **4f**

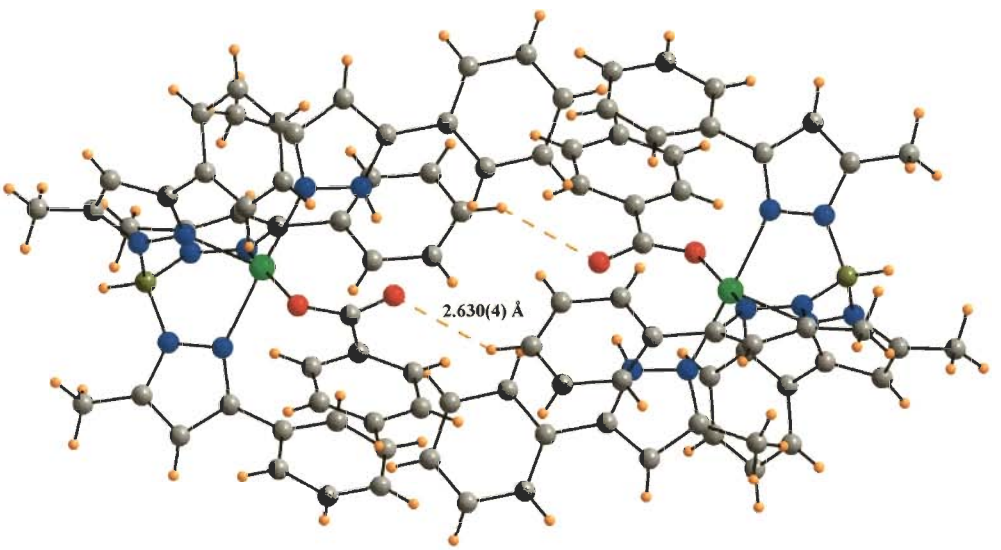

Fig. 4-36 Intermolecular interaction of complex [$Tp^{Ph,Me}$Ni(OBz)$Pz^{Ph,Me}$H] **4f** showing C-H···O interactions.

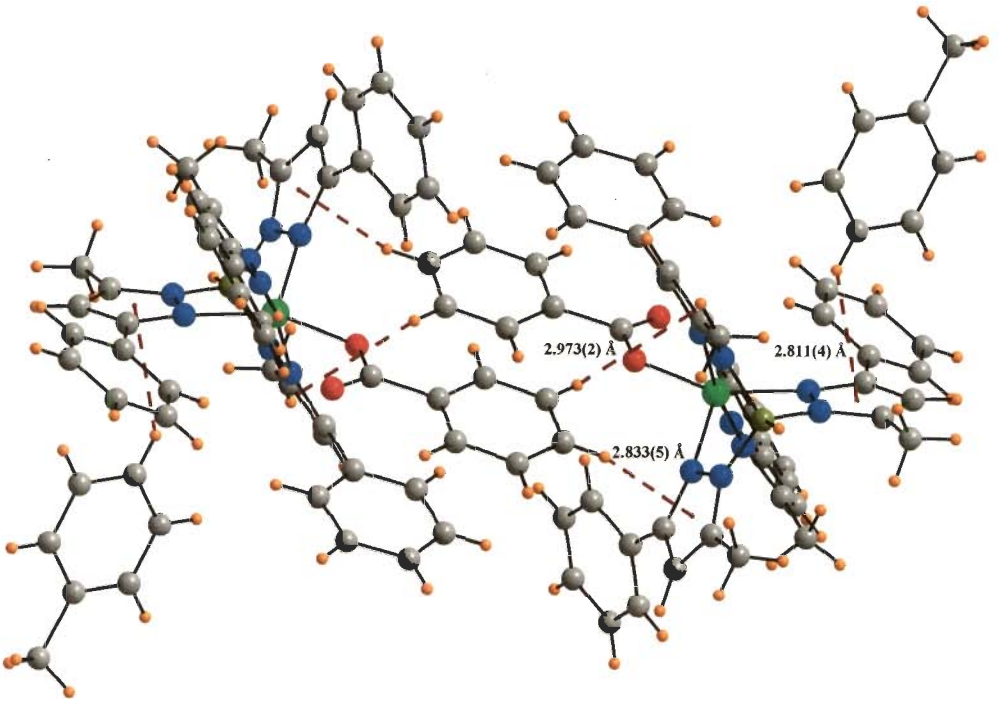

Fig. 4-37 Intermolecular C-H···π interactions present in complex **4f**

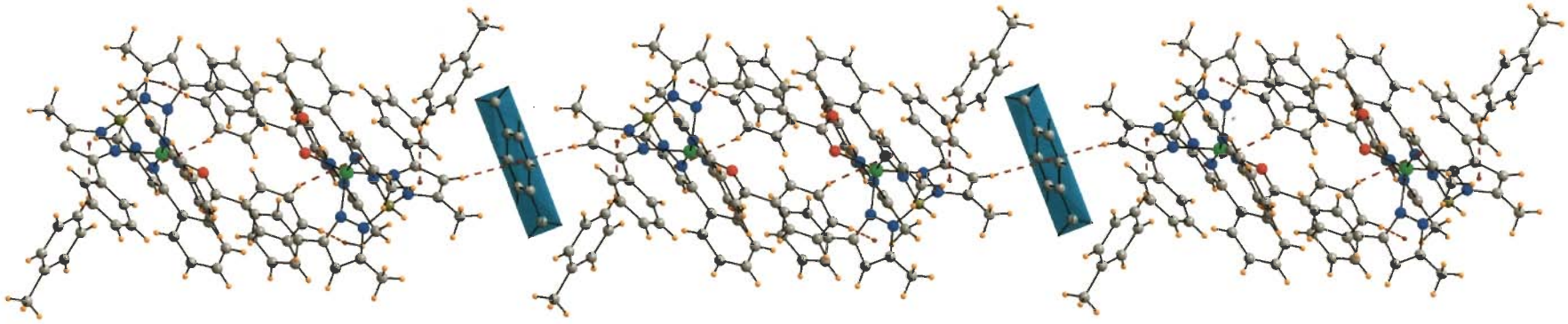

Fig. 4-38 One dimensional chain in complex **4f** formed by toluene molecule through C-H···π (brown dotted) interactions. Color code: C, grey; H, orange; N, blue; O, red; B, sea green; Ni, green.

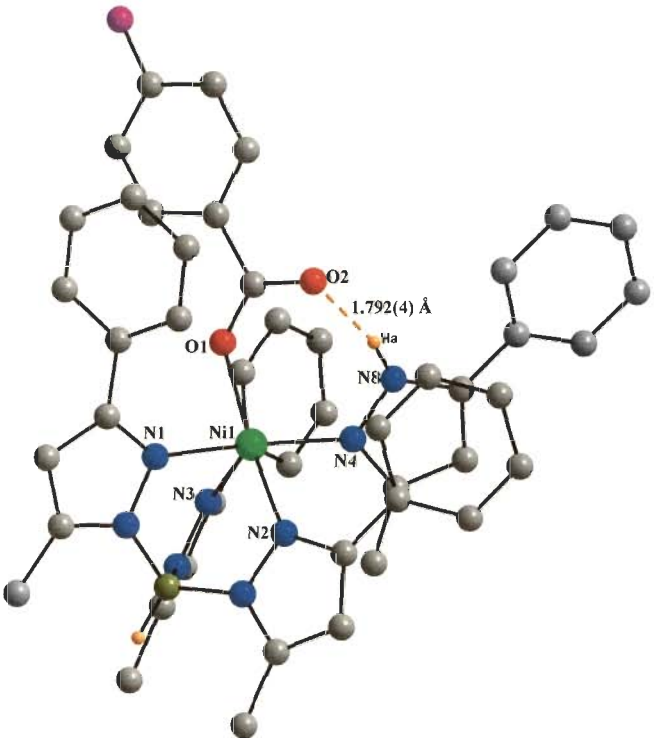

Fig. 4-39 Crystal structure of [$Tp^{Ph,Me}$Ni(*p*-F-OBz)$Pz^{Ph,Me}$H] **4g**

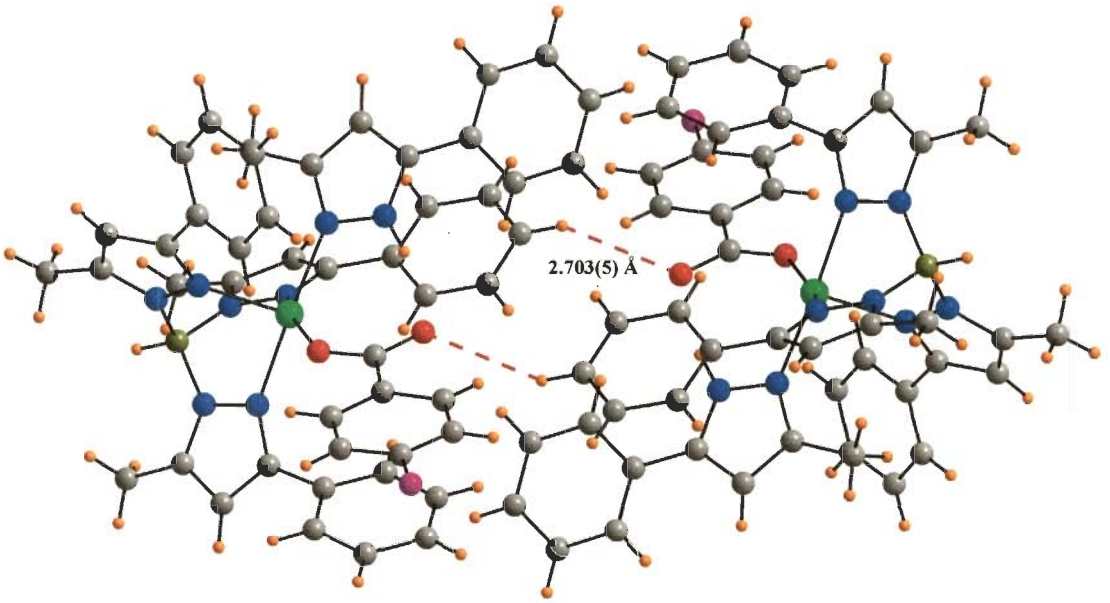

Fig. 4-40 Intermolecular C-H···O interactions present in complex **4g**

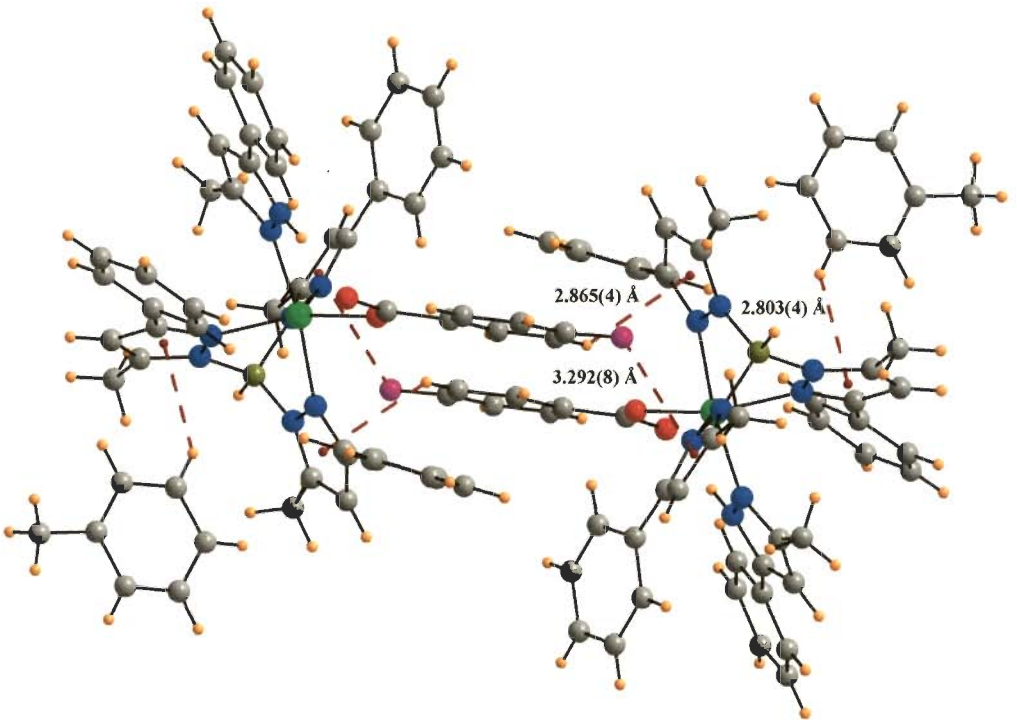

Fig. 4-41 Intermolecular C-H··· π and C-F···π interactions present in complex **4g**

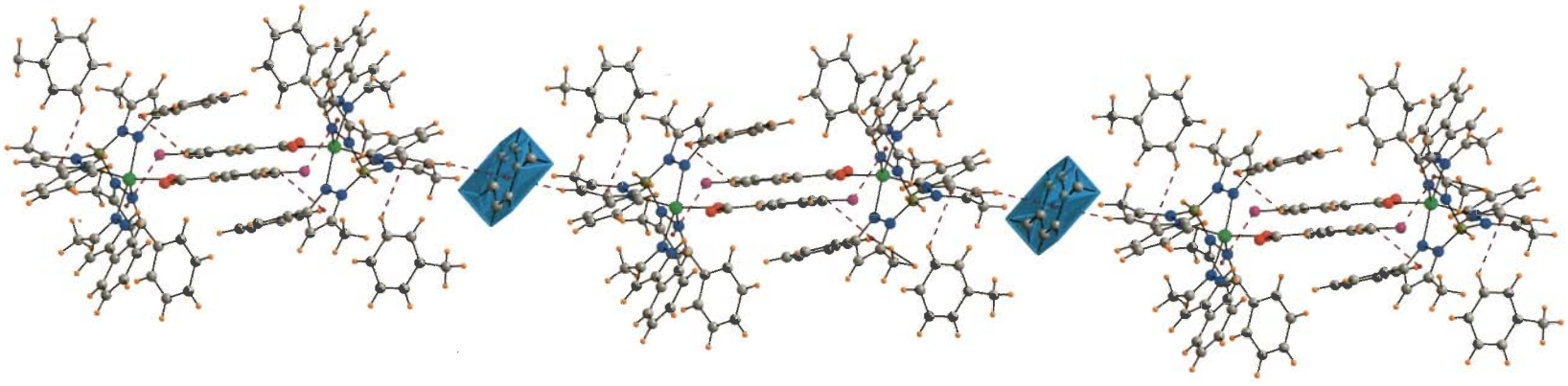

Fig. 4-42 One dimensional chain in complex **4g** formed by toluene molecule through C-H···π interactions. Color code: C, grey; H, orange; N, blue; O, red; B, sea green; F, purple; Ni, green.

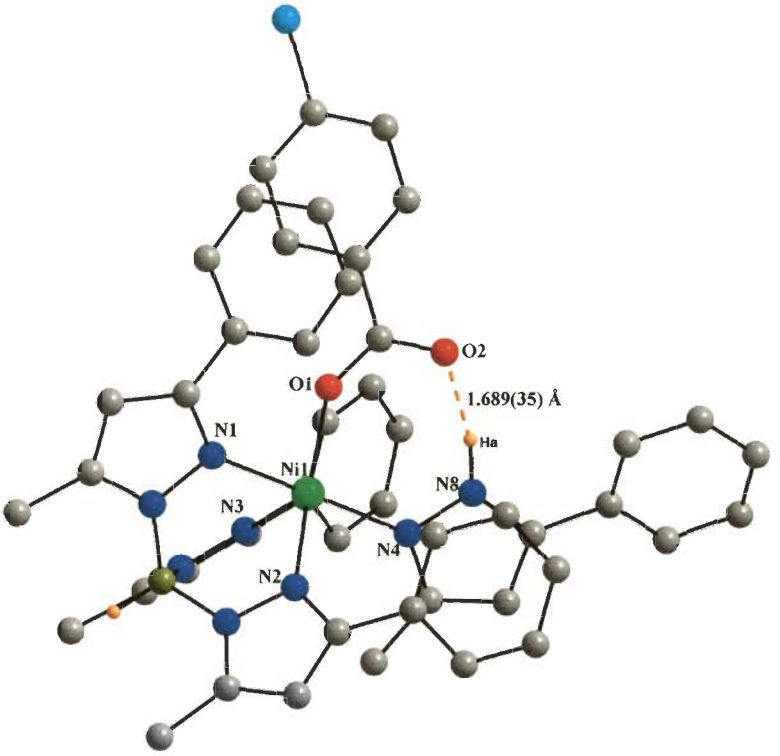

Fig. 4-43 Crystal structure of [$Tp^{Ph,Me}$Ni(*p*-Cl-OBz)$Pz^{Ph,Me}$H] **4h**

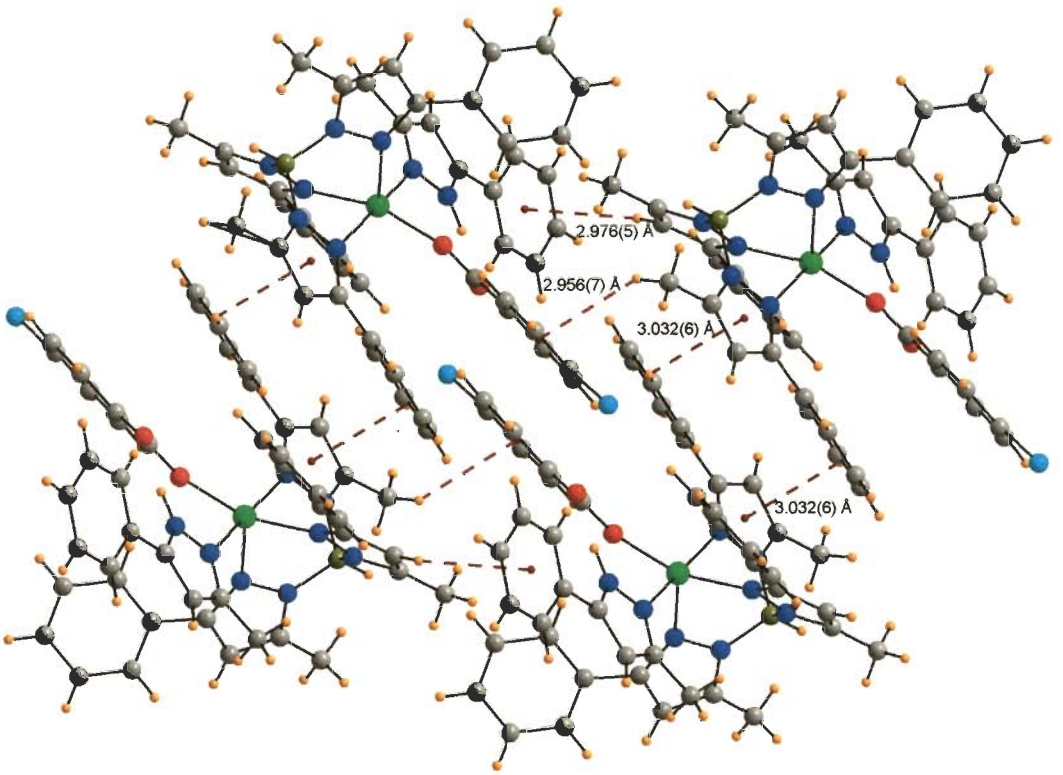

Fig.4-44 Intermolecular $CH_3\cdots\pi$ and C-H$\cdots\pi$ interactions present in complex **4h**

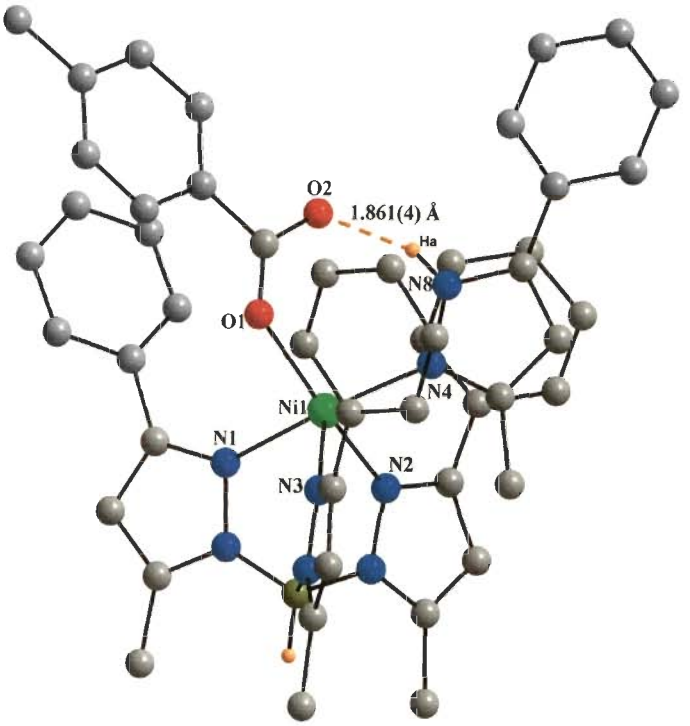

Fig. 4-45 Crystal structure of [$Tp^{Ph,Me}$Ni(*p*-CH_3-OBz)$Pz^{Ph,Me}$H] **4j**

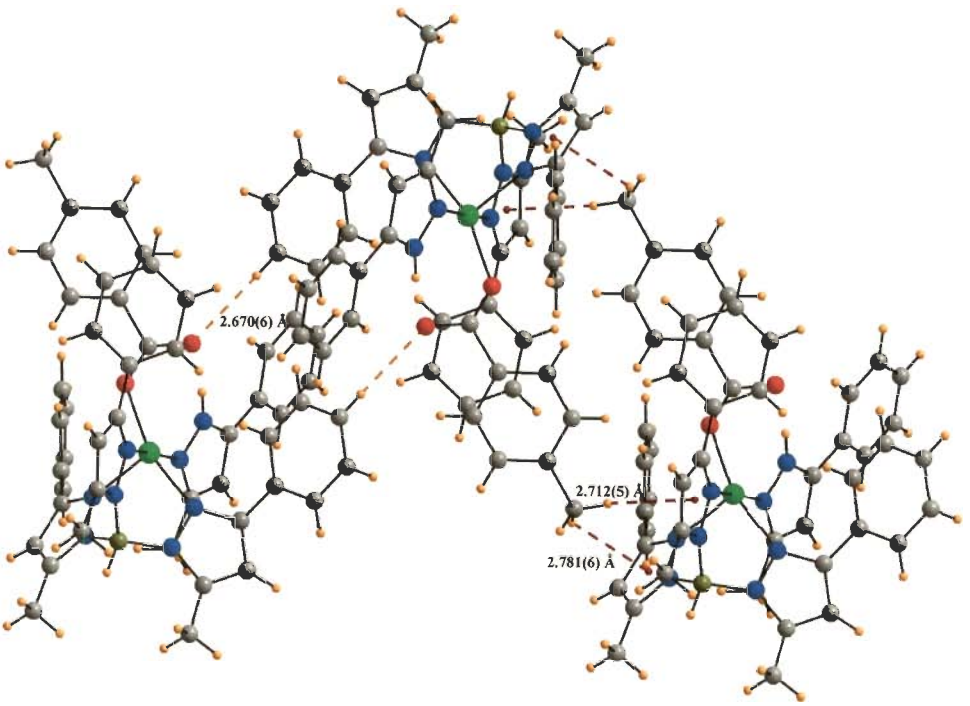

Fig. 4-46 Intermolecular C-H···O and CH_3···π interactions present in complex **4j**

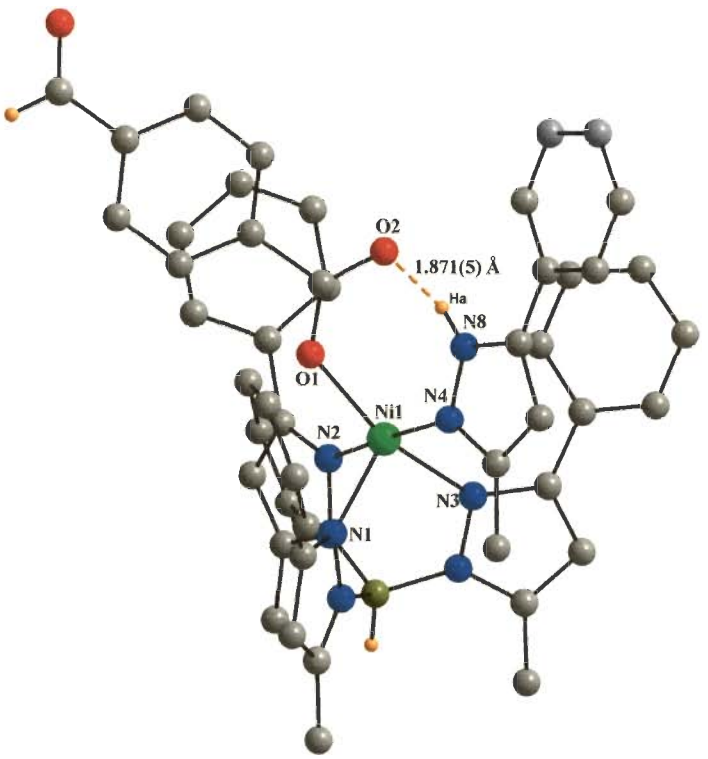

Fig. 4-47 Crystal structure of [$Tp^{Ph,Me}$Ni(*p*-CHO-OBz)$Pz^{Ph,Me}$H] **4m**

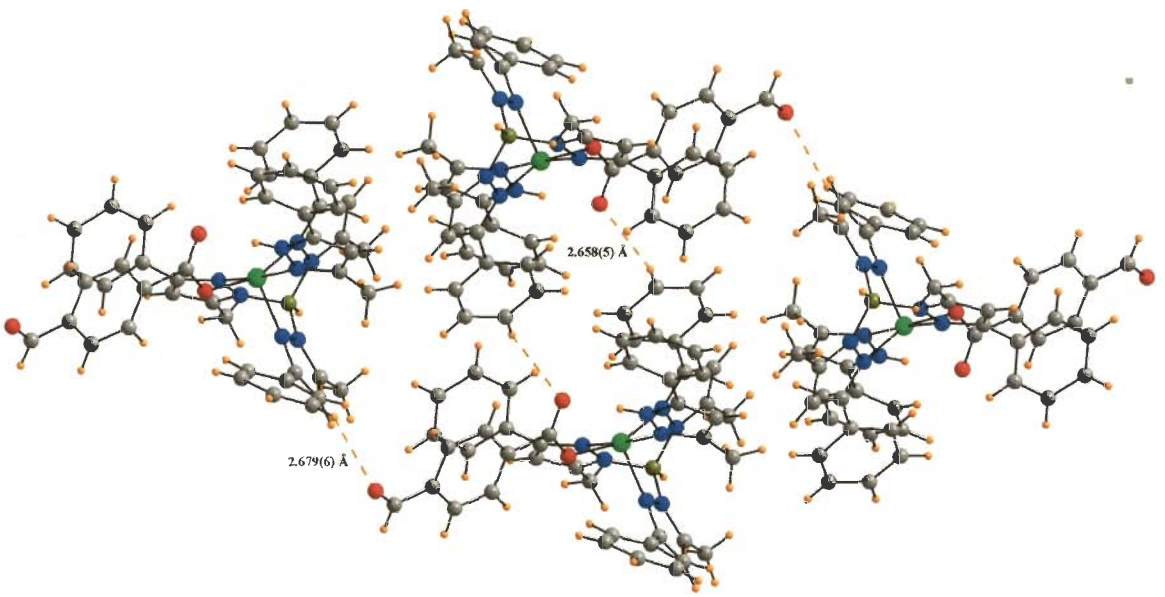

Fig. 4-48 Intermolecular C-H···O interactions present in complex **4m**

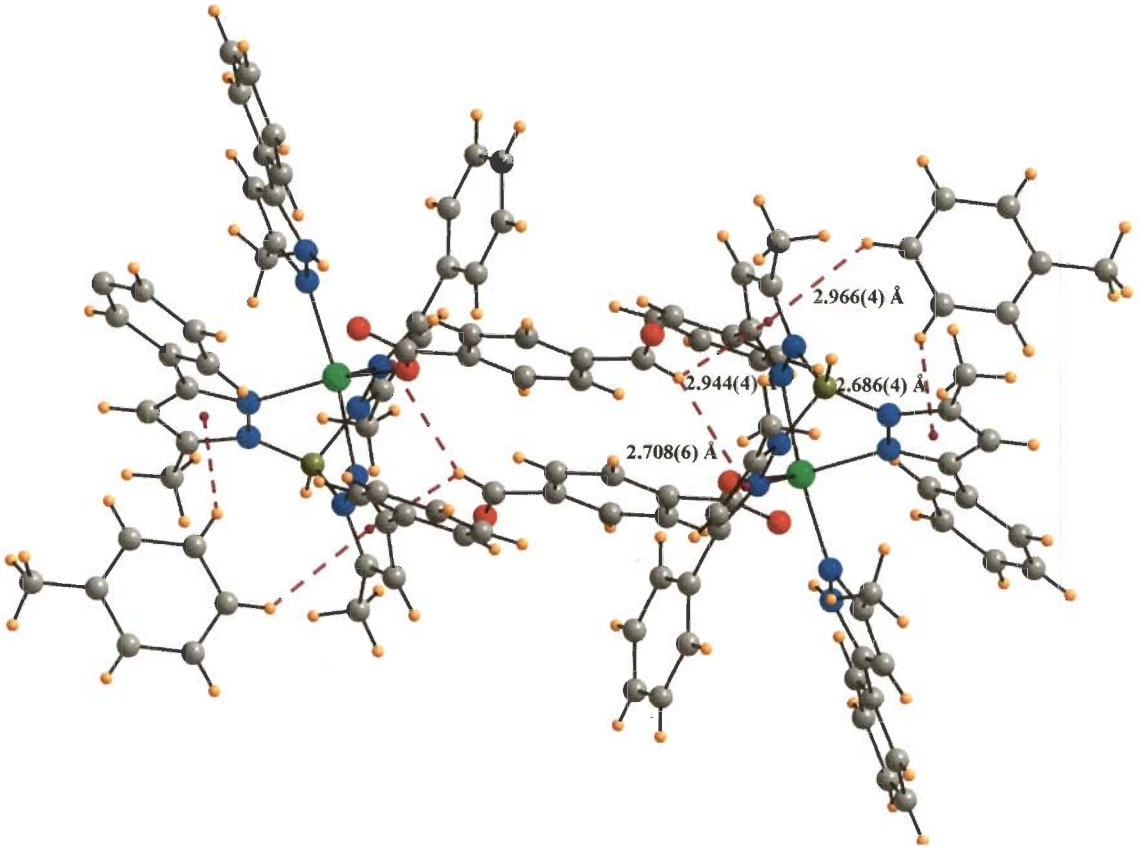

Fig. 4-49 Intermolecular C-H···π interactions present in complex **4m**

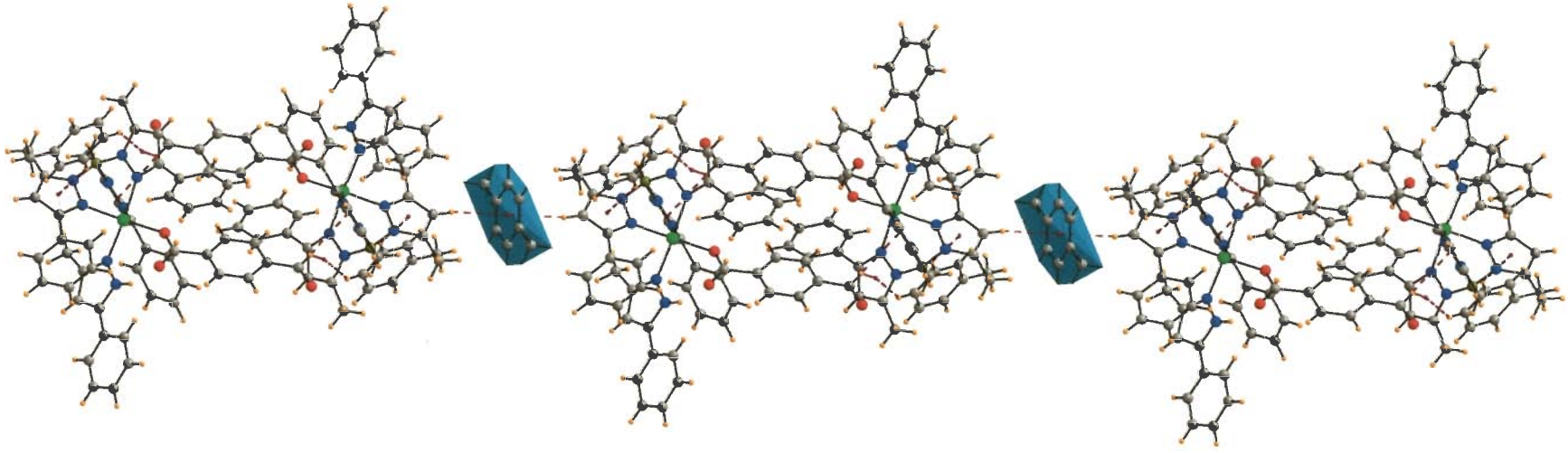

Fig. 4-50 One dimensional chain in complex **4m** formed by toluene molecule through C-H···π interactions. Color code: C, grey; H, orange; N, blue; O, red; B, sea green; Ni, green.

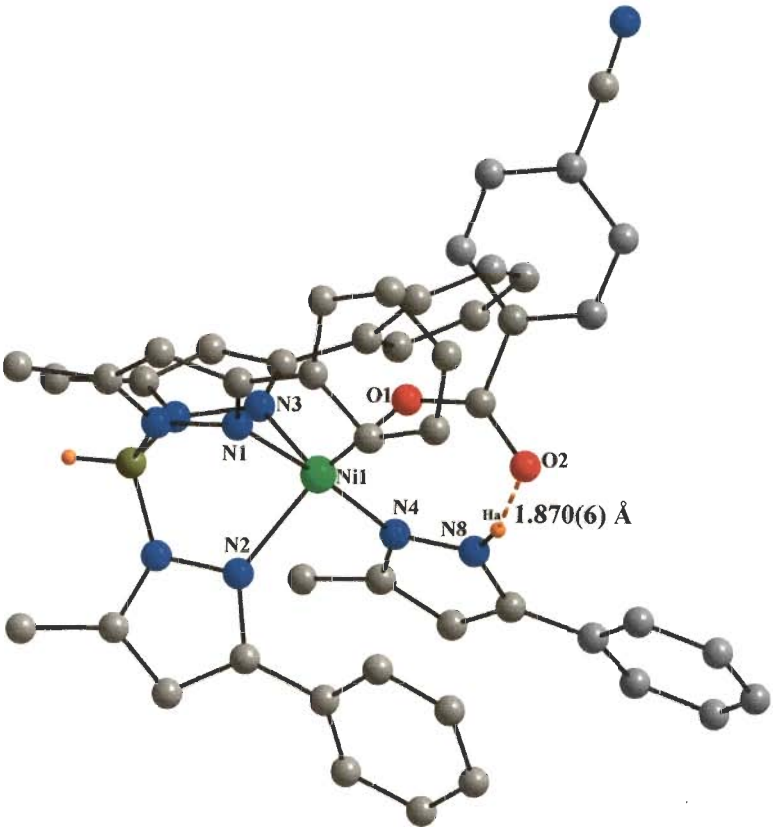

Fig. 4-51 Crystal structure of [$Tp^{Ph,Me}$Ni(*p*-CN-OBz)$Pz^{Ph,Me}$H] **4n**

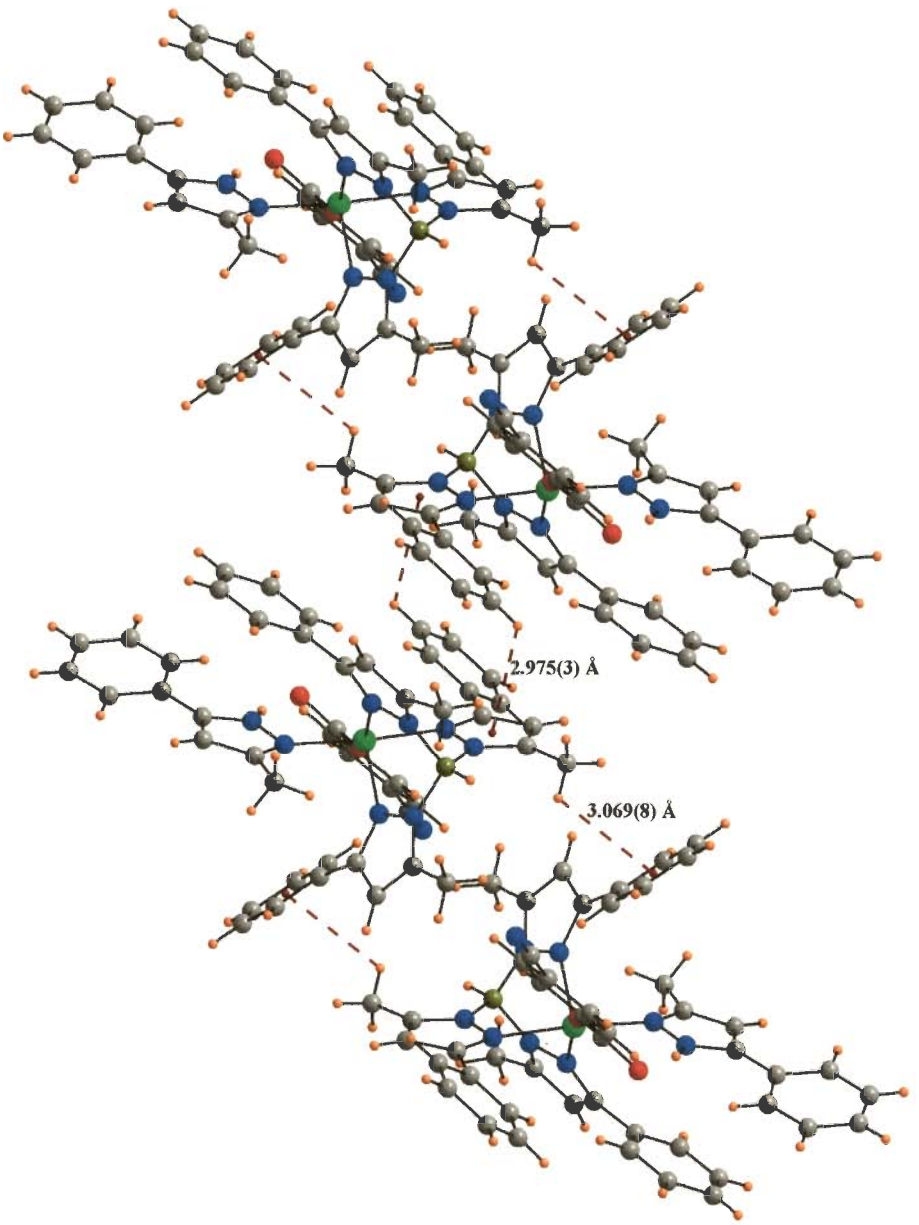

Fig. 4-52 One-dimensional chain in complex **4n** formed by C-H··· π interactions.

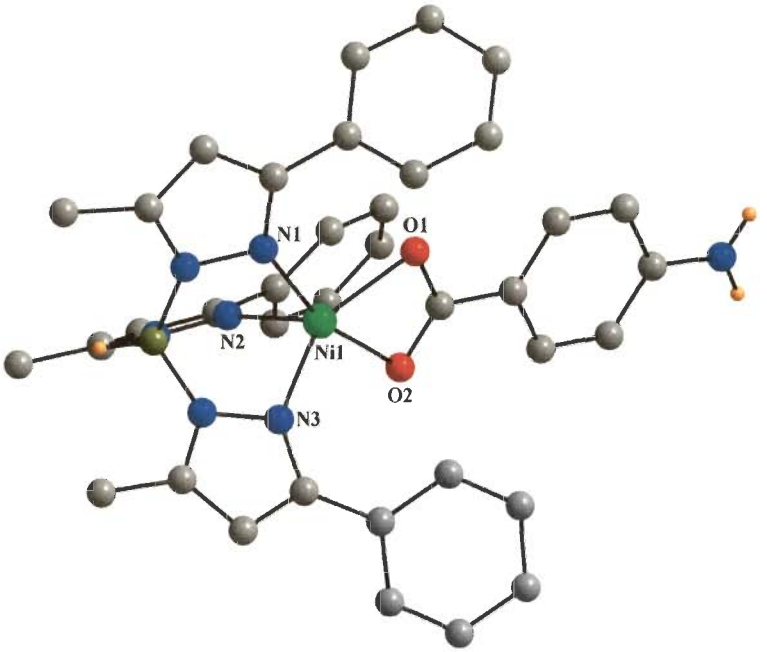

Fig. 4-53 Crystal structure of [$Tp^{Ph,Me}$Ni(*p*-NH_2-OBz)] **4o**

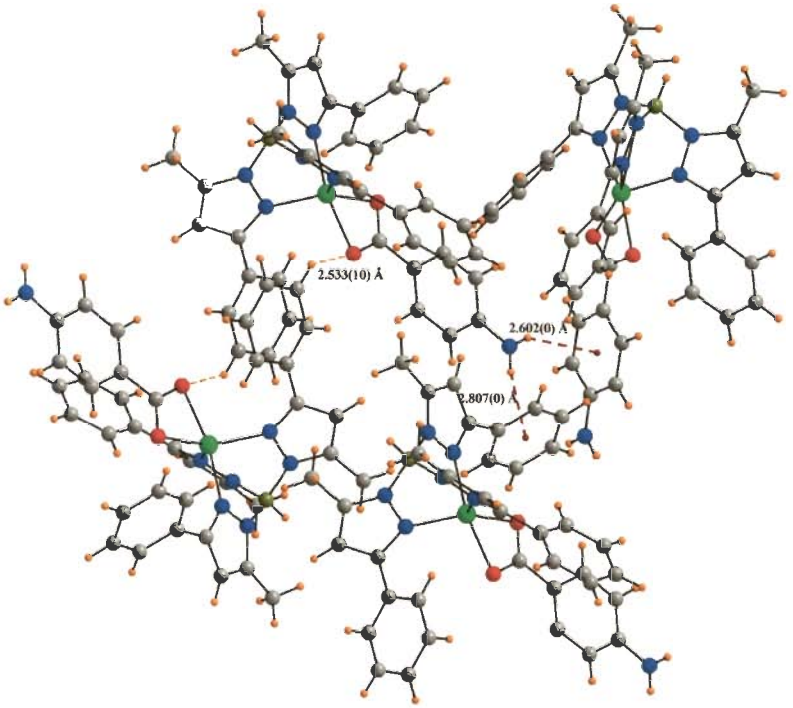

Fig. 4-54 Intermolecular C-H···O and N-H···π interactions present in complex **4o**

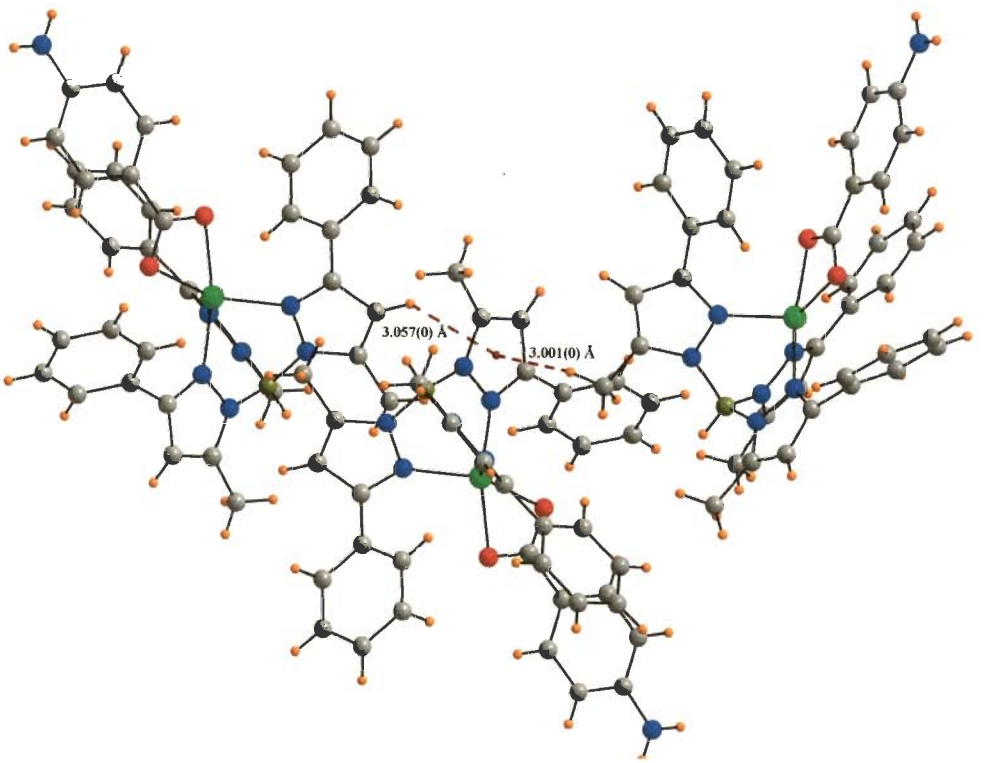

Fig. 4-55 Intermolecular $CH_3\cdots\pi$ and C-H$\cdots\pi$ interactions present in complex **4o**

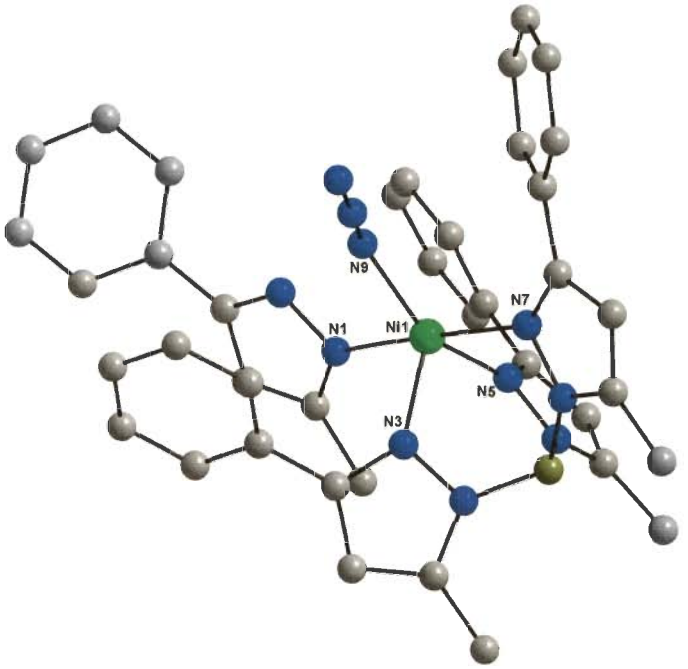

Fig. 4-56 Crystal structure of [$Tp^{Ph,Me}Ni(N_3)Pz^{Ph,Me}H$] **4p**

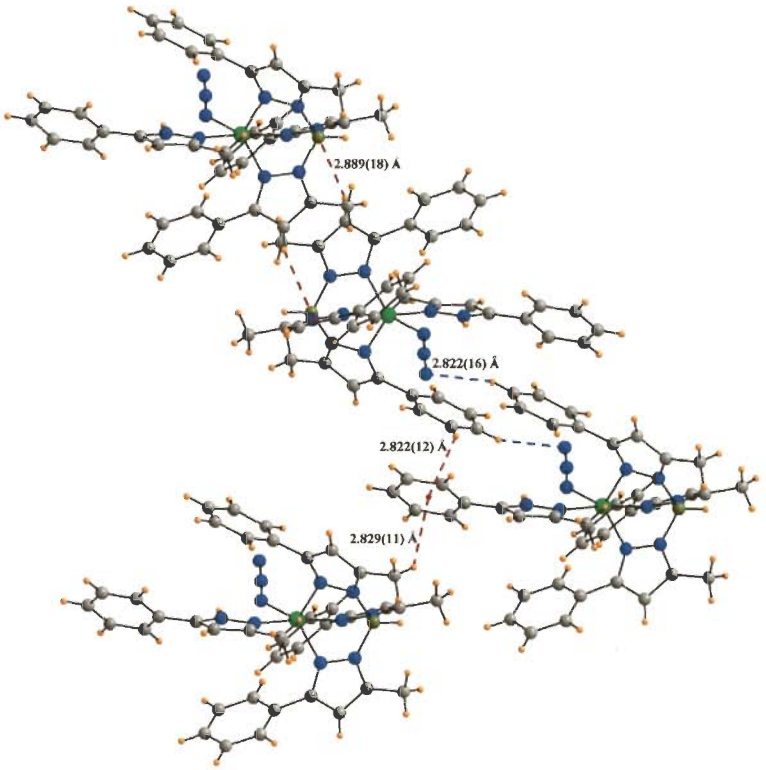

Fig. 4-57 Intermolecular C-H···N and C-H···π interactions present in complex **4p**

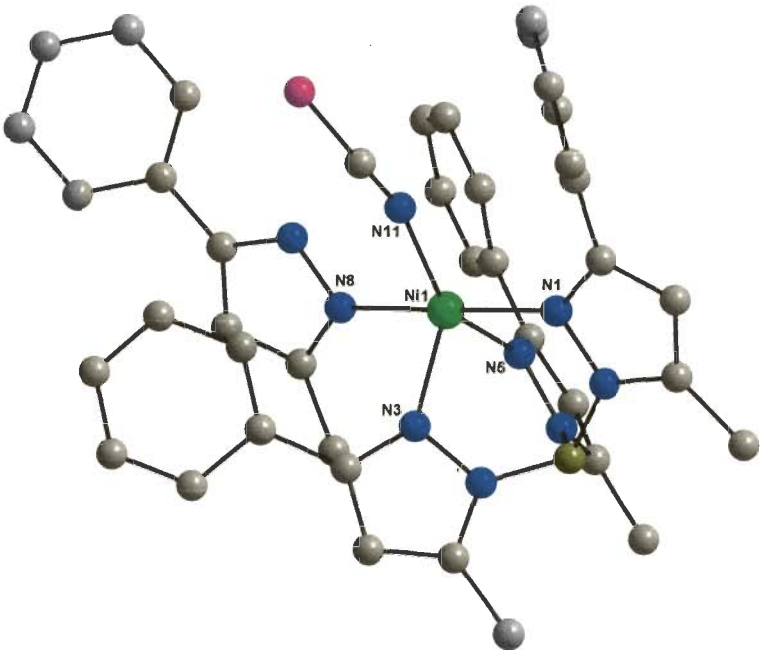

Fig. 4-58 Crystal structure of [$Tp^{Ph,Me}$Ni(NCS)$Pz^{Ph,Me}$H] **4q**

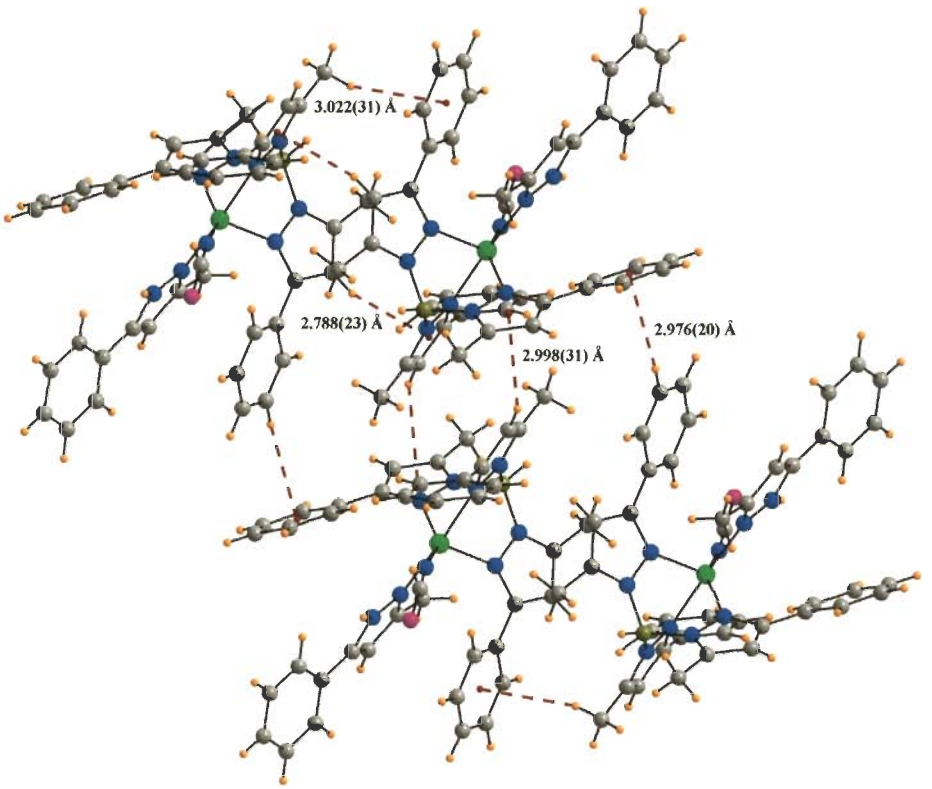

Fig. 4-59 Intermolecular C-H···π interactions present in complex **4q**

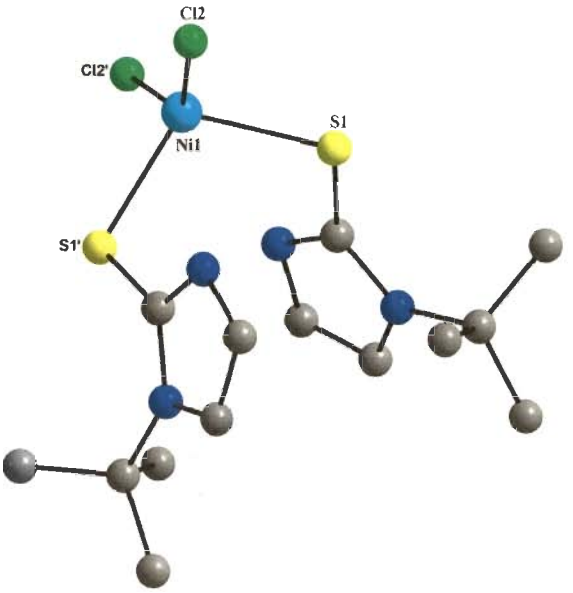

Fig. 4-60 Crystal structure of $Ni(tm^{t\text{-}Bu})_2Cl_2$ **4r**

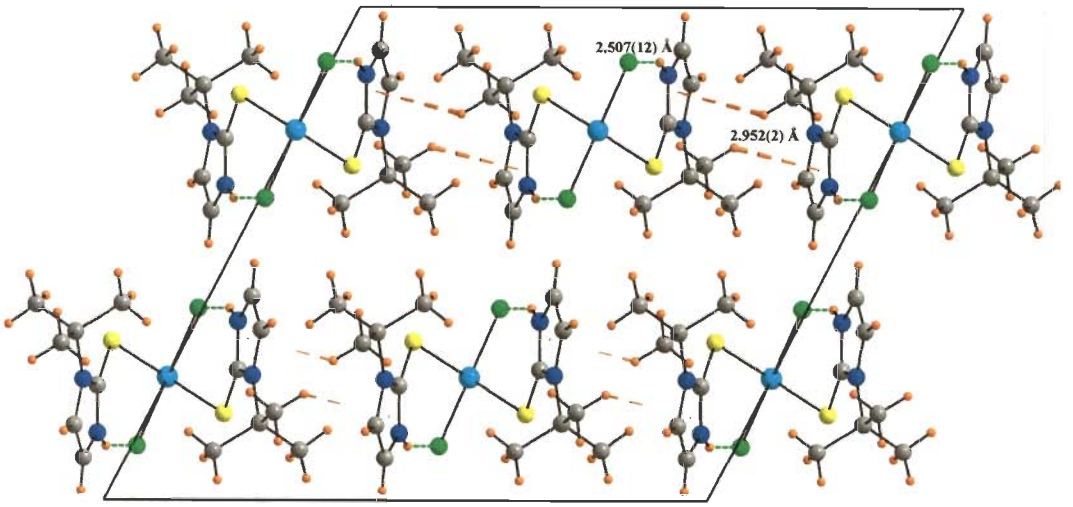

Fig. 4-61 Non-covalent interaction in complex **4r** showing $CH_3\cdots$ π and intramolecular N-H…Cl interactions in unit cell packing

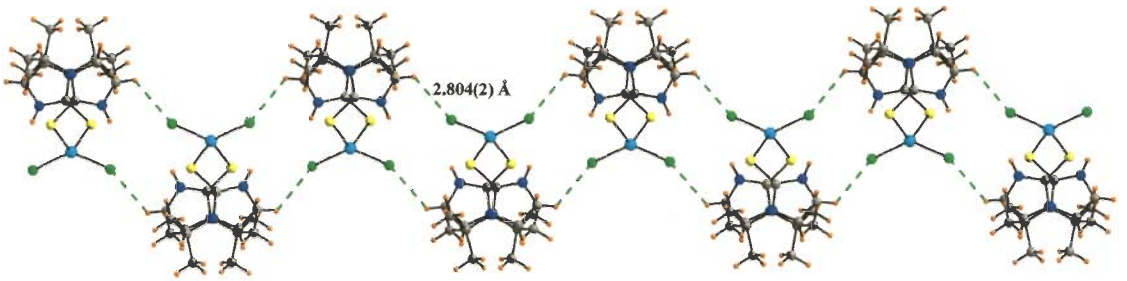

Fig. 4-62 Zig-zag chain formation in complex **4r** due to C-H···Cl interactions.

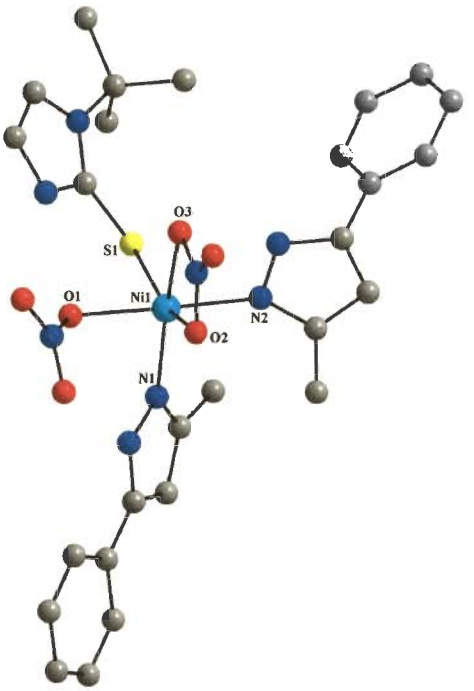

Fig. 4-63 Crystal structure of $[(tm^{t\text{-}Bu})Ni(Pz^{Ph,Me}H)_2(NO_3)_2]$ 4s

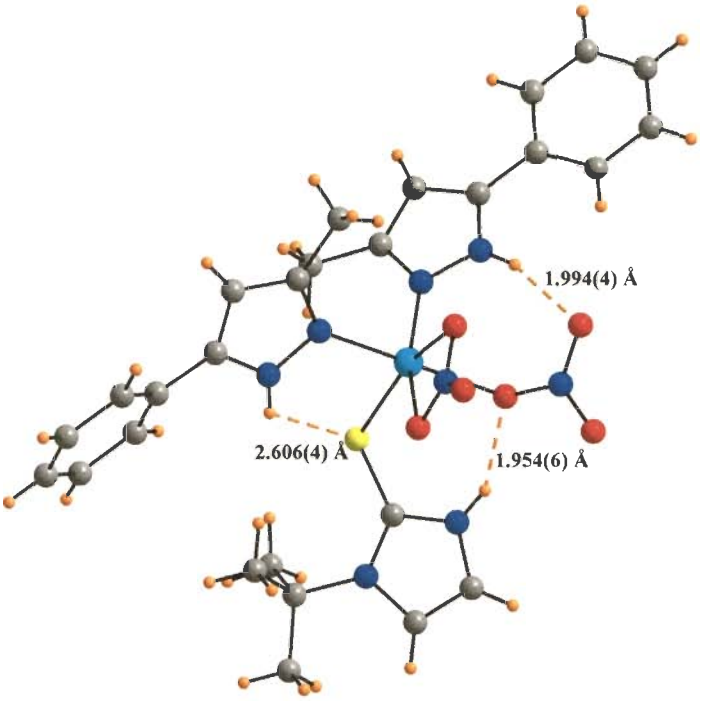

Fig. 4-64 Intramolecular N-H···O and N-H···S interactions present in complex **4s**

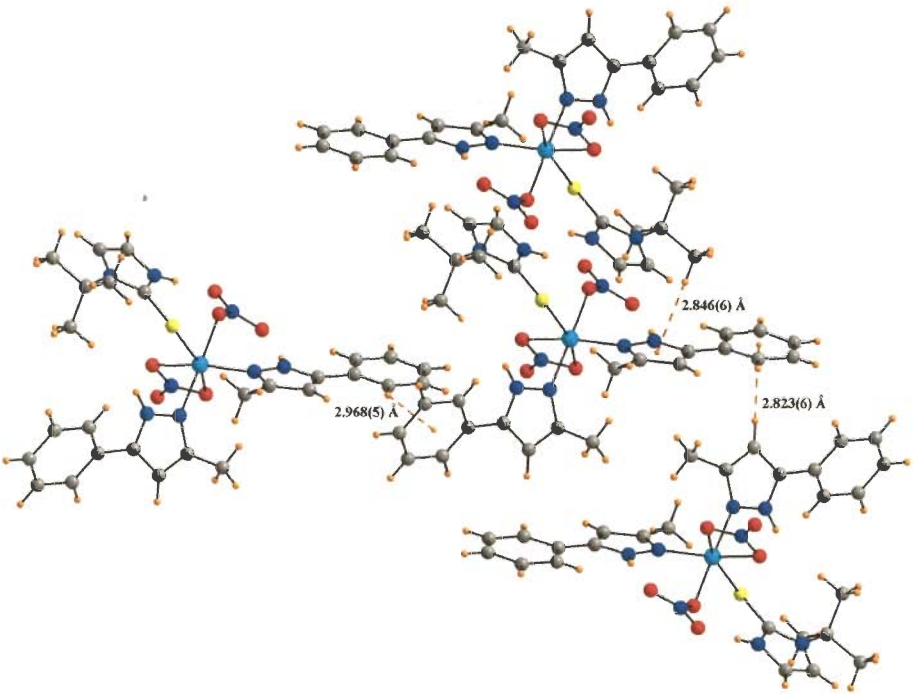

Fig. 4-65 Intermolecular C-H···π interactions present in complex **4s**

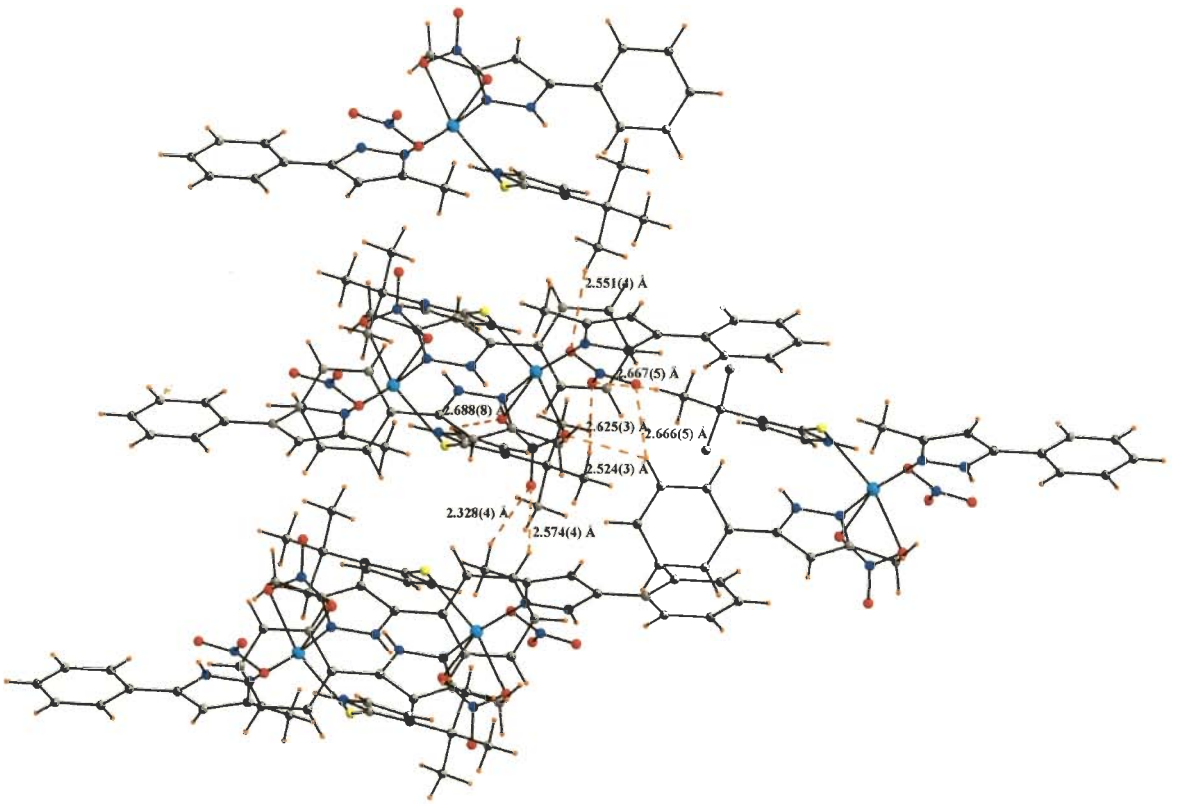

Fig. 4-66 Intermolecular C-H···O interactions present in complex **4s**

References

1. Arthur, J.R., Bremner, I. and Chesters, J.K., "Trace elements in animal nutrition", Inorg. Biochemistry, H. A. O. Hill (Ed.), **2,** 283 (1979).
2. Dixon, N.E., Gazzola, C., Blakeley, R.L. and Zerner, B., "Jack bean urease (EC 3.5.1.5). metalloenzyme. Simple biological role for nickel", J. Am. Chem. Soc., **97,** 4131 (1975).
3. Scott, B.M. and Robert, P.H., "Nickel uptake and utilization by microorganisms", Nat Struct Biol., **10,** 234 (2003).
4. Bible, K.C., Buytendrop, M., Zierath, P.D. and Rinehart, K.L., "Tunichlorin: a nickel chlorin isolated from the *caribbean tunicate tridemnum soalidum*", Proc. Natl. Acad. Sci. USA, **85,** 4582 (1988).
5. Malcolm, A.H. and Christou, G., "Bioinorganic chemistry of nickel", Chem. Rev., **94,** 2421 (1994).
6. Pearson, M.A., Hausinger, R.P. and Karplus, P.A., "Crystallographic studies of the nickel metalloenzyme urease and insight into the catalytic mechanism", J. Inorg. Biochem., **67,** 179 (1997).
7. Jabri, E., Carr, M.B., Hausinger, R.P. and Karplus, P.A., "The crystal structure of urease from *Klebsiella aerogene*", Science, **268,** 998 (1995).
8. Day, E.P., Sendova, M.S., Todd, M.J. and Hausinger, R.P., "Saturation magnetization of urease from *Klehsiella aerogenes* and Jack bean: No evidence for exchange coupling between the two active site nickel ions in native enzymes", Inorg. Chem., **32,** 634 (1993).
9. Wages, R.H.F., Tan, K.L. and Lippard, S.J., "$[Ni_2(OAc)_3(urea)$-$(tmen)_2](Otf)$ and $Ni(OAc)(urea)_2(tmen)](Otf)$, model complexes for the enzyme urease", Inorg. Chem., **32,** 4985 (1993).
10. Chaudhuri, P., Kuppers, H., Wieghardt, K., Gehring, S., Haase, W., Nuber, B. and Weiss, J., "Synthesis, magnetic properties, redox behaviour and crystal structure of the bridged binuclear nickel (II) complex $[Ni_2(\mu\text{-}OH)(\mu\text{-}O_2CCH_3)_2L_2](ClO_4).H_2O$", J. Chem. Soc., Dalton Trans., 1367 (1988).
11. Buchanan, R.M., Mashuta, M.S., Oberhausen, K.J., Richardson, J.F., Li, Q. and Hendrickson, D.N., "Active site model of urease: Synthesis, structure and magnetic properties of a binuclear Ni(II) complex containing a polyirnidazole

ligand", J. Am. Chem. Soc., **111,** 4497 (1989).

12. Holman, T.R., Hendrich, M.P. and Que, L., Jr., "EPR studies of a dinickel complex in its II, II and II, III oxidation states", Inorg. Chem., **31,** 937 (1992).
13. Holligan, B.M., Jeffery, C. and Ward, M.D., "The coordination chemistry of mixed pyridine-phenol and phenantharoline-phenolligands, Effects of π-stacking interactions and ligand rigidity on complex structures", J. Chem. Soc., Dalton Trans., 3337 (1992).
14. Mikuriya, M., Murase, I., Asato, E. and Kida, S., "A novel Mn-carbonato-bridged binuclear nickel (II) complex with N, N', N'', N'''- tetrakis(2-aminoethyl)-1 ,4,8,11-trazaazacyc1otetradecane", Chem. Lett., 497 (1989).
15. Rawle, S.C., Harding, C.J., Moore, P. and Alcock, N.W., "Crystal structure of an antiferromagnetically coupled μ-carboxylato-bridged dinickel (II) complex containing the pendent-arm macrocycle 1-(3-dimethylaminopropyl)-1,5,9-triazacycldodecane (L'); a system which readily sequesters carbon dioxide from air", J. Chem. Soc., Chem. Comm., 1701 (1992).
16. Eemler, U., Grabarse, W., Shima, S., Goubeaud, M. and Thauer, R.K., "Crystal structure of methyl-CoM reductase containing a Ni-porphinoid", J. Inorg. Biochem., **67,** 180 (1997).
17. Thauer, R.K., "Structure and function of the nickel enzyme methyl coenzyme M-reductase", J. Inorg. Biochem., **74,** 54 (1999).
18. Higuchi, Y. and Yasuoka, N., "Novel nickel-iron active center found in hydrogenase", J. Inorg. Biochem., **67,** 190 (1997).
19. Cammack, R., Fernandez, V.M. and Schneider, K., "The Bioinorganic chemistry of nickel", Wiley-VCH Publishers (1988).
20. Lindahl, P.A., "The Ni-containing carbon monoxide dehydrogenase family: light at the end of the tunnel ?", Biochemistry, **41**, 2097 (2002).
21. Ragsdale, W.E. and Kumar, M., "Nickel-containing carbon monoxide dehydrogenase / acetyl-CoA synthase", Chem. Rev., **96**, 2515 (1996).
22. Ferry, J.G., "CO dehydrogenase", Annu. Rev. Microbiol., **49**, 305 (1995).
23. Dobbek, H., Svetlitchnyi, V., Gremer, L., Huber, R. and Meyer, O., "Crystal structure of a carbon monoxide dehydrogenase reveals a [Ni-4Fe-5S] cluster", Science, **293**, 1281 (2001).

24. Drennan, C.L., Heo, J., Sintchak, M.D., Schreiter, E. and Ludden, P.W., "Life on carbon monoxide: X-ray structure of *Rhodospirillum rubrum* Ni-Fe-S carbon monoxide dehydrogenase", Proc. Natl. Acad. Sci. USA, **98**, 11973 (2001).

25. Murakami, E. and Ragsdale, S.W., "Evidence for intersubunit communication during acetyl-CoA cleavage by the multienzyme CO dehydrogenase / acetyl-CoA synthase complex from *Methanosarcina thermophila*. Evidence that the L subunit catalyzes C-C and C-S bond cleavage", J. Biol. Chem., **275**, 4699 (2000).

26. Bhaskar, B., DeMoll, E. and Grahame, D.A., "Redox-independent acetyl transfer partial reaction of the acetyl-CoA decarbonylase / synthase complex kinetics and mechanism", Biochemistry, **37**, 14491 (1998).

27. Tan, X.S., Sewell, C. and Lindahl, P.A., "Stopped-flow kinetics of methyl group transfer between the corrinoid-iron-sulfur protein and acetyl-coenzyme A synthase from *Clostridium thermoaceticum*", J. Am. Chem. Soc., **124**, 6277 (2002).

28. Seravalli, J., Kumar, M. and Ragsdale, S.W., "Rapid kinetic studies of acetyl-CoA synthesis evidence supporting the catalytic intermediacy of a paramagnetic NiFeC species in the autotrophic Wood-Ljungdahl pathway", Biochemistry, **41**, 1807 (2002).

29. Maynard, E.L. and Lindahl, P.A., "Evidence of a molecular tunnel connecting the active sites for CO_2 reduction and acetyl-CoA synthesis in acetyl-CoA synthase from *Clostridium thermoaceticum*", J. Am. Chem. Soc., **121**, 9221 (1999).

30. Seravalli, J. and Ragsdale, S.W., "Channeling of carbon monoxide during anaerobic carbon dioxide fixation", Biochemistry, **39**, 1274 (2000).

31. Doukov, T.I., Iverson, T.M., Seravalli, J., Ragsdale, S.W. and Drennan, C.L., "A Ni-Fe-Cu center in a bifunctional carbon monoxide dehydrogenase / acetyl-CoA synthase", Science, **298**, 567 (2002).

32. Darnault, C., Volbeda, A., Kim, E.J., Legrand, P., Verne'de, X., Lindahl, P.A. and Fontecilla-Camps, J.C., "Ni-Zn-[Fe_4-S_4] and Ni-Ni-[Fe_4-S_4] clusters in closed and open K subunits of acetyl-CoA synthase / carbon monoxide dehydrogenase", Nat. Struct. Biol, **10**, 271 (2003).

33. Fridovich, I., "Superoxide dismutases. An adaptation to a paramagnetic gas", J.

Biol. Chem., **264,** 7761 (1989).

34. Fridovich, I., "Oxygen toxicity: A radical explanation", J. Exp. Biol., **201,** 1203 (1998).

35. Bordo, D., Pesce, A., Bolognesi, M., Stroppolo, M.E., Falconi, M. and Desideri, A., "Copper-zinc superoxide dismutase in prokaryotes and eukaryotes". In Handbook of Metalloproteins, Messerschmidt, A., Huber, R., Poulos, T., and Wieghardt, K., Eds.; Wiley & Sons: Chicester, New York, Weinheim, Brisbane, Singapore, Toronto., **2,** 1284 (2001).

36. Youn, H.-D., Youn, H., Lee, J.-W., Yim, Y.-I., Lee, J.-K., Hah, Y.C. and Kang, S.-O., "Unique isozymes of superoxide dismutase in *Streptomyces griseus*", Arch. Biochem. Biophys., **334,** 341 (1996).

37. Youn, H.-D., Kim, E.-J., Roe, J.-H., Hah, Y.C. and Kang, S.-O., "A novel nickel-containing superoxide dismutase from *Streptomyces spp.*", Biochem. J., **318,** 889 (1996).

38. Kim, E.-J., Kim, H.-P., Hah, Y.C. and Roe, J.-H., "Differential expression of superoxide dismutases containing Ni and Fe / Zn in *Streptomyces coelicolor*", Eur. J. Biochem., **241,** 178 (1996).

39. Palenik, B., Brahamsha, B., Larimer, F.W., Land, M., Hauser, L., Chain, P., Lamerdin, J., Regala, W., Allen, E.E., McCarren, J., Paulsen, I., Dufresne, A., Partensky, F., Webb, E.A. and Waterbury, J., "The genome of a motile marine synechococcus", Nature, **424,** 1037 (2003).

40. Maroney, M.J., Choudhary, S.B., Lee, J.-W., Davidson, G., Yim, Y.-I., Bose, K., Sharma, M.L., Kang, S.-O. and Cabelli, D.E., "A SOD story: The structure and function of the NiSOD active site", J. Inorg. Biochem ., **74,** 39 (1999).

41. Wuerges, J., Lee, J.-W., Yim, Y.-I., Yim, H.-S., Kang, S.-O. and Carugo, K.D., "Crystal structure of nickel-containing superoxide dismutase reveals another type of active site", Proc. Natl. Acad. Sci. U.S.A., **101,** 8569 (2004).

42. Barondeau, D.P., Kassmann, C.J., Bruns, C.K., Tainer, J.A. and Getzoff, E.D., "Nickel superoxide dismutase structure and mechanism", Biochemistry, **43,** 8038 (2004).

43. Barondeau, D.P. and Getzoff, E.D., "Structural insights into protein-metal ion

partnerships", Curr. Opin. Struct. Biol., **14,** 765 (2004).

44. Vladimir, P. and Siegbahn, P.E.M., "Nickel superoxide dismutase reaction mechanism studied by hybrid density functional methods", J. Am. Chem. Soc., **23,** 7475 (2006).

45. Clugston, S.L., Barnard, J.F.J., Kinach, R., Miedema, D., Ruman, R., Daub, E. and Honek, J.F., "Overproduction and characterization of a dimeric non-zinc glyoxylase I from *Escherichia coli* evidence for optimal activation by nickel ions", Biochemistry, **37**, 8754 (1998).

46. He, M.M., Clugston, S.L., Honek, J.F. and Matthews, B.W., "Determination of the structure of *Escherichia coli* glyoxylase I suggests a structural basis for differential metal activation", Biochemistry, **39**, 8719 (2000).

47. Davidson, G., Clugston, S.L., Honek, J.F. and Maroney, M.J., "An XAS investigation of product and inhibitor complexes of Ni-containing GlxI from *Escherichia coli* mechanistic implications", Biochemistry, **40**, 4569 (2001).

48. Clugston, S.L. and Honek, J.F., "Identification of sequences encoding the detoxification metalloisomerase glyoxylase I in microbial genomes from several pathogenic organisms", J. Mol. Evol., **50**, 491 (2000).

49. Dai, Y., Wensink, P.C. and Abeles, R.H., "One protein, two enzymes", J. Biol. Chem., **274**, 1193 (1999).

50. Chai, S.C., Ju, T., Dang, M., Goldsmith, R.B., Maroney, M.J. and Pochapsky, T.C., "Characterization of metal binding in the active sites of acireductone dioxygenase isoforms from *Klebsiella* ATCC 8724", Biochemistry, **47**, 2428 (2008).

51. Al-Mjeni, F., Ju, T., Pochapsky, T.C. and Maroney, M.J., "XAS investigation of the structure and function of Ni in acireductone dioxygenase", Biochemistry, **41**, 6761 (2002).

52. Pochapsky, T.C., Pochapsky, S.S., Ju, T., Mo, H., Al-Mjeni, F. and Maroney, M.J., "Modeling and experiment yields the structure of acireductone dioxygenase from *Klebsiella pneumoniae*", Nat. Struct. Biol., **9**, 966 (2002).

53. Pochapsky, T.C., Pochapsky, S.S., Ju, T., Hoefler, C. and Liang, J., "A refined model for the structure of acireductone dioxygenase from *Klebsiella ATCC 8724* incorporating residual dipolar couplings", J. Biomol. NMR, **34**, 117

(2006).

54. Ewen, H. and Jahns, T., "Bacterial degradation of methyleneureas as slow-release fertilizer", Rec. Res. Dev. Microbiol., **4**, 255 (2000).

55. Christianson, D.V. and Lipscomb, W.N., "Carboxypeptidase A", Acc. Chem. Res., **22,** 62 (1989).

56. Bertini, J., Donaire, A., Monnanni, R., Moratal, J.M. and Salgado, J., "Spectroscopic characterization of nickel (II) carboxypeptidase", J. Chem. Soc., Dalton Trans., 1443 (1992).

57. Moratal, J.M., Castells, J., Donaire, A., Salgado, J. and Jimenez, H.R., "Interaction of carboxylate inhibitors with the active site of nickel (II) carboxypeptidase A", J. Chem. Soc., Dalton Trans., 3317 (1992).

58. Dudev, T. and Lim, C., "Effect of carboxylate-binding mode on metal binding / selectivity and function in proteins", Acc. Chem. Res., **40**, 85 (2007).

59. Busch, D.H. and Stephenson, N.A., "Molecular organization, portal to supramolecular chemistry: Structural analysis of the factors associated with molecular organization in coordination and inclusion chemistry, including the coordination template effect", Coord. Chem. Rev., **100**, 119 (1990).

60. Lynch, D.E., Lad, J., Smith, G. and Parsons, S., "Molecular complexes of 3-hydroxypyridine with nitro-substituted aromatic and heterocyclic carboxylic acids", Crystal Engg., **2**, 65 (1999).

61. Santana, M.D., Lozano, A.A., Garcia, G., Lopez, G. and Perez, J., "Five-coordinate nickel (II) complexes with carboxylate anions and derivatives of 1,5,9-triazacyclododec-1-ene: structural and ^{1}H NMR spectroscopic studies", Dalton Trans., 104 (2005).

62. Santana, M.D., Garcia, G., Lopez, G., Lozano, A., Vicente, C., Garcia, L. and Perez, J., "Preparation, crystal structures and NMR characterization of substituted-benzoate complexes Nickel(II)-N_3-macrocycles", Polyhedron, **26**, 1029 (2007).

63. Li, X., Musie, G.T. and Powell, D.R., "Hexacoordinated cobalt (II) and nickel (II) complexes of a novel mixed ligand, N-(2-methylpyridine)-2-aminomethyl benzoic acid: structures, spectroscopic characterizations and redox studies", Inorg. Chim. Acta, **355**, 328 (2003).

64. Hammes, B.S. and Carrano, C.J., "The synthesis and characterization of 4, 5,

and 6 coordinate Ni(II) complexes of the "Heteroscorpionate" ligand (3-tert-Butyl-2-hydroxy-5-methylphenyl)bis(3,5-dimethylpyrazolyl)methane", Inorg. Chem., **38**, 3562 (1999).

65. Eremenko, I.L., Nefedov, S.E., Sidorov, A.A., Golubnichaya, M.A., Danilov, P.V., Ikorskii, V.N., Shvedenkov, Y.G., Novotortsev, V.M. and Moiseev, I.I., "Bi- and mononuclear nickel (II) trimethylacetate complexes with pyridine bases as ligands", Inorg. Chem., **38**, 3764 (1999).

66. Szajna-Fuller, E., Chambers, B.M., Arif, A.M. and Berreau, L.M., "Carboxylate coordination chemistry of a mononuclear Ni(II) center in a hydrophobic or hydrogen bond donor secondary environment: Relevance to acireductone dioxygenase", Inorg. Chem., **46**, 5486 (2007).

67. Szajna-Fuller, E., Rudzka, K., Arif, A.M. and Berreau, L.M., "Acireductone dioxygenase-(ARD-) type reactivity of a nickel (II) complex having monoanionic coordination of a model substrate: Product identification and comparisons to unreactive analogues", Inorg. Chem., **46**, 5499 (2007).

68. Carlsson, H., Haukka, M., Bousseksou, A., Latour, J.-M. and Nordlander, E., "Nickel complexes of carboxylate-containing polydentate ligands as models for the active site of urease", Inorg. Chem., **43**, 8252 (2004).

69. Yamaguchi, K., Koshino, S., Akagi, F., Suzuki, M., Uehara, A. and Suzuki, S., "Structures and catalytic activities of carboxylate-bridged dinickel (II) complexes as models for the metal center of urease", J. Am. Chem. Soc., **119**, 5752 (1997).

70. Rochon, F.D. and Massarweh, G., "Study of the aqueous reactions of metallic ions with benzenetetracarboxylate ions Part 1. Crystal structures of compounds of the types $[M(H_2O)_6][C_6H_2(COO)_2(COOH)_2]$ (M = Mn, Co and Ni) and $Ni(H_2O)_5(m\text{-}C_6H_2(COO)_4)Ni(H_2O)_5{\cdot}6H_2O$", Inorg. Chim. Acta, **304**, 190 (2000).

71. Ivanikova, R., Boca, R., Dlhan, L., Fuess, H., Maslejova, A., Mrazova, V., Svoboda, I. and Titis, J., "Heteroleptic nickel (II) complexes formed from N-donor bases, carboxylic acids and water: Magnetostructural correlations", Polyhedron, **25**, 3261 (2006).

72. Hong, C.S. and You, Y.S., "Synthesis, crystal structures and magnetic studies of

terephthalato-bridged binuclear nickel (II) complexes", Polyhedron, **23,** 1379 (2004).

73. Fan, J., Zhang, Y.-A., Okamura, T., Zou, Z.-H., Ueyama, N. and Sun, W.-Y., "Synthesis and crystal structure of a one-dimensional coordination polymer of nickel (II) with 4′-(imidazole-1-yl-methyl)benzoate anion", Inorg. Chem. Comm., **4**, 501 (2001).

74. Baruah, A.M., Karmakar, A. and Baruah, J.B., "Ring opening reactions of pyromellitic dianhydride for the synthesis of first row transition metal dicarboxylate complexes", Polyhedron, **26,** 4479 (2007).

75. Choi, K.-Y. and Kim, K.-J., "Self-assembly of 1D coordination polymers from nickel (II) tetraaza macrocycle and carboxylate ligands", Polyhedron, **27**, 1311 (2008).

76. Sileoa, E.E., Araujob, A.S., Rigottic, G., Piroc, O.E. and Castellano, E.E., "Solid state coordination chemistry of pyridinedicarboxylic acid isomers. III Synthesis and crystal structures of complexes of Zn and Ni with lutidinic acid (lutidinic = 2,4-pyridinedicarboxylic)", J. Mol. Struct., **644,** 67 (2003).

77. Maslejova, A., Ivanikova, R., Svoboda, I., Papankova, B., Dlhan, L., Miklos, D., Fuess, H. and Boca, R., "Structural characterization and magnetic properties of hexakis(imidazole)nickel (II) bis(formate), bis(chloroacetate), bis(2-chloropropionate) and hexakis(1-methyl-imidazole)nickel (II) chloride dehydrate", Polyhedron, **25,** 1823 (2006).

78. Huang, Y.-G., Zhou, Y.-F., Yuan, D.-Q., Wu, B.-L., Jiang, F.-L. and Hong, M.-C., "Syntheses, crystal structures and magnetic properties of Ni(II)–2,4-pyridine-dicarboxylates", J. Mol. Struct., **830**, 85 (2007).

79. Wang, E., Ohashi, K. and Kamata, S., "Coated carbon-rod anion electrodes using bis(diphenylphosphino)propane-metal complexes", Anal. Sci., **7**, 755 (1991).

80. Webber, P.R.A., Drew, M.G.B., Hibbert, R. and Beer, P.D., "Transition metal-directed self-assembly of calix[4]arene based dithiocarbamate ligands", Dalton Trans., 1127 (2004).

81. Segui, M.J., Lizondo-Sabater, J., Martinez-Manez, R., Sancenon, F. and Soto, J., "Linear polyamines as carriers in thiocyanate-selective membrane

electrodes", Talanta, **68**, 1182 (2006).

82. Behzad, R., Soraya, M., Vajihe, N. and Saeid, B, "Highly thiocyanate-selective membrane electrode based on the bis(benzoylacetone) propylenediimine copper (II) complex", Annal. di Chim., **97**, 1191 (2007).

83. Singh, A.K., Singh, U.P., Mehtab, S. and Aggarwal, V., "Thiocyanate selective sensor based on tripodal zinc complex for direct determination of thiocyanate in biological samples", Sens. Actuat. B, **125(2)**, 453 (2007).

84. Prasad, R., Gupta, V.K. and Kumar, A., "Metallo-tetraazaporphyrin based anion sensors: regulation of sensor characteristics through central metal ion coordination", Anal. Chim. Acta, **508**, 61 (2004).

85. Hassan, S.S.M., Zawawy, F.M., Marzouk, S.A.M. and Elnemma, E.M., "Poly(vinyl chloride) matrix membrane electrodes for manual and flow injection determination of metal azides", Analyst, **117,** 1683 (1992).

86. Harding, D.J., Harding, P., Adams, H. and Tuntulani, T., "Synthesis and characterization of sterically hindered tris(pyrazolyl)borate Ni complexes", Inorg. Chim. Acta, **360**, 3335 (2007).

87. Matsunaga, Y., Fujisawa, K., Ibi, N., Miyashita, Y. and Okamoto, K., "Structural and spectroscopic characterization of first-row transition metal (II) substituted blue copper model complexes with hydrotris(pyrazolyl)borate", Inorg. Chem., **44**, 325 (2005).

88. Konrad, M., Meyer, F., Heinze, K. and Zsolnai, L., "Unsymmetrically substituted pyrazolates: nickel (II) complexes of a novel dinucleating ligand providing both N- and S-rich co-ordination spheres", Dalton Trans., 199 (1998).

89. Yang, X., Kumar, N., Chi, H., Hibbert, D.B. and Alexander, P.W., "Lead-selective membrane electrodes based on dithiophenediazacrown ether derivatives", Electroanalysis, **9**, 549 (1997).

90. Dakovic, M., Popovic, Z., Giester, G. and Rajic-Linaric, M., "Synthesis, spectroscopic and structural investigation of $Zn(NCS)_2(nicotinamide)_2$ and $[Hg(SCN)_2(nicotinamide)]_n$", Polyhedron, **27**, 465 (2008).

91. Desiraju, G.R. and Steiner, T., "The Weak Hydrogen Bond: In Structural Chemistry and Biology", Oxford Univ. Press (1999).

92. Goher, M.A.S., Escuer, A., Mautner, F.A. and Al-Salem, N.A., "A new series of 1D polymeric nickel (II) complex cations of pyridine derivative ligands with a

single μ-1,3 azide bridge and X-ray crystal structure and magnetic properties of polymeric {[Ni(4-ethylpyridine)$_4$(N_3)$_n$](PF_6)$_n$}", Polyhedron, **21**, 1871 (2002).

93. Graziani, R., Vidali, M., Casellato, U. and Vigato, P.A., "Synthesis and crystal structure of bis(dimethylthioacetonedicarboxylate)nickel (II)", Transition Met. Chem., **6**, 166 (1981).

94. Ibrahim, M.M., Seebacher, J., Steinfeld, G. and Vahrenkamp, H., "Tris(thioimidazolyl)borate-zinc-thiolate complexes for the modeling of biological thiolate alkylations", Inorg. Chem., **44**, 8531 (2005)

95. Ibrahim, M.M., He, G., Seebacher, J., Benkmil, B. and Vahrenkamp, H., "Biomimetic thiolate alkylation with zinc pyrazolylbis(thioimidazolyl)borate complexes", Eur. J. Inorg. Chem., 4070 (2005).

96. Benkmil, B., Ji, M. and Vahrenkamp, H., "Bis(pyrazolyl)(thioimidazolyl)borate ligands: The missing member in the N_3...S_3 scorpionate series", Inorg. Chem., **43**, 8212 (2004).

97. Ji, M., Benkmil, B. and Vahrenkamp, H., "Zinc-thiolate complexes of the bis(pyrazolyl)(thioimidazolyl)hydroborate tripods for the modeling of thiolate alkylating enzymes", Inorg. Chem., **44**, 3518 (2005).

98. Seebacher, J., Shu, M. and Vahrenkamp, H., "The best structural model of ADH so far: A pyrazolylbis(thioimidazolyl)borate zinc ethanol complex", Chem. Comm., 1026 (2001).

Chapter 5

Experimental

Materials

All manipulations were carried out under an inert atmosphere using standard Schlenk tube techniques unless otherwise stated. Prior to use dichloromethane, toluene, methanol, acetonitrile, diethylether, tetrahydrofuran and pentane were purified and distilled under nitrogen by a reported method [1]. $MnCl_2.4H_2O$, $FeCl_3.6H_2O$, $NiCl_2.6H_2O$, $CoCl_2.6H_2O$, $Co(NO_3)_2.6H_2O$ and $ZnCl_2$ (reagent grade) were purchased from Aldrich. Sodium azide, potassium thiocyanate, sodium acetylacetonate and potassium picolinate were purchased from s.d. fine, India. Lithium amide, isopropylmethylketone, methylisobutyrate, benzoylacetone, 1,10-phenanthroline monohydrate, 2-methylpropan-2-amine, bromoacetaldehydediethylacetal, pyrazole (PzH) and 3,5-dimethylpyrazole ($Pz^{Me2}H$) were purchased from Aldrich chemical company, Germany. For membrane preparation, high molecular weight poly (vinyl chloride) (PVC), *o*-nitrophenyloctyl ether (*o*-NPOE), dioctylphthalate (DOP), dibutylphthalate (DBP), benzylacetate (BA) and hexadecyltrimethylammonium bromide (HTAB) were used as received from Fluka. Reagent grade sodium salts of all anions used were of highest purity available from SRL (Mumbai, INDIA) and used without any further purification except for vacuum drying over P_2O_5. Tris-hydroxymethylaminomethane (TRIS), glycine (gly) and 2-morpholinoethanesulfonic acid (MES) were purchased from Fluka. Other reagents were of the highest grade commercially available grade and used without further purification.

Instrumentation

Carbon, hydrogen, nitrogen and sulphur were analyzed with a Vario EL III elemental analyzer after carefully drying the samples under vacuum for several hours.

The UV/vis spectra were recorded on Perkin–Elmer Lambda 35 UV/vis spectrophotometer. IR spectra were obtained on a Thermo Nikolet Nexus FT-IR spectrometer in KBr. NMR spectra were recorderd on a Bruker-DRX 500 spectrometer with Fourier transformation technique. The chemical shifts for ^{1}H-NMR were reported in ppm relative to the TMS (tetramethylsilane) as internal standards. Room temperature magnetic susceptibility measurements were done on a Princeton applied research vibrating sample magnetometer Model 155 whereas the magnetic susceptibility measurements at variable temperature (from liquid helium to room temperature) were performed on Quantum Design Squid Magnetometer Model MPMS. The TG-DTG experiments were performed on Perkin-Elmer's (Pyris Diamond) thermogravimetry analyzer under air atmosphere. Cyclic voltammetry and differential pulse voltammetry were performed using an BAS Epsilon electrochemical workstation with DMSO / acetonitrile solution of samples containing 0.10 M $[N(n\text{-}Bu)_4]ClO_4$ as supporting electrolyte. The working electrode was a BAS glassy carbon disk electrode of radius 3 mm, the reference electrode was Ag / AgCl and the auxiliary electrode was a Pt wire. All potential measurements were preformed at ambient temperature using a Century scientific-digital pH / milivoltmeter (Model CP 901). The X-ray data collection and processing for the complexes were performed on a Kappa Apex Bruker CCD detector with MoKα radiation (λ = 0.71070 Å). Crystal structures were solved by direct / Patterson methods with the SHELX program suite [2]. All non-hydrogen atoms were refined anisotropically. Hydrogen atoms were placed in geometrically calculated positions and refined using a riding model. Images were created with the DIAMOND program [3].

Preparation of Membranes

Preparation of poly(vinyl chloride) based membranes

The ion sensitive membranes of the PVC matrix were fabricated according to the procedure described by Craggs et al. [4]. An important requirement for making PVC membranes of an ion selective sensor is that the ionophore, PVC, plasticizers and anionic additives should be soluble in some fast evaporating solvent. The ionophores, PVC, plasticizers and anionic additives used in the present investigations were found to be sufficiently soluble in THF. Therefore, THF was used for preparing the membranes. Thus, membrane cocktails were formulated by dissolving appropriate amounts of ionophores, anionic additives and plasticizers. The components were added in terms of weight percentages. After thorough dissolution, the homogeneous mixture was concentrated by evaporating THF and poured into polyacrylates rings placed on a smooth glass plate. The solution was poured gently so as to avoid the formation of air bubbles. A pad of filter papers and a heavy weight were then placed on top of the ring and the assembly was left for one day to allow the solvent to evaporate slowly at room temperature. After 24 h of evaporation, the transparent membranes of 0.4 mm thickness were removed carefully from the glass plate and glued to one end of pyrex glass tube. It is known that the sensitivity, linearity and selectivity of ion selective electrode depend significantly on the membrane composition. Thus, optimization was performed after a good deal of experimentation to provide membranes, that generated reproducible and stable potentials. The membranes having only PVC as membrane ingredient (dummy membranes) were also prepare to observe any background potentials being produced due to the binding material.

Preparation of Sandwich Membranes

Ion-selective electrode membranes were cast by the above mentioned procedure. Blank membranes (without ionophore) having same composition were also prepared. The sandwich membrane was prepared by pressing two individual membranes (ordinarily one without ionophore and one with the same components and an additional ionophore) together, after blotting them individually dry with a tissue paper. The obtained sandwich membrane was visibly checked for air bubbles before mounting on the electrode body. The combined segmented membrane was then rapidly mounted on to the electrode body, such that ionophore-containing segment faces the sample solution. Subsequently, the measurements were carried out [5].

Chapter-2

Potassium hydrotris(1-pyrazolyl) borate [KTp] (**2a**), Potassium hydrotris(3,5-dimethyl-1-pyrazolyl)borate [KTp^{Me2}] (**2b**) (Ref. [2] of chapter 1), N-tert-butyl-2-thioimidazole [$tm^{t\text{-}Bu}$] (**2n**) (Ref. [75] of chapter 2) and $[Ni(phen)_3]Cl_2.2H_2O$ (**2o**) (Ref. [76] of chapter 2) were synthesized by the literature method.

Synthesis of Potassium hydrotris(1-pyrazolyl) borate [KTp] (2a)

A mixture of pyrazole (12.24 g, 0.18 mol) and KBH_4 (3.24 g, 0.06 mol) was heated in an oil bath with stirring. The temperature was elevated gradually. After the temperature of the oil bath reached 220 °C, heating was continued at the same temperature until no hydrogen evolution was observed. The mixture was allowed to cool at room temperature and the resulting solid was refluxed in toluene, filtered in hot condition and dried under vacuum for several hours. Yield was 75 % (10.08 g, 0.04 mol). Anal. Calcd. (%) for $C_9H_{10}N_6BK$ (252): C, 42.87; H, 4.00; N, 33.33.

Found: C, 42.92; H, 4.09; N, 33.42. IR (KBr, cm^{-1}): ν(BH) 2400. ^1H NMR ($(CD_3)_2CO$, 500 MHz) δ, 6.60 (s, 9H, CH).

Synthesis of Potassium hydrotris(3,5-dimethyl-1-pyrazolyl)borate [KTp^{Me2}] (2b)

The ligand **2b** was prepared in 68 % (12.09 g, 0.036 mol) yield by the same procedure as outlined above for **2a**. Anal. Calcd. (%) for $C_{15}H_{22}N_6BK$ (336): C, 53.57; H, 6.59; N, 24.99. Found: C, 53.72; H, 6.71; N, 25.08. IR (KBr, cm^{-1}): ν(BH) 2480. ^1H NMR ($(CD_3)_2CO$, 500 MHz) δ, 2.70 (d, 18H, CH_3), 5.67 (q, 3H, Pz).

[TpFe(pic)Cl] (2c)

A methanolic solution of iron (III) chloride hexahydrate (0.20 g, 0.75 mmol) and potassium picolinate (0.12 g, 0.75 mmol) was stirred for 1 h. KTp (0.18 g, 0.75 mmol) in dichloromethane (10 ml) was added to this solution and the resultant solution was stirred for additional 2 h. The reaction mixture was filtered over celite, evaporated to dryness and obtained brown colored compound in 73 % (0.23 g, 0.54 mmol) yield. Anal. Calcd. (%) for $C_{15}H_{13}N_7O_2BClFe$ (425): C, 42.35; H, 3.05; N, 23.05. Found: C, 42.61; H, 3.17; N, 23.42. IR (KBr, cm^{-1}): ν(BH) 2496, ν_{as}(COO) 1642, ν_s(COO) 1371. UV / vis (acetonitrile, nm, ε/$M^{-1}cm^{-1}$): 282 (1748), 521 (163). Magnetic moment μ_{eff} (295 K) = 5.91 B.M.

[Tp^{Me2}Fe(pic)Cl] (2d)

This complex was prepared in 65 % (0.24 g, 0.48 mmol) yield by the same procedure as outlined above for **2c**. Anal. Calcd. (%) for $C_{21}H_{26}N_7O_2BClFe$ (510): C, 49.31; H, 5.08; N, 19.17. Found: C, 49.43; H, 5.15; N, 19.31. IR (KBr, cm^{-1}): ν(BH) 2532, ν_{as}(COO) 1636, ν_s(COO) 1378. UV / vis (acetonitrile, nm, ε/$M^{-1}cm^{-1}$): 285 (1732), 531 (164). Magnetic moment μ_{eff} (295 K) = 5.85 B.M.

[TpFe(acac)Cl] (2e)

This complex was prepared in 73 % (0.22 g, 0.54 mmol) yield by the same procedure as outlined above for **2c**. Anal. Calcd. (%) for $C_{14}H_{17}N_6O_2BClFe$ (403): C, 41.68; H, 4.21; N, 20.84. Found: C, 41.79; H, 4.34; N, 20.93. IR (KBr, cm^{-1}): ν(BH) 2498, ν(CO) 1584. UV / vis (acetonitrile, nm, $\varepsilon/M^{-1}cm^{-1}$): 286 (1871), 528 (174). Magnetic moment μ_{eff}(295 K) = 5.96 B.M.

[Tp^{Me2}Fe(acac)Cl] (2f)

This complex was prepared in 68 % (0.25 g, 0.51 mmol) yield by the same procedure as outlined above for **2c**. The brown colored crystals were obtained from a mixture of acetonitrile and dichloromethane at –20 °C. Anal. Calcd. (%) for $C_{20}H_{29}N_6O_2BClFe$ (488): C, 49.18; H, 5.94; N, 17.23. Found: C, 49.03; H, 5.76; N, 17.11. IR (KBr, cm^{-1}): ν(BH) 2540, ν(CO)1588. UV / vis (acetonitrile, nm, $\varepsilon/M^{-1}cm^{-1}$): 283 (1868), 521 (152). Magnetic moment μ_{eff}(295 K) = 5.91 B.M.

[TpFe(pic)N$_3$] (2g)

A methanolic solution of sodium azide (0.03 g, 0.50 mmol) was added to the solution of **2c** (0.21 g, 0.50 mmol) in acetonitrile and the mixture was stirred for 1 h. The resultant brown colored solution was filtered over celite and dried under vacuum to give the compound in 72 % (0.16 g, 0.36 mmol) yield. Anal. Calcd. (%) for $C_{15}H_{13}N_{10}O_2BFe$ (432): C, 41.67; H, 3.00; N, 32.40. Found C, 41.72; H, 3.16; N, 32.58. IR (KBr, cm^{-1}): ν(BH) 2497 $\nu(N_3)$ 2051, ν_{as}(COO) 1640, ν_s(COO) 1373. UV / vis (acetonitrile, nm, $\varepsilon/M^{-1}cm^{-1}$): 289 (1852), 444 (714), 564 (178). Magnetic moment μ_{eff}(295 K): 5.94 B.M.

[Tp^{Me2}Fe(pic)N$_3$] (2h)

This complex was prepared in 71 % (0.18 g, 0.36 mmol) yield by the same procedure as outlined above for **2g**. Anal. Calcd. (%) for $C_{21}H_{26}N_{10}O_2BFe$ (518):

C, 48.64; H, 5.01; N, 27.02. Found C, 48.73; H, 5.14; N, 27.23. IR (KBr, cm^{-1}): ν(BH) 2547 ν(N_3) 2046, ν_{as}(COO) 1632, ν_s(COO) 1375. UV / vis (acetonitrile, nm, ε/$M^{-1}cm^{-1}$): 281 (1782), 442 (694), 581 (168). Magnetic moment μ_{eff}(295 K): 5.91 B.M.

[TpFe(acac)N_3] (2i)

This complex was prepared in 67 % (0.14 g, 0.34 mmol) yield by the same procedure as outlined above for **2g**. Anal. Calcd. (%) for $C_{14}H_{17}N_9O_2BFe$ (410): C, 41.01; H, 4.18; N, 13.62. Found C, 41.23; H, 4.24; N, 13.73. IR (KBr, cm^{-1}): ν(BH) 2494, ν(N_3) 2049, ν(CO) 1586. UV / vis (acetonitrile, nm, ε/$M^{-1}cm^{-1}$): 289 (1952), 440 (684), 581 (168). Magnetic moment μ_{eff}(295 K): 5.93 B.M.

[Tp^{Me2}Fe(acac)N_3] (2j)

This complex was prepared in 63 % (0.16 g, 0.32 mmol) yield by the same procedure as outlined above for **2g.** The brown colored crystals were obtained from a mixture of pentane and dichloromethane at –20 °C. Anal. Calcd. (%) for $C_{20}H_{29}N_9O_2BFe$ (494): C, 48.61; H, 5.92; N, 25.50. Found C, 48.73; H, 5.94; N, 25.63. IR (KBr, cm^{-1}): ν(BH) 2530, ν(N_3) 2056, ν(CO) 1589. UV / vis (acetonitrile, nm, ε/$M^{-1}cm^{-1}$): 289 (1952), 440 (684), 581 (168). Magnetic moment μ_{eff}(295 K): 5.92 B.M.

[TpFe(PzH)(N_3)$_2$] (2k)

The compound **2k** was synthesized by the reaction of iron (III) chloride (0.21 g, 0.78 mmol), KTp (0.19 g, 0.78 mmol), PzH (0.07 g, 0.78 mmol) and sodium azide (0.10 g, 1.56 mmol) in methanol. The reaction mixture was refluxed for 2 h. The resultant solution was filtered over celite and the solvent was evacuated to dryness under vaccum to give the compound in 66 % (0.51 mmol) yield. Anal. Calcd. (%) for $C_{12}H_{21}N_{14}BFe$ (428): C, 33.67; H, 4.94; N, 45.81. Found C, 33.72; H, 5.02; N, 45.93. IR (KBr, cm^{-1}):

ν(NH) 3354, ν(BH) 2494, ν(N_3) 2046. UV / vis (acetonitrile, nm, ε/$M^{-1}cm^{-1}$): 284 (1987), 442 (697), 574 (171). Magnetic moment μ_{eff} (295 K): 5.90 B.M.

[$Tp^{Me2}Fe(Pz^{Me2}H)(N_3)_2$] (2l)

This complex was prepared in 69 % (0.16 g, 0.54 mmol) yield by the same procedure as outlined above for **2k.** The crystallization of this compound from CH_3CN (5ml) at -20 °C led to the formation of suitable brown colored crystals for X-ray data collection. Anal. Calcd. (%) for $C_{20}H_{30}N_{14}BFe$ (533): C, 45.02; H, 5.62; N, 36.77. Found C, 45.13; H, 5.74; N, 36.84. IR (KBr, cm^{-1}): ν(NH) 3358, ν(BH) 2547, ν(N_3) 2052. UV / vis (acetonitrile, nm, ε/$M^{-1}cm^{-1}$): 284 (1987), 442 (697), 574 (171). Magnetic moment μ_{eff} (295 K): 5.93 B.M.

[$(Tp^{Me2})_2Fe$][$FeCl_4$] (2m)

The compound **2m** was obtained by the electrochemical reduction of compound **2l** (0.446 g, 0.84 mmol) in acetonitrile and single crystals suitable for X-ray data collection was obtained in aerobic condition by cooling the acetonitrile solution at -20 °C in presence of lithium chloride. Yield was 55 % (0.39 g, 0.46 mmol). Anal. Calcd. (%) for $C_{30}H_{42}N_{12}B_2Cl_4Fe_2$ (844): C, 42.60; H, 4.99; N, 19.85. Found C, 42.73; H, 5.09; N, 19.91. IR (KBr, cm^{-1}): ν(BH)2540. UV / vis (acetonitrile, nm, ε/$M^{-1}cm^{-1}$): 282 (1932), 571 (167). Magnetic moment μ_{eff} (295 K): 6.32 B.M.

Synthesis of N-tert-butyl-2-thioimidazole [tm^{t-Bu}] (2n)

2-methylpropan-2-amine (7.30 g, 0.10 mol) and bromoacetaldehydediethylacetal (19.60 g, 0.10 mol) were refluxed in ethanol for 6 d. After refluxing, aqueous and organic layers were separated and extracted with ether. Further organic layer was extracted with distilled water and dried using Na_2SO_4. N-(2,2-diethoxyethyl)-2-methylpropan-2-amine was obtained in 72 % (13.62 g, 0.72 mol) yield after the

removal of ether under vaccum. KSCN (6.79 g, 70.0 mmol) and HCl (75 mL, 2N) were added to an ethanolic (130 mL) solution of N-(2,2-diethoxyethyl)-2-methylpropan-2-amine (11.34 g, 60.0 mmol) and the reaction mixture was refluxed for 24 h. The solvent was evaporated to dryness and the residue was dissolved in 500 mL hot water. The solution was allowed to cool to room temperature to obtain a pale yellow compound that was filtered, dried and recrystallized from methanol by using activated charcoal. White compound was obtained in 33% yield (4.54 g, 29.6 mmol) and single crystals suitable for X-ray data collection were obtained at -20 °C in acetonitrile. Anal. Calcd. (%) for $C_7H_{12}N_2S$ (156): C, 53.81; H, 7.74; N, 17.93; S, 20.52; C, 53.94; H, 7.89; N, 17.99; S, 20.61. IR (KBr, cm^{-1}) ν(C=S) 1117, ν(NH) 3413. ^1H NMR ($CDCl_3$, 500 MHz): δ = 1.13 (s, 9H, Me), 6.64 (d, J = 2.2 Hz, 1H, Im), 6.85 (d, J = 1.8 Hz, 1H, Im), 12.32 (s, 1H, NH).

$[Ni(phen)_3]Cl_2.2H_2O$ (2o)

A solution of $NiCl_2.6H_2O$ (0.24 g, 1.0 mmol) in 10 mL methanol was added dropwise to a solution of 1,10-phenanthroline monohydrate (0.59 g, 3.0 mmol) in 5 mL of the same solvent. The resultant mixture was stirred for one hour. The clear pink solution was filtered and evaporated to dryness under vacuum in 71 % (0.50 g, 0.71 mmol) yield. Anal. Calcd. (%) for $C_{36}H_{28}N_6O_2Cl_2Ni$ (704): C, 61.22; H, 4.01; N, 11.90; Found: C, 61.43; H, 4.07; N, 11.98. IR (KBr, cm^{-1}): ν(C=N) 1623. UV / vis (acetonitrile, nm, $\varepsilon/M^{-1}cm^{-1}$): 245 (954), 532 (236).

$[Ni(phen)_3]$ $[MnCl_4]$ (2p)

A solution of $[Ni(phen)_3]Cl_2.2H_2O$ (0.71 g, 1.0 mmol) in 10 mL methanol was added dropwise to a solution of $MnCl_2.6H_2O$ (0.19 g, 1.0 mmol) in 5 mL of the same solvent. The resultant mixture was stirred for 30 min. The clear solution was filtered

and evaporated to dryness under vacuum in 71 % (0.56 g, 0.71 mmol) yield. The solid compound was dissolved in acetonitrile and pink colored single crystals suitable for X-ray data collection were obtained by slow evaporation at room temperature. Anal. Calcd. (%) for $C_{36}H_{24}N_8Cl_4MnNi$ (821): C, 52.47; H, 2.94; N, 13.60; Found: C, 52.84; H, 3.07; N, 13.72. IR (KBr, cm^{-1}): ν(C=N) 1623. UV / vis (methanol, nm, $\varepsilon/M^{-1}cm^{-1}$): 242 (882), 516 (272).

$[Ni(phen)_3]$ $[Co(tm^{t\text{-}Bu})Cl_3]_2$ (2q)

A solution of $[Ni(phen)_3]Cl_2.2H_2O$ (0.71 g, 1.0 mmol) in 10 mL methanol was added dropwise to a solution of $Co(tm^{t\text{-}Bu})Cl_3$ obtained by the reaction of $CoCl_2.6H_2O$ (0.24 g, 1.0 mmol) and N-tert-butyl-2-thioimidazole (0.16 g, 1.0 mmol) in 5 mL of methanol (40 min. reaction time). The resultant mixture was further stirred for 30 min and filtered on celite. The solvent was evaporated to dryness and the compound was dissolved in acetonitrile for crystallization. The green colored crystals suitable for X-ray data collection were obtained by slow evaporation at room temperature. The yield was 68 % (0.84 g, 0.68 mmol). Anal. Calcd. (%) for $C_{50}H_{48}N_{10}S_2Cl_6Co_2Ni$ (1238): C, 48.30; H, 3.86; N, 11.27; S, 5.15. Found: C, 48.24; H, 3.78; N, 11.21; S, 5.12. IR (KBr, cm^{-1}): ν(N-H) 3391, ν(C-H) 3044, ν(C=N) 1627, ν(C=S) 1089. UV / vis (acetonitrile, nm, $\varepsilon/M^{-1}cm^{-1}$): 245 (876), 522 (264).

$[Ni(phen)_3]$ $[Ni(tm^{t\text{-}Bu})Cl_3]_2$ (2r)

This complex was prepared in 64 % (0.78 g, 0.64 mmol) yield by the same procedure as outlined above for **2q.** The green colored crystals suitable for X-ray data collection were obtained by slow evaporation of acetonitrile solution at room temperature. Anal. Calcd. (%) for $C_{50}H_{48}N_{10}S_2Cl_6Ni_3$ (1236): C 48.30, H 3.86, N 11.27,

S 5.15; Found: C 48.24, H 3.78, N 11.21, S 5.12. IR (KBr, cm^{-1}): ν(N-H) 3386, ν(C-H) 3038, ν(C=N) 1625, ν(C=S) 1087. UV / vis (acetonitrile, nm, $\varepsilon/M^{-1}cm^{-1}$): 241 (912), 528 (255).

$[Ni(phen)_2(tm^{t\text{-}Bu})Cl)]Cl$ (2s)

A methanolic solution (15 mL) of $NiCl_2.6H_2O$ (0.24 g, 1.0 mmol), 1,10-phenanthroline (0.39 g, 2.0 mmol) and N-tert-butyl-2-thioimidazole (0.16 g, 1.0 mmol) were stirred for 1 h. The reaction mixture was filtered over celite and evaporated to dryness under vacuum. Yield was 72 % (0.46 g, 0.72 mmol). Anal. Calcd. (%) for $C_{31}H_{28}N_6SCl_2Ni$ (644): C, 57.67; H, 4.34; N, 13.02; S, 4.96. Found: C, 57.73; H, 4.39; N, 13.11; S, 5.05. IR (KBr, cm^{-1}): ν(N-H) 3382, ν(C-H) 3053, ν(C=N) 1618, ν(C=S) 1082. UV / vis (acetonitrile, nm, $\varepsilon/M^{-1}cm^{-1}$): 245 (943), 531 (276).

$[Ni(phen)_2(tm^{t\text{-}Bu})Cl)]$ $[Zn(tm^{t\text{-}Bu})Cl_3]$ (2t)

The solution of $[Ni(phen)_2(tm^{t\text{-}Bu})Cl)]Cl$ (0.32 g, 0.5 mmol) in 10 mL methanol was added dropwise to a methanolic solution (5 mL) of $Zn(tm^{t\text{-}Bu})Cl_3$ obtained from the reaction of $ZnCl_2$ (0.07 g, 0.5 mmol) and N-tert-butyl-2-thioimidazole (0.08 g, 0.5 mmol). The resultant solution was further stirred for 30 min. The green colored solution was filtered and evaporated to dryness. The solid compound was dissolved in acetonitrile and light green colored crystals suitable for X-ray data collection were obtained by slow evaporation at room temperature. Yield was 64 % (0.60 g, 0.32 mmol). Anal. Calcd. (%) for $C_{38}H_{48}N_8S_2Cl_4NiZn$ (942): C, 48.61; H, 5.11; N, 11.94; S, 3.41 %. Found: C, 48.53; H, 5.18; N, 11.85; S, 3.48 %. IR (KBr, cm^{-1}): ν(N-H) 3379, ν(C-H) 3053, ν(C=N) 1621, ν(C=S) 1084. UV / vis (methanol, nm, $\varepsilon/M^{-1}cm^{-1}$): 241 (832), 526 (282).

Chapter-3

Synthesis of 3,5-diisopropylpyrazole [$Pz^{iPr2}H$] (3a)

Diisobutrylmethane used for the preparation of 3,5-diisopropylpyrazole was synthesized by the following method:

Lithium amide (25.00 g, 1.08 mol) and diethyl ether (80 mL) were taken in three necked flask round bottom flask. To the mixture, a solution of isopropylmethylketone (58.82 g, 0.68 mol) was added dropwise over a period of 60 min. Methylisobutyrate (56.62 g, 0.55 mol) was then added dropwise to the above mixture over a period of 90 min. After being refluxed for 10 h, a dilute HCl solution was added to the mixture to hydrolyze the unreacted lithium amide and the water layer was extracted with diethyl ether (3 x 100 mL). The ether layer was washed three times with saturated NaCl aqueous solution and after drying over $MgSO_4$, diethyl ether was removed by evaporation. The resulting solution was distilled under reduced pressure at 140 °C affording 44.96 g diisobutrylmethane.

In a two-necked round bottom flask, aqueous hydrazine monohydrate (23.00 g, 0.46 mol) was added dropwise to a solution of diisobutrylmethane (42.49 g, 0.27 mol) dissolved in 60 mL ethanol. After refluxing for 10 h, the mixture was allowed to cool at room temperature and 100 ml saturated aqueous NaCl solution was added. The compound was extracted with diethyl ether (3 x 100 mL) and the organic layer was washed with saturated NaCl solution (three times). After being dried over $MgSO_4$ for 6 h the solvent was evaporated to dryness. The resultant white solid was recrystallized from acetonitrile to afford 3,5-diisopropylpyrazole as white needles in 48.24 % (19.69 g, 0.13 mol) yield. Anal. Calcd. (%) for $C_9H_{16}N_2$ (152): C, 71.01; H, 10.59; N 18.40. Found: C, 70.33; H, 10.49; N, 17.95. ^{1}H NMR ($(CD_3)_2CO$, 500 MHz) δ, 1.22 (d, 12 H, CH*Me*2), 2.91 (m, 2 H, *CH*Me2), 5.80 (s, 1 H, Pz), 11.31 (s, br, 1H, NH).

Synthesis of potassium hydrotris(3,5-diisopropyl-1-pyrazolyl)borate [KTp^{ipr2}] (3b)

A mixture of 3,5-diisopropylpyrazole (13.00 g, 0.08 mol) and KBH_4 (1.53 g, 0.027 mol) was warmed gradually while monitoring hydrogen evolution. The mixture was heated to 240 °C and heating continued until no hydrogen evolution was observed. The solution was allowed to cool at room temperature; the solid mass was dissolved in dichloromethane and filtered over celite. The solvent was evaporated under vacuum and the resultant solid was carefully recrystallized from acetonitrile, affording KTp^{ipr2} as a white crystalline solid in 25.65 % (10.08 g, 0.02 mol) yield. Anal. Calcd. (%) for $C_{27}H_{46}N_6BK$ (504): C, 64.27; H, 9.19; N, 16.65. Found: C, 64.20 ; H, 9.26; N,16.65. IR (KBr, cm^{-1}): ν(BH), 2453. ^1H NMR (500 MHz, $(CD_3)_2CO$,) δ (ppm) = 1.10 (d, 18H, $CHMe_2$), 1.15 (d, 18H, $CHMe_2$), 2.96-3.14 (m, 6H, $CHMe_2$), 5.67 (s, 3H, Pz).

[$Tp^{iPr2}Co(NO_3)$] (3c)

(0.29 g, 1.0 mmol) $Co(NO_3)_2.6H_2O$ and (0.50 g, 1.0 mmol) KTp^{iPr2} were stirred in 30 mL CH_2Cl_2 for 6 h. The mixture was filtered over celite and solvent was evaporated to dryness under vacuum. The compound was recrystallized from acetronitrile at -20 °C and the purple crystals were obtained in 75 % (0.47 g, 0.75 mmol) yield. Anal. Calcd. (%) for $C_{29}H_{49}N_8O_3BCo$ (627): C, 55.51; H, 7.87; N, 17.86. Found: C, 55.12; H, 7.65; N, 16.97. IR (KBr, cm^{-1}): ν(BH) 2535, $\nu_{as}(NO_3)$ 1530, $\nu_s(NO_3)$ 1261. UV / vis (toluene, nm, $\varepsilon/M^{-1}cm^{-1}$) 243 (823), 532 (127). Magnetic moment μ_{eff} (295 K): 3.60 B.M.

[$Tp^{iPr2}Co$(*p*-F-OBz)] (3d)

To the toluene solution (15 mL) of **3c** (0.51 g, 0.81 mmol), acetonitrile solution (10 mL) of sodium *p*-fluorobenzoate (0.13 g, 0.81 mmol) was added drop-wise and the

reaction mixture was stirred for 10 h. The resultant mixture was filtered over celite and solvent was evaporated to dryness under vacuum. The compound was dissolved in a mixture of acetonitrile and dichloromethane solvent and the purple colored crystals were obtained at –20 °C in 52 % (0.28 g, 0.42 mmol) yield. Anal. Calcd. (%) for $C_{34}H_{50}N_6O_2BFCo$ (663): C, 61.54; H, 7.60; N, 12.67. Found: C, 61.49; H, 7.72; N, 12.59. IR (KBr, cm^{-1}): ν(BH) 2532, ν_{as}(COO) 1602, ν_s(COO) 1432. UV / vis (toluene, nm, $\varepsilon/M^{-1}cm^{-1}$): 290 (1837), 576 (112). Magnetic moment μ_{eff} (295 K): 3.89 B.M.

[Tp^{iPr2}Co(*p*-Cl-OBz)] (3e)

This complex was prepared in 55 % (0.30 g, 0.44 mmol) yield by the same procedure as outlined above for **3d**. Anal. Calcd. (%) for $C_{34}H_{50}N_6O_2BClCo$ (679): C, 61.05; H, 7.41; N, 12.36. Found: C, 61.09; H, 7.47; N, 12.39. IR (KBr, cm^{-1}): ν(BH) 2536, ν_{as}(COO) 1605, ν_s(COO) 1428. UV / vis (toluene, nm, $\varepsilon/M^{-1}cm^{-1}$): 290 (1837), 576 (112). Magnetic moment μ_{eff} (295 K): 3.93 B.M.

[Co(*p*-F-OBz){HB(3-OCMe$_2$-5-Pz^{iPr})(3,5-Pz^{iPr2})$_2$}(3,5-Pz^{iPr2}H)] (3f)

To dichloromethane solution (15 mL) of **3d** (0.46 g, 0.70 mmol), 1 equivalent of 3,5-Pz^{iPr2}H (0.11 g, 0.70 mmol) and 30 equivalent of aqueous 30 % H_2O_2 (2.15 mL, 21.0 mmol) was added drop-wise at room temperature with continuous stirring. The reaction mixture was further stirred for 1 h, cooled at -20 °C for 10 min and filtered on celite in cold condition. The solution was evaporated to dryness and the brown colored crystals were obtained from the mixture of acetonitrile and dichloromethane at –20 °C in 71 % (0.41 g, 0.50 mmol) yield. Anal. Calcd. (%) for $C_{43}H_{65}N_8O_3BFCo$ (830): C, 62.17; H, 7.89; N, 13.49. Found: C, 62.23; H, 7.94; N, 13.56. IR (KBr, cm^{-1}): ν(NH)

3354, ν(BH) 2541, ν_{as}(COO) 1592, ν_{s}(COO) 1381. UV / vis (toluene, nm, ε/$M^{-1}cm^{-1}$): 289 (885).

[Co(*p*-Cl-OBz){HB(3-OCMe$_2$-5-Pz^{iPr})(3,5-Pz^{iPr2})$_2$}(3,5-Pz^{iPr2}H)] (3g)

This complex was prepared in 68 % (0.30 g, 0.47 mmol) yield by the same procedure as outlined above for **3f**. Anal. Calcd. (%) for $C_{43}H_{65}N_8O_3BClCo$ (846): C, 59.94; H, 7.73; N, 14.07. Found: C, 60.05; H, 7.84; N, 14.19. IR (KBr, cm^{-1}): ν(NH) 3362, ν(BH) 2537, ν_{as}(COO) 1589, ν_{s}(COO) 1378. UV / vis (toluene, nm, ε/$M^{-1}cm^{-1}$): 286 (967).

[(3,5-Pz^{iPr2}H)$_2$Co$_2$(μ-3,5-Pz^{iPr2})$_2$(*p*-F-OBz)$_2$] (3h)

$CoCl_2.6H_2O$ (0.29 g, 1.0 mmol), 3,5-Pz^{iPr2}H (0.30 g, 2.0 mmol) and sodium *p*-fluorobenzoate (0.16 g, 1.0 mmol) were stirred in a mixture of dichloromethane (20 mL) and acetonitrile (5 mL) for 8 h. The solution was filtered over celite and the solvent was evaporated to dryness under vacuum in 75% (0.76 g, 0.75 mmol) yield. Violet colored crystals were obtained by slow cooling of acetonitrile solution at -20 °C. Anal. Calcd. (%) for $C_{50}H_{70}N_8O_4F_2Co_2$ (1002): C, 59.87; H, 7.03; N, 11.17. Found: C, 59.91; H, 7.15; N, 11.29. IR (KBr, cm^{-1}): ν(NH) 3367, ν_{as}(COO) 1590, ν_{s}(COO) 1382. Magnetic moment μ_{eff}(295 K): 5.78 B.M.

[(3,5-iPr$^{i}_2$pzH)$_2$Co$_2$(μ-3,5-Pr$^{i}_2$pz)$_2$(Cl-OBz)$_2$] (3i):

This complex was prepared in 72 % (0.30 g, 0.72 mmol) yield by the same procedure as outlined above for **3h**. Anal. Calcd. (%) for $C_{50}H_{70}N_8O_4Cl_2Co_2$ (1034): C, 57.97; H, 6.81; N, 11.38; Found: C, 58.06; H, 6.90; N, 11.43. IR (KBr, cm^{-1}), ν(NH) 3374, ν_{as}(COO) 1588, ν_{s}(COO) 1374. Magnetic moment μ_{eff}(295 K): 5.78 B.M.

[Co(3-OCMe$_2$-5-Pz^{iPr}H)$_3$]. 2(*p*-F-OBz) (3j)

$CoCl_2.6H_2O$ (0.29 g, 1.0 mmol) and 3,5-Pz^{iPr2}H (0.45 g, 3.0 mmol) were stirred for 2 h in dichloromethane. A methanolic solution of sodium *p*-fluorobenzoate (0.33 g, 2.0 mmol) and 50 equivalents of 30 % H_2O_2 (5.12 mL, 50 mmol) was added to the reaction mixture and the color change from blue to purple was observed at -40 °C. The reaction mixture was stirred for additional 20 min and extracted with dichloromethane. The solvent layer was dried on anhydrous sodium sulphate and filtered over celite. The solution was evaporated to dryness and purple colored compound was obtained in 64.2 % (0.54 g, 0.64 mmol) yield. Suitable single crystals for X-ray data collection were obtained from acetonitrile solution at -20 °C. Anal. Calcd. (%) for $C_{41}H_{52}N_6O_7F_2Co$ (837): C, 58.78; H, 6.26; N, 10.03; Found: C, 58.82; H, 6.31; N, 10.06. IR (KBr, cm^{-1}), ν(NH) 3368, ν_{as}(COO) 1681, ν_s(COO) 1464. UV / vis (acetonitrile, nm, $\varepsilon/M^{-1}cm^{-1}$): 246 (943).

[Co(3-OCMe$_2$-5-Pz^{iPr}H)$_3$]. 2(*p*-Cl-OBz) (3k)

This complex was prepared in 65.4 % (0.57 g, 0.65 mmol) yield by the same procedure as outlined above for **3j**. Anal. Calcd. (%) for $C_{41}H_{53}N_6O_7Cl_2Co$ (870): C, 56.49; H, 6.13; N, 9.64. Found: C, 56.56; H, 6.16; N, 9.68. IR (KBr, cm^{-1}): ν(NH) 3363, ν_{as}(COO) 1676, ν_s(COO) 1468. UV / vis (acetonitrile, nm, $\varepsilon/M^{-1}cm^{-1}$): 249 (939).

[Co(3-OCMe$_2$-5-Pz^{iPr}H)$_3$]. 2(*p*-CH$_3$-OBz) (3l)

This complex was prepared in 62.4 % (0.51 g, 0.62 mmol) yield by the same procedure as outlined above for **3j**. Anal. Calcd. (%) for $C_{43}H_{59}N_6O_7Co$ (830): C, 62.16; H, 7.16; N, 10.11. Found: C, 62.21; H, 7.26; N, 10.19. IR (KBr, cm^{-1}): ν(NH) 3371, ν_{as}(COO) 1681, ν_s(COO) 1472. UV / vis (acetonitrile, nm, $\varepsilon/M^{-1}cm^{-1}$): 246 (969).

[Co(3-OCMe$_2$-5-Pz^{iPr}H)$_3$]. 2(*p*-NO$_2$-OBz) (3m)

This complex was prepared in 63.8 % (0.54 g, 0.64 mmol) yield by the same procedure as outlined above for **3j**. Anal. Calcd. (%) for $C_{41}H_{53}N_8O_{11}Co$ (892): C, 55.15; H, 5.98; N, 12.55. Found: C, 55.21; H, 6.04; N, 12.63. IR (KBr, cm^{-1}): ν(NH) 3364, ν_{as}(COO) 1682, ν_s(COO) 1465. UV / vis (acetonitrile, nm, $\varepsilon/M^{-1}cm^{-1}$): 248 (823).

[Co(3-OCMe$_2$-5-Pz^{iPr}H)$_3$]. 2(*p*-CN-OBz) (3n)

This complex was prepared in 66.4 % (0.56 g, 0.66 mmol) yield by the same procedure as outlined above for **3j**. Anal. Calcd. (%) for $C_{43}H_{53}N_8O_7Co$ (852): C, 60.56; H, 6.26; N, 13.14. Found: C, 60.63; H, 6.34; N, 13.19. IR (KBr, cm^{-1}): ν(NH) 3370, ν(CN) 2278, ν_{as}(COO) 1689, ν_s(COO) 1469. UV / vis (acetonitrile, nm, $\varepsilon/M^{-1}cm^{-1}$): 242 (987).

[Co(3-OCMe$_2$-5-Pz^{iPr}H)$_3$]. 2(*p*-CHO-OBz) (3o)

This complex was prepared in 61.7 % (0.54 g, 0.62 mmol) yield by the same procedure as outlined above for **3j**. Anal. Calcd. (%) for $C_{43}H_{55}N_6O_9Co$ (858): C, 60.13; H, 6.45; N, 9.79. Found: C, 60.19; H, 6.51; N, 9.86. IR (KBr, cm^{-1}): ν(NH) 3365, ν_{as}(COO) 1685, ν_s(COO) 1471. UV / vis (acetonitrile, nm, $\varepsilon/M^{-1}cm^{-1}$): 246 (841).

[Co(3-OCMe$_2$-5-Pz^{iPr}H)$_3$] (3p)

$CoCl_2.6H_2O$ (0.29 g, 1.0 mmol) and 3,5-Pz^{iPr2}H (0.45 g, 3.0 mmol) were stirred for 2 h in dichloromethane. 100 equivalents of 30 % H_2O_2 (10.02 mL, 100 mmol) was added to the reaction mixture and the color change from blue to purple was observed at -40 °C. The reaction mixture was stirred for additional 20 min and extracted with dichloromethane. The solvent layer was dried on anhydrous sodium sulphate and

filtered over celite. The solution was evaporated to dryness in 52.1 % (0.54 g, 0.52 mmol) yield. Anal. Calcd. (%) for $C_{27}H_{44}N_6O_3Co$ (559): C, 57.95; H, 7.93; N, 15.02; Found: C, 58.03; H, 8.11; N, 15.16. IR (KBr, cm^{-1}), ν(NH) 3374. UV / vis (acetonitrile, nm, $\varepsilon/M^{-1}cm^{-1}$): 242 (759).

$[_k^2(tm^{t\text{-}Bu})_2CoCl_2]$ (3q)

$CoCl_2.6H_2O$ (0.12 g, 0.5 mmol) and N-tert-butyl-2-thioimidazole (0.16 g, 1 mmol) were stirred in 15 mL CH_2Cl_2 and 3 mL CH_3OH for 2 h. The mixture was filtered over celite and solvent was evaporated to dryness under vacuum. The compound obtained in 78.8% (0.17 g, 0.39 mmol) yield was dissolved in 5 mL CH_3CN and green crystals were obtained at -20 °C. Anal. Calcd. (%) for $C_{14}H_{22}N_4S_2Cl_2Co$ (439): C, 38.18; H, 5.00; N, 12.72. Found: C, 38.12; H, 5.08; N, 12.54. IR (KBr, cm^{-1}): ν(C=S) 1092. UV / vis (acetonitrile, nm, $\varepsilon/M^{-1}cm^{-1}$): 284 (832), 514 (272). Magnetic moment μ_{eff} (295 K): 3.86 B.M.

$[(tm^{t\text{-}Bu})_2Co_2(\mu\text{-}tm^{t\text{-}Bu})_2Cl_2]$ (3r)

(0.24 g, 1 mmol) $CoCl_2.6H_2O$ and (0.32 g, 2 mmol) of N-tert-butyl-2-thioimidazole were stirred in 15 mL CH_2Cl_2 and 3 mL CH_3OH for 8 h. The mixture was filtered over celite and the solvent was evaporated to dryness under vacuum. The compound obtained in 62.4% (0.49 g, 0.62 mmol) yield was dissolved in 5 mL CH_3CN and green crystals were obtained at -20 °C. Anal. Calcd. (%) for $C_{28}H_{46}N_8S_4Cl_2Co_2$ (810): C, 41.43; H, 5.67; N, 13.81. Found: C, 41.16; H, 5.76; N, 13.93. IR (KBr, cm^{-1}): ν(C=S) 1097. UV / vis (acetonitrile, nm, $\varepsilon/M^{-1}cm^{-1}$): 287 (954), 518 (291). Magnetic moment μ_{eff} (295 K): 5.81 B.M.

Chapter-4

Synthesis of 3-phenyl-5-methylpyrazole [$Pz^{Ph,Me}H$] (4a)

To the ethanolic solution (150 mL) of benzoylacetone (25 g, 0.15 mol) in two necked round bottom flask, hydrazine hydrate (13 mL, 0.22 mmol) was added over a period of 40 min. The reaction mixture was refluxed (110-140 °C) for 10 h. The solution was allowed to cool at room temperature and the solid mass was transferred on bucker funnel, washed with distilled water and eventually with hexane for 2-3 times. It was dried completely under vacuum for several hours. The white powdered 3-phenyl-5-methylpyrazole was obtained in 73.03 % (16.85 g, 0.10 mol) yield. Anal. Calcd. (%) for $C_{10}H_{10}N_2$ (158): C, 75.92; H, 6.37; N, 17.72. Found: C, 76.03; H, 6.43; N, 17.83. IR (KBr, cm^{-1}): ν (NH) 3406. ^1H NMR (CD_3OD, 500 MHz) δ, 2.69 (s, 3H, CH_3), 6.28 (s, 1H, Pz), 7.20-7.54 (m, 5 H, C_6H_5), 13.72 (s, br, 1H, NH).

Synthesis of Potassium hydrotris(3-phenyl-5-methyl-1-pyrazolyl)borate [$KTp^{Ph,Me}$] (4b)

A mixture of 3-phenyl-5-methylpyrazole (10.39 g, 0.07 mol) and KBH_4 (1.17g, 0.02 mol) was heated upto 240 °C and the heating continued until no hydrogen evolution was observed. The solution was allowed to cool at room temperature. The solid product was dissolved in dichloromethane and filtered over celite. The solvent was evaporated and the resultant solid was carefully recrystallized from acetonitrile affording $KTp^{Ph,Me}$ as a white crystalline solid in 69 % (7.20 g, 0.01 mol) yield. Anal. Calcd. (%) for $C_{30}H_{28}N_6BK$ (522): C, 68.96; H, 5.40; N, 16.08; Found: C, 69.05; H, 5.48; N, 16.17. IR (KBr, cm^{-1}): ν(BH) 2428. ^1H NMR (CD_3OD, 500 MHz) δ, 2.52 (s, 9H, CH_3), 6.34 (s, 3H, Pz), 7.15-7.36 (m, 15H, C_6H_5).

[$(Tp^{Ph,Me})_2Ni$] (4c)

$NiCl_2.6H_2O$ (0.20 g, 0.85 mmol) and $KTp^{Ph,Me}$ (0.88 g, 1.70 mmol) were stirred in 25 mL CH_2Cl_2 and 5 mL CH_3OH for 6 h. The mixture was filtered over celite and the solvent was evaporated to dryness under vacuum. The resultant compound in 67.6 % (0.58 g, 0.56 mmol) yield was dissolved in 5 mL toluene and yellow crystals suitable for X-ray data collection were obtained at -20 °C. Anal. Calcd. (%) for $C_{60}H_{56}N_{12}B_2Ni$ (1024): C, 70.27; H, 5.50; N, 16.39. Found: C, 70.38; H, 5.57; N, 16.46. IR (KBr, cm^{-1}): ν(BH) 2546. UV / vis (dichloromethane, λ_{max}, nm, $\varepsilon/M^{-1}cm^{-1}$): 287 (1048), 594 (373). Magnetic moment μ_{eff} (295 K): 3.52 B.M.

[$(Tp)_2Ni$] (4d)

$NiCl_2.6H_2O$ (0.16 g, 0.65 mmol) and KTp (0.31 g, 1.30 mmol) were stirred in CH_2Cl_2 (25 mL) and CH_3OH (5 mL) for 6 h. The mixture was filtered over celite and the solvent was evaporated to dryness under vacuum. The resultant compound in 80 % (0.25 g, 0.52 mmol) yield was dissolved in CH_3CN (5 mL) and pink crystals suitable for X-ray data collection were obtained at -20 °C. Anal. Calcd. (%) for $C_{18}H_{20}B_2N_{12}Ni$ (484): C, 44.53; H, 4.12; N, 34.64. Found: C, 44.62; H, 4.18; N, 34.69. IR (KBr, cm^{-1}): ν(BH) 2541. UV / vis (dichloromethane, λ_{max}, nm, $\varepsilon/M^{-1}cm^{-1}$): 287 (1048), 564 (373). Magnetic moment μ_{eff} (295 K): 3.16 B.M.

[$Tp^{Ph,Me}Ni(Cl)Pz^{Ph,Me}H$] (4e)

$NiCl_2.6H_2O$ (0.47 g, 2.0 mmol), $Pz^{Ph,Me}H$ (0.32 g, 2.0 mmol) and $KTp^{Ph,Me}$ (1.04 g, 2.0 mmol) were stirred in 25 mL CH_2Cl_2 and 5 mL CH_3OH for 6 h. The mixture was filtered over celite and solvent was evaporated to dryness under vacuum. The compound in 84.8 % (1.24 g, 1.69 mmol) yield was dissolved in 5 mL toluene and

yellow crystals were obtained at -20 °C. Anal. Calcd. (%) for $C_{40}H_{38}N_8BClNi$ (734): C, 65.30; H, 5.21; N, 15.23. Found: C, 65.38; H, 5.28; N, 15.29. IR (KBr, cm^{-1}): ν(NH) 3382, ν(BH) 2532. UV / vis (toluene, λ_{max}, nm, $\varepsilon/M^{-1}cm^{-1}$): 289 (832), 484 (272). Magnetic moment μ_{eff} (295 K): 3.49 B.M.

[$Tp^{Ph,Me}$Ni(OBz)$Pz^{Ph,Me}$H] (4f)

To a 20 mL toluene solution of **4e** (0.36 g, 0.64 mmol), 10 mL acetonitrile solution of sodium benzoate (0.09 g, 0.64 mmol) was added and the reaction mixture was stirred for 10 h. After filtration, the filtrate was dried under vacuum and green compound in 73.2 % (0.38 g, 0.46 mmol) yield was obtained. The colored compound was recrystallized from toluene at -20 °C. Anal. Calcd. (%) for $C_{47}H_{43}N_8O_2BNi$ (820): C, 68.72; H, 5.28; N, 13.64. Found: C, 68.83; H, 5.31; N, 13.72. IR (KBr, cm^{-1}): ν(NH) 3364, ν(BH) 2534, ν_{as}(COO) 1596, ν_s(COO) 1388. UV / vis (toluene, λ_{max}, nm, $\varepsilon/M^{-1}cm^{-1}$): 285 (842), 518 (287). Magnetic moment μ_{eff} (295 K): 3.59 B.M.

[$Tp^{Ph,Me}$Ni(*p*-F-OBz)$Pz^{Ph,Me}$H] (4g)

This complex was prepared in 63.4 % (0.53 g, 0.63 mmol) yield by the same procedure as outlined above for **4f**. Anal. Calcd. (%) for $C_{47}H_{42}N_8O_2BFNi$ (838): C, 67.25; H, 5.04; N, 13.35. Found: C, 67.33; H, 5.11; N, 13.46. IR (KBr, cm^{-1}): ν(NH) 3364, ν(BH) 2534, ν_{as}(COO) 1606, ν_s(COO) 1391. UV / vis (toluene, λ_{max}, nm, $\varepsilon/M^{-1}cm^{-1}$): 289 (739), 516 (340). Magnetic moment μ_{eff} (295 K): 3.52 B.M.

[$Tp^{Ph,Me}$Ni(*p*-Cl-OBz)$Pz^{Ph,Me}$H] (4h)

This complex was prepared in 68.3% (0.58 g, 0.68 mmol) yield by the same procedure as outlined above for **4f**. Anal. Calcd. (%) for $C_{47}H_{42}N_8O_2BClNi$ (854): C, 65.96; H, 4.95; N, 13.09. Found: C, 66.13; H, 5.08; N, 13.14. IR (KBr, cm^{-1}): ν(NH)

3368, ν(BH) 2543, ν_{as}(COO) 1598, ν_{s}(COO) 1396. UV / vis (toluene, λ_{max}, nm, $\varepsilon/M^{-1}cm^{-1}$): 282 (856), 512 (407). Magnetic moment μ_{eff} (295 K): 3.61 B.M.

[$Tp^{Ph,Me}$Ni(*p*-NO_2-OBz)$Pz^{Ph,Me}$H] (4i)

This complex was prepared in 67.3 % (0.58 g, 0.67 mmol) yield by the same procedure as outlined above for **4f**. Anal. Calcd. (%) for $C_{47}H_{42}N_9O_4BNi$ (865): C, 65.55; H, 4.92; N, 13.83. Found: C, 65.63; H, 4.98; N, 13.89. IR (KBr, cm^{-1}): ν(NH) 3362, ν(BH) 2537, ν_{as}(COO) 1605, ν_{s}(COO) 1398, ν(NO_2) 1342. UV / vis (dichloromethane, λ_{max}, nm, $\varepsilon/M^{-1}cm^{-1}$): 286 (684), 519 (124). Magnetic moment μ_{eff} (295 K): 3.65 B.M.

[$Tp^{Ph,Me}$Ni(*p*-Me-OBz)$Pz^{Ph,Me}$H] (4j)

This complex was prepared in 71.1 % (0.59 g, 0.70 mmol) yield by the same procedure as outlined above for **4f**. Anal. Calcd. (%) for $C_{48}H_{45}N_8O_2BNi$ (834): C, 69.01; H, 5.43; N, 13.41. Found: C, 69.12; H, 5.58; N, 13.56. IR (KBr, cm^{-1}): ν(NH) 3361, ν(BH) 2540, ν_{as}(COO) 1605, ν_{s}(COO) 1401. UV / vis (toluene, λ_{max}, nm, $\varepsilon/M^{-1}cm^{-1}$): 285 (556), 514 (251). Magnetic moment μ_{eff} (295 K): 3.49 B.M.

[$Tp^{Ph,Me}$Ni(*p*-OMe-OBz)$Pz^{Ph,Me}$H] (4k)

This complex was prepared in 74.8 % (0.63 g, 0.74 mmol) yield by the same procedure as outlined above for **4f**. Anal. Calcd. (%) for $C_{48}H_{45}N_8O_3BNi$ (850): C, 67.71; H, 5.33; N, 13.16. Found: C, 67.83; H, 5.39; N, 13.28. IR (KBr, cm^{-1}): ν(NH) 3369, ν(BH) 2533, ν_{as}(COO) 1598, ν_{s}(COO) 1388. UV / vis (toluene, λ_{max}, nm, $\varepsilon/M^{-1}cm^{-1}$): 284 (871), 517 (412). Magnetic moment μ_{eff} (295 K): 3.59 B.M.

[$Tp^{Ph,Me}$Ni(*p*-HO-OBz)$Pz^{Ph,Me}$H] (4l)

This complex was prepared in 70.7 % (0.59 g, 0.70 mmol) yield by the same procedure as outlined above for **4f**. Anal. Calcd. (%) for $C_{47}H_{43}N_8O_3BNi$ (836): C, 67.41; H, 5.18; N, 13.38. Found: C, 67.56; H, 5.26; N, 13.47. IR (KBr, cm^{-1}): ν(NH) 3364, ν(BH) 2539, ν_{as}(COO) 1601, ν_s(COO) 1396, ν(OH) 3521. UV / vis (acetonitrile, λ_{max}, nm, $\varepsilon/M^{-1}cm^{-1}$): 283 (421), 523 (158). Magnetic moment μ_{eff}(295 K): 3.52 B.M.

[$Tp^{Ph,Me}$Ni(*p*-CHO-OBz)$Pz^{Ph,Me}$H] (4m)

This complex was prepared in 68.9 % (0.58 g, 0.68 mmol) yield by the same procedure as outlined above for **4f**. Anal. Calcd. (%) for $C_{48}H_{43}N_8O_3BNi$ (848): C, 67.87; H, 5.10; N, 13.19. Found: C, 67.96; H, 5.16; N, 13.22. IR (KBr, cm^{-1}): ν(NH) 3360, ν(BH) 2542, ν(CO) 1698, ν_{as}(COO) 1592, ν_s(COO) 1373. UV / vis (toluene, λ_{max}, nm, $\varepsilon/M^{-1}cm^{-1}$): 285 (1514), 513 (265). Magnetic moment μ_{eff}(295 K): 3.60 B.M.

[$Tp^{Ph,Me}$Ni(*p*-CN-OBz)$Pz^{Ph,Me}$H] (4n)

This complex was prepared in 73.8 % (0.62 g, 0.73 mmol) yield by the same procedure as outlined above for **4f**. Anal. Calcd. (%) for $C_{48}H_{43}N_9O_2BNi$ (846): C, 68.03; H, 5.11; N, 14.88. Found: C, 68.16; H, 5.16; N, 14.92. IR (KBr, cm^{-1}): ν(NH) 3365, ν(BH) 2539, ν(CN) 2267, ν_{as}(COO) 1589, ν_s(COO) 1374. UV / vis (toluene, λ_{max}, nm, $\varepsilon/M^{-1}cm^{-1}$): 286 (824), 516 (231). Magnetic moment μ_{eff}(295 K): 3.58 B.M.

[$Tp^{Ph,Me}$Ni(*p*-NH_2-OBz)] (4o)

This complex was prepared in 72.4 % (0.49 g, 0.72 mmol) yield by the same procedure as outlined above for **4f**. Anal. Calcd. (%) for $C_{37}H_{34}N_7O_2BNi$ (677):

C, 65.52; H, 5.05; N, 14.46. Found: C, 65.59; H, 5.18; N, 14.52. IR (KBr, cm^{-1}): ν(NH) 3132, ν(BH) 2544, ν_{as}(COO) 1548, ν_{s}(COO) 1374. UV / vis (toluene, λ_{max}, nm, $\varepsilon/M^{-1}cm^{-1}$): 283 (932), 519 (365). Magnetic moment μ_{eff} (295 K): 3.57 B.M.

[$Tp^{Ph,Me}Ni(N_3)Pz^{Ph,Me}H$] (4p)

Complex **4e** (0.22 g, 0.30 mmol) and sodium azide (0.02 g, 0.30 mmol) were allowed to react in a mixture of 5 mL methanol and 10 mL toluene for 1 h. The mixture was filtered over celite and the solvent was evaporated to dryness. The green colored compound in 74.8 % (0.16 g, 0.21 mmol) yield was recrystallized from acetonitrile at -20 °C. Anal. Calcd. (%) for $C_{40}H_{38}N_{11}BNi$ (741): C, 64.72; H, 5.16; N, 20.76. Found: C, 64.77; H, 5.22; N, 20.88. IR (KBr, cm^{-1}): ν(NH) 3363, ν(BH) 2524, ν(N_3) 2075. UV / vis (acetonitrile, λ_{max}, nm, $\varepsilon/M^{-1}cm^{-1}$): 294 (375), 544 (194). Magnetic moment μ_{eff} (295 K): 3.53 B.M.

[$Tp^{Ph,Me}Ni(NCS)Pz^{Ph,Me}H$] (4q)

This complex was prepared in 71.7 % (0.54 g, 0.71 mmol) yield by the same procedure as outlined above for **4p**. Anal. Calcd. (%) for $C_{41}H_{38}N_9BSNi$ (757): C, 64.93; H, 5.05; N, 16.62; S, 4.23. Found: C, 64.97; H, 5.13; N, 16.76; S, 4.34. IR (KBr, cm^{-1}): ν(NH) 3368, ν(BH) 2529, ν(NCS) 2058. UV / vis (acetonitrile, λ_{max}, nm, $\varepsilon/M^{-1}cm^{-1}$): 292 (426), 518 (176). Magnetic moment μ_{eff} (295 K): 3.55 B.M.

[$Ni(tm^{t\text{-}Bu})_2Cl_2$] (4r)

$NiCl_2.6H_2O$ (0.12 g, 0.5 mmol) and N-tert-butyl-2-thioimidazole (0.16 g, 1.0 mmol) were stirred in CH_2Cl_2 (10 mL) and CH_3OH (3 mL) for 1 h. The mixture was filtered over celite and the solvent was evaporated to dryness under vacuum. The

compound in 76.4 % (0.17 g, 0.38 mmol) yield was dissolved in CH_3CN (5 mL) and green crystals were obtained at -20 °C. Anal. Calcd. (%) for $C_{14}H_{24}N_4S_2Cl_2Ni$ (440): C, 38.03; H, 5.47; N, 12.67; S, 14.51. Found: C, 38.06; H, 5.54; N, 12.71; S, 14.62. IR (KBr, cm^{-1}): ν(C=S) 1089. UV / vis (acetonitrile, λ_{max}, nm, $\varepsilon/M^{-1}cm^{-1}$): 282 (867), 517 (253). Magnetic moment μ_{eff} (295 K): 3.94 B.M.

$[Ni(Pz^{Ph,Me}H)_2(tm^{t\text{-}Bu})(NO_3)_2]$ (4s)

$Ni(NO_3)_2.6H_2O$ (0.14 g, 0.5 mmol), N-tert-butyl-2-thioimidazole (0.08 g, 0.5 mmol) and 3-phenyl-5-methyl pyrazole (0.16 g, 1.0 mmol) were stirred in CH_2Cl_2 (15 mL) and CH_3OH (5 mL) for 2 h. The mixture was filtered over celite and solvent was evaporated to dryness under vacuum. The compound in 82.1 % (0.27 g, 0.41 mmol) yield was dissolved in CH_3CN (5 mL) and green crystals were obtained at -20 °C. Anal. Calcd. (%) for $C_{27}H_{32}N_8O_6SNi$ (654): C, 49.48; H, 4.92; N, 17.10; S, 4.89. Found: C, 49.53; H, 4.99; N, 17.16; S, 4.96. IR (KBr, cm^{-1}): ν(NH) 3373, $\nu_{as}(NO_3)$ 1532, ν(C=S) 1095, $\nu_s(NO_3)$ 1262. UV / vis (acetonitrile, λ_{max}, nm, $\varepsilon/M^{-1}cm^{-1}$): 286 (874), 523 (242). Magnetic moment μ_{eff} (295 K): 3.24 B.M.

References

1. Perrin, D.D., Armarego, W.L. and Perrin, D.R., "Purification of laboratory chemicals" 2nd ed., Pergamon, New York, (1980).

2. (a) Sheldrick, G.M., "Phase annealing in SHELX-90: direct methods for larger structures", Acta Cryst., **A46**, 467 (1990). (b) Sheldrick, G.M., "SHELXTL-NT 2000 version 6.12, reference manual", University of Göttingen, Göttingen, Germany.

3. Klaus, B., "DIAMOND, Ver. 1.2c", University of Bonn, Germany (1999).

4. Craggs, A., Keil, L., Moody, G.J. and Thomas, J.D.R., "Evaluation of solvent mediators for ion-selective electrode membranes based on calcium bis(dialkylphosphate) sensors trapped in poly(vinyl chloride) matrixes", Talanta, **22**, 907 (1975).

5. Shultz, M.M., Stefanova, O.K., Mokrov, S.B. and Mikhelson, K.N., "Potentiometric estimation of the stability constants of ion-lonophore complexes in ion-selective membranes by the sandwich membrane method: theory, advantages, and limitations", Anal. Chem., **74**, 510 (2002).